This electronic thesis or dissertation has been downloaded from the King's Research Portal at https://kclpure.kcl.ac.uk/portal/

KING'S College LONDON

The Synthesis and Characterisation of Novel Peptidomimetic Foldamers

Stendall, Ryan

Awarding institution:
King's College London

The copyright of this thesis rests with the author and no quotation from it or information derived from it may be published without proper acknowledgement.

END USER LICENCE AGREEMENT

Unless another licence is stated on the immediately following page this work is licensed

under a Creative Commons Attribution-NonCommercial-NoDerivatives 4.0 International

licence. https://creativecommons.org/licenses/by-nc-nd/4.0/

You are free to copy, distribute and transmit the work

Under the following conditions:

- Attribution: You must attribute the work in the manner specified by the author (but not in any way that suggests that they endorse you or your use of the work).
- Non Commercial: You may not use this work for commercial purposes.
- No Derivative Works - You may not alter, transform, or build upon this work.

Any of these conditions can be waived if you receive permission from the author. Your fair dealings and other rights are in no way affected by the above.

Take down policy

If you believe that this document breaches copyright please contact librarypure@kcl.ac.uk providing details, and we will remove access to the work immediately and investigate your claim.

Download date: 08. Oct. 2023

The Synthesis and Characterisation of Novel Peptidomimetic Foldamers

King's College London

Ryan Stendall

A thesis submitted for the degree of
Doctor of Philosophy in Chemistry

September 2022

Department of Chemistry, King's College London

Abstract

For the past three decades, chemists have sought to synthesise oligomeric structures that adopt single, well-defined conformations in solution. Known as foldamers, these structures have the potential to be able to replicate and perhaps even improve upon the function of biopolymers, with applications in areas such as catalysis and information storage. Peptidomimetic foldamers – those that mimic the structure and behaviour of natural peptides – have received a great deal of attention in particular, with the synthesis and use of extended, unnatural amino acids a common method in order to access molecules with novel secondary structures.

This thesis first describes the synthesis of novel, cyclically-constrained δ-amino acid monomers. Two δ-amino acid targets were synthesised, with the required stereochemistry embedded via previously described organocatalytic procedures. The *trans* monomer was achieved in an overall yield of 4%, whilst the *cis* monomer was achieved in a 29% overall yield.

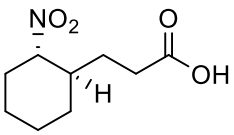

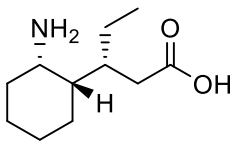

The *cis* monomer was then incorporated into a series of α/δ foldamers, which were subsequently characterised in order to probe their secondary structure. The 1:1 α/δ foldamers with D-Alanine α-residues showed a strong propensity for folding and were found to populate either a 13/11- or 11/13-helical conformation, depending on their length.

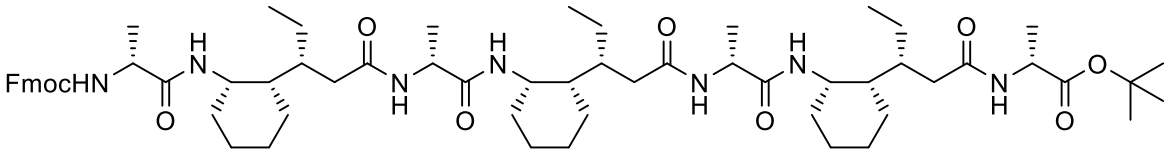

Finally, the syntheses of two previously described cyclically-constrained γ-amino acid precursors was optimised, after which they were incorporated into a series of novel dipeptide building blocks that could be used to for the construction of potentially catalytic α/γ foldamers.

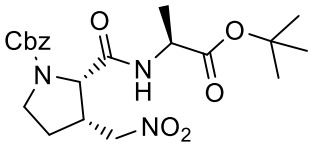

Acknowledgements

I would first like to thank my supervisors - Dr Andre Cobb and Dr Manuel Müller - for their expertise and guidance throughout this project, and a huge thank you to Graeme Hogarth and Cairn Macfaland for their help and support during some difficult times. A big thank you in particular to Dan, Laura and Rossana who welcomed me so warmly into the group, as well as László, Qi, Callum, Ariane and Damien for their helpful contributions and for making life in the lab much more palatable. Ines, thank you for being a fantastic master's student/colleague and for providing all of the many wild, chaotic stories from your everyday life.

A big shout out to my fellow cohort members Steven and Mark for keeping me entertained throughout my time at King's, in addition to all of those I played football with on Fridays. To Jesame and Brie, my housemates for the first two years, thank you for putting up for me and for all the fun times.

Gina and Janette, thank you for all the greatly appreciated encouragement and pep talks, and for providing such a constant source of support. Fred, Ollie, Katie and Mike, thank you for all the fun times and supportive video calls. Thanks to the whole group for not responding to my antics with explosive rage. You're the best!

To my parents, Eliza and Tim, thank you very much for your unwavering support, even in the face of such difficult circumstances. It's fair to say that we faced some significant challenges during my PhD, and we got through them together. Thanks also to Chris and Helen for your support in these times, and in general.

Finally, thank you so much to the most important of them all, Barbara. First for your excellent work that contributed to this thesis, and then for your constant support and companionship thereafter. You suffered almost as much as I did during the write up of this thesis, and I greatly appreciate your patience and encouragement. I look forward to returning the favour in due course!

Declaration of material from a previously submitted thesis, and work done in conjunction with others

The synthesis of compounds **80, 81, 77** and **60** (chapter 2) were first carried out and optimised in conjunction with Barbara Dworakowska (MSci Student, October 2018 – May 2019) as part of her master's project and were included in her master's dissertation.[116]

All CD spectra (chapter 3) were obtained by Fred Martin at the University of Bristol (2022).

All other work in this thesis is entirely my own and has not been submitted previously for any other degree at King's College London or at any other university.

Contents

List of Abbreviations

Ala – Alanine

ACHA - *trans*-2-Aminocyclohexanecarboxylic acid

ACPA - (R)-3-((1S,2S)-2-aminocyclohexyl)pentanoic acid

AMCP - (1S,2R)-2-(nitromethyl)cyclopentane-1-carboxylic acid

Ar – Aryl

Bn – Benzyl

Boc – *tert*-Butyloxycarbonyl

*n*BuLi – *n*-Butyllithium

Cbz - Carbobenzyloxy

CD – Circular dichroism

DAN - 1,5-dialkoxynaphthalene

DCE – Dichloroethane

DCM - Dichloromethane

DIBAL-H - Diisobutylaluminum hydride

DIPEA - N,N-Diisopropylethylamine

DMF - N,N-Dimethylformamide

DMSO - Dimethyl sulfoxide

dr – Diastereomeric ratio

EDCI - 1-Ethyl-3-(3-dimethylaminopropyl)carbodiimide

ee - Enantiomeric excess

EtOAc – Ethyl acetate

Fmoc – Fluorenylmethoxycarbonyl

GABA - γ-aminobutyric acid

HOBt - 1-Hydroxybenzotriazole hydrate

HMBC - Heteronuclear Multiple Bond Correlation

HRMS - High Resolution Mass Spectrometry

HSQC - Heteronuclear Single Quantum Coherence Spectroscopy

IR – Infrared spectroscopy

MeCN – Acetonitrile

MeOH – Methanol

$MgSO_4$ – Magnesium sulfate

MHz – Megahertz

mp – Melting point

NEt_3 - Triethylamine

Ni – Nickel

NMR - Nuclear Magnetic Resonance

NOE – Nuclear Overhauser Effect

NOESY - Nuclear Overhauser Effect Spectroscopy

PCC - Pyridinium chlorochromate

PDI - Pyromellitic diimide

PNA – Peptide nucleic acid

ppm – parts per million

Psi – Pound per square inch

R – Alkyl group

ROESY - Rotating Frame Overhauser Enhancement Spectroscopy

rt – Room temperature

TBAI - Tetra-n-butylammonium iodide

TEMPO - (2,2,6,6-Tetramethylpiperidin-1-yl)oxyl

TFA - Trifluoroacetic acid

THF – Tetrahydrofuran

TLC – Thin Layer Chromatography

TMS – Tetramethylsilyl

TOCSY - Total Correlation Spectroscopy

Trt – Trityl

List of Figures

List of Tables

Chapter 1 - Introduction

Nature utilizes a vast array of macromolecules in order to perform the complicated functions required for life. Many of these can be categorized as structural biopolymers (collagen, cellulose, etc), providing form and shape to cells, tissues and organs whilst contributing to the mechanical properties of the organism.[1] Others, such as enzymes, DNA and antibodies, are responsible for performing sophisticated chemical operations. These "biomolecular structures" fold into intricate, three-dimensional shapes that are vital to their function. This folding is governed both by inherent properties of the molecule itself – such as the type and sequence of monomeric subunit and the subsequent intermolecular forces that are present between them - and by external factors such as pH, temperature, and the presence of cofactors. Although often inert, biopolymer misfolding can introduce toxic functionality. The foundation of many neurodegenerative diseases is underpinned by the aggregation of misfolded proteins, known as prions.

Additionally, many genetic disorders will result in the formation of misshapen and ill-functioning proteins, with sickle cell anemia and cystic fibrosis being prominent examples. However, when functioning as intended, the folding of biomolecular structures unlocks tremendous potential for chemical functionality, including catalysis, information storage and energy capture. The best performing enzymes are capable of accelerating reactions by a factor of 10^{17} (Scheme 1.1), whilst DNA has been demonstrated to hold up to 215 petabytes of data per gram.[2,3] It is no wonder that chemists have long sought to synthetically replicate or even improve upon this fundamental biological phenomenon in the lab.

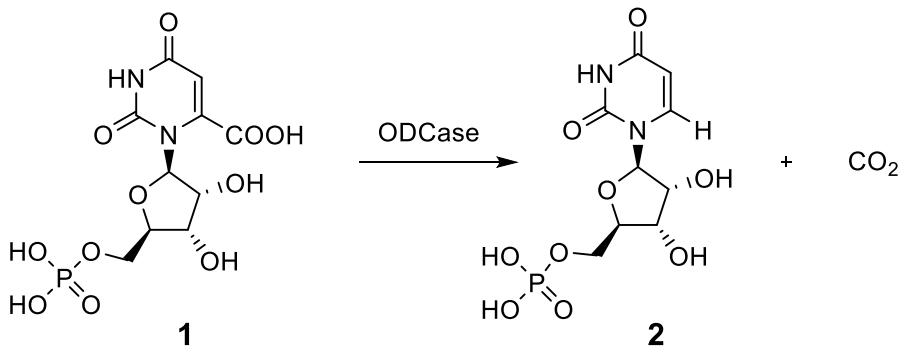

Scheme 1.1: The decarboxylation of Orotidine 5'-monophosphate **1** (OMP) which, in the presence of the enzyme ODCase, has a half-life of 18 ms. Without ODCase, the half-life is 78 million years.[4]

1.1. Foldamers

In 1996, Professor Samuel Gellman was the first to use the term “foldamer” and he went on to provide a definition two years later.[5,6] He described foldamers as synthetic oligomers that have a strong tendency to adopt a specific, compact conformation in solution. This was built upon by Professor Jeffrey Moore, who provided perhaps the most comprehensive definition to date: “a foldamer is any oligomer that folds into a conformationally ordered state in solution, the structures of which are stabilized by a collection of noncovalent interactions between nonadjacent monomer units”.[7] Their ideas were supplemented by the modelling work undertaken by Chan and Dill, which helped to shed some light on the propensity for novel oligomers to adopt secondary structures, predicted to be achieved through the delicate balance of attractive and repulsive forces between monomers.[8]

The first foldamers predated the term; one of the earliest was reported in 1992 by Schreiber *et al.*, who developed a series of vinylogous peptides.[9] They sought to promote the formation of sheet-like structures via the restriction of the β, γ-carbon-carbon bond in the key vinylogous γ-amino acid monomer by the presence of bulky side groups on the γ-carbon. They succeeded in achieving a highly ordered, parallel β-sheet structure - determined by x-ray crystallography – in several tripeptides, such as **3** (Figure 1.1) . They were also able to synthesis a series of foldamers that adopted the alternative antiparallel β-sheet structure by the insertion of a proline-glycine dipeptide subunit, which acted effectively as a β-turn. Crucially, this conformation was observed in solution, via NMR.

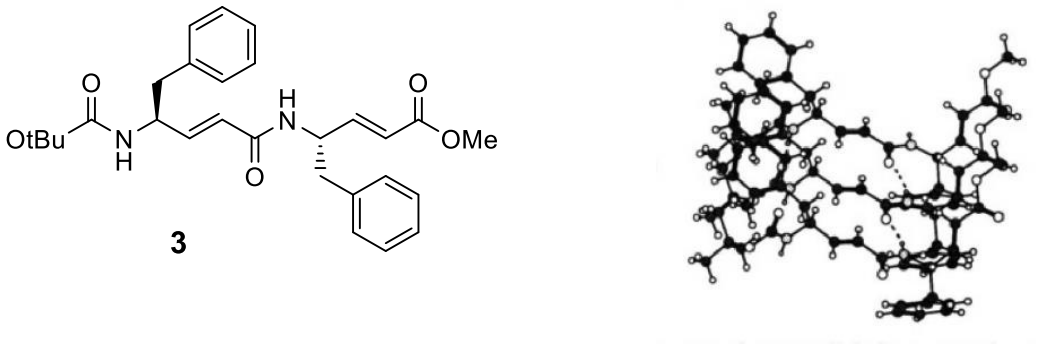

Figure 1.1: The structure of the vinylogous peptide **3**, and the x-ray crystal structure of the parallel β-sheet conformation it adopts.

An early example was provided by Gennari and co-workers in 1994, with their development of sulfonamido-pseudopeptides.[10] They were motivated by the enhanced metabolic stability of the sulfonamide bond when compared to the peptide bond, as well as its significant difference in polarity and the potentially novel structures this might result in. Since α-aminosulfonamides are known to be unstable - readily decomposing via fragmentation - the group sought to make use of β- and γ-aminosulfonic acid monomers in order to construct stable oligomers. The β-aminosulfonic derivatives were found preferentially form 12-membered rings (Figure 1.2) whilst the γ-aminosulfonic derivatives formed 14-membered rings, both facilitated by the formation of a single, well aligned hydrogen bond.

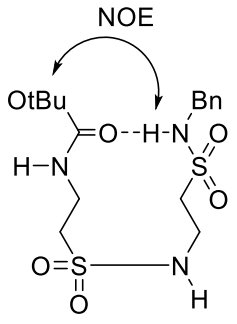

4

Figure 1.2: The 12-membered ring formed by the β-aminosulfonic pseudopeptide **4**, confirmed by NOE signals.

As the decade progressed, interest in the synthesis and study of new foldamers increased rapidly. Since the turn of the century, the field has expanded into a vast array of different foldamer classes, most of which can be grouped into three main categories: abiotic, nucleotidomimetic and peptidomimetic.[7,11]

1.1.1. Abiotic Foldamers

Abiotic foldamers are defined as those which are not derived from or inspired by biological materials. This "*ab initio*" approach to foldamer design allows for a greater level of creativity and diversity of structure, which has led to a broad field of examples, often exhibiting distinctly different properties from those that are bio-inspired.

The use of aromatic monomers is a very common approach and an attractive proposition due to the potential for beneficial, non-covalent interactions (such as pi stacking) to form between aromatic sub-units. Lehn *et al.* provided an elegant example, creating an achiral polyheterocyclic oligomer that folds into a helix.[12] Consisting of an alternating sequence of pyridine and pyrimidine units, the stabilization of the helical conformation was thought to be due to both the formation of favorable aromatic stacking interactions and the preference for the *transoid* geometry of the single bonds within the backbone. To aid the solubility of the foldamer in organic solvents, six thiopropyl side chains were carefully incorporated, all orientated outwards from the helix in order to not disrupt its formation. Thus, the group were able to elucidate its conformation in solution, which closely matched its helical solid-state structure (Figure 1.3).

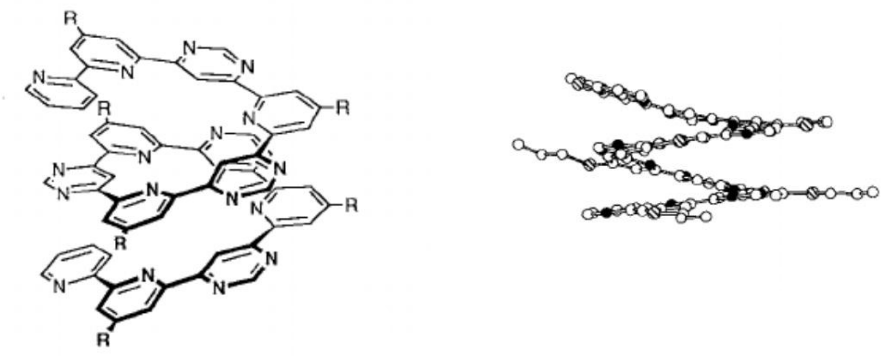

Figure 1.3: From left to right, the solution and solid-phase structures of the polyheterocyclic oligomer developed by Lehn and co-workers.[13]

In 1995, Iverson and co-workers described the first aromatic foldamer in an aqueous environment.[13] He made use of electron-rich donor groups (DAN) and electron-deficient groups (NDI) strung together with peptide linkers to produce a unique, pleated structure (Figure 1.4). Aspartic acid residues were chosen to link the donor and acceptor groups, in order to increase water solubility and to aggregation.

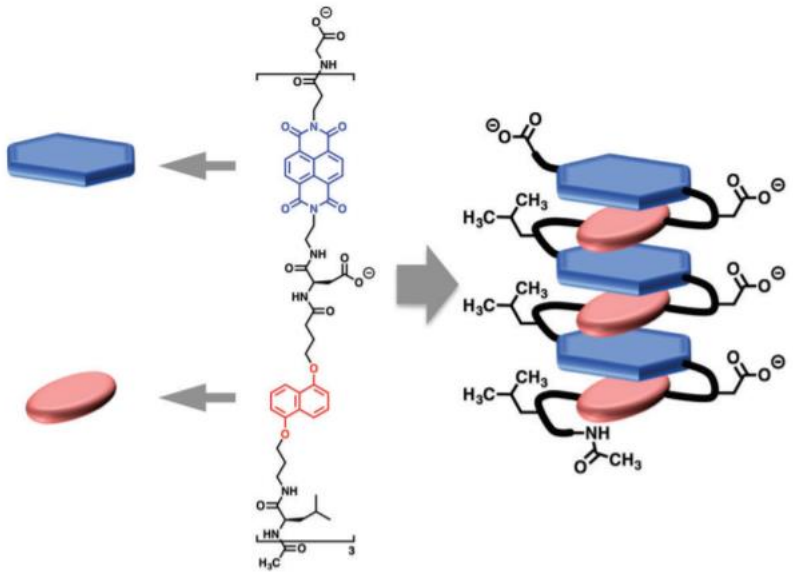

Figure 1.4: The structure and diagram of the single stranded, water soluble foldamer developed by Iverson, showing the electron-rich donor groups (red) and the electron-deficient groups (blue).[14]

This concept was taken further by the group in order to create multiple-stranded complexes. By bringing together two distinctive oligomers – one with only electron-rich DAN groups and the other just electron-deficient NDI groups - they were able to produce an intertwined, heteroduplex foldamer (Figure 1.5).[15]

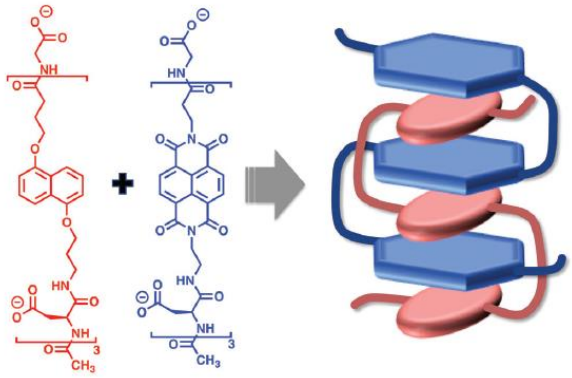

Figure 1.5: The double-stranded DAN/NDI foldamer, showing the overall intertwined structure.[14]

It is worth mentioning that some abiotic structures at first glance appear to be foldamers, but in fact do not qualify according to the definitions previously outlined. Helicenes are a prominent example (Figure 1.6), defined as polycyclic aromatic compounds comprised of

sequentially ortho-fused benzene or other aromatic rings.[16] As the name suggests, they are helical in nature, as the rings tilts in order to prevent steric collisions.[17] Despite the lack of any asymmetric carbons or chiral centers, their shape renders them chiral, possessing axial chirality. They cannot be considered foldamers, however, as their conformational structure is not "stabilized by a collection of noncovalent interactions between nonadjacent monomer units".[7] Instead, their shape is an inherent property of the molecule itself, uninfluenceable and rigid, with no structure-defining bonding interactions between monomers.

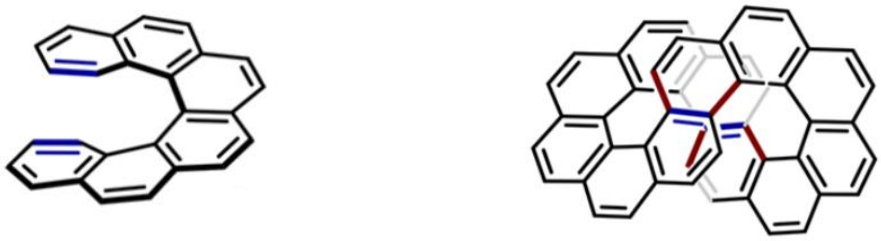

Figure 1.6: [6] Helicene and the elaborately twisted Infinitene.[18]

Other abiotic structures that do not qualify as foldamers for similar reasons include polyoxapolyspiroalkanones and oligonaphthalenes.[11]

1.1.2. Nucleotidomimetic Foldamers

Chemists engaged in the synthesis and research of nucleotidomimetic foldamers make use of the natural building blocks of DNA and RNA to create novel structures. They are often motivated by a desire to gain a deeper understanding of natural oligonucleotides and to find answers for some of the fundamental mysteries in biology, such as the origin of life.[7]

Modifications to natural oligonucleotides have come in several different forms, including changes to the sugar ring,[19] nucleotide bases[20,21] and the phosphate group.[22] Often, very simple changes will have a big effect on the properties of the oligonucleotide, as demonstrated by Gryaznov and co-workers, who replaced the 3'-oxygen with nitrogen (Figure 1.7).[23,24] The resultant phosphoramidates (named np-DNA) showed enhanced thermal stability for duplexes with complimentary DNA and in particular RNA strands. It was theorized

that their higher stability when compared to natural phosphodiester DNA was due to a change in the 2'-deoxyribose conformation, which resulted in the strengthening of the hydrogen bonds between the bases, leading to the adoption of the less common A-form of the double helix.[24]

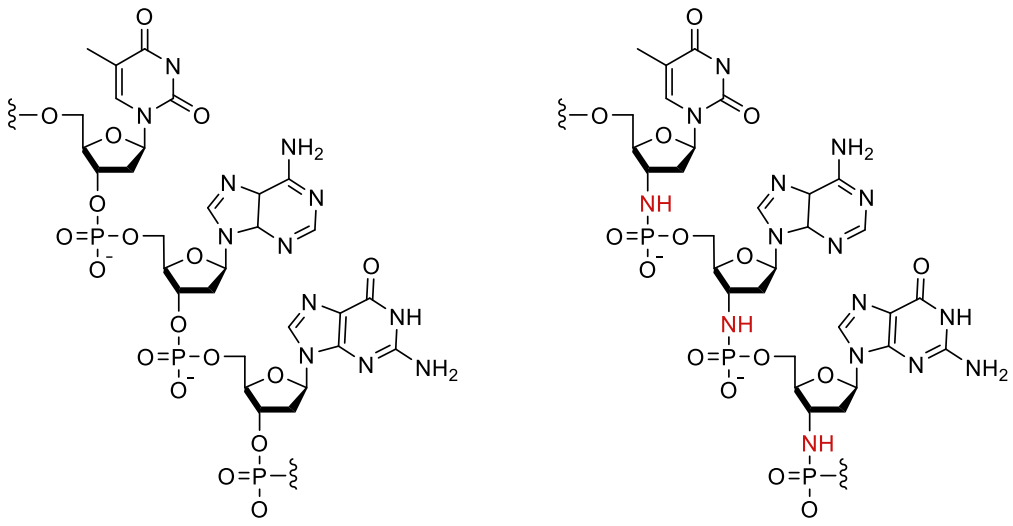

Figure 1.7: The general structure of a natural oligonucleotide (left) compared to the modified phosphoramidate (right).

By far the most studied class of nucleotidomimetics are peptide nucleic acids (PNAs). First introduced by Nielsen *et al.*,[25] they are DNA/RNA analogues whereby the sugar-phosphate backbone is replaced with a δ-peptide backbone, with nucleobases extending outwards via carboxymethyl linkers (Figure 1.8).[26] The lack of charged phosphate groups result in a lack of electrostatic repulsion when binding to DNA/RNA, enhancing specificity and stability.[27] Consequently, they are not easy cleaved by either chemical or enzymatic means, making them particularly suitable for biomedical applications. It has even been postulated that they were in fact the first genetic material, a potential precursor to RNA.[28]

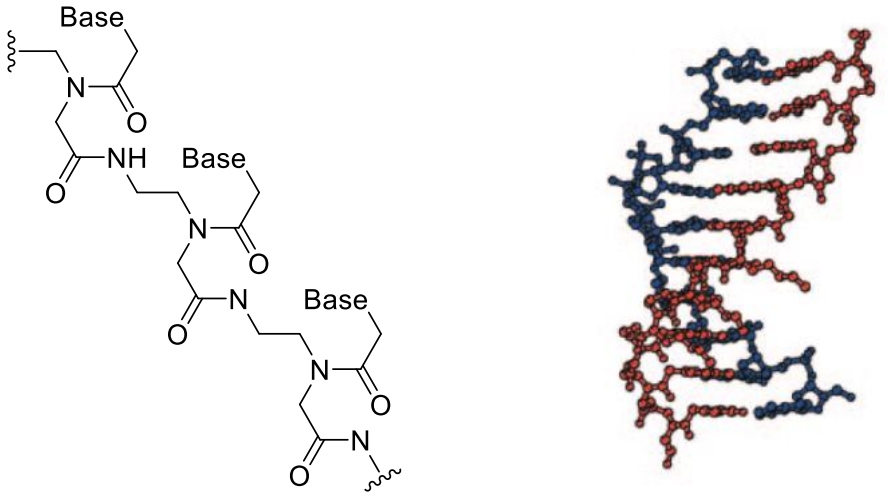

Figure 1.8: The general structure of a peptide nucleic acid (left) and the structure of a PNA-DNA complex, with the PNA strand in red (right).[27,29]

Due to their superior binding affinity, peptide nucleic acids have been used extensively as nucleic probes for genomic analysis, resulting in ever-more sensitive and sophisticated DNA sequencing technologies.[30,31] An enthusiasm for further improvement has inspired several PNA modifications, often resulting in the increase of PNA-DNA duplex stability.[27] One such modification was pioneered by Appella and co-workers, who inserted a varying number of *trans*-cyclopentane units within the backbone of a series of PNA sequences (Figure 1.9).[32]

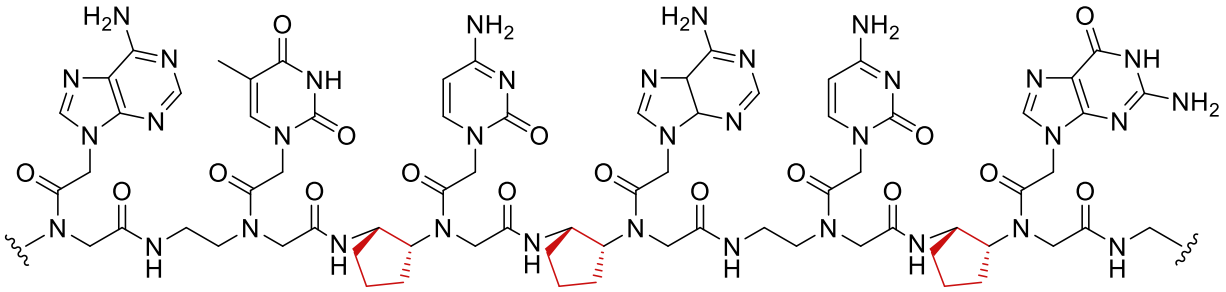

Figure 1.9: A partial PNA sequence, with trans-cyclopentane units inserted in the backbone.

The binding affinity of the modified PNA sequences to complementary DNA was found to be higher than that of the corresponding unmodified PNA sequence. Increasing the number of cyclopentane units was found to amplify the effects, leading to even higher melting points for

the PNA-DNA duplexes (Table 1.1).[32] The increase in stability was thought to be entropically driven, with the conformational flexibility of the unbound PNA strand significantly reduced, lowering the energy cost required to form the PNA-DNA complexes.[33] Interestingly, the stereochemistry of the cyclopentane ring insertion was found to be crucial, with the PNA sequences containing (*R*,*R*)-*trans*-cyclopentane units lacking a defined melting transition temperature, suggesting binding was either poor or non-existent.

Entry[a]	Sequence	T_m (°C) for DNA-PNA duplex	ΔT_m (°C)[b]
1	GTAGATCACT-Lys	48.9	-
2	GTAGA**T***CACT-Lys	54.9	6.0
3	GTAGATC**A***CT-Lys	54.5	5.6
4	GTAGAT**C***ACT-Lys	54.2	5.3
5	GTAGA**T*C***ACT-Lys	60.2	11.3
6	G**T***AGA**T***CACT-Lys	59.6	10.7
7	G**T***AGA**T***C**A***CT-Lys	63.2	14.3
8	GTAG**A*T*C***ACT-Lys	64.4	15.5
9	G**T***AG**A*T***C**A***CT-Lys	70.3	21.4
10	GTAGA**T*^{R}**CACT-Lys	n/a	n/a

(a) Stereochemistry of the cyclopentane units is (*S,S*), unless stated otherwise. (b) ΔT_m is the difference in melting temperature between unmodified PNA-DNA duplex (entry 1) and the modified PNA-DNA duplex. **B*** = *trans*-cyclopentane unit. **B*^{R} =** *trans*-cyclopentane unit with (*R,R*) stereochemistry.

Table 1.1: The melting temperature data for a series of PNA-DNA duplexes, with duplexes containing higher numbers of cyclopentane units exhibiting higher melting temperatures, and thus increased binding affinities.

1.2. Peptidomimetics

1.2.1. Peptides and Proteins

Proteins display by far the most variety in terms of both structure and function of all the biopolymers. It is unsurprising therefore that the field of peptidomimetics is the largest and most intensively studied within foldamer research. Twenty two genetically encoded (proteinogenic) amino acids are utilised by nature, in addition to approximately 140 non-proteinogenic amino acids, usually formed via post-translational modification.[34] This allows

for a huge number of possible peptide and protein structures, with 3.5×10^4 coded in the human genome alone.[35]

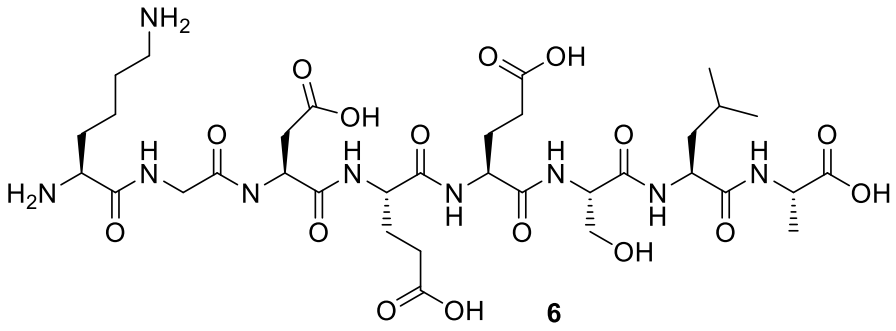

Figure 1.10: The beefy meaty peptide, an example of a naturally occurring peptide containing proteinogenic amino acids (KGDEESLA).[36] It is responsible for the umami taste of beef.

The functional, energetically favorable 3D structure of a protein is referred to as its native state. It is fundamentally determined by the linear sequence of amino acids, known as the primary structure. Spontaneous folding of this sequence will occur, directed by a combination of factors, of which two are particularly dominant: hydrogen bonding and hydrophobic interactions. The formation of numerous hydrogen bonds between non-adjacent monomers will provide most of the directional influence for folding, whilst contributing greatly to the stability of the protein.[37] Hydrophobic interactions will tend to result in the amino acids containing hydrophobic side-chains (such as alanine or tyrosine) to be found buried deep within the protein - so as to avoid unfavorable interactions with water - in a phenomenon known as the hydrophobic effect.[38] Other contributors to folding include the formation of covalent, disulfide bridges between cysteine residues, ionic interactions between charged amino acid side groups, and van der Waal forces.

The resultant folding governed by these processes is known as the secondary structure. There are a relatively small number of distinct, characterizable secondary conformations found within natural proteins, of which two dominate: alpha helices and beta sheets. Together, they account for approximately 60% of all residues found in globular proteins.[39] Other, less common types of secondary structures include beta turns and omega loops. There are also alternatives to the alpha helix such as the 3_{10} helix (defined as a helix with three residues per

turn and 10 atoms in the ring formed by the hydrogen bonding patterns) which are rarely found in natural proteins but become more relevant in the field of peptidomimetics.[37]

The different regions of secondary structure within a protein – often known as domains – will come together to form the three-dimensional, tertiary structure (Figure 1.11). When more than one polypeptide chain come together to form a protein complex such as hemoglobin, it is described as a quaternary structure. The resultant global structure of a protein is not static, and will undergo rapid, reversible conformational changes in order to perform its biological function.[40] The correct folding and overall shape for proteins is vital, especially for globular and membrane proteins. Exposure to environmental stresses outside of the operating window such as temperature, pH and salinity may denature the protein, resulting in a loss of secondary, tertiary and/or quaternary structure, and thus biological function.

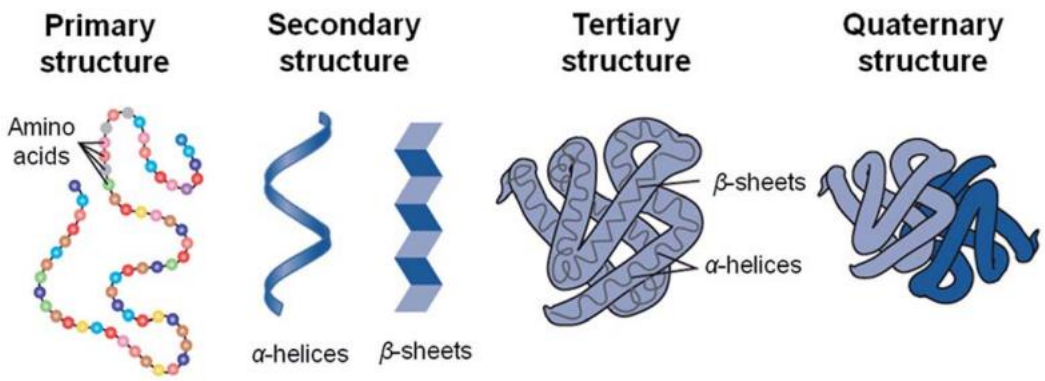

Figure 1.11: The hierarchal levels of protein structure.[41]

1.2.2. Peptidomimetic Foldamers

Despite the endless number of possible proteinogenic amino acid combinations, chemists have readily sought to diversify the pool of monomers available to them, creating an ever-increasing amount of synthetic amino acid monomers. This has allowed for the creation of a class of foldamer that maintain general features analogous to peptides, but with often significant differences in structure and functionality. The modification of amino acids can come in many different forms, such as the movement of side chains to a different position,

the introduction of novel side chains, and the use of extended amino acids. An early example of the first was presented by Bartlett and co-workers in 1992, who endeavored to create oligomers of *N*-substituted glycines – a new class of peptidomimetic foldamers known as peptoids.[42] They established a simple two-step synthetic procedure capable of producing a wide range of glycine monomers (scheme 1.2). The first step is the reductive amination of the amine bearing the relevant side chain with glyoxylic acid. Where necessary, the side chain is appropriately protected with either Boc, ^{t}Bu or Trt groups. The second step is to simply Fmoc protect the naked amine. The monomer is then ready to undergo oligomerization via solid-phase peptide synthesis (SPPS).

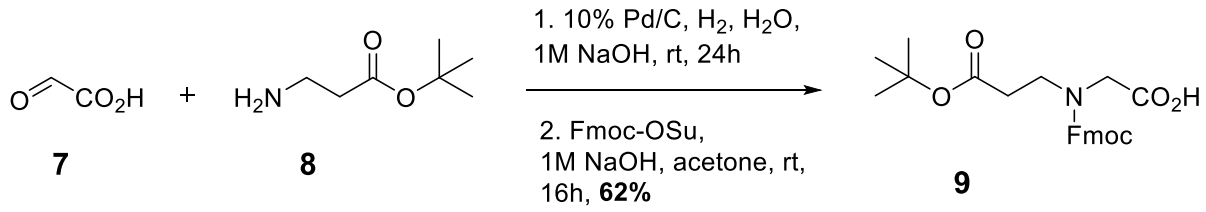

Scheme 1.2: The two-step procedure to produce the N-substituted glycine peptoid monomer **5**.

A range of peptoid oligomers were synthesized, including the one shown in Figure 1.12. As a consequence of the N-substituted side chains, peptoids exhibit some stark differences from their peptide counterparts. Perhaps the most impactful is the absence of stabilizing hydrogen bonds between carbonyl and amine groups in the oligomer backbone. Additionally, peptoids are devoid of stereocentres, and will contain flexible methylene groups instead. It is projected that these factors would contribute to an increased difficulty in forming secondary structures, making them more susceptible to denaturation. Nevertheless, peptoids in this study were found to complex to RNA in a similar fashion to corresponding peptide residues, suggesting that the formation of similar secondary structure is possible. Furthermore, the oligomers were found to be significantly resistant to proteolysis, with no cleavage detected when introduced to peptidases such as chymotrypsin, papain and thermolysin. Due to this biological robustness and their ease of synthesis, the therapeutic potential of peptoids has since been explored.[43,44]

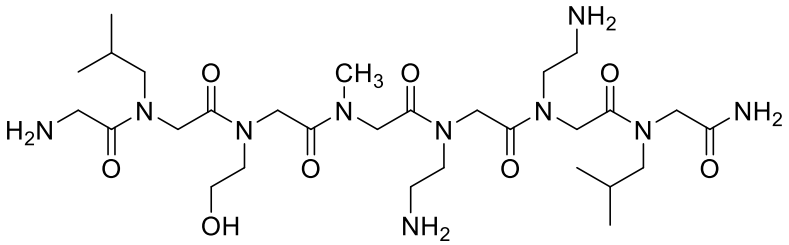

10

Figure 1.12: One of the peptoids developed by Bartlett and co-workers.

Peptoids belong to the α-peptide family, in that they are made up of monomers that have only one carbon atom between the terminal amino and carboxyl groups. Many other classes of foldamer belong to this family, such as oligopyrrolinones, oxazolidin-2-ones and azatides.[7] The majority of peptidomimetic foldamers however will consist - at least partially - of extended (homologated) amino acids, namely β, γ or δ-amino acids (Figure 1.13). The use of such monomers is an attractive proposition due to the potential formation of less common or even novel secondary structures. This is facilitated by substantial changes in the distances and alignments between the amine and carboxyl groups of the foldamer backbone, leading to significant differences in hydrogen bond patterns. Extended amino acids also present an opportunity for further functionalisation, either with additional side chains or inherent changes to the backbone itself, such as the introduction of double bonds or ring systems – features that would introduce conformational constraints and likely favour the formation of secondary structure.

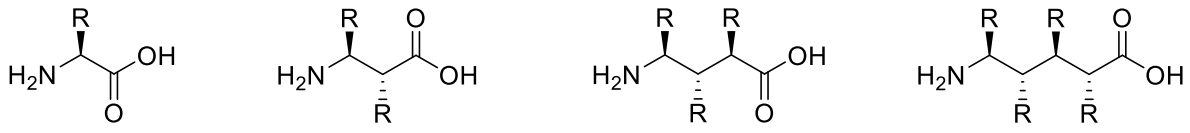

α-amino acid **β-amino acid** **γ-amino acid** **δ-amino acid**

Figure 1.13: The general structure of an α-amino acid compared to extended amino acids, showing the increasing propensity for additional side chains/functionalization.

Gellman himself presented one of the earliest rationally designed β-peptide foldamers in 1996, which coincidently made use of conformationally constraining infrastructure in order to promote secondary structure formation.[45] He envisioned the exclusive use of carbocyclic β-amino acid monomers in order to introduce the desired structural rigidity. The monomer itself was prepared via a procedure first reported by Miyashita and co-workers in 1970 (Scheme 1.3).[46] A racemic mixture of (±)-*trans*-2-aminocyclohexanecarboxylic acid **12** was first obtained by the reaction of anthranilic acid with sodium, which was then benzoylated to give the racemic mixture **13**. The desired enantiomer was isolated via the co-crystallisation with enantiopure quinine to isolate **14.** This was then hydrolysed and esterified to give **15** and then hydrolysed again to give the final, enantiopure *trans*-ACHC product, **16**.

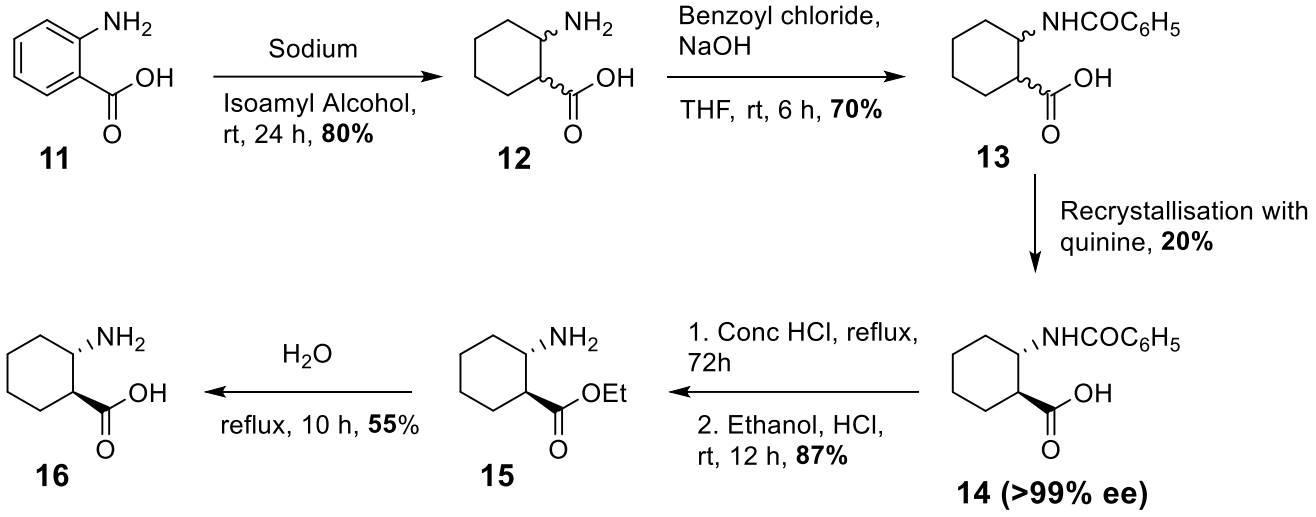

Scheme 1.3: The asymmetric synthesis of *trans*-ACHC as developed by Miyashita and co-workers.

With the monomer in hand, Gellman synthesized oligomers of varying length via solid-phase peptide synthesis, from dipeptide to hexamer. The crystal structures of the tetramer and the pentamer showed that they adopted a 14-helical conformation in the solid state, characterized by hydrogen bonds forming between amide protons at residue (*i)* with backbone carbonyl oxygen atoms two residue further along in the sequence (*i*+2).[47] To probe the conformational stability of the foldamers, amide proton exchange studies were carried out, comparing the dipeptide and hexamer. NH/ND exchange was found to be complete within 6 minutes for the dipeptide, an expected result considering that it is too small to form internal hydrogen bonding. In contrast, three of the six amide protons of the hexamer were

found to exchange very slowly, requiring over two days to reach completion. Their participation in 14-helical hydrogen bonding and the subsequent secondary structure formation provides these amides substantial protection from solvent effects and reveals the inherent stability of the foldamer itself (Figure 1.14).

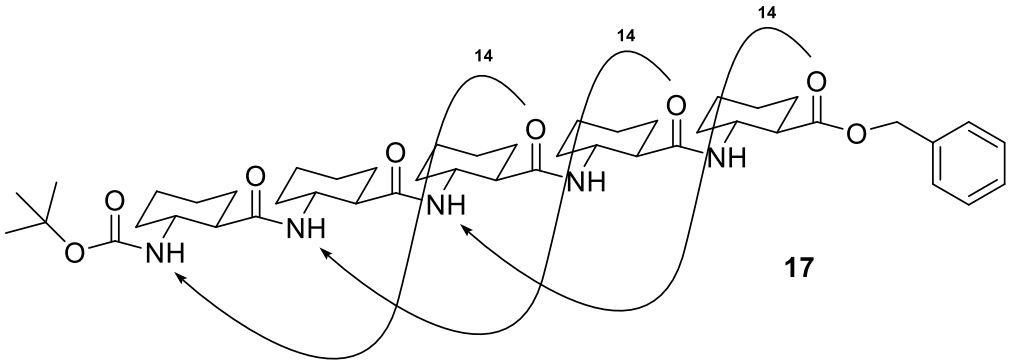

Figure 1.14: A pentamer consisting of *trans*-ACHC monomer units, showing the 14-helical hydrogen bonding.

Seebach took a different approach to the modification of β-foldamers, introducing side chains instead of conformational rigidity.[48] His group aimed to create a water soluble β-peptide through the use of ionically charged residues. Additionally, with careful placement of these residues and their side-chains, the group postulated that salt-bridges would form, stabilising the helix of the foldamer. β-Heptapeptide **18** was synthesised via SPPS and was shown to exhibit excellent solubility in both methanol and water. Circular Dichroism was used to investigate its helicity, with a minimum at *ca.* 216 nm and maximum at *ca.* 198 nm in both methanol and aqueous solution - characteristic of a 3_{14}-helix (Figure 1.15). The CD spectra also provided strong evidence for the formation of the two salt bridges and the increased stability they provide, with the strongest "molar ellipticity" observed at 5.5 pH, where all ionic groups are expected to be charged.

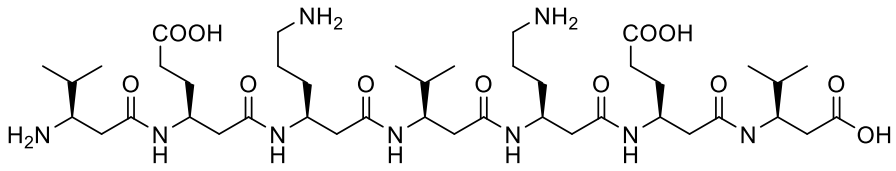

18

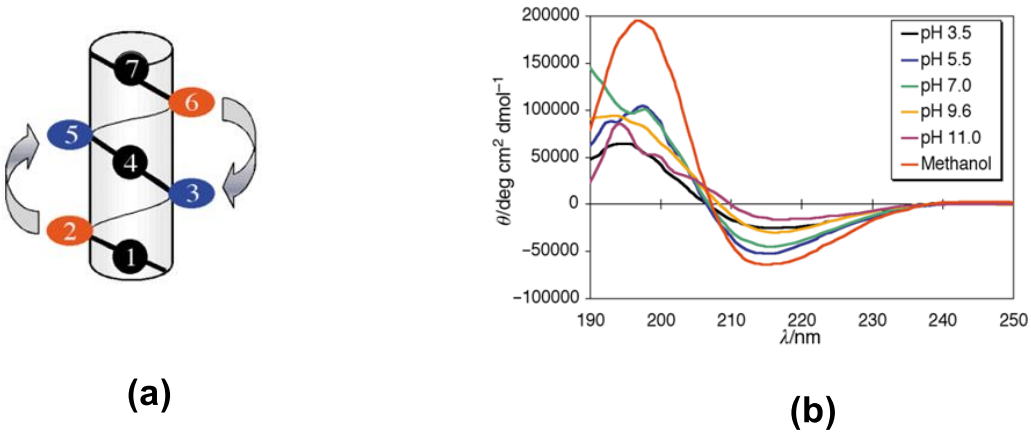

Figure 1.15: . The β-heptapeptide **18** developed by Seebach and co-workers, alongside the schematic representation of its helical structure and salt bridges **(a)** and its CD spectra in methanol and aqueous solutions **(b)**.[48]

As the number of examples of β-amino acid containing foldamers steadily increased, attention inevitably turned to the synthesis and utilisation of γ-amino acids within foldamers. A particularly interesting example was given by the Guichard group, who synthesised hybrid foldamers consisting of both urea and γ-amino acid monomers (Figure 1.16).[49] The group had previously demonstrated that oligoureas were able to mimic the activity of α-helical host-defence peptides in disrupting the phospholipid membranes of bacteria, revealing their potential as antimicrobial agents.[50] A range of oligomers with differing ratios of urea and amino acid monomers was synthesised, and their antimicrobial activity compared. It was generally found that antimicrobial activity decreased as the number of γ-amino acid residues inserted into the backbone increased. When the corresponding γ-peptide was synthesised and tested, it was found to be virtually inactive towards both gram-positive and gram-negative bacteria. Additionally, the insertion of amino acid residues was found to have a destabilising effect on the helical conformation, as characteristic ellipticities in the CD spectra reduced significantly.

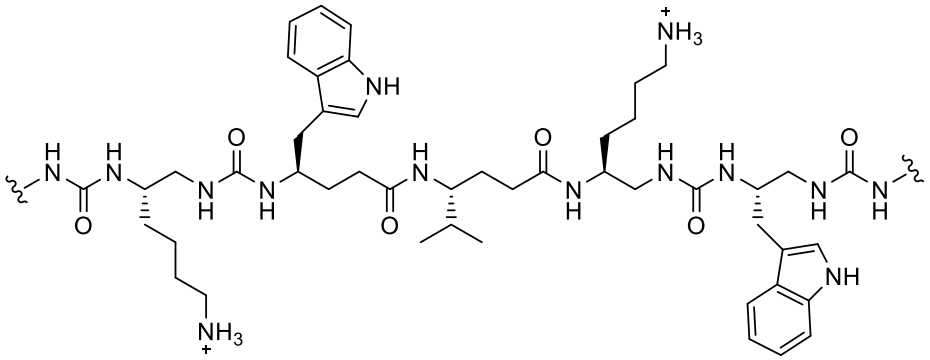

Figure 1.16: A section of the urea/amide hybrid foldamer, with the general structure UUAAUU.

Despite these disappointing trends, the group were still able to build upon this work and develop amide/urea foldamers with a strong propensity for helical formation. They found that by implementing an alternating pattern of urea and amino acid residues in a 1:1 ratio, in addition to the use of consistent, uniformly distributed benzyl side chains, they could create a foldamer that clearly demonstrated secondary structure formation.[51] This was confirmed by NMR by the presence of several NOE interactions consistent with helical folding, in addition to the crystal structure, which revealed a helical structure much like that of the equivalent urea homooligomer (Figure 1.17).

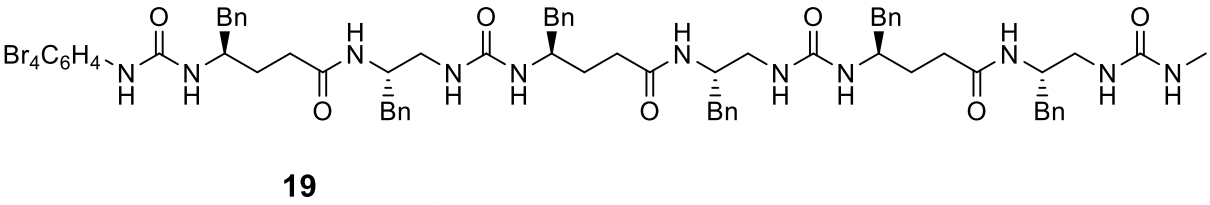

19

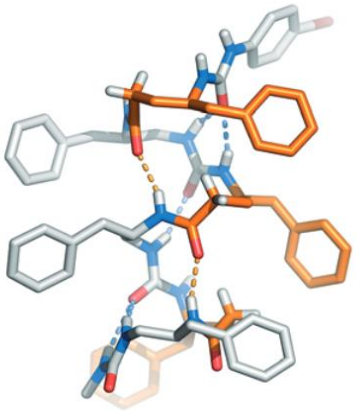

Figure 1.17: The structure of the alternating urea/amide foldamer **19** presented by Guichard and co-workers (above), which displays a helical structure in both the solution and solid-state (below).[51]

A more detailed discussion on the synthesis and use of γ-amino acids within foldamers is given in Chapter 4.

The development of foldamers containing δ-amino acid residues is a recently emerging trend in the field, with a very small yet steadily growing list of examples. One of the very first examples was published by Li and co-workers in 2003, who developed a series of δ-foldamers containing electron-deficient and electron-rich side chain units, in order to facilitate donor-acceptor interactions between monomers.[52] The group hoped to harness these interactions in order to generate foldamers with a "zipper-like" secondary structure (Figure 1.18).

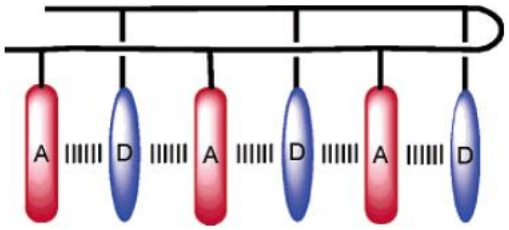

Figure 1.18: A representation of the "zipper-like" structure sought by the Li group for their δ-foldamers.[52]

The δ-monomers were derived from L-ornithine, with the appropriately protected versions reacting with either the electron-rich 1,5-dialkoxynaphthalene (DAN) unit or the electron-deficient pyromellitic diimide (PDI) unit, to give the two required monomers (Scheme 1.4).

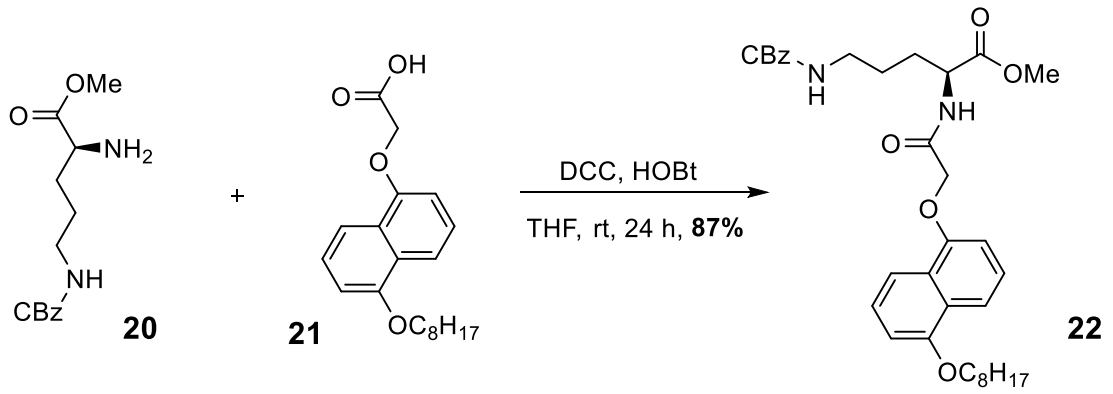

Scheme 1.4: The synthesis of the electron-rich δ-residue **22**, containing a 1,5-dialkoxynaphthalene (DAN) side chain unit.

With the monomers synthesised, the group could then begin to construct the target foldamers. This was achieved by liquid-phase synthesis (LPPS) in a sequential fashion, in order to create a series of oligomers, from dipeptide to hexapeptide (Figure 1.19).

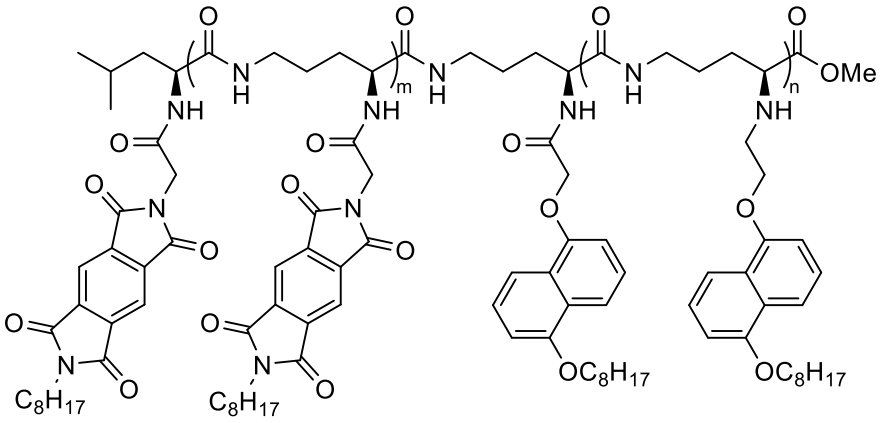

23: m = n = 0
24: m = 1, n = 0
25: m = 0, n = 1
26: m = n = 1
27: m = 2, n = 1
28: m = 1, n = 2
29: m = n = 2

Figure 1.19: The structures of the foldamers developed by Li, from dipeptide to hexapeptide.

2D-NOSEY NMR experiments were carried out in order to provide evidence for intramolecular donor-acceptor interactions – the proposed mechanism for secondary structure formation. NOE signals were found between a proton of the PDI units and the ortho and para protons of the DAN units of the tetrapeptide **26**, although poor resolution prevented the same to be found for the longer peptides **27-29**. Crucially, the chemical shifts of these protons in **26** were found to be essentially concentration independent, eliminating the possibility of intermolecular interactions. Further evidence of conformational ordering was provided by a UV-vis spectral study. Significant hypochromism was observed in the ultraviolet absorption bands for all peptides, especially when compared to a 1:1 mixture – an effect only possible when chromophores are positioned close together and are correctly orientated.[53]

1.2.3. Catalytic Peptidomimetic Foldamers

Due to the desire to mimic and perhaps improve upon the function of enzymes, catalysis has naturally become a main focus of peptidomimetic research. Natural enzymes are exceedingly efficient and work under mild, aqueous conditions (most often at close-to-neutral pH and physiological temperatures). They also offer excellent stereoselectivity, being largely responsible for the conversion of chirality in living organisms.[54] However, they are denatured easily and will often have a very narrow substrate scope. Appropriately designed foldamers will have the potential to work under similarly green conditions, but with an increased chemical robustness and a significantly expanded substrate scope.[55, 56]

An early example of foldamer catalysis was reported by Hilvert *et al*. in 2009.[57] They synthesised a β-peptide foldamer containing β^3-homolysine residues, allowing for amine-mediated catalysis (Figure 1.20). It also contained the same *trans*-ACHC cyclic monomer used by Gellman to produce cyclically-strained oligomers.[45] With careful placement of the homolysine residues in the *i, i+3, i+6* positions, alongside the projected formation of the 14-helix as seen in similar β-peptides, the amine-containing side-chains could be aligned along one side of the helix, facilitating amine catalysis via a decrease in the ammonium pK_a values. The N terminus was capped with a heptanoyl moity to promote self-assembly.

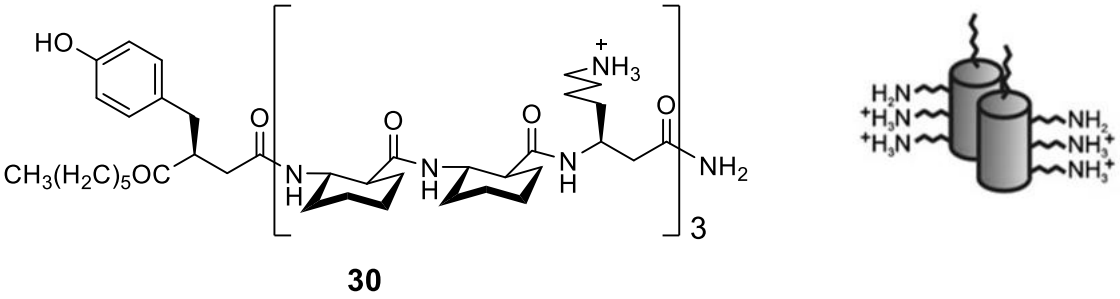

30

Figure 1.20: The structure of the catalytic foldamer **30** created by Hilvert and co-workers, and a cartoon showing the alignment of amine side chains and the propensity of the peptide to self-assemble.

The formation of the expected 14-helix and the self-assembly of **30** was confirmed via CD measurements, 2D NMR spectroscopy and analytical ultracentrifugation (AU). The model reaction selected to probe the catalytic ability of the foldamer was the retroaldol cleavage of **31** (Scheme 1.4). The foldamer catalysed reaction was found to proceed with multiple

turnovers and was significantly accelerated when compared to the uncatalysed reaction. Interestingly, self-assembly was shown to be crucial for catalysis. When the heptanoyl group was replaced by an acetyl group, the characteristic CD signature for self-assembly was lost, and this was accompanied by a drop in catalytic activity, by an order of magnitude. It was suggested that the interface between clustered helical β-peptides could act as a primitive substrate binding pocket.

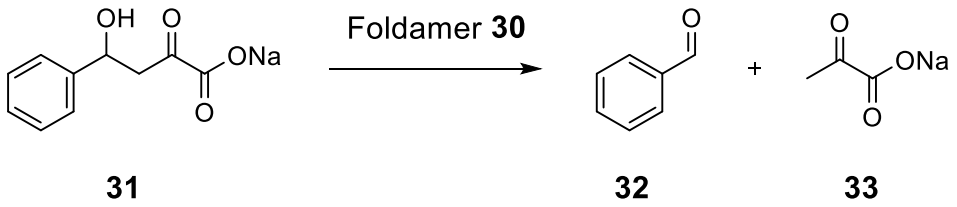

31 **32** **33**

Scheme 1.4: The retroaldol cleavage promoted by foldamer **30**, facilitated by its secondary structure self-assembled network.

Perhaps the most elaborate and impressive example of foldamer-mediated catalysis to date was published by Gellman *et al.* in 2019.[58] They described the α/β-Peptide foldamer **34** capable of performing bifunctional catalysis – specifically aldol condensations - in order to produce macrocyclic compounds (Figure 1.21). The foldamer itself consists of two distinct catalytic units, one being a primary amine side chain and the other a pyrrolidine residue. These are carefully spaced in an *i, i+3* arrangement, causing them to appropriately align upon helical folding. The choice of these two different catalytic units is crucial for the success of the aldol condensation, as primary amines favour imine adducts with aldehydes, whereas secondary amines favour enamine adducts.[59,60]

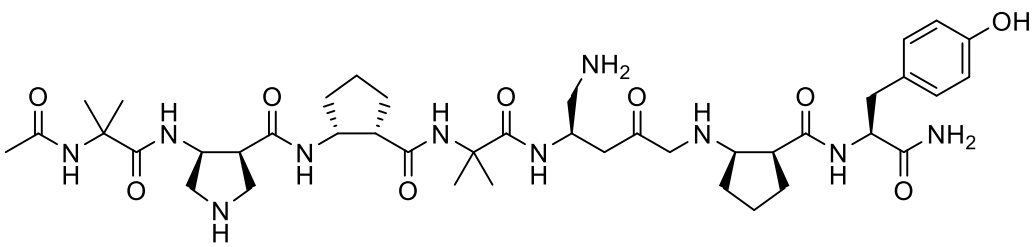

34

Figure 1.21: The catalytic α/β foldamer developed by Gellman and co-workers.

The foldamer proved to be a versatile catalyst, successfully catalysing a range of substrates in high yields, producing macrocyclic compounds with ring sizes between 12 and 22. A particular example is given in Scheme 1.5, with the 16-membered macrocyclic product **36** being produced in a 97% yield from **35**. A control reaction with pyrrolidine and n-butylamine produced only trace amounts of cyclized product in the same time frame. The group were also able to utilize the same foldamer-mediated macrocyclization as part of the total synthesis of robustol, creating the required 22-membered ring in an 84% yield.

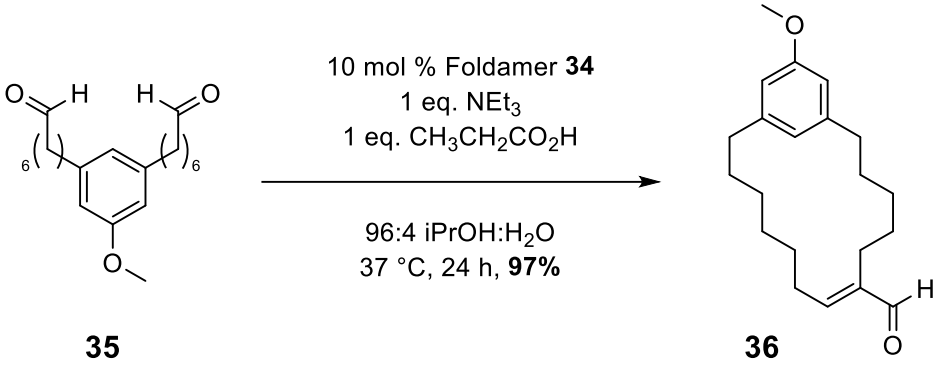

Scheme 1.5: An example of the foldamer-mediated macrocyclization developed by the Gellman group, resulting in a 16-membered ring.

One crucial, property of enzymes that has yet to be translated into peptidomimetic foldamer catalysis research (barring one peptoid example presented by Kirshenbaum)[61] is the ability for enantioselective synthesis. So far, foldamer examples have lacked enough of a well-defined, asymmetric environment needed in order to impart stereochemistry control on substrates. Efforts to achieve this will first require the discovery and careful development of novel helical structures, facilitated by the use of new building blocks – most specifically the less explored, higher homologue γ- and δ-amino acid monomers.

1.2.4. δ-amino acid monomers

The use of δ-amino acids in peptidomimetics is an attractive proposition due the increased potential for functionalisation and their propensity to act as dipeptide mimics, increasing the likelihood for successful secondary structure formation.[62] The synthesis of enantiopure δ-amino acid monomers remains a challenge, although an increasingly diverse number of approaches are being now reported.[63-65] One strategy is to simply homologate existing enantiopure molecules – making use of the "chiral pool". A pertinent example of this was provided by Fujii and co-workers within the synthesis of antimetastatic peptides (Scheme 1.6).[66] Using D-Serine as a starting point, the aziridine **39** was produced in 3 simple steps.[67] After treatment with DIBAL, a (*Z*)-selective Horner-Wadsworth-Emmons reaction was undertaken to give the enaote ester **40**. A final copper mediated ring-opening of the aziridine gave the final, protected δ-amino acid **41**.

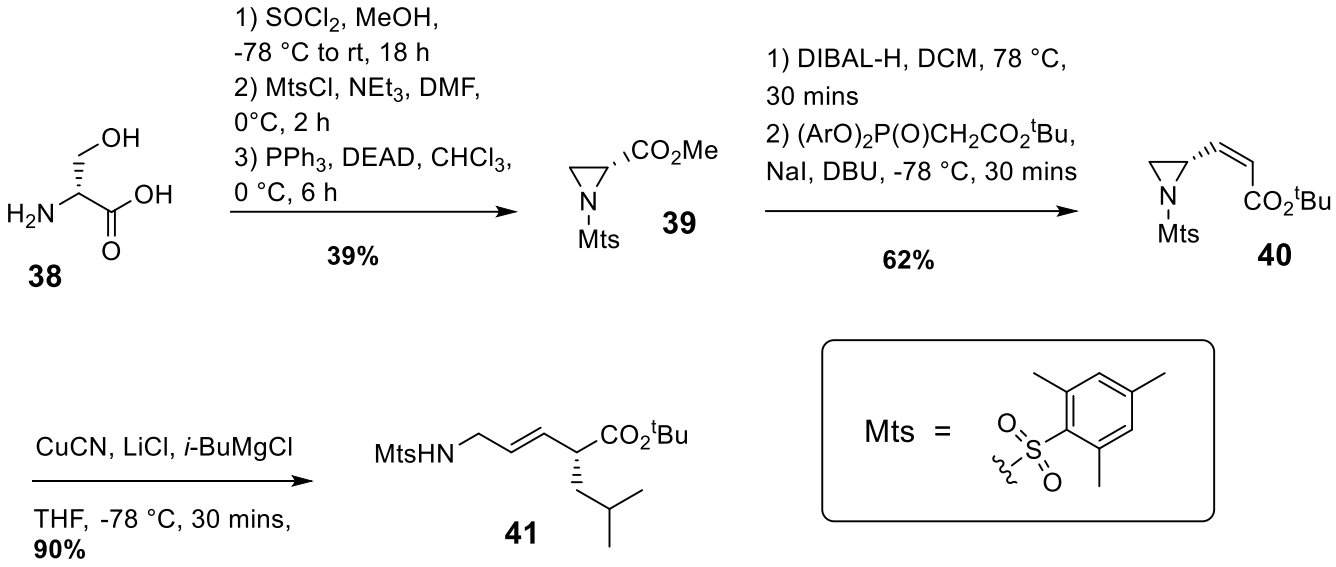

Scheme 1.6: Fujii's synthesis of the δ-amino acid monomer **41**, for use in antimetastatic peptides.

Another important method for the creation of enantiopure δ-amino acids and their analogues is asymmetric catalysis. Transition-metal based catalysts bearing chiral ligands are often used for this purpose, an excellent example of which was provided by the Feng group, who reported a scandium complex-catalysed vinylogous Mannich reaction (Scheme 1.7).[68] The reaction brings together the general aldehyde **42**, amino alcohol **43** and the acyclic silyl dienol ester **44** in the presence of $Sc(OTf)_3$ and the chiral ligand **45**, producing the δ-amino acid

precursor **46**. A variety of aromatic aldehydes were found to be suitable substrates for the reaction, all achieving high yields (90-99%) and good to excellent enantioselectivities (80-99% *ee*).

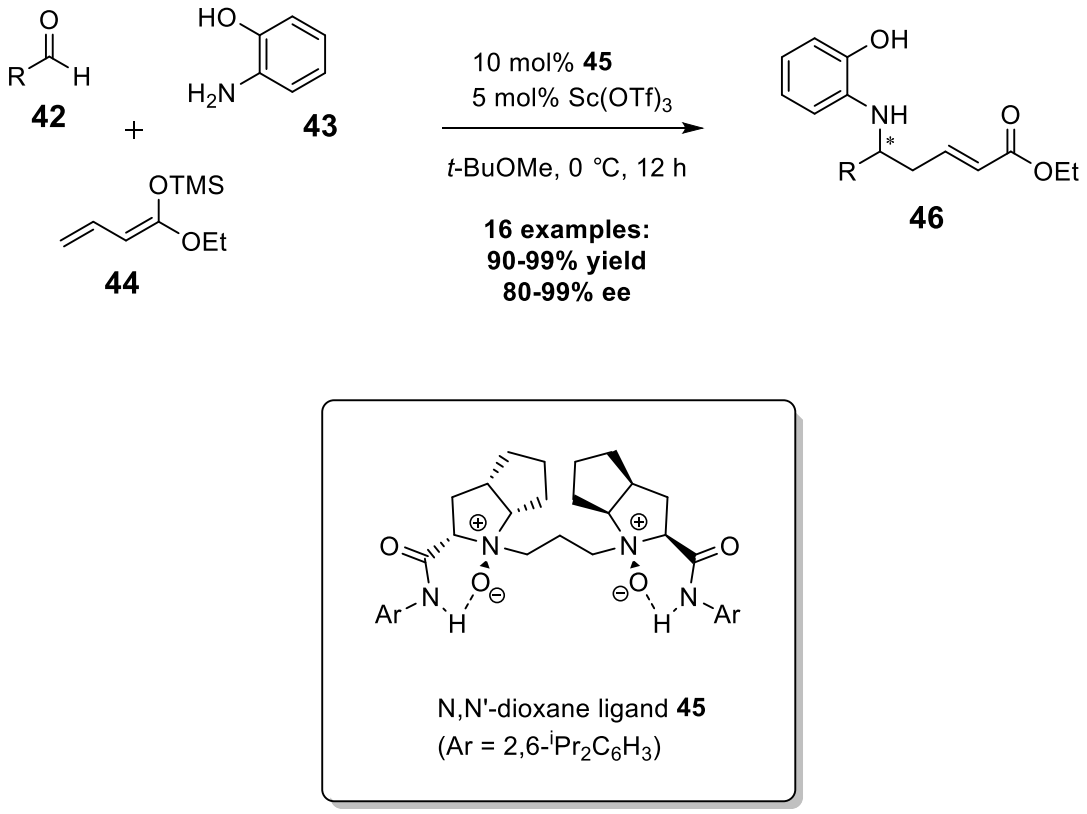

Scheme 1.7: The scandium complex-catalsyed synthesis of δ-amino acid precursors, pioneered by the Feng group.

Asymmetric catalysis is not limited to the use of transition metal-based catalysts, with organocatalytic methods offering the potential for enantioselective transformations in mild, ambient conditions without the use of potentially toxic heavy metals. There are several examples for the organocatalytic production of δ-amino acid precursors, one of which is given by the Cobb group, who were able to make use of a bifunctional thiourea catalyst to produce a range of complex, cyclic δ-monomers (Scheme 1.8).[69] The transformation is described as a cascade reaction, as an initial Michael addition between the conjugated cyanosulfone **47** and the nitro-α,β-unsaturated ester **48** is followed by a subsequent ring-closing Michael addition - both occurring asymmetrically – to give the cyclic amino acid precursor **50**.

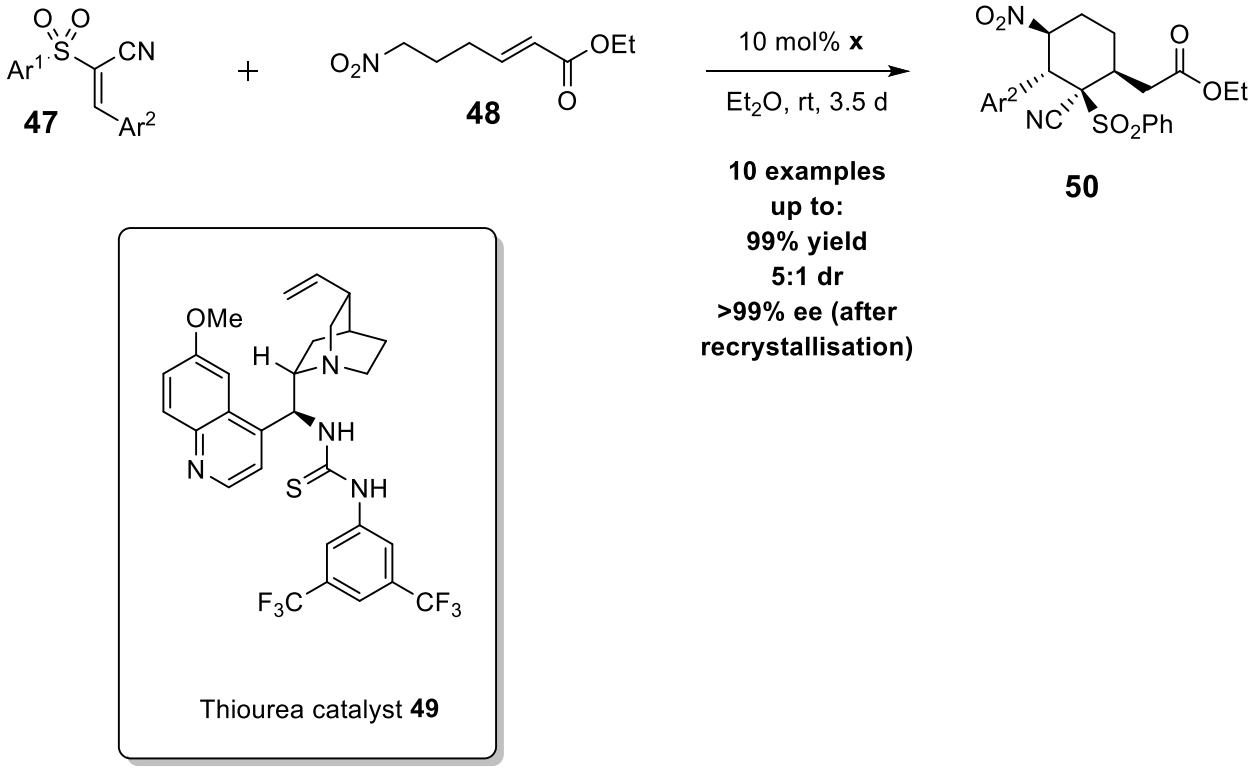

Scheme 1.8: The organocatalytic domino reaction of cyanosulfones, creating amino acid precursors.

The reaction was found to be versatile for a variety of aromatic appendages in the two relevant positions within the cyanosulfone **47**, with good yields (67-99%), diastereoselectivities (5:3-5:1) and enantioselectivities (83->99%, after recrystallisation) across the 10 examples given. Most strikingly, the resultant compounds can be considered both δ and ε amino acid precursors, depending on which orthogonally reactive N-termini is harnessed for peptide chemistry. This, combined with their inherent complexity – bearing a quaternary carbon centre, a ring system and substantial functionalization – makes the resultant compounds particularly useful within the field of peptidomimetics.

Although the numbers of δ-amino acid syntheses are steadily increasing, their utilization within foldamers remains scarce. In addition to the previously mentioned δ-foldamer presented by Li, there only exists a mere handful of examples. One of these is given by Fleet and co-workers, who developed the synthesis of 2,4-*cis*-oxetane amino acid monomers and their oligomerization (Scheme 1.9).[70] The monomer synthesis begins with the partially protected furanose **51**, which is first tosylated and then treated with sodium azide to give **52**. This was followed by acidic hydrolysis to give the lactol and then oxidation with bromine to

give the lactone **53**. Protection of the free alcohol with a triflate group was followed by the crucial ring-contraction step, facilitated by the addition of basic methanol, gave the final protected oxetane monomer **54**.

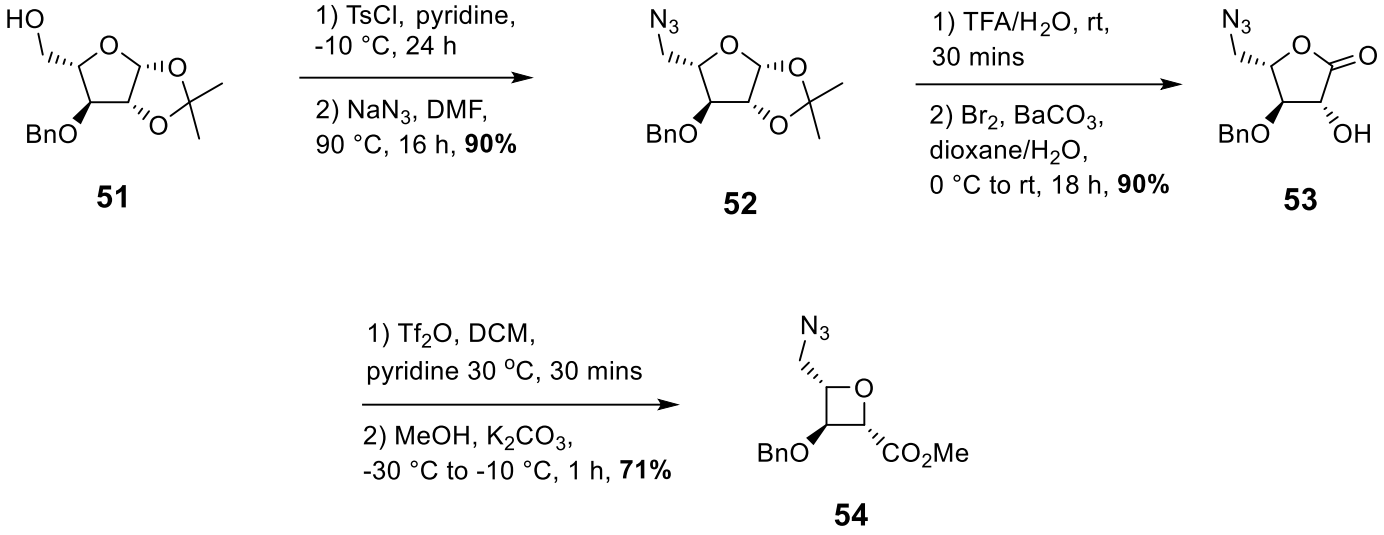

Scheme 1.9: The synthesis of the protected oxetane amino acid monomer **54**, by Fleet *et al.*

The desired oligomers, namely the dipeptide, tetrapeptide and the hexapeptide were synthesised via liquid-phase peptide synthesis in an iterative procedure, with TBTU selected as the coupling reagent. The secondary structural preferences of earlier foldamer examples bearing similar oxetane monomers were found to favour turn type structures, and the same was anticipated for these newer examples.[71] Characterisation of the three peptides was explored in a separate paper, mostly relying on NMR data.[72] For the hexapeptide **55**, four of the six amide protons were found to have resonance shifts well above 7ppm, indicative of their participation in intramolecular hydrogen-bonding. A DMSO titration experiment provided further evidence for this, with the four protons in question remaining virtually unchanged on the addition of increasing amounts of DMSO, suggesting that these protons are not solvent exposed, and are protected by their involvement in internal hydrogen-bonding. More detailed evidence for the secondary structure as provided by 2D NMR, with the NOEs for the tetramer and hexamer showing the formation of 10-membered rings, by virtue of hydrogen bond formation between the amide proton of residue *i* and the carbonyl of group *i-2*. This results in a repeating β-turn structure, as shown in Figure 1.22.

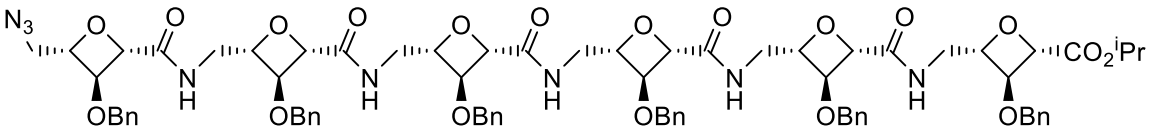

55

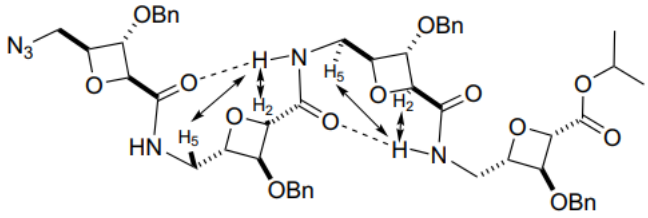

Figure 1.22: The structure of the hexamer **55** (above) and a schematic of the β-turn structure of the tetramer (below).[72]

1.2.5. α/δ-Foldamers

δ-amino acids can be considered isosteres of α-amino acid dipeptides - therefore it is logical to assume that α/δ-peptides would be highly likely to successfully fold into conformationally ordered states, perhaps forming similar folding systems to α-peptides. In 2009, Hofmann and co-workers utilised *ab initio* MO theory in order to predict the most stable helical secondary structures that would form for α/δ hybrid peptides with a 1:1 alternating backbone.[73] The lowest energy and thus most stable structure was predicted to be the 13/11-Helix - where the amide protons of the α-residues take part in the hydrogen bonding of 13-membered rings, and those of the δ-residues in 11-membered rings.

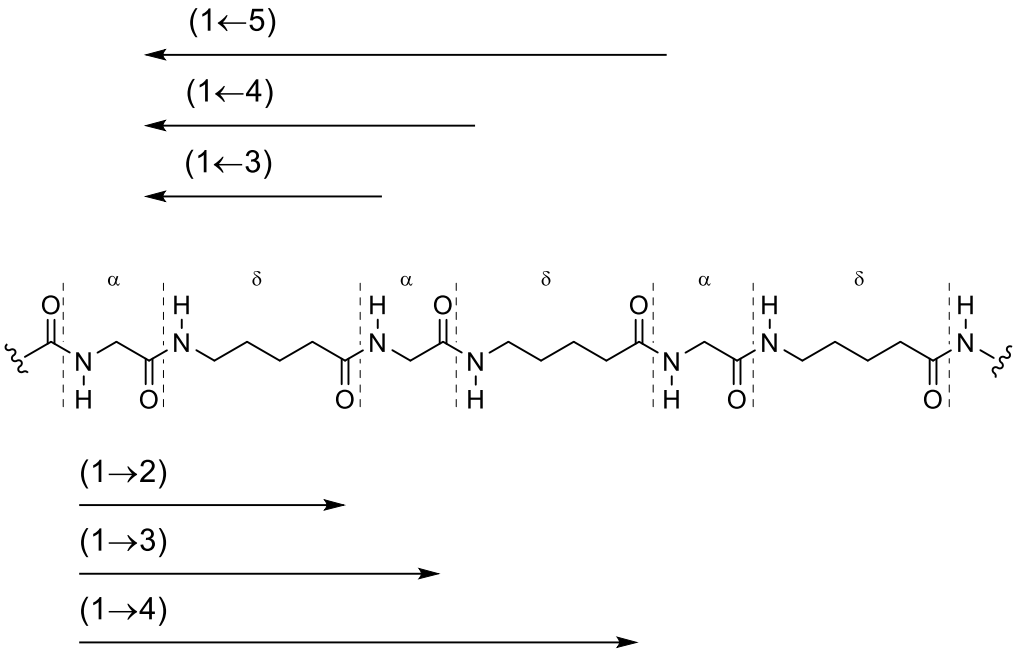

Figure 1.23: Possible hydrogen-bonding patterns for 1:1 hybrid α/δ-peptides, as studied by Hofmann and co-workers.

The Hofmann group were eager to supplement their theoretical work with experimental data and looked to create a 1:1 hybrid α/δ-peptides upon which conformational analysis could be performed. Alanine was selected as the α-residue, and **58** chosen as the δ-residue. The furanose side chain is intended to introduce rigidity to the structure and further promote secondary structure formation. The synthesis of **58** started with the previously synthesised aldehyde **56**, which underwent a Wittig reaction with (methoxycarbonylmethylene)triphenylphosphorane to give the α,β-unsaturated ester **57**.[74] This was then hydrogenated to give the final protected monomer, **58** (Scheme 1.10). This two-procedure represents one of many homologation techniques that can be used to synthesis extended amino acids in an easy and convenient manner.

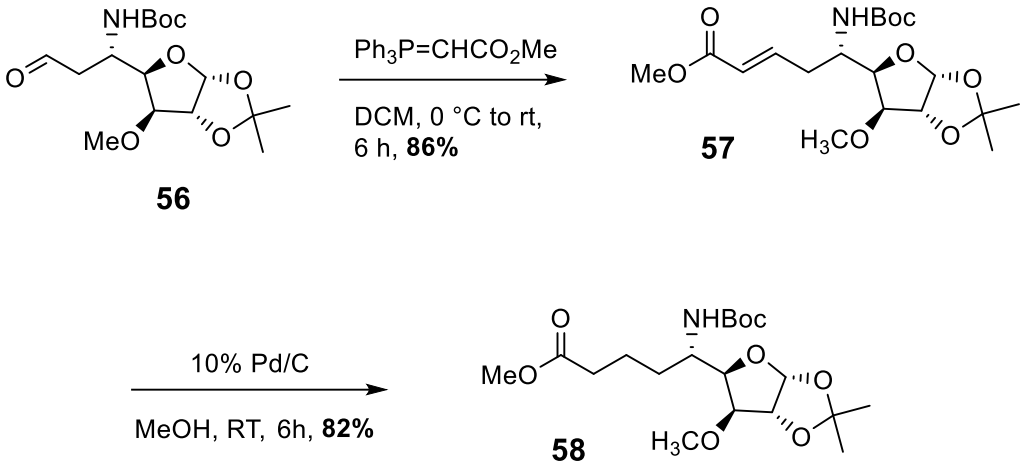

Scheme 1.10: The synthesis of the delta monomer **58**, homologating the β-amino acid precursor **56.**

Peptide synthesis was achieved via liquid-phase peptide synthesis, with the delta monomer **58** first deprotected and coupled with L-Alanine to give the dipeptide. Sequential couplings with alternating monomers gave rise to a range of peptides of varying lengths, up to the hexamer **59** (Figure 1.24).

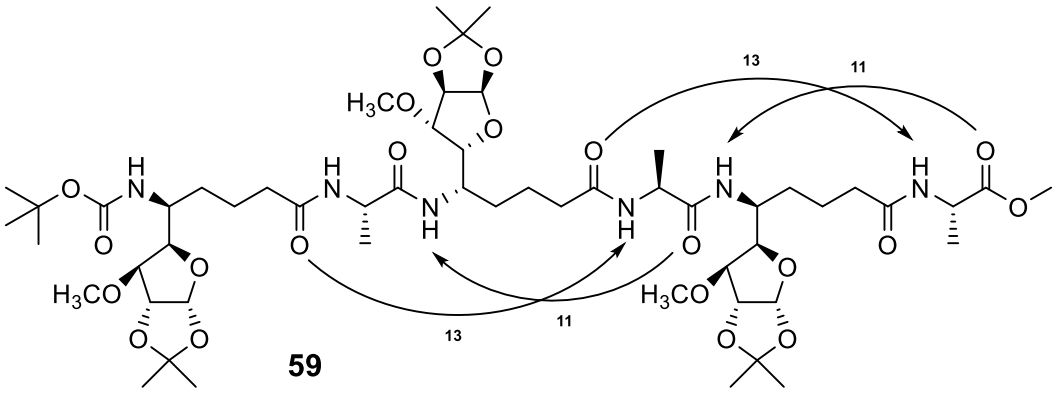

Figure 1.24: Hexamer **59**, showing the hydrogen bonding characteristic of an 11/13 helix.

Conformational analysis confirmed the formation of a 13/11-helix in all peptides synthesized, including **59.** Most notably, the characteristic hydrogen bonding could be determined by 2D NMR, with NOE correlations indicating the formation of the required 13 and 11 membered rings. DMSO titration studies were also carried out, which showed that the amide protons of **59** were participating in hydrogen bonding, by virtue of their modest change in ppm on addition of DMSO ($\Delta\delta < 0.5$ ppm).

1.3. Aims of the Study

The overall aim of this study is the discovery and utilisation of novel carbocyclic amino acid monomers and building blocks in order to generate new peptidomimetic foldamers. Many of the previously described foldamer examples contain carbocyclic monomer residues, promoting secondary structure by providing substantial rigidity and reducing the conformational degrees of freedom.[45, 57, 58]

The first goal of this thesis was the asymmetric synthesis of one or more cyclically-constrained δ-amino acid residues for use in peptide synthesis (Figure 1.25).

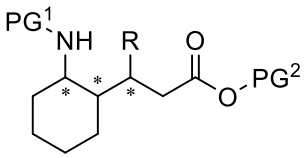

Figure 1.25: The general structure for the target δ-amino acid residues.

The next priority was to develop and fully characterise novel α/δ peptidomimetic foldamers, investigating the effect of changes in amino acid sequence and chirality on the secondary structure (Figure 1.26).

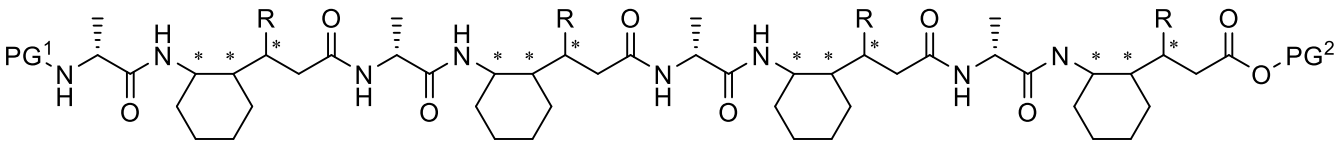

Figure 1.26: The general structure for a target α/δ peptidomimetic foldamer.

The final goal was to optimise the synthesis of previously described cyclically-constrained γ-amino acid precursors and utilising them to construct novel dipeptide building blocks for the construction of potentially catalytic foldamers (Figure 1.27).

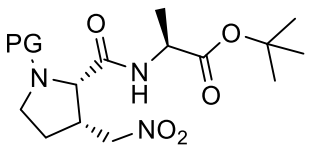

Figure 1.27: The target pyrrolidine-based dipeptide.

Chapter 2 - The synthesis of novel cyclically-constrained δ-amino acid monomers and α/δ-foldamers

2.1. Background

As discussed in the previous chapter, 1:1 α/δ-foldamers have been predicted by Hofmann – and in one example, experimentally shown – to fold into stable confirmations, adopting a 13/11-helical structure.[62, 73] Interestingly, the initial modelling work also predicted that these foldamers would possess two unique and potentially useful features. Firstly, the extra length of the δ-monomers leads to a more tightly packed helix when compared to the corresponding α/γ systems. This can be clearly seen by comparing two closely related α/γ and α/δ octameric systems side-by-side, with the α/δ system having a smaller pitch - the height of one complete helical turn (Figure 2.1). This results in the side chains being brought closer together. The second feature is the α-residues being found closer to the helix centre when compared to the α/γ system, resulting in deep grooves in the helix itself. These two features combined may allow for the creation of binding cavities – missing in previous foldamer catalyst examples - within the helical structure of the foldamer, potentially mimicking the structure and function of an enzyme active site and therefore allow stereochemical control when appropriately functionalized and used as a catalyst. This ultimate goal first necessitates the continued exploration of simple 1:1 α/δ foldamer scaffolds, with a view for further development and diversification to achieve catalytically active examples in the future.

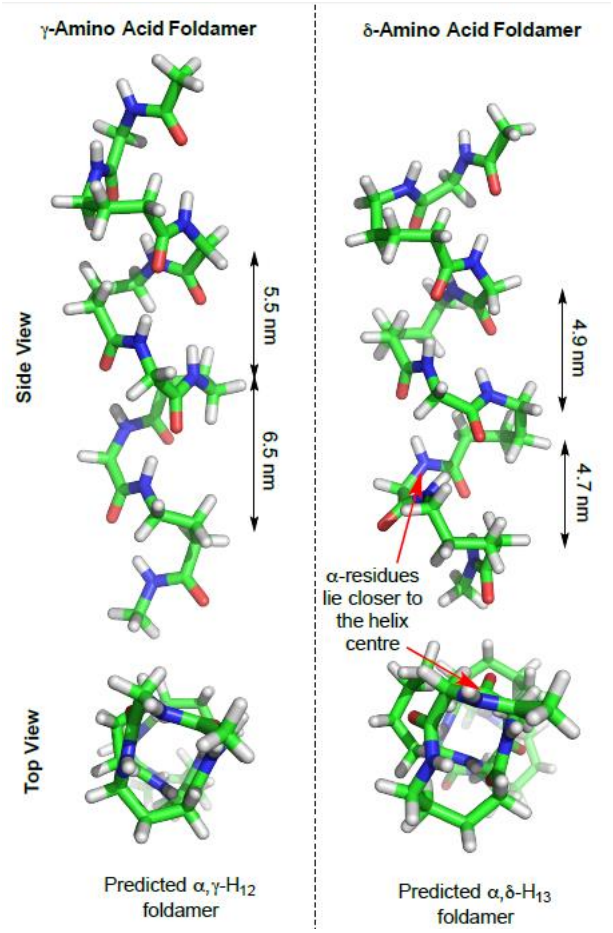

Figure 2.1: The side-by-side comparison of corresponding 1:1 α/γ and α/δ octameric systems.[62]

2.2. Aims and Objectives

The aim of this chapter was to synthesis novel, cyclically-constrained δ-amino acid monomers and to incorporate them into hybrid 1:1 α/δ-peptides. The synthesis of both the *trans* and *cis* δ-residues **60** and **61** is described first, starting with the organocatalytic synthesis of the corresponding γ-amino acid precursors and then the efforts to homologate up to the δ-systems. Then, the protection efforts and subsequent incorporation of **61** (*cis*-ACPA) into a range of foldamers via liquid-phase peptide synthesis is discussed (Figure 2.2).

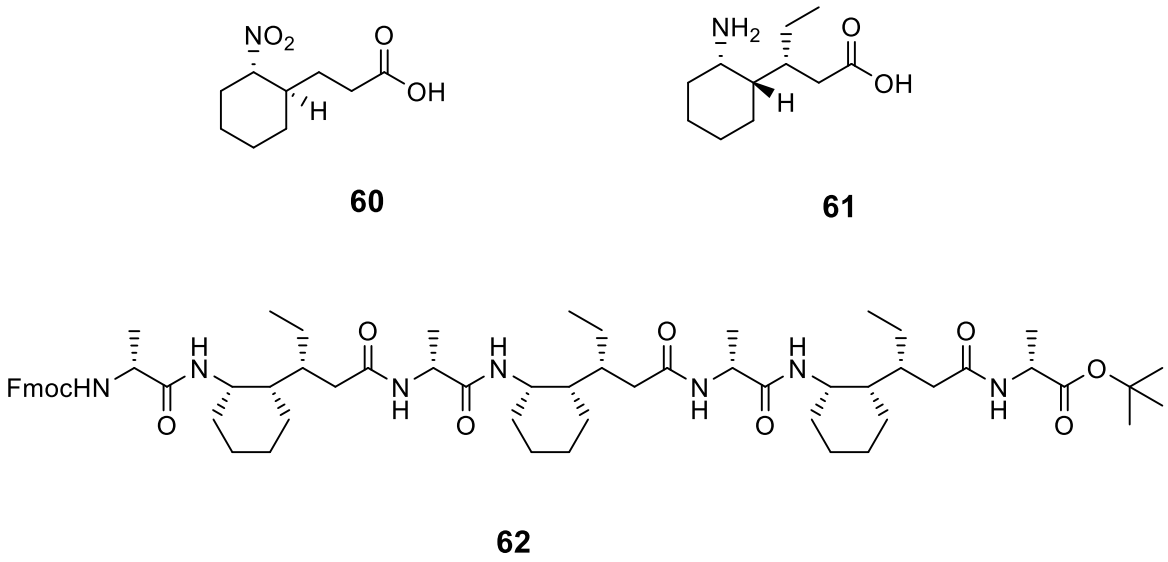

Figure 2.2: The target *cis* **60** and *trans* **61** δ-amino acid systems, and the heptamer **62**, one of the final foldamer targets.

2.3. Results and Discussion

2.3.1. Synthesis of *trans* δ-amino acid precursor 60

Previously published work by the Cobb group provided the starting point for the synthesis of **60**. This work described the enantioselective, organocatalytic synthesis of a range of cyclically-strained *trans* γ-amino acid precursors (Scheme 2.1).[75] It made use of the bifunctional thiourea catalyst **63** to promote the intramolecular Michael addition of a nitronate to a conjugated ester, with stereochemical control over the formation of three contiguous stereocenters. Long reaction times are used in order to allow the system to equilibrate to the desired and thermodynamically more stable *trans* isomer **65**.

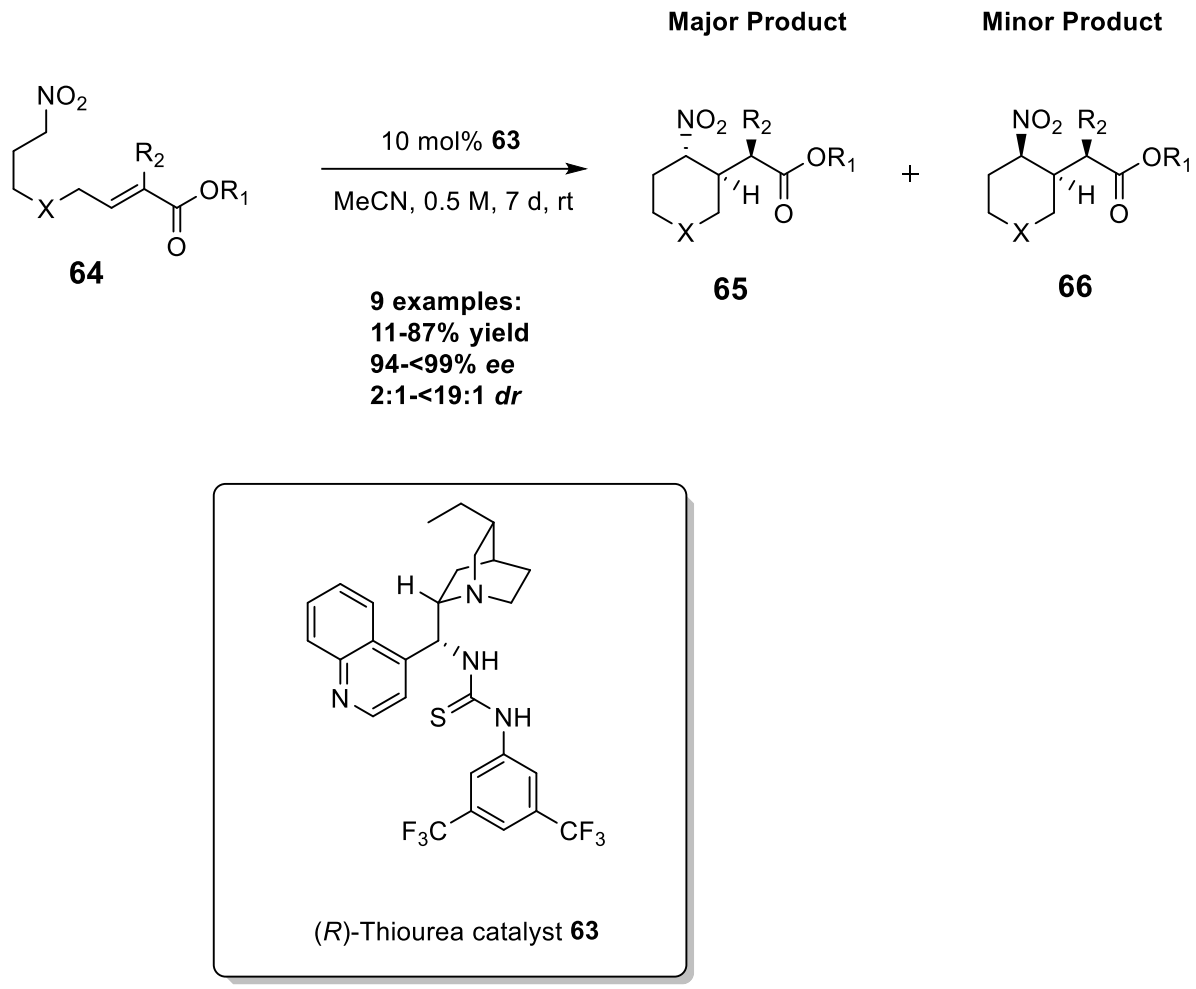

Scheme 2.1: The organocatalytic synthesis of cyclic γ-amino acid precursors, developed by Cobb and co-workers.

The *trans* isomer is the more thermodynamically favorable because of the possibility to place both the nitro group and the alkyl chain in the equatorial position on the cyclohexane ring, avoiding destabilizing interactions with the axial protons, known as 1,3-diaxial interactions. In the *cis* system, at least one of the substituents (most likely the nitro group) will have to be in the axial position and the unfavorable 1,3-diaxial interactions will occur (Figure 2.3).

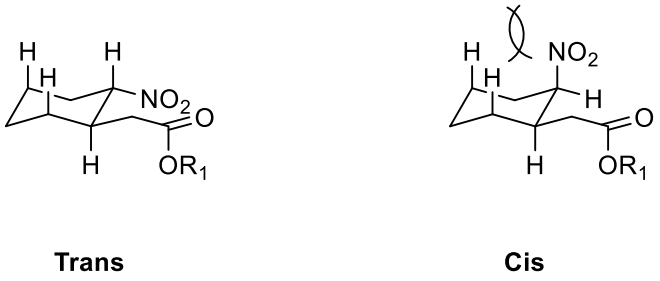

Figure 2.3: A diagram showing the destabilizing 1,3-diaxial interactions of the *cis* isomer (R_2 removed for clarity).

The required nitro ester starting material **70** was synthesised in three steps, beginning with the nitration of ethyl 6-bromohexanoate **67** with sodium nitrite in a 44% yield, followed by the DIBAL-H reduction of the ester **68** to aldehyde **69** in a 78% yield. A Wittig reaction was then performed, with **69** reacting with (carbmethoxymethylene)triphenylphosphorane to give the α,β-unsaturated ester **70** in a 70% yield (Scheme 2.2)

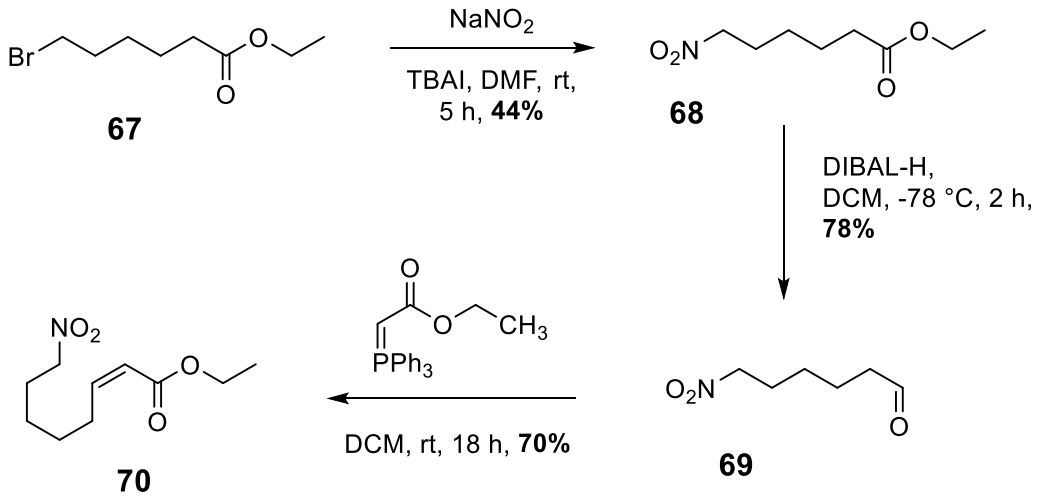

Scheme 2.2: The synthesis of the α,β-unsaturated ester **70**.

The organocatalytic Michael addition was then undertaken, with **70** converted to the cyclic ester **71** upon addition of the (R)-thiourea catalyst **63** and the reaction mixture being stirred for 7 days (Scheme 2.3). Whereas the yield of 87% was the same as the literature value, the *dr* for the trans isomer was substantially worse (10:3 compared to >19:1). This was probably due to the moderate solubility of the catalyst, with the issue being compounded by the much larger scale of the reaction when compared to the literature example. This resulted in a much

longer reaction time, taking much longer to equilibrate to the more stable trans isomer. Leaving the reaction even longer would solve this issue, but this was not considered a practical solution considering the reaction time was already at 7 days, so the decision was made to re-address the diastereomeric ratio at a later point in the synthesis.

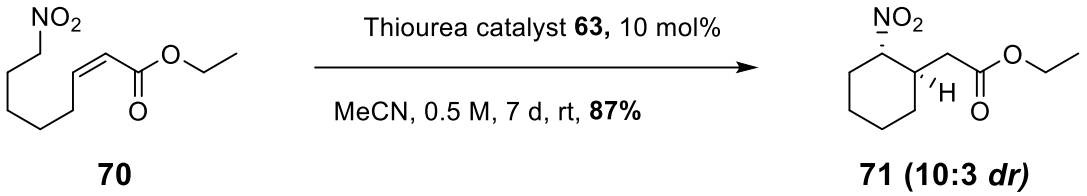

70 **71 (10:3 *dr*)**

Scheme 2.3: The organocatalytic synthesis of **71**.

Having acquired the γ-amino acid precursor **71**, the next step was to homologate it up to an equivalent δ-system. The first strategy considered for this was the Arndt–Eistert reaction, which is commonly utilized in order to achieve a one-carbon homologation of carboxylic acids.[76] This approach has been used before in the homologation of amino acids, with Seebach and co-workers homologating Boc-protected α-amino acids to their β-equivalents.[77] Due to the highly toxic and explosive nature of diazomethane, it was decided that the procedure should be attempted first with trimethylsilyldiazomethane, a safer alternative.[78]

The ester **71** was first converted to the carboxylic acid **72** by treatment with hydrochloric acid and refluxing overnight, resulting in a 66% yield after purification. This was then treated with triethylamine and ethyl chloroformate in order to form the acyl chloride **73** *in situ*. Shortly after, TMS-diazomethane was added and left to stir for 22 hours, in an attempt to form the desired diazo compound **73** (Scheme 2.4). TLC analysis of the reaction mixture indicated that the starting material had been consumed and that a major product had formed, alongside several side-products. However, **73** was not isolated after the work-up and purification, indicating that it may have broken down due to the aqueous conditions of the work-up or, more likely, due to interactions with the silica gel used in the flash chromatography purification.

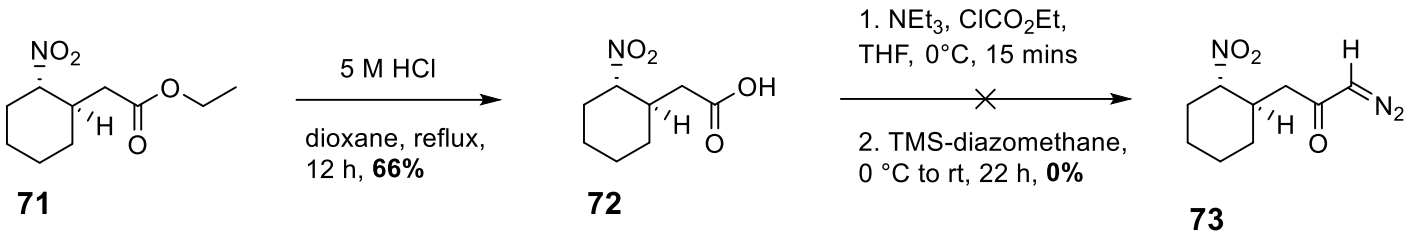

Scheme 2.4: The attempted synthesis of the diazo compound **73**.

In an attempt to circumvent the isolation issue of **73**, the crude product was collected and fed directly into the next step of the homologation. The crude reaction mixture of **73** was taken up in THF and a mixture of silver benzoate in triethylamine was slowly added whilst the solution was sonicated, followed by the addition of water (Scheme 2.5). TLC analysis indicated the presence of a complex mixture of products, and the desired carboxylic acid **74** was not isolated after purification. It was speculated that the presence of side-products that had been brought through with the crude mixture interfered with the formation of **74**.

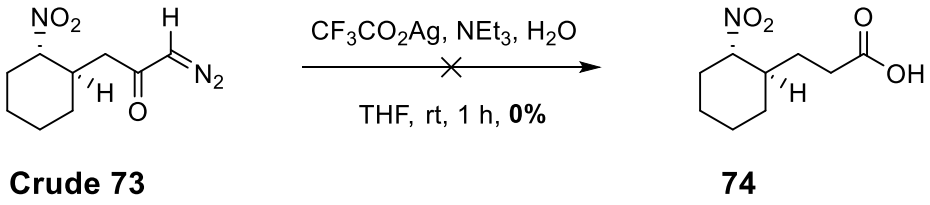

Scheme 2.5: The attempted synthesis of the homologated carboxylic acid **74**.

Due to the difficulties encountered with this homologation method, the decision was made to design a new synthetic route. Attention turned towards the Wittig reaction as a possible alternative. A one-carbon homologation can be achieved by reaction with the simplest Wittig reagent, methylenetriphenylphosphorane, which will convert an aldehyde to a terminal alkene. A subsequent hydroboration and oxidation can be performed to restore the aldehyde functionality, as shown in Scheme 2.6.

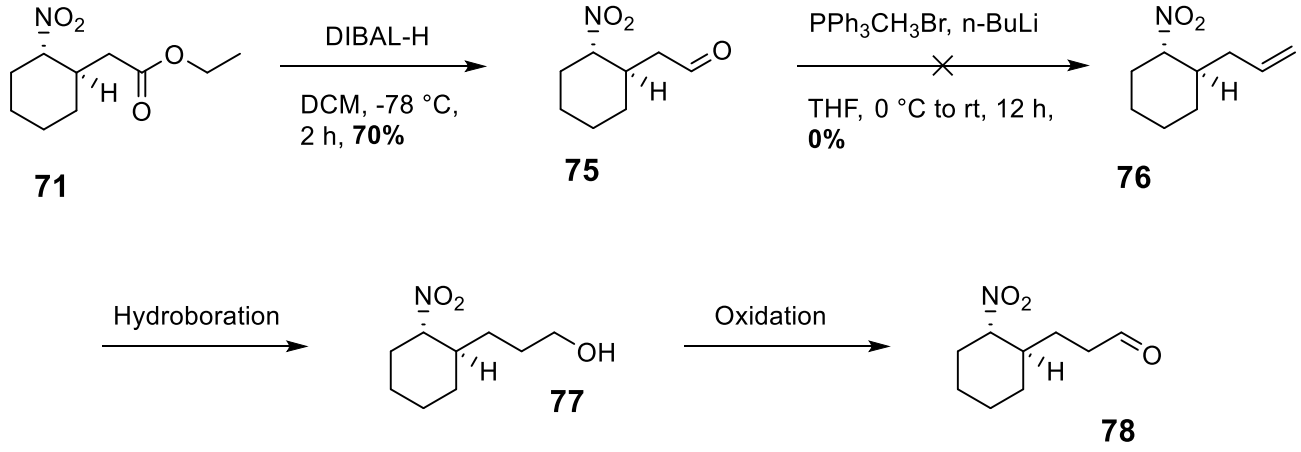

Scheme 2.6: The proposed synthetic route to the homologated aldehyde **78**, showing the unsuccessful Wittig reaction of **75**.

The ester **71** was successfully converted to the required aldehyde **75** by treatment with DIBAL-H, achieved in a 70% yield. In the next step, methylenetriphenylphosphorane was prepared *in situ* by the addition of *n*-BuLi to the corresponding phosphonium salt. **75** was then added, and the reaction allowed to warm to room temperature. Unexpectedly, the reaction did not proceed, even at extended reaction times. Difficulties in the use of Methylenetriphenylphosphorane for Wittig reactions have been reported for sterically hindered ketones, but not for aldehydes.[79,80] It is still unclear why this reaction failed, and further investigation would be needed to discover why.

Instead of abandoning the Wittig reaction as a method of homologation, it was decided that the use of an alternative Wittig reagent should be attempted and an alternative synthetic route towards the synthesis of **60** pursued - developed in conjunction with Barbara Dworakowska as part of her master's project. The methoxy ylide **79** can also be used to homologate aldehydes as part of a two-step procedure. The first Wittig step is followed by the hydrolysis of the resultant methoxy compound, resulting in a one-carbon homologation. Again, the active phosphorane ylide **79** was generated in situ by the addition of *n*-BuLi to the corresponding phosphonium salt. **75** was added and the reaction allowed to stir for 2 hours. This time, TLC analysis indicated consumption of the starting material and the likely formation of *E* and *Z* isomers of the methoxy product. The reaction was quenched and worked-up, and

the crude product taken up in THF and 8M HCl added. After purification, the homologated aldehyde **80** was obtained in a yield of 75% (Scheme 2.7).

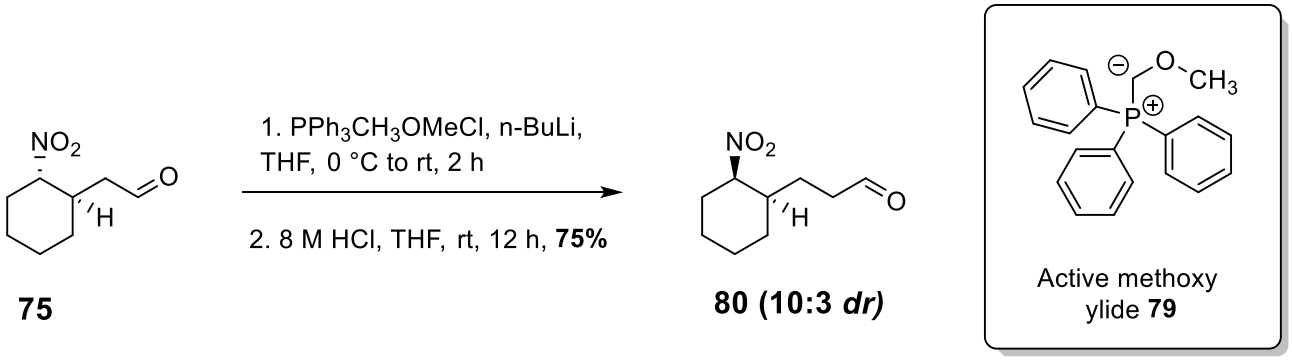

75

80 (10:3 *dr)*

Scheme 2.7: The homologation of **75** to give aldehyde **80**, showing the active methoxy ylide that is produced *in situ*.

Unfortunately, it was the *cis* isomer that was predominantly formed, with a diastereomeric ratio of 10:3. The strong base added in the first step of the homologation is capable of deprotonating at the position alpha to the nitro group, by virtue of the formation of a stabilizing nitronate ion. Any subsequent restorative protonation that occurs will approach from either the concave or convex side, with the concave side sterically blocked by 1,3-diaxial interactions.[81] It will instead occur from the "freer" convex side, resulting in the epimerization of the stereocentre and the preferential formation of the *cis* product, despite it being less thermodynamically stable than the *trans* system (Figure 2.4).

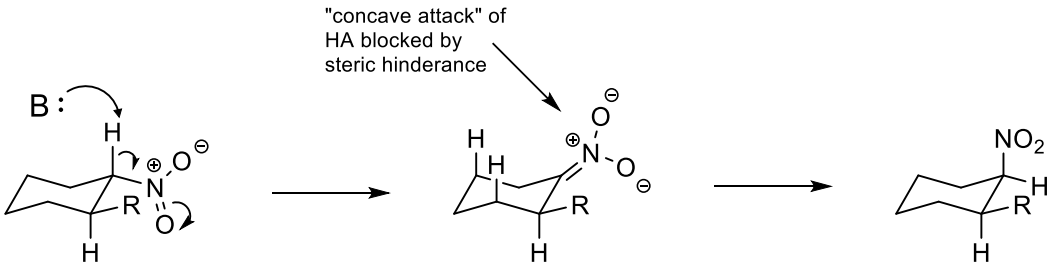

Figure 2.4: The base-promoted epimerisation of the nitro group, showing the blocked concave protonation due to steric hinderance.

The addition of a weak, aqueous base to **80** should result in the conversion back to the desired *trans* isomer **78**. The slower, more reversible nature of the proton exchange would allow for

the system to equilibrate to its more stable form, facilitating the selective epimerisation of the aforementioned stereocentre. The presence of both a nitro and aldehyde group could result in unwanted side-reactions under these conditions however, most notably the Henry reaction. Therefore, **80** was converted to the alcohol **81** by reduction with sodium borohydride, achieved in a 61% yield. The epimerisation was then performed, with sodium bicarbonate added and the mixture allowed to stir overnight. The *trans* alcohol **77** was isolated in a yield of 79% and a diastereomeric ratio of 16:1. This was then converted to the carboxylic acid in a TEMPO-catalysed oxidation, using sodium chlorite as the oxidant, resulting in the *trans* δ-amino acid precursor **60** in a yield of 58% and a final diastereomeric ratio of 16:1 (Scheme 2.8).[82]

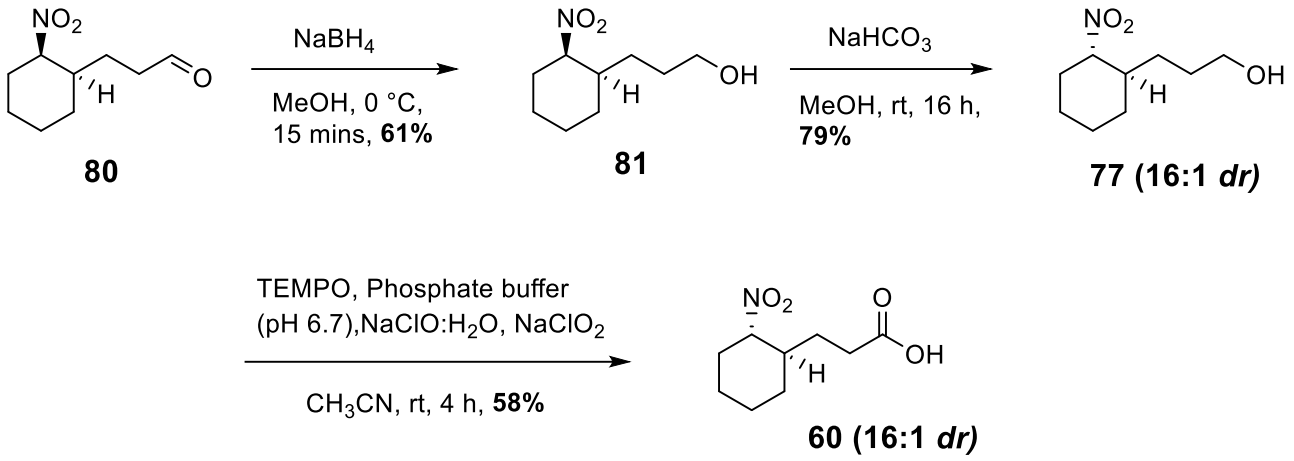

Scheme 2.8: The synthesis of the *trans* δ-amino acid precursor **60**, including the successful epimerisation of **81** to the *trans* isomer **77**.

Due to the lengthy nature of the synthesis of **60**, both in terms of synthetic steps and time, the decision was made to prioritise the synthesis and optimisation of the *cis* δ-residue **61** and its incorporation into peptidomimetic foldamers.

2.3.2. Synthesis of *cis* δ-amino acid 61

The starting point for the synthesis of **61** is provided by Gellman and co-workers, who developed the enantioselective, organocatalytic synthesis of a range of cyclically-strained *cis* γ-amino acid monomers (Scheme 2.9).[83] It describes the pyrrolidine-catalsyed Michael addition of a series of aldehydes to 1-nitrocyclohexene, all with high diastereo- and

enantioselectivities. Much like the previously described example provided by Cobb, the reaction delivers stereochemical control over the formation of three contiguous stereocentres.

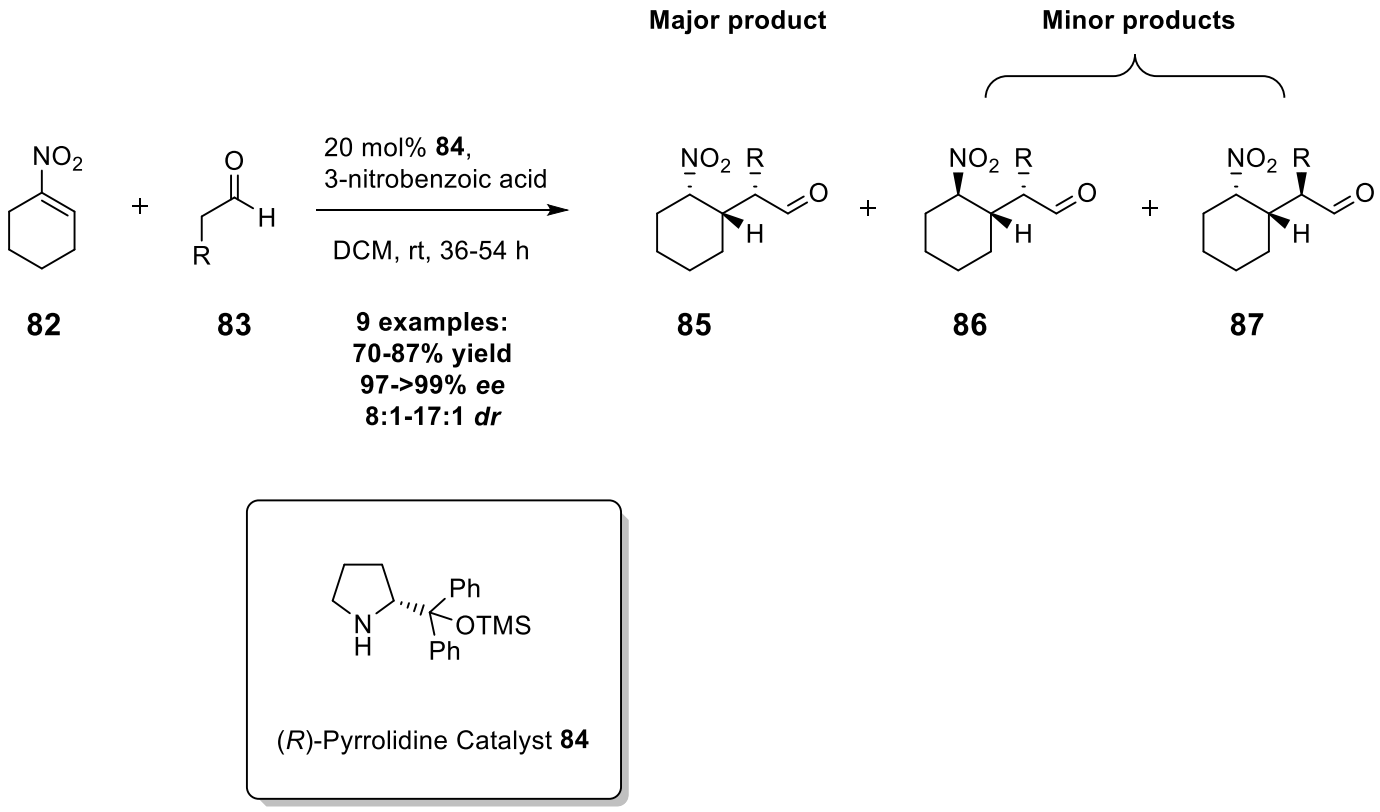

Scheme 2.9: The organocatalytic synthesis of cyclic γ-amino acid precursors, developed by Gellman and co-workers.

Three of the possible eight diastereoisomers were routinely observed in the examples provided, most notably the desired *cis* compound **85** and the *trans* epimer **86**. Compound **87** was detected only in negligible amounts and was therefore omitted from the calculated *dr* values.

Butyraldehyde **88** was selected to be the aldehyde of choice for the synthesis of our amino acid precursor, offering the best yield and diasteresoselectivity of all the examples, whilst also resulting in one of the least bulky and potentially disruptive R group side chains. As shown in Scheme 2.10, the γ-amino acid precursor **89** was produced as a mixture of diastereoisomers in a yield of 62%, a *dr* of 11:2 and an *ee* of 98% (established at a later point of the synthetic route). The yield and diastereomeric ratio were notably worse than the literature values,

again as a consequence of the much larger scale (~20 times) required to produce synthetically useful amounts. As we are now interested in producing the thermodynamically less stable *cis* isomer, it is not possible to improve the diastereomeric ratio in a reversible manner, as achieved in the synthesis of. Therefore, the priority throughout the synthesis of **61** was to preserve the *dr* as much as possible.

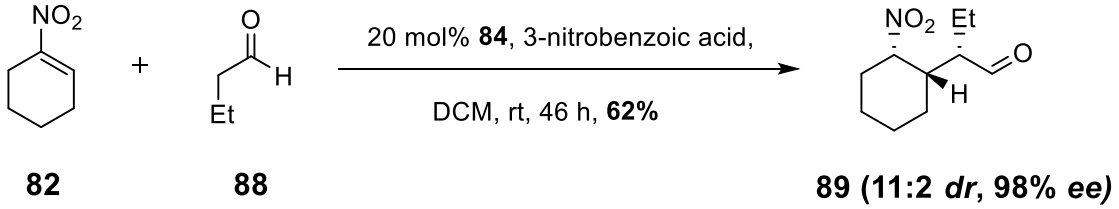

82 **88** **89 (11:2 *dr*, 98% *ee)***

Scheme 2.10: The organocatalytic synthesis of **89**.

Through careful analysis of the ^{1}H NMR spectrum and the coupling constants of the H^1 proton, Gellman and co-workers were able to determine the exact configuration of each of the two important *cis* and *trans* epimers **89** and **90** (Figure 2.5). The magnitude of coupling between two protons is influenced by their spatial relationship and the dihedral angle between the two - known as the Karplus relationship. In the context of cyclohexane rings, large coupling constants (10-14 Hz) are reported for protons with a relative 180^{o} dihedral angle, found in axial-axial relationships. Smaller coupling constants (2-5 Hz) are reported for protons with a relative 60^{o} dihedral angle, found in both axial-equatorial and equatorial-equatorial relationships.[84]

For **89**, the coupling constants between H^1 and neighbouring protons are consistently small (J = 3.8, 3.8, 3.8 Hz), indicating equatorial-equatorial and equatorial-axial relationships. H^2 must therefore be in an equatorial position, leaving the nitro group in an axial position. For **90**, H^2 was found to possess one small and two large coupling constants (J = 11.3, 11.3, 3.8 Hz) with neighbouring protons, indicating that both H^1 and H^2 are occupying axial positions, leaving both the nitro group and the aldehyde-bearing side chain in equatorial positions. These findings and the resultant stereochemical assignments are consistent with the

structures that the group obtained from the X-ray crystallography of derivates of both compounds.

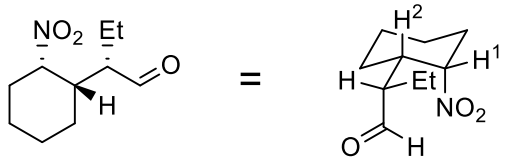

89

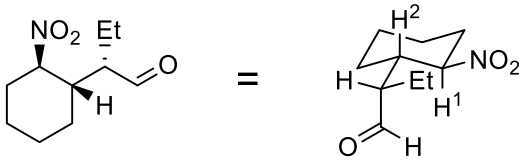

90

Figure 2.5: The axial and equatorial configurations for **89** and **90**, as determined by H^1 NMR.

The same homologation method that was developed for the Cobb-derived system **75** was employed for **89**. The Wittig reaction was performed, resulting in a mixture of *E* and *Z* alkenes in a yield of 80% (Scheme 2.11). This time, the *E*- and *Z*-alkene proved to be separable by flash chromatography and were both isolated and characterised. Interestingly, 1H NMR analysis showed that the *Z*-alkene (distinguishable from the *E*-alkene by its lower coupling constants for the two vinylogous protons) was formed selectively from the desired *cis* isomer **90** , resulting in the single diastereomer **92**. The *E*-alkene **91** however was indiscriminate in its formation, representing a complex mixture of both diastereomers.

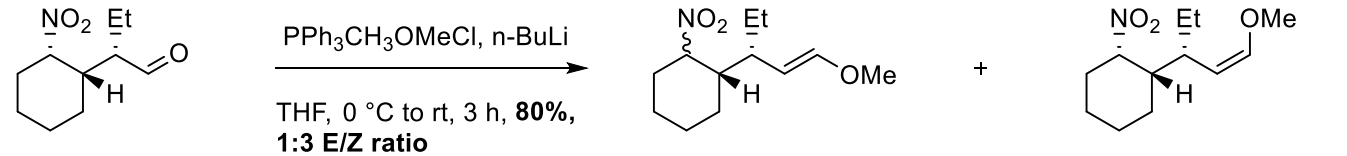

89 (*dr* 11:2)

91
diastereomeric mixture

92
single distereoisomer formed

Scheme 2.11: The Wittig reaction of **89**, showing the formation of *E* and *Z* methoxy isomers **91** and **92**.

The selective nature of formation for the *Z*-alkene **92** might be explained by the different configurations of the *cis* and *trans* isomers. For the *cis* isomer, the nitro group is in an axial position, pointing away from the end of the equatorial side chain and thus positioned far away from the methoxy group, no matter how the side chain rotates. For the *trans* isomer, however, the nitro and methoxy group can come together in close proximity as the side chain rotates, increasing steric repulsions and discouraging its formation. This selective pressure does not exist for the E-alkene, as the methoxy group is pointing much further away, meaning that steric hinderance is no longer an issue for either *cis* or *trans* isomer and both can form easily (Figure 2.6).

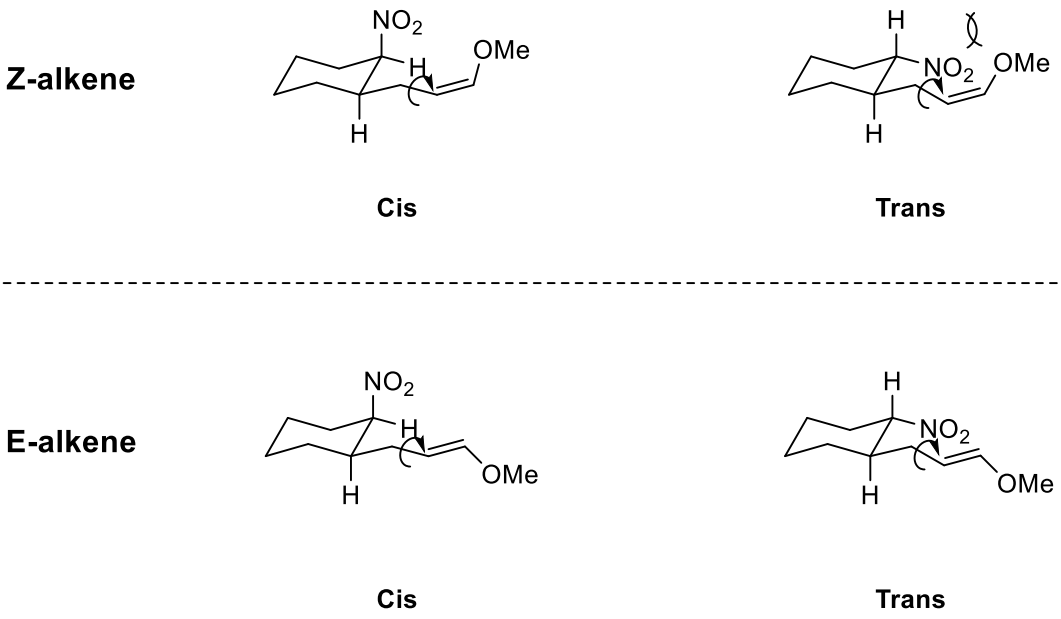

Figure 2.6: A rationale for the single diastereoisomer formation of the Z-alkene, with steric repulsions in the *trans* isomer discouraging its formation (ethyl group removed for clarity).

It might have been decided to carry forward only the *Z*-alkene **92** due to its diastereomeric purity, but this would have resulted in a considerable loss of material, as the *E*-alkene also contained plenty of the *cis* isomer. It was also speculated that the *cis* and *trans* isomers could be more easily separated at a later stage in the synthesis. **91** and **92** were therefore combined and subjected to the second step of the homologation, with 8M HCl added and the reaction stirred for 12 hours. The homologated aldehyde **93** was produced in a yield of 90% (giving a yield of 72% for the overall two-step homologation) and a *dr* of 9:2. It was at this stage - having successfully homologated the system – that the enantiomeric excess was established, to check that the stereochemical integrity was maintained. The aldehyde **93** was reduced down

to the alcohol **94** using sodium borohydride and chiral HPLC analysis performed alongside the racemic equivalent (produced via a racemic organocatalytic first step and following the same synthetic route). The *ee* was found to be 98%. The carboxylic acid **95** was then produced from the aldehyde **93** by a Pinnick oxidation in a yield of 92% and a slightly deteriorated *dr* of 7:2 (Scheme 2.12).

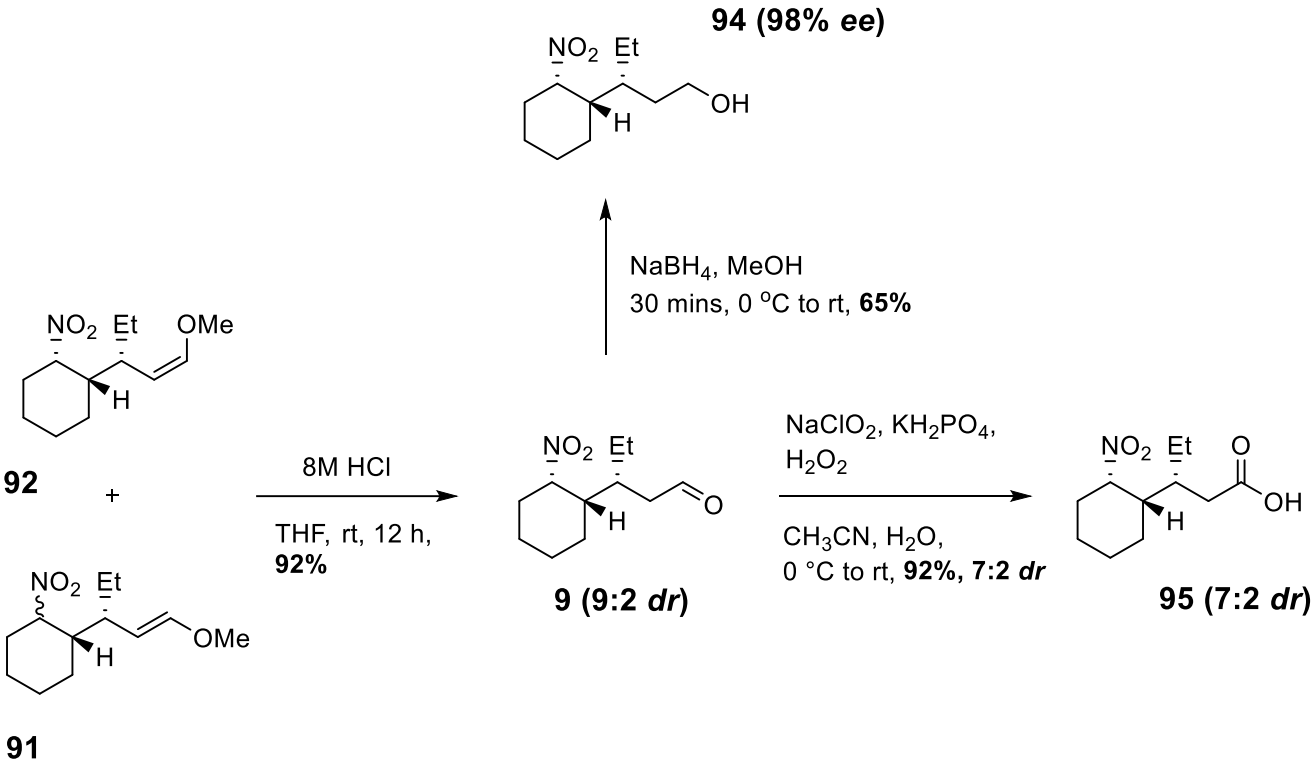

Scheme 2.12: The synthesis of carboxylic acid **95**, as well as the alcohol **94**.

With the homologated nitro acid system **95** in hand, attention could turn to monomer preparation for peptide synthesis. Solid-phase peptide synthesis (SPPS) was the first strategy considered and aimed for, due to its high efficiency, simplicity and speed when compared to liquid-phase peptide synthesis.[85] The process makes use of a solid resin bead support, upon which the amino-protected amino acid is covalently bound to via the carbonyl group. The amino group will then be deprotected and coupled to the next protected amino acid and the process repeated until the desired sequence is complete. The completed peptide can then simply be cleaved from the resin and collected. The process is automated and will all take place in a single reaction vessel. The easiest and most commonly used protection strategy for SPPS employs the Fmoc and *t*Bu protection groups, due to their ease of removal under mild

conditions, especially for the Fmoc group. It is therefore necessary to produce the Fmoc protected *cis* amino acid **96**, as shown in Scheme 2.13.

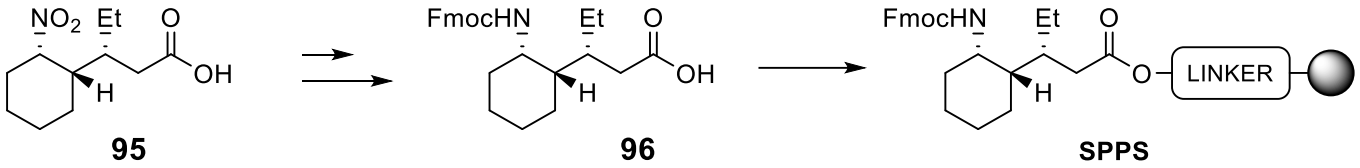

Scheme 2.13: A schematic showing the necessary Fmoc-protected amino acid **96** for Solid-phase peptide synthesis.

The reduction of the nitro group and thus production of the naked amino acid **97** (*cis*-ACPA) is the first required step towards the synthesis of **96** (Scheme 2.14). The reaction proved challenging at first, with efforts employing palladium on carbon as the reducing agent failing to produce any of the amino acid, regardless of any changes in pressure or the use of a hydrogen transfer-agent. The use of Raney Nickel saw improved yet still modest results, with the best example achieving a yield of 32% at a pressure of 40 Psi. Transfer catalytic hydrogenation with zinc offered the best yields, achieving 70% with the use of ammonium chloride as the hydrogen transfer-agent (Table 2.1). The failed use of palladium on carbon might have been due to incomplete hydrogenation, leading to the formation of the corresponding hydroxylamine instead of the desired amino acid **97**. This has been previously reported for the use of Pd catalysts when reducing aliphatic groups, particularly those which are hindered.[86,87]

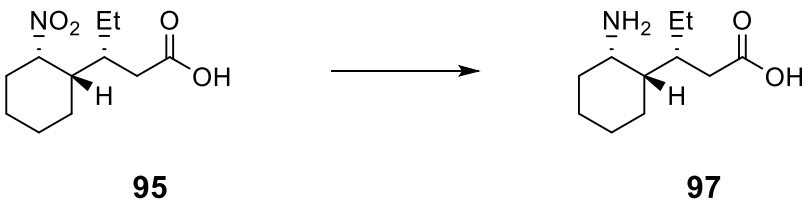

Scheme 2.14: The reduction of the nitro acid **95** to the amino acid **97**.

(a) Reactions conducted at room temperature, with between 0.8 and 3 mmol of **95**. (b) Isolated yield.

Entry[a]	Reagents	Solvent	Pressure [Psi]	Time [h]	Yield[b] [%]
1	10% Pd/C, H_2	MeOH	14.7	12	0
2	10% Pd/C, H_2	MeOH	40	5	0
3	10% Pd/C, NH_4HCO_2	MeOH	14.7	6	0
4	Raney Ni, H_2	MeOH	14.7	12	25
5	Raney Ni, H_2	MeOH	40	5	32
6	Raney Ni, H_2	MeOH	50	5	22
7	**Zn, NH_4Cl**	**MeOH/THF**	**14.7**	**3**	**70**
8	Zn, CH_3COOH	MeOH	14.7	6	45

Table 2.1: The attempted reaction conditions for the reduction of compound **95** to compound **97**.

Unfortunately, all attempts to Fmoc protect the amino acid **97** failed, despite considerable efforts to optimise the reaction (Table 2.2). The use of two different Fmoc derivatizing agents was tested, Fmoc-chloroformate and Fmoc-succinimidyl carbonate. Together, these account for the vast majority of successful Fmoc protection procedures found in literature.[86] Regardless of the base and solvent used, the reaction consistently failed, even at elevated temperatures and extended reaction times. Steric effects might be an obvious answer for these failures, especially considering the sizeable steric bulk of the Fmoc group and the clustered nature of the secondary amine - bound directly to a cyclohexane ring which bears a lengthy side chain on the adjacent carbon. However, examples of successful Fmoc protections of similar and arguably even more sterically hindered amine compounds can be found in literature, using similarly mild reaction conditions.[88]

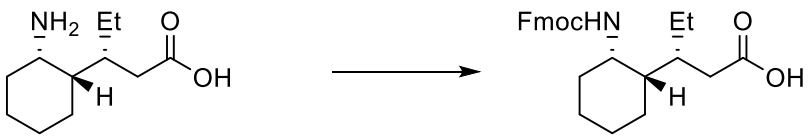

97 **96**

Scheme 2.15: The Fmoc protection of **97** to give **96**.

Entry[a]	Fmoc Source	Base	Solvent	Temperature [°C]	Time [h]	Yield[b] [%]
1	Fmoc-Cl	DIPEA	DCM	rt	6	0
2	Fmoc-Cl	Na_2CO_3 (10%)	Dioxane	0 to rt	12	0
3	Fmoc-Cl	NaOH	Dioxane/MeOH	rt	6	0
4	Fmoc-Cl	DIPEA	Dioxane	50	16	0
5	Fmoc-OSu	Na_2CO_3 (10%)	Dioxane	rt	16	0
6	Fmoc-OSu	DIPEA	Dioxane	0 to rt	16	0
7	Fmoc-OSu	DIPEA	Dioxane	50	24	0

(a) Reactions conducted with between 1 and 3 mmol of **97**. (b) Isolated yield

Table 2.2: The attempted reaction conditions for the Fmoc protection of **97.**

Another contributing reason for the failure to achieve the Fmoc protection might be the interfering nature of the carboxylic acid. It has been noted by several investigators that the preparation of Fmoc-protected amino acids that a pseudo-polymerisation process can occur, resulting in the formation of significant quantities of di- and tripeptides.[89,90] The general mechanism of this process is shown in Scheme 2.16, with the carboxylate of the successfully formed Fmoc-protected amino acid **100** going on to react with a second equivalent of the Fmoc agent **98**, resulting in the mixed carbonic carboxylic anhydride **101**. This activated species can then be subjected to nucleophilic attack by a second equivalent of the naked amino acid **99**, resulting in the formation of the dipeptide **102**. The process can continue unabated to form even longer peptidic impurities.

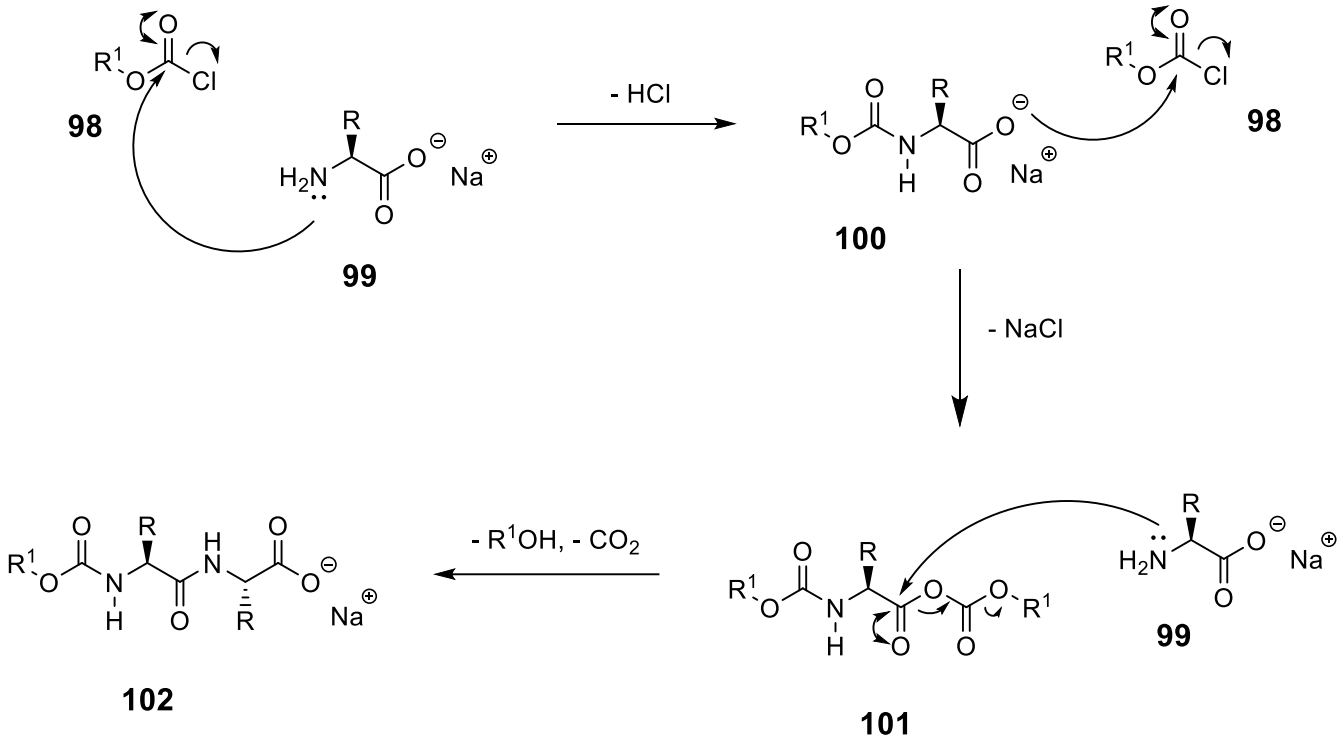

Scheme 2.16: The mechanism for the formation of impurities during the Fmoc protection of an amino acid.

Meienhofer and co-workers developed an Fmoc protection procedure that addresses this issue, which has seen considerable success when used to synthesis particularly sterically hindered amino acids.[87,91,92] It involves the initial addition of trimethylsilyl chloride and an appropriate base, in order to facilitate the *in situ* silylation of both the amine and the carboxylic acid groups (Scheme 2.17). This will effectively protect the carboxylic acid moiety whilst still allowing the amine to react once the Fmoc agent is introduced (by virtue of the amines stronger nucleophilic character). An aqueous work up will yield the desired Fmoc-protected amino acid.

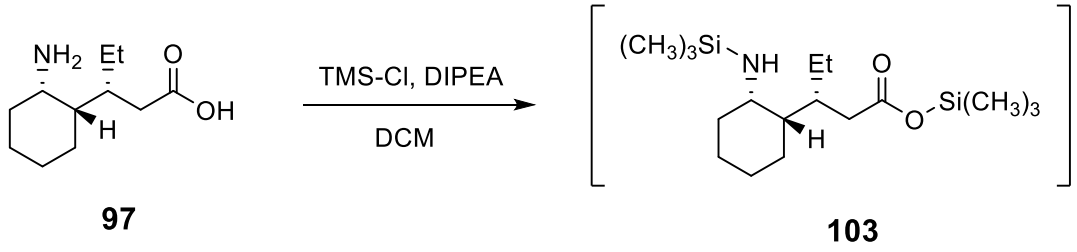

Scheme 2.17: The *in situ* silylation of the amino acid **97**.

The procedure was attempted with both Fmoc-chloroformate and Fmoc-succinimidyl carbonate, with 2 equivalents of TMS-Cl and DIPEA having been added to **97** beforehand in the hope of generating the *O,N-bis*-trimethylsilyl-amino acid **103** (Scheme 2.18). In both instances, no product was formed, despite lengthy reaction times. This suggests that the interference of the carboxylic acid moiety was not the primary reason for the failure to achieve the Fmoc protection.

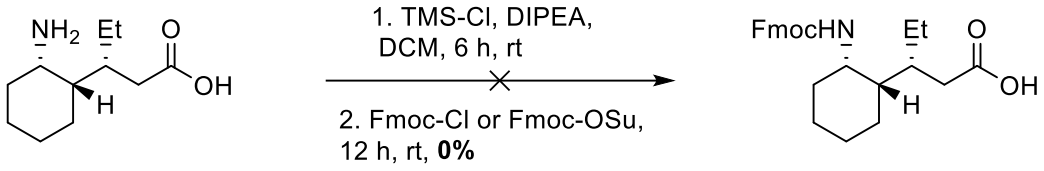

97 **96**

Scheme 2.18: The attempted Fmoc protection of **97**, via *in situ* silylation.

Having failed to produce the Fmoc-protected amino acid **96**, the prospect of utilising SPPS in order to synthesis the foldamers became more challenging. The only other widely used alternative method to the Fmoc/tBu protection strategy in SPPS requires Boc- and benzyl-protected amino acids.[85] However, it involves the use of hydrogen fluoride in order to cleave the completed peptide from the resin, increasing safety concerns and necessitating the use of apparatus we did not have to hand.[93] Therefore, the decision was made to instead focus on the use of liquid-phase peptide synthesis (LPPS), despite the inevitable detrimental impact reaction yields and the time required to produce the foldamers.[84] There are advantages associated with LPPS however, including improved results at higher reaction scales and a greater level of control/optimisation possible over each individual step.

2.3.3. Synthesis of α/δ foldamers

The initial foldamer targets were α/δ hybrid peptides of varying length with a 1:1 alternating backbone, as predicted by Hofmann and co-workers to form the most stable helical secondary structures.[73] Alanine was selected to be the sole α-residue used, chosen for the small size of its methyl side chain, making it unlikely to interfere with secondary structure formation. Alanine was chosen over glycine in particular due to its lower conformational entropy, making it a greater helix stabiliser.[94] D-Ala was used in the first instance, in accordance with the foldamers produced by Gellman and co-workers that incorporated the corresponding γ-amino acid monomers.[83]

A common problem in peptide coupling is the potential for racemization, as a consequence of the necessary activation of the carboxyl group by the introduction of an electron-withdrawing group. The two potential pathways for this process are shown in Scheme 2.19.[95]

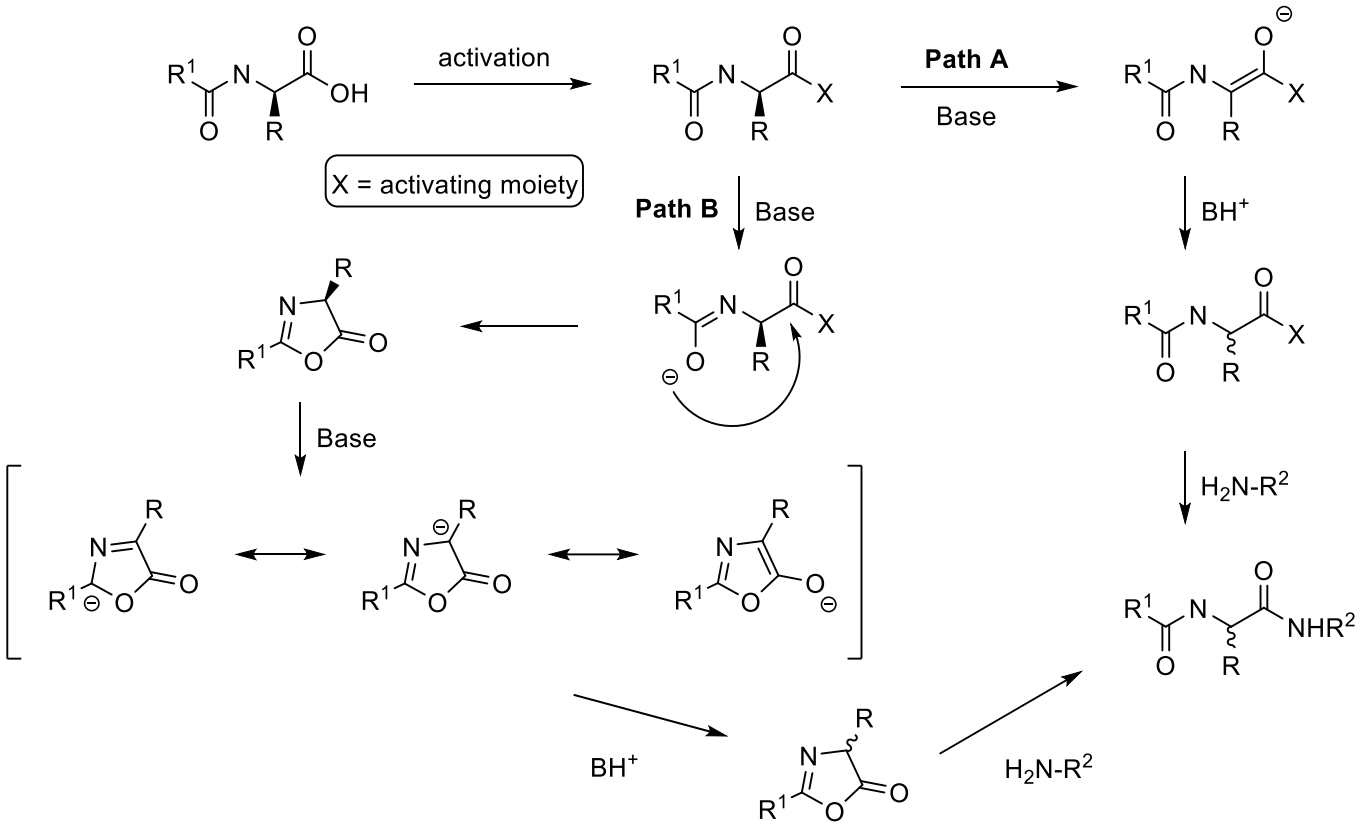

Scheme 2.19: The two major pathways for racemisation in peptide coupling reactions.[95]

Pathway B shows the formation of an oxazolone ring and the subsequent base-catalysed loss of chiral integrity at the α-position. Pathway A shows the simpler, direct enolization that can cause racemisation at the same position. Both pathways are possible for carbodiimide-mediated peptide coupling, by far the most popular and frequently used technique. These pathways can be supressed and sometimes eliminated altogether by the addition of coupling additives such as HOBt, Oxyma, etc.[96] In addition to preventing racemisation, these additives will also inhibit side reactions and accelerate the coupling reaction itself, making them useful additions even in the absence of a vulnerable stereocentre. This is the case for our first coupling reaction between the nitro acid **95** and D-Ala, with the reaction proceeding via the c-terminus of the δ-residue to produce the dipeptide. Racemisation will not be possible through the traditional pathways just mentioned, although it might still be possible at the nitro position in the usual base-promoted fashion (through the formation of the stabilised nitronate ion). Racemisation via pathways A and B will become more relevant in subsequent couplings, due to the unavoidable use and activation of the α-residue C-terminus.

The coupling of **95** and D-Alanine tert-butyl ester hydrochloride was achieved in a 69% yield, with a 3:1 ratio of *cis* and *trans* dipeptide products, **104** and **105**, respectively (Scheme 2.20). The formation of the *trans* dipeptide can be explained by the presence of the *trans* nitro acid isomer in the starting material. Pleasingly, the two diastereoisomers were easily separable by flash chromatography. The use of oxyma as the coupling additive was also investigated, resulting in a lower overall yield of 47%. Therefore, the use of HOBt was maintained for subsequent coupling reactions.

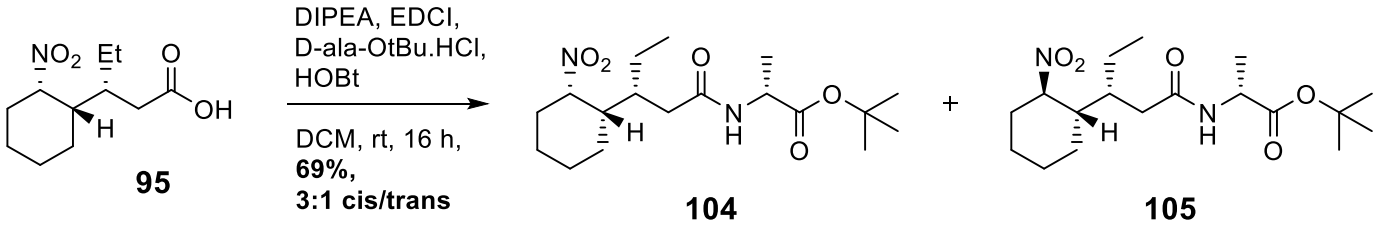

Scheme 2.20: Synthesis of the *cis* and *trans* nitro-dipeptides **104** and **105**.

Having obtained the *cis* nitro-dipeptide **104,** the next priority was to reduce the nitro group to the amine and to install a suitable protecting group, so that the dipeptide could be used to eventually generate an octamer via sequential peptide coupling. The reduction of **104** proved troublesome, even more so than the reduction of **95**. The use of zinc and ammonium chloride resulted in a yield of only 18%, markedly different to the yield of 70% for the production of the amino acid **97** (Scheme 2.21). The best result was achieved with Raney nickel at high pressure (40 Psi), yielding 32% of the amine **106**. The increased difficulty in reduction was attributed to the larger size of the starting material and the associated steric bulk preventing the molecule from effectively adsorbing onto the metal surface. The isolated yield may have also been impacted by the difficulty in purifying the compound due to the attraction between the basic amine and the acidic silica gel.

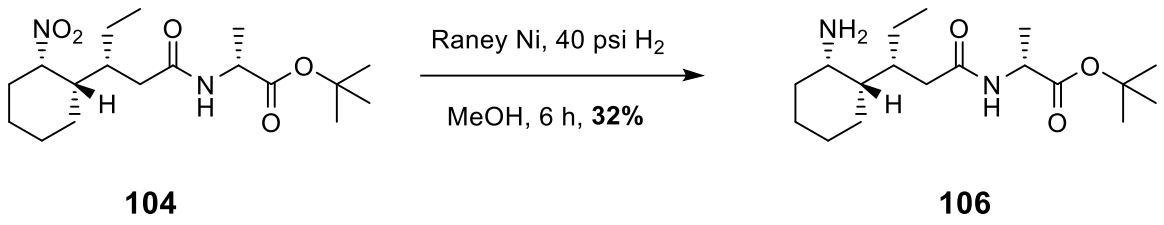

104 **106**

Scheme 2.21: The reduction of nitro-dipeptide **104** to give **106**.

The protection of **106** with both a Cbz and Fmoc group was attempted, with neither being successful. The failure to install an Fmoc group came as no surprise, considering the failed attempts to do the same for the amino acid **96**. The failed Cbz protection was disappointing however, especially considering its reduced size and steric bulk when compared to Fmoc. One solution to these difficulties could have been to directly couple **106** with the deprotected form of the nitro-dipeptide **104** in order to produce the nitro-tetramer. This was not considered suitable however due to the persistence of the troublesome nitro group and the associated reduction/isolation problems. An alternative strategy was therefore devised, which involved the direct coupling of **106** with Fmoc-protected alanine in order to produce the fully protected trimer **107** (Scheme 2.22). The potential for racemisation (as mentioned in Scheme 2.24) became relevant here, as the coupling reaction proceeds via the C-terminus of the Alanine α-residue. The reaction proceeded successfully with a yield of 61% and with no observable formation of the epimer.

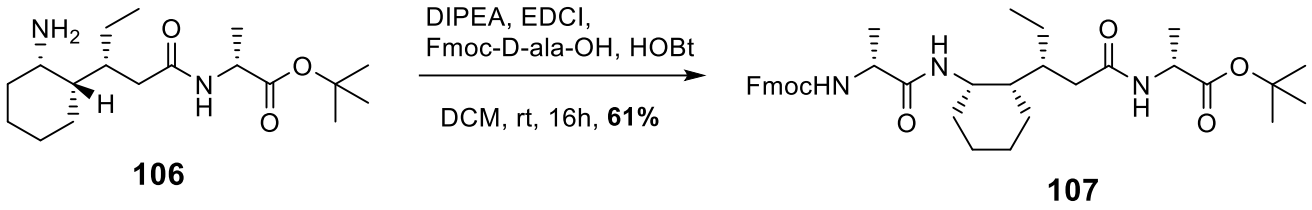

Scheme 2.22: The synthesis of the Fmoc-protected trimer **107**, with D-ala residues.

Having formed the trimer **107** with the incorporation of D-ala α-residues, the next priority was to form the corresponding trimer with L-ala residues. This would allow us to compare and evaluate both for initial signs of secondary structure formation, allowing for one of the systems to be prioritised for the creation of longer peptidic foldamers. The coupling of the nitro acid **95** and L-alanine tert-butyl ester hydrochloride was performed, and the required *cis* dipeptide product **108** separated from the *trans* product, resulting in a 44% yield. This was reduced and the crude product carried directly into the next coupling reaction, achieving the trimer **109** in a yield of 12% over the two steps (Scheme 2.23).

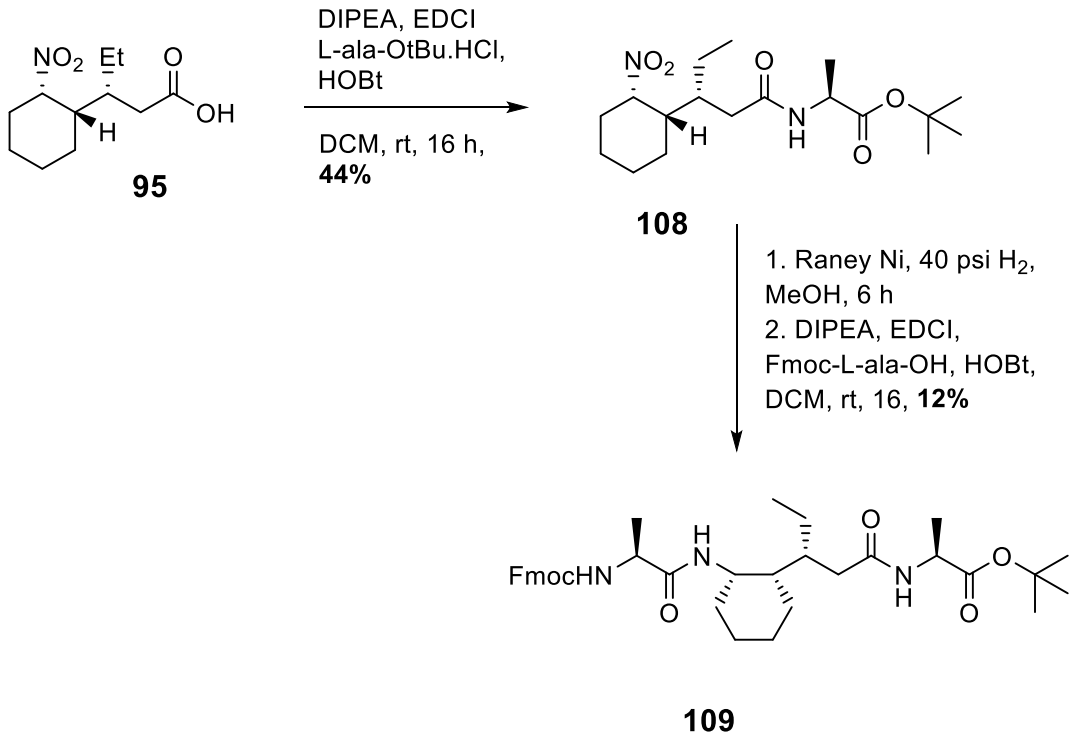

Scheme 2.23: The synthesis of the Fmoc-protected trimer **109**, with L-ala residues.

The ^{1}H NMR spectrum of both trimers were compared, with close attention paid to the chemical shift of the three amide protons for each. Amide protons that partake in hydrogen bonding will be found further downfield than those that do not. A chemical shift of 7 ppm or above is generally found to be the threshold that strongly suggests involvement in intramolecular hydrogen bonding and thus secondary structure formation.

For trimer **107**, two of its three amide protons were found to have a chemical shift above 7 ppm, contrasting considerably with **109**, which had none of its amide protons above 7 ppm (Figure 2.7). The system containing D-alanine residues displays a greater propensity for secondary structure formation, and thus was selected as the starting point for longer peptidic targets. More detailed characterisation and comparison of the two trimers is given in chapter 3.

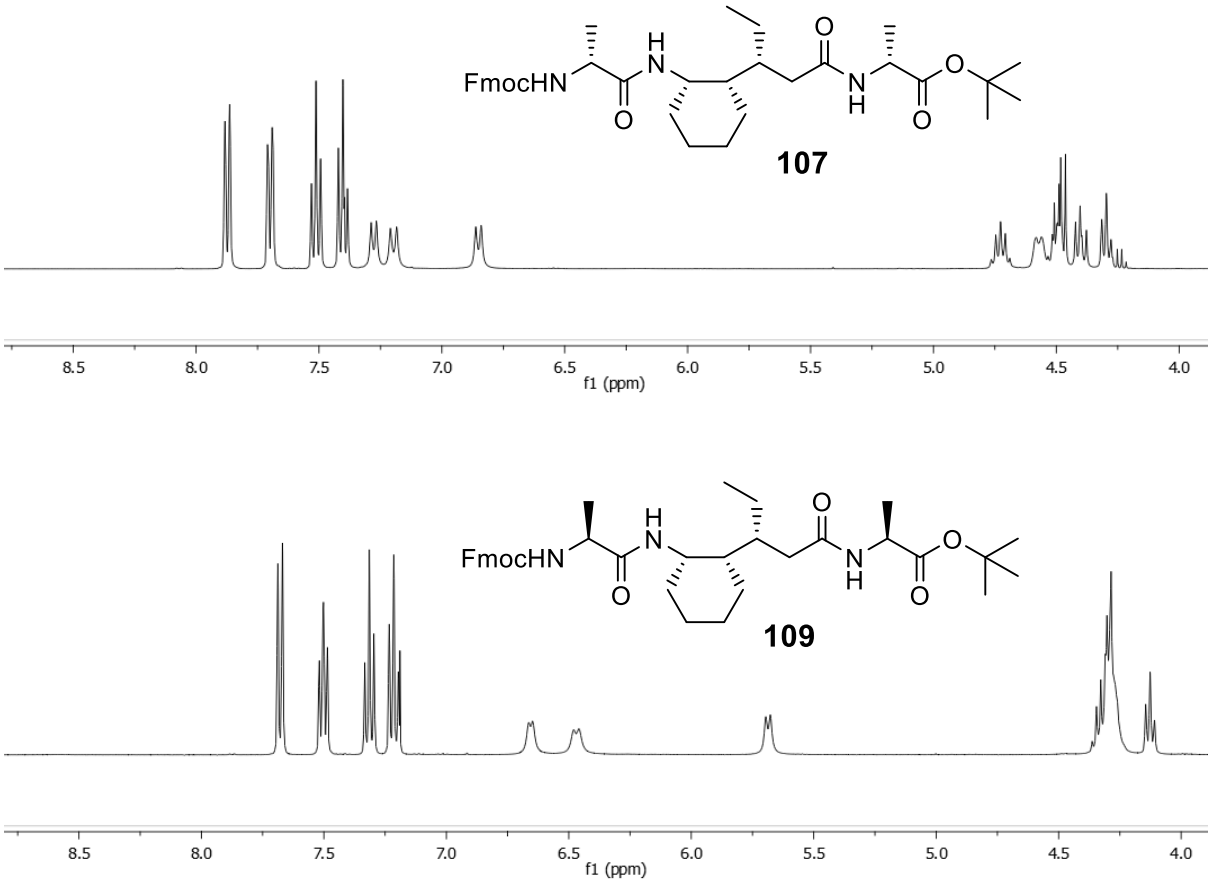

Figure 2.7: The ^{1}H NMR spectrum for trimers **107** and **109**, showing differences in chemical shift for the three respective amide protons.

As a consequence of the difficulties in producing the fully protected dipeptide and the resultant decision to synthesis the trimer instead, it no longer became feasible to produce the final target octamer product, and thus the pentamer and heptamer were targeted instead (Scheme 2.24). Firstly, the C-terminus of the trimer **107** was deprotected by the addition of TFA, resulting in the free acid **110** in a quantitative yield. This was then coupled with the free amine **106** to give the pentamer **111** in a yield of 37%. The process was then repeated, with **111** deprotected in a quantitative yield and the resultant free acid coupled with **106**, resulting in the heptamer **112** in a 32% yield. For both the pentamer and the heptamer, only negligible amounts of the epimer were detected, easily separable from the desired product.

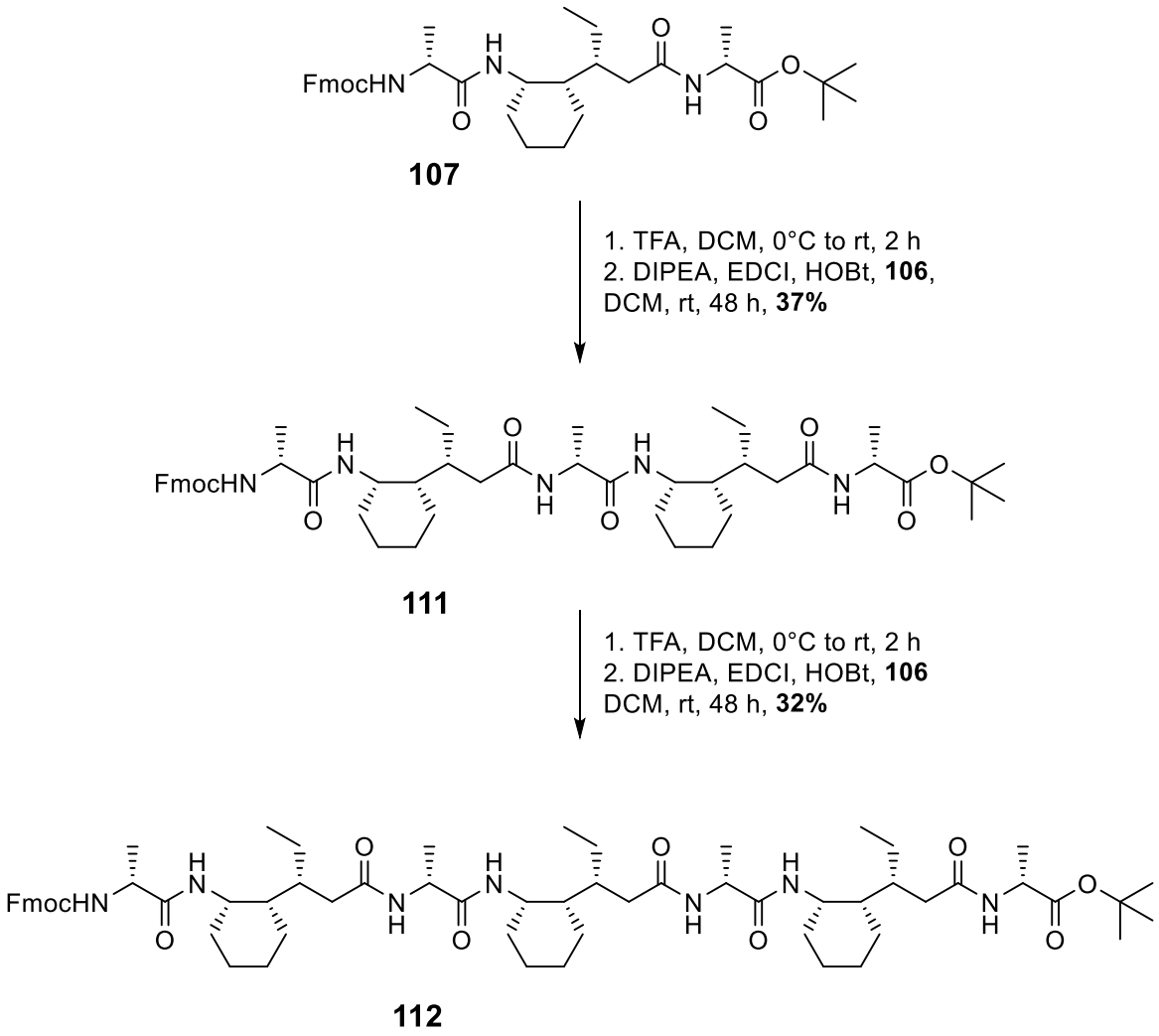

Scheme 2.24: The synthesis of the pentamer **111** and the heptamer **112.**

In addition to α/δ peptides with a 1:1 alternating sequence, the synthesis of a peptide with an alternative sequence was pursued. This was achieved by the coupling of the trimer **107** with itself, resulting in a hexamer with a αδα sequence (Scheme 2.25).

The free amine **113** was produced by the addition of piperidine to **107**, achieving a yield of 90%. This was then coupled with the free acid **110** to give the hexamer **114** in a yield of 20%.

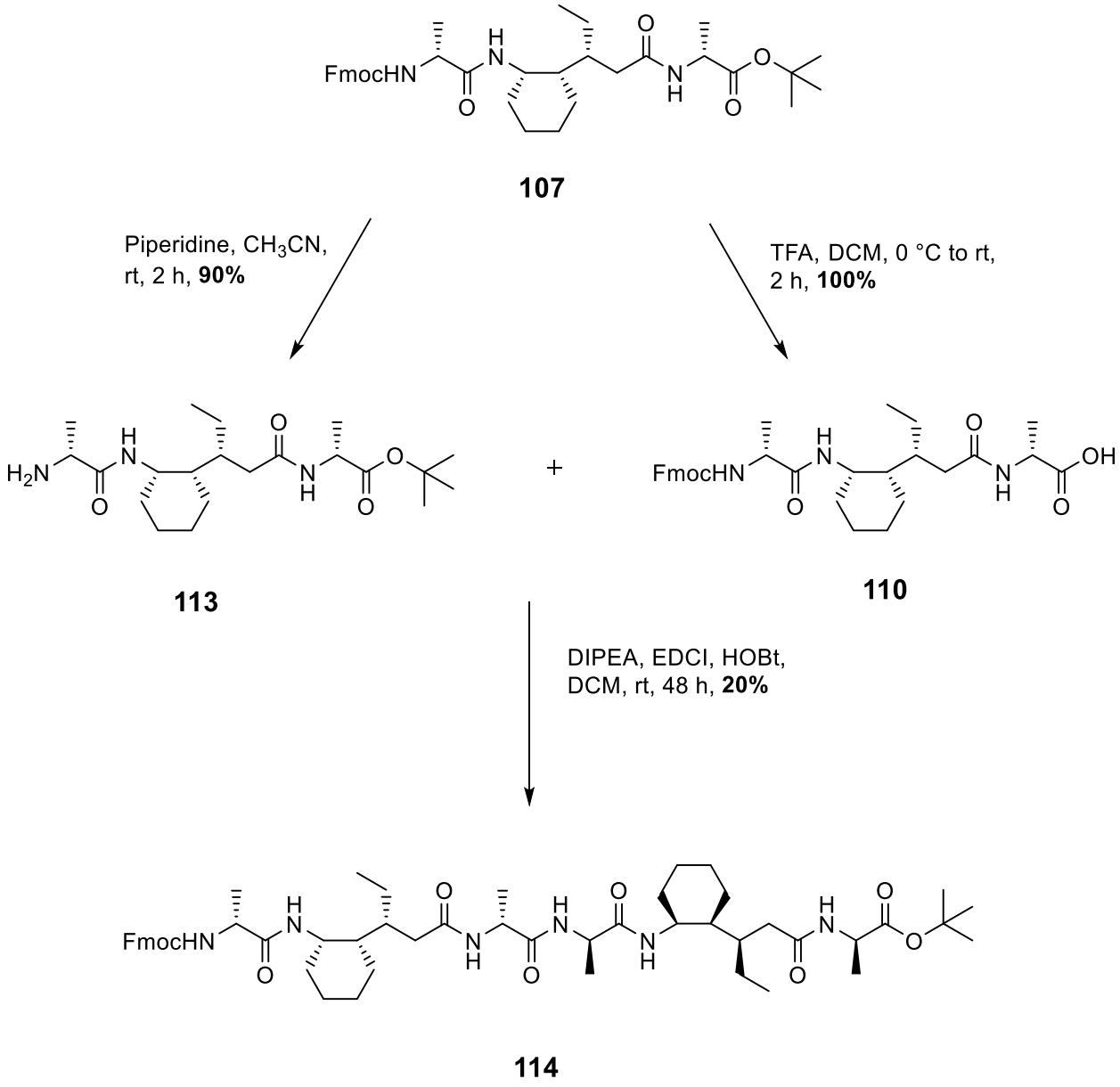

Scheme 2.25: The synthesis of the hexamer **114**.

2.4. Conclusion

In this chapter, the synthesis of the cyclically-constrained *trans* δ-amino acid precursor **60** was achieved in a 4% yield over 9 steps. The final diastereomeric ratio was 16:1, achieved by the help of a crucial base-promoted epimerisation step in order to generate the desired thermodynamically favoured *trans* system.

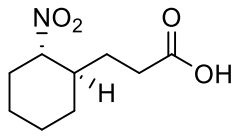

60

Figure 2.8: The *trans* δ-amino acid precursor **60**.

The cyclically-constrained *cis* δ-amino acid **97** (ACPA) was also successfully synthesised in a 29% overall yield in 5 steps. However, due to unsuccessful Fmoc protection attempts, the nitro acid **95** was utilised instead for peptide synthesis. The use of both D- and L-alanine α-residues was examined, with the trimer containing D-alanine monomers **107** displaying a greater propensity for secondary structure formation.

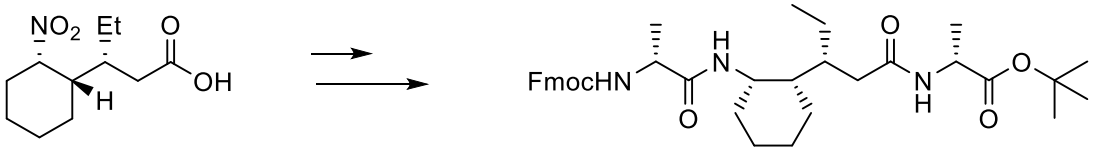

95 **107**

Scheme 2.26: The *cis* δ-amino acid precursor **95** and the resultant trimer **107**.

Finally, a range of final foldamer targets were synthesised including the pentamer **111** and heptamer **112** with a 1:1 α/δ alternating sequence, and the hexamer **114** with an αδα sequence.

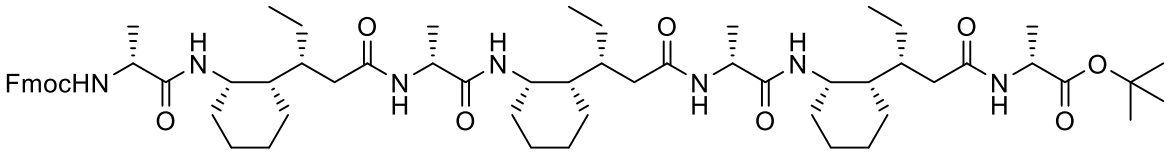

112

Figure 2.9: The α/δ heptamer **112**.

2.5. Future work

Having synthesised a small range of α/δ foldamers containing cyclically-constrained residues, any future studies might look to create more diverse and sophisticated structures. This could be achieved by increasing the number of unique residues or introducing additional elements such as ionisable side chains and studying the effect they might have on secondary structure formation and other physical properties. A quick and obvious way to achieve the former would be to synthesis peptides containing both the *cis* and *trans* δ-systems developed in this chapter, creating a peptide such as **115**, shown in Figure 2.10.

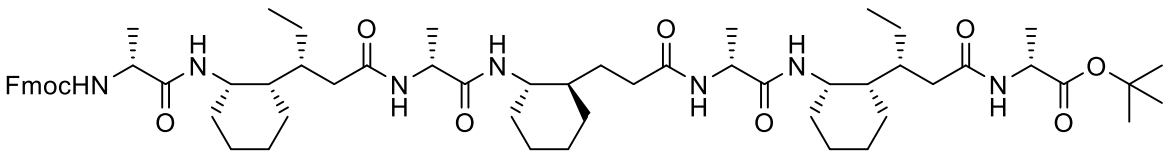

115

Figure 2.10: An α/δ peptide containing both *cis* and *trans* residues.

To achieve the latter, alternative α-residues could be used in place of alanine, such as lysine or aspartic acid, likely to enhance a foldamers solubility in aqueous solution (Figure 2.11).

Both of these were previously used in good effect by Gellman to generate a water-soluble α/β/γ foldamer.[97]

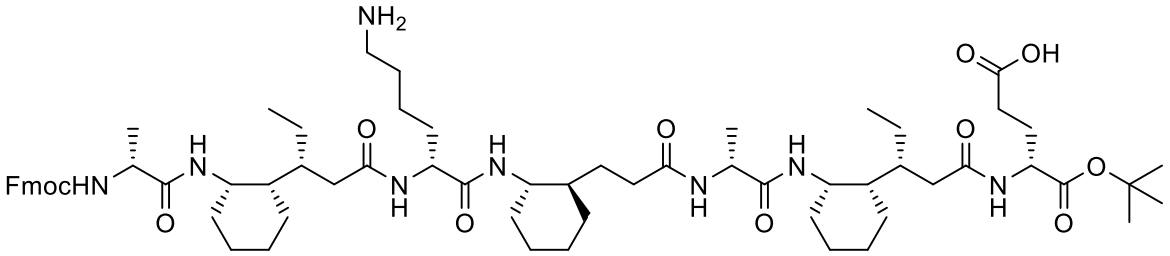

116

Figure 2.11: An α/δ peptide containing lysine and aspartic acid α-residues.

The introduction of ionisable groups can also be facilitated by the modification of the δ-residues themselves, making use of a different starting material for the initial organocatalytic reactions. An obvious way to do this would be to synthesis the nitrogen-embedded *trans* amino acid precursor **119** and incorporate it into a foldamer (Scheme 2.27).

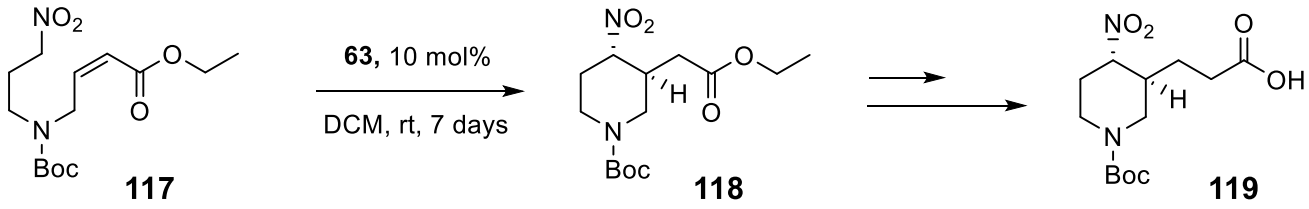

117 **118** **119**

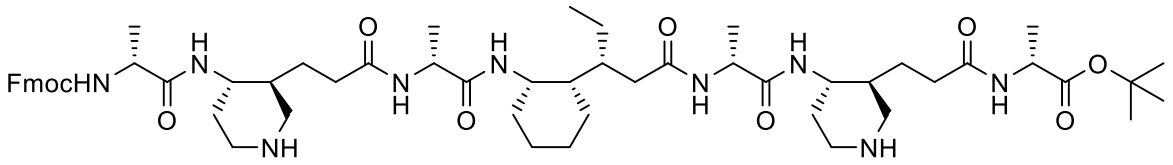

120

Scheme 2.27: The proposed nitrogen-embedded *trans* δ-amino acid precursor **119** , and it's incorporation into foldamer **120**.

Chapter 3 – The structural characterisation of novel α/δ-foldamers

3.1. Background

There are several methods available for probing the secondary structure of a given peptidomimetic foldamer. A multitude of NMR techniques are commonly used, including both 1D and 2D methods. A simple analysis of the amide chemical shifts in the ^{1}H NMR will provide the first tentative piece of evidence for their involvement in hydrogen bonding.[72] DMSO titration and aggregation studies can also be performed via ^{1}H NMR in order to explore the extent of hydrogen bonding and to rule out intermolecular hydrogen bonding, respectively.[74, 98] 2D NMR techniques such as HSQC, TOCSY and HMBC will often be required in order to sufficiently assign the proton and carbon environments of a foldamer, whereas NOESY and/or ROESY experiments will be important for characterising the through-space NOE signals between atoms coupling together within the molecule.[52, 73]

Circular Dichroism (CD) is another commonly used spectroscopic technique in order to investigate the secondary structure of both proteins and foldamers, with a particular propensity for characterising helical structures.[48] Other techniques that have been used include x-ray crystallography (3D arrangement of atoms in the solid state), Infrared (aggregation and hydrogen bonding) and UV-vis/fluorescence spectroscopy (chromophore interactions).[7]

3.2. Aims and Objectives

The aim of this chapter was to provide evidence for and characterise the secondary structure of peptides **107**, **109**, **111**, **112**, and **114**. 1D and 2D NMR spectra and circular dichroism for all five are analysed and discussed, with close attention paid to the differences between trimers **107** and **109**. For the 1:1 hybrid α/δ-peptides, evidence for the formation of a 13/11 (or 11/13) helix was sought where possible, as predicted and subsequently demonstrated by Hofmann and co-workers for their previously described 1:1 hybrid α/δ-peptides.[73]

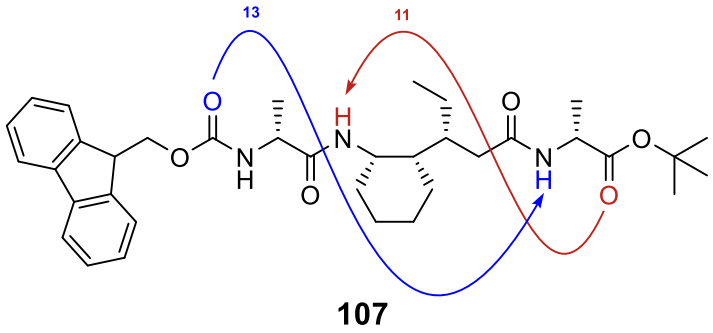

107

Figure 3.1: The characteristic 13/11 hydrogen bonding pattern in trimer **107**. 13-membered rings are shown in blue, with 11-membered rings in red.

3.3. Results and Discussion

3.3.1. Trimers 107 and 109

3.3.1.1. NMR Characterisation

As mentioned in the previous chapter, the ^{1}H NMR spectra of **107** provided evidence for the presence of secondary structure, as two of the three amide protons were shown to have a chemical shift above 7 ppm (Figure 3.2). With the help of ^{13}C and 2D NMR spectra (TOCSY, HSQC and HMBC), the structure was fully assigned, with the key assignments listed in table **3.1** below. The amide proton of residue D-Ala (1) was first identified via a HMBC cross peak with the Fmoc methylene, which then allowed for the identification of the α and β protons in

the D-Ala (1) residue by TOCSY cross peaks. These protons communicate with the carbonyl carbon of the D-Ala (1) residue via HMBC cross peaks, which in turn will selectively communicate with the ACPA (3) amide proton and not the D-Ala (3) amide proton, allowing for all to be distinguished and identified. The rest of the assignments can be assigned by a combination of TOCSY and HMBC correlations.

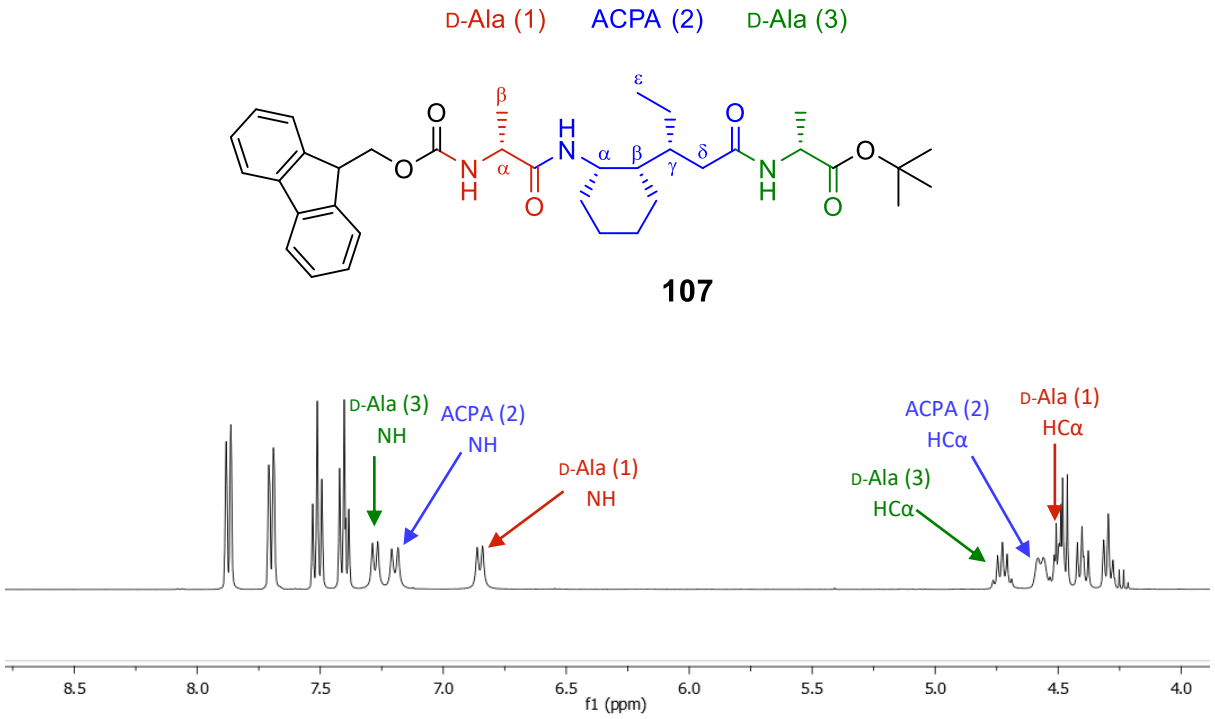

Figure 3.2: The structure and ^{1}H NMR spectra for trimer **107**, showing the peaks for the key assignments (400 MHz).

Residue	NH [ppm]	Hα [ppm]	Hβ [ppm]	Hγ [ppm]	Hδ1 [ppm]	Hδ2 [ppm]	Hε [ppm]
D-Ala (1)	6.71	4.36	1.38	-	-	-	-
ACPA (2)	7.06	4.44	1.31	1.45	1.94	2.59	0.71
D-Ala (3)	7.14	4.59	1.38	-	-	-	-

Table 3.1 The chemical shifts for the key assignments of trimer **107** (400 MHz).

The chemical shifts of the three amide protons agrees with the 13/11-helix hydrogen bonding prediction, with the ACPA (2) and D-Ala (3) amide protons being found downfield of 7 ppm, and the Ala (1) being found further upfield. The ACPA (2) amide proton is perhaps engaging in an 11-membered hydrogen bonding ring with the carbonyl oxygen of residue D-Ala (3), with the D-Ala (3) amide proton engaging in a 13-membered hydrogen bonding ring with the Fmoc carbonyl. The D-Ala (2) amide proton would be unable to form a 13-membered ring (or 11-membered ring) with any carbonyl oxygen within the molecule, leaving the proton more shielded and thus further upfield (Figure 3.3).[99]

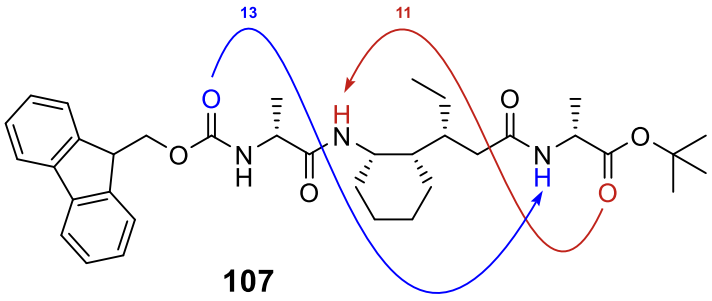

Figure 3.3: The 13/11 hydrogen bonding pattern in trimer **107** that would explain the chemical shifts for the amide protons.

For secondary structure elucidation, ROESY NMR was used for the analysis of NOE signal within all the synthesised peptides, including **107**. Like NOESY, ROESY NMR will show cross peaks between atoms that are spatially close rather than those that are coupled through covalent bonds. ROESY NMR was the selected technique instead of NOESY primarily due its superior suitability for medium-sized molecules (between 600-1200 Da). A larger molecular weight is correlated with an increased rotational correction time, which has a direct influence on the nuclear Overhauser effect. In NOESY, this will result in the NOE tending towards zero for medium-sized molecules, making the signals too weak to detect. For ROESY however, the correlation between the rotational correction time and nuclear Overhauser effect is different, and the NOE signals will stay consistently positive.[100, 101]

To investigate the potential formation of the 13/11-helix, the ROESY cross peaks of the synthesised 1:1 hybrid α/δ-peptides will be compared with those of the previously characterised Hofmann 1:1 α/δ-peptides.[73] The characteristic NOEs for the Hofmann trimer **121** are listed and shown below (Figure 3.4):

I. HCα of residue 1 (i) to NH of residue 3 (i +2)

II. NH of residue 2 (i) to NH of residue 3 (i +1)

III. HCδ of residue 2 (i) to HCα of residue 2 (i)

IV. HCδ of residue 2 (i) to HCβ to residue 2 (i)

V. HCα of residue 2 (i) to NH of residue 3 (i +1)

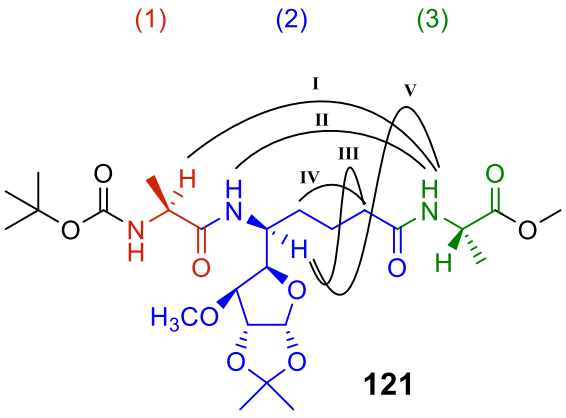

Figure 3.4: The characteristic proton NOE signals for the Hofmann trimer **121**, indicating the presence of a 13/11-helix.

The ROESY NMR spectrum for **107** is shown below (Figure 3.5), with the observed proton cross peaks listed in Table 3.2. The cross peaks that correspond with those found in the Hofmann trimer **121** are highlighted. Spectral overlap was minimal, with only the signals from the Alanine methyl groups HC_{β} (1) and HC_{β} (3) overlapping sufficiently to prevent distinction. Cross peaks between protons within the same residue are omitted, apart from those that correspond with the characteristic Hofmann cross peaks.

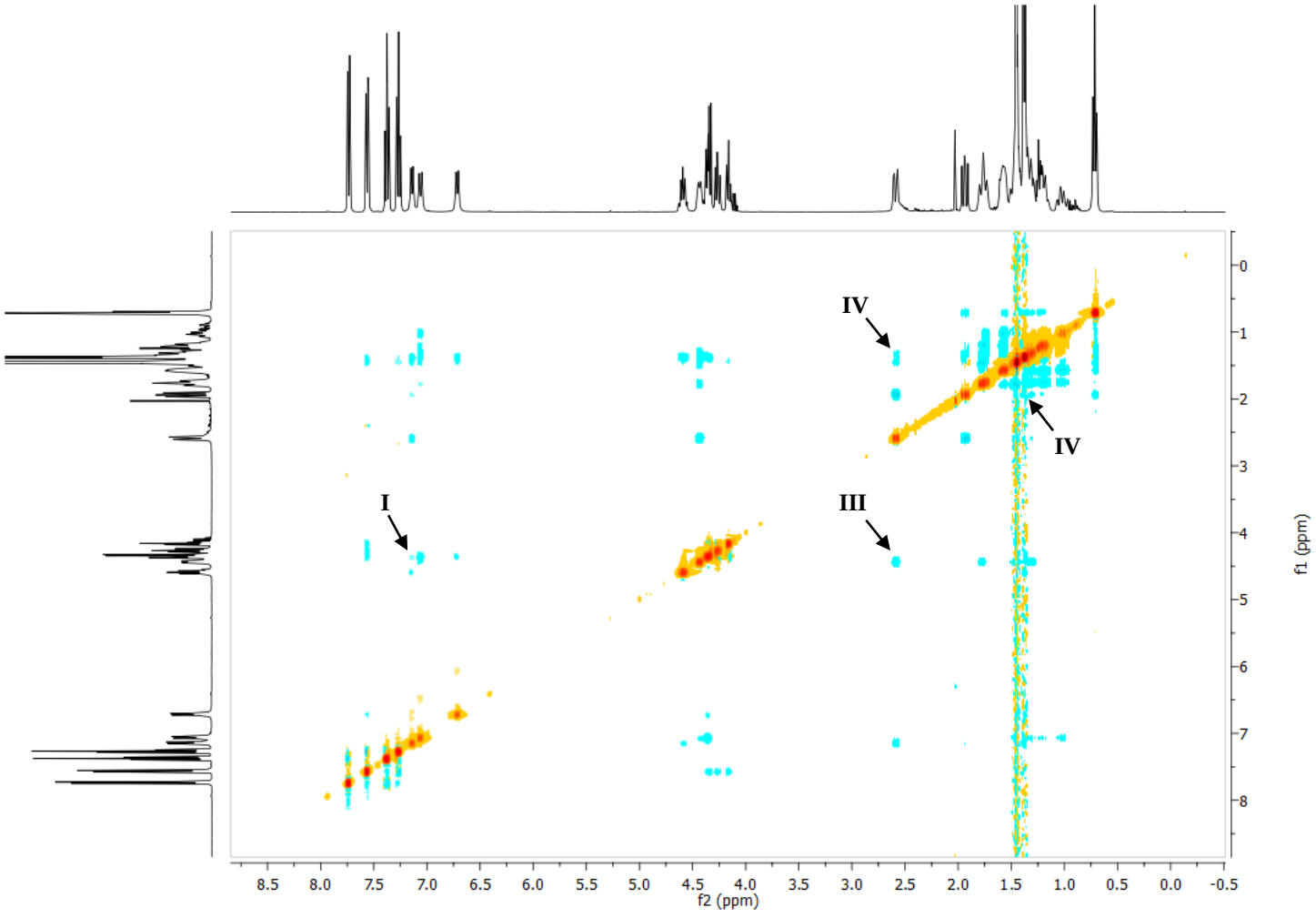

Figure 3.5: The 2D ROESY NMR spectrum for **107**, with the corresponding 13/11 Hoffman cross peaks highlighted. Recorded at rt, in an 8.0 mM solution in $CDCl_3$ (400 MHz).

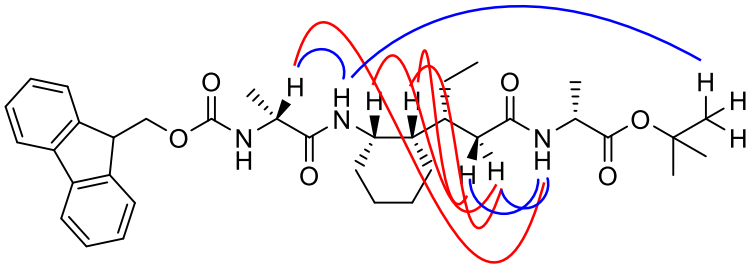

107

NOE Cross Peak	Corresponding 13/11 Hofmann Cross Peak
HCα (1) – NH (2)	-
HCα (1) – NH (3)	**I**
NH (2) – O^{t}Bu	-
HCα (2) – HCδ'' (2)	**III**
HCβ (2) – HCδ' (2)	**IV**
HCβ (2) – HCδ'' (2)	**IV**
HCδ' (2) – NH (3)	-
HCδ'' (2) – NH (3)	-

Table 3.2: Unambiguous NOE cross peaks observed for trimer **107**. Characteristic 13/11-helix cross peaks are shown in red.

Characteristic cross peaks of 13/11-helical structures for 1:1 hybrid α/δ-peptides **I**, **III** and **IV** were observed for **107**, in a total of four interactions. The absence of cross peaks **II** and **V** might be explained by the cyclically-strained nature of the ACPA residue and the associated reduction in conformational freedom when compared to **121**. The carbocycle of ACPA (and to a lesser extent, the ethyl side-chain in the γ-position) will "lock" the molecule in a certain conformation, enhancing the propensity for folding, but perhaps preventing certain atoms becoming spatially close. Nevertheless, the adoption of a 13/11-helix seems to be most likely for trimer **107**.

In contrast to **107**, the ^{1}H NMR spectra for **109** suggested a lesser degree of secondary structure formation, with the chemical shift of all three amide protons being below 7 ppm (Figure 3.6). The full structure was assigned in the same manner as **107,** with the key assignments listed in Table 3.3. Considerable overlap between the α-protons of each residue did not allow for their visual distinction, at least on the ^{1}H NMR spectra.

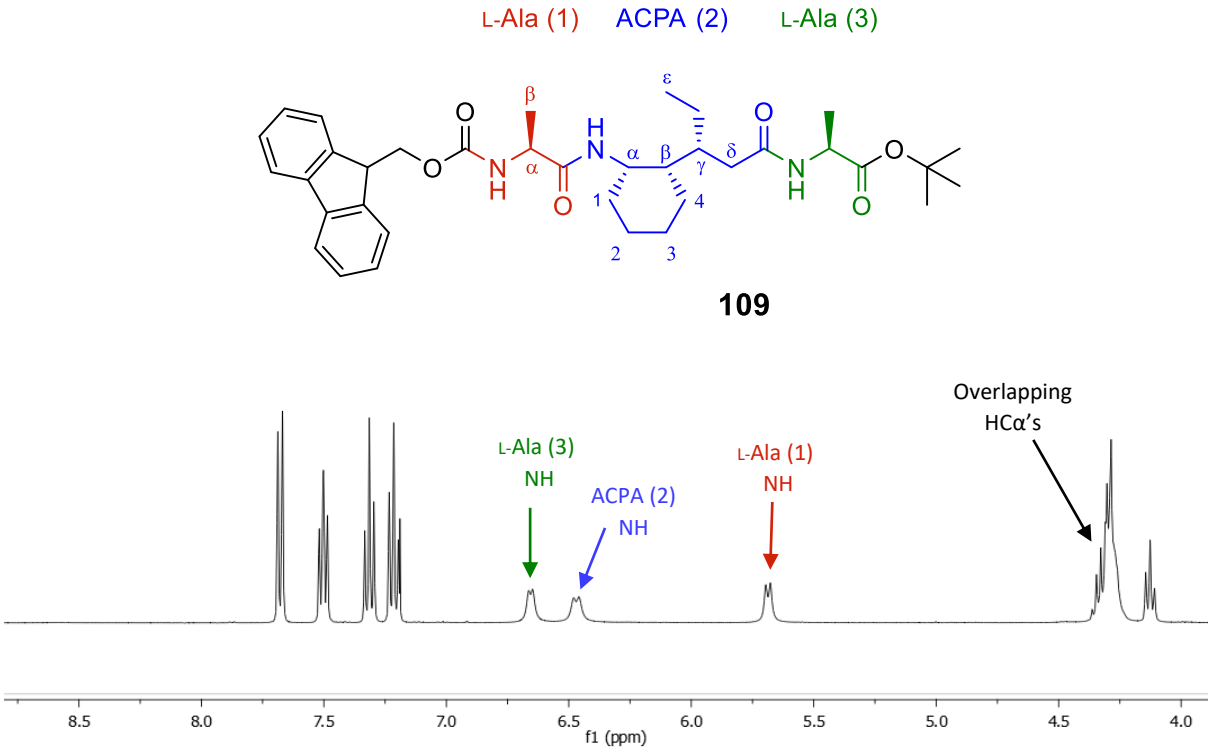

Figure 3.6: The structure and ^{1}H NMR spectra for trimer **109**, showing the peaks for the key assignments (400 MHz).

Residue	NH [ppm]	Hα [ppm]	Hβ [ppm]	Hγ [ppm]	Hδ' [ppm]	Hδ'' [ppm]	Hε [ppm]
L-Ala (1)	5.76	4.39	1.41	-	-	-	-
ACPA (2)	6.54	4.34	1.39	1.49	1.95	2.56	0.80
L-Ala (3)	6.73	4.27	1.30	-	-	-	-

Table 3.3: The ^{1}H NMR spectra and chemical shifts for the key assignments of trimer **109** (400 MHz).

The chemical shifts of the three amide protons for **109** are in the same order as for **107**, with the L-Ala (1) amide proton even further adrift upfield from the other two, again suggesting that it is not taking part in hydrogen bonding to the same degree as the other two.

The ROESY NMR spectrum for **109** is shown below (Figure 3.7), with the observed proton cross peaks listed in Table 3.4 and the characteristic 13/11 Hofmann cross peaks highlighted. Spectral overlap was even better than for **107**, with distinction between all signals, including the two Alanine methyl groups.

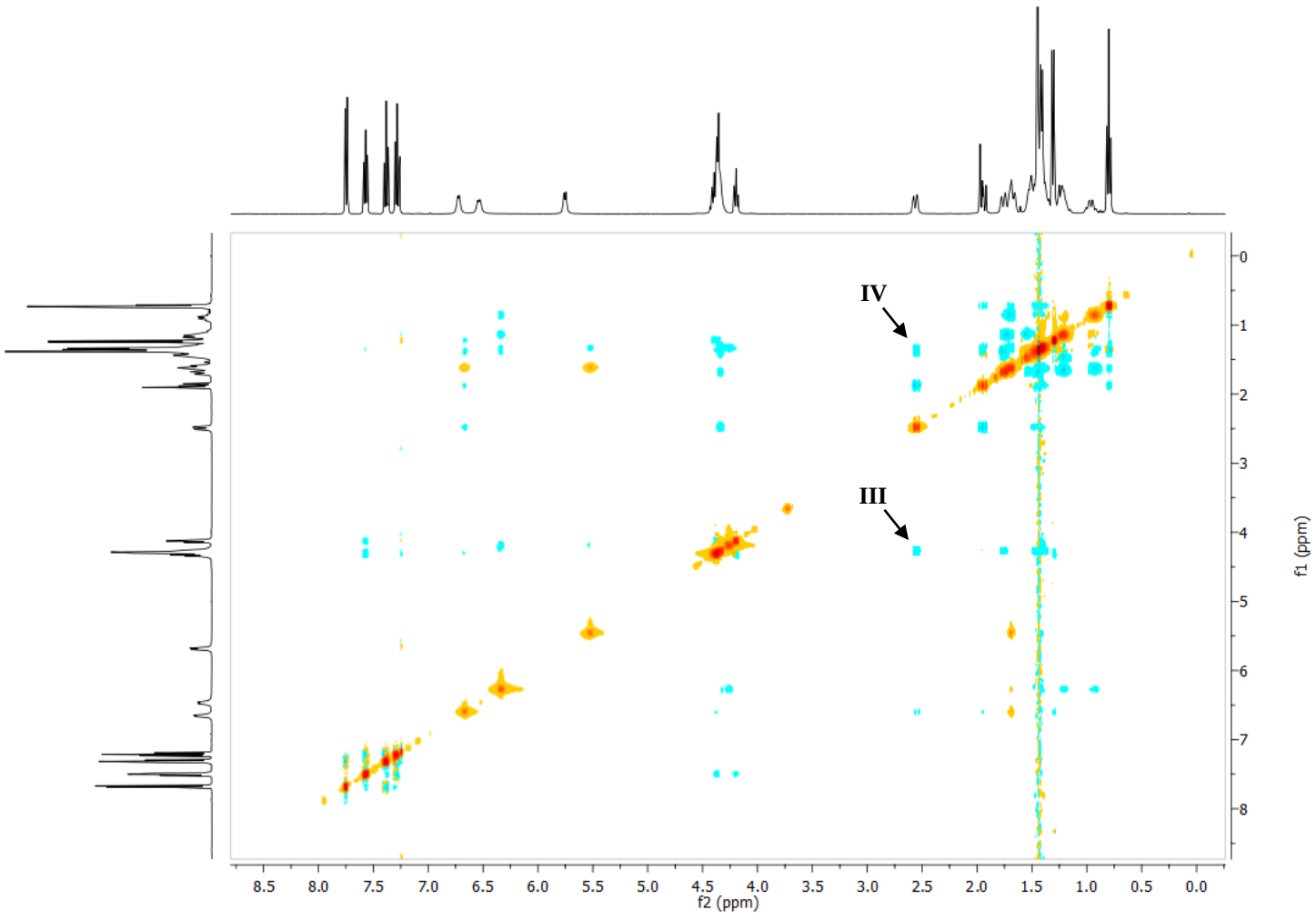

Figure 3.7: The 2D ROESY NMR spectrum for **109,** with the corresponding 13/11 Hoffman cross peaks highlighted. Recorded at rt, in an 8.0 mM solution in $CDCl_3$ (400 MHz).

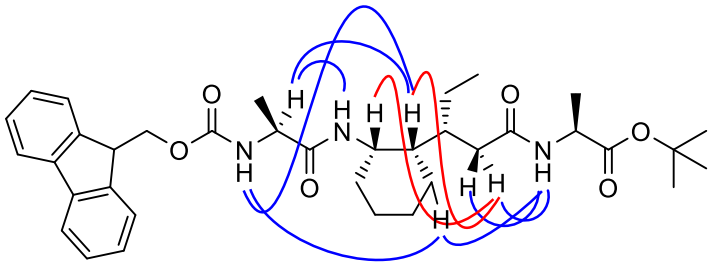

109

NOE Cross Peak	Corresponding 13/11 Hofmann Cross Peak
HCα (1) – NH (2)	-
HCα (1) – HCβ (2)	-
HCα (2) – HCδ'' (2)	**III**
HCβ (2) – HCδ'' (2)	**IV**
HCβ (2) – NH (1)	-
HCδ' (2) – NH (3)	-
HCδ'' (2) – NH (3)	-
HC_4'' (2) – NH (1)	-
HC_4'' (2) – NH (3)	-

Table 3.4: Unambiguous NOE cross peaks observed for trimer **109**. Characteristic 13/11-helix cross peaks are shown in red.

Only two characteristic 13/11-helix cross peaks were observed for **109**, **III** and **IV**, in a total of two interactions. It is worth noting that there are more NOE signals for the interactions *between* residues for **109** than there is for **107**, including the distinct involvement of the Ala (1) amide proton. It seems likely that despite a relatively small difference in structure (the inversion of two stereocentres), **109** is adopting a markedly different conformation than **107**. In fact, the increased number and variety of NOE signals might be due to the structure interconverting between two or more different conformations (perhaps the 13/11-helix and a more random, "unbound" conformation), explaining the apparent reduction in hydrogen bonding observed by the amide protons. This "conformational averaging" could also explain

the high degree of overlap for the HCα protons of each residue, a phenomenon that has been previously described.[98]

3.3.1.2. Circular Dichroism

Circular dichroism is a spectroscopic technique that has been used extensively for the evaluation of secondary structure within proteins and foldamers.[48, 102] It is a technique that measures the difference in absorbance of right- and left-circularly polarized light by a substance. Asymmetric molecules will absorb the two to different extents, leaving the resultant plane of light tellingly rotated when compared to the incident light (referred to as elliptical polarization).[103] The resultant CD spectra will exhibit telltale absorption bands, either positive or negative. The different types of secondary structure will be recognizable by their signature spectra patterns, such as the characteristic negative bands at 208 and 222 nm for α-helices (Figure 3.8).[102]

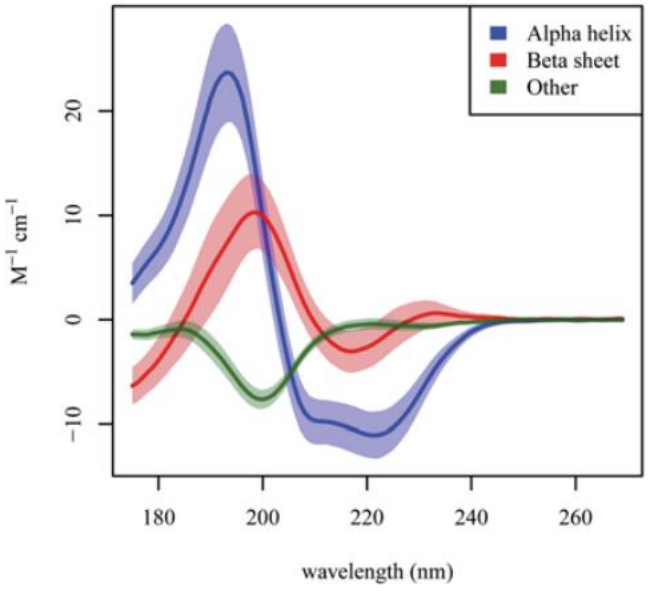

Figure 3.8: The characteristic CD spectra for an alpha helix and a beta sheet.[104]

Unfortunately, due to the lack of examples within literature, foldamers containing δ-amino acids lack a distinct signature CD spectra to compare with. Useful information can still be gained however by observing the *intensity* of the resultant absorption bands, especially when directly comparing two or more foldamer examples.[105] The presence of secondary structure

can also be investigated by taking an additional CD measurement at an elevated temperature and comparing this spectra to the original. If the molecule resides in a single, well-defined conformation, the absorption bands of the CD spectra recorded at the higher temperature would be expected to be less intense, as the structure-defining hydrogen bonds are disrupted, and the population of other conformations becomes more favored.[106]

All CD measurements described in this study were carried out by Fred Martin at the University of Bristol. The CD of trimers **107** and **109** were measured in methanol in a 0.25 mM concentration, at 20°C and 60°C (Figure 3.9). The CD spectra at 20°C for **107** presented a broad, intense negative band at approximately 215 nm. The 60°C CD spectra displayed the same band but with a notable reduction in intensity, indicative of a reduction of the defined secondary structure. Interestingly, the 20°C CD spectra of **109** shows bands at *ca.* 202 and 222 nm, potentially indicating at least a partial population of an α-helix-like conformation. The intensity of both bands is considerably less than the band found for **107**, consistent with the evidence provided so far that suggests a lesser degree of secondary structure formation for **109**. This hypothesis is strengthened further when looking at the 60°C CD spectra for **109**, which shows little to no change in intensity for the absorption bands. Since **109** is already found to populate more than one conformation, a rise in temperature would not have the same effect on the extent of secondary structure as it would for a molecule that exists in a single, well-defined conformation.

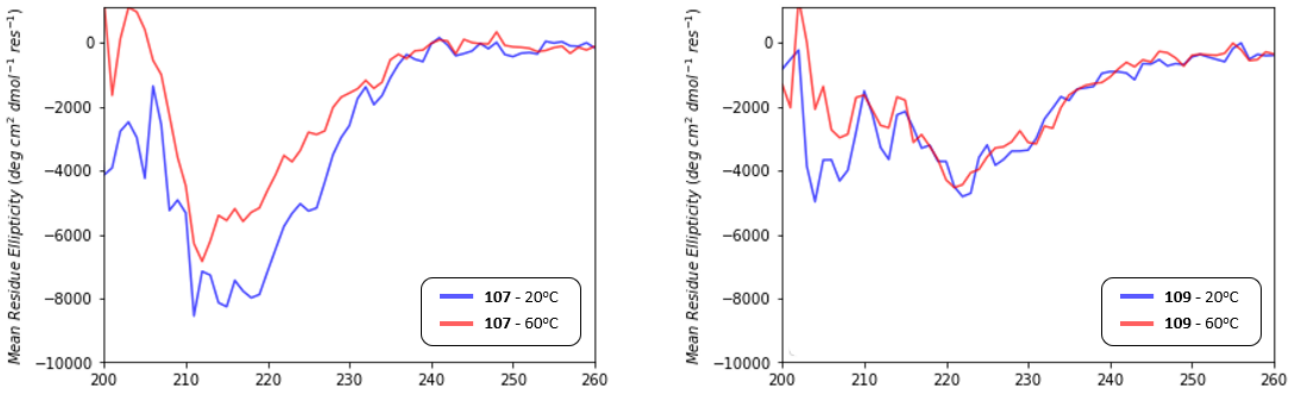

Figure 3.9: The CD spectra at 20°C and 60°C for **107** (left) and **109** (right). Recorded at rt in MeOH, in a 0.25 mM solution.

3.3.2. Pentamer 111

3.3.2.1. NMR Characterisation

All five amide protons for pentamer **111** are shown to have a chemical shift above 7 ppm, indicative of secondary structure formation (Figure 3.10). Unfortunately, due to the extensive overlap of key protons within the two ACPA residues and two of the three D-Ala residues, combined with the apparent lack of a HMBC cross peak between the Fmoc methylene carbon and the amide proton of the D-Ala (1) residue (and an ambiguous HMBC cross peak between the Fmoc methylene carbon and the HCα proton of Ala (1)), the structure could not be fully assigned, and the different residues could not be distinguished. It was possible however to designate the amide and HCα protons as belonging to either an D-Ala or an ACPA residue, by virtue of the TOCSY cross peaks between the D-Ala HCα protons and the HCβ protons of the Alanine methyl groups, and the cross peaks between those identified HCα protons and the relevant amine peaks.

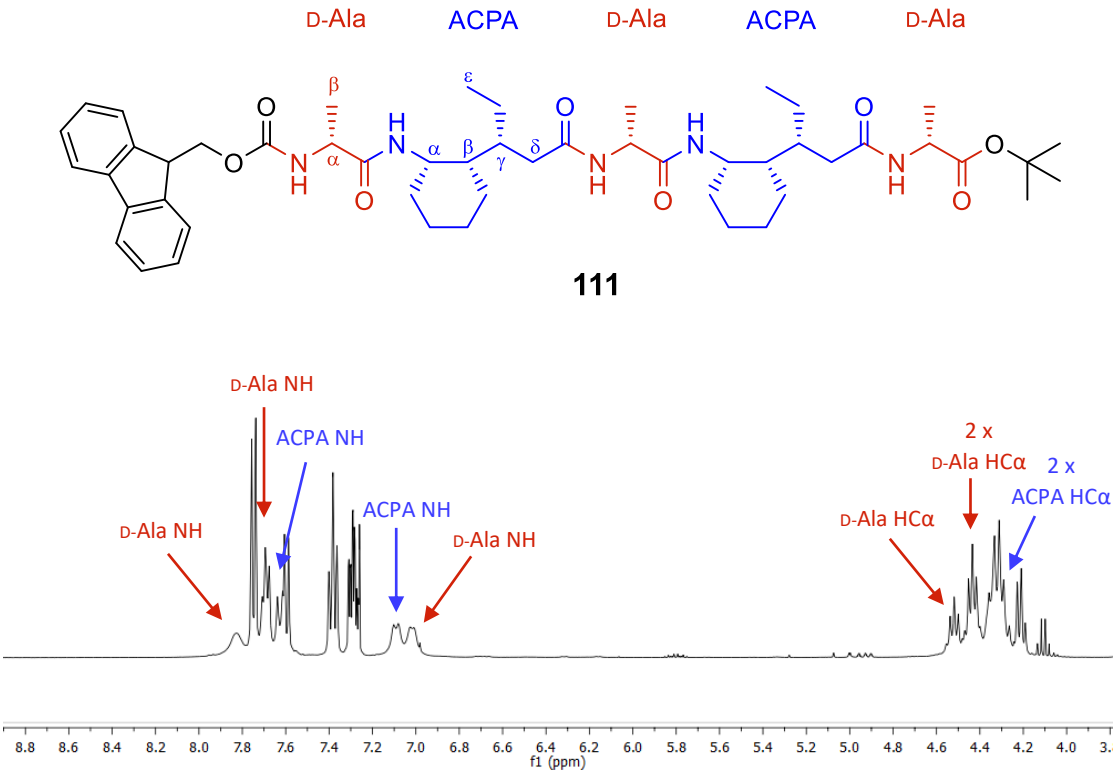

Figure 3.10: The ^{1}H NMR spectra of **111**, showing the chemical shifts of amide and HCα protons within either Ala or ACPA residues (400 MHz).

The amide protons of **111** exist in two distinct groups, with two being found at approximately 7.0-7.1 ppm (one from an ACPA residue, the other from an D-Ala residue), with the other three found between 7.6-7.9 ppm. A possible explanation for this would be the adoption of an 11/13 helix (where the amide protons of the α-residues take part in the hydrogen bonding of 11-membered rings, and those of the δ-residues in 13-membered rings), a switch from the 13/11-helix found for the trimer **107**. This would invert the direction of the hydrogen bonds, leaving one ACPA and one Ala amide proton uninvolved in hydrogen bonding (or at least participating to a lesser degree), resulting in their chemical shift being further upfield than the other three. The reason why the switch to an 11/13 helix might happen remains unclear, especially considering that a 13/11-helix for **111** would perhaps be more favourable, engaging four amide protons within its characteristic hydrogen bonding pattern instead of three. With a full NMR assignment of **111** not possible, the proposed 11/13 helix remains speculative and unfortunately cannot be confirmed.

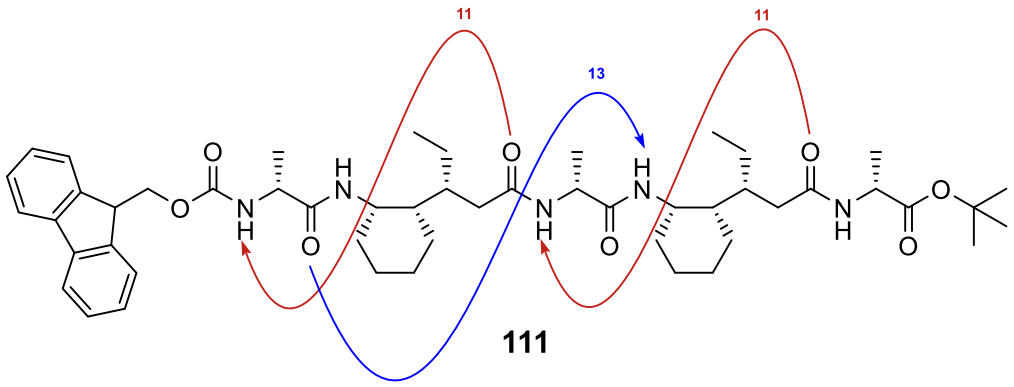

Figure 3.11: The proposed 11/13 helix hydrogen bonding pattern for **111** that would explain the chemical shifts for the amide protons.

Having not been able to conclusively assign the structure of **111**, it is not possible to analysis the ROESY NMR for specific proton cross peaks. An estimation on the presence/degree of secondary structure can be made however by looking at the number and general type of cross peaks present. The ROESY NMR spectra for **111** is shown below (Figure 3.12).

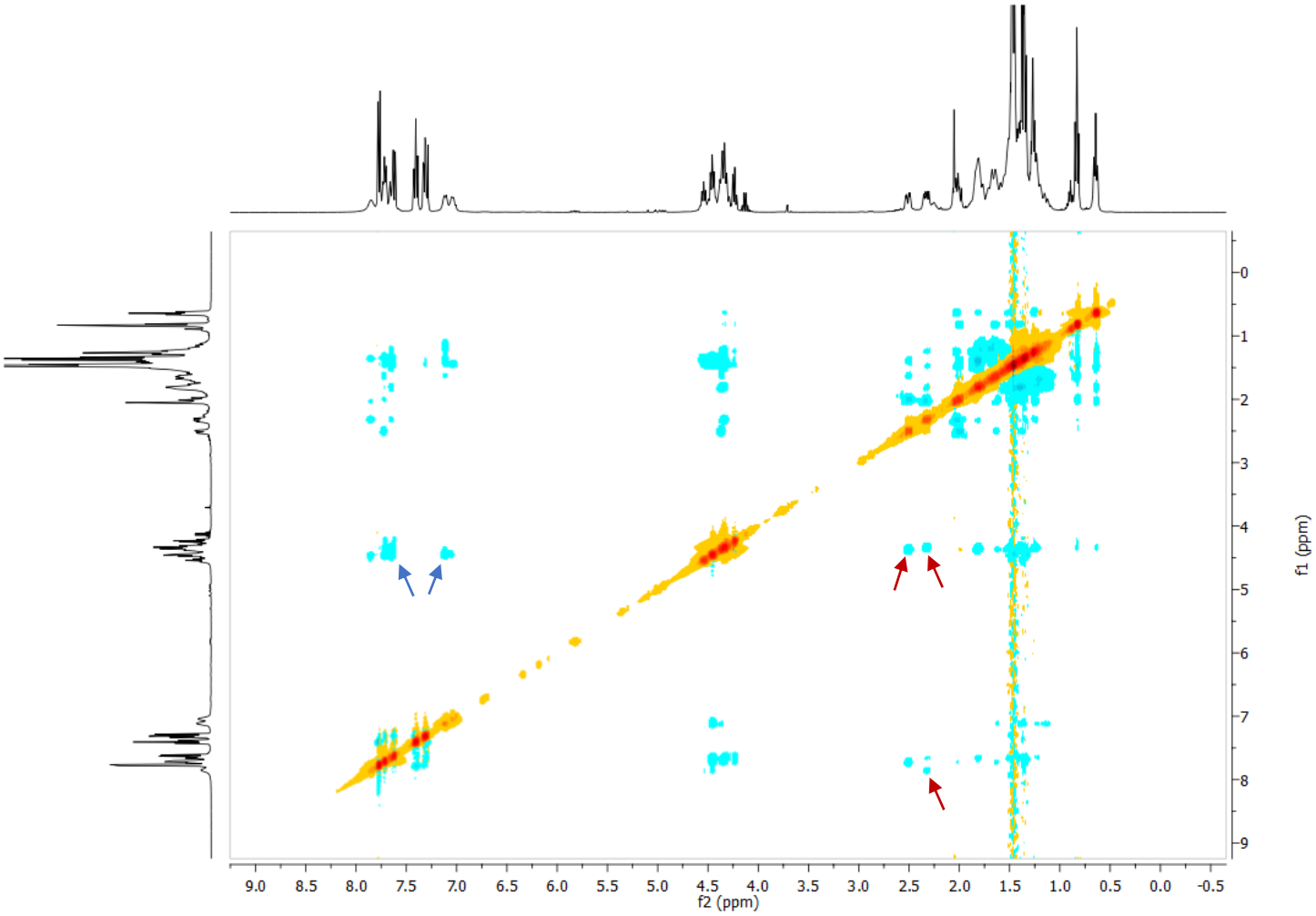

Figure 3.12: The 2D ROESY NMR spectrum for **111**. Recorded at rt, in an 8.0 mM solution in $CDCl_3$ (400 MHz).

A good number of cross peaks was observed, with the spectra indicating plenty of interactions between protons of *different* residues. This includes communication between HCα protons of the D-Ala residues with the amide protons of the ACPA residues (blue arrows), as well as the HCδ protons of the ACPA residues with the HCα and amide protons of the D-Ala residues (red arrows).

3.3.2.2. Aggregation Control Experiment

Aggregation studies can be undertaken to determine whether the downfield chemical shift of the amide protons is due to intermolecular interactions, rather than intramolecular interactions.[98] The ^{1}H NMR of the chosen compound is recorded at a range of different concentrations (1 mM - 16 mM) and the chemical shifts of the amides compared. Any drastic changes in chemical shift would indicate that they are participating in intermolecular hydrogen bonds. The aggregation study for **111** showed minimal changes in chemical shift for the amide protons (Figure 3.13). Only one ACPA amide (denoted with a red arrow) experienced any notable shift (Δδ - 0.12 ppm), which is still much too small to be attributed solely to intermolecular hydrogen bonding.

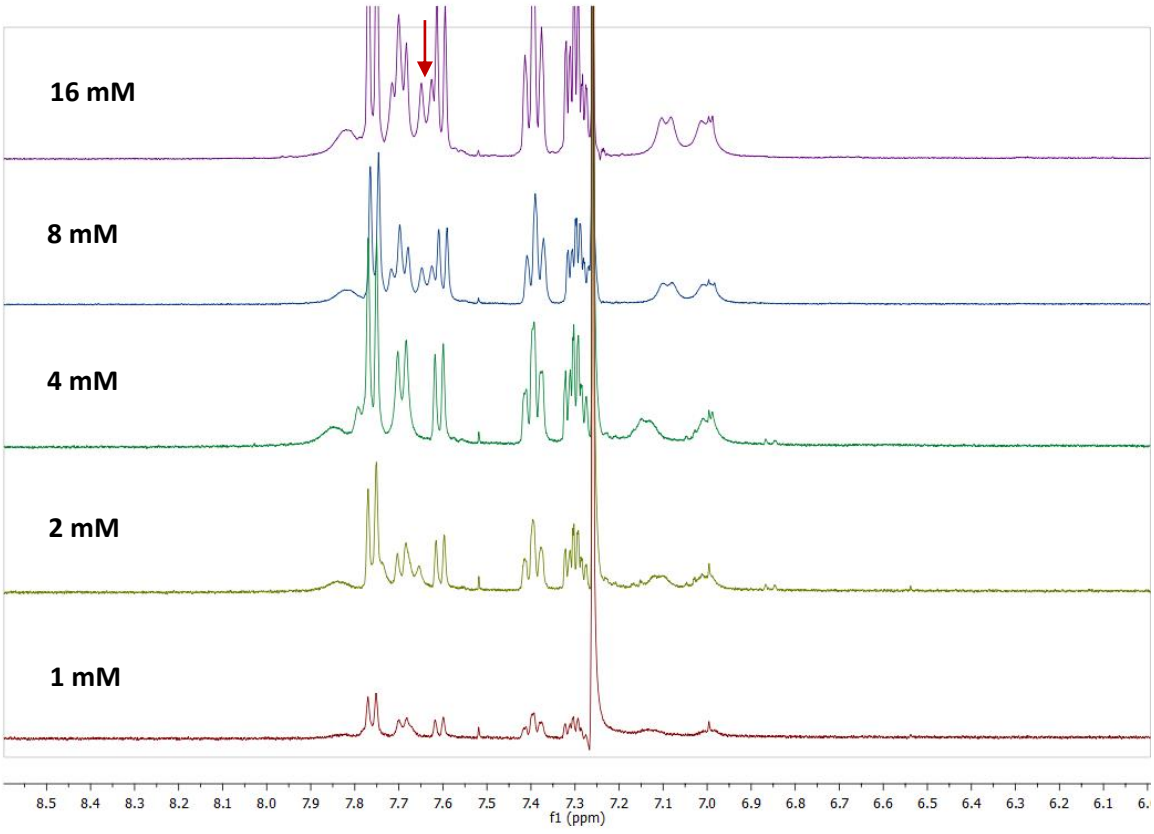

Figure 3.13: The ^{1}H NMR spectra for **111** at concentrations 16, 8, 4, 2 and 1 mM. Recorded at rt in $CDCl_3$ (400 MHz).

3.3.2.3. DMSO Titration Experiment

Similar in principle to the aggregation studies, a DMSO titration experiment investigates the nature of hydrogen bonding for amide protons. It entails the recording of the ^{1}H NMR spectra of a chosen compound with increasing amounts of d_6-DMSO. Because DMSO is a strong hydrogen bond acceptor, it should readily form hydrogen bonds with any "exposed" amide protons in the structure that are not participating in intramolecular hydrogen bonding. This will result in a large downfield shift of its resonance. By contrast, any amide proton that is participating in intramolecular hydrogen bonding will shift to a much lesser degree, sometimes in the upfield direction.[98]

The ^{1}H NMR of a 4 mM solution of pentamer **111** in $CDCl_3$ was first measured (Figure 3.14), followed by a series of spectra with 5, 10, 25, 50 and 100 µL of d_6-DMSO added. The resultant amide proton chemical shifts are shown in Table 3.5.

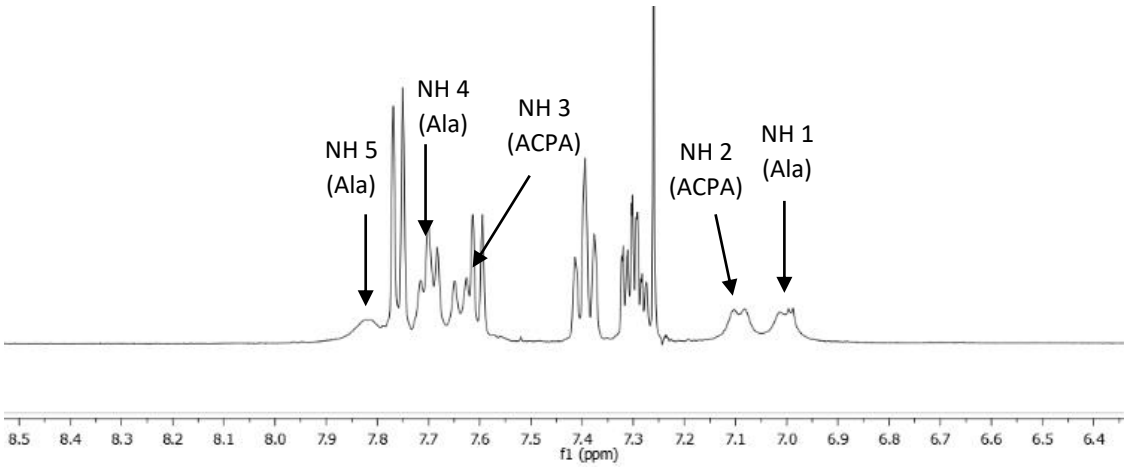

Figure 3.14: The 4 mM d_6-DMSO-free ^{1}H NMR spectra of **111**, showing the numbered amide protons. Recorded at rt in $CDCl_3$ (400 MHz).

Volume of d_6-DMSO added [µL]	NH 1 (D-Ala) [ppm]	NH 2 (ACPA) [ppm]	NH 3 (ACPA) [ppm]	NH 4 (D-Ala) [ppm]	NH 5 (D-Ala) [ppm]
0	7.00	7.09	7.63	7.70	7.82
5	7.00	7.12	7.69	-	7.83
10	6.99	7.12	7.66	-	7.83
25	6.99	7.12	7.65	-	7.83
50	6.99	7.15	7.70	7.80	7.85
100	6.99	7.16	7.70	7.81	7.85
Δ [ppm]	-0.01	+0.07	+0.07	+0.11	+0.03

Table 3.5: The chemical shifts of the amide protons of **111**, with increasing concentrations of d_6-DMSO. Dashed entries indicate resonances that could not be unambiguously assigned due to spectral overlap.

Much like the aggregation control experiment, the chemical shifts of all amide protons showed minimal changes upon addition of d_6-DMSO, further indicating their involvement in intramolecular hydrogen bonding.

3.3.2.4. Circular Dichroism

The CD spectra for **111** at 20°C and 60°C is shown below (Figure 3.15), with the 20°C spectra showing a broad negative band with a minima at approximately 215 nm, very similar to the one found in the corresponding spectra for **107**. The 60°C spectra shows the same negative band, but with a marked reduction in intensity, again similar to **107**. This data suggests that **111** exists in a single, well-defined conformation which is similar to that populated by **107**.

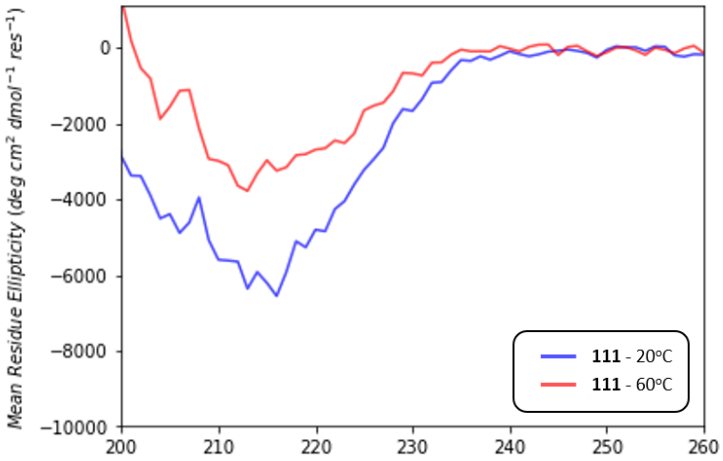

Figure 3.15: The CD spectra at 20°C and 60°C for **111.** Recorded at rt in MeOH, in a 0.25 mM solution.

3.3.3. Heptamer 112

3.3.3.1. NMR Characterisation

Five of the seven amide protons for heptamer **112** display a chemical shift above 7 ppm, with two of those five being found above 8 ppm, suggesting the presence of secondary structure formation (Figure 3.16). Again, much like pentamer **111**, extensive spectral overlap and a lack of the required HMBC cross peaks prevents the full NMR assignment of **112**, and the individual residues were not able to be distinguished. This is despite the use of a 700 MHz NMR Spectrometer, with the increased magnetic field strength failing to provide the required resolution for unambiguous assignments. Nevertheless, it was again possible to determine which *type* of residue that each amide proton belonged to on the ^{1}H NMR spectrum, using the same method as for **111**. The level of signal overlap for the HCα protons on the ^{1}H NMR spectra prevented any meaningful visual distinction.

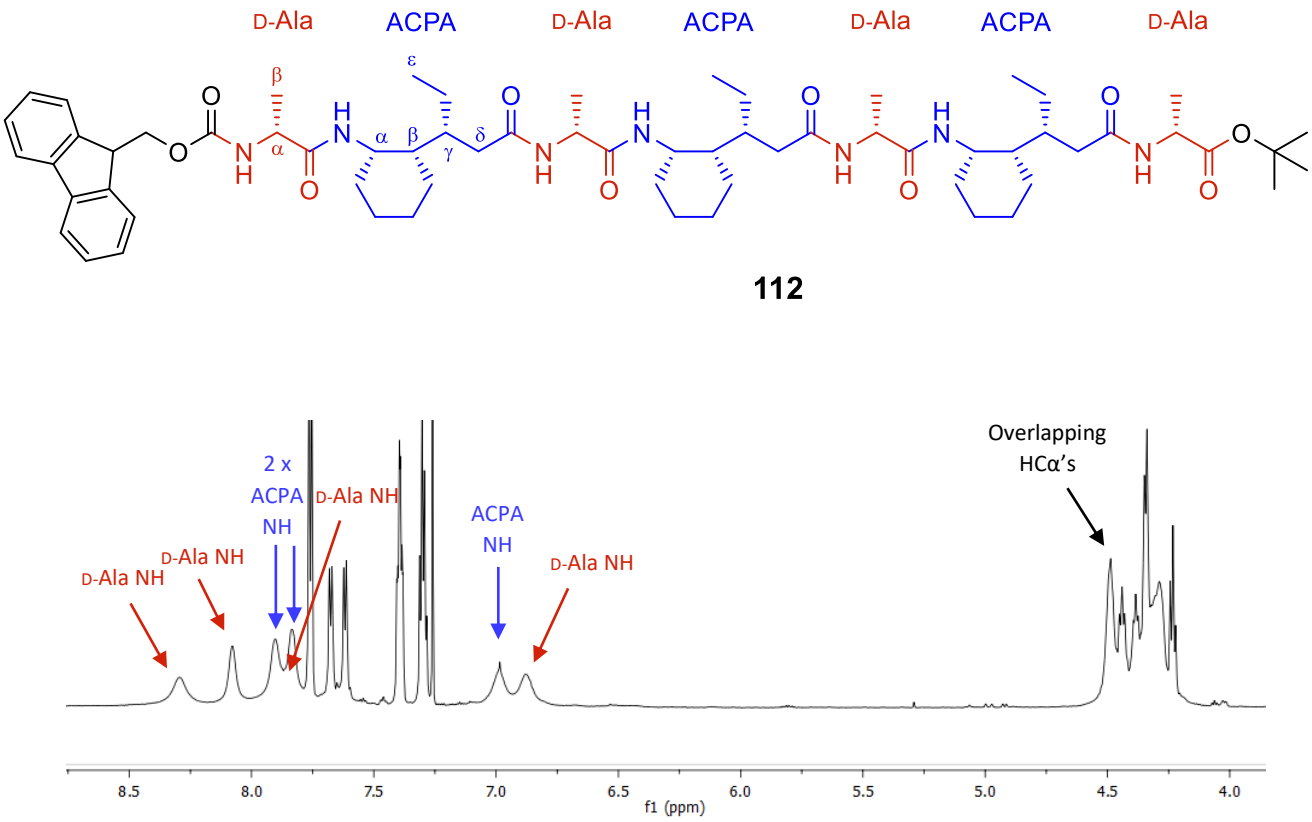

Figure 3.16: The ^{1}H NMR spectra of **112**, showing the chemical shifts of amide protons within either Ala or ACPA residues (700 MHz).

Like pentamer **111**, the amide protons of **112** exist in two distinct groups, with one ACPA and one D-Ala amide proton found close together, further upfield from the rest. This provides tentative evidence that **112** might also be adopting an 11/13 helix (Figure 3.17). Again, without a full NMR assignment, it is not possible to confirm this finding.

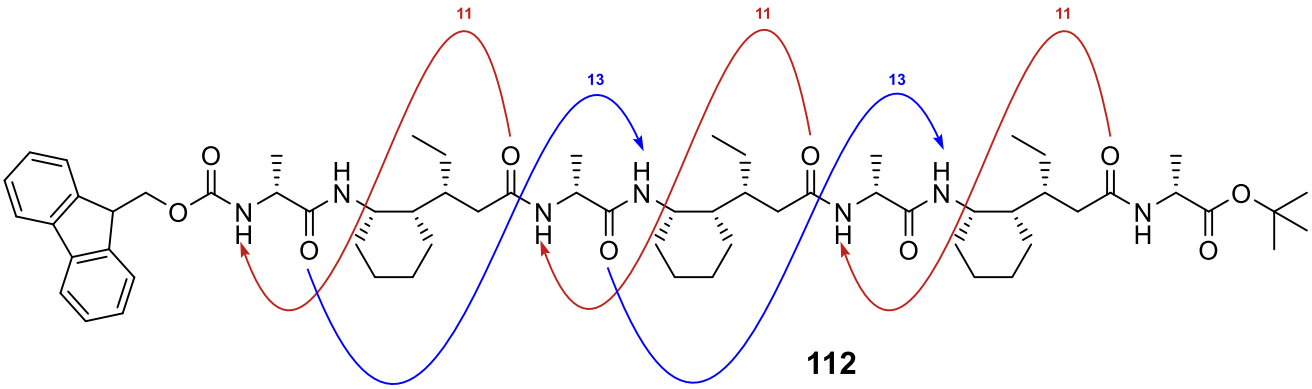

Figure 3.17: The proposed 11/13 helix hydrogen bonding pattern for **112** that would explain the chemical shifts for the amide protons.

The ROESY NMR for heptamer **112** is shown below (Figure 3.18), with attention paid to the number and general type of cross peaks observed, the same as for **111**. Similarly to the ^{1}H NMR, a 700 MHz NMR spectrometer was initially used for the 2D NMR acquisition. However, it provided minimal improvement for spectral overlap, and displayed a much weaker signal-to-noise ratio than the corresponding 400 MHz spectra. Therefore, the 400 MHz spectra for 2D NMR experiments are given for **112**.

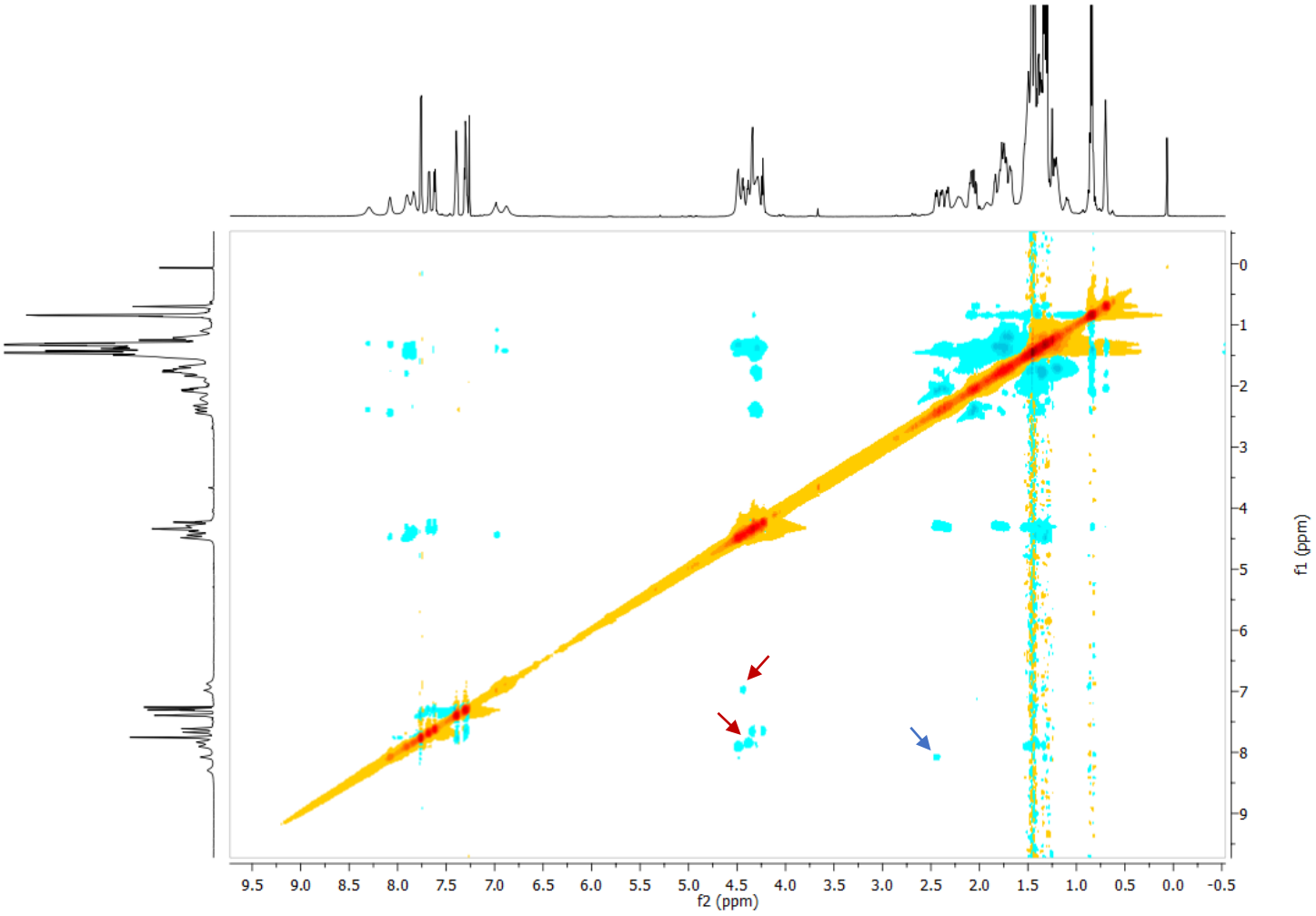

Figure 3.18: The 2D ROESY NMR spectrum for **112**. Recorded at rt, in an 8.0 mM solution in $CDCl_3$ (400 MHz).

Similar to **111,** a good number of cross peaks was observed, with the spectra indicating interactions between protons of different residues. This includes communication between HCα protons of the D-Ala residues with the amide protons of the ACPA residues (red arrows), as well as the HCδ protons of the ACPA residues with the amide protons of the D-Ala residues

(blue arrow). In fact, the ROESY NMR spectrum for **112** shares many of the same interactions as for **111**, suggesting very similar secondary structures.

3.3.3.2. Aggregation Control Experiment

The aggregation study for **112** showed minimal changes in shift for all amide protons, suggesting that they are not involved in intermolecular bonding, and that the foldamer is not aggregating (Figure 3.19). Note that one of the D-Ala amide protons (at approximately 7.85 ppm) is consistently undistinguishable due to spectral overlap but is also assumed to experience minimal changes in chemical shift.

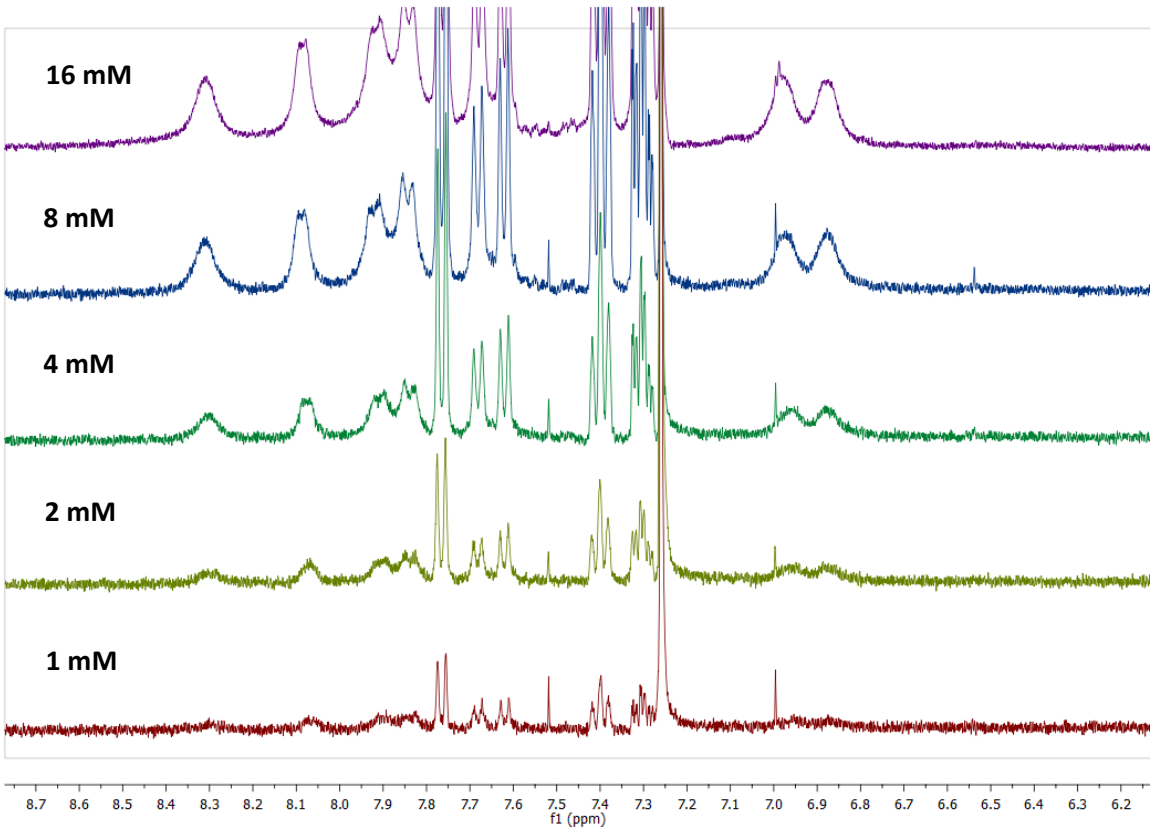

Figure 3.19: The ^{1}H NMR spectra for **112** at concentrations 16, 8, 4, 2 and 1 mM. Recorded at rt in $CDCl_3$ (400 MHz).

3.3.3.3. DMSO Titration Experiment

The ^{1}H NMR of a 4 mM solution of pentamer **112** in $CDCl_3$ was first measured (Figure 3.20), followed by a series of spectra with 5, 10, 25, 50 and 100 µL of d_6-DMSO added. The resultant amide proton chemical shifts are shown in Table **3.6**.

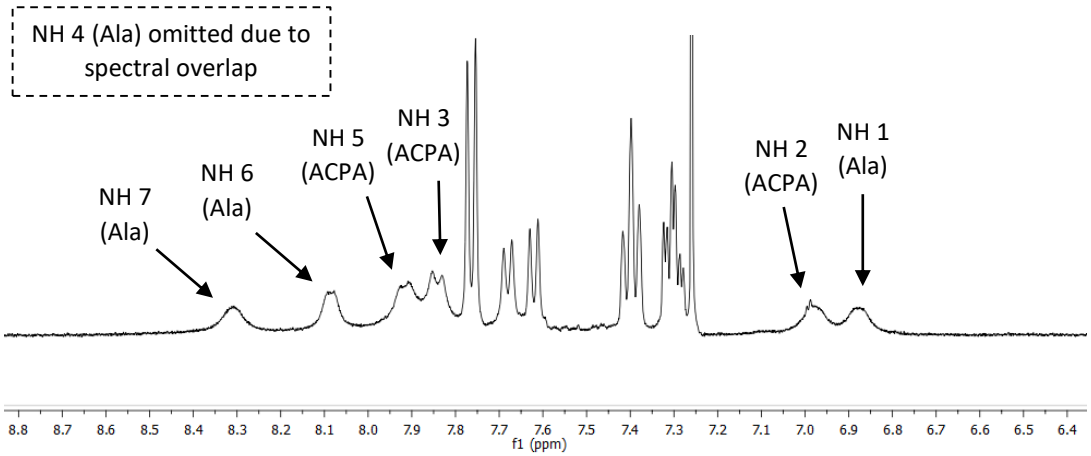

Figure 3.20: The 4 mM d_6-DMSO-free ^{1}H NMR spectra of **112**, showing the numbered amide protons. Recorded at rt in $CDCl_3$ (400 MHz).

Volume of d_6-DMSO added [µL]	NH 1 (D-Ala) [ppm]	NH 2 (ACPA) [ppm]	NH 3 (ACPA) [ppm]	NH 4 (D-Ala) [ppm]	NH 5 (ACPA) [ppm]	NH 6 (D-Ala) [ppm]	NH 7 (D-Ala) [ppm]
0	6.88	6.98	7.84	-	7.92	8.09	8.31
5	6.89	7.04	7.86	-	7.96	8.15	8.34
10	6.89	6.96	7.70	-	7.78	7.91	8.09
25	6.86	6.94	7.60	-	7.70	7.80	7.98
50	6.81	6.90	7.45	-	7.60	7.67	7.82
100	6.80	6.89	7.35	-	7.53	7.55	7.71
Δ [ppm]	-0.08	-0.09	-0.49	-	-0.39	-0.54	-0.60

Table 3.6: The chemical shifts of the amide protons of **112**, with increasing concentrations of d_6-DMSO. Dashed entries indicate resonances that could not be unambiguously assigned due to spectral overlap.

There was some substantial shifting for four of the seven amide protons of **112** upon the addition of d_6-DMSO, but in the upfield direction, suggesting that they are indeed participating in intramolecular hydrogen bonding. The two amide protons found further upfield, NH 1 and NH 2, displayed a much more subtle change in chemical shift (also in the upfield direction), distinguishing them from the others and strengthening the hypothesis that they are at least participating in intramolecular to a lesser degree than the others. Spectral overlap for NH 4 (with either the other amide protons or Fmoc protons) prevented a conclusive identification of its chemical shift for any of the spectra.

3.3.3.4. Circular Dichroism

The CD spectra for **112** at 20°C and 60°C is shown below (Figure 3.21), with the 20°C spectra showing the same broad, negative band as found in the corresponding spectra for **107** and **111**, with a remarkably similar intensity to the one found for **111** in particular. Again, the 60°C spectra shows the same negative band but with diminished intensity, indicative of a loss/reduction of defined secondary structure.

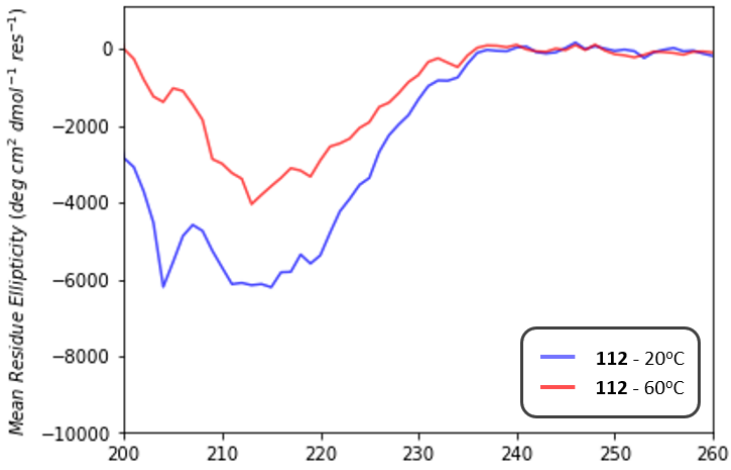

Figure 3.21: The CD spectra at 20°C and 60°C for **112.** Recorded at rt in MeOH, in a 0.25 mM solution.

3.3.4. Hexamer 114

3.3.4.1. NMR Characterisation

Four of the six amide protons for hexamer **114** are found above 7ppm on the ^{1}H NMR spectra, indicating a certain level of secondary structure formation (Figure 3.22). The distribution of these amide protons is notably different than for **111** or **112** however, with more of an even spread instead of two distinct groups, suggesting that participation in hydrogen bonding is more evenly distributed in **114**. Spectral overlap was considerably better than for **111** or **112** (aided by the use of a 700 MHz NMR Spectrometer), with four of the six residues identifiable, at least with regard to the amide and the HCα protons. Only the D-Ala (3) and D-Ala (6) residues were completely indistinguishable from each other, due to the NMR equivalence of their carbonyl carbons in particular (and the equivalence of the ACPA carbonyl carbons preventing the distinction between adjacent the D-Ala (3) and D-Ala (6) amide protons).

The key, unambiguous ^{1}H NMR assignments of **114** are listed in table 3.7, below. The D-Ala (1) amide proton was first identified due to the characteristic *absence* of a HMBC cross peak with any of the residue carbonyl carbons. The HCα and HCβ protons of the D-Ala (1) residue were then identified via TOCSY cross peaks, and the D-Ala (1) carbonyl carbon then identified by the HMBC cross peak with those HCβ protons. The ACPA (2) amide proton was then assigned via a HMBC cross peak with the D-Ala (1) carbonyl carbon, which in turn allowed for the ACPA (5) amide proton to also be identified (as the only other amide proton not interacting with an Alanine methyl group via TOCSY NMR). The adjacent D-Ala (4) residue can then be worked out via a mixture of HMBC and TOCSY interactions. Only the amide and HCα protons of the two ACPA residues could be unambiguously assigned, with the other key protons (and carbons) being too similar in chemical shift to be distinguished.

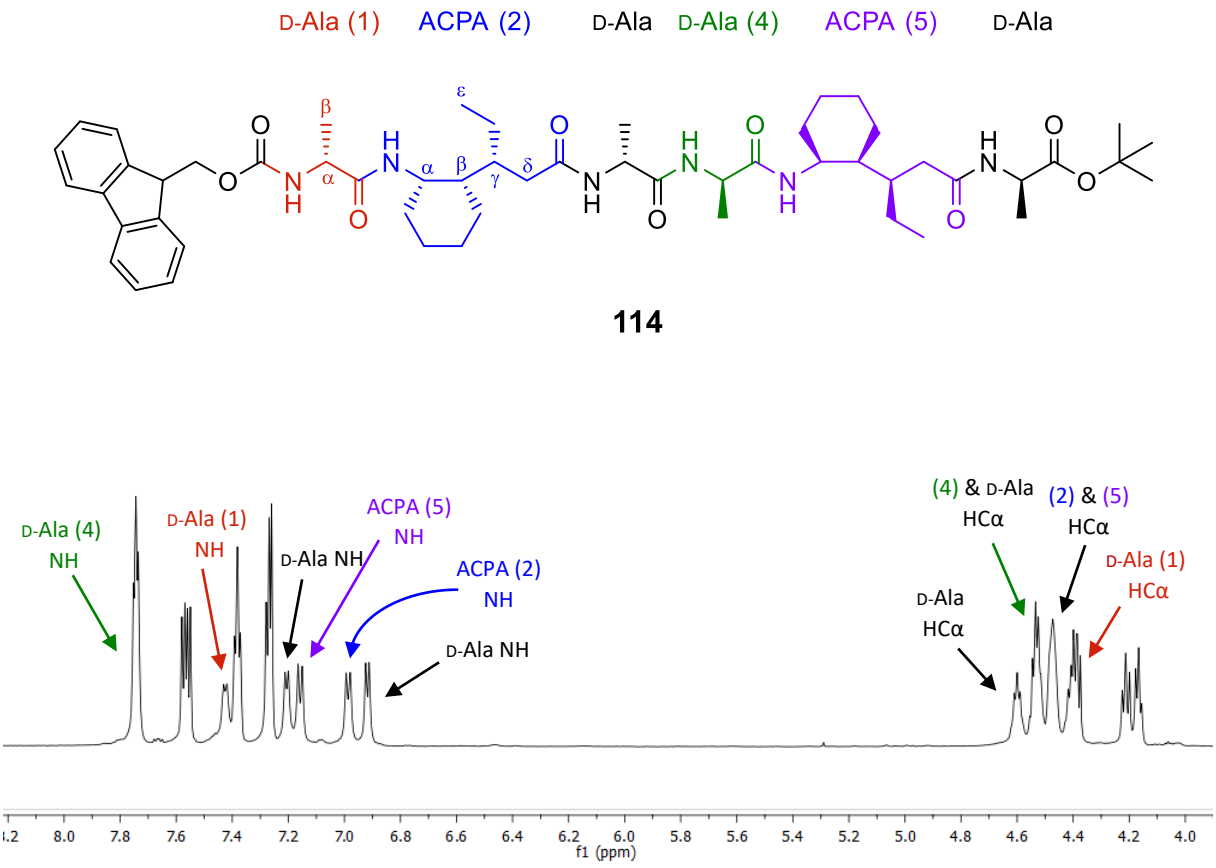

Figure 3.22: The structure and ^{1}H NMR spectra for hexamer **114**, showing the peaks for the key assignments (400 MHz).

Residue	NH [ppm]	Hα [ppm]	Hβ [ppm]	Hγ [ppm]	Hδ1 [ppm]	Hδ2 [ppm]	Hε [ppm]
D-Ala (1)	7.42	4.40	1.45	-	-	-	-
ACPA (2)	6.99	4.47	-	-	-	-	-
D-Ala (4)	7.75	4.53	1.18	-	-	-	-
ACPA (5)	7.16	4.47	-	-	-	-	-

Table 3.7: The ^{1}H NMR spectra and chemical shifts for the key assignments of hexamer **114** (700 MHz).

Without literature examples of α/δ-foldamers with an αδα repeating sequence, in addition to a lack of a fully unambiguous NMR assignment for **114**, it is difficult to predict and confirm a probable secondary structure conformation. However, if we assume that like 1:1 α/δ

foldamers, the amide protons of **114** would also favour the formation either 11- or 13-membered hydrogen bonding rings, we can hypothesis the potential hydrogen bonding interactions (Figure 3.23). The ACPA residues are capable of 11-membered rings only, with the Ala residues capable of either 11- or 13-membered rings. The amide proton of the Ala (4) residue (highlighted in bold) is notable as it is the only one that is capable of forming hydrogen bonding rings of both sizes, perhaps accounting for its chemical shift being the most downfield of all the amide protons. It is important to note however that if **114** does indeed adopt 11- and 13-membered hydrogen bonding rings, these interactions are unlikely to be found in their entirety (in the same way that the 1:1 α/δ-foldamers will adopt *either* a 13/11 or 11/13 helical conformation).

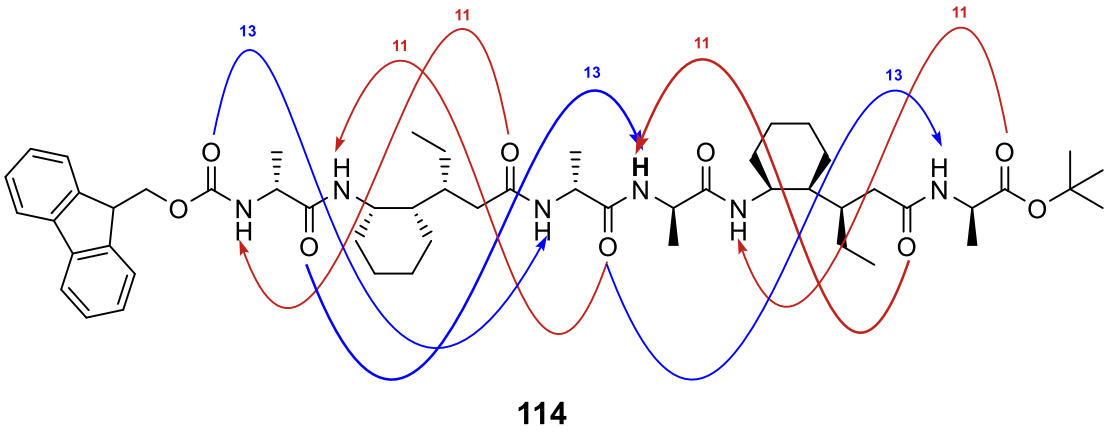

114

Figure 3.23: The possible 11- and 13-membered hydrogen bonding rings for **114.**

The ROESY NMR for hexamer **114** is shown below (Figure 3.24). Despite the improved NMR assignments of **114** when compared to **111** and **112**, the identification of ROESY cross peaks was still challenging, with many of the key proton environments lacking unambiguous assignment, in addition to prohibitive overlap between the HCα protons. Therefore, analysis of the ROESY NMR spectra of **114** was mostly limited to simply observing the number and type of interactions observed.

Again, a 700 MHz NMR spectrometer was used for the acquisition for 2D data but did not provide a sufficient improvement in spectral overlap and presented with a much worse signal-to-noise ratio, so the 400 MHz spectra were used instead.

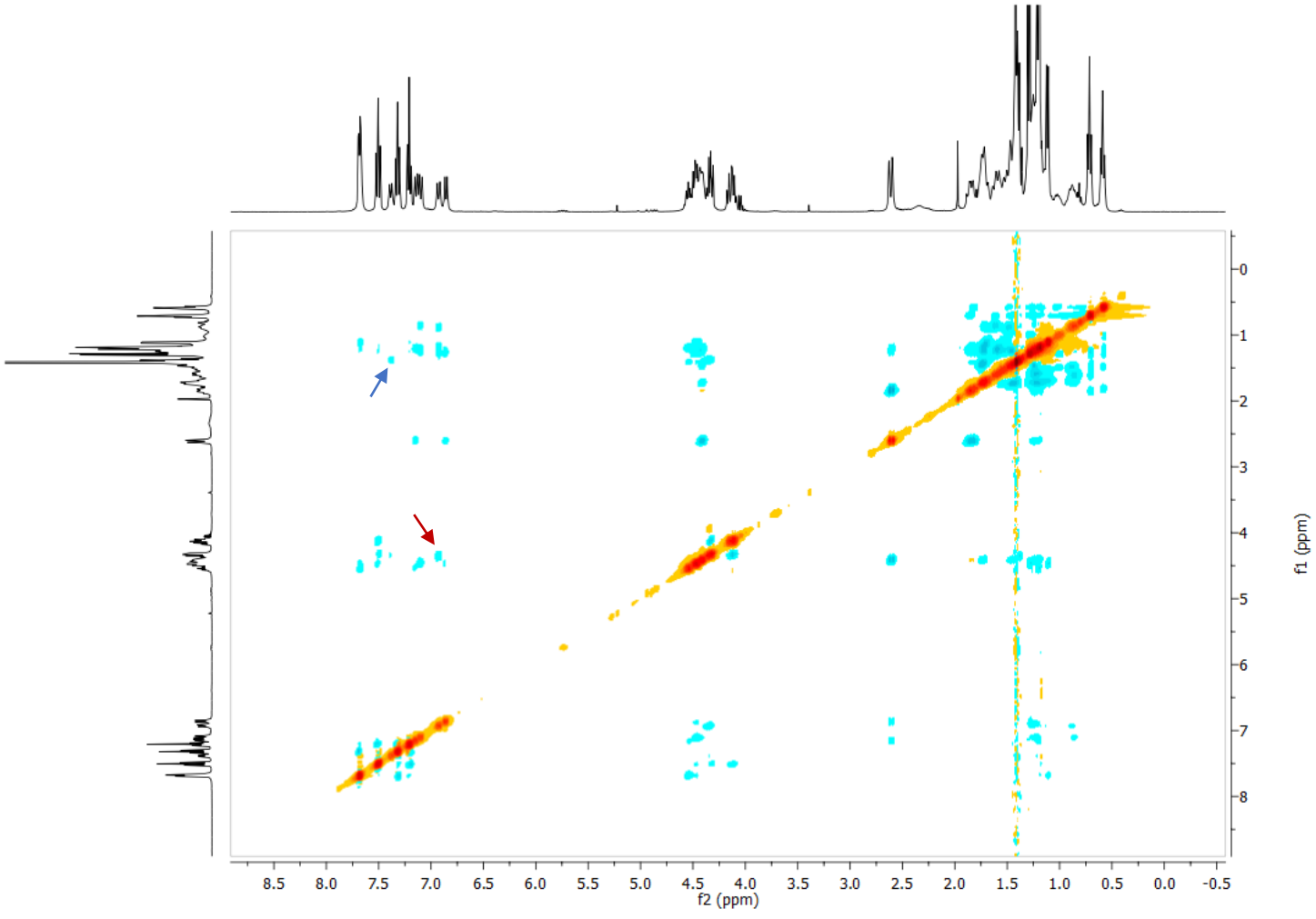

Figure 3.24: The 2D ROESY NMR spectrum for **114**. Recorded at rt, in an 8.0 mM solution in $CDCl_3$ (400 MHz).

A good number of ROESY cross peaks for **114** was observed, although certainly with less interactions between *different* residues than for **111** and **114**. For instance, there is less communication between the HCα protons of the D-Ala residues with the amide protons of the ACPA residues than for both **111** and **112**, and no interactions at all between the HCδ protons of the ACPA residues and the HCα protons of the D-Ala residues. Interactions tend to be between protons of the same residue, which suggests that there might be a lower degree of folding for **114** than for **111** and **112**. However, there were a couple of unambiguous cross peaks between different residues identified, including an interaction between the ACPA (2) amide proton with the HCα proton of the D-Ala (1) residue (red arrow), as well as an interaction between the D-Ala (1) amide proton with the proton(s) of the *tert*-butyl group at the terminus of the foldamer (blue arrow), showing that longer-distance interactions are indeed present (Figure 3.25).

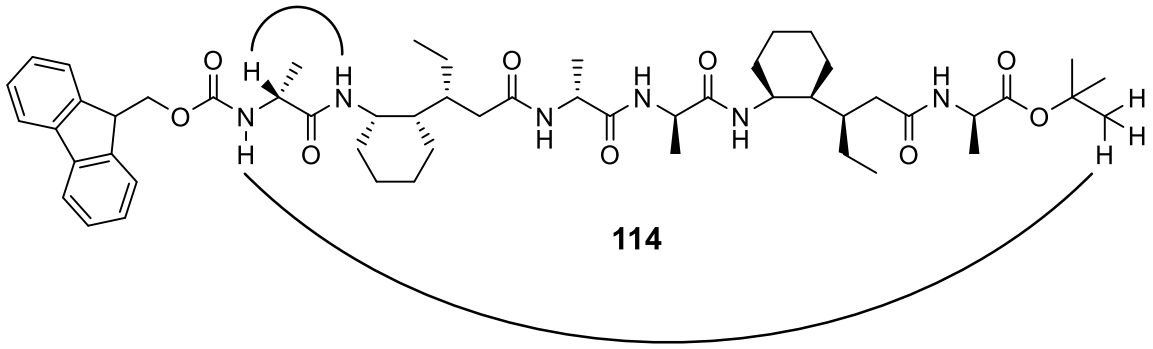

Figure 3.25: The two unambiguous NOE cross peaks between different residues observed for heptamer **114**.

3.3.4.2. Aggregation Control Experiment

The aggregation study for **114** (Figure 3.26) showed minimal changes in shift for all amide protons, suggesting that they are not involved in intermolecular bonding, and that the foldamer is not aggregating.

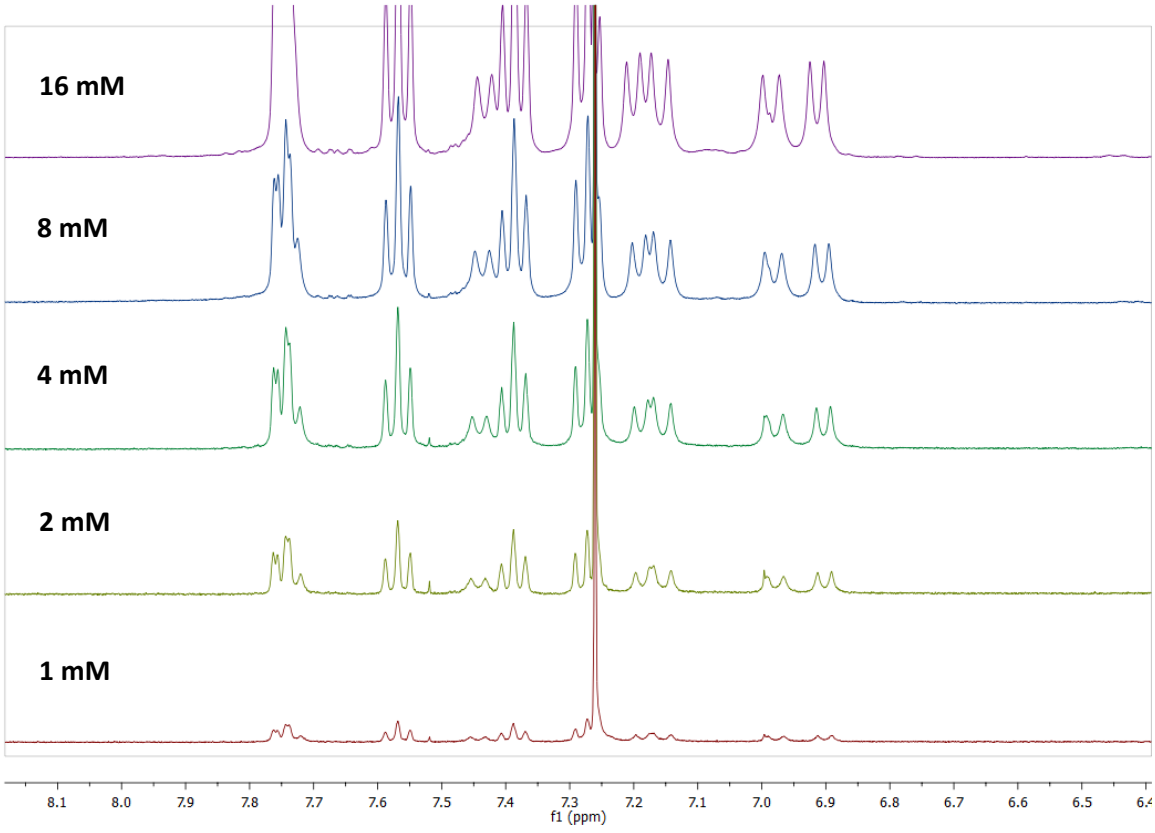

Figure 3.26: The ^{1}H NMR spectra for **114** at concentrations 16, 8, 4, 2 and 1 mM. Recorded at rt in $CDCl_3$ (400 MHz).

3.3.4.3. DMSO Titration Experiment

The ^{1}H NMR of a 4 mM solution of pentamer **114** in $CDCl_3$ was first measured (Figure 3.27), followed by a series of spectra with 5, 10, 25, 50 and 100 µL of d_6-DMSO added. The resultant amide proton chemical shifts are shown in table **3.28**. Note that the two unassigned amides have arbitrarily been designated Ala NH 3 and Ala NH 6.

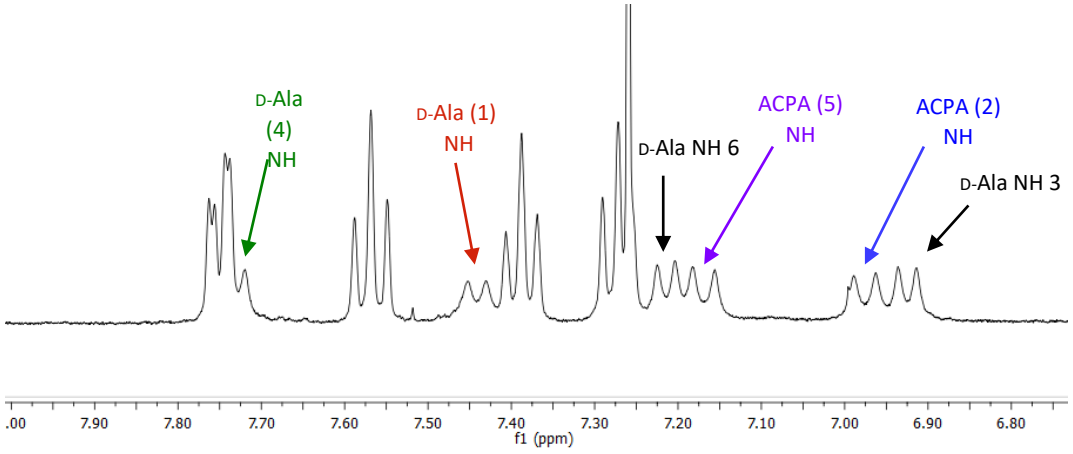

Figure 3.27: The 4 mM d_6-DMSO-free ^{1}H NMR spectra of **112**, showing the numbered amide protons. Recorded at rt in $CDCl_3$ (400 MHz).

Volume of d_6-DMSO added [µL]	D-Ala NH 3 [ppm]	ACPA (2) NH [ppm]	ACPA (5) NH [ppm]	D-Ala NH 6 [ppm]	D-Ala (1) NH [ppm]	D-Ala (4) NH [ppm]
0	6.92	6.98	7.17	7.22	7.44	7.73
5	6.93	6.99	7.17	7.22	7.42	-
10	6.93	6.99	7.17	7.22	7.42	-
25	6.94	6.99	7.17	7.23	7.41	-
50	6.94	6.99	7.17	7.23	7.41	-
100	7.25	7.32	-	-	-	7.91
Δ [ppm]	+0.33	+0.34	0.00	+0.01	-0.03	+0.18

Table 3.8: The chemical shifts of the amide protons of **114**, with increasing concentrations of d_6-DMSO. Dashed entries indicate resonances that could not be unambiguously assigned due to spectral overlap.

Up until the addition of 50 µL d_6-DMSO, all of the amide protons experienced little to no change in their chemical shift, suggesting that they are all participating in intramolecular hydrogen bonds. Upon the addition of 100 µL, a sudden and considerable downfield shift for all of the amide protons was observed (although three of the amide protons were undistinguishable due to spectral overlap). The higher concentration of d_6-DMSO may have disrupted and severely compromised the secondary structure of the foldamer. This is an indication that whilst there is evidence for secondary structure formation for hexamer **114**, it may be less robust and more sensitive to external environmental factors than that of **111** and **112.**

3.3.4.4. Circular Dichroism

The CD spectra for **114** at 20°C and 60°C is shown below (Figure 3.28), with the 20°C spectra showing the same broad, negative band as found in the corresponding spectra for **107**, **111** and **112**, but with a marked reduction in intensity, again suggesting a lesser degree of secondary structure formation for **114**. Again, the 60°C spectra shows the same negative band but with diminished intensity, indicative of a loss/reduction of defined secondary structure.

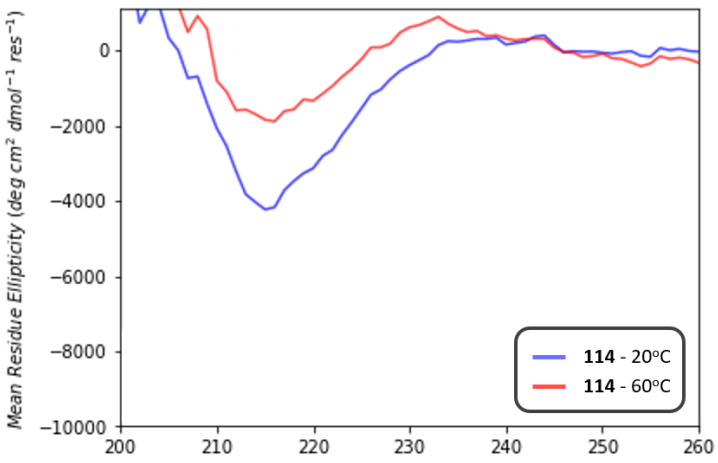

Figure 3.28: The CD spectra at 20˚C and 60˚C for **114.** Recorded at rt in MeOH, in a 0.25 mM solution.

3.4. Conclusion

In this chapter, the structural characterisation of foldamers **107, 109, 111, 112** and **114** was achieved, most notably through the use of 1D and 2D NMR techniques, in addition to circular dichroism. Tripeptides **107** and **109** were first compared, with the evidence suggesting that **107** adopts a single, well-defined 13/11-helical structure (Figure 3.29), whereas **109** lacks a well-defined secondary structure, populating two or more different conformations (including the 13/11-helix).

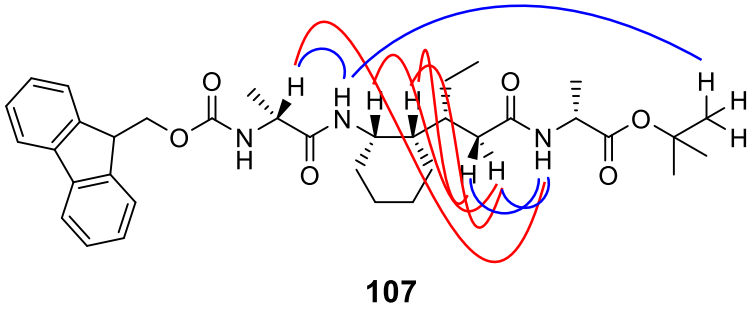

107

Figure 3.29: The unambiguous NOE cross peaks observed for trimer **107**. Characteristic 13/11-helix cross peaks are shown in red.

Pentamer **111** was found to possess a high degree of secondary structure, with the chemical shifts of the amide protons tentatively pointing towards an 11/13 helical structure (Figure 3.30). The same was found for heptamer **112,** with both also having similar ROESY NMR and CD spectra. Aggregation and DMSO titration studies confirmed that the amide protons were engaging in intramolecular hydrogen bonds.

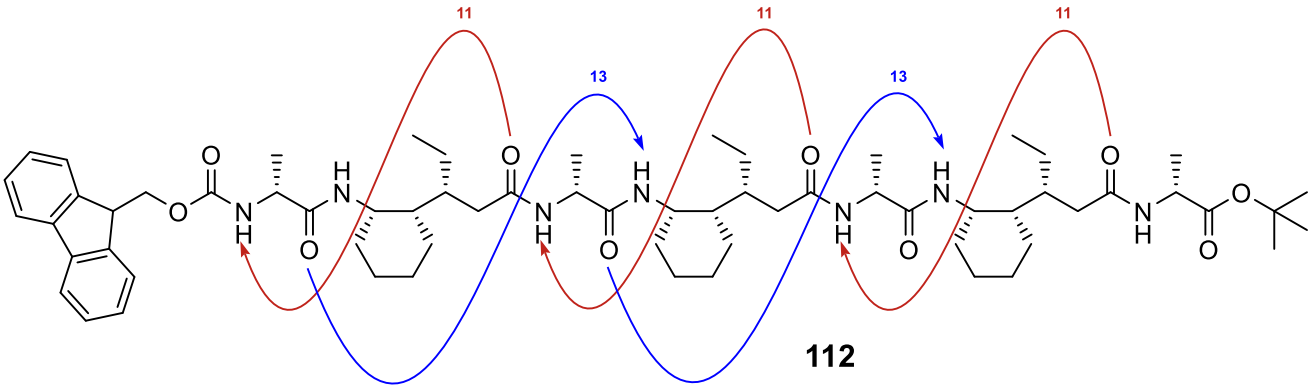

112

Figure 3.30: The proposed 11/13 helix hydrogen bonding pattern for **112**.

Finally, hexamer **114** was also found to display the formation of secondary structure, but perhaps to a lesser degree than **107, 111** and **112**. The ROESY NMR spectra showed the presence of some longer distance inter-residue interactions (Figure 3.31), but less than those found in **111** and **112** in particular. Additionally, the CD spectra displayed the same negative band as found in the other foldamer examples, but with a marked reduction in intensity.

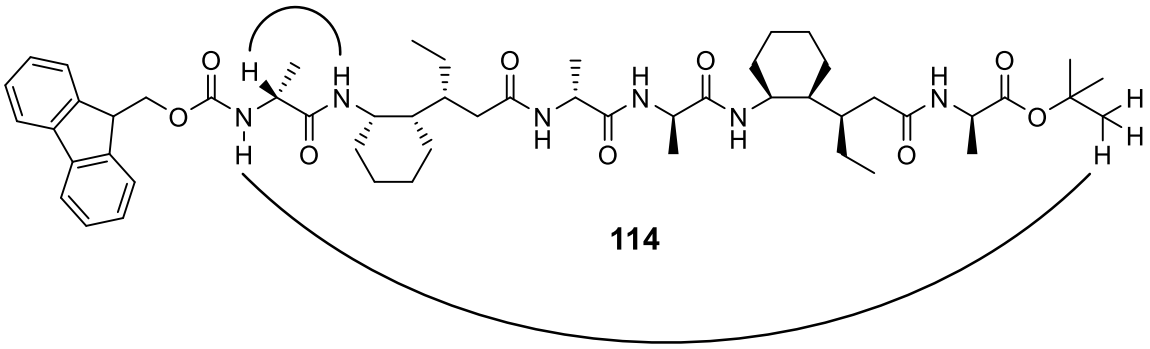

Figure 3.31: The two unambiguous NOE cross peaks between different residues observed for heptamer **114**.

3.5. Future Work

Unfortunately, attempts to grow crystals for all of the foldamers were unsuccessful, and therefore the X-ray structures could not be obtained. This would have provided insightful information on the solid-phase structure of the foldamers, as well as allowing for the measurement of the distances between interacting atoms in the ROESY NMR structure, through the cross-peak integration and extrapolation of a known bond-distance within the structure. Any future studies would greatly benefit from the successful acquisition of crystal structures in order to obtain this data.

As mentioned previously, spectral overlap was a considerable problem for the NMR characterisation of the foldamers, for **111** and **112** in particular, and to a lesser extent **114**. This problem was substantial enough that an increase in magnetic field strength from 400 MHz to 700 MHz saw minimal improvement. A solution to this might be to incorporate tyrosine or phenylalanine residues into the foldamers (in place of some Alanine residues) in order to promote the diversity and dispersion of NMR resonances (Figure 3.30).[107] This would hopefully allow for the individual α-residues and thus the adjacent δ-residues to be picked out and identified. Of course, there is the potential for these changes to have an effect on the secondary structure through steric effects, and so would have to be carefully managed in order to minimise structural disruption. To avoid this problem, DFT calculations could be carried out instead, which would provide predictions for the ^{1}H chemical shifts which can be compared to the real-life spectra, helping to shed light on the likely conformation.[11]

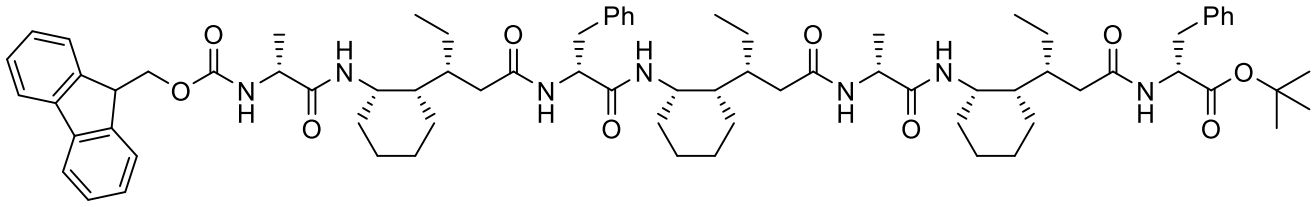

122

Figure 3.32: The example heptamer **122** with a variety of α-amino acid residues.

Chapter 4 – The synthesis of novel α/γ-dipeptide building blocks

4.1. Background

4.1.1. Cyclic γ-amino acid monomers and their use in α/γ-foldamers

The synthesis of γ-amino acids had already received a great deal of attention before their use within foldamers was even realised, as a consequence of their therapeutic potential - chiefly as analogues of the neurotransmitter GABA.[108] As the field of peptidomimetic foldamers grew, the synthesis and use of cyclic γ-amino acid monomers in particular quickly became a popular choice, due to the previously mentioned propensity for cyclically-restrained residues to promote secondary structure formation.[109-111] Two prominent have already been mentioned in chapter 2, with the cyclic γ-amino acid precursors **71** and **89** serving as a starting point for the synthesis of the eventual δ-amino acid residue targets **60** and **61**, respectively.[75,83] In the original study, the opposite enantiomer of **89** (produced by switching from the (*R*) to the (*S*)-pyrrolidine catalyst in the initial organocatalytic step) was converted to the corresponding protected carboxylic acid and successfully incorporated into a series of 1:1 α/γ-foldamers. They were predicted and subsequently shown to adopt 12-helical conformations in solution, as determined by the observation of characteristic NOE interactions in the ROESY NMR (Figure 4.1) Crystal structures were obtained which showed that the 12-helical conformation was also adopted in the solid state (Figure 4.2).

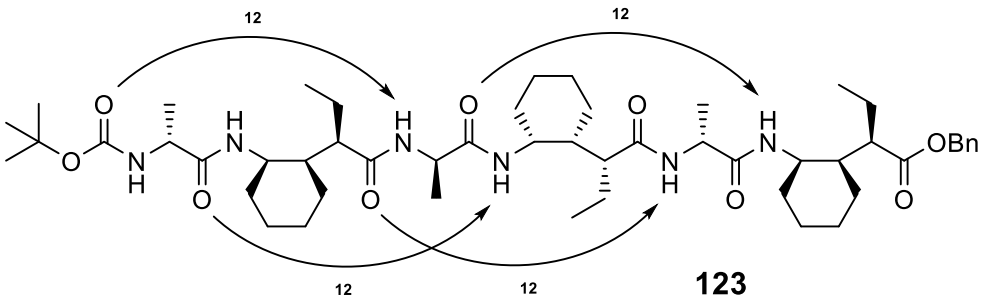

Figure 4.1: The hexamer **123** as produced by Gellman and co-workers, showing the characteristic 12-helical hydrogen bonding pattern.

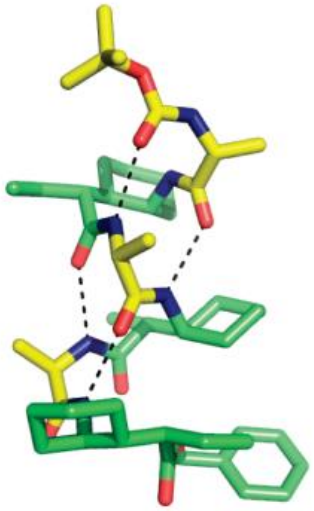

Figure 4.2: The crystal structure of hexamer **123**.[83]

Gellman and co-workers subsequently built upon this work by investigating the use of alternative cyclic γ-amino acid monomers within α/γ-foldamers. Moving away from cyclohexyl-based γ-residues, they developed the stereoselective synthesis of the *trans* cyclopentyl-based residue **124** (AMCP).[98] This was achieved via the organocatalytic asymmetric Michael addition of nitromethane **125** to cyclopentane1-carboxaldehyde **126** to exclusively give the *trans* δ-nitro alcohol **127** in a 99% yield, with an *ee* of >99%. The nitro group was then reduced, the subsequent amine group boc-protected and the primary alcohol oxidised to the carboxylic acid to give the desired protected γ-amino acid **128** (Scheme 4.1).

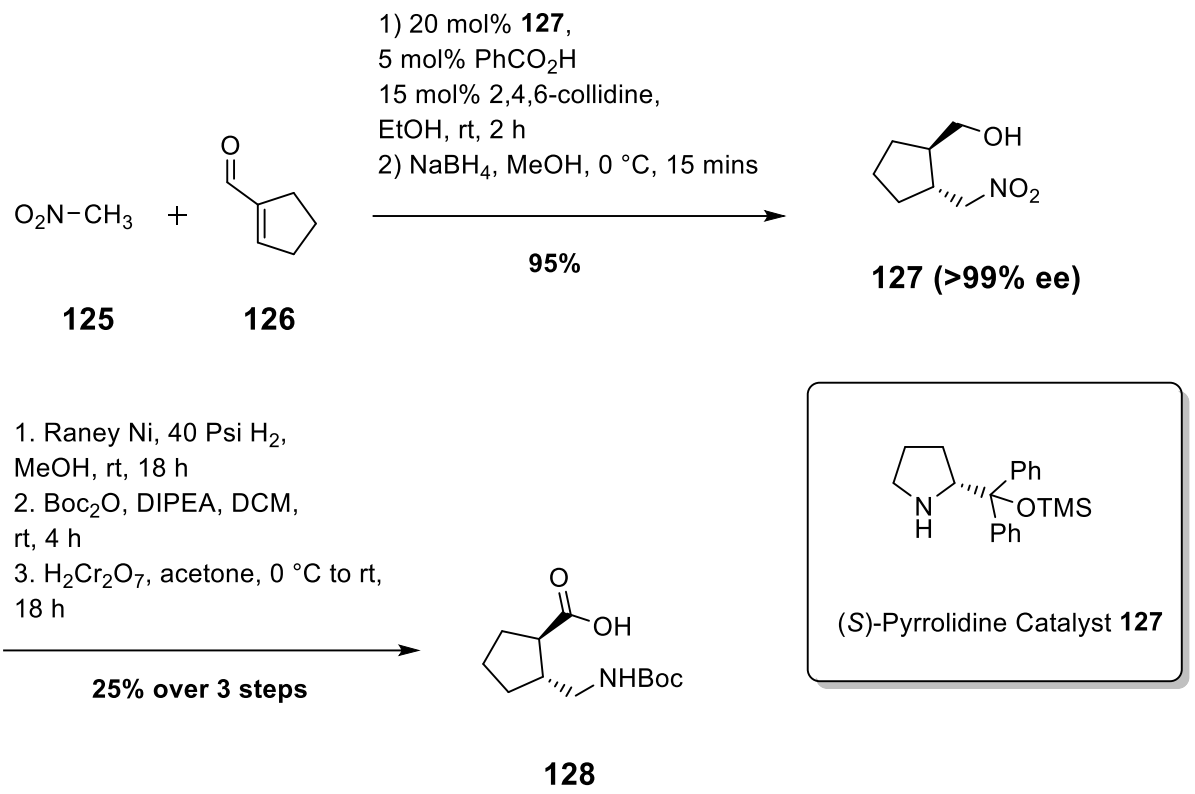

Scheme 4.1: The asymmetric synthesis of the protected *trans*-AMCP residue **128**.

The group incorporated **128** into a series of 1:1 α/γ-peptides, using D-Alanine as the α-reside for the tetramer, hexamer **129** and octamer (with D-phenylalanine also used in the construction of the decamer). The structural characterisation data for the peptides indicated only a modest propensity for folding, with each failing to adopt a single, highly populated secondary structure in solution. The ROESY NMR spectra for all four lacked several (but not all) of the characteristic NOE interactions for the expected 12/10-helix. In addition, NOE-restrained simulated-annealing calculations were carried out for the three longest peptides, showing the ten conformations with the lowest energy for each. The resultant structural ensembles showed a diverse range of possible conformations, mostly lacking a contiguous network of hydrogen bonds. However, a DMSO titration experiment the decamer indicated at least a partial population of the 12/10-helical conformation, with the resonances of the amide protons at each terminus of the peptide experiencing a strong downfield shift relative to the others, indicating their absence from the network of hydrogen bonds – as they would be in a 12/10 helix. These two amide protons are also found further upfield than the rest in the native ^{1}H NMR, strengthening the hypothesis of a partial 12/10-helical conformation. The

group speculated that the lack of a substituent at the Cγ position caused the residue to retain considerable flexibility, despite the carbocyclic constraint.

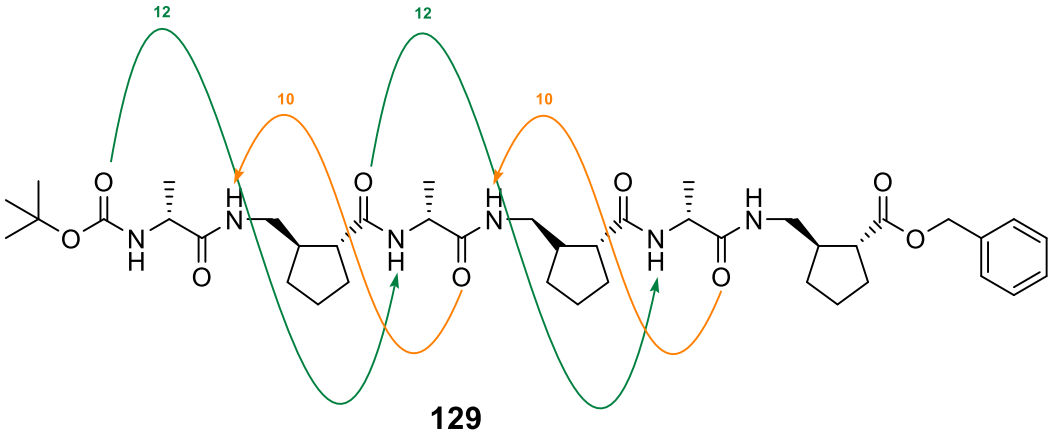

Figure 4.3: Hexamer **128** as developed by Gellman and co-workers, showing the hydrogen bonding pattern for the 12/10-helix it is purported to partially populate. 12-membered rings are shown in green, with 10-membered rings in orange.

4.1.2. *Cis*-AMCP residues and their use in 1:1 α/γ-foldamers

The Cobb group were keen to investigate the synthesis and foldermeric use of AMCP residues further, hoping to discover how a stereochemical change in the structure might affect and hopefully enhance the folding properties of any resultant foldamer.[112] They first sought to develop a reliable synthetic route towards the *cis*-AMCP system, something that was up until that point lacking in the relevant literature. They would then incorporate this system into α/γ-peptides equivalent to the ones created by Gellman for the *trans* system, in order to compare their folding propensities.

An asymmetric, organocatalytic process was developed for the synthesis of the *cis* δ-nitro alcohol **132**, which employed the tetrazolic catalyst **131** in order to promote the intramolecular Michael addition of 7-nitro-hept-6-en-1-al **130,** followed by the reduction of the aldehyde to the alcohol (Scheme 4.2) The organocatalytic reaction was successfully optimised, achieving a high level of selectivity for the formation of desired *cis* product with a

diasteresoselectivity of 9:1, in addition to a good yield (74%) and an excellent enantiomeric excess (92%).

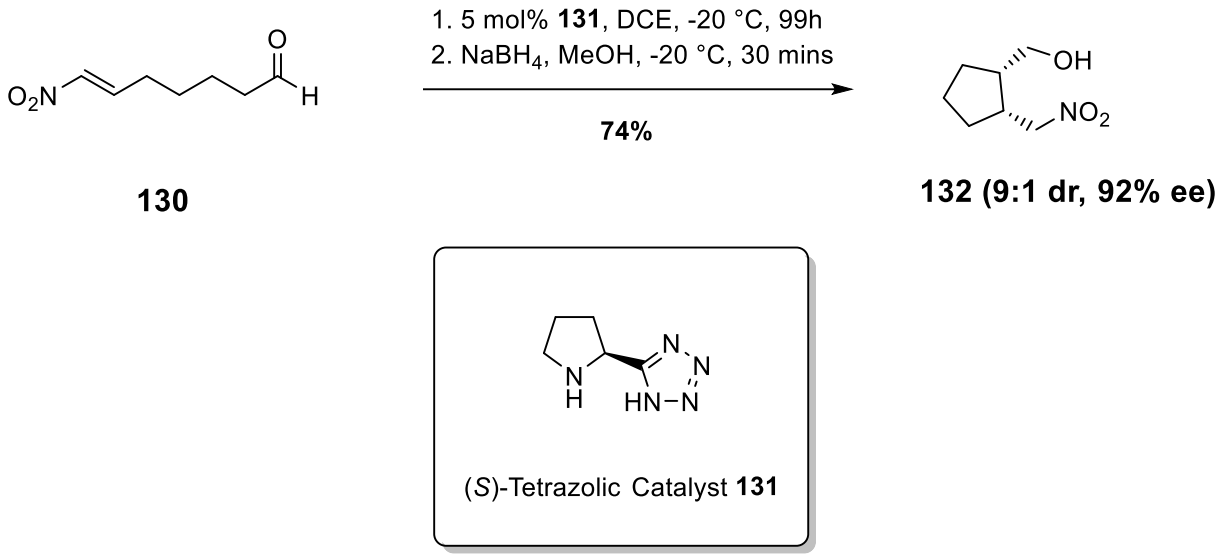

Scheme 4.2: The organocatalytic synthesis of the *cis* δ-nitro alcohol **132**, developed by Cobb and co-workers.

It was found that whilst the *cis*-system forms faster and with a superior enantioselectivity, it will slowly epimierize to the *trans*-system under the reaction conditions. The reaction time is therefore finely balanced between maximizing the yield and preserving the diasteresoselectivity of the product.

Having established access to the *cis* δ-nitro alcohol **132**, focus could turn to its utilisation within 1:1 α/γ-peptides (Scheme 4.3). It was first oxidised to the carboxylic acid **133**, and then coupled with benzyl-protected L-Alanine to give the dipeptide **134**. The nitro group can be readily reduced to produce the free amine **135** in a quantitative yield, which was subsequently boc-protected to give **136**. This can now be deprotected at the carboxyl terminus to give the free carboxylic acid **137**, via a palladium-mediated hydrogenation. The group now had all of the necessary building blocks to generate the tetramer **138** and the final hexamer target **139**, achieved via iterative peptide couplings between the appropriately deprotected subunits.

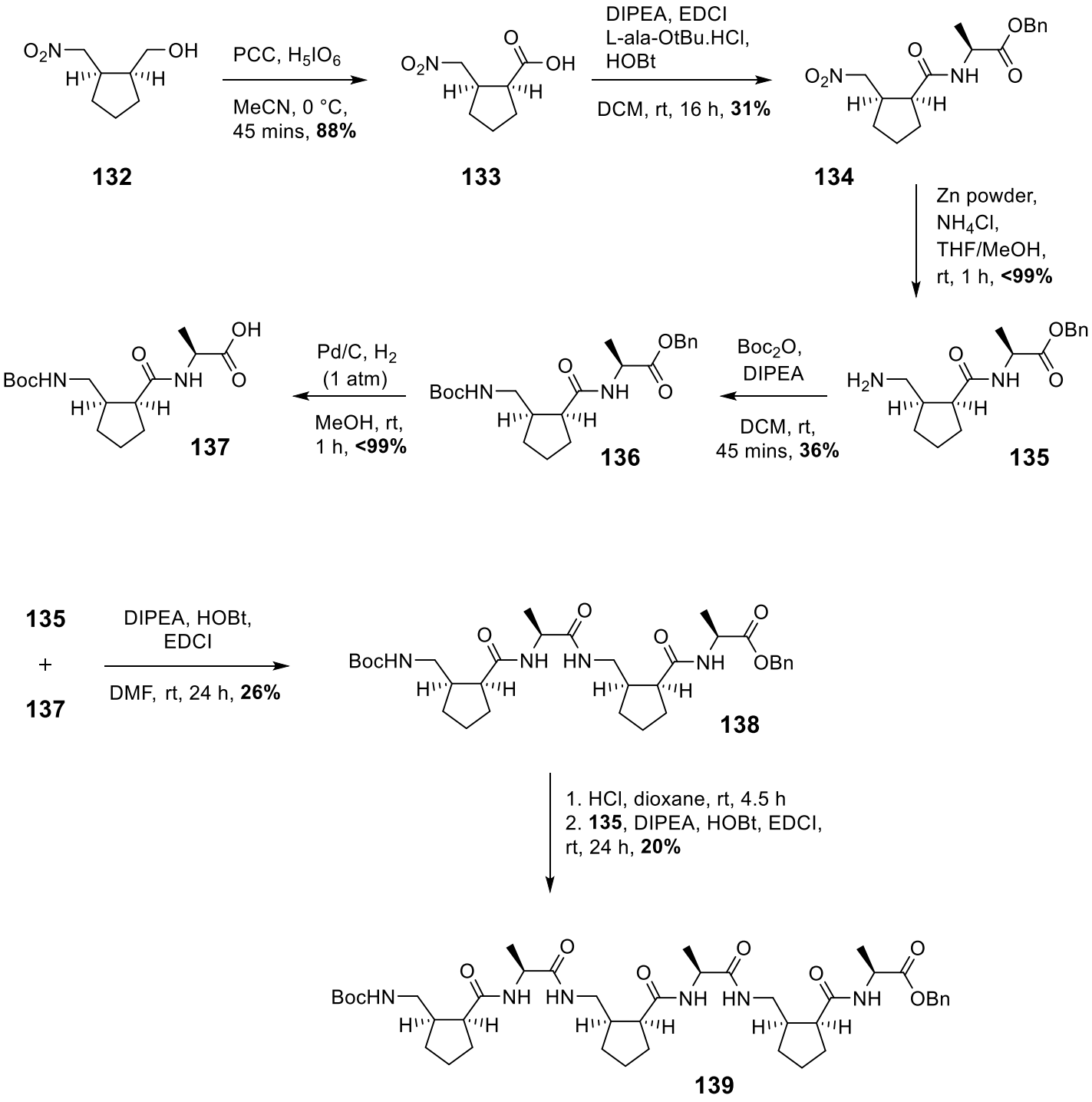

Scheme 4.3: The synthesis of tetramer **138** and hexamer **139**.

In contrast to the foldamers based on the *trans*-AMCP residues developed by Gellman, hexamer **139** was found to have strong propensity for folding, adopting a single, well-defined 12/10-helical conformation. This was confirmed by the greater number of characteristic 12/10 NOE interactions in the ROESY NMR, in addition to the findings from a NOE-restrained simulated-annealing computational study, which showed that the nine conformations with

the lowest energy agreed with the prediction of a 12/10-helical structure (Figure 4.4). Interestingly, this study allowed the group to elucidate the reason for the difference in folding propensity between the *trans*-AMCP and *cis*-AMCP derived foldamers. For the *cis* foldamers, they found that the backbone torsion angle ζ - defined as rotation about the Cα-Cβ bond of the AMCP residue - is strongly restricted, with only a relatively small range of values possible. This is not the case with the *trans* foldamers, with a much larger range of torsion angle ζ values possible, meaning that the foldamers are inherently more flexible. This would allow them to access a much greater number of possible competing conformations, reducing the likelihood of the adoption of a single, well-defined structure.

Figure 4.4: The overlap of the nine lowest energy conformations of hexamer **139**, showing the likely adoption of a 12/10-helix (side chains and terminal protecting groups removed for clarity).

Having established that α/γ-foldamers based upon the *cis*-AMCP residues exhibited superior secondary structure formation, work could begin towards the construction of catalytic foldamers. This would entail the insertion of a secondary amine into one or more of the cyclopentyl rings, allowing for enamine or iminium catalysis that would have the potential for enantioselective control (Figure 4.5). This would be facilitated by the asymmetric nature of the foldamers helix, as the helical chirality of the foldamer induces point chirality in the eventual product.

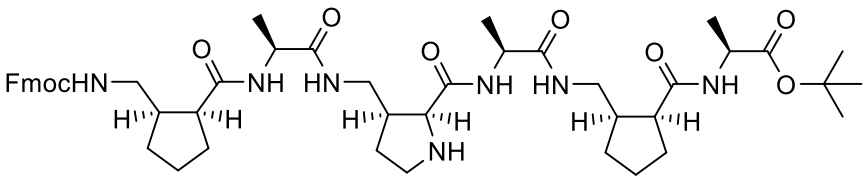

140

Figure 4.5: The potentially catalytic foldamer **140**, with the pyrrolidine-based residue in the centre.

4.2. Aims and Objectives

The aim of this chapter was to synthesis the novel dipeptide building blocks that would be required to create the catalytic foldamer **140**. The improved synthesis of the cyclopentyl-based *cis* γ-amino acid precursor **132** and the pyrrolidine-based equivalent **141** is described first, followed by their incorporation into the novel target dipeptides, **143** and **144** (Scheme 4.4).

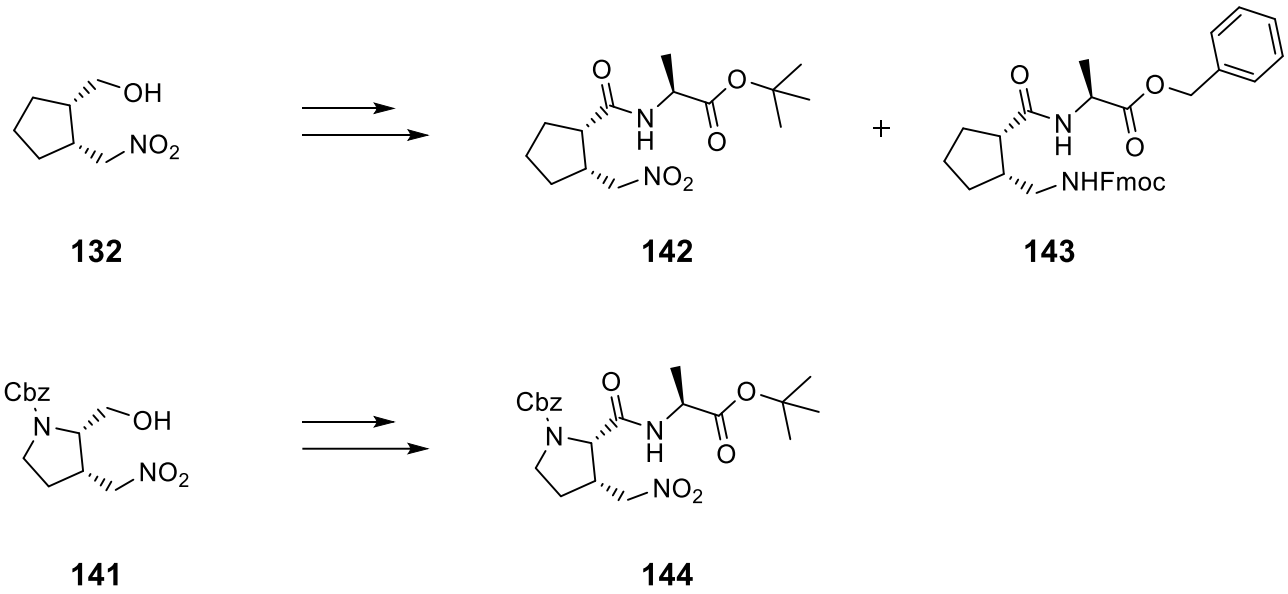

Scheme 4.4: The δ-nitro alcohols **132** and **141**, and the target dipeptides **142**, **143** and **144**.

The final aim was to synthesis the dipeptide **145** (Figure 4.6), which could be used as a starting point/benchmark for the investigation of catalytic ability for pyrrolidine-based foldamers.

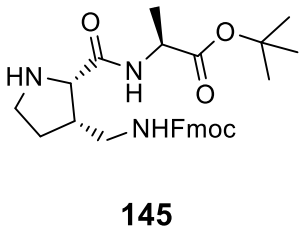

Figure 4.6: The target catalytic dipeptide **145**.

4.3. Results and Discussion

4.3.1. Synthesis of *cis* δ-nitro alcohol 132

The synthesis of the required nitro aldehyde starting product **130** for the organocatalytic generation of **132** has been previously described by Cobb and co-workers.[112] It entails the radical nitration of Ethyl-6-heptenoate **146**, followed by the DIBAL-H reduction of **147** to give **130** in an overall yield of 22% (Scheme 4.5). The procedure suffers from the generation of hard-to-separate impurities, considerably hampering the purity of the final product. This was speculated to occur during the DIBAL-H reduction, or possibly as a result of the silica-induced cyclisation of the product during the column chromatography.[113]

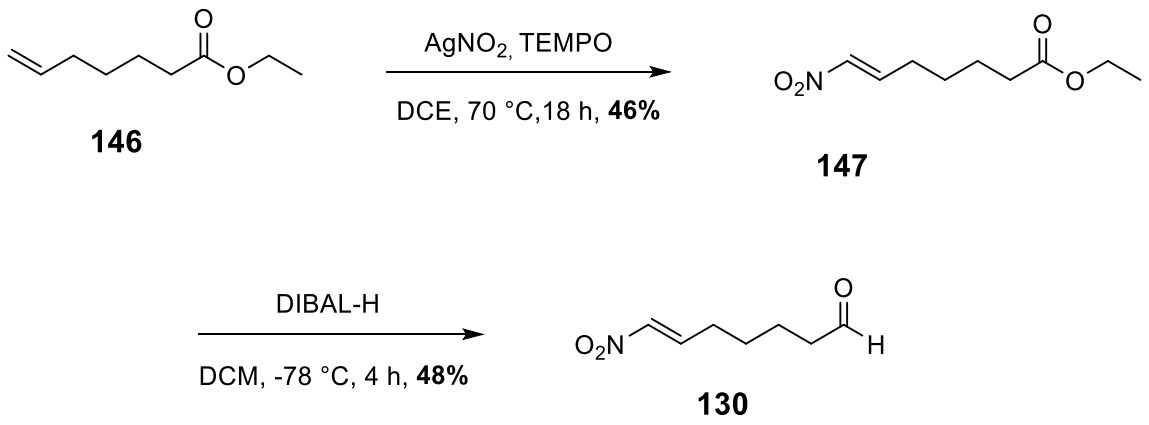

Scheme 4.5: The previously described synthesis of the nitro aldehyde **130**.

A modified version of this synthetic route was the first attempted in this study for the synthesis of **130** (Scheme 4.6). Instead of using $AgNO_2$, tert-butyl nitrile was instead utilised as the nitrile source, with dioxane as the solvent.[114] This resulted in a much improved yield of 74%, resulting in a 35% yield overall for the two-step process. As expected however, the purity of **130** was low, with the H^1 NMR indicating the presence of a high level of impurities. The decision was made to devise a new route that could minimise or eliminate the generation of these impurities.

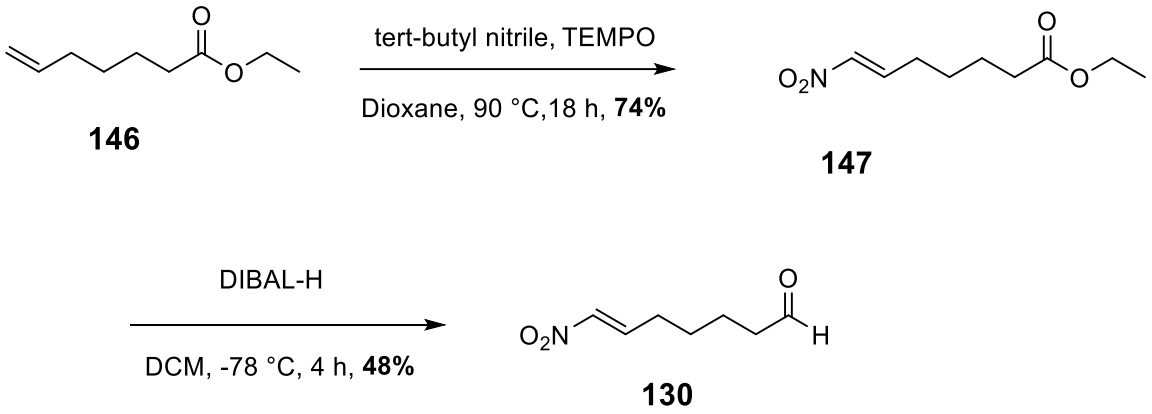

Scheme 4.6: The first attempted synthesis of **130**.

Considering that the impurities were generated during either the formation or purification of the nitro ester **147**, it would be pertinent to avoid its formation in any new synthetic route. It was also noted that the reaction conditions for the improved nitration of **146** could also be used for the oxidation of alcohols to aldehydes.[115] It might be possible to simultaneously - yet independently – nitrate and oxidise the alcohol olefin **148** in order to produce the desired product **130** (Scheme 4.7).

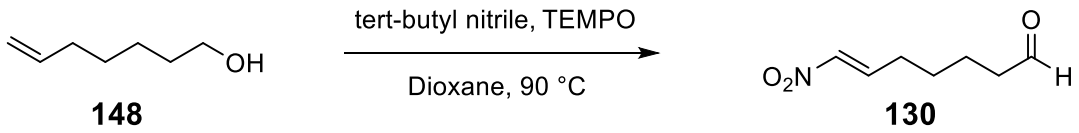

Scheme 4.7: The proposed radical-mediated transformation of **148** to **130**.

A new synthetic route was therefore established (Scheme 4.8), with **146** first reduced to the alcohol olefin **148** with excess DIBAL-H in a yield of 97%. **130** was then successfully produced in a yield of 37% via the radical-mediated nitration/oxidation, giving an overall yield of 36%. Crucially, the ^{1}H NMR spectra showed the purity to be excellent, with the presence of impurities extremely low, especially when compared to the sample produced in the first attempted synthetic route.

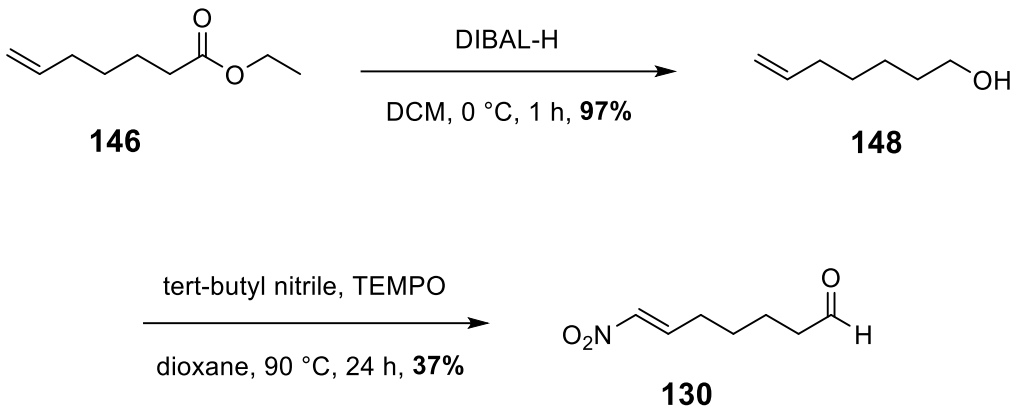

Scheme 4.8: The improved synthesis of nitro aldehyde **130**.

The organocatalytic step was next, and this was carried out in the same fashion as described in the literature, giving the *cis*-nitro alcohol **132** in a slightly improved yield and a comparable *dr* to the literature values (Scheme 4.9). Note that the *ee* of the reaction was not checked but was assumed to match the literature value.

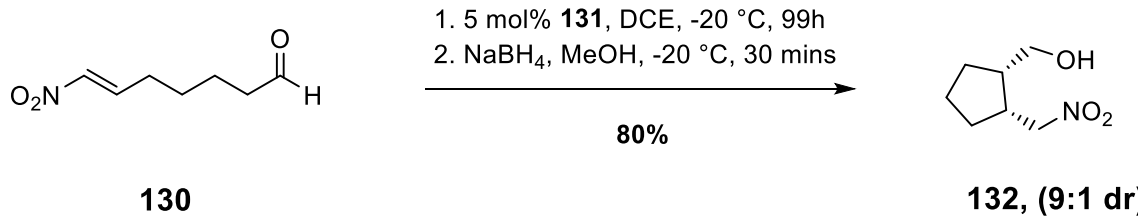

Scheme 4.9: The organocatalytic synthesis of the *cis* δ-nitro alcohol **132**.

4.3.2. Synthesis of pyrrolidine-based *cis* δ-nitro alcohol 141

The synthesis of the required nitro aldehyde starting product **154** for the organocatalytic generation of **141** was carried out using the same method as described by Cobb and co-workers.[113] It began with the nucleophilic substitution of diethoxyethylamine **150** to 4-bromo-1-butene **149** in the presence of potassium carbonate to give the amine **151**. This was followed by a Cbz protection and then a TEMPO radical-mediated nitration with silver nitrite

as the source of NO_2, with the final step being an aldehyde deprotection with acetic acid and HCl, to give the nitro aldehyde **154** (Scheme 4.10). All of the yields were comparable to the literature values except for the aldehyde concentration step, which was considerably better (68% vs 33%).

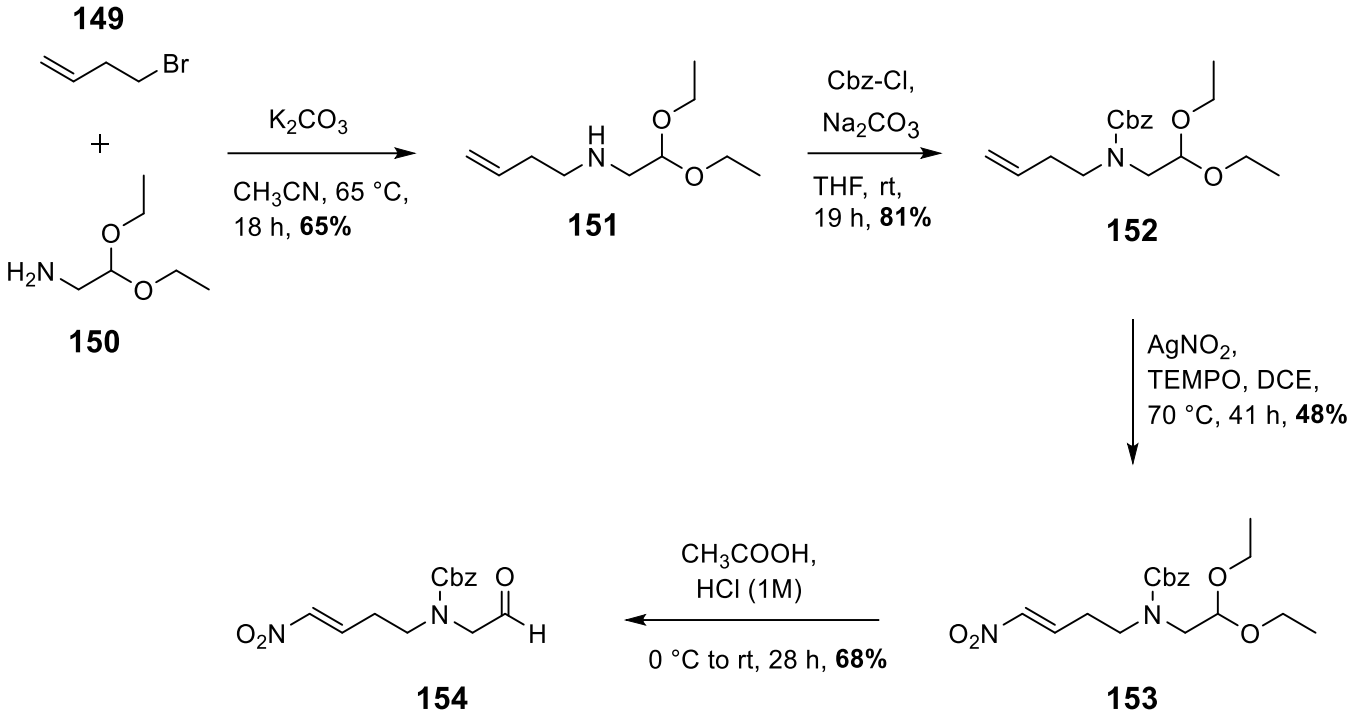

Scheme 4.10: The synthesis of nitro aldehyde **154**.

The previously described organocatalytic reaction of **154** to form the cyclised, pyrrolidine-based *cis* δ-nitro alcohol **141** was based upon the same reaction to form **132**, albeit with a longer reaction time of seven days in order for the reaction to go to completion.[113] **141** was reported to be synthesised in a 46% yield, with a *dr* of 1:1 and an ee of 77% for the desired *cis* product. It was hoped that the reaction could be optimised to improve these results, particularly the diastereomeric ratio. The reaction should undergo the same mechanism described for substrate **130**, meaning that the *cis* product will quickly form, but then slowly start to epimierize to the *trans* product over time. It was therefore decided to attempt the reaction with a shorter reaction time in order to preserve the *dr*. The reaction was carried out over the course of four days instead of seven, leading to **141** forming in an identical yield, but with a much improved *dr* of 5:1 and a slightly improved *ee* of 80% (Scheme 4.11).

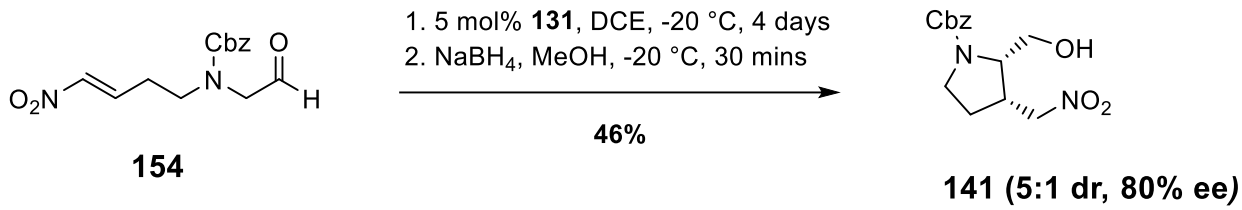

154

141 (5:1 dr, 80% ee)

Scheme 4.11: The optimised organocatalytic synthesis of **141**.

4.3.3. Synthesis of dipeptides 142 and 143

With the secondary amine of the pyrrolidine-based residue protected with the hydrogenolysis labile Cbz group, the terminal protecting groups of the eventual foldamer should be orthogonal, with one being acid labile and the other base labile, in order for the Cbz group to be selectively removed. The commonly used Fmoc/O^{t}Bu protection strategy would therefore be the most effective method. The protected dipeptide **155** (Figure 4.7) would be a logical target, as it could be used to couple at both ends of an equivalent pyrrolidine-based dipeptide whilst maintaining orthogonality.

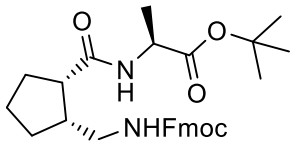

155

Figure 4.7: The initial dipeptide target **155**.

The nitro alcohol **130** was first oxidised to the nitro acid **133** via the literature procedure, achieving a comparable yield of 85%. This was then coupled with L-Alanine tert-butyl ester hydrochloride to form the dipeptide **142** (Scheme 4.12). Unfortunately, the yield was very low, at only 14%.

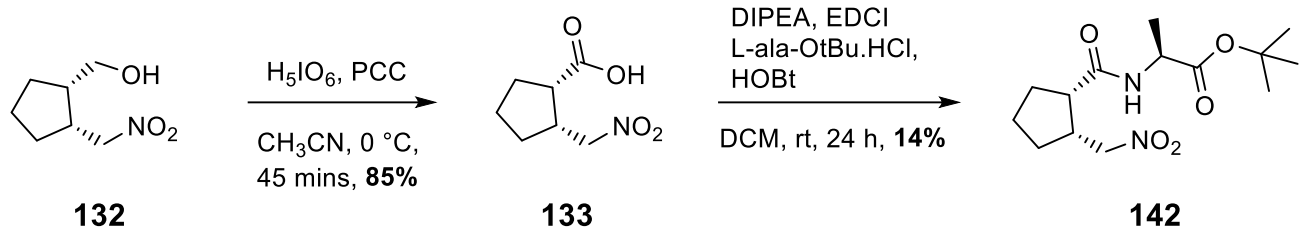

132 **133** **142**

Scheme 4.12: The synthesis of dipeptide **142**.

With **142** forming in such a low yield, it becomes impractical to carry it forward to produce the target dipeptide **155**, especially when considering the quantity needed in order for it to form both ends of the resultant foldamer. **142** can still be used to form the C-terminus of the foldamer however, with the synthesis of an alternative dipeptide building block required for the N-terminus. Dipeptide **134 –** with the Alanine protected with the benzyl instead of *tert*-butyl group - can be produced and appropriately modified for this purpose, as it was formed in a higher, more synthetically useful yield in the original study. **132** was therefore coupled with L-Alanine benzyl ester p-toluenesulfonate salt to give **134** in a yield of 37%. The nitro group was then selectively reduced via the literature procedure to give the free amine **135** in a quantitative yield, which was then Fmoc protected to give the required dipeptide **143** (Scheme 4.13).

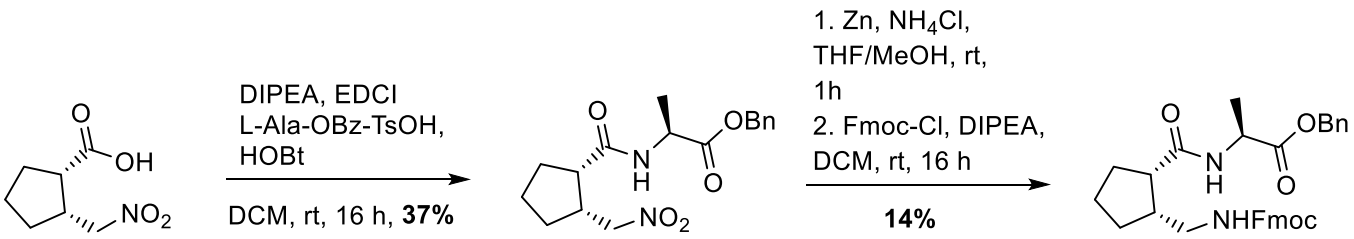

133 **134** **143**

Scheme 4.13: The synthesis of the protected dipeptide **143**.

4.3.4. Synthesis of pyrrolidine-based dipeptide 144

The target pyrrolidine-based dipeptide **144** can be produced in the same manner as **142**, with the nitro alcohol **141** oxidised to the nitro acid **156** in a yield of 52% via the addition of periodic acid and PCC. This was then coupled with L-Alanine tert-butyl ester hydrochloride to form dipeptide **144** in a yield of 27% (Scheme 4.14).

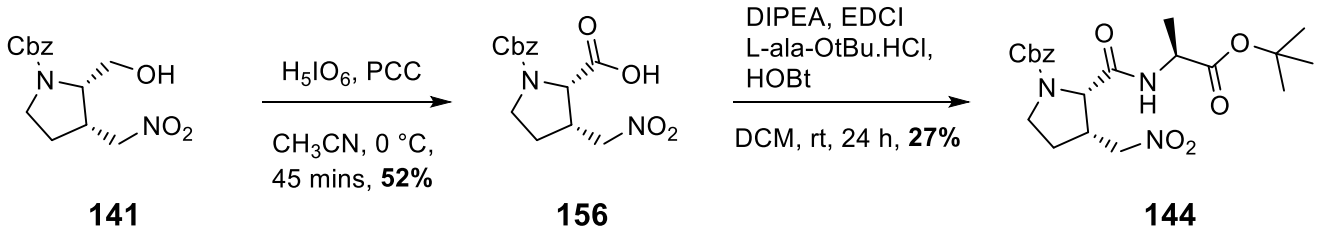

Scheme 4.14: The synthesis of the dipeptide **144**.

4.3.5. Synthesis of catalytic dipeptide 145

In order to produce the catalytic dipeptide **145**, the nitro group of **144** needs to be reduced and suitably protected, so that the Cbz to be selectively removed via hydrogenation. This was carried out in the same fashion as for **134**, with the free amine produced in a quantitative yield, followed by the Fmoc protection, giving the fully protected dipeptide **157** in a yield of 37%. The Cbz group was then removed by hydrogenation catalysed by Pd/C, to give the target dipeptide **145** in a yield of 93% (Scheme 4.15).

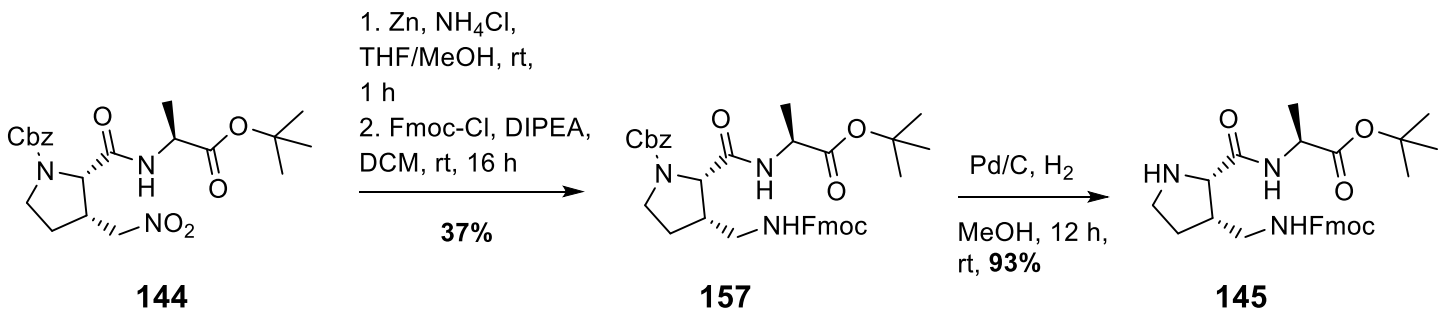

Scheme 4.15: The synthesis of the catalytic dipeptide **145**.

4.4. Conclusion

In this chapter, the syntheses of the previously described δ-nitro alcohols **132** and **141** were improved, with a modified synthetic route towards **132** resulting in a higher overall yield, and the optimisation of the reaction time for the organocatalytic production of **141** leading to a much improved diasteresoselectivity. These monomers were then converted to the corresponding nitro acids and then incorporated into the dipeptide building blocks – **142**, **143** and **144** - that would be required to synthesis the catalytic foldamer **140**. Finally, the catalytic dipeptide **145** was synthesis in a 3-step process from **144**, ready for further studies.

4.5. Future Work

The obvious next steps for this work would be to synthesis the foldamer **140** and to confirm its propensity for secondary structure via the usual characterisation methods. Its catalytic ability can then be investigated, alongside the dipeptide **144**. A model reaction, such as the organocatalytic iminium indole alkylation as developed by MacMillan and co-workers, could be employed for this purpose (Scheme 4.16). The level of stereochemical control achieved by both (if any) would make for an interesting comparison, with **144** representing a more typical organocatalyst such as proline and its derivatives, and **140** representing an example of the lesser-explored class of foldermeric catalysts. The activity of both would help to direct the future development of even more potent catalytic foldamers.

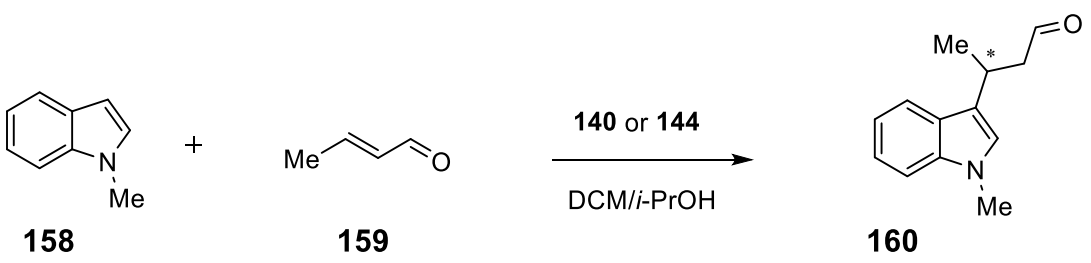

158 159 160

Scheme 4.16: The enantioselective indole alkylation reaction that could serve as model for the investigation of catalytic ability of **140** and **144**.

4.6. General Conclusions

In conclusion, the enantioselective synthesis of the novel, cyclically-constrained δ-amino acid monomers **60** and **61** was achieved, with **61** being successfully incorporated into a series of hybrid α/δ-peptidomimetic foldamers. Structural characterisation was then performed on these peptides in order to probe their propensity for secondary structure formation. A direct comparison was made between the tripeptides **107** and **109**, which made use of D- and L-Alanine residues, respectively. The distribution and downfield nature of the amide chemical shifts in the ^{1}H NMR, in addition to the NOEs analysis of the ROESY NMR spectra, indicated that **107** adopted a single, well-defined 13/11 helical conformation. In contrast, the secondary structure of **109** was shown to be much less well-defined, probably adopting more than one conformation. The longer foldamers **111**, **112** and **114** were therefore constructed using D-Ala as the α-residue, with **107** being used as the starting building block for all. The characterisation of pentamer **111** and heptamer **112** was challenging due to spectral overlap, although tentative evidence for the adoption of an 11/13-helical conformation was obtained. Otherwise, both foldamers demonstrated a good level of secondary structure formation, evidenced by the downfield chemical shift of the amide protons, the number and type of NOE cross peak interactions found in their ROESY NMR spectra, as well as characteristic bands in the CD spectra. Results from the aggregation and DMSO titration experiments for both showed that the amide protons were engaging in intramolecular hydrogen bonding, strengthening these findings. The hexamer **114** - with its different residue backbone sequence - also displayed secondary structure formation, but perhaps to a lesser degree than **111** and **112**.

Finally, the syntheses of the previously described γ-amino acid precursors **132** and **141** was improved, with the overall yield of **132** increasing through the use of an alternative synthetic route, and the *dr* of the organocatalytic production of **141** improved via an optimised reaction time. Both were used to synthesis novel dipeptide building blocks that could go on to create the potentially catalytic foldamer **140**, in addition to the synthesis of the novel catalytic pyrrolidine-based dipeptide **145**.

Chapter 5 – Experimental Section

5.1. Specifications

Materials and methods: All reactions were performed under ambient conditions and magnetically stirred, unless stated otherwise. For air/moisture sensitive reactions, glassware was dried with a heat gun and the system flushed and maintained with the use of a nitrogen filled balloon. Reactions were cooled by the use of cooling baths for reactions at 0°C (ice/water) and -78°C (dry ice/acetone) or a cooling reactor module for reactions at -20°C or -30°C (Polar Bear Plus). Reactions were heated by the use of heat-on blocks or silicone oil baths. Hydrogenation reactions at increased pressure were performed using a Parr Hydrogenation Apparatus 3916EGX and magnetically stirred. Anhydrous MeOH, THF, DCM, DMF and toluene were obtained from a dry solvent machine, with all other examples supplied by Sigma-Aldrich in Sureseal® bottles. All reagents were purchased from commercial sources (Sigma-Aldrich, Fluorochem, Fisher, Alfa Aeser, VWR).

Chromatography: Reactions were monitored by thin-layer chromatography using Silica Gel 60 F254, Merck aluminium backed sheets. UV irradiation (254 nm) or potassium permanganate stain was used for visualization. Column chromatography was performed by hand on silica gel (60 Å, 230-400 mesh, 40-63 µm).

NMR data: ^{1}H, ^{13}C and two-dimensional NMR spectroscopy measurements were recorded using a Bruker Ascend 400 (400 MHz) or Bruker AVIII 700 (700 MHz) spectrometer using TMS as the internal standard.

MS data: High-resolution mass spectra were recorded on a Waters Xevo G2-XS QTof Mass Spectrometer by the Department of Chemistry at King's College London.

IR data: Infra-red spectra were recorded on a Shimadzu IRAffinity-1S FTIR Spectrophotometer.

Optical Rotation: Optical rotation readings were recorded using an Anton Parr MCP100 Polarimeter. Readings were recorded at 20^{o}C and in DCM, unless otherwise stated. Specific rotation units - deg cm^{2} g^{-1}. Concentration units (c) – 10^{-2} g mL^{-1}.

Melting point: Melting points were recorded using a Stuart SMP30 melting point apparatus and are uncorrected.

HPLC: HPLC analysis performed on an Agilent Technologies 1200 Series HPLC using a chiral ADH column. A ratio of HPLC grade hexane and propan-1-ol was used as the eluent. Detection was achieved by UV at 254 nm.

Circular Dichroism: Circular dichroism spectra were collected on a JASCO J-810 spectropolarimeter. Foldamer ampules were made up at concentrations of 250 μM in methanol. Spectra were recorded in a 1 mm path length quartz cuvette. Data were collected at a 1 nm interval, at a scan rate of 100 nm min-1, 1 nm bandwidth, and scans are the average of 8 scans. Data were normalised by subtracting a blank of the methanol without foldamer from the data. The ellipticity (deg) was then normalised to the concentration of the sample, the pathlength, and the number of amide bonds to return the mean residue ellipticity (MRE, deg cm^{2} dmol^{-1} res^{-1}.

5.2. Chapter 2

5.2.1. Synthesis of *trans* δ-amino acid precursor 60

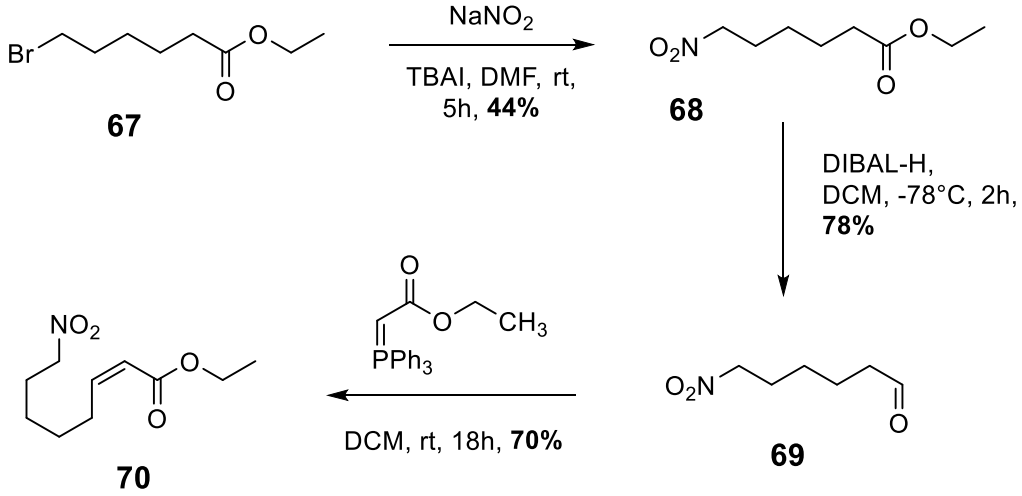

Ethyl 6-nitrohexanoate **68**

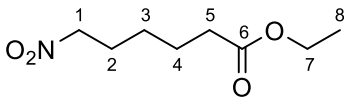

68

To a solution of ethyl 6-bromohexanoate **67** (5.00 g, 22.41 mmol) in DMF (200 mL) was added sodium nitrite (2.32 g, 33.62 mmol) and *tert*-butyl ammonium iodide (1.66 g, 4.48 mmol) and the reaction stirred for 5 hours. The reaction was then quenched by the addition of ice water (100 mL) and the mixture was extracted with diethyl ether (3 x 125 mL). The combined organic layers were washed with saturated aqueous LiCl solution (2 x 125 mL) and brine (1 x 125 mL), dried over $MgSO_4$ and concentrated *in vacuo*. The crude product was purified by column chromatography (40% diethyl ether in hexane) to give compound **68** as a pale yellow oil (44% yield, 1.87 g). ^{1}H NMR ($CDCl_3$, 400 MHz): δ 1.22 (3H, t, J = 7.5 Hz, H-8), 1.35-1.44 (2H, m, H-3),

1.60-1.70 (2H, m, H-4), 1.95-2.05 (2H, m, H-2), 2.29 (2H, t, J = 7.4 Hz, H-5), 4.09 (2H, q, J = 7.4 MHz, H-7), 4.36 (2H, t, J = 7.4 MHz, H-1). ^{13}C NMR ($CDCl_3$, 100 MHz): δ 14.3 (C-8), 24.2 (C-3), 25.8 (C-4), 27.1 (C-2), 33.9 (C-5), 60.5 (C-7), 75.5 (C-1), 173.3 (C-6).

6-Nitrobutanal **68**

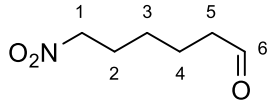

69

To a solution of ethyl 6-nitrohexanoate **68** (3.00 g, 15.86 mmol) in anhydrous dichloromethane (90 ml) at -78°C under nitrogen was added DIBAL-H (1M) in hexane (16.65 mL, 16.65 mmol) dropwise over 20 minutes. After 2 hours the reaction was quenched with 2M aqueous hydrochloric acid (75 mL) and water (100 mL), and the solution stirred for 5 hours. The aqueous phase was extracted with dichloromethane (3 x 60 mL), dried over $MgSO_4$, filtered and concentrated *in vacuo*. The crude product was purified by column chromatography (25% ethyl acetate in hexane) to give compound **69** as a colourless oil (75%, 1.73 g). ^{1}H NMR ($CDCl_3$, 400 MHz): δ 1.29-1.39 (2H, m, H-3), 1.55-1.64 (2H, m, H-4), 1.90-1.99 (2H, m, H-2), 2.38-2.44 (2H, td, J = 7.2 & 1.4 Hz, H-5), 4.30-4.35 (2H, t, J = 7.0 Hz, H-1), 9.66-9.99 (1H, t, J = 1.4 Hz, H-6). ^{13}C NMR ($CDCl_3$, 100 MHz): δ 21.1 (C-4), 25.7 (C-3), 27.0 (C-2), 43.3 (C-5), 75.3 (C-1), 202.0 (C-6).

Ethyl (*Z*)-8-nitrooct-2-enoate **70**

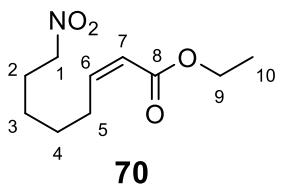

70

To a solution of 6-nitrobutanal **69** (1.75 g, 12.09 mmol) in anhydrous dichloromethane (50 mL) was added (carbethoxymethylene)triphenylphosphorane (5.06 g, 14.51 mmol) and the reaction left to stir at rt overnight. The reaction was then quenched with saturated aqueous

ammonium chloride (60 mL), and the aqueous layer extracted with dichloromethane (2 X 60 mL). The combined organic layers were washed with water, dried over $MgSO_4$, filtered and concentrated *in vacuo*. The crude product was purified by column chromatography (25% ethyl acetate in hexane) to give compound **70** as a yellow oil (70%, 1.82 g). ^{1}H NMR ($CDCl_3$, 400 MHz): δ 1.20-1.29 (3H, m, H-10), 1.32-1.55 (4H, m, H-3 & H-4), 1.93-2.04 (2H, m, H-2), 2.14-2.23 (2H, m, H-5), 4.10-4.18 (2H, m, H-9), 4.32-4.38 (2H, m, H-1), 5.78 (1H, dt, J = 14.8 & 2.5 Hz, H-7), 6.83-6.93 (1H, m, H-6). ^{13}C NMR ($CDCl_3$, 100 MHz): δ 14.2 (C-10), 25.7 (C-2), 27.1 (C-3), 27.3 (C-5), 31.7 (C-4), 60.2 (C-1), 75.1 (C-1), 121.8 (C-7), 148.2 (C-6), 166.5 (C-8).

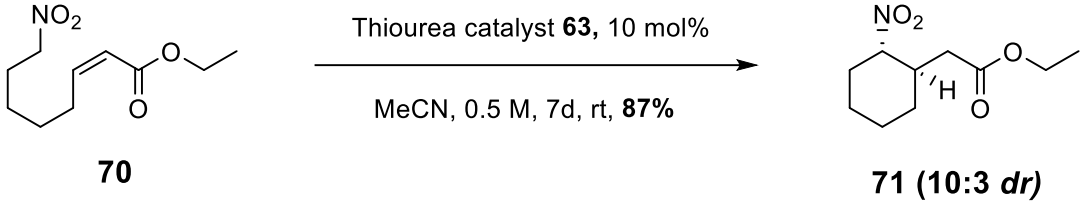

70 **71 (10:3 *dr*)**

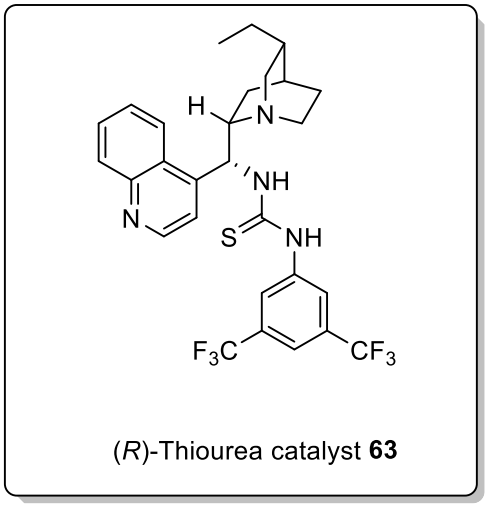

(*R*)-Thiourea catalyst **63**

Ethyl 2-((1*R*,2*S*)-2-nitrocyclohexyl)acetate **71**

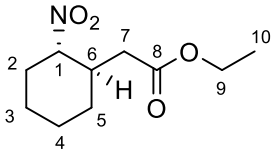

71

To a solution of Ethyl (*Z*)-8-nitrooct-2-enoate **70** (1.82 g, 8.47 mmol) in acetonitrile (2.8 mL) was added (*R*)-thiourea catalyst **63** (0.51 g, 0.85 mmol) and the reaction stirred for 7 days, after which the solution was concentrated *in vacuo*. The crude product was purified by column chromatography (30% diethyl ether in hexane) to give compound **71** as a pale yellow oil (87%, 1.59 g, 10:3 *dr*) ^{1}H NMR ($CDCl_3$, 400 MHz): δ 1.05-1.17 (1H, m, H-5), 1.17-1.22 (3H, t, J = 7.2 Hz, H-10), 1.25-1.34 (2H, m, H-4), 1.65-1.72 (1H, m, H-3), 1.79-1.86 (2H, m, H-3 & H-2), 1.88-1.95 (1H, m, H-5), 2.10-2.17 (1H, m, H-7), 2.18-2.25 (1H, m, H-2), 2.27-2.35 (2H, m, H-7 & H-6), 4.05-4.11 (2H, m, H-9), 4.26-4.36 (1H, td, J = 11.3 & 4.1 Hz, H-1, major *trans* isomer), 4.66-4.71 (minor *cis* isomer). ^{13}C NMR ($CDCl_3$, 100 MHz): δ 13.2 (C-10), 23.2 (C-3), 23.6 (C-4), 29.1 (C-5), 30.8 (C-2), 36.3 (C-7), 36.8 (C-6), 59.6 (C-9), 88.6 (C-1), 170.2 (C-8). IR (neat, cm^{-1}): 737, 856, 901, 975, 1026, 1225, 1290, 1369, 1450, 1543, 1732, 2860, 2940. $[\alpha]_D^{20}$ +19 (c = 0.1, dichloromethane).

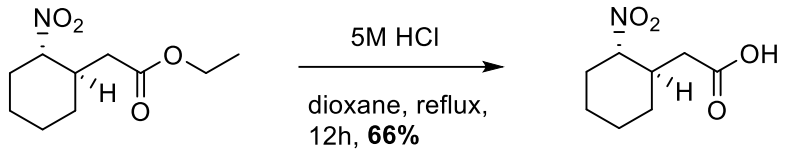

71 **72**

2-((1*R*,2*S*)-2-nitrocyclohexyl)acetic acid **72**

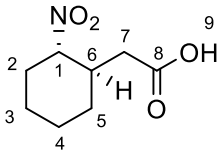

72

To a solution of the nitro ester **71** (0.200 g, 0.930 mmol) in dioxane (2.30 mL) was added 5M HCl (2.30 mL) and the reaction mixture heated under reflux and left to stir overnight. After cooling to rt, the reaction mixture was diluted with 5% aqueous sodium carbonate solution (30 mL) and washed with diethyl ether (3 x 18 mL). The aqueous layer was then acidified to pH 1 with concentrated HCl and extracted with dichloromethane (3 x 18 mL). The organic

layers were combined, dried over $MgSO_4$, filtered and concentrated *in vacuo*. The crude product was purified by column chromatography (50% ethyl acetate in hexane with 0.15% acetic acid additive) to give compound **72** as a pale yellow solid (66%, 0.115g). ^1H NMR ($CDCl_3$, 400 MHz): δ 1.11-1.25 (1H, m, H-5), 1.29-1.42 (2H, m, H-4), 1.68-1.79 (1H, m, H-3), 1.81-1.94 (2H, m, H-3 & H-2), 1.96-2.04 (1H, m, H-5), 2.18-2.30 (2H, m, H-2 & H-7), 2.36-2.46 (2H, m, H-6 & H-7), 4.35 (1H, td, J = 11.2 & 4.1, H-1, trans isomer), 10.39 (1H, s, H-9). ^{13}C NMR ($CDCl_3$, 100 MHz): δ 24.3 (C-3), 24.6 (C-4), 30.2 (C-5), 31.9 (C-2), 37.3 (C-7), 37.6 (C-6), 89.5 (C-1), 177.1 (C-8). IR (neat, cm^{-1}): 737, 900, 1110, 1183, 1246, 1294, 1374, 1412, 1450, 1541, 1705, 2860, 2938. $[\alpha]_D^{20}$ +43 (c = 0.1, dichloromethane). mp = 58.2 - 60.3°C. HRMS required for $C_8H_{13}NO_4$ $[M-H]^-$ 186.0771, found 186.0791.

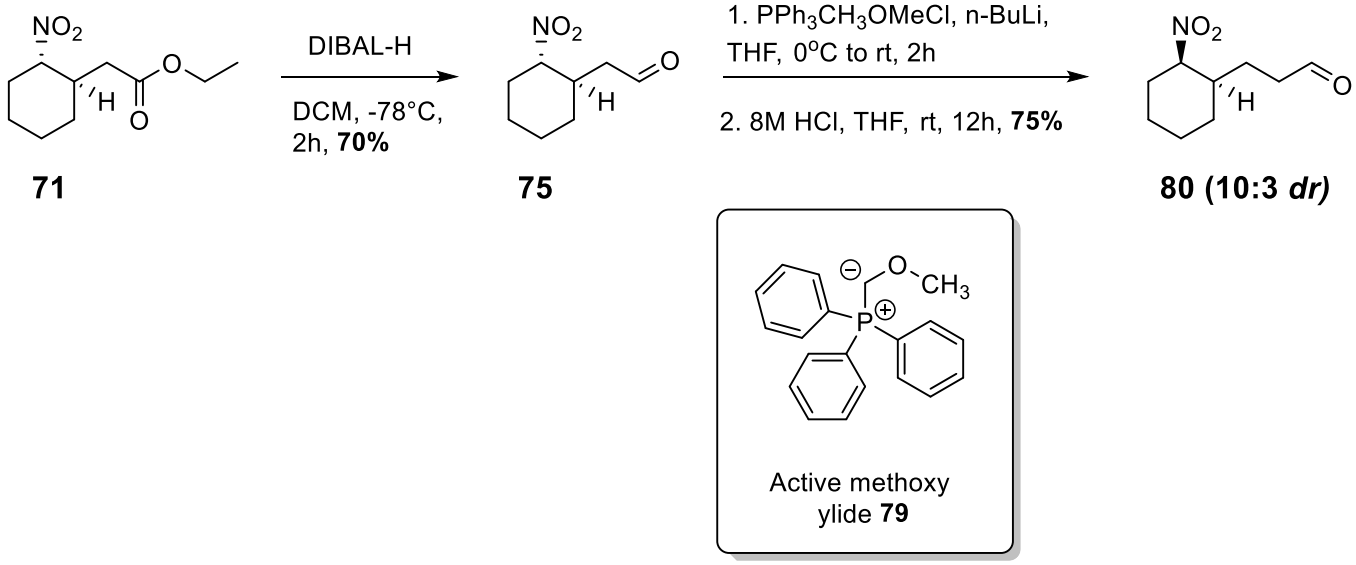

2-((1*R*,2*S*)-2-nitrocyclohexyl)acetaldehyde **75**

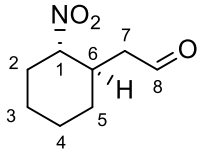

75

To a solution of the nitro ester **71** (2.00 g, 9.30 mmol) in anhydrous dichloromethane (64 mL) at -78°C under nitrogen was added DIBAL-H (1M) in hexane (9.75 mL, 9.75 mmol) dropwise

over 20 minutes. After 2 hours the reaction was quenched with 2M aqueous hydrochloric acid (50 mL) and water (75 mL), and the solution stirred for 2 hours. The aqueous phase was extracted with dichloromethane (3 x 40 mL) and the combined organic layers then dried over $MgSO_4$, filtered and concentrated *in vacuo*. The crude product was purified by column chromatography (20% ethyl acetate in hexane) to give compound **75** as a yellow oil (70%, 1.11 g). ^{1}H NMR ($CDCl_3$, 400 MHz): δ 1.02-1.14 (1H, m, H-5), 1.22-1.34 (2H, m, H-4), 1.60-1.70 (1H, m, H-3), 1.77-1.90 (3H, m, H23, H-3 & H-5), 2.14-2.22 (1H, m, H-2), 2.24-2.34 (1H, m, H-7), 2.37-2.50 (2H, m, H-6 & H-7), 4.25 (1H, H-1, td, J = 11.2 & 4.0 Hz, major *trans* isomer), 4.62 (minor *cis* isomer), 9.61 (1H, dd, J = 1.9 & 1.0 Hz, H-8, major *trans* isomer), 9.64 (minor *cis* isomer). ^{13}C NMR ($CDCl_3$, 100 MHz): δ 24.1 (C-3), 24.5 (C-4), 30.5 (C-5), 31.7 (C-2), 35.7 (C-6), 46.4 (C-7), 89.6 (C-1), 198.8 (C-8). IR (neat, cm^{-1}): 736, 899, 1128, 1246, 1298, 1376, 1450, 1541, 1720, 2730, 2860, 2935. $[\alpha]_D^{20}$ +32 (c = 0.1, dichloromethane). HRMS required for $C_8H_{13}NO_3$ $[M+H]^+$ 173.0968, found 173.0990.

3-((1*R*,2*R*)-2-nitrocyclohexyl)propanal **80**

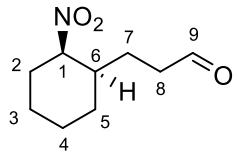

80

A suspension of (methoxymethyl)triphenylphosphonium chloride (5.55 g, 15.23 mmol) in dry THF (26 mL) under nitrogen was cooled to 0°C and treated with *n*-BuLi (2.5M) in hexane (5.41 mL, 13.53 mmol). The reaction was stirred for 30 minutes, after which a solution the nitro aldehyde **75** (1.16 g, 6.78 mmol) in dry THF (2 mL) was added and the reaction mixture allowed to warm to rt and then left to stir for 5 hours. The reaction was then quenched with saturated ammonium chloride solution (30 mL) and the aqueous phase extracted with dichloromethane (3 x 75 mL). The combined organic layers were then washed with saturated aqueous sodium bicarbonate solution (1 x 75 mL) and brine (1 x 75 mL), dried over $MgSO_4$, filtered and concentrated *in vacuo.* The crude product was then taken up in THF (27 mL) and 8M HCl (2.75

mL) added dropwise over 2 minutes. The reaction was allowed to stir overnight, after which the reaction mixture was diluted with water (30 mL) and extracted with ethyl acetate (3 x 50 mL). The combined organic layers were washed with brine (1 x 50 mL), dried over $MgSO_4$, filtered and concentrated *in vacuo*. The crude product was purified by column chromatography (10% ethyl acetate in hexane) to give compound **80** as a yellow oil (75%, 0.94 g, 10:3 *dr*). ^{1}H NMR ($CDCl_3$, 400 MHz): δ 1.27-1.40 (2H, m, H-3 & H-4), 1.47-1.60 (3H, m, H-4, H-5 & H-7), 1.67-1.86 (4H, m, H-2, H-3, H-4 & H-5), 1.96-2.02 (1H, m, H-6), 2.03-2.11 (1H, m, H-2), 2.43 (2H, tdd, J = 8.1, 2.7 & 1.4 Hz, H-8), 4.13-4.20 (minor *trans* isomer), 4.53-4.59 (1H, m, H-1, major *cis* isomer), 9.65-9.67 (minor *trans* isomer), 9.67-9.69 (1H, t, J = 1.4 Hz, H-9 major *cis* isomer). ^{13}C NMR ($CDCl_3$, 100 MHz): δ 21.6 (C-7), 21.8 (C-3), 22.1 (C-4), 26.8 (C-5), 27.2 (C-2), 38.2 (C-6), 46.4 (C-7), 89.6 (C-1), 199.8 (C-9). IR (neat, cm^{-1}): 1377, 1450, 1541, 1721, 2725, 2860, 2934. $[\alpha]_D^{20}$ +39 (c = 0.1, dichloromethane). HRMS required for $C_9H_{15}NO_3$ $[M+Na]^+$ 208.0944, found 208.0931.

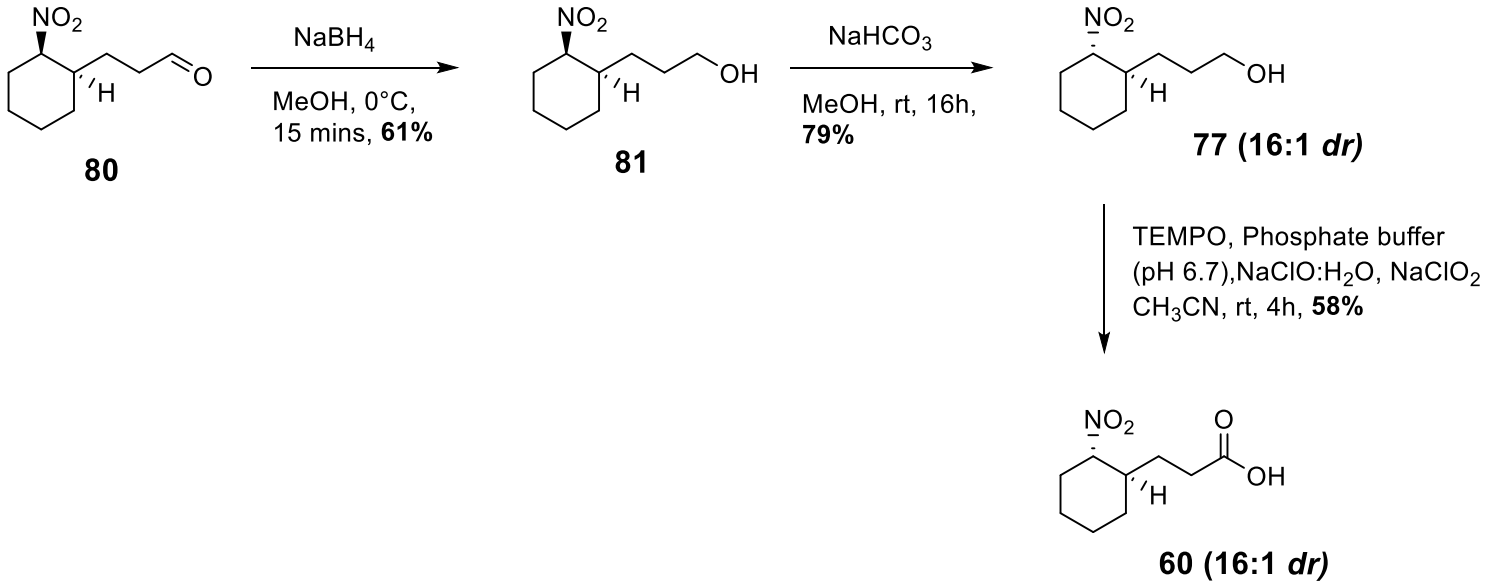

3-((1*R*,2*R*)-2-nitrocyclohexyl)propan-1-ol **81**

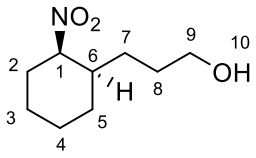

81

To a solution of the nitro aldehyde **80** (0.200 g, 1.080 mmol) in anhydrous MeOH (10 mL) at 0°C was added $NaBH_4$ (0.068 g, 1.819 mmol) and the reaction stirred for 15 minutes. A saturated aqueous solution of ammonium chloride (10 mL) was then added and the aqueous layer extracted with dichloromethane (3 x 15 mL). The combined organic layers were then dried over $MgSO_4$, filtered and concentrated *in vacuo*. The crude product was purified by column chromatography (50% ethyl acetate in hexane) to give compound **81** as a colourless oil (61%, 0.123 g, 10:1 *dr*). ^{1}H NMR ($CDCl_3$, 400 MHz): δ 1.21-1.29 (1H, m, H-7), 1.32-1.46 (3H, m, H-4 & H-7), 1.47-1.67 (4H, m, H-3, H-5 & H-8), 1.75-1.87 (4H, m, H-2, H-3, H-5, H-10), 2.01-2.15 (2H, m, H-2 & H-6), 3.55-3.62 (2H, m, H-9), 4.57-4.63 (1H, m, H-1). ^{13}C NMR ($CDCl_3$, 100 MHz): δ 22.1 (C-3), 22.2 (C-4), 25.3 (C-7), 27.1 (C-5), 27.3 (C-2), 30.2 (C-8), 38.8 (C-6), 62.7 (C-1), 86.5 (C-1). IR (neat, cm^{-1}): 735, 760, 1059, 1375, 1449, 1537, 2862, 2936, 3350. $[\alpha]_D^{20}$ +10 (c = 0.1, dichloromethane). HRMS required for $C_9H_{17}NO_3$ $[M+Na]^+$ 210.1101, found 210.1109.

3-((1*R*,2*S*)-2-nitrocyclohexyl)propan-1-ol **77**

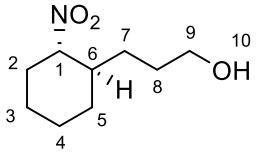

77

To a solution of the nitro alcohol **81** (0.123 g, 0.657 mmol) in MeOH (2.5 mL) was added sodium bicarbonate (0.56 g) and the reaction stirred overnight. The reaction mixture was then

diluted with water (2.5 mL) and extracted with dichloromethane (3 x 5 mL). The combined organic layers were then dried over $MgSO_4$, filtered and concentrated *in vacuo*. The crude product was purified by column chromatography (50% ethyl acetate in hexane) to give compound **77** as a colourless oil (79%, 0.098 g, 16:1 *dr*). ^{1}H NMR ($CDCl_3$, 400 MHz): δ 0.88-1.02 (1H, m, H-7), 1.10-1.20 (1H, m, H-3), 1.22-1.43 (4H, m, H-3, H-5 H-7 & H-8), 1.53-1.62 (1H, m, H-8), 1.65-1.72 (1H, m, H-4), 1.76-1.95 (4H, m, H-2, H-4, H-5 & H-6), 2.08-2.21 (1H, m, H-2), 2.48 (1H, s, H-10), 3.49 (2H, td, J = 6.5 & 2.9 Hz, H-9), 4.16 (1H, td, J = 11.1 & 4.0 Hz, H-1). ^{13}C NMR ($CDCl_3$, 100 MHz): δ 24.3 (C-3), 24.7 (C-4), 28.7 (C-7), 28.9 (C-5), 29.6 (C-2), 32.0 (C-8), 40.5 (C-6), 62.4 (C-9), 91.3 (C-1). IR (neat, cm^{-1}): 520, 735, 899, 1013, 1055, 1246, 1371, 1450, 1541, 2862, 2938. $[\alpha]_D^{20}$ +24 (c = 0.1, dichloromethane). HRMS required for $C_9H_{17}NO_3$ [M+Na]+ 210.1101, found 210.1102.

3-((1*R*,2*S*)-2-nitrocyclohexyl)propanoic acid **60**

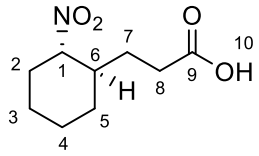

60

To a solution of the nitro alcohol **77** (0.098 g, 0.524 mmol) and TEMPO (0.008 g, 0.052 mmol) in CH_3CN (2.80 mL) was added a 0.67M sodium phosphate buffer (2.80 mL). Then, a solution of sodium chlorite (0.094 g, 1.039 mmol) in water (0.19 mL) and a 1:1 solution of 12.5% sodium hypochlorite and water (0.28 mL) was added simultaneously over 20 minutes. The reaction was stirred at rt for 4 hours, after which water was added (4 mL). The pH was adjusted to 10.0 by the addition of sodium hydroxide, and the aqueous phase washed with diethyl ether (2 x 5 mL). The pH was then adjusted to 3.0 by the addition of concentrated HCl, and the aqueous phase extracted with dichloromethane (3 x 10 mL). The combined organic layers were washed with water (1 x 10 mL), dried over $MgSO_4$, filtered and concentrated *in vacuo*. The crude product was purified by column chromatography (50% ethyl acetate in hexane with 0.15% acetic acid additive) to give compound **60** as an off-white solid (58%, 0.061

g, 16:1 *dr*). ^{1}H NMR ($CDCl_3$, 400 MHz): δ 1.00 (1H, m, qd, J = 12.7 & 6.2 Hz, H-7), 1.25-1.34 (2H, m, H-4), 1.41-1.50 (1H, m, H-5), 1.66-1.76 (2H, m, H-3 & H-5), 1.81-1.89 (2H, m, H-3 & H-8), 1.90-2.00 (2H, m, H-6 & H-7), 2.18-2.24 (1H, m, H-8), 2.28-2.46 (2H, m, H-2), 4.20 (1H, td, J = 11.0 & 4.0 Hz, H-1 major *trans* isomer), 4.59-4.63 (minor *cis* isomer), 9.80-10.40 (1H, s, H-10). ^{13}C NMR ($CDCl_3$, 100 MHz): δ 24.3 (C-3), 24.7 (C-4), 27.4 (C-5), 29.4 (C-7), 30.8 (C-2), 32.0 (C-8), 40.1 (C-6), 91.0 (C-1), 179.5 (C-9). IR (neat, cm^{-1}): 505, 735, 901, 938, 1225, 1285, 1308, 1368, 1450, 1541, 1697, 2860, 2933. $[\alpha]_D^{20}$ +39 (c = 0.1, dichloromethane). mp = 70.8-71.9 °C. HRMS required for $C_9H_{15}NO_4$ [M+Na]+ 233.0993, found 233.1005.

5.2.2. Synthesis of *cis* δ-amino acid 61

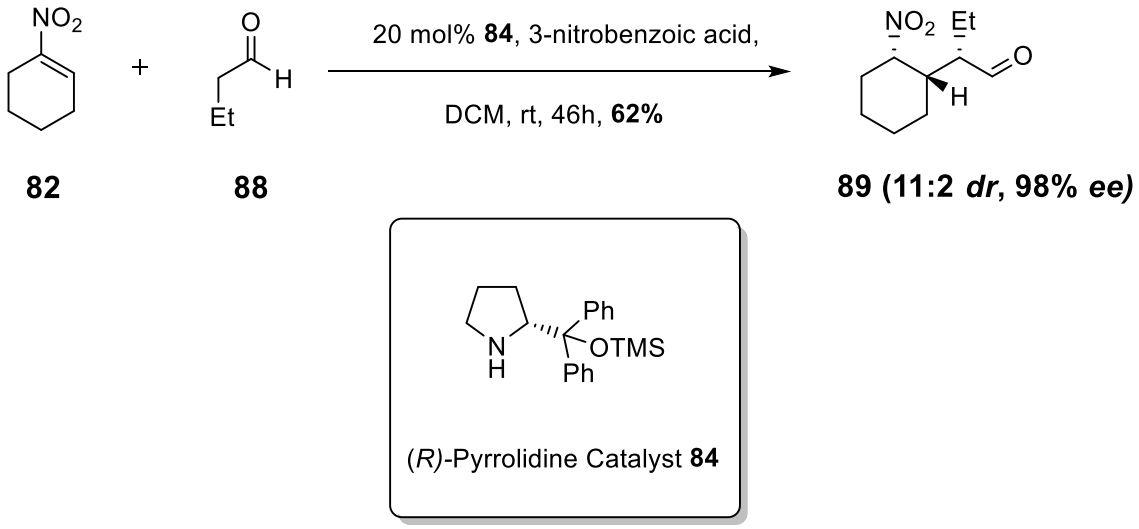

(*S*)-2-((1*S*,2*S*)-2-nitrocyclohexyl)butanal **89**

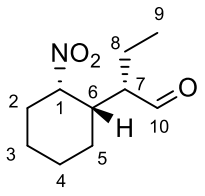

89

To a solution of (*R*)-pyrrolidine catalyst **84** (1.28 g, 4.12 mmol) in dichloromethane (20 mL) was added 3-nitrobenzoic acid (0.33 g, 1.96 mmol) and butanal **88** (7.08 g, 98.15 mmol) and the resultant mixture stirred at rt for 2 minutes. Then, 1-nitrocyclohexene **82** (2.50 g, 19.66 mmol) was added and the reaction stirred for 46 hours. The reaction mixture was then concentrated *in vacuo* and the crude product purified by column chromatography (10% ethyl acetate in hexane) to give compound **89** as a light orange oil (62%, 2.42 g, 11:2 *dr*, 98% *ee*). ^{1}H NMR ($CDCl_3$, 400 MHz): δ 0.77 (3H, t, J = 7.5 Hz, H-9 major *cis* isomer), 0.87 (3H, t, J = 7.4 Hz, minor *trans* isomer), 1.22-1.28 (1H, m, H-5), 1.48-1.52 (1H, m, H-3), 1.54-1.62 (3H, m, H-4 & H-8), 1.64-1.72 (3H, m, H-3, H-4 & H-2), 1.77-1.83 (1H, m, H-5), 2.02 (1H, m, H-6), 2.17-2.23 (1H, m, H-2), 2.38-2.45 (1H, m, H-7), 4.38-4.46 (minor *trans* isomer), 4.79 (1H, dd, J = 6.9 & 3.5 Hz, H-1), 9.50 (minor *trans* isomer), 9.59 (1H, d, J = 1.9 Hz, H-10). ^{13}C NMR ($CDCl_3$, 100 MHz): δ 9.9 (C-9), 19.2 (C-4), 20.1 (C-3), 23.2 (C-8), 24.8 (C-5), 29.6 (C-2), 37.3 (C-6), 53.1 (C-7), 83.5 (C-1), 203.5 (C-10). IR (neat, cm^{-1}): 735, 776, 829, 978, 1244, 1358, 1448, 1541, 1717, 2865, 2938. $[\alpha]_D^{20}$ -36 (c = 0.1, dichloromethane). HRMS required for $C_{10}H_{17}NO_3$ $[M+H]^+$ 200.1281, found 200.1277.

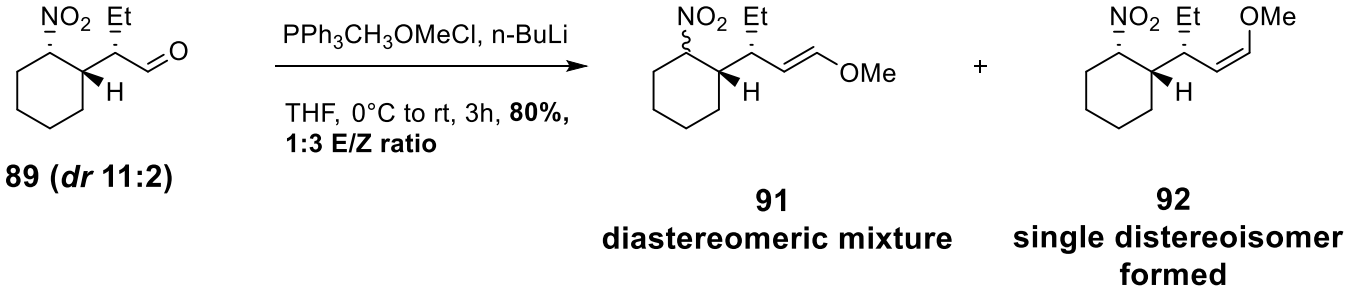

89 (*dr* 11:2)

91
diastereomeric mixture

92
single distereoisomer formed

(1*S*,2*S*)-1-((*S*,*Z*)-1-methoxypent-1-en-3-yl)-2-nitrocyclohexane **92**

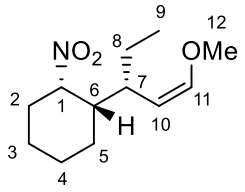

92

A suspension of (methoxymethyl)triphenylphosphonium chloride (11.41 g, 31.31 mmol) in dry THF (50 mL) under nitrogen was cooled to 0˚C and treated with *n*-BuLi (2.5M) in hexane (11.83 mL, 29.58 mmol). The reaction was stirred for 30 minutes, after which a solution of the nitro aldehyde **89** (2.95 g, 14.80 mmol) in dry THF (5 mL) was added and the reaction mixture allowed to warm to rt and then left to stir for 3 hours. The reaction was then quenched with saturated ammonium chloride solution (60 mL) and the aqueous phase extracted with dichloromethane (3 x 125 mL). The combined organic layers were then washed with saturated aqueous sodium bicarbonate solution (1 x 125 mL) and brine (1 x 125 mL), dried over $MgSO_4$, filtered and concentrated *in vacuo.* The crude product was purified by column chromatography (10% ethyl acetate in hexane) to give compound **91** (0.67 g, pale yellow oil) as a diastereomeric mixture, and compound **92** (2.02 g, colourless oil) as a single diastereoisomer (80% yield for both products). **92** data: ^{1}H NMR ($CDCl_3$, 400 MHz): δ 0.81 (3H, t, J = 7.4 Hz, H-9), 1.04-1.13 (1H, m, H-8), 1.25-1.34 (1H, m, H-5), 1.40-1.46 (1H, m, H-6), 1.51-1.59 (2H, m, H-3), 1.66-1.80 (3H, m, H-2, H-4 & H-8), 1.82-1.90 (3H, m, H-4, H-5 & H-6), 2.26-2.33 (1H, m, H-2), 3.49 (3H, s, H-12), 4.33 (1H, dd, J = 12.5 & 10.4 Hz, H-10), 4.81 (1H, q, J = 7.4 Hz, H-1), 6.11 (1H, d, J = 12.5 Hz, H-11). ^{13}C NMR ($CDCl_3$, 100 MHz): δ 11.5 (C-9), 20.6 (C-3), 24.3 (C-4), 25.3 (C-5), 25.8 (C-8), 31.3 (C-2), 42.0 (C-7), 44.0 (C-6), 56.5 (C-12), 84.8 (C-10), 104.1 (C-1), 148.9 (C-11). IR (neat, cm^{-1}): 631, 740, 781, 831, 939, 1157, 1207, 1244, 1356, 1448, 1541, 1651, 2868, 2933. $[\alpha]_D^{20}$ +14 (c = 0.1, dichloromethane). HRMS required for $C_{12}H_{21}NO_3$ $[M+H]^+$ 228.1594, found 228.1635.

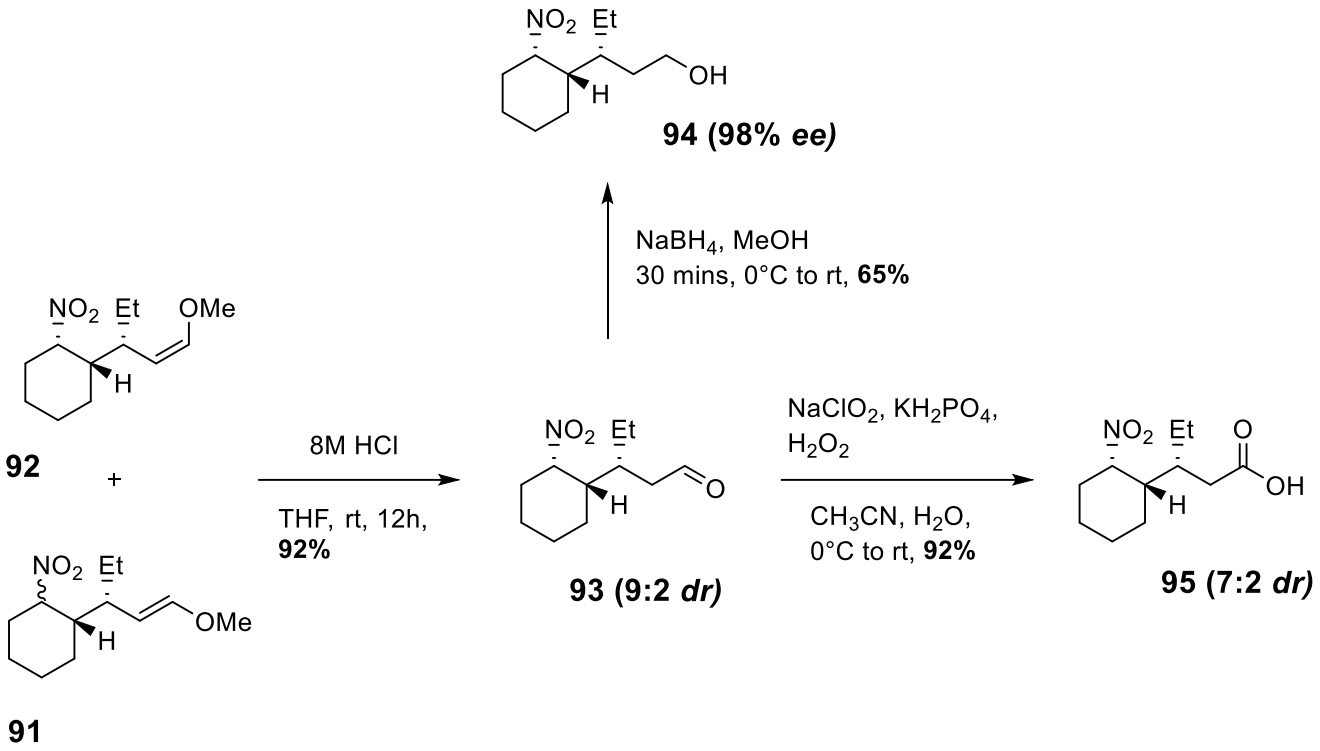

(*R*)-3-((1*S*,2*S*)-2-nitrocyclohexyl)pentanal **93**

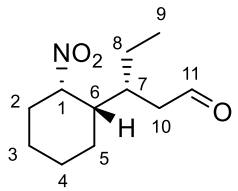

93

To a solution of the combined E/Z nitro methoxy compounds **91** and **92** (3.00 g, 13.21 mmol) in THF (60 mL) was added 8M HCl (4.25 mL) dropwise over 2 minutes. The reaction was stirred overnight, after which the reaction mixture was diluted with water (50 mL) and extracted with ethyl acetate (3 x 100 mL). The combined organic layers were washed with brine (1 x 100 mL), dried over $MgSO_4$, filtered and concentrated *in vacuo*. The crude product was purified by column chromatography (15% ethyl acetate in hexane) to give compound **93** as a pale yellow oil (92%, 2.59 g, 9:2 *dr*). ^{1}H NMR ($CDCl_3$, 400 MHz): δ 0.71 (3H, t, J = 7.5 Hz, H-9), 0.76 (3H, t, J = 7.4 Hz, minor *trans* isomer), 1.11-1.20 (1H, m, H-8), 1.23-1.39 (2H, m, H-5), 1.42-1.49 (1H,

m, H-3), 1.52-1.64 (5H, m, H-2, H-3, H-4 & H-6), 1.72-1.78 (1H, m, H-8), 1.82-1.90 (1H, m, H-7), 2.10-2.16 (1H, m, H-2), 2.24 (1H, ddd, J = 16.9, 7.5 & 2.7 Hz, H-10), 2.43 (1H, ddd, J = 16.9, 4.7 & 0.9 Hz, H-10), 4.35-4.43 (minor *trans* isomer), 4.72-4.75 (1H, m, H-1), 9.52-9.54 (minor *trans* isomer), 9.57 (1H, dd, J = 2.6 & 1.1 Hz, H-11). ^{13}C NMR ($CDCl_3$, 100 MHz): δ 10.1 (C-9), 19.9 (C-3), 23.1 (C-5), 23.4 (C-4), 25.1 (C-8), 30.3 (C-2), 35.9 (C-7), 41.8 (C-6), 44.2 (C-10), 83.7 (C-1), 202.0 (C-11). IR (neat, cm^{-1}): 735, 830, 1150, 1246, 1337, 1358, 1450, 1541, 1721, 2723, 2868, 2937. $[\alpha]_D^{20}$ +9 (c = 0.1, dichloromethane). HRMS required for $C_{11}H_{19}NO_3$ 188.1281, found 188.1264.

(*R*)-3-((1*S*,2*S*)-2-nitrocyclohexyl)pentan-1-ol **94**

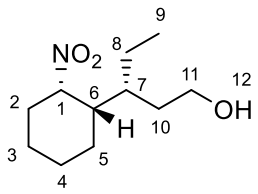

94

To a solution of the nitro aldehyde **93** (0.176 g, 0.826 mmol) in anhydrous MeOH (9 mL) at 0°C was added $NaBH_4$ (0.061 g, 1.60 mmol) and the reaction stirred for 30 minutes. A saturated aqueous solution of ammonium chloride (10 mL) was then added and the aqueous layer extracted with dichloromethane (3 x 15 mL). The combined organic layers were then dried over $MgSO_4$, filtered and concentrated *in vacuo*. The crude product was purified by column chromatography (40% ethyl acetate in hexane) to give compound **94** as a colourless oil (65%, 0.116 g, 98% *ee*). ^{1}H NMR ($CDCl_3$, 400 MHz): δ 0.81 (3H, t, J = 7.4 Hz), 1.20-1.30 (1H, m, H-4), 1.32-1.46 (2H, m, H-8), 1.46-1.52 (2H, m, H-7 & H-10), 1.54-1.62 (3H, m, H-6, H-8, H-12), 1.64-1.80 (5H, m, H-2, H-5, H-8 & H-10), 1.85-1.92 (1H, m, H-4), 2.22-2.31 (1H, m, H-2), 3.54-3.70 (2H, m, H-11), 4.91-4.96 (1H, m, H-1). ^{13}C NMR ($CDCl_3$, 100 MHz): δ 9.6 (C-9), 20.2 (C-3), 21.8 (C-8), 23.6 (C-5), 25.5 (C-4), 30.9 (C-2), 32.4 (C-10), 37.2 (C-7), 42.1 (C-6), 60.9 (C-11), 84.2 (C-1). IR (neat, cm^{-1}): 827, 1044, 1246, 1358, 1446, 1539, 2872, 2936. $[\alpha]_D^{20}$ +75 (c = 0.1, dichloromethane). HRMS required for $C_{11}H_{21}NO_3$ $[M+H]^+$ 216.1594, found 216.1582. HPLC analysis: Chiralpack AD-H, 7.5% isopropanol in hexane, flow rate = 1.0 mL/min, λ = 280 nm.

3-(2-nitrocyclohexyl)pentan-1-ol **94-rac**

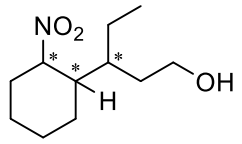

94-rac

The production of the racemic product **94-rac** was achieved by following the same synthetic route as for **94**, but with an equal amount of (*R*)- and (*S*)-thiourea catalyst used in the first organocatalytic step. All other reagents/quantities/conditions for the remaining synthetic steps were the same.

(*R*)-3-((1*S*,2*S*)-2-nitrocyclohexyl)pentanoic acid **95**

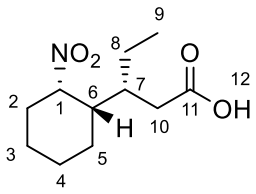

95

To a solution of the nitro aldehyde **93** (1.02 g, 4.80 mmol) in CH_3CN (25 mL) at 0°C was added a solution of KH_2PO_4 (0.50 g, 3.65 mmol) in water (12.50 mL) and H_2O_2 (30%, 0.65 mL) and left to stir rigorously for 2 minutes. A solution of sodium chlorite (1.24 g, 13.73 mmol) in water (24.82 mL) was then added and the reaction mixture stirred for 3 hours whilst warming to rt. The reaction was then quenched with saturated aqueous $Na_2S_2O_3$ solution (25 mL) and acidified to pH 2 with concentrated HCl. The aqueous phase was extracted with dichloromethane (3 x 40 mL) and the combined organic layers were then dried over $MgSO_4$, filtered and concentrated *in vacuo*. The crude product was purified by column chromatography (50% ethyl acetate in hexane with 0.15% acetic acid additive) to give compound **95** as a yellow oil (92%, 1.10 g, 7:2 *dr*). ^1H NMR ($CDCl_3$, 400 MHz): δ 0.87 (3H, t, J =

7.4 Hz, H-9), 1.27-1.36 (2H, m, H-3 & H-5), 1.50-1.62 (2H, m, H-3 & H-8), 1.65-1.76 (5H, m, H-3, H-5, H-6 & H-7), 1.81-1.89 (2H, m, H-4 & H-7), 2.24-2.31 (1H, m, H-2), 2.37 (1H, dd, J = 15.8 & 6.6 Hz, H-10), 2.48 (1H, dd, J = 15.8 & 5.2 Hz, H-10), 4.43-4.53 (minor *trans* isomer), 4.89-4.95 (1H, m, H-1), 10.37 (1H, s, H-12). ^{13}C NMR ($CDCl_3$, 100 MHz): δ 10.7 (C-9), 20.1 (C-3), 23.0 (C-8), 23.4 (C-5), 25.4 (C-4), 30.7 (C-2), 34.6 (C-10), 38.2 (C-7), 42.0 (C-6), 84.2 (C-1), 179.5 (C-11). IR (neat, cm^{-1}): 733, 830, 923, 1246, 1285, 1360, 1414, 1447, 1541, 1703, 2867, 2936. $[\alpha]_D^{20}$ +2 (c = 0.1, dichloromethane). HRMS found for $C_{11}H_{19}O_4$ $[M-H]^-$ 228.1241, found 228.1166.

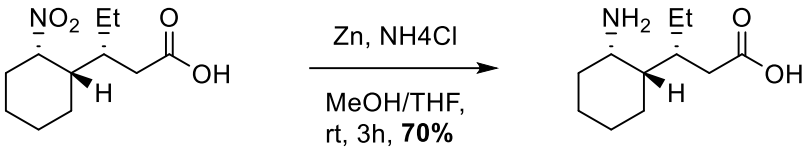

95 **97**

(*R*)-3-((1*S*,2*S*)-2-aminocyclohexyl)pentanoic acid (ACPA) **97**

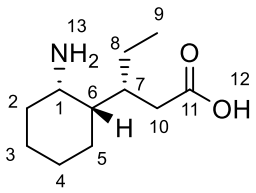

97

To a solution of the nitro ester **95** (0.426 g, 1.859 mmol) in MeOH (35 mL) and THF (35 mL) was added zinc powder (1.72 g, 26.30 mmol) and ammonium chloride (1.405 g, 26.30 mmol) and the reaction stirred for 3 hours. The reaction mixture was then diluted with ethyl acetate (15 mL), filtered over celite and concentrated *in vacuo.* . The crude product was purified by column chromatography (40% methanol in ethyl acetate with 0.20% acetic acid additive) to give compound **97** as a white solid (70%, 0.259 g). ^{1}H NMR (CD_3OD, 400 MHz): δ 0.89 (3H, m, H-9), 1.24-1.43 (4H, m, H-3, H-4 & H-8), 1.47-1.53 (1H, m, H-6), 1.57-1.74 (4H, m, H-2, H-3, H-5 & H-7), 1.80-1.90 (2H, m, H-4 & H-5), 1.99-2.07 (1H, m, H-2), 2.22-2.38 (2H, m, H-10), 3.55

(1H, d, J = 2.1 Hz, H-1). ^{13}C NMR ($CDCl_3$, 100 MHz): δ 9.8 (C-9), 14.3 (C-3), 20.3 (C-4), 24.9 (C-8), 26.3 (C-5), 30.8 (C-2), 38.6 (C-7), 41.2 (C-10), 43.7 (C-6), 49.8 (C-1), 183.2 (C-11). IR (neat, cm^{-1}): 982, 1063, 1399, 1501, 1550, 1651, 2926, 3220. $[\alpha]_D^{20}$ +18 (c = 0.1, MeOH). HRMS found for $C_{11}H_{21}NO_2$ $[M+H]^+$ 200.1645, found 200.1667.

5.2.3. Synthesis of α/δ foldamers

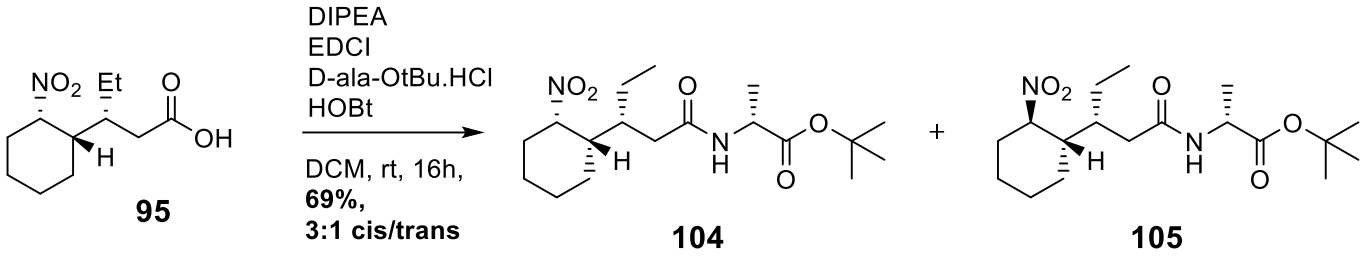

Tert-butyl ((*R*)-3-((1*S*,2*S*)-2-aminocyclohexyl)pentanoyl)-D-alaninate **104**

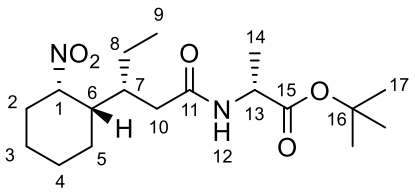

104

To a solution of the nitro acid **95** (1.00 g, 4.362 mmol) in dichloromethane (42 mL), DIPEA (0.911 mL, 5.234 mmol), $HOBt.H_2O$ (0.802 g, 5.234 mmol) and EDCI (0.926 mL, 5.234 mmol) were added and the reaction mixture stirred for 5 minutes. D-Ala tert-butyl ester hydrochloride (0.951 g, 5.234 mmol) was then added and the reaction stirred for 16 hours. The reaction mixture was then diluted with excess ethyl acetate and washed with aqueous 10% citric acid (50 mL), aqueous saturated sodium bicarbonate (50 mL) and brine (50 mL). The organic layer was dried over $MgSO_4$, filtered and concentrated *in vacuo*. The crude

product was purified by column chromatography (25% ethyl acetate in hexane) to give compound **104** as a white foam (51%, 0.804 g) and compound **105** as a white solid (17%, 0.268 g). 3:1 *cis/trans* ratio, 69% yield for both diastereoisomers. **104** data: ^{1}H NMR ($CDCl_3$, 400 MHz): δ 0.80 (3H, t, J = 7.4 Hz, H-9), 1.19-1.30 (5H, m, H-4, H-8 & H-14), 1.38 (9H, s, H-17), 1.41-1.54 (2H, m, H-3 & H-8), 1.55-1.72 (4H, m, H-2, H-3 & H-5), 1.74-1.85 (3H, m, H-4, H-6 & H-7), 2.09-2.27 (3H, m, H-2 & H-10), 4.35 (1H, qu, J = 7.2 Hz, H-13), 4.90-4.94 (1H, m, H-1), 6.16 (1H, d, J = 7.4 Hz, H-12). ^{13}C NMR ($CDCl_3$, 100 MHz): δ 10.8 (C-9), 18.4 (C-14), 20.1 (C-3), 22.8 (C-8), 23.3 (C-5), 25.3 (C-4), 27.9 (C-17), 30.5 (C-2), 36.4 (C-10), 38.9 (C-7), 41.8 (C-6), 48.5 (C-13), 81.8 (C-16), 84.3 (C-1), 171.4 (C-11), 172.2 (C-15). IR (neat, cm^{-1}): 849, 1051, 1148, 1225, 1368, 1449, 1541, 1643, 1734, 2873, 2936, 3309. $[\alpha]_D^{20}$ +39 (c = 0.1, dichloromethane). mp = 74.0-75.2°C. HRMS required for $C_{18}H_{32}N_2O_5$ $[M+Na]^+$ 379.2203, found 379.2090.

Tert-butyl ((*R*)-3-((1*S*,2*R*)-2-nitrocyclohexyl)pentanoyl)-D-alaninate **105**

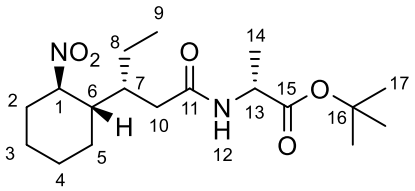

105

^{1}H NMR ($CDCl_3$, 400 MHz): δ 0.89 (3H, t, J = 7.3 Hz, H-9), 1.01-1.12 (2H, m, H-4 & H-8), 1.24-1.31 (2H, m, H-5), 1.36 (3H, d, J = 7.1 Hz, H-14), 1.44-1.46 (9H, s, H-17), 1.46-1.50 (1H, m, H-8), 1.54-1.61 (1H, m, H-7), 1.72-1.77 (1H, m, H-4), 1.79-1.87 (3H, m, H-2 & H-3), 2.01-2.12 (2H, m, H-6 & H-10), 2.18-2.24 (1H, m, H-2), 2.34 (1H, dd, J = 14.3 & 5.5 Hz, H-10), 4.41-4.52 (2H, m, H-1 & H-13), 6.00 (1H, d, J = 7.2 Hz, H-12). ^{13}C NMR ($CDCl_3$, 100 MHz): δ 12.7 (C-9), 18.6 (C-14), 22.4 (C-8), 24.6 (C-3), 24.6 (C-5), 25.0 (C-4), 28.1 (C-17), 32.4 C-2), 38.4 (C-10), 38.5 (C-7), 43.4 (C-6), 48.6 (C-13), 82.1 (C-16), 88.5 (C-1), 171.1 (C-11), 172.6 (C-15). IR (neat, cm^{-1}): 629, 735, 845, 1146, 1223, 1366, 1454, 1545, 1636, 1728, 2868, 2935, 3283. $[\alpha]_D^{20}$ -22 (c = 0.1, dichloromethane). mp = 87.1-89.2°C. HRMS required for $C_{18}H_{32}N_2O_5$ $[M+H]^+$ 357.2384, found 357.2315.

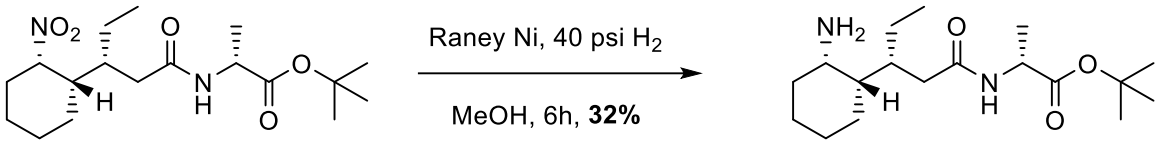

104 **106**

Tert-butyl ((*R*)-3-((1*S*,2*S*)-2-aminocyclohexyl)pentanoyl)-D-alaninate **106**

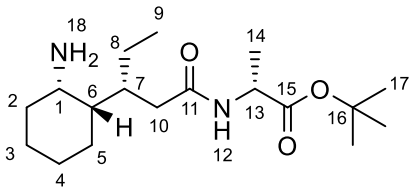

106

To a solution of the dipeptide **104** (0.400 g, 1.122 mmol) in MeOH (50 mL) was added Raney Nickel (0.800 g). The flask was attached to a parr apparatus and the reaction stirred for 6 hours at a H_2 pressure of 40 psi. After TLC analysis indicated reaction completion, the reaction mixture was filtered through celite and concentrated *in vacuo.* The crude product was purified by column chromatography (60% dichloromethane in methanol with 0.15% triethylamine additive) to give compound **106** as a white solid (32%, 0.117 g). ^{1}H NMR ($CDCl_3$, 400 MHz): δ 0.82 (3H, t, J = 7.4 Hz, H-9), 1.13-1.25 (2H, m, H-4 & H-5), 1.25-1.31 (1H, m, H-6), 1.31-1.35 (3H, d, J = 7.2 Hz, H-14), 1.35-1.41 (1H, m, H-8), 1.43-1.52 (13H, m, H-2, H-3, H-8 & H-17), 1.58-1.63 (1H, m, H-5), 1.68-1.77 (2H, m, H-2 & H-4), 1.81-1.88 (1H, m, H-7), 1.90-2.30 (2H, s, H-18), 2.03 (1H, dd, J = 14.5 & 7.9 Hz, H-10), 2.41 (1H, dd, J = 14.5 & 4.5 Hz, H-10), 3.18 (1H, s, H-1), 4.43 (1H, qu, J = 7.1 Hz, H-13), 7.12 (1H, s, H-12). ^{13}C NMR ($CDCl_3$, 100 MHz): δ 9.4 (C-9), 18.6 (C-14), 19.6 (C-3), 23.5 (C-8), 23.8 (C-5), 26.4 (C-4), 28.1 (C-17), 34.8 (C-2), 37.7 (C-7), 38.0 (C-10), 42.8 (C-6), 47.1 (C-1), 48.7 (C-13), 81.7 (C-16), 172.8 (C-11), 173.3 (C-15). IR (neat, cm^{-1}): 849, 1150, 1368, 1449, 1541, 1645, 1732, 2928. $[\alpha]_D^{20}$ -2 (c = 0.1, dichloromethane). HRMS required for $C_{18}H_{34}N_2O_3$ [M] 326.2569, found 326.2566.

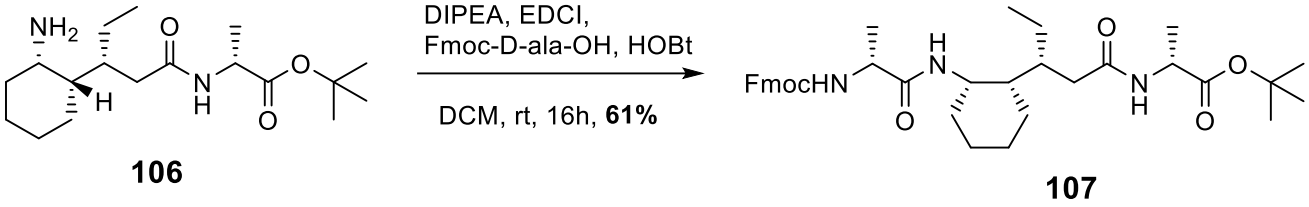

106 **107**

α/δ-peptide FmocNH-(L-Ala-ACPA)-L-Ala-O^{t}Bu **107**

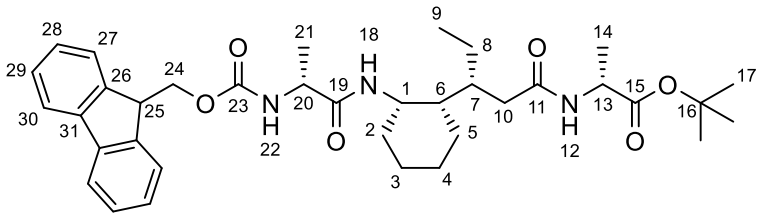

107

To a solution of dipeptide **106** (0.321 g, 0.982 mmol) in dichloromethane (10 mL), DIPEA (0.205 mL, 1.178 mmol), HOBt.H_2O (0.181 g, 1.178 mmol) and EDCI (0.209 mL, 1.178 mmol) were added and the reaction mixture stirred for 5 minutes. Fmoc-D-Ala-OH (0.306 g, 0.982 mmol) was then added and the reaction mixture stirred for 16 hours. The reaction mixture was then diluted with excess ethyl acetate and washed with aqueous 10% citric acid (20 mL), aqueous saturated sodium bicarbonate (20 mL) and brine (20 mL). The organic layer was dried over $MgSO_4$, filtered and concentrated *in vacuo*. The crude product was purified by column chromatography (40% ethyl acetate in hexane) to give compound **107** as a white foam (61%, 0.372 g). ^{1}H NMR ($CDCl_3$, 400 MHz): δ 0.71 (3H, t, J = 7.3 Hz, H-9), 0.97-1.09 (1H, m, H-5), 1.13-1.24 (2H, m, H-4 & H-8), 1.28-1.35 (2H, m, H-3 & H-6), 1.35-1.41 (7H, m, H-8, H-14 & H-21), 1.42-1.49 (11H, m, H-2, H-7 & H-17), 1.53-1.62 (2H, m, H-3 & H-5), 1.70-1.82 (2H, m, H-2 & H-4), 1.94 (1H, dd, J = 12.8 & 10.3 Hz, H-10), 2.59 (1H, dd, J = 12.9 & 3.1 Hz, H-10), 4.16 (1H, t, J = 7.5 Hz, H-25), 4.23-4.30 (1H, m, H-24), 4.31-4.39 (2H, m, H-20 & H-24), 4.44 (1H, d, J = 8.0 Hz, H-1), 4.59 (1H, qu, J = 7.3 Hz, H-13), 6.71 (1H, d, J = 8.7 Hz, H-22), 7.06 (1H, d, J = 10.1 Hz, H-18), 7.14 (1H, d, J = 8.5 Hz, H-12), 7.27 (2H, t, J = 7.5 Hz, H-28), 7.38 (2H, t, J = 7.5 Hz, H-29), 7.56 (2H, dd, J = 7.5 & 0.9 Hz, H-27), 7.74 (2H, d, J = 7.6 Hz, H-30). ^{13}C NMR ($CDCl_3$, 100 MHz):

δ 8.7 (C-9), 16.1 (C-21), 18.6 (C-14), 20.7 (C-3), 22.1 (C-8), 24.8 (C-5), 26.1 (C-4), 28.0 (C-17), 31.7 (C-2), 37.3 (C-10), 38.6 (C-7), 42.9 (C-6), 44.9 (C-1), 47.1 (C-25), 47.9 (C-13), 50.2 (C-20), 67.6 (C-24), 82.1 (C-16), 120.0 (C-30), 125.2 (C-27), 127.1 (C-28), 127.3 (C-28), 127.8 (C-29), 141.2 (C-31), 141.3 (C-31), 143.7 (C-26), 143.8 (C-26), 157.4 (C-23), 172.8 (C-19), 173.3 (C-11), 174.2 (C-15). IR (neat, cm^{-1}): 739, 758, 847, 1034, 1079, 1149, 1236, 1368, 1449, 1525, 1647, 1717, 2930, 3310. $[\alpha]_D^{20}$ +53 (c = 0.1, dichloromethane). mp = 78.8-79.5°C. HRMS required for $C_{36}H_{49}N_3O_6$ $[M+H]^+$ 620.3694, found 620.3690.

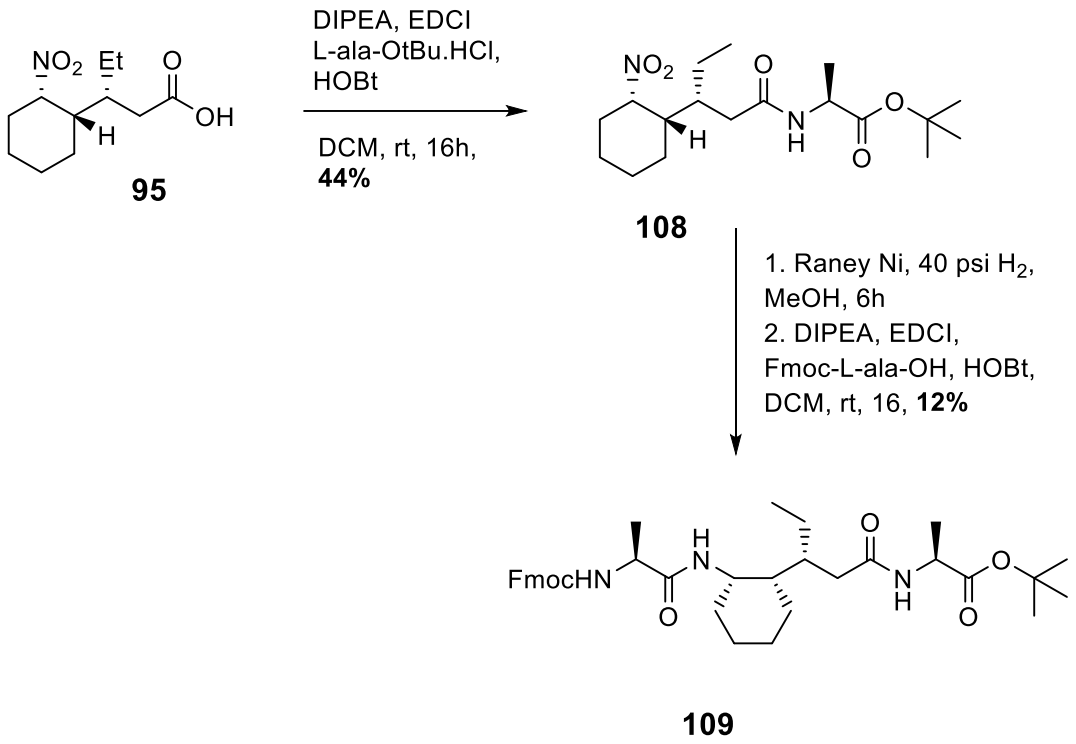

Tert-butyl ((*R*)-3-((1*S*,2*S*)-2-nitrocyclohexyl)pentanoyl)-L-alaninate **108**

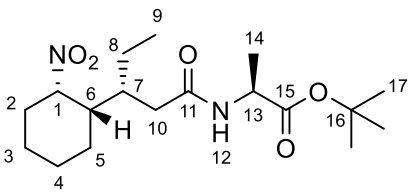

108

To a solution of the nitro acid **95** (1.400 g, 6.110 mmol) in dichloromethane (42 mL), DIPEA (0.911 mL, 5.234 mmol), HOBt.H_2O (0.802 g, 5.234 mmol) and EDCI (0.926 mL, 5.234 mmol)

were added and the reaction mixture stirred for 5 minutes. L-Ala tert-butyl ester hydrochloride (1.332 g, 7.332 mmol) was then added and the reaction stirred for 16 hours. The reaction mixture was then diluted with excess ethyl acetate and washed with aqueous 10% citric acid (50 mL), aqueous saturated sodium bicarbonate (50 mL) and brine (50 mL). The organic layer was dried over $MgSO_4$, filtered and concentrated *in vacuo*. The crude product was purified by column chromatography (25% ethyl acetate in hexane) to give compound **108** as a white solid (44%, 0.804 g). ^{1}H NMR ($CDCl_3$, 400 MHz): δ 0.81 (3H, t, J = 7.4 Hz, H-9), 1.20-1.31 (5H, m, H-4, H-8 & H-14), 1.40 (9H, s, H-17), 1.43-1.55 (2H, m, H-3 & H-8), 1.55-1.72 (4H, m, H-2, H-3 & H-5), 1.72-1.83 (3H, m, H-4, H-6 & H-7), 2.11-2.27 (3H, m, H-2 & H-10), 4.36 (1H, qu, J = 7.2 Hz, H-13), 4.92-4.98 (1H, m, H-1), 6.15 (1H, d, J = 7.0 Hz, H-12). ^{13}C NMR ($CDCl_3$, 100 MHz): δ 11.0 (C-9), 18.5 (C-14), 20.1 (C-3), 22.9 (C-8), 23.4 (C-5), 25.4 (C-4), 27.9 (C-17), 30.5 (C-2), 36.2 (C-10), 39.1 (C-7), 41.8 (C-6), 48.5 (C-13), 81.9 (C-16), 84.2 (C-1), 171.5 (C-11), 172.3 (C-15). IR (neat, cm^{-1}): 559, 588, 629, 689, 779, 833, 847, 922, 960, 985, 1040, 1072, 1108, 1155, 1248, 1300, 1369, 1458, 1539, 1637, 1721, 2880, 2934, 3313. $[\alpha]_D^{20}$ +22 (c = 0.1, dichloromethane). mp = 138.1-138.9°C. HRMS required for $C_{18}H_{32}N_2O_5$ $[M+Na]^+$ 379.2203, found 379.2208.

α/δ-peptide FmocNH-(D-Ala-ACPA)-D-Ala-O^{t}Bu **109**

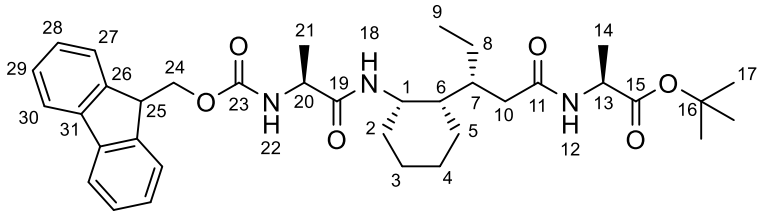

109

To a solution of the dipeptide **108** (0.600g, 1.683mmol) in MeOH (75 mL) was added Raney Nickel (1.20g). The flask was attached to a parr apparatus and the reaction stirred for 6 hours at a H_2 pressure of 40 psi. After TLC analysis indicated reaction completion, the reaction mixture was filtered through celite and concentrated *in vacuo.* The crude product was then

taken up in dichloromethane (15 mL) and DIPEA (0.325 mL, 1.869 mmol), HOBt.H_2O (0.286g, 1.869 mmol) and EDCI (0.331 mL, 1.869 mmol) were added and the reaction mixture stirred for 5 minutes. Fmoc-L-Ala-OH (0.485 g, 1.558 mmol) was then added and the reaction mixture stirred for 16 hours. The reaction mixture was then diluted with excess ethyl acetate and washed with aqueous 10% citric acid (25 mL), aqueous saturated sodium bicarbonate (25 mL) and brine (25 mL). The organic layer was dried over $MgSO_4$, filtered and concentrated *in vacuo*. The crude product was purified by column chromatography (40% ethyl acetate in hexane) to give compound **109** as a white solid (12% over two steps, 0.125 g). ^{1}H NMR ($CDCl_3$, 400 MHz): δ 0.80 (3H, t, J = 7.4 Hz, H-9), 0.90-1.03 (1H, m, H-5), 1.18-1.27 (2H, m, H-3 & H-4), 1.28-1.33 (3H, d, J = 7.1 Hz, H-14), 1.33-1.44 (6H, m, H-6, H-8 & H-21), 1.44-1.48 (10H, m, H-2 & H-17), 1.49-1.57 (2H, m, H-3 & H-7), 1.64-1.80 (3H, m, H-2, H-4 & H-5), 1.95 (1H, dd, J = 12.5 & 9.4 Hz, H-10), 2.56 (1H, dd, J = 13.2 & 1.9 Hz, H-10), 4.20 (1H, t, J = 7.1 Hz, H-25), 4.28-4.45 (5H, m, H-1, H-13, H-20 & H-24), 5.76 (1H, d, J = 7.4 Hz, H-22), 6.54 (1H, d, J = 8.5 Hz, H-18), 6.73 (1H, d, J = 6.3 Hz, H-12), 7.29 (2H, t, J = 7.4 Hz, H-28), 7.39 (2H, t, J = 7.5 Hz, H-29), 7.57 (2H, t, J = 6.6 Hz, H-27), 7.75 (2H, d, J = 7.5 Hz, H-30). ^{13}C NMR ($CDCl_3$, 100 MHz): δ 9.0 (C-9), 18.6 (C-14), 19.0 (C-21), 20.6 (C-3), 21.9 (C-8), 24.9 (C-5), 26.0 (C-4), 28.1 (C-17), 31.5 (C-2), 37.1 (C-10), 38.4 (C-7), 42.1 (C-6), 45.5 (C-1), 47.2 (C-25), 48.7 (C-13), 50.8 (C-20), 67.3 (C-24), 81.7 (C-16), 120.1 (C-30), 125.2 (C-27), 127.2 (C-28), 127.9 (C-29), 141.4 (C-31), 143.8 (C-26), 156.4 (C-23), 172.3 (C-19), 172.6 (C-11), 172.9 (C-15). IR (neat, cm^{-1}): 984, 1065, 1150, 1220, 1253, 1377, 1398, 1451, 1506, 1540, 1643, 1745, 2929, 3260. $[\alpha]_D^{20}$ +4 (c = 0.1, dichloromethane). mp = 170.6-171.5^{o}C. HRMS required for $C_{36}H_{49}N_3O_6$ $[M+H]^+$ 620.3694, found 620.3643.

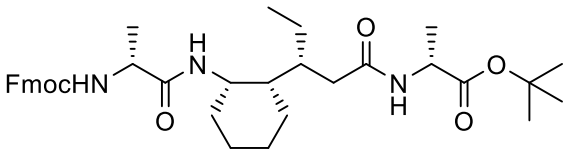

107

1. TFA, DCM, 0°C to rt, 2h
2. DIPEA, EDCI, HOBt, **106**,
DCM, rt, 48h, **37%**

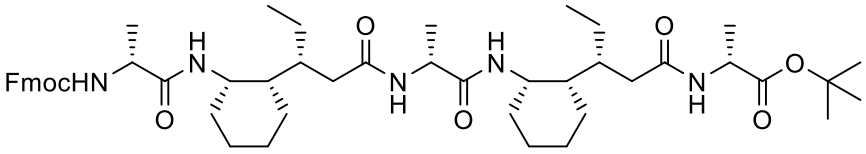

111

1. TFA, DCM, 0°C to rt, 2h
2. DIPEA, EDCI, HOBt, **106**
DCM, rt, 48h, **32%**

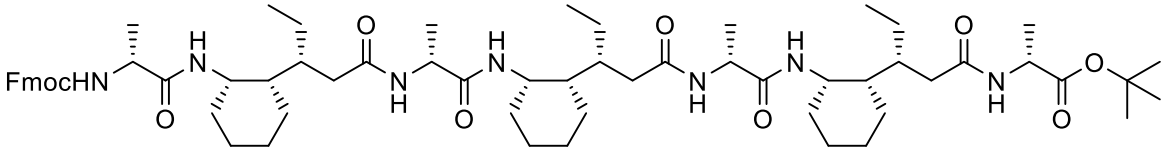

112

α/δ-peptide FmocNH-(D-Ala-ACPA)$_2$-D-Ala-O^{t}Bu **111**

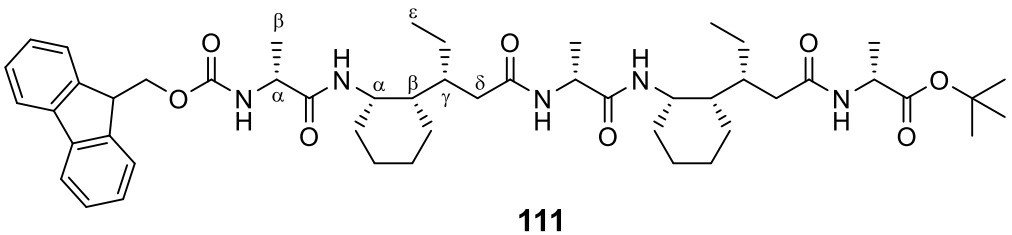

111

To a solution of trimer **107** (0.375 g, 0.605 mmol) in anhydrous dichloromethane (5.5 mL) at 0°C was added trifluoroacetic acid (1.38 mL, 18.034 mmol) dropwise over 10 minutes, and the

reaction stirred for 2 hours whilst warming to rt. The reaction mixture was then concentrated *in vacuo* 3 times, co-evaporating with toluene each time (3 x 5 mL). The crude product was then taken up in dichloromethane (6 mL) and DIPEA (0.126 mL, 0.724 mmol), HOBt.H_2O (0.111 g, 0.724 mmol) and EDCI (0.128 mL, 0.724 mmol) were added and the reaction mixture stirred for 5 minutes. Amine **106** (0.394 g, 1.210 mmol) was then added and the reaction stirred for 48 hours. The reaction mixture was then diluted with excess ethyl acetate and washed with aqueous 10% citric acid (15 mL), aqueous saturated sodium bicarbonate (15 mL) and brine (15 mL). The organic layer was dried over $MgSO_4$, filtered and concentrated *in vacuo*. The crude product was purified by column chromatography (60% ethyl acetate in hexane) to give compound **111** as a white foam (37%, 0.195 g). ^{1}H NMR ($CDCl_3$, 400 MHz): δ 0.62 (3H, t, J = 7.3, H-ε), 0.81 (3H, t, J = 7.4, H-ε), 1.19-1.27 (5H, m), 1.30-1.37 (9H, m), 1.41-1.48 (18H, m), 1.51-1.58 (2H, m), 1.59-1.67 (2H, m), 1.74-1.84 (4H, m), 1.96-2.04 (2H, m, H-δ), 2.30 (1H, dd, J = 13.8 & 7.2 Hz, H-δ), 2.49 (1H, dd, J = 13.5 & 5.0 Hz, H-δ), 4.18-4.24 (1H, m, H-Fmoc), 4.25-4.38 (4H, m), 4.40-4.47 (2H, m, Ala H-α), 4.48-4.56 (1H, m, Ala H-α), 7.02 (1H, d, J = 6.8 Hz, Ala-NH), 7.09 (1H, d, J = 8.3 Hz, ACPA-NH), 7.29 (2H, tdd, J = 7.5, 3.5 & 1.1 Hz, H-Fmoc), 7.38 (2H, t, J = 7.5 Hz, H-Fmoc), 7.58-7.64 (2H, m, ACPA-NH & H-Fmoc), 7.66-7.72 (2H, m, Ala-NH & H-Fmoc), 7.75 (2H, d, J = 7.6 Hz), 7.83 (1H, s, Ala-NH). ^{13}C NMR ($CDCl_3$, 100 MHz): δ 9.8 (C-ε), 10.4 (C-ε), 16.9 (2 x Ala C-β), 17.7 (Ala C-β), 20.8, 21.1, 23.8, 25.2, 25.4, 26.2, 26.7, 28.0, (C-O^{t}Bu), 29.8, 31.8, 37.5 (C-δ), 37.9 (C-δ), 38.5 (2 x C-γ), 42.7 (ACPA C-β), 43.5 (ACPA C-β), 45.3 (2 x ACPA C-α), 47.2 (C-Fmoc), 48.3 (Ala C-α), 49.1 (Ala C-α), 50.3 (Ala C-α), 67.5 (C-Fmoc), 82.0 (C-O^{t}Bu), 120.0 (2 x C-Fmoc), 125.3 (C-Fmoc), 125.5 (C-Fmoc), 127.1 (C-Fmoc), 127.2 (C-Fmoc), 127.8 (2 x C-Fmoc), 141.4 (2 x C-Fmoc), 143.8 (C-Fmoc), 144.1 (C-Fmoc), 157.5 (CO-Fmoc), 172.7 (CO-Ala), 172.9 (CO-Ala), 173.5 (CO-ACPA), 174.2 (CO-ACPA), 174.6 (CO-ACPA). IR (neat, cm^{-1}): 739, 758, 847, 1034, 1079, 1149, 1236, 1368, 1449, 1525, 1647, 1717, 2930, 3310. $[\alpha]_D^{20}$ +53 (c = 0.1, dichloromethane). mp = 95.9-97.2°C. HRMS required for $C_{50}H_{73}N_5O_8$ $[M+H]^+$ 872.5532, found 872.5510.

α/δ-peptide FmocNH-(D-Ala-ACPA)$_3$-D-Ala-O^{t}Bu **112**

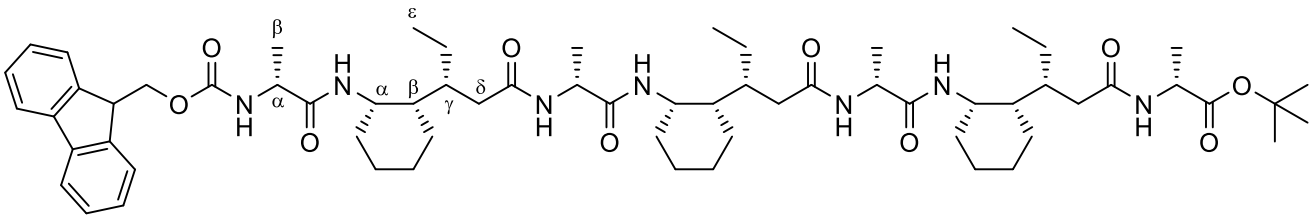

112

To a solution of pentamer **111** (0.105 g, 0.120 mmol) in anhydrous dichloromethane (1.0 mL) at 0°C was added trifluoroacetic acid (0.27 mL, 3.528 mmol) dropwise over 5 minutes, and the reaction stirred for 2 hours whilst warming to rt. The reaction mixture was then concentrated *in vacuo* 3 times, co-evaporating with toluene each time (3 x 3 mL). The crude product was then taken up in dichloromethane (1.4 mL) and DIPEA (0.0293 mL, 0.168 mmol), HOBt.H_2O (0.0258 g, 0.168 mmol) and EDCI (0.0297 mL, 0.168 mmol) were added and the reaction mixture stirred for 5 minutes. Amine **106** (0.1500 g, 0.460 mmol) was then added and the reaction stirred for 48 hours. The reaction mixture was then diluted with excess ethyl acetate and washed with aqueous 10% citric acid (5 mL), aqueous saturated sodium bicarbonate (5 mL) and brine (5 mL). The organic layer was dried over $MgSO_4$, filtered and concentrated *in vacuo*. The crude product was purified by column chromatography (100% ethyl acetate) to give compound **112** as a white foam (32%, 0.044 g). ^{1}H NMR ($CDCl_3$, 700 MHz): δ 0.70 (3H, t, J = 6.9 Hz, H-ε), 0.84 (6H, dd, J = 15.7 & 7.7 Hz, H-ε), 1.19-1.35 (21H, m), 1.37-1.44 (13H, m), 1.44-1.47 (13H, m), 1.54-1.56 (1H, m), 1.66-1.82 (9H, m), 2.07 (3H, ddd, J = 20.7, 13.9 & 6.2 Hz, H-δ), 2.33 (1H, dd, J = 13.9 & 7.3 Hz, H-δ), 2.42 (2H, ddd, J = 20.5, 13.8 & 6.0 Hz), 4.20-4.50 (10H, m, Ala H-α, ACPA H-α, H-Fmoc), 6.88 (1H, s, Ala-NH), 6.99 (1H, s, ACPA-NH), 7.30 (2H, dd, J = 13.2 & 6.9 Hz, H-Fmoc), 7.39 (2H, td, J = 7.3 & 2.8 Hz, H-Fmoc), 7.62 (1H, d, J = 7.4 Hz, H-Fmoc), 7.68 (1H, d, J = 7.3 Hz, H-Fmoc), 7.76 (2H, d, J = 7.5 Hz, H-Fmoc), 7.81-7.93 (3H, m, 2 x ACPA-NH & Ala-NH), 8.08 (1H, s, Ala-NH), 8.29 (1H, s, Ala-NH). ^{13}C NMR ($CDCl_3$, 175 MHz): δ 9.8 (C-ε), 10.2 (C-ε), 10.7 (C-ε), 16.9 (2 x Ala C-β), 17.1 (Ala C-β), 17.5 (Ala C-β), 20.7, 24.4, 25.3, 25.6, 26.2, 26.8, 28.0 (C-O^{t}Bu), 29.8, 31.8, 32.6, 37.3 (C-δ), 38.0 (ACPA C-β), 38.3 (C-δ),

42.8 (C-γ), 43.5 (C-γ), 45.6 (3 x ACPA C-α), 47.2 (C-Fmoc), 48.5 (Ala C-α), 49.2 (Ala C-α), 49.5 (Ala C-α), 50.4 (Ala C-α), 67.5 (C-Fmoc), 82.1 (C-O^{t}Bu), 120.1 (C-Fmoc), 125.3 (C-Fmoc), 125.5 (C-Fmoc), 127.2 (C-Fmoc), 127.8 (C-Fmoc), 141.4 (C-Fmoc), 143.9 (C-Fmoc), 144.1 (C-Fmoc), 157.4 (CO-Fmoc), 172.5 (2 x CO-Ala), 173.0 (CO-Ala), 173.7 (2 x CO-ACPA), 174.1 (CO-ACPA), 174.6 (CO-Ala). IR (neat, cm^{-1}): 739, 758, 847, 1035, 1081, 1150, 1250, 1320, 1449, 1539, 1641, 2860, 2930, 3281. $[\alpha]_D^{20}$ +55 (c = 0.1, dichloromethane). mp = 115.2°C. HRMS required for $C_{64}H_{97}N_7O_{10}$ $[M+H]^+$ 1124.7370, found 1124.7228.

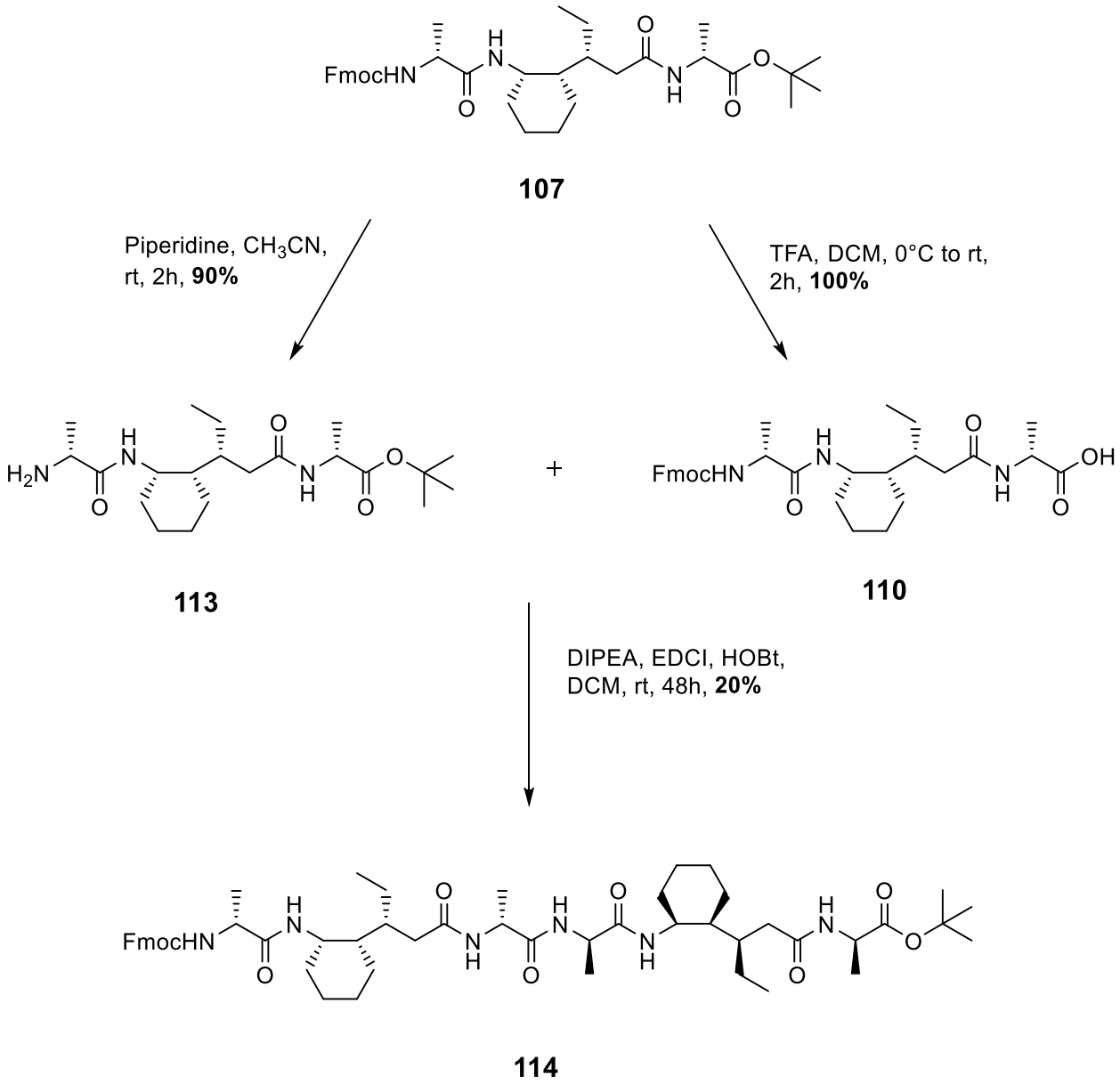

α/δ-peptide FmocNH-(D-Ala-ACPA-D-Ala)$_2$-O^{t}Bu **114**

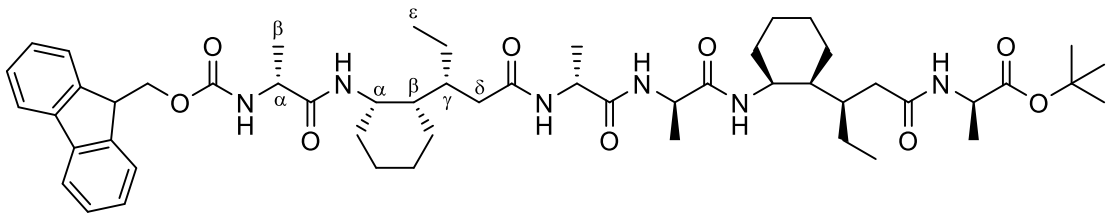

114

To a solution of trimer **107** (0.200 g, 0.323 mmol) in anhydrous dichloromethane (3.0 mL) at 0°C was added trifluoroacetic acid (0.74 mL, 9.670 mmol) dropwise over 10 minutes, and the reaction stirred for 2 hours whilst warming to rt. The reaction mixture was then concentrated *in vacuo* 3 times, co-evaporating with toluene each time (3 x 5 mL) to give the crude product **110**, which was set aside. Meanwhile, to a solution of trimer **107** (0.400 g, 0.646 mmol) in anhydrous CH_3CN (4.30 mL) under nitrogen was added piperidine (1.08 mL, 10.933 mmol) and the reaction allowed to stir for 30 minutes. The reaction was then concentrated *in vacuo* 3 times, co-evaporating with toluene each time (3 x 5 mL). The crude product was then taken up in diethyl ether (8 mL) and triturated, with the solution then filtered to collect the solid crude product **113**. Both crude products were then taken up in dichloromethane (3.2 mL) and DIPEA (0.069 mL, 0.396 mmol), HOBt.H_2O (0.060 g, 0.391 mmol) and EDCI (0.070 mL, 0.396 mmol) added and the reaction left to stir for 48 hours. The reaction mixture was then diluted with excess ethyl acetate and washed with aqueous 10% citric acid (5 mL), aqueous saturated sodium bicarbonate (5 mL) and brine (5 mL). The organic layer was dried over $MgSO_4$, filtered and concentrated *in vacuo*. The crude product was purified by column chromatography (80% ethyl acetate in hexane) to give compound **114** as a white foam (20%, 0.058 g). ^{1}H NMR ($CDCl_3$, 700 MHz): δ 0.65 (3H, t, J = 7.1 Hz, H-ε), 0.77 (3H, t, J = 7.1 Hz, H-ε), 0.91-0.98 (2H, m), 1.06-1.10 (1H, m), 1.18 (3H, d, J = 6.4 Hz, Ala (4) H-β), 1.24-1.28 (9H, m), 1.33-1.37 (6H, m), 1.45 (3H, d, J = 6.7 Hz, Ala (1) H-β), 1.47-1.52 (12H, m), 1.58-1.70 (4H, m), 1.73-1.84 (5H, m), 1.86-1.95 (2H, m, H-δ), 2.67 (2H, d, J = 12.3 Hz, H-δ), 4.17 (1H, t, J = 7.3 Hz, H-Fmoc), 4.21 (1H, t, J = 9.0 Hz, H-Fmoc), 4.37-4.43 (2H, m, Ala (1) H-α & H-Fmoc), 4.45-4.50 (2H, m, 2 x ACPA H-α), 4.51-4.56 (2H, m, Ala (4) H-α & Ala H-α), 4.60 (1H, qu, J = 7.0 Hz, Ala H-α), 6.92 (1H, d, J = 8.2

Hz, Ala-NH), 6.99 (1H, d, J = 10.1 Hz, ACPA (2)-NH), 7.16 (1H, d, J = 10.3 Hz, ACPA (5)-NH), 7.21 (1H, d, J = 7.9 Hz, Ala-NH), 7.27 (2H, t, J = 7.4 Hz, H-Fmoc), 7.38 (2H, t, J = 7.0 Hz, H-Fmoc), 7.42 (1H, d, J = 8.0 Hz, Ala (1)-NH), 7.56 (2H, dd, J = 13.8 & 7.5 Hz, H-Fmoc), 7.72-7.78 (3H, m, H-Fmoc & Ala (4)-NH). ^{13}C NMR ($CDCl_3$, 175 MHz): δ 7.0 (C-ε), 7.8 (C-ε), 15.2 (Ala (4) C-β), 15.8 (Ala (1) C-β), 18.8 (Ala C-β), 19.0 (C-β), 20.6, 20.7, 21.2, 24.4, 24.5, 26.0, 26.1, 28.2 (C-O^{t}Bu), 29.8, 31.7, 31.8, 36.1 (C-δ), 36.8 (C-δ), 37.9, 38.3, 41.9, 42.7, 44.8 (2 x ACPA C-α), 47.2 (C-Fmoc), 47.9 (Ala C-α), 48.3 (Ala C-α), 48.5 (Ala (4) C-α), 50.2 (Ala (1) C-α), 67.7 (C-Fmoc), 82.5 (C-O^{t}Bu), 120.1 (C-Fmoc), 125.2 (C-Fmoc), 125.3 (C-Fmoc), 127.2 (C-Fmoc), 127.4 (C-Fmoc), 127.9 (C-Fmoc), 141.3 (C-Fmoc), 141.4 (C-Fmoc), 143.6 (C-Fmoc), 143.9 (C-Fmoc), 157.6 (CO-Fmoc), 172.1 (CO-Ala (4)), 173.0 (CO-Ala (1)), 173.3 (2 x CO-Ala), 174.7 (2 x CO-ACPA). IR (neat, cm^{-1}): 739, 848, 1035, 1080, 1150, 1245, 1319, 1368, 1449, 1521, 1638, 2855, 2928, 3301. $[\alpha]_D^{20}$ +150 (c = 0.1, dichloromethane). mp = 106.2-107.3°C. HRMS required for $C_{53}H_{78}N_6O_9$ $[M+Na]^+$ 965.5722, found 965.5698.

5.3. Chapter 4

5.3.1. Synthesis of *cis* δ-nitro alcohol 132

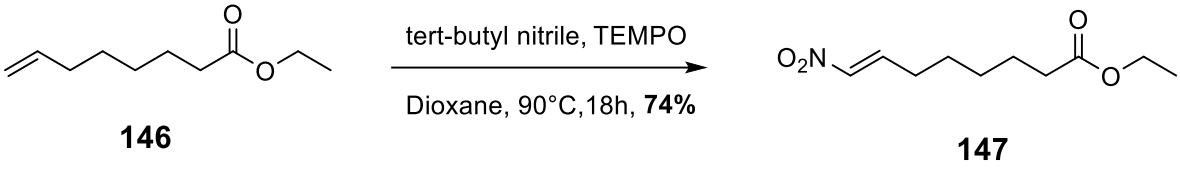

146 **147**

Ethyl (*E*)-8-nitrooct-7-enoate **147**

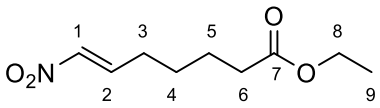

147

To a solution of Ethyl-6-heptenoate **146** (1.000 g, 5.878 mmol) in dioxane (16.5 ml) was added TEMPO (0.246 g, 1.574 mmol) and tert-butyl nitrile (1.630 ml, 13.722 mmol) and the reaction mixture heated under reflux and stirred for 18 hours. The reaction mixture was then allowed to cool to rt, filtered through a pad of celite and concentrated *in vacuo*. The crude product was purified by column chromatography (20% ethyl acetate in hexane) to give compound **147** as a colourless oil (74%, 0.936 g). ^{1}H NMR ($CDCl_3$, 400 MHz): δ 1.25 (3H, t, J = 7.1 Hz, H-9), 1.51-1.61 (2H, m, H-5), 1.64-1.73 (2H, m, H-4), 2.27-2.36 (4H, m, H-3 & H-6), 4.13 (2H, q, J = 7.1 Hz, H-8), 7.00 (1H, dt, J = 13.4 & 1.5 Hz, H-2), 7.21-7.32 (1H, m, H-1). ^{13}C NMR ($CDCl_3$, 125 MHz): δ 14.2 (C-9), 24.3 (C-4), 27.1 (C-5), 28.1 (C-3), 33.8 (C-6), 60.4 (C-8), 139.8 (C-1), 142.1 (C-2), 173.1 (C-7). IR (neat, cm^{-1}): 731, 962, 1030, 1097, 1151, 1180, 1350, 1521, 1651, 1728, 2869, 2940, 2983, 3106.

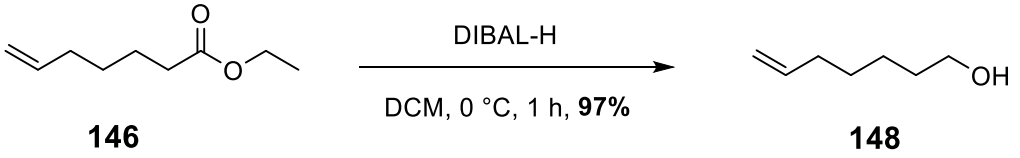

146 **148**

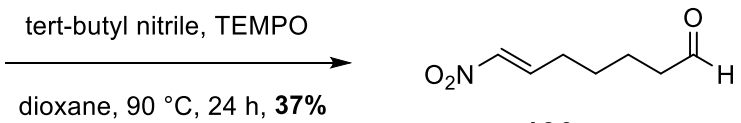

130

Hept-6-en-1-ol **148**

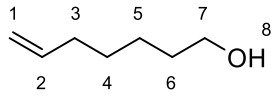

148

To a solution of Ethyl-6-heptenoate **146** (5.000 g, 32.026 mmol) in anhydrous dichloromethane (375 ml) at 0˚C under nitrogen was added DIBAL-H (1M) in hexane (68.0 ml, 68.0 mmol) over the course of 10 minutes. After 1 hour the reaction was quenched with 2M aqueous hydrochloric acid (300 ml) and water (150 ml). The aqueous layer was extracted with dichloromethane (3 x 100 ml) and the combined organic layers then dried over $MgSO_4$, filtered and concentrated *in vacuo* to give the pure product **148** as a pale yellow oil. (97%, 3.545 g). ^{1}H NMR ($CDCl_3$, 400 MHz): δ 1.28-1.42 (4H, m, H-4 & H-5), 1.46-1.55 (2H, m, H-6), 1.97-2.05 (2H, m, H-3), 3.32 (1H, s, H-8), 3.53 (2H, t, J = 6.8 Hz, H-7), 4.89 (1H, ddt, J = 10.2, 2.2 & 1.2 Hz, H-1), 4.95 (1H, ddd, J = 17.1, 3.6 & 1.6 Hz), 5.75 (1H, ddt, J = 16.9, 10.2 & 6.7 Hz, H-2). ^{13}C NMR ($CDCl_3$, 125 MHz): δ 25.2 (C-5), 28.7 (C-4), 32.4 (C-8), 33.7 (C-3), 62.4 (C-7), 114.3 (C-1), 138.8 (C-2). IR (neat, cm^{-1}): 633, 735, 908, 993, 1053, 1460, 1641, 1718, 1736, 2858, 2930, 3076, 3330.

(*E*)-7-nitrohept-6-enal **130**

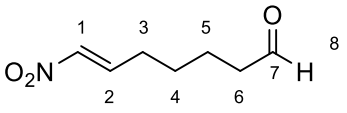

130

To a solution of Hept-6-en-1-ol **147** (2.000 g, 17.515 mmol) in dioxane (44 ml) was added TEMPO (0.673 g, 4.307 mmol) and tert-butyl nitrile (4.44 ml, 37.378 mmol) and the reaction mixture heated under reflux and stirred for 24 hours. The reaction mixture was then allowed

to cool to rt, filtered through a pad of celite and concentrated *in vacuo*. The crude product was purified by column chromatography (20% ethyl acetate in hexane) to give compound **146** as a colourless oil (37%, 1.019 g). ^{1}H NMR ($CDCl_3$, 400 MHz): δ 1.54-1.62 (2H, m, H-4), 1.65-1.74 (2H, m, H-5), 2.31 (2H, ddd, J = 14.7, 7.3 & 1.6 Hz, H-3), 2.51 (2H, m, td, J = 7.1 & 1.4 Hz, H-6), 7.01 (1H, m, dt, J = 13.4 & 1.6 Hz, H-1), 7.22-7.30 (1H, m, H-2), 9.78 (1H, t, J = 1.4 Hz, H-8). ^{13}C NMR ($CDCl_3$, 125 MHz): δ 21.5 (C-5), 27.2 (C-4), 28.3 (C-3), 43.4 (C-6), 139.9 (C-1), 141.9 (C-2), 201.8 (C-7). IR (neat, cm^{-1}): 731, 961, 1348, 1518, 1647, 1719, 2725, 2859, 2932, 3105.

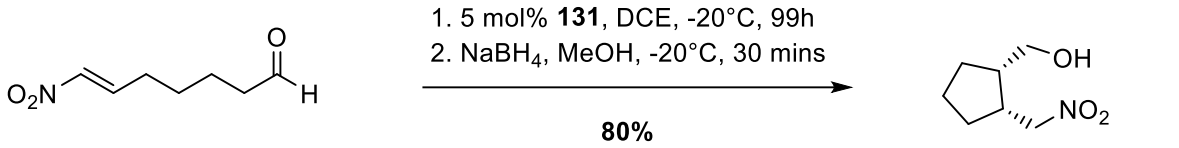

130 **132 (9:1 *dr*)**

((1*S*,2*R*)-2-(nitromethyl)cyclopentyl)methanol **132**

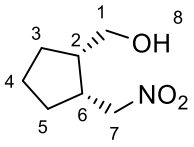

132

A solution of (*S*)-(-)-5-(2-pyrrolidinyl)-1H-tetrazole **131** (0.0800 g, 0.575 mmol) in DCE (100 mL) was sonicated for 30 minutes and then cooled to -20˚C, after which a solution of (*E*)-7-nitrohept-6-enal **130** (0.857 g, 5.456 mmol) in DCE (2 mL) was added dropwise over the course of 3 minutes. The reaction mixture was then left stirring at -20˚C for 99 hours. $NaBH_4$ (0.320 g, 8.459 mmol) was then added in one portion, followed by MeOH (8.2 mL) and the reaction left to stir for 1 hour. The reaction was then quenched via the addition of a saturated aqueous solution of ammonium chloride (10 mL), followed by brine (40 mL). The organic phase was

first extracted with a 3:1 mixture of chloroform and isopropanol (3 x 80 mL) and then with ethyl acetate (3 x 100 mL). The combined organic layers were dried over $MgSO_4$, filtered and concentrated *in vacuo*. The crude product was purified by column chromatography (25% ethyl acetate in hexane) to separately give the *cis* and *trans* diastereoisomers (80%, 0.694 g, 9:1 *dr*). *Cis*-**132** data: ^{1}H NMR ($CDCl_3$, 400 MHz): δ 1.28-1.43 (2H, m, H-3 & H-5), 1.49-1.61 (1H, m, H-4), 1.63-1.72 (1H, m, H-4), 1.73-1.83 (2H, m, H-3 & H-5), 2.22-2.32 (1H, m, H-2), 2.48 (1H, s, H-8), 2.67-2.79 (1H, m, H-6), 3.43-3.54 (2H, m, H-1), 4.30 (1H, dd, J = 12.8 & 9.3 Hz, H-7), 4.64 (1H, dd, J = 12.8 & 6.6 Hz, H-7). ^{13}C NMR ($CDCl_3$, 125 MHz): δ 22.9 (C-4), 27.7 (C-3), 29.0 (C-5), 40.1 (C-6), 42.9 (C-2), 62.8 (C-1), 77.0 (C-7). IR (neat, cm^{-1}): 1020, 1383, 1431, 1543, 2874, 2953. $[\alpha]_D^{20}$ -12 (c = 0.1, dichloromethane).

5.3.2. Synthesis of pyrrolidine-based *cis* δ-nitro alcohol 141

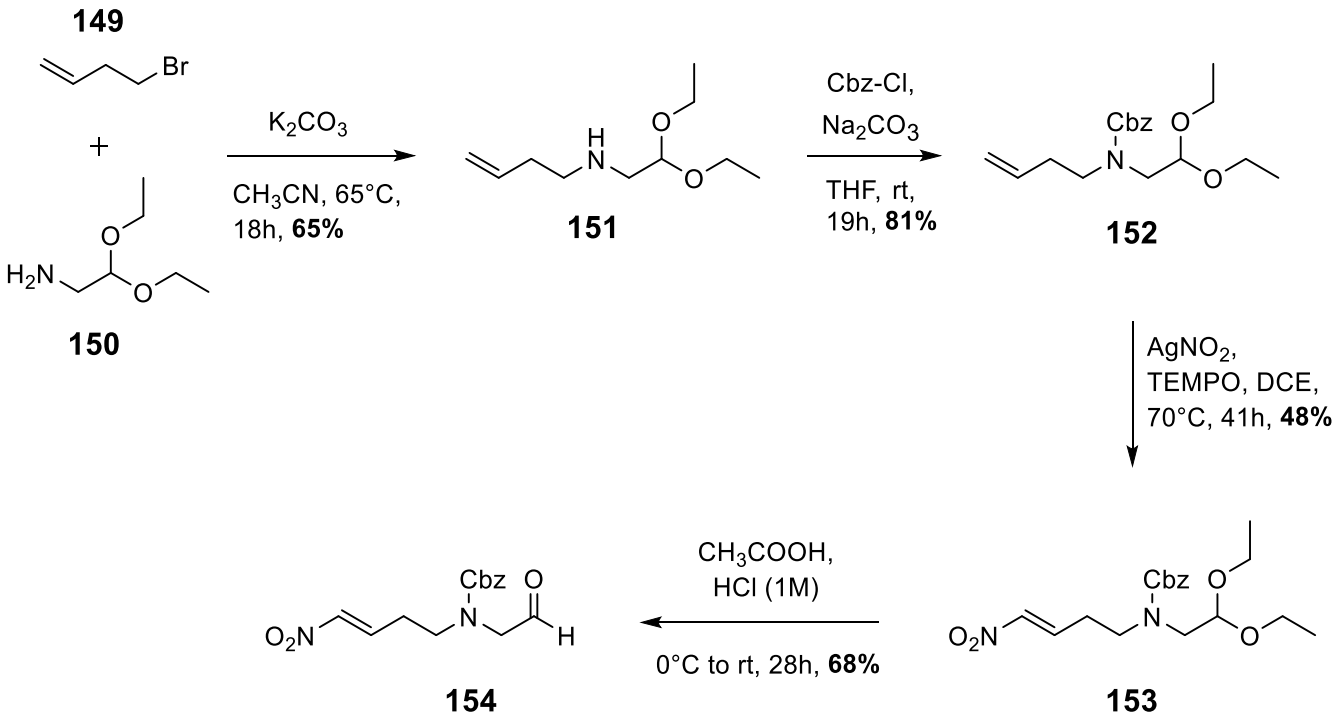

N-(2,2-diethoxyethyl)but-3-en-1-amine **151**

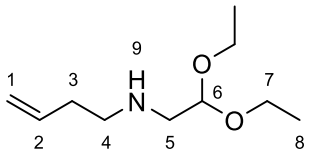

151

To a solution of aminoacetaldehyde diethyl acetal (7.5 mL, 51.580 mmol) in acetonitrile (180 mL), K_2CO_3 (5.36 g, 38.783 mmol) and 4-bromobutene (2.59 mL, 25.516 mmol) were added and the reaction mixture stirred at 65°C for 18 hours. The reaction mixture was then concentrated *in vacuo* and the residue diluted with ethyl acetate (75 mL) and washed first with H_20 (75 mL) and then brine (75 mL). The organic phase was dried over $MgSO_4$, filtered and concentrated *in vacuo*. The crude product was purified by column chromatography (40% ethyl acetate in hexane) to give compound **150** as a pale yellow oil (65%, 3.106 g). ^{1}H NMR ($CDCl_3$, 400 MHz): δ 1.20 (6H, t, J = 7.1 Hz, H-8), 1.68 (1H, s, H-9), 2.25 (2H, qt, J = 6.9 & 1.2 Hz, H-3), 2.69 (2H, t, J = 6.9 Hz, H-4), 2.72 (2H, d, J = 5.6 Hz, H-5), 3.61 (4H, ddq, J = 64.7, 9.4 & 7.1 Hz, H-8), 4.60 (1H, t, J = 5.6 Hz, H-6), 5.00-5.12 (2H, m, H-1), 5.77 (1H, ddt, J = 17.1, 10.2 & 6.9 Hz, H-2). ^{13}C NMR ($CDCl_3$, 125 MHz): δ 15.5 (C-8), 34.4 (C-3), 48.9 (C-4), 52.1 (C-5), 62.6 (C-7), 102.2 (C-6), 116.5 (C-1), 136.4 (C-2). IR (neat, cm^{-1}): 2978, 1457, 1372, 1060, 990, 913, 751.

benzyl but-3-en-1-yl(2,2-diethoxyethyl)carbamate **152**

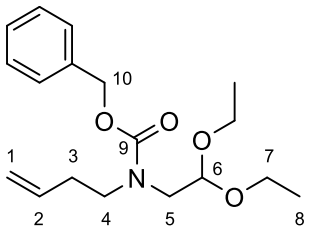

152

To a solution of N-(2,2-diethoxyethyl)but-3-en-1-amine **151** (5.51 g, 29.44 mmol) in THF (120 mL) was added sodium carbonate (9.00 g, 84.91 mmol) and benzyl chloroformate (5.10 mL, 35.89 mmol) and the reaction mixture left to stir at rt for 19 hours. H_2O (60 mL) was then added and the organic phase extracted with ethyl acetate (3 x 80 mL). The combined organic layers were then washed with brine (3 x 60 mL), dried over $MgSO_4$, filtered and concentrated *in vacuo*. The crude product was purified by column chromatography (20% ethyl acetate in hexane) to give compound **152** as a yellow oil (81%, 7.66 g). ^{1}H NMR ($CDCl_3$, 400 MHz): δ 1.13 & 1.18 (split because of N-Cbz rotamers, 6H, t, J = 7.0 Hz, H-8), 2.28 (2H, td, J = 14.7 & 7.1 Hz, H-3), 3.29 & 3.32 (2H, d, J = 5.3 Hz, H-5), 3.37-3.76 (6H, m, H-4 & H-7), 4.48 & 4.63 (1H, t, J = 5.3 Hz, H-6), 4.92-5.09 (2H, m, H-1), 5.13 (2H, s, H-10), 5.63-5.82 (1H, m, H-2), 7.22-7.42 (5H, m, H-Ar). ^{13}C NMR ($CDCl_3$, 125 MHz): δ 15.4 (C-8), 32.4 & 33.1 (C-3), 48.1 & 48.4 (C-4), 50.3 & 50.9 (C-5), 63.4 & 63.5 (C-7), 67.0 (C-10), 101.7 & 102.2 (C-6), 116.7 (C-1), 127.8 (C-Ar), 128.0 (C-Ar), 128.5 (C-Ar), 135.3 & 136.8 (C-2), 155.9 & 156.4 (C-9). IR (neat, cm^{-1}): 698, 735, 769, 914, 1059, 1121, 1160, 1239, 1285, 1373, 1416, 1473, 1697, 2900, 2976.

benzyl (*E*)-(2,2-diethoxyethyl)(4-nitrobut-3-en-1-yl)carbamate **153**

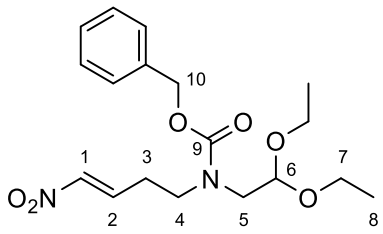

153

To an oven-dried round bottom flask was added activated 4Å molecular sieves (0.8g), DCE (77 mL), **152** (8.00 g, 24.91 mmol), $AgNO_2$ (20.27 g, 119.36 mmol) and TEMPO (2.34 g, 14.99 mmol). The reaction mixture was heated to 70°C and allowed to stir for 41 hours. The reaction was then allowed to cool to rt, filtered through a pad of celite, washed with ethyl acetate (500 mL) and concentrated *in vacuo*. The crude product was purified by column chromatography (30% ethyl acetate in hexane) to give compound **153** as a pale orange oil (48%, 4.38 g). ^{1}H

NMR ($CDCl_3$, 400 MHz): δ 1.11 & 1.17 (6H, t, J = 7.0 Hz, H-8), 2.42-2.57 (2H, m, H-3), 3.27 & 3.31 (2H, d, J = 5.2 Hz, H-5), 3.35-3.75 (6H, m, H-4 & H-7), 4.45 & 4.62 (1H, t, J = 5.1 Hz, H-6), 5.09-5.12 (2H, m, H-10), 6.87 & 6.96 (1H, d, J = 13.4 Hz, H-1), 7.09-7.24 (1H, m, H-2), 7.27-7.36 (5H, m, H-Ar). ^{13}C NMR ($CDCl_3$, 125 MHz): δ 15.2 (C-8), 27.3 & 27.9 (C-3), 47.0 & 47.4 (C-5), 50.8 & 51.2 (C-4), 63.4 & 63.6 (C-7), 67.4 (C-10), 101.4 & 101.9 (C-6), 128.0 & 128.2 (C-Ar), 128.5 (C-Ar), 136.3 (C-Ar), 139.2 & 139.3 (C-2), 140.4 (C-1), 155.9 (C-9). IR (neat, cm^{-1}): 698, 740, 7634, 962, 1057, 1117, 1240, 1348, 1416, 1469, 1526, 1697, 2882, 2976.

Benzyl (*E*)-(4-nitrobut-3-en-1-yl)(2-oxoethyl)carbamate **154**

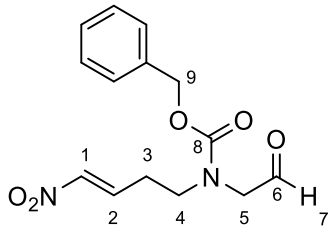

154

153 (3.06 g, 8.36 mmol) was added to a round bottom flask and cooled to 0˚C. Acetic acid (8.33 ml) was added and once the solution started to freeze, 1M HCl (2.74 mL) added and the reaction stirred at rt for 28 hours. Dichloromethane (30 mL) was then added and the organic phase washed with H_2O (2 x 30 mL) and saturated aqueous sodium bicarbonate (50 mL). The aqueous phase was back extracted with dichloromethane (3 x 40 mL) and the combined organic layers dried over $MgSO_4$, filtered and concentrated *in vacuo*. The crude product was purified by column chromatography (60% ethyl acetate in hexane) to give compound **154** as a colourless oil (68%, 1.66 g). ^1H NMR ($CDCl_3$, 400 MHz): δ 2.49 & 2.54 (2H, q, J = 7.2 Hz, H-3), 3.48-3.55 (2H, m, H-4), 4.08 & 4.12 (1H, s, H-5), 5.11 & 5.16 (2H, s, H-9), 6.96 & 7.03 (1H, d, J = 13.5 Hz, H-1), 7.14-7.25 (1H, m, H-2), 7.30-7.40 (5H, m, H-Ar), 9.56 & 9.60 (1H, s, H-7). ^{13}C NMR ($CDCl_3$, 125 MHz): δ 27.6 & 28.1 (C-3), 47.1 & 47.7 (C-4), 57.9 & 58.1 (C-5), 67.9 & 68.1 (C-9), 128.0 (C-Ar), 128.2 (C-Ar), 128.3 (C-Ar), 128.5 (C-Ar), 128.6 (C-Ar), 128.7 (C-Ar), 135.9 (C-Ar), 138.5 & 138.8 (C-2), 140.8 (C-1), 155.7 & 156.1 (C-8), 197.1 (C-6). IR (neat, cm^{-1}): 458, 547, 603, 696, 733, 770, 838, 957, 1028, 1132, 1232, 1348, 1423, 1520, 1694, 2851, 2923.

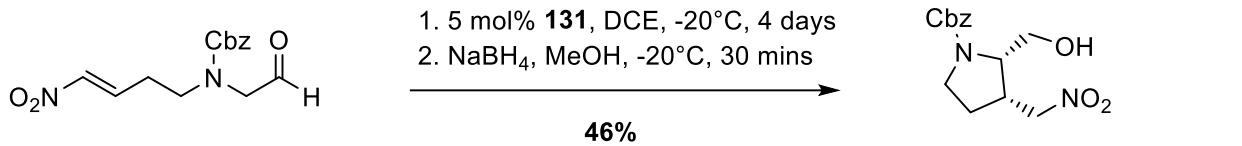

154

141 (5:1 *dr*, 80% *ee*)

benzyl (2*S*,3*S*)-2-(hydroxymethyl)-3-(nitromethyl)pyrrolidine-1-carboxylate **141**

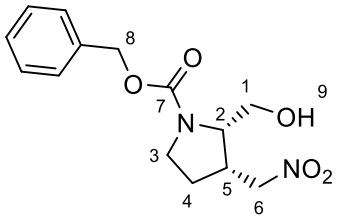

141

A solution of (*S*)-(-)-5-(2-pyrrolidinyl)-1H-tetrazole **131** (0.117 g, 0.841 mmol) in DCE (80 mL) was sonicated for 30 minutes and then cooled to -20°C, after which a solution of **154** (1.158 g, 3.96 mmol) in DCE (4 mL) was added dropwise over the course of 5 minutes. The reaction mixture was then left stirring at -20°C for 96 hours. $NaBH_4$ (0.224 g, 5.921 mmol) was then added in one portion, followed by MeOH (10 mL) and the reaction left to stir for 1 hour. The reaction was then quenched via the addition of a saturated aqueous solution of ammonium chloride (10 mL), followed by brine (40 mL). The organic phase was first extracted with a 3:1 mixture of chloroform and isopropanol (3 x 80 mL) and then with ethyl acetate (3 x 100 mL). The combined organic layers were dried over $MgSO_4$, filtered and concentrated *in vacuo*. The crude product was purified by column chromatography (50% ethyl acetate in hexane) to separately give the *cis* and *trans* diastereoisomers (46%, 0.536 g, 5:1 *dr*, 80% *ee*). *Cis*-**141** data: ^{1}H NMR ($CDCl_3$, 400 MHz): δ 1.86-2.08 (2H, m, H-4), 2.47 (1H, s, H-9), 2.96-3.10 (1H, m, H-3), 2.96-3.10 (1H, m, H-5), 3.36-3.48 (1H, m, H-5), 3.55-3.62 (1H, m, H-1), 3.62-3.70 (1H, m, H-1), 3.73-3.86 (2H, m, H-2), 4.05-4.16 (1H, m H-6), 4.45-4.57 (1H, m, H-6), 4.70-4.79 (2H, m, H-8), 7.31-7.38 (5H, m, H-Ar). ^{13}C NMR ($CDCl_3$, 125 MHz): δ 27.0 & 27.8 (C-4), 38.7 & 39.4 (C-2), 45.4 & 45.7 (C-5), 61.0 & 61.3 (C-1), 67.2 (C-8), 74.9 (C-6), 127.9 (C-Ar), 128.1 (C-Ar), 128.2 (C-Ar),

128.6 (C-Ar), 136.4 (C-Ar), 154.8 & 155.4 (C-7). IR (neat, cm^{-1}): 605, 696, 737, 768, 1003, 1040, 1111, 1325, 1358, 1414, 1549, 1674, 2888, 2953, 3420. $[\alpha]_D^{20}$ +9 (c = 0.1, dichloromethane). HPLC analysis: Chiralpack AD-H, 10% isopropanol in hexane, flow rate = 1 mL/min, λ = 254 nm.

benzyl (2*S*,3*S*)-2-(hydroxymethyl)-3-(nitromethyl)pyrrolidine-1-carboxylate **141-rac**

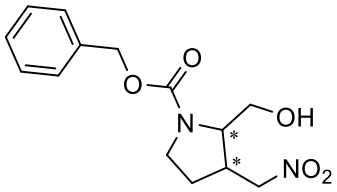

141-rac

The production of the racemic product **141-rac** was achieved by following the same synthetic route as for **141**, but with an equal amount of *D*- and *L*-proline used as the catalyst for the organocatalytic reaction.

5.3.3. Synthesis of dipeptides 142 and 143

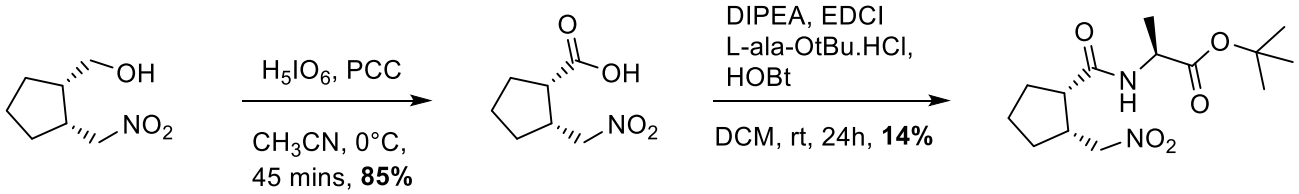

132 **133** **142**

(1*S*,2*R*)-2-(nitromethyl)cyclopentane-1-carboxylic acid **133**

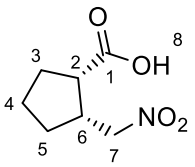

133

A solution of H_5IO_6 (0.874 g, 3.834 mmol) in anhydrous acetonitrile (7.5 mL) was stirred at rt for 15 minutes, after which the reaction mixture was cooled to 0˚C and a solution of the nitro alcohol **132** (0.278 g, 1.747 mmol) in anhydrous acetonitrile (0.8 mL) added, followed by PCC (0.008 g, 0.037 mmol) in anhydrous acetonitrile (1.6 mL). The reaction was stirred at 0°C for 45 minutes, after which ethyl acetate (20 ml) was added and the organic phase washed with brine (20 mL), then with a saturated aqueous sodium bicarbonate solution (30 mL) and then brine again (20 mL). The combined organic layers were then dried over $MgSO_4$, filtered and concentrated *in vacuo* to give compound **133** as a pale yellow oil (85%, 0.257 g). ^{1}H NMR ($CDCl_3$, 400 MHz): δ 1.54-1.64 (1H, m, H-5), 1.65-1.76 (1H, m, H-4), 1.84-1.95 (2H, m, H-4 & H-5), 1.97-2.05 (2H, m, H-3), 2.83-2.94 (1H, m, H-6), 3.01-3.08 (1H, m, H-2), 4.43 (1H, dd, J = 13.3 & 8.1 Hz, H-7), 4.67 (1H, dd, J = 13.3 & 7.3 Hz, H-7), 11.47 (1H, s, H-8). ^{13}C NMR ($CDCl_3$, 125 MHz): δ 23.3 (C-4), 29.1 (C-5), 29.3 (C-3), 40.6 (C-6), 45.6 (C-2), 76.4 (C-7), 180.8 (C-1). IR (neat, cm^{-1}): 662, 920, 1151, 1240, 1381, 1429, 1547, 1699, 2875, 2954. $[\alpha]_D^{20}$ +17 (c = 0.1, dichloromethane).

Tert-butyl ((1*S*,2*R*)-2-(nitromethyl)cyclopentane-1-carbonyl)-L-alaninate **142**

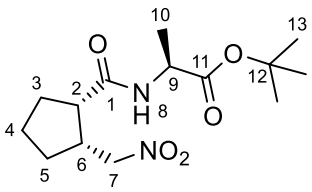

142

To a solution of the nitro acid **133** (0.700 g, 4.045 mmol) in dichloromethane (29 mL), DIPEA (0.840 mL, 4.826 mmol), HOBt.H_2O (0.739 g, 4.826 mmol) and EDCI (0.749 g, 4.826 mmol) were added and the reaction mixture stirred for 5 minutes. L-Ala tert-butyl ester hydrochloride (0.738 g, 4.06 mmol) was then added and the reaction stirred for 24 hours. The reaction mixture was then diluted with excess ethyl acetate and washed with aqueous 10% citric acid (30 mL), aqueous saturated sodium bicarbonate (30 mL) and brine (30 mL). The organic layer was dried over $MgSO_4$, filtered and concentrated *in vacuo*. The crude product was purified by column chromatography (40% ethyl acetate in hexane) to give compound **142** as a white solid (14%, 0.170 g). ^{1}H NMR ($CDCl_3$, 400 MHz): δ 1.33 (3H, d, J = 7.2 Hz, H-10), 1.44 (9H, s, H-13), 1.57-1.68 (2H, m, H-4 & H-5), 1.78-1.85 (1H, m, H-5), 1.87-1.98 (3H, m, H-3 & H-4), 2.73-2.89 (2H, m, H-2 & H-6), 4.29-4.44 (2H, m, H-7 & H-9), 4.70 (1H, dd, J = 13.4 & 7.5 Hz, H-7), 6.18 (1H, d, J = 6.7 Hz, H-8). ^{13}C NMR ($CDCl_3$, 125 MHz): δ 18.3 (C-10), 23.9 (C-4), 28.0 (C-13), 29.6 (C-3), 29.8 (C-5), 41.6 (C-6), 46.9 (C-2), 48.8 (C-9), 76.6 (C-7), 82.1 (C-12), 172.2 (C-11), 173.1 (C-1). IR (neat, cm^{-1}): 695, 847, 1149, 1223, 1334, 1370, 1448, 1549. 1639, 1738, 2979, 3304, 3374. $[\alpha]_D^{20}$ +21 (c = 0.1, dichloromethane). mp = 75.6°C. HRMS required for $C_{14}H_{24}N_2O_5$ $[M+Na]^+$ 323.1592, found 323.1546.

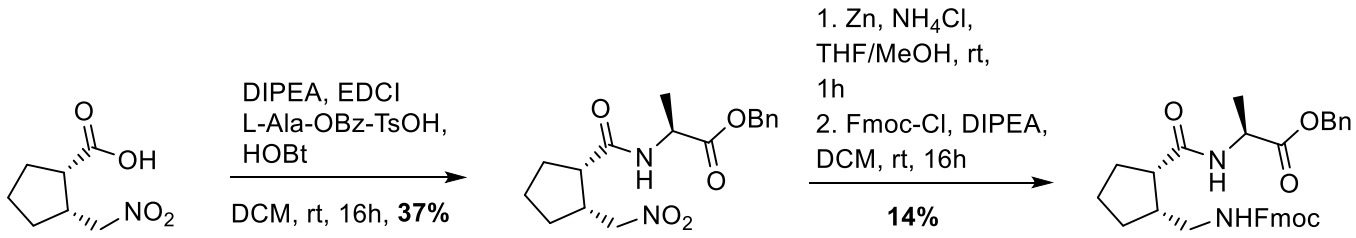

133 **134** **143**

Benzyl ((1*S*,2*R*)-2-(nitromethyl)cyclopentane-1-carbonyl)-L-alaninate **134**

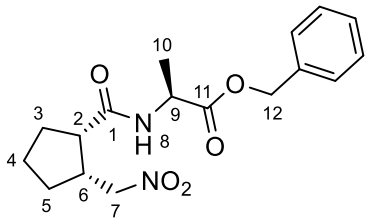

134

To a solution of the nitro acid **133** (0.522 g, 3.016 mmol) in dichloromethane (21 mL), DIPEA (0.630 mL, 3.620 mmol), HOBt.H_2O (0.554 g, 3.620 mmol) and EDCI (0.562 g, 4.826 mmol) were added and the reaction mixture stirred for 5 minutes. L-Ala benzyl ester p-toluene sulfonate salt (1.062 g, 3.016 mmol) was then added and the reaction stirred for 16 hours. The reaction mixture was then diluted with excess ethyl acetate and washed with aqueous 10% citric acid (20 mL), aqueous saturated sodium bicarbonate (20 mL) and brine (20 mL). The organic layer was dried over $MgSO_4$, filtered and concentrated *in vacuo*. The crude product was purified by column chromatography (40% ethyl acetate in hexane) to give compound **134** as a white solid (37%, 0.373 g). ^{1}H NMR ($CDCl_3$, 400 MHz): δ 1.37 (3H, d, J = 7.3 Hz, H-10), 1.55-1.66 (2H, m, H-4 & H-5), 1.75-1.84 (1H, m, H-5), 1.86-1.99 (3H, m, H-3 & H-4), 2.70-2.81 (1H, m, H-6), 2.84-2.91 (1H, m, H-2), 4.35 (1H, dd, J = 13.5 & 7.1 Hz, H-7), 4.51 (1H, p, J = 7.3 Hz, H-9), 4.65 (1H, dd, J = 13.5 & 7.8 Hz, H-7), 5.14 (2H, dd, J = 28.9 & 12.2 Hz, H-12), 6.33 (1H, d, J = 7.1 Hz, H-8), 7.27-7.37 (5H, m, H-Ar). ^{13}C NMR ($CDCl_3$, 125 MHz): δ 17.7 (C-10), 23.7 (C-4), 29.3 (C-3), 29.6 (C-5), 41.6 (C-6), 46.6 (C-2), 48.2 (C-9), 67.2 (C-12), 76.4 (C-7), 128.2 (C-Ar), 128.4 (C-Ar), 128.6 (C-Ar), 135.3 (C-Ar), 172.7 (C-11), 173.4 (C-1). IR (neat, cm^{-1}): 597, 700, 742, 912, 962, 1151, 1188, 1347, 1387, 1454, 1526, 1640, 1744, 2959, 3316. $[\alpha]_D^{20}$ +17 (c = 0.1, dichloromethane). mp = 96.1-97.5°C.

benzyl ((1*S*,2*R*)-2-(((((9H-fluoren-9-yl)methoxy)carbonyl)amino)methyl)cyclopentane-1-carbonyl)-L-alaninate **143**

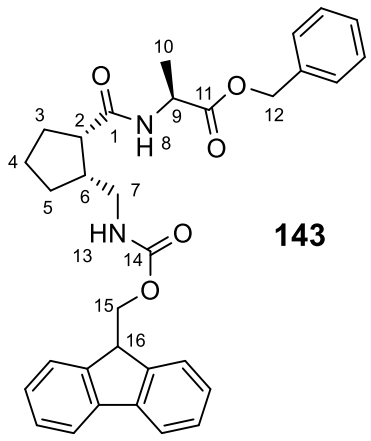

143

To a solution of dipeptide **134** (0.324 g, 0.970 mmol) in anhydrous MeOH (21 mL) and anhydrous THF (21 mL) was added Zn powder (1.04 g, 15.82 mmol) and ammonium chloride (0.847 g, 15.82 mmol), and the reaction mixture stirred for 1 hour at rt. Ethyl acetate was then added (200 mL) and the solution filtered through a pad of celite. The white solid that was obtained was then dissolved in dichloromethane and filtered through cotton wool. The crude product was then taken up in dichloromethane (6 mL) and DIPEA (0.302 ml, 1.734 mmol) added, followed by Fmoc-Cl (0.449 g, 1.734 mmol). The reaction was stirred for 16 hours at room temperature after which excess ethyl acetate was added, and the organic phase washed with saturated aqueous sodium bicarbonate solution (2 x 25 mL). The organic layer was dried over $MgSO_4$, filtered and concentrated *in vacuo* to give compound **143** as a white solid (14%, 0.071 g). ^{1}H NMR ($CDCl_3$, 400 MHz): δ 1.24-1.27 (1H, m, H-3), 1.40-1.44 (3H, m, H-10), 1.50-1.62 (2H, m, H-4 & H-5), 1.72-1.78 (2H, m, H-3 & H-4), 2.41-2.49 (1H, m, H-6), 2.52-2.61 (1H, m, H-2), 2.98-3.06 (1H, m, H-7), 3.29-3.39 (1H, m, H-7), 4.22 (1H, t, J = 6.8 Hz, H-16), 4.42 (1H, dd, J = 6.9 & 2.0 Hz, H-15), 4.53-4.63 (2H, m, H-9 & H-15), 5.08-5.24 (2H, m, H-12), 5.99 (1H, d, J = 7.1 Hz, H-8), 6.16 (1H, t, J = 5.9 Hz, H-13), 7.28-7.42 (m, H-Ar), 7.56-7.69 (3H, m, H-Ar), 7.76 (2H, d, J = 7.5 Hz, H-Ar). ^{13}C NMR ($CDCl_3$, 125 MHz): δ 17.9 (C-10), 24.8 (C-4), 29.8 (C-3), 30.0 (C-5), 42.3 (C-7), 44.0 (C-6), 46.9 (C-2), 47.6 (C-16), 48.1 (C-9), 66.2 (C-15), 67.5 (C-12), 120.0 (C-Ar), 125.3 (C-Ar), 125.4 (C-Ar), 127.1 (C-Ar), 127.7 (C-Ar), 128.3 (C-Ar), 128.7 (C-Ar), 135.3 (C-Ar), 141.4 (C-Ar), 144.2 (C-Ar), 144.4 (C-Ar), 156.8 (C-14), 173.8 (C-11), 175.0 (C-1). IR (neat, cm^{-1}): 694, 736, 756, 1107, 1146, 1196, 1265, 1379, 1447, 1539, 1640, 1694, 1736, 2929, 3322. $[\alpha]_D^{20}$ +45 (c = 0.1, dichloromethane). mp = 62.4°C. HRMS required for $C_{32}H_{34}N_2O_5$ 527.2573, found 527.2617.

5.3.4. Synthesis of pyrrolidine-based dipeptide 144

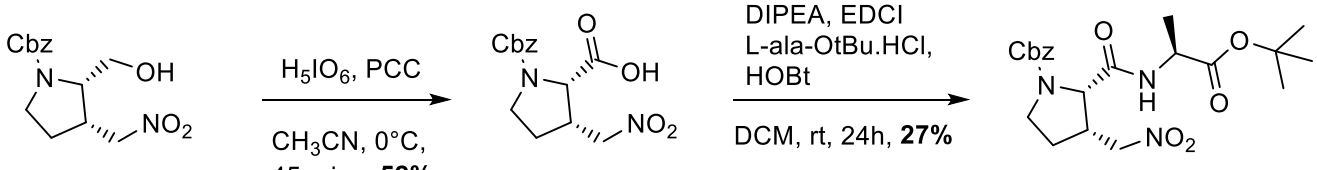

141 **156** **144**

(2*S*,3*S*)-1-((benzyloxy)carbonyl)-3-(nitromethyl)pyrrolidine-2-carboxylic acid **156**

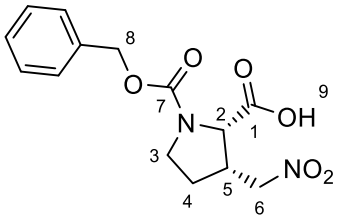

156

A solution of H_5IO_6 (0.968 g, 4.247 mmol) in anhydrous acetonitrile (8.5 mL) was stirred at rt for 15 minutes, after which the reaction mixture was cooled to 0°C and a solution of the nitro alcohol **141** (0.569 g, 1.935 mmol) in anhydrous acetonitrile (0.9 mL) added, followed by PCC (0.009 g, 0.041 mmol) in anhydrous acetonitrile (1.8 mL). The reaction was stirred at 0°C for 45 minutes, after which ethyl acetate (20 ml) was added and the organic phase washed with brine (20 mL), then with a saturated aqueous sodium bicarbonate solution (30 mL) and then brine again (20 mL). The combined organic layers were then dried over $MgSO_4$, filtered and concentrated *in vacuo* to give compound **156** as a white solid (52%, 0.312 g). ^{1}H NMR ($CDCl_3$, 400 MHz): δ 1.75-1.95 (1H, m, H-4), 2.03-2.09 (1H, m, H-4), 3.05-3.26 (1H, m, H-5), 3.38-2.50 (1H, m, H-3), 3.66-3.80 (1H, m, H-3), 4.29-4.42 (1H, dd, J = 14.5 & 7.2 Hz, H-6), 4.48-4.68 (2H, m, H-2 & H-6), 5.00-5.21 (2H, m, H-8), 7.22-7.38 (5H, m, H-Ar), 10.65 (1H, s, H-9). ^{13}C NMR ($CDCl_3$, 125 MHz): δ 26.5 & 27.7 (C-4), 38.6 & 39.4 (C-5), 45.4 & 45.7 (C-3), 60.7 (C-2), 67.6 (C-8), 74.7 (C-6), 127.6 (C-Ar), 127.8 (C-Ar), 128.2 (C-Ar), 128.5 (C-Ar), 128.6 (C-Ar), 136.2 (C-Ar), 154.4 & 155.3 (C-7), 171.7 & 174.0 (C-1). IR (neat, cm^{-1}): 698, 735, 770, 1128, 1210, 1360, 1382, 1418, 1553, 1698, 2900, 2959. $[\alpha]_D^{20}$ -17 (c = 0.1, dichloromethane). mp = 51.7°C. HRMS required for $C_{14}H_{16}N_2O_6$ $[M-H]^-$ 307.0927, found 308.0938.

benzyl (2*S*,3*S*)-2-(((*S*)-1-(tert-butoxy)-1-oxopropan-2-yl)carbamoyl)-3-(nitromethyl)pyrrolidine-1-carboxylate **144**

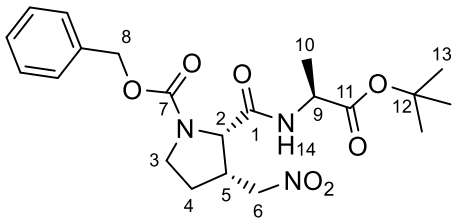

144

To a solution of the nitro acid **156** (0.326 g, 1.058 mmol) in dichloromethane (7 mL), DIPEA (0.215 mL, 1.235 mmol), HOBt.H_2O (0.190 g, 1.241 mmol) and EDCI (0.192 g, 1.235 mmol) were added and the reaction mixture stirred for 5 minutes. L-Ala tert-butyl ester hydrochloride (0.198 g, 1.089 mmol) was then added and the reaction stirred for 24 hours. The reaction mixture was then diluted with excess ethyl acetate and washed with aqueous 10% citric acid (10 mL), aqueous saturated sodium bicarbonate (10 mL) and brine (10 mL). The organic layer was dried over $MgSO_4$, filtered and concentrated *in vacuo*. The crude product was purified by column chromatography (60% ethyl acetate in hexane) to give compound **144** as a white solid (27%, 0.124 g). ^{1}H NMR ($CDCl_3$, 400 MHz): δ 1.12 &1.21 (3H, d, J = 7.0 Hz, H-10), 1.37 (9H, s, H-13), 1.84-2.04 (2H, m, H-4), 2.88-3.03 (1H, m, H-5), 3.33-3.44 (1H, m, H-3), 3.62-3.74 (1H, m, H-3), 4.19 (1H, p, J = 7.0 Hz, H-9), 4.30-4.88 (3H, m, H-2 & H-6), 4.94-5.11 (2H, m, H-8), 6.38 & 7.01 (1H, d, J = 6.0 Hz, H-14), 7.18-7.31 (5H, m, H-Ar). ^{13}C NMR ($CDCl_3$, 125 MHz): δ 17.4 & 17.8 (C-10), 26.8 & 27.7 (C-4), 27.9 (C-13), 39.5 & 40.2 (C-5), 45.4 & 45.8 (C-3), 48.8 & 49.1 (C-9), 61.3 (C-2), 67.4 (C-8), 74.6 (C-6), 127.9 (C-Ar), 128.1 (C-Ar), 128.2 (C-Ar), 128.5 (C-Ar), 136.2 (C-Ar), 136.4 (C-Ar), 154.2 & 154.9 (C-7), 169.0 & 169.3 (C-11), 171.4 & 171.6 (C-1). $[\alpha]_D^{20}$ -69 (c = 0.1, dichloromethane). mp = 42.8-49.9°C. HRMS required for $C_{21}H_{29}N_3O_7$ $[M+H]^+$ 436.2073, found 436.1995.

5.3.5. Synthesis of catalytic dipeptide 145

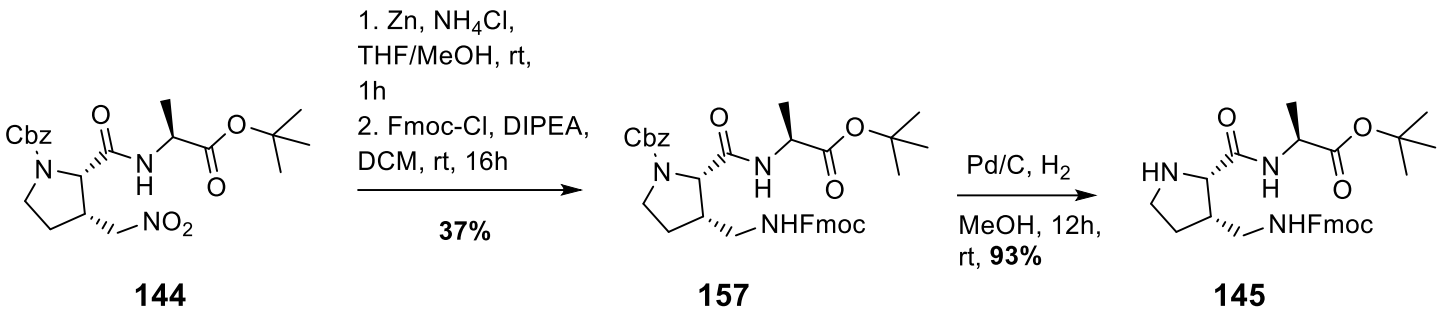

144 **157** **145**

Benzyl (2*S*,3*S*)-3-(((((9H-fluoren-9-yl)methoxy)carbonyl)amino)methyl)-2-(((*S*)-1-(tert-butoxy)-1-oxopropan-2-yl)carbamoyl)pyrrolidine-1-carboxylate **157**

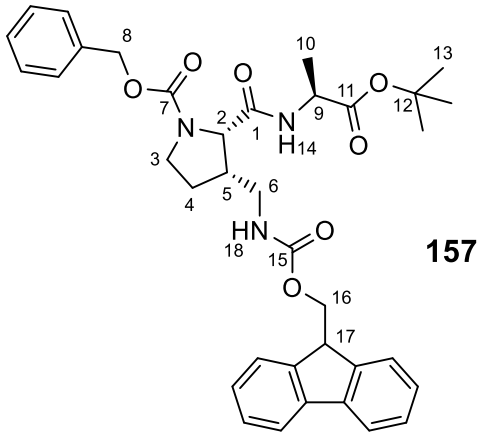

157

To a solution of dipeptide **144** (0.122 g, 0.396 mmol) in anhydrous MeOH (7.7 mL) and anhydrous THF (7.7 mL) was added Zn powder (0.391 g, 5.796 mmol) and ammonium chloride (0.0.314 g, 5.796 mmol), and the reaction mixture stirred for 1 hour at rt. Ethyl acetate was then added (70 mL) and the solution filtered through a pad of celite. The white solid that was obtained was then dissolved in dichloromethane and filtered through cotton wool. The crude product was then taken up in dichloromethane (2.50 mL) and DIPEA (0.122 ml, 0.700 mmol)

added, followed by Fmoc-Cl (0.119 g, 0.460 mmol). The reaction was stirred for 12 hours at room temperature after which excess ethyl acetate was added, and the organic phase washed with saturated aqueous sodium bicarbonate solution (2 x 15 mL). The organic layer was dried over $MgSO_4$, filtered and concentrated *in vacuo* to give compound **157** as a white solid (37%, 0.092 g). ^{1}H NMR ($CDCl_3$, 400 MHz): δ 1.20-1.52 (12H, m, H-10 & H-13), 1.70-1.97 (2H, m, H-4), 2.66-2.98 (2H, m, H-3 & H-5), 3.33-3.50 (1H, m, H-6), 3.52-3.66 (1H, m, H-3), 3.68-3.82 (1H, m, H-6), 4.18 (1H, t, J = 6.7 Hz, H-17), 4.25-4.86 (3H, m, H-2, H-9 & H-16), 5.04-5.22 (2H, m, H-8), 6.20-7.01 (2H, m, H-14 & H-18), 7.24-7.77 (13H, m, H-Ar). ^{13}C NMR ($CDCl_3$, 125 MHz): δ 18.1 (C-10), 27.0 & 27.8 (C-4), 28.0 (C-13), 41.1 (C-3), 42.7 & 43.5 (C-5), 46.3 & 46.6 (C-6), 47.4 (C-17), 48.6 (C-9), 62.4 (C-2), 66.5 (C-16), 67.2 (C-8), 82.4 (C-12), 120.0 (C-Ar), 125.3 (C-Ar), 127.0 (C-Ar), 127.7 (C-Ar), 128.0 (C-Ar), 128.5 (C-Ar), 141.3 (C-Ar), 143.9 (C-Ar), 154.6 & 155.1 (C-7), 156.7 (C-15), 170.3 (C-11), 172.4 & 173.0 (C-1). IR (neat, cm^{-1}): 694, 733, 757, 845, 907, 991, 1110, 1140, 1264, 1352, 1416, 1538, 1650, 1693, 2947, 3325. $[\alpha]_D^{20}$ +44 (c = 0.1, dichloromethane). mp = 119.5-122.1°C. HRMS – unstable when ionised.

Tert-butyl ((2*S*,3*S*)-3-(((((9H-fluoren-9-yl)methoxy)carbonyl)amino)methyl)pyrrolidine-2-carbonyl)-L-alaninate **145**

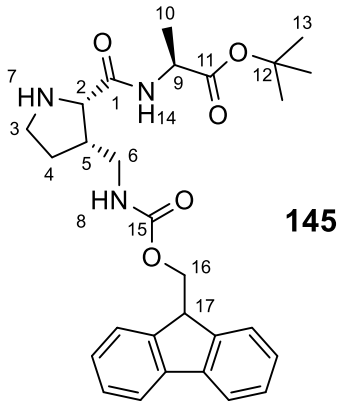

145

To a solution of **157** (0.077 g, 0.123 mmol) in anhydrous MeOH (2.5 mL) was added Pd/C (7.5 mg). The reaction vessel was allowed to flush with H_2 for 5 minutes, through the use of a H_2 balloon and a venting needle. The venting needle was then removed and a fresh H_2 balloon

added, after which the reaction was allowed to stir at rt for 12 hours. The reaction mixture was then filtered through a pad of celite and the solvent removed *in vacuo* to give the product as a white solid (93%, 0.0564 g). ^{1}H NMR (CD_3OD, 400 MHz): δ 1.38 (3H, d, J = 7.3 Hz, H-10), 1.47 (9H, s, H-13), 1.61-1.72 (1H, m, H-4), 1.92-2.02 (1H, m, H-4), 2.59-2.69 (H-5), 2.94-3.02 (1H, m, H-6), 3.06-3.14 (1H, m, H-3), 3.21-3.31 (2H, m, H-3 & H-6), 3.90 (1H, d, J = 8.1 Hz, H-2), 4.18 (1H, t, J = 6.8 Hz, H-17), 4.28-4.42 (3H, m, H-9 & H-18), 7.29 (2H, t, J = 7.5 Hz, H-Fmoc), 7.38 (2H, t, J = 7.5 Hz, H-Fmoc), 7.64 (2H, d, J = 7.4 Hz, H-Fmoc), 7.79 (2H, d, J = 7.5 Hz, H-Fmoc). ^{13}C NMR ($CDCl_3$, 125 MHz): δ 17.6 (C-10), 28.2 (C-13), 30.3 (C-4), 41.5 (C-3), 43.8 (C-5), 46.2 (C-6), 48.5 (C-17), 50.2 (C-9), 63.0 (C-2), 67.6 (C-16), 83.1 (C-12), 120.9 (C-Ar), 126.2 (C-Ar), 128.1 (C-Ar), 128.8 (C-Ar), 142.6 (C-Ar), 145.3 (C-Ar), 158.9 (C-15), 171.8 (C-11), 173.5 (C-1). IR (neat, cm^{-1}): 574, 740, 800, 841, 1050, 1136, 1450, 1679, 2932. $[\alpha]_D^{20}$ +8 (c = 0.1, dichloromethane). mp = 138.6^{o}C. HRMS required for $C_{28}H_{35}N_3O_5$ $[M+Na]^+$ 516.2492, found 516.2425.

References

(1)K. Numata, *Polymer Journal.*, 2020, **52**, 1043-1056.

(2) A. Radzicka and R. Wolfenden, *Science*., 1995, **267**, 90-93.

(3) Y. Erlich and D. Zielinski, *Science*., 2017, **355**, 950-954.

(4) B. Callahan and B. Miller, *Bioorganic Chemistry.,* 2007, **35**, 465-469.

(5) D. Appella, L. Christianson, I. Karle, D. Powell, S. Gellman, *J. Am. Chem. Soc.,* 1996, **118**, 13071-13072.

(6) S. Gellman, *Acc. Chem. Res.,* 1998, **31**, 173-180.

(7) D. Hill, M. Milo, R. Prince, T. Hughes, J. Moore, *Chem. Rev.,* 2001, **101**, 3893-4011.

(8) K. Dill and H. Chan, *Proteins*., 1996, **24**, 335-344.

(9)M. Hagihara, N. Anthony, T. Stout, J. Clardy, S. Schreiber, *J. Am. Chem. Soc*., 1992, **114**, 6568-6570.

(10) C. Gennari, B. Salom, D. Potenza, A. Williams, *Angew. Chem. Int. Ed.,* 1994, **33**, 2067-2069.

(11) S. Rinaldi, *Molecules*., 2020, **25**, 3276-3343.

(12) D. Bassani, J. Lehn, G. Baum, D. Fenske, *Angew. Chem. Int. Ed. Engl.,* 1997, **36**, 1845-1847.

(13) R. Lokey, B. Iverson, *Nature*., 1995, **375**, 303-305.

(14) B. Ikkanda, B. Iverson, *Chem. Commun*., 2016, **52**, 7752-7759.

(15) G. Gabriel, B. Iverson, *J. Am. Chem. Soc.,* 2002, **124**, 15174-15175.

(16) T. Khattab, S. Kamel, *Egypt. J. Chem*., 2021, **64**, 593-604.

(17) Y. Shen, C. Chen, *Chem. Rev.,* 2012*,* **112**, 1463-1535.

(18) M. Krzeszewski, H. Ito, K. Itami, *J. Am. Chem. Soc.,* 2022, **144**, 862-871.

(19) K. Shoning, P. Scholz, S. Guntha, X. Wu, R. Krishnamurthy, A. Eschenmoser, *A. Science.*, 2000, **290**, 1347-1351.

(20) E. Kool, J. Morales, K. Guckian, *Angew. Chem. Int. Ed*., 2000, **39**, 990-1009.

(21) A. Cobb, *Org. Biomol. Chem*., 2007, **5**, 3260–3275.

(22) B. Musicki, T. Widlanski, *Tetrahedron Lett.*, 1991, **32**, 1267-1270.

(23) J. Chen, R. Schultz, D. Lloyd, S. Gryaznov, *Nucleic Acids Research*., 1995, **23**, 2661-2668.

(24) S. Gryaznov, J. Chen, *J. Am. Chem. Soc.,* 1994, **115**, 3143-3144.

(25) P. Nielsen, M. Egholm, R. Berg, O. Buchardt, *Science*., 1991, **254**, 1497-1500.

(26) B. Hyrup, P. Nielsen, *Bioorganic & Medicinal Chemistry*., 1996, **4**, 5-23.

(27) A. Gupta, A. Mishra, N. Puri, *Journal of Biotechnology*., 2017, **259**, 148-159.

(28) K. Nelson, M. Levy, S. Miller, *PNAS*., 2000, **97**, 3868-3871.

(29) V. Menchise, G. De Simone, T. Tedeschi, R. Corranini, S. Sforza, R. Marchelli, D. Capasso, M. Saviano, C. Pedone, *PNAS*., 2003, **100**, 12021-12026.

(30) K. Mach, A. Kaushik, K. Hsiech, P. Wong, T. Wang, J. Liao, *Analyst.,* 2019, **144**, 1565-1574.

(31) K. Kroger, A. Jung, S. Reder, G. Gauglitz, *Analytica Chimica Acta.,* 2002, **469**, 37-48.

(32) J. Pokorski, M. Witschi, B. Purnell, D. Appella, *J. Am. Chem. Soc.,* 2004, **126**, 15067-15073.

(33) L. Marky, K. Breslauer, *Biopolymers.,* 1987, **26**, 1601-1620.

(34) A. Ambrogelly, S. Palioura, D. Söll, *Nature Chemical Biology.,* 2007, **3**, 29-35.

(35) J. Otaki, S. Ienaka, T. Gotoh, H. Yamamoto, *Protein Science.,* 2005, **14**, 617-625.

(36) J. Hau, D. Cazes, L. Fay, *J. Agric. Food Chem.,* 1997, **45**, 1351-1355.

(37) R. Hubbard, M. Haider, Hydrogen Bonds in Proteins: Role and Strength, *Encyclopedia of Life Sciences*., John Wiley & Sons, Ltd, 2010, 1-7.

(38) R. Spolar, J. Ha, M. Thomas Record, *Proc. Natl. Acad. Sci.,* 1989, **86**, 8382-8385.

(39) N. Darby, T. Creighton, Protein Structure: In Focus, *IRL Press,* Oxford University Press, 1993, 97.

(40) J. Ha, S. Loh, *Chem. Eur. J*., 2012, **18**, 7984 – 7999.

(41) N. Silva, C. Viela, I. Marrucho, C. Freire, C. Neto, A. Silvestre, *J. Mater. Chem. B*., 2014, **2**, 3715-3740.

(42) R. Simon, R. Kania, R. Zuckermann, V. Huebner, D. Jewell, S. Banville, S. Ng, L. Wang, S. Rosenberg, C. Marlowe, D. Spellmeyer, R. Tan, A. Frankel, D. Santi, F. Cohen, P. Bartlett, *Proc. Nad. Acad. Sci.,* 1992, **89**, 9367-9371.

(43) K. Bicker, S. Cobb, *Chem. Commun.,* 2020, **56**, 11158-11168.

(44) L. Wolf, S. Servoss, M. Moss, *Journal of Neurology & Neuromedicine.,* 2017, **2**, 1-5.

(45) D. Appella, L. Christianson, I. Karle, D. Powell, S. Gellman, *J. Am. Chem. Soc.,* 1996, **118**, 13071-13072.

(46) H. Nohira, K. Ehara, A. Miyashita, *Bull. Chem. Soc. Jpn.,* 1970, **43**, 2230-2233.

(47) J. Kritzer, J. Tirado-Rives, S. Hart, J. Lear, W. Jorgensen, A. Schepartz, *J. Am. Chem. Soc.,* 2005, **127**, 167-178.

(48) P. Arvidsson, M. Rueping, D. Seebach, *Chem. Commun.,* 2001, 649-650.

(49) P. Claudon, Aude. Violette, K. Lamour, M. Decossas, S. Fournel, B. Heurtault, J. Godet, Y. Mely, B. Jamart-Gregoire, M. Averlant-Petit, J. Briand, G. Duportail, H. Monteil, G. Guichard, *Angew. Chem. Int. Ed.*, 2010, **49**, 333 –336.

(50) A. Violette, S. Fournal, K. Lamour, O. Chaloin, B. Frisch, J. Briand, H. Monteil, G. Guichard, *Chemistry & Biology.,* 2006, **13**, 531-538.

(51) N. Pendem, Y. Reddy Nelli, C. Douat, L. Fischer, M. Laguerre, E. Ennifar, B. Kauffmann, G. Guichard, *Angew. Chem. Int. Ed.,* 2013, **52**, 4147-4151.

(52) X. Zhao, M. Jia, X. Jiang, L. Wu, Z. Li, G. Chen, *J. Org. Chem.,* 2004, **69**, 270-279.

(53) C. Cantor, P. Schimmel, Biophysical Chemistry, *Freeman*: *New York*, 1980, 47.

(54) M. Hall, RSC. *Chem. Biol.,* 2021, **2**, 958-989.

(55) B. Legrand, J. Aguesseau-Kondrotas, M. Simon, L. Maillard, *Catalysts*., 2020, **10**, 700-720.

(56) E. John, C. Massena, O. Berryman, *Chemical Reviews.,* 2020, **120**, 2759-2782.

(57) M. Muller, M. Windsor, W. Pomerantz, S. Gellman, D. Hilvert, *Angew. Chem. Int. Ed.,* 2009, **48**, 922-925.

(58) Z. Girvin, M. Andrews, X. Li, S. Gellman, *Science*., 2019, **366**, 1528-1531.

(59) A. Erkkilä, I. Majander, P. M. Pihko, *Chem. Rev.,* 2007, **107**, 5416-5470.

(60) S. Mukherjee, J. W. Yang, S. Hoffmann, B. List, *Chem. Rev.,* 2007, **107**, 5471-5569.

(61) G. Maayan, M. Ward, K. Kirshenbaum, *PNAS*., 2009, **106**, 13679-13684.

(62) C. Baldauf, R. Gunther, H. Hofmann, *J. Org. Chem.,* 2004, **69**, 6214-6220.

(63) R. Stendall, A. Cobb, *Tetrahedron*, 2018, **74**, 4917-4925.

(64) E. O'Reilly, L. Pes, Y. Ortin, H. Muller-Bunz, F. Paradisi, *Amino Acids.,* 2013, **44**, 511-518.

(65) A. Trabocchi, G. Menchi, E. Danieli, A. Guarna, *Amino Acids.,* 2008, **35**, 37-44.

(66) K. Tomita, S. Oishi, H. Ohno, S. Peiper, N. Fujii, *J. Med. Chem.,* 2008, **51**, 7645-7649.

(67) H. Tamamura, T. Tanaka, H. Tsutsumi, K. Nemoto, S. Mizokami, N. Ohashi, S. Oishi, N. Fujii, *Tetrahedron*., 2007, **63**, 9243-9254.

(68) Q. Zhang, Y. Hui, X. Zhou, L. Lin, X. Liu, X. Feng, *Adv. Synth. Catal.,* 2010, **352**, 976-980.

(69) S. Rajkumar, K. Shankland, J. Goodman, A. Cobb, *Org Lett.,* 2013, **15**, 1386-1389.

(70) B. Lopez-Ortega, S. Jenkinson, T. Claridge, G. Fleet, *Tetrahedron Asymmetry.,* 2008, **18**, 976-983.

(71) T. Claridge, J. Goodman, A. Moreno, D. Angus, S. Barker, C. Taillefumier, M. Watterson, G. Fleet, *Tetrahedron Letters.,* 2001, **42**, 4251-4255.

(72) T. Claridge, B. Lopez-Ortega, S. Jenkinson, G. Fleet, *Tetrahedron Asymmetry.,* 2008, **19**, 984-988.

(73) G. Sharma, B. Babu, K. Ramakrishna, P. Nagendar, A. Kunwar, P. Schramm, C. Baldauf, H. Hofmann, *Chem. Eur. J.,* 2009, **15**, 5552-5566.

(74) G. Sharma, V. Reddy, A. Chander, K. Reddy, *Tetrehedron Asymmetry.,* 2002, **13**, 21-24.

(75) D. Nutt, A. Chippindale, A. Cobb, *J. Am. Chem. Soc.,* 2009, **131**, 16016-16017.

(76) A. Wilds, A. Meader, *Journal of Organic Chemistry.,* 1948, **13**, 763-779.

(77) K. Gademann, M. Ernst, D. Hoyer, D. Seebach, *Angew. Chem. Int. Ed.,* 1999, **38**, 1223-1226.

(78) N. Hodnett, *Synlett.,* 2003, **13**, 2095-2096.

(79) A. Ghosh, I. Chakraborty, N. Adarsh, S. Lahiri, *Tetrahedron*., 2010, **66**, 164-171.

(80) Z. Valiullina, L. Khasanova, N. Selezneva, F. Gimalova, K. Pivnitsky, M. Miftakhov, *Mendeleev Commun*., 2014, **24**, 272–273.

(81) F. Bordwell, K. Yee, *J. Am. Chem. Soc.,* 1970, **92**, 5939-5944.

(82) M. Zhao, J. Li, E. Mano, Z. Song, D. Tschaen, E. Grabowski, P. Reider, *J. Org. Chem*., 1999, **64**, 2564-2566.

(83) L. Guo, Y. Chi, A. Almeida, I. Guzei, B. Parker, S. Gellman, *J. Am. Chem. Soc.,* 2009, **131**, 16018-16020.

(84) M. Minch, *Concepts in Magnetic Resonance.,* 1994, **6**, 41-56.

(85) J. Palomo, *RSC Adv*., 2014, **4**, 32658-32672.

(86) D. Boger, R. Lerner, B. Cravett, *J. Org. Chem.,* 1994, **59**, 5078-5079.

(87) Y. Fu, L. Hammarstrom, T. Miller, F. Fronczek, M. Mclaughlin, R. Hammer, *J. Org. Chem.,* 2001, **66**, 7118-7124.

(88) S. Kavanagh, D. Gilheany, *Org. Lett.,* 2020, **22**, 8198-8203.

(89) N. Benoiton, F.Chen, R. Steinauer, M. Chouinard, *Int. J. Peptide. Protein. Res.,* 1986, **27**, 28-33.

(90) G. Sigler, W. Fuller, N. Chaturvedi, M. Goodman, M. Verlander, *Biopolymers.,* 1983, **22**, 2157-2162.

(91) D. Bolin, I. Sytwu, F. Humiec, J. Meienhofer, *Int. J. Peptide. Protein. Res.* 1989, **33**, 353-359.

(92) B. Fisher, S. Gellman, *J. Am. Chem. Soc*., 2016, **138**, 10766−10769.

(93) M. Muttenthaler, F. Albericio, P. Dawson, *Nature Protocols.,* 2015, **10**, 1067-1083.

(94) J. Lopez-Llano, L.A. Campos, J. Sancho, *Proteins.,* 2006, **64**, 769-778.

(95) Ayman El-Faham, F. Albericio, *Chem. Rev.,* 2011, **111**, 6557-6602.

(96) R. Suiros-Funosas, R. Prohens, R. Barbas, A. El-Faham, F. Albericio, *Chem. Eur. J.,* 2009, **15**, 9394-9403.

(97) T. Sawada, S. Gellman, *J. Am. Chem. Soc.,* 2011, **133**, 7336-7339.

(98) M. Giuliano, S. Maynard, A. Almeida, A. Reidenbach, L. Guo, E. Ulrich, I. Guzei, S. Gellman, *J. Org. Chem*., 2013, **78**, 12351-12361.

(99) M. Natalia, C. Zarycz, C. Guerra, *J. Phys. Chem. Lett.,* 2018, **9**, 3720-3724.

(100) J. Decatur, *NOESY on the 400 and 500 Using Topspin*, 2007.

(101) K. Nakanishi, *One-dimensional and two-dimensional NMR spectra by modern pulse techniques*, Mill Valley, Cal., 1990, 619.

(102) N. Greenfield, *Nature Protocols.,* 2006, **1**, 2876-2890.

(103) S. Kelly, T. Jess, N. Price, *Biochimica et Biophysica Acta.,* 2005, **1751**, 119-139.

(104) S. Spencer, A. Rodger, *Anal. Methods.,* 2021, **13**, 359.

(105) Y. Shin, S. Gellman, *J. Am. Chem. Soc*., 2018, **140**, 1394−1400.

(106) R. Katoono, Y. Obara, K. Fujiwara, T. Suzuki, *Chem. Sci.,* 2018, **9**, 2222-2229.

(107) A. Hayen, M.Schmitt, F. Ngassa, K. Thomasson, S. Gellman, *Angew. Chem. Int. Ed.,* 2004, **43**, 505–510.

(108) P. Yogeeswari, J. Vaigunda Ragavendran, D. Sriram, *Recent Patents on CNS Drug Discovery*., 2006, **1**, 113-118.

(109) M. Woll, J. Lai, I. Guzei, S. Taylor, M. Smith, S. Gellman, *J. Am. Chem. Soc.,* 2001, **123**, 11077-11078.

(110) M. Khurram, N. Qureshi, M. Smith, *Chem. Commun*., 2006, 5006-5008.

(111) C. Jones, M. Khurram, F. Truscott, S. Hsu, A. Morrison, M. Smith, *Angew. Chem. Int. Ed.*, 2008, **48**, 7099-7102.

(112) R. Fanelli, D. Berta, T. Foldes, E. Rosta, R. Atkinson, H. Hofmann, K. Shankland, A. Cobb, *J. Am. Chem. Soc.,* 2020, **142**, 1382-1393.

(113) R. Fanelli, *Organocatalytic Access to γ-Amino Acids as Building Blocks for the Synthesis of Foldamers*, 2019, PhD thesis, King's College London.

(114) S. Maity, T. Naveen, U. Sharma, D. Maiti, *Org. Lett*., 2013, **15**, 3384-3387.

(115) X. He, Z. Shen, W. Mo, N. Sun, B. Hu, X. *Hu, Adv. Synth. Catal.,* 2009, **351**, 89 – 92.

(116) B. Dworakowska, *The enantioselective synthesis of 3-((1R,2S)-2 aminocyclohexyl)propanoic acid – a novel δ-amino acid*, 2019, master's dissertation, King's College London.

The synthesis and characterisation of novel peptidomimetic foldamers - Appendix

King's College London

Ryan Stendall

September 2022

7.1 – NMR’s

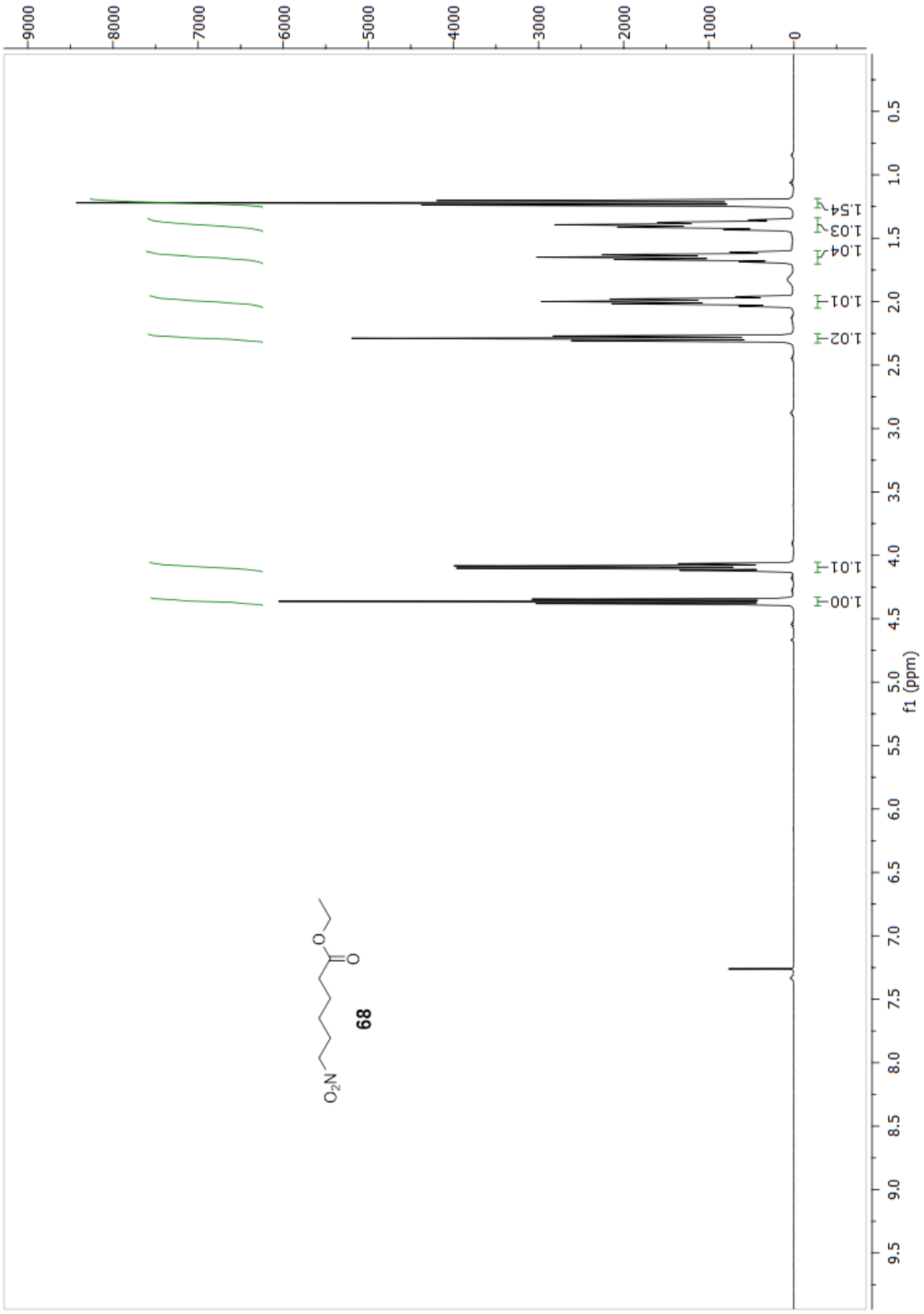
9000
8000
7000
6000
5000
4000
3000
2000
1000
0
0.5
1.0
1.5
2.0
2.5
3.0
3.5
4.0
4.5
5.0
5.5
6.0
6.5
7.0
7.5
8.0
8.5
9.0
9.5
f1 (ppm)
1.54
1.03
1.04
1.01
1.02
1.01
1.00
O
O
O2N
68

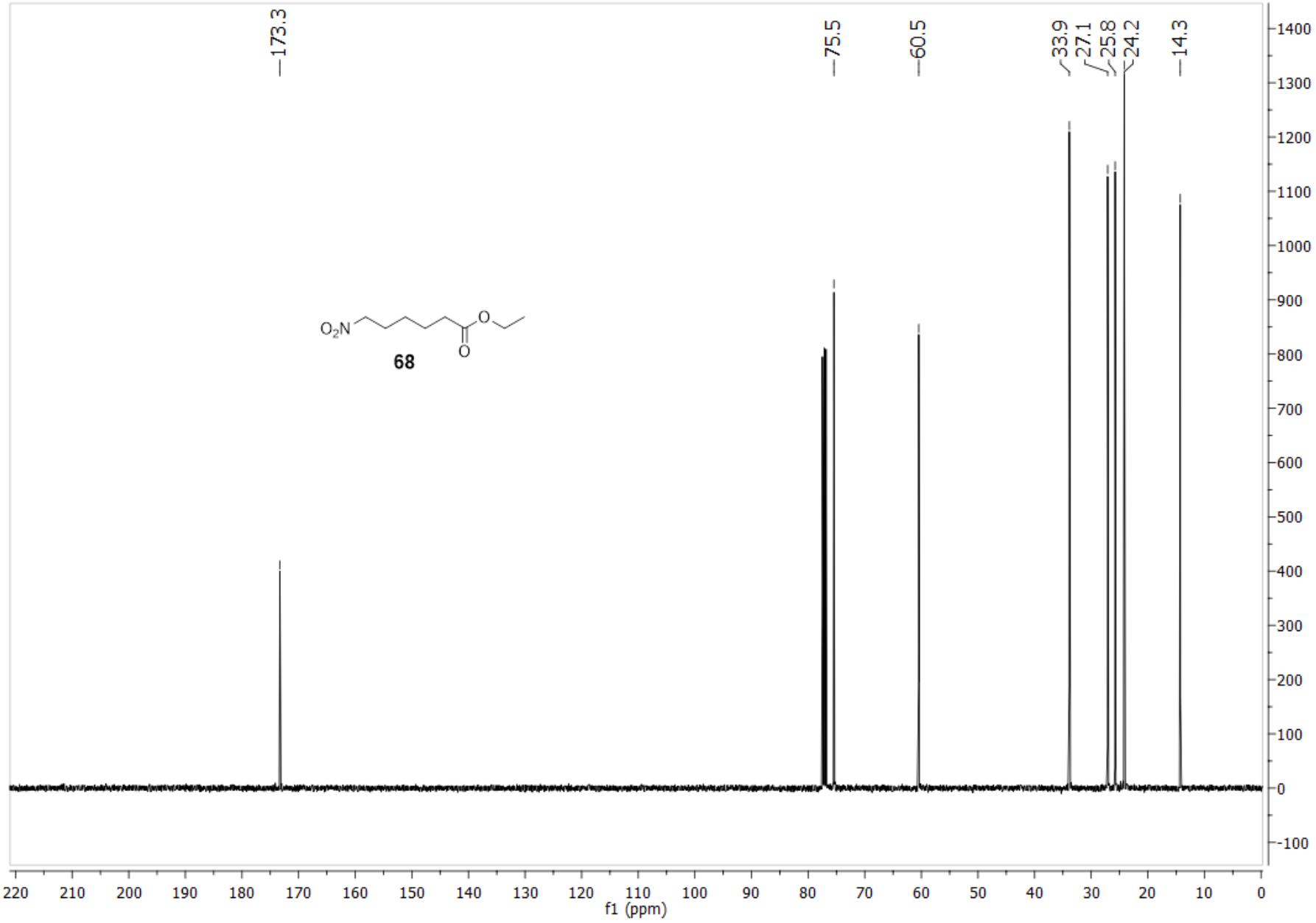
173.3
75.5
60.5
33.9
27.1
25.8
24.2
14.3
O2N
O
O
68
1400
1300
1200
1100
1000
900
800
700
600
500
400
300
200
100
0
-100
220
210
200
190
180
170
160
150
140
130
120
110
100
90
80
70
60
50
40
30
20
10
0
f1 (ppm)

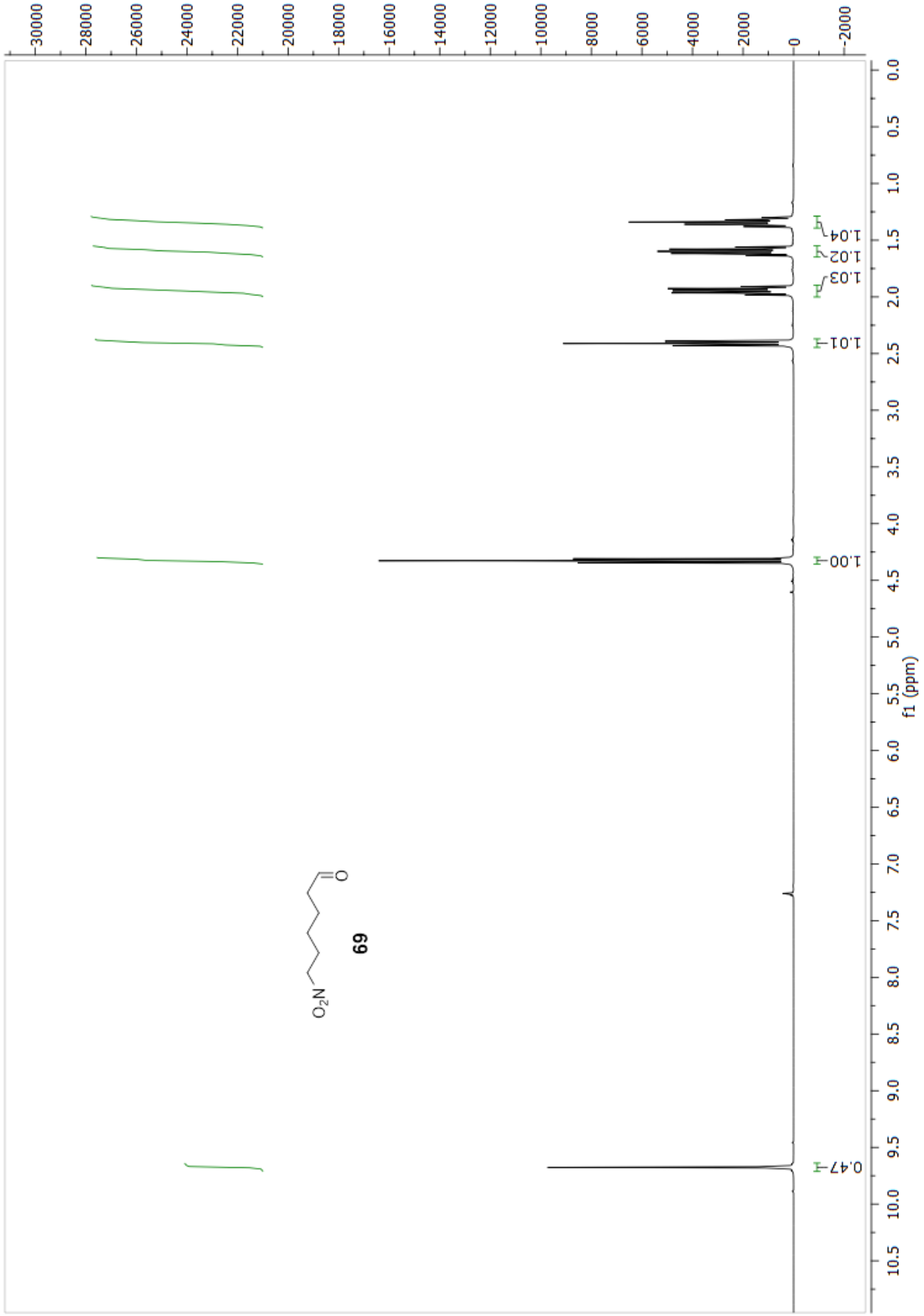
69
O2N
O
1.04
1.02
1.03
1.01
1.00
0.47
f1 (ppm)

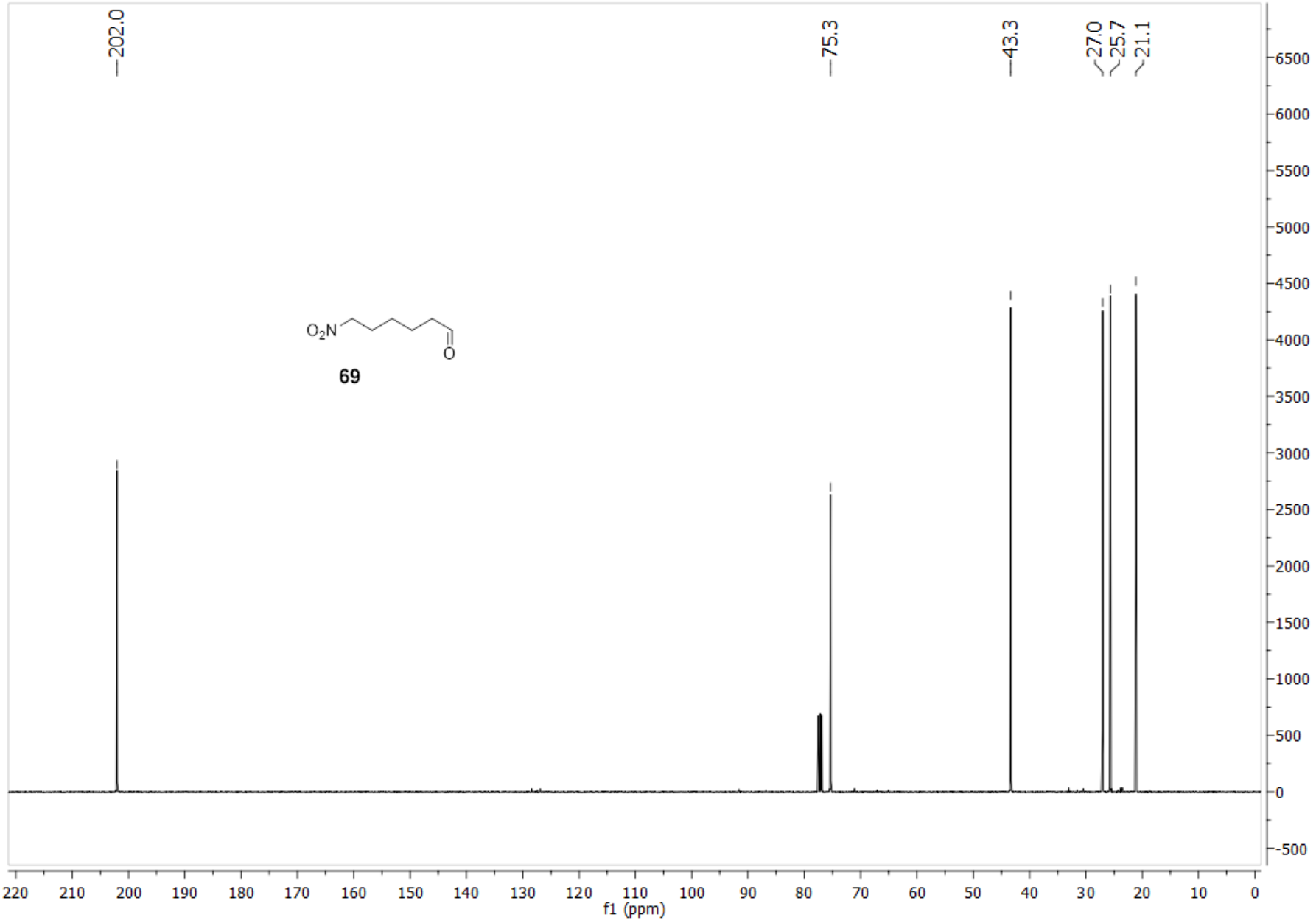
202.0
75.3
43.3
27.0
25.7
21.1
O2N
O
69
6500
6000
5500
5000
4500
4000
3500
3000
2500
2000
1500
1000
500
0
-500
220 210 200 190 180 170 160 150 140 130 120 110 100 90 80 70 60 50 40 30 20 10 0
f1 (ppm)

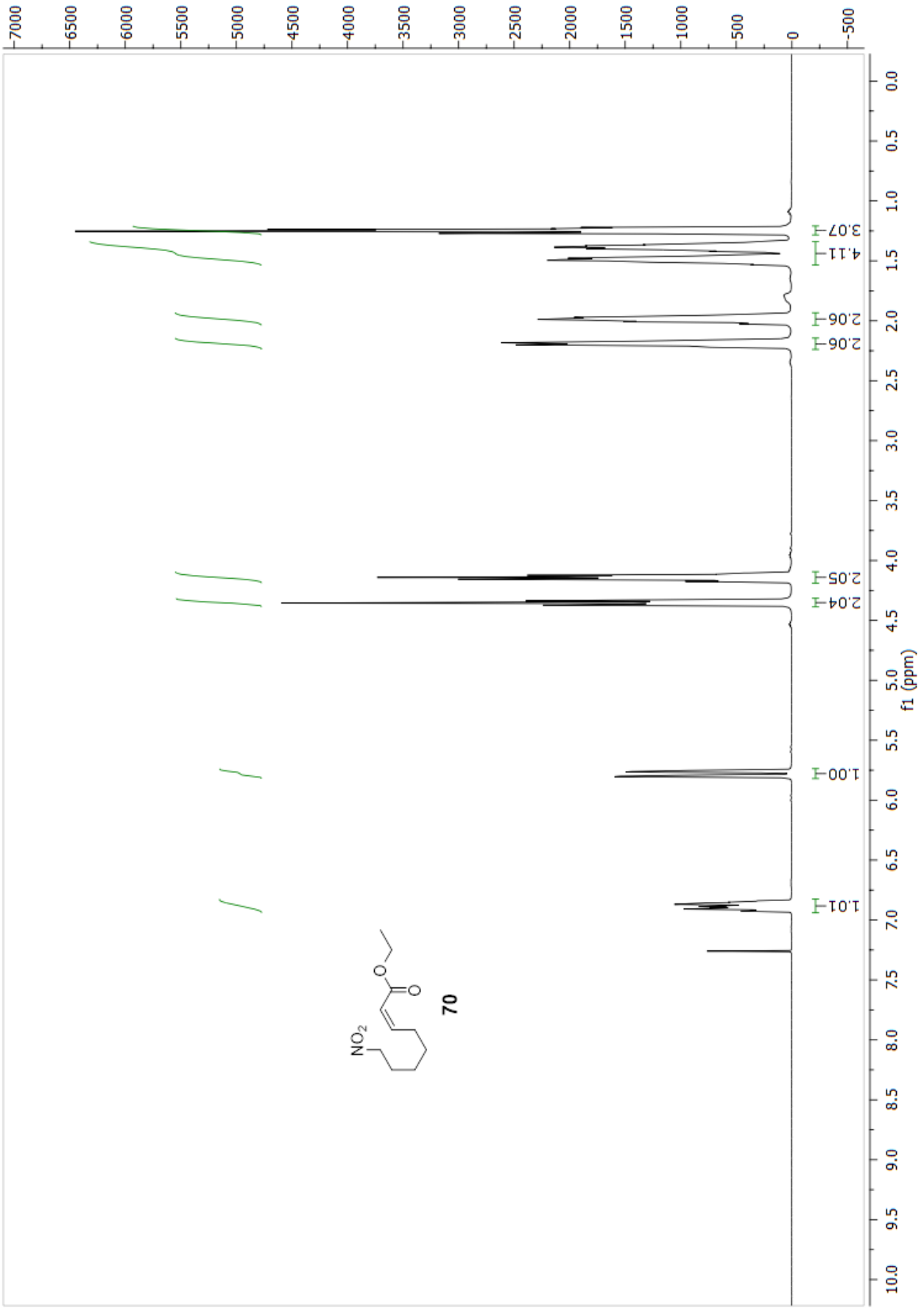
3.07
4.11
2.06
2.06
2.05
2.04
1.00
1.01
f1 (ppm)
70

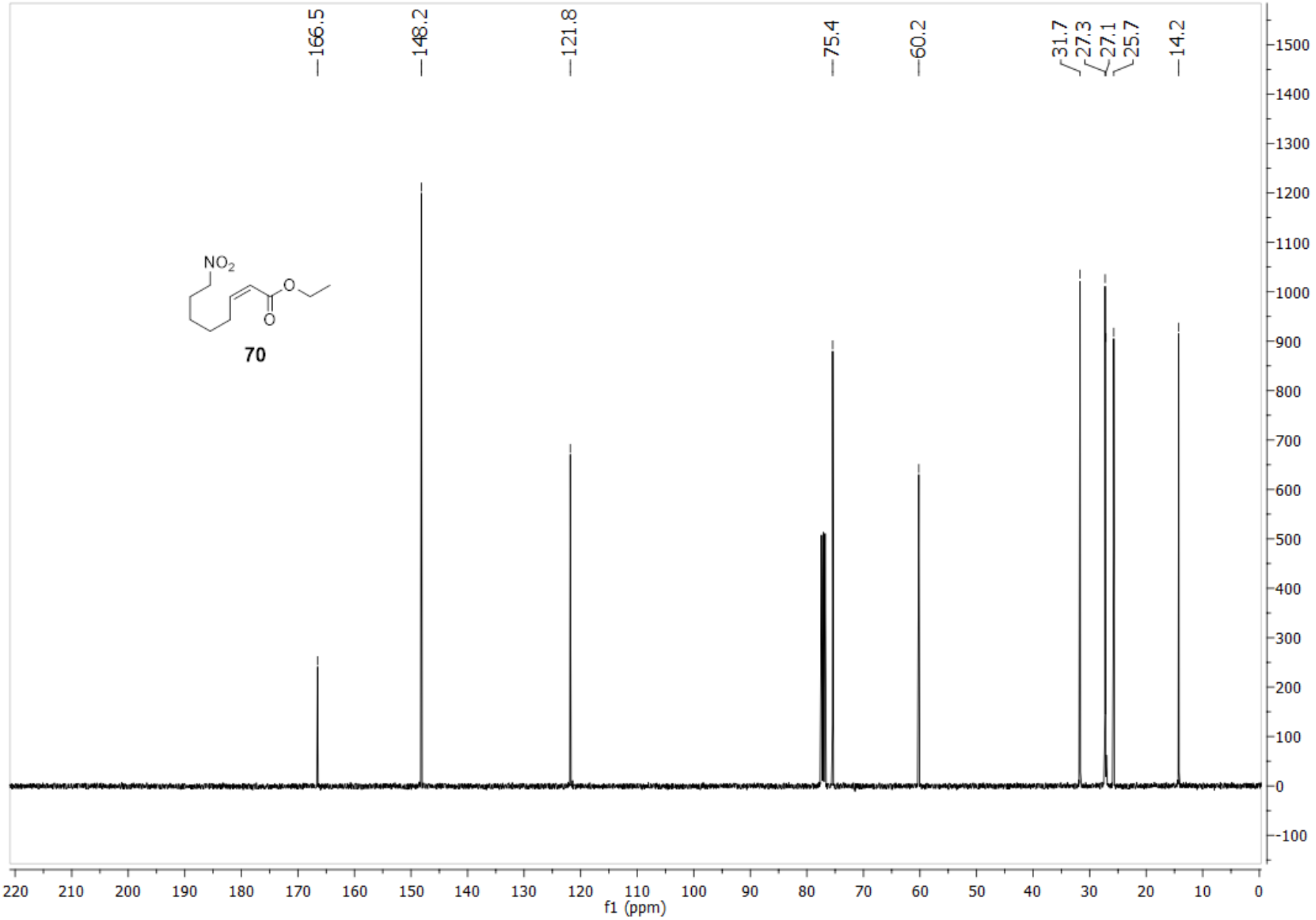
166.5
148.2
121.8
75.4
60.2
31.7
27.3
27.1
25.7
14.2
NO2
O
O
70
f1 (ppm)

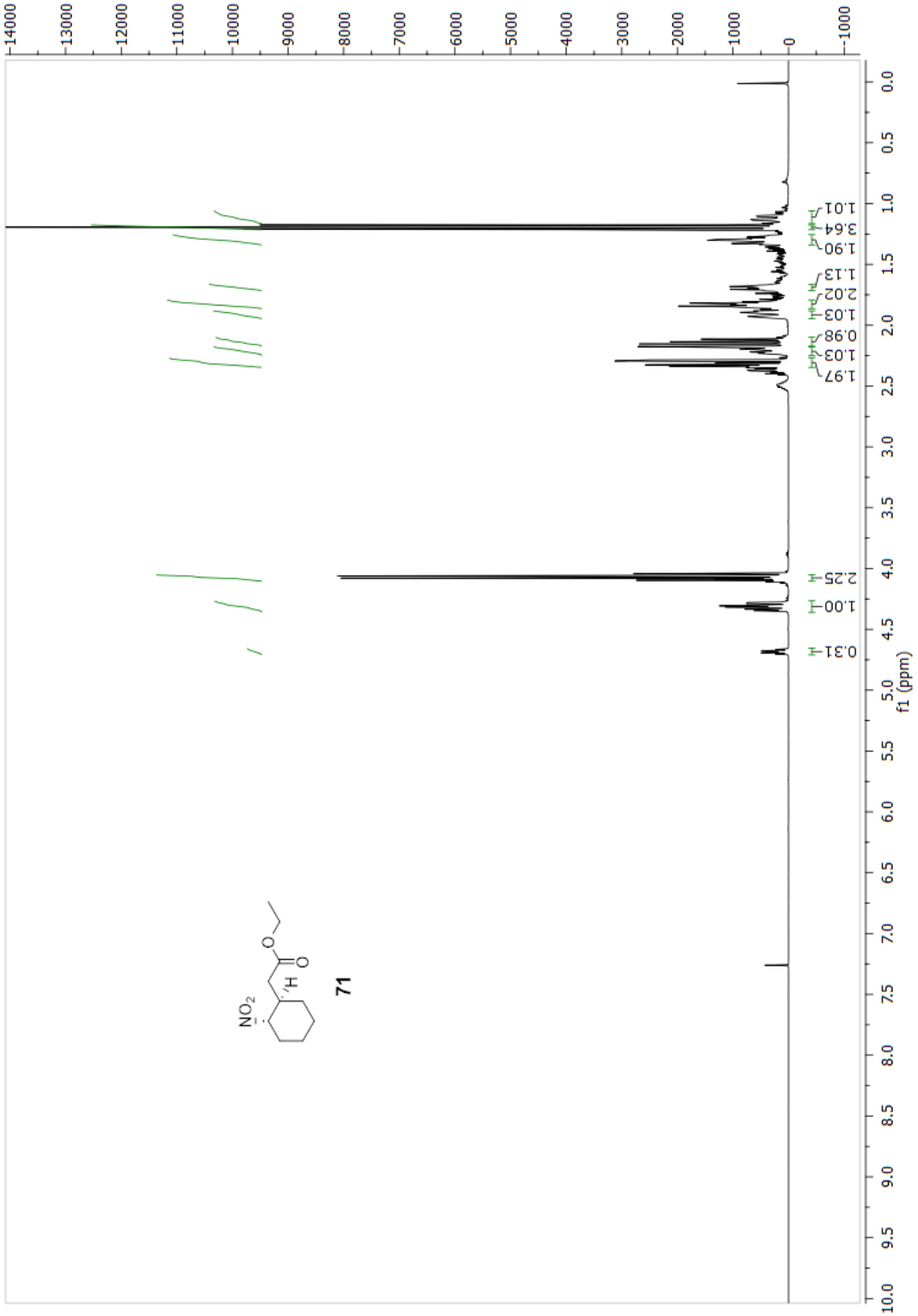
14000
13000
12000
11000
10000
9000
8000
7000
6000
5000
4000
3000
2000
1000
0
-1000
0.0
0.5
1.0
1.5
2.0
2.5
3.0
3.5
4.0
4.5
5.0
5.5
6.0
6.5
7.0
7.5
8.0
8.5
9.0
9.5
10.0
f1 (ppm)
1.01
3.64
1.90
1.13
2.02
1.03
0.98
1.03
1.97
2.25
1.00
0.31
NO2
H
O
O
71

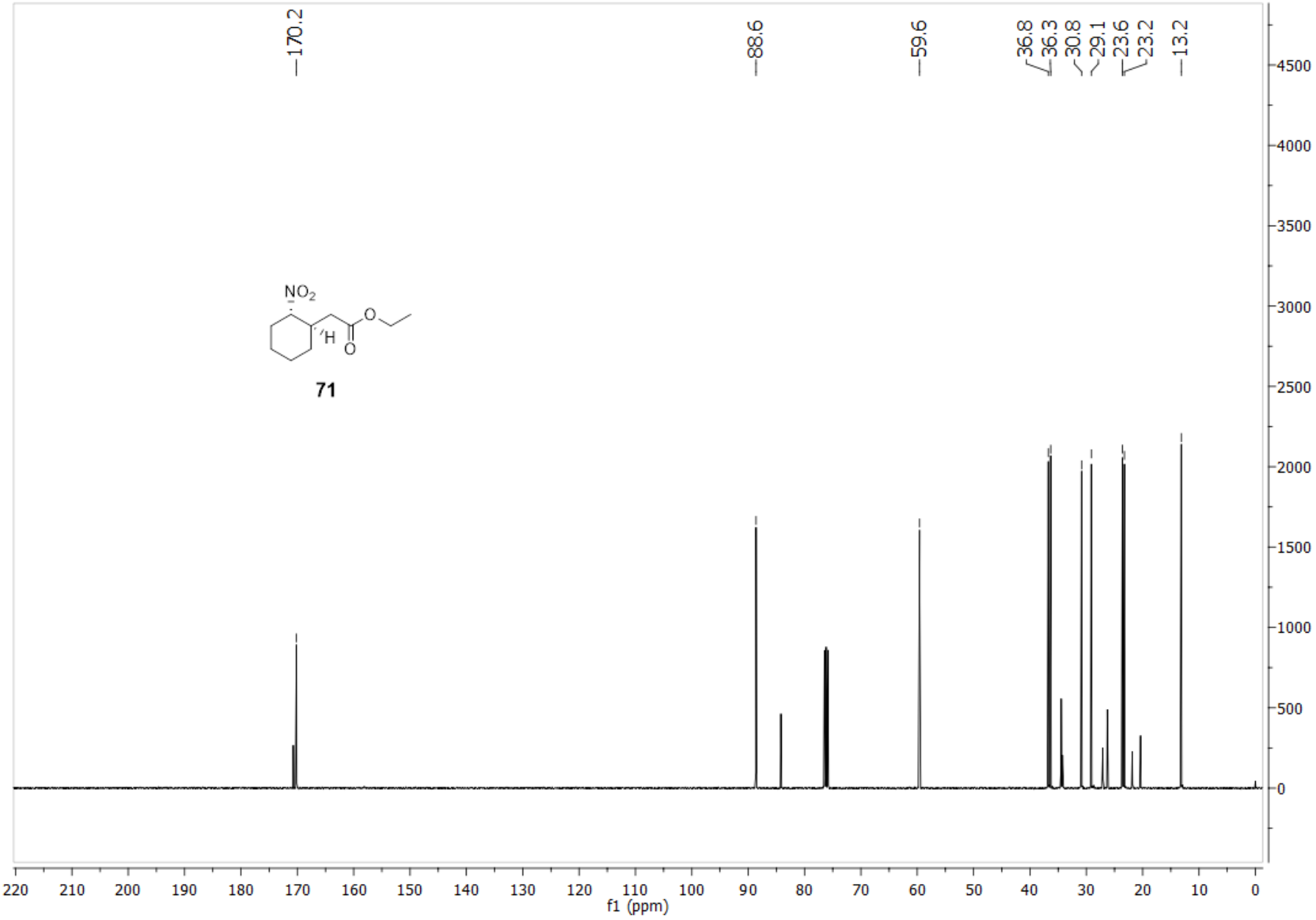
170.2
88.6
59.6
36.8
36.3
30.8
29.1
23.6
23.2
13.2
NO2
H
O
O
71
4500
4000
3500
3000
2500
2000
1500
1000
500
0
220 210 200 190 180 170 160 150 140 130 120 110 100 90 80 70 60 50 40 30 20 10 0
f1 (ppm)

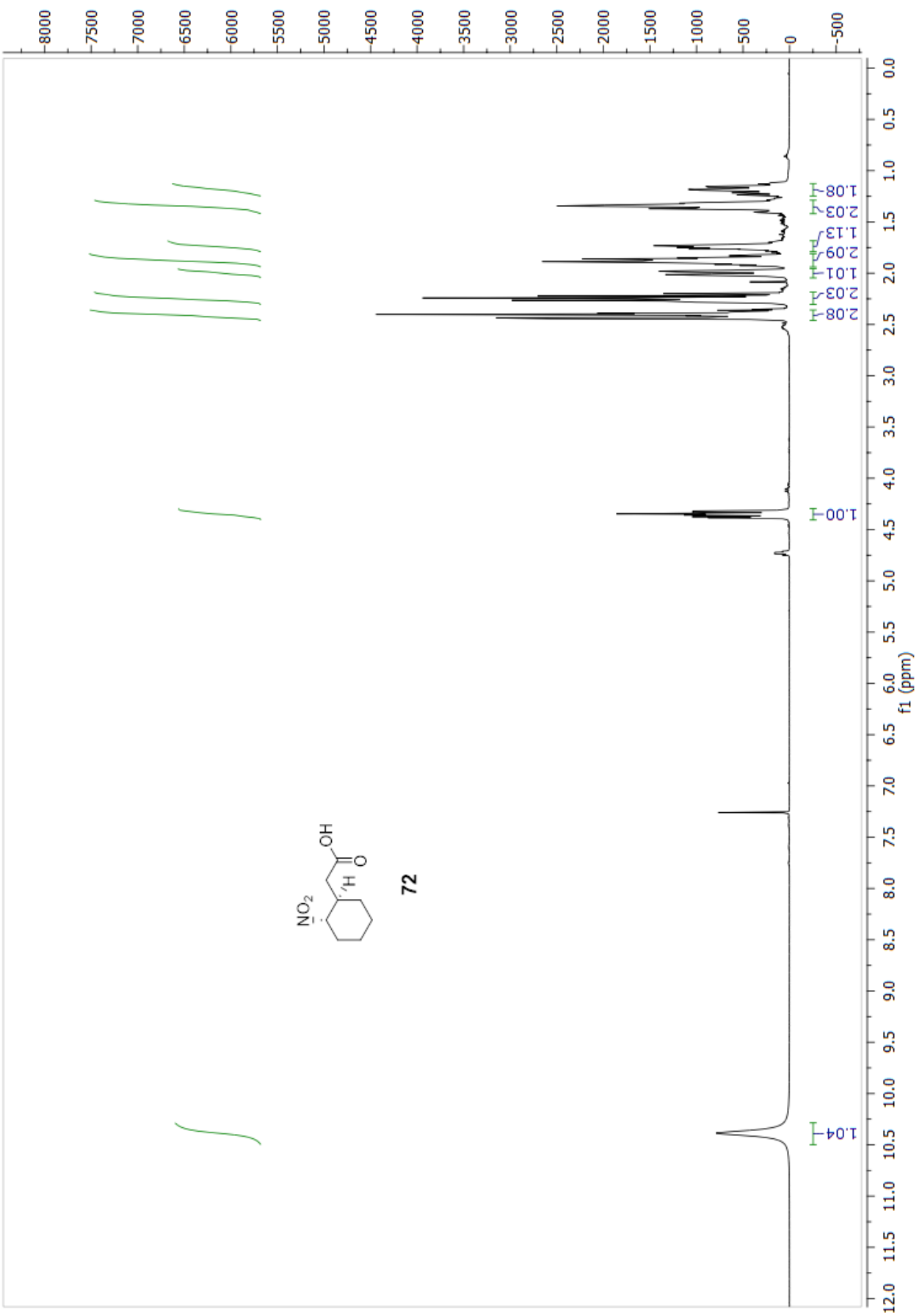
OH
O
H
NO2
72
1.08
2.03
1.13
2.09
1.01
2.03
2.08
1.00
1.04
f1 (ppm)

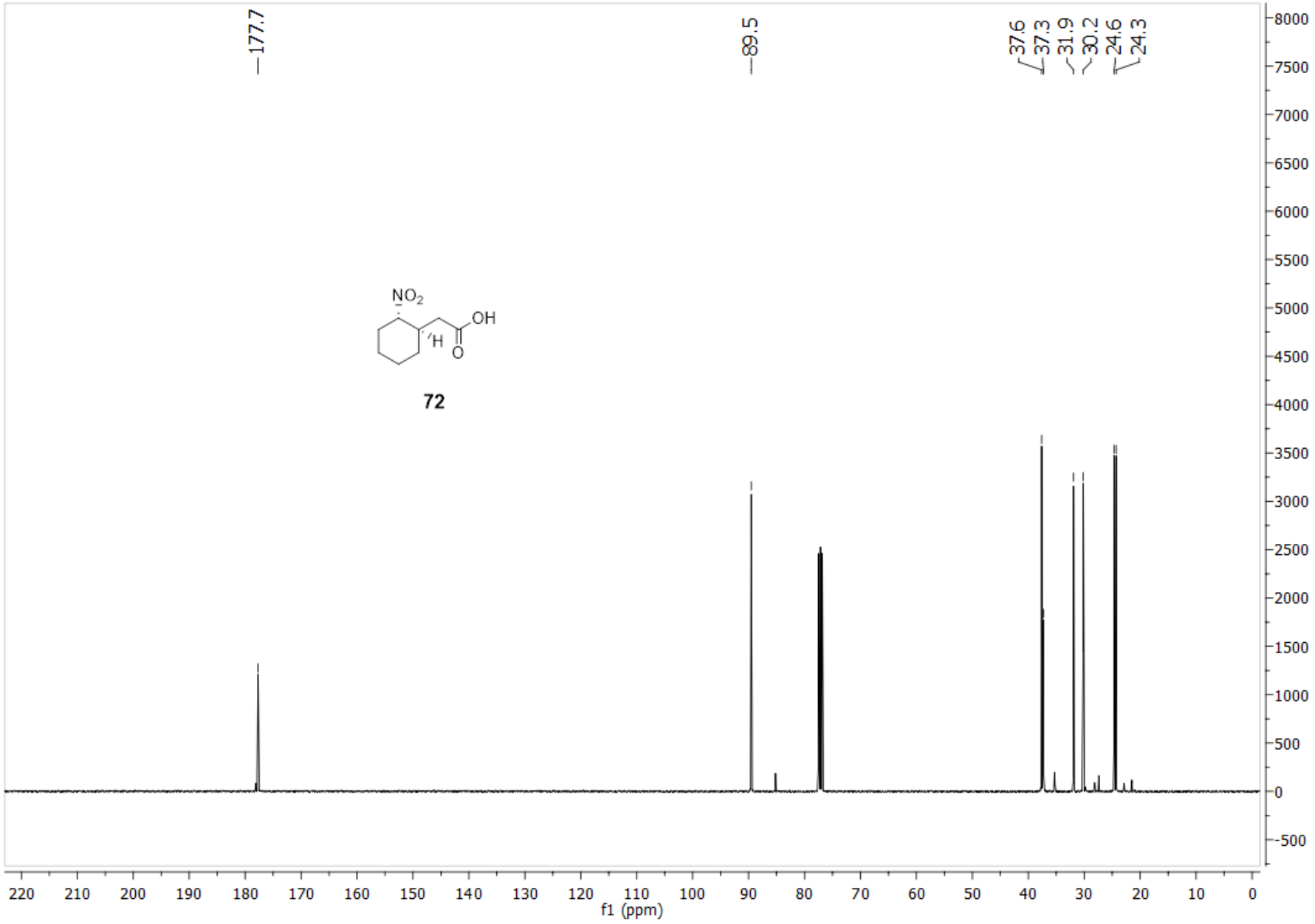
177.7
89.5
37.6
37.3
31.9
30.2
24.6
24.3
NO2
OH
H
O
72
f1 (ppm)

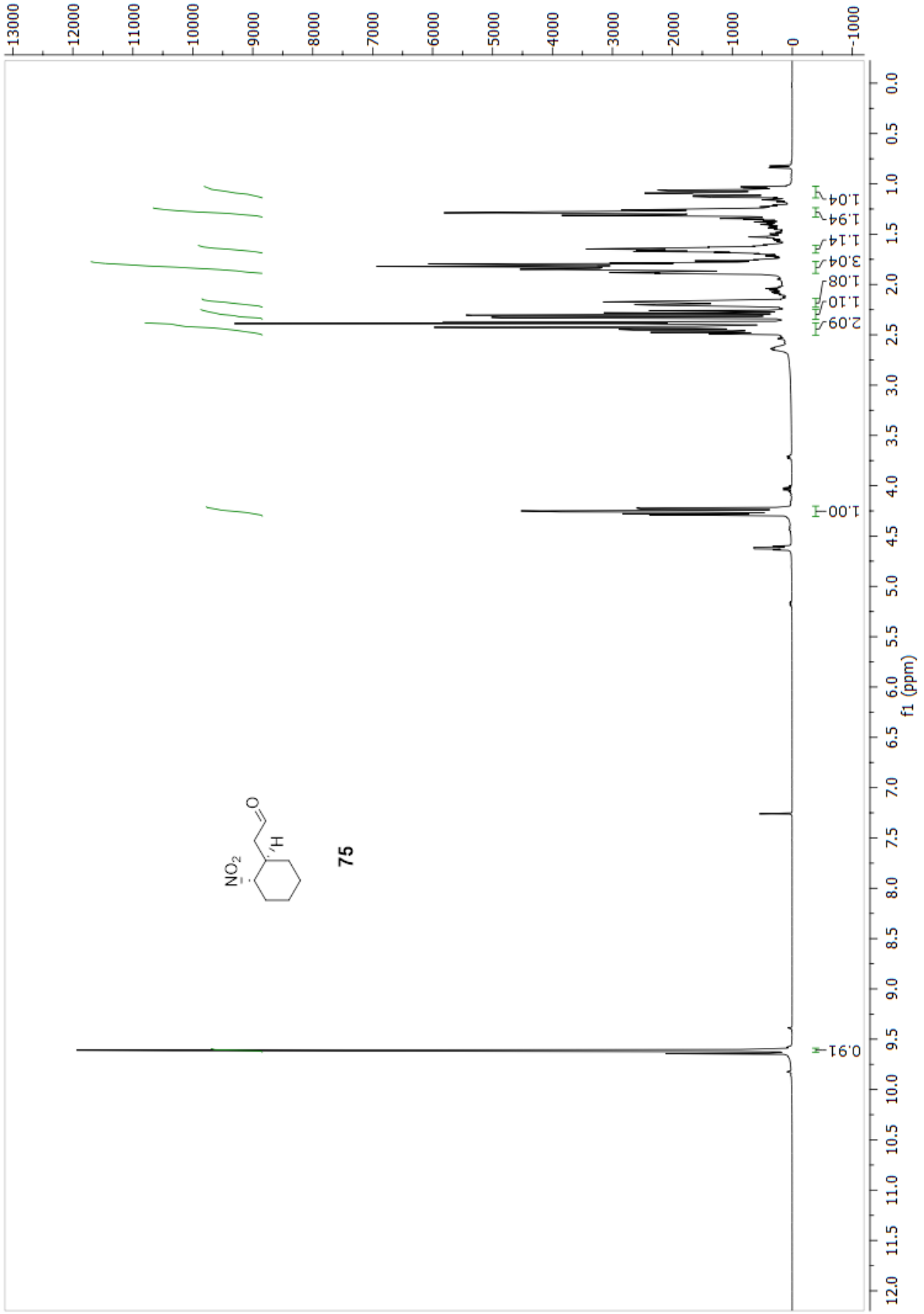
13000
12000
11000
10000
9000
8000
7000
6000
5000
4000
3000
2000
1000
0
-1000
0.0
0.5
1.0
1.5
2.0
2.5
3.0
3.5
4.0
4.5
5.0
5.5
6.0
6.5
7.0
7.5
8.0
8.5
9.0
9.5
10.0
10.5
11.0
11.5
12.0
f1 (ppm)
1.04
1.94
1.14
3.04
1.08
1.10
2.09
1.00
0.91
O
H
NO2
75

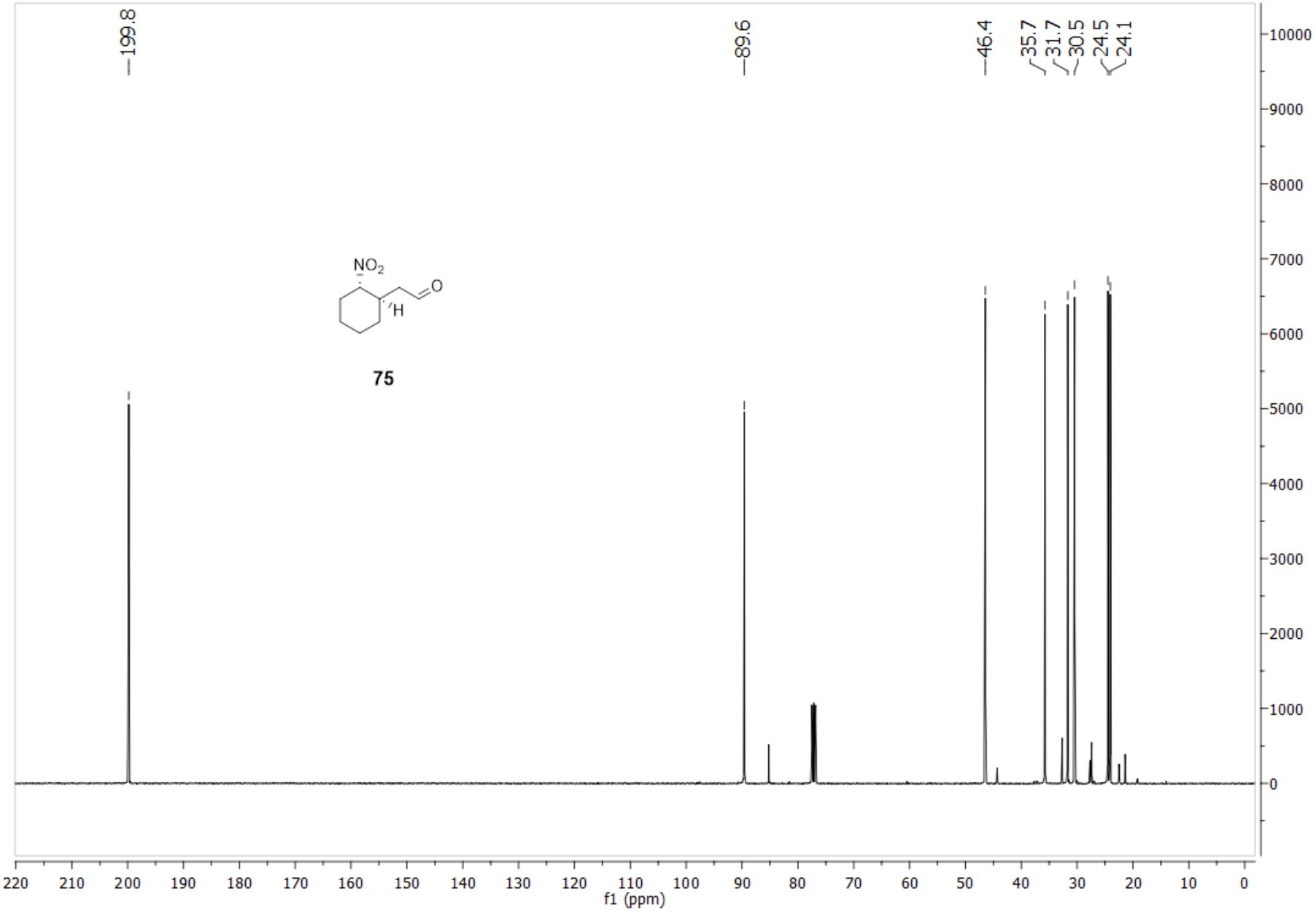
199.8
89.6
46.4
35.7
31.7
30.5
24.5
24.1
NO2
O
H
75
10000
9000
8000
7000
6000
5000
4000
3000
2000
1000
0
220 210 200 190 180 170 160 150 140 130 120 110 100 90 80 70 60 50 40 30 20 10 0
f1 (ppm)

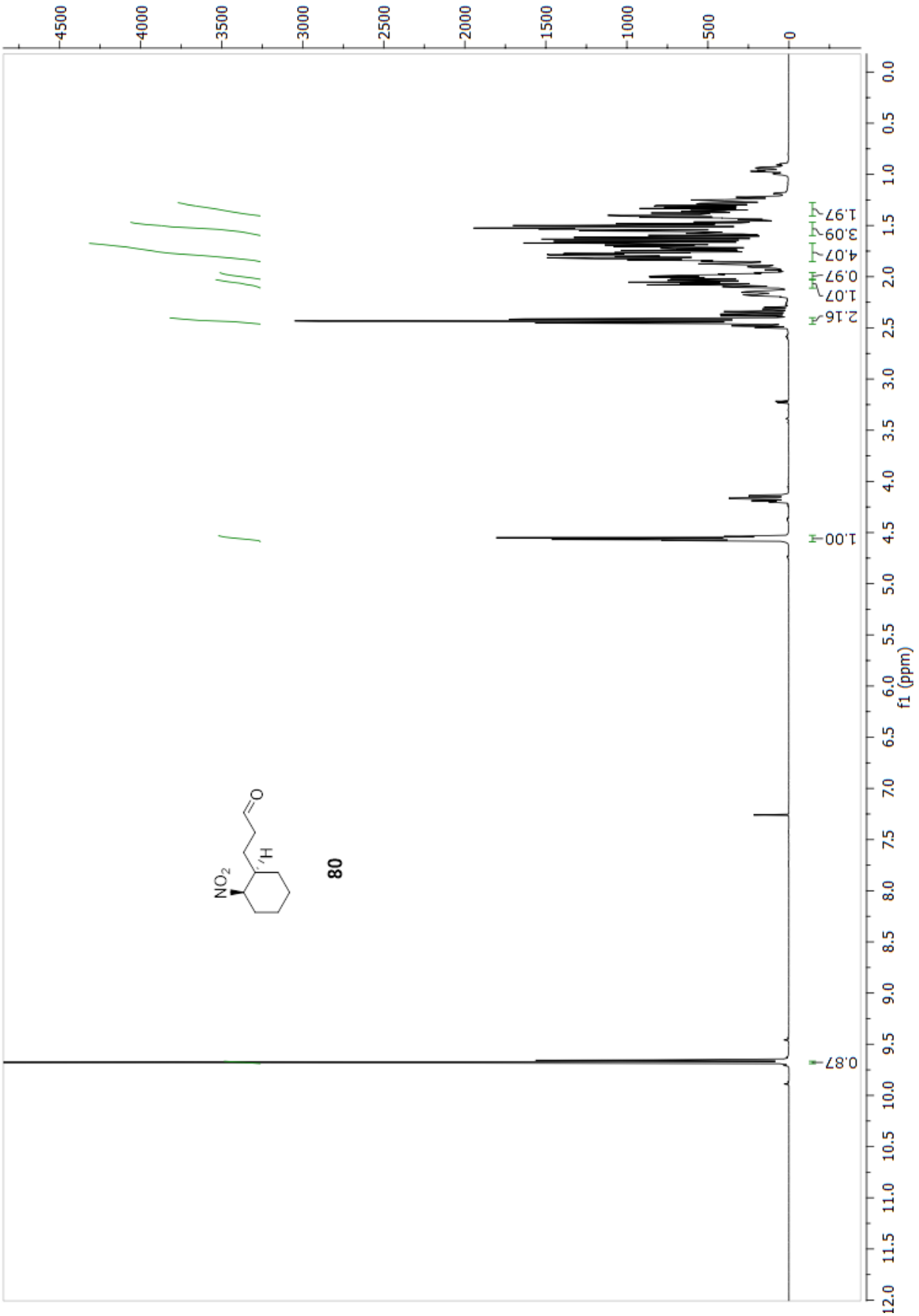
80
NO2
O
H
f1 (ppm)
1.97
3.09
4.07
0.97
1.07
2.16
1.00
0.87

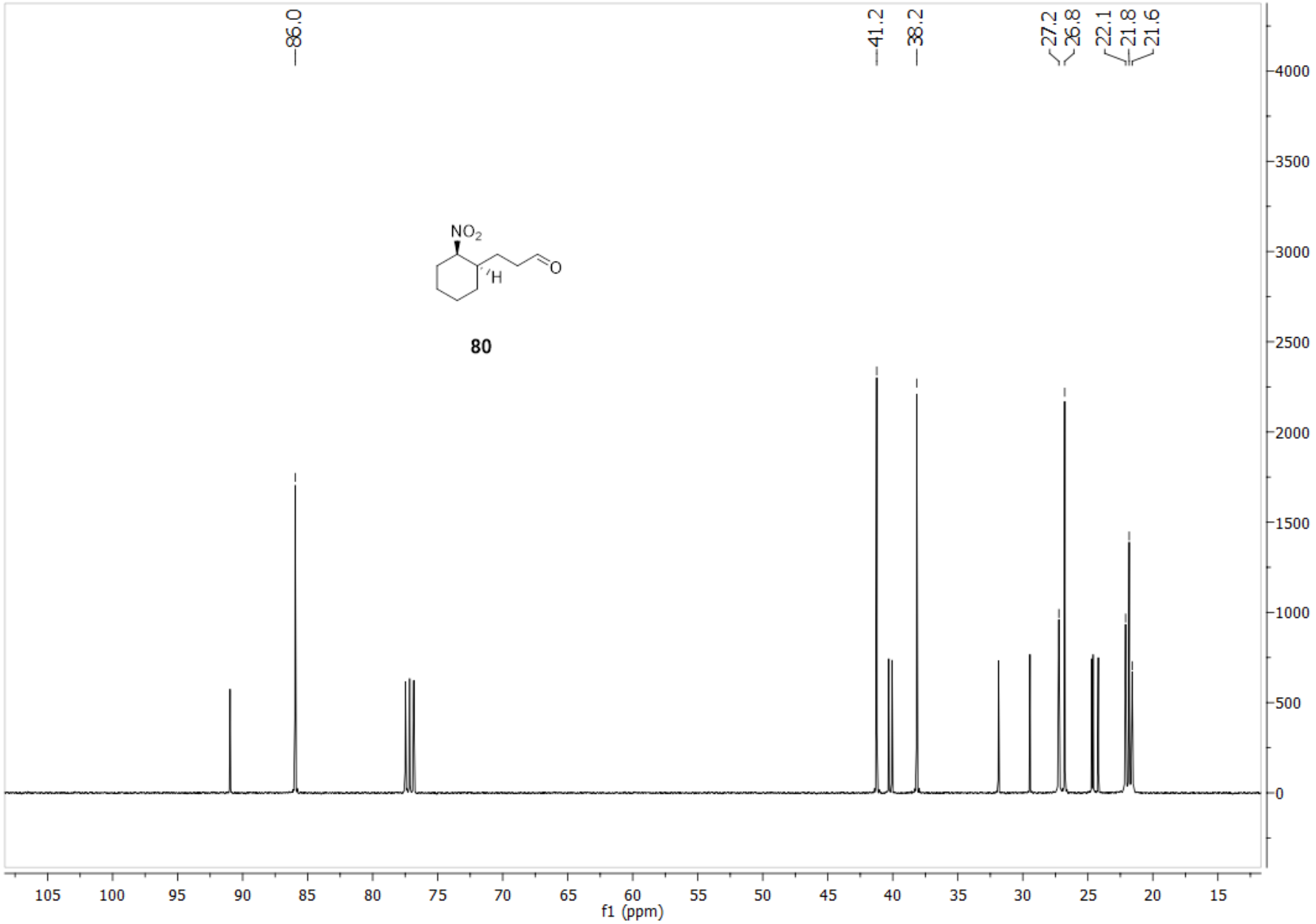
86.0
41.2
38.2
27.2
26.8
22.1
21.8
21.6
NO2
H
O
80
4000
3500
3000
2500
2000
1500
1000
500
0
105
100
95
90
85
80
75
70
65
60
55
50
45
40
35
30
25
20
15
f1 (ppm)

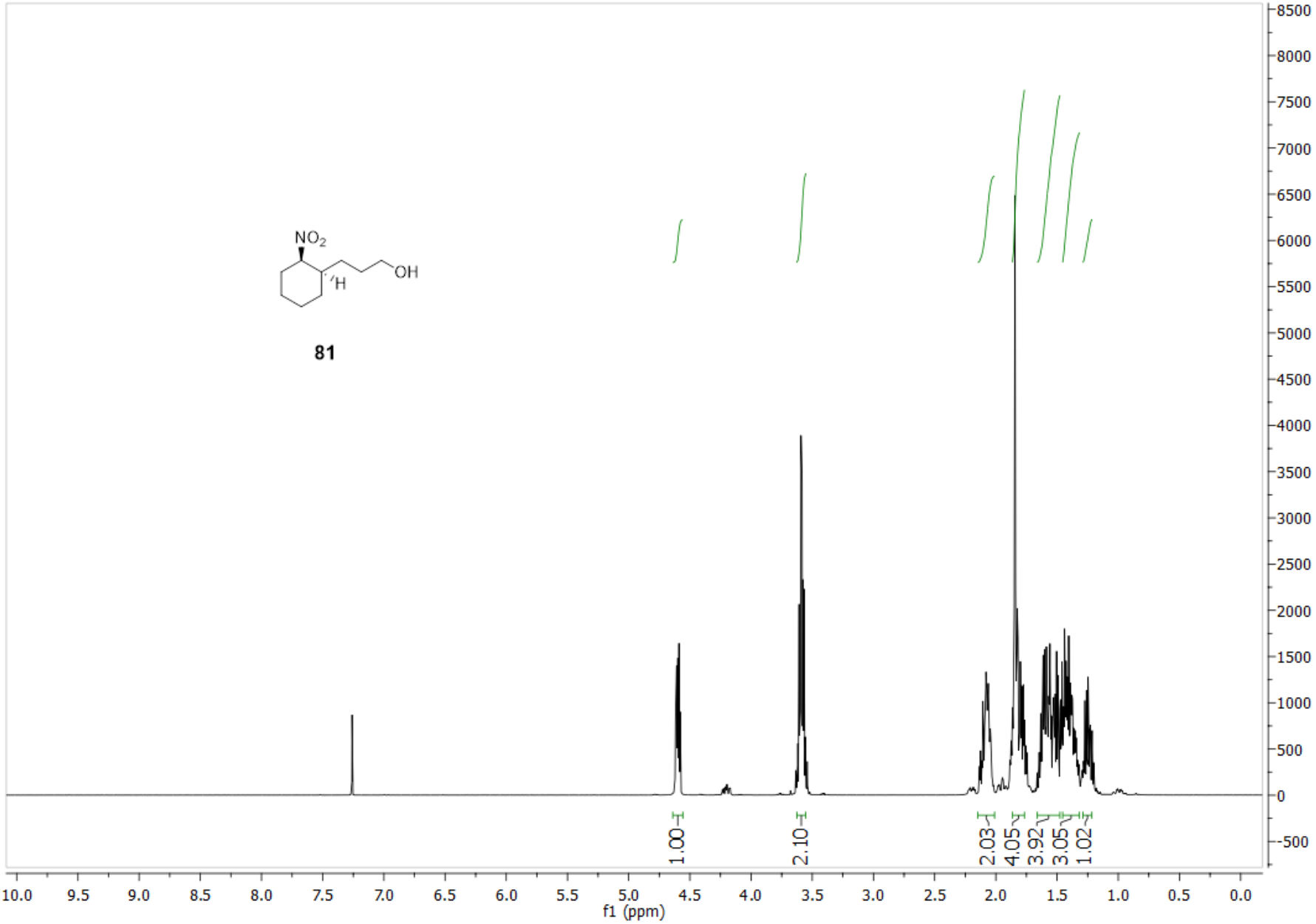
NO2
OH
H
81
1.00
2.10
2.03
4.05
3.92
3.05
1.02
f1 (ppm)

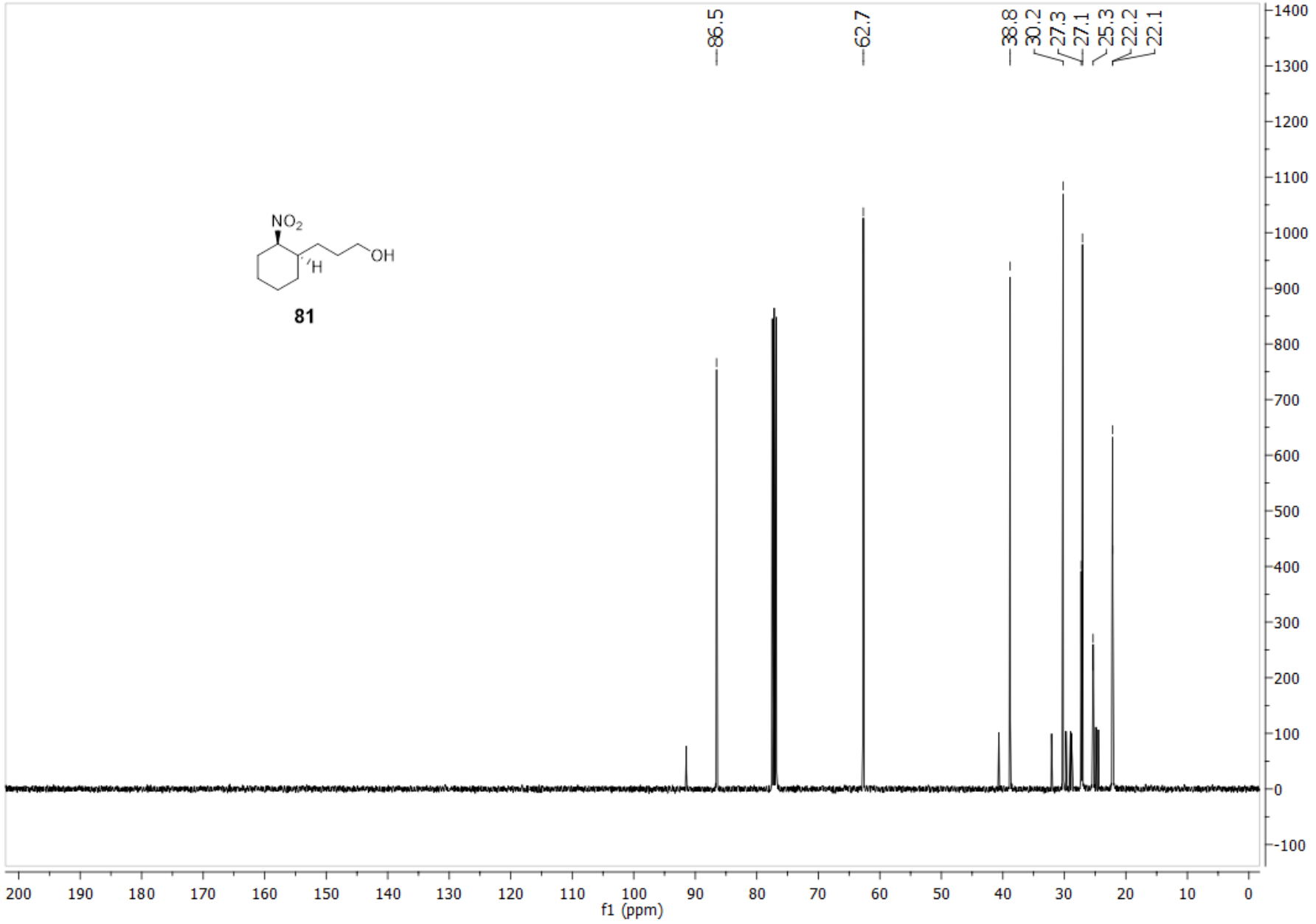
86.5
62.7
38.8
30.2
27.3
27.1
25.3
22.2
22.1
NO2
OH
H
81
f1 (ppm)

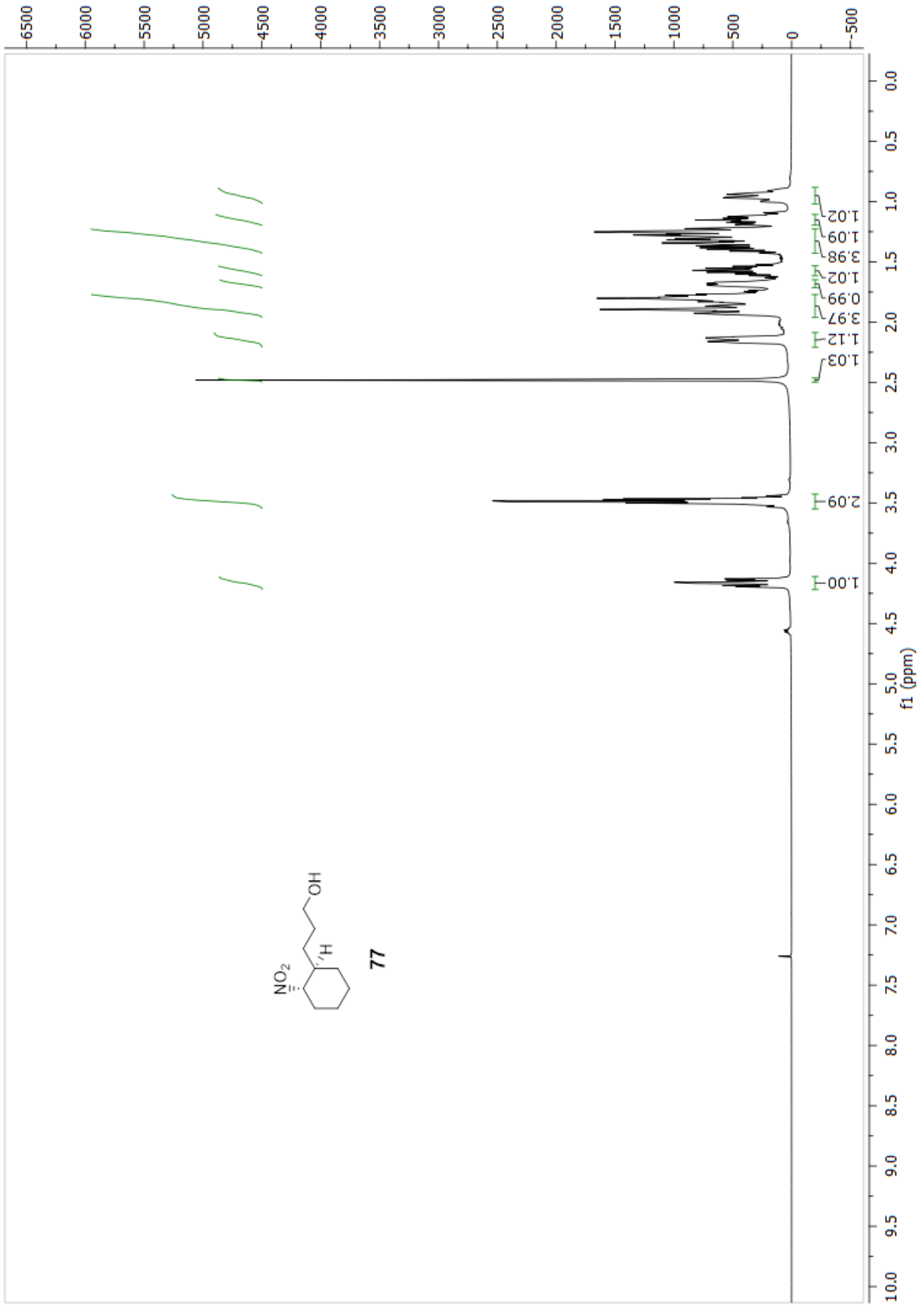
77
NO2
OH
H
1.00
2.09
1.03
1.12
3.97
0.99
1.02
3.98
1.09
1.02
f1 (ppm)

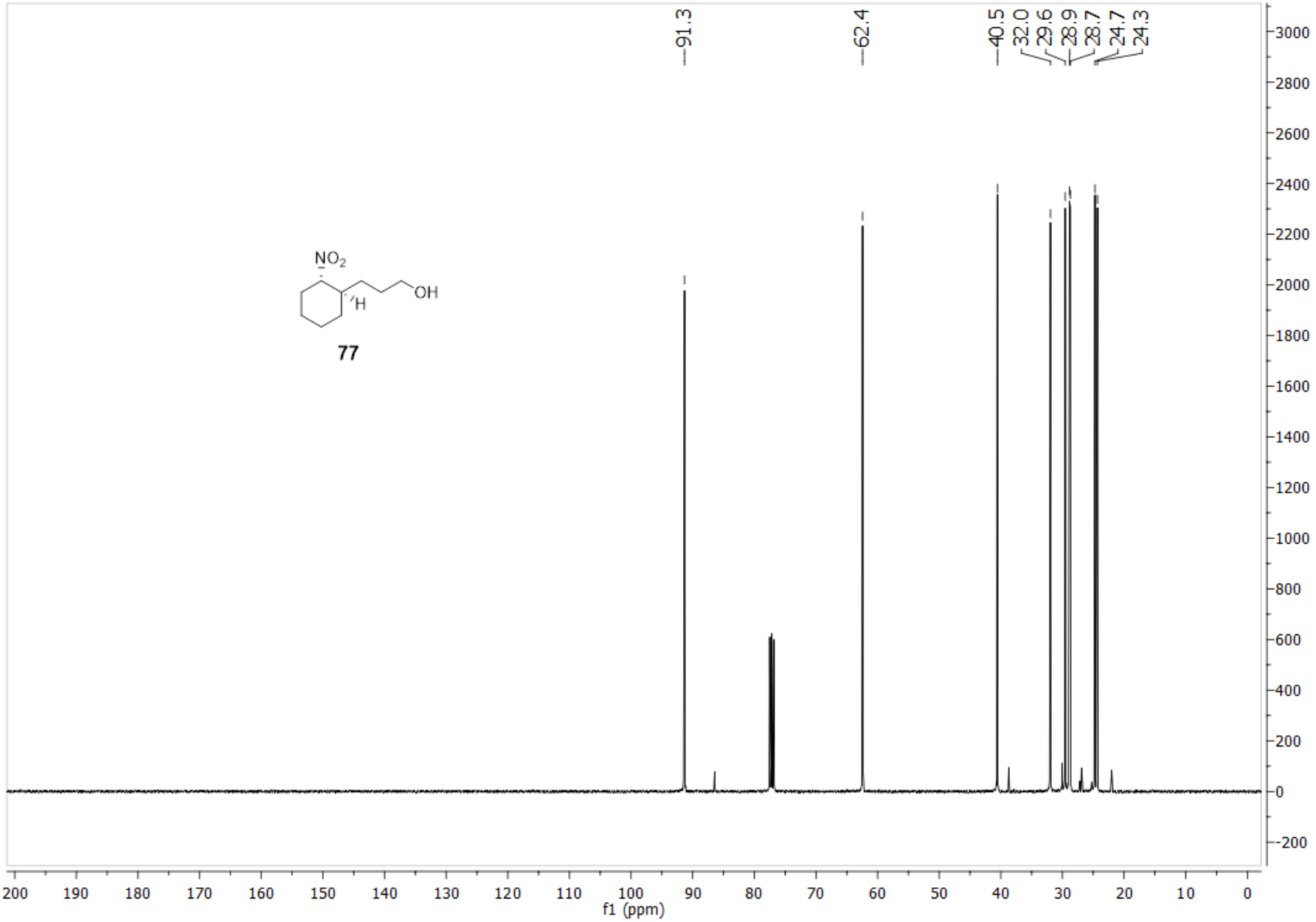
91.3
62.4
40.5
32.0
29.6
28.9
28.7
24.7
24.3
NO2
OH
H
77
f1 (ppm)

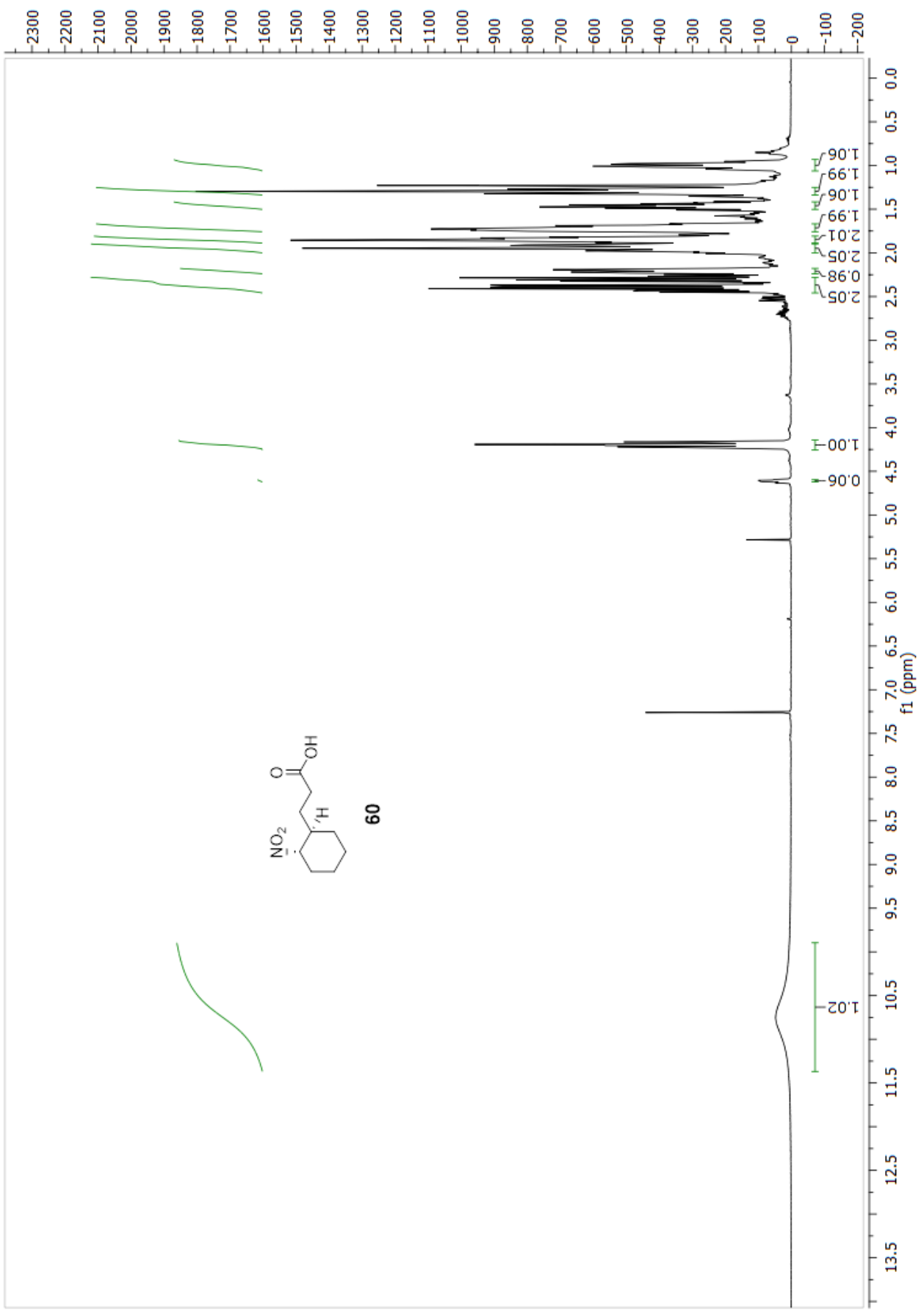
60
f1 (ppm)

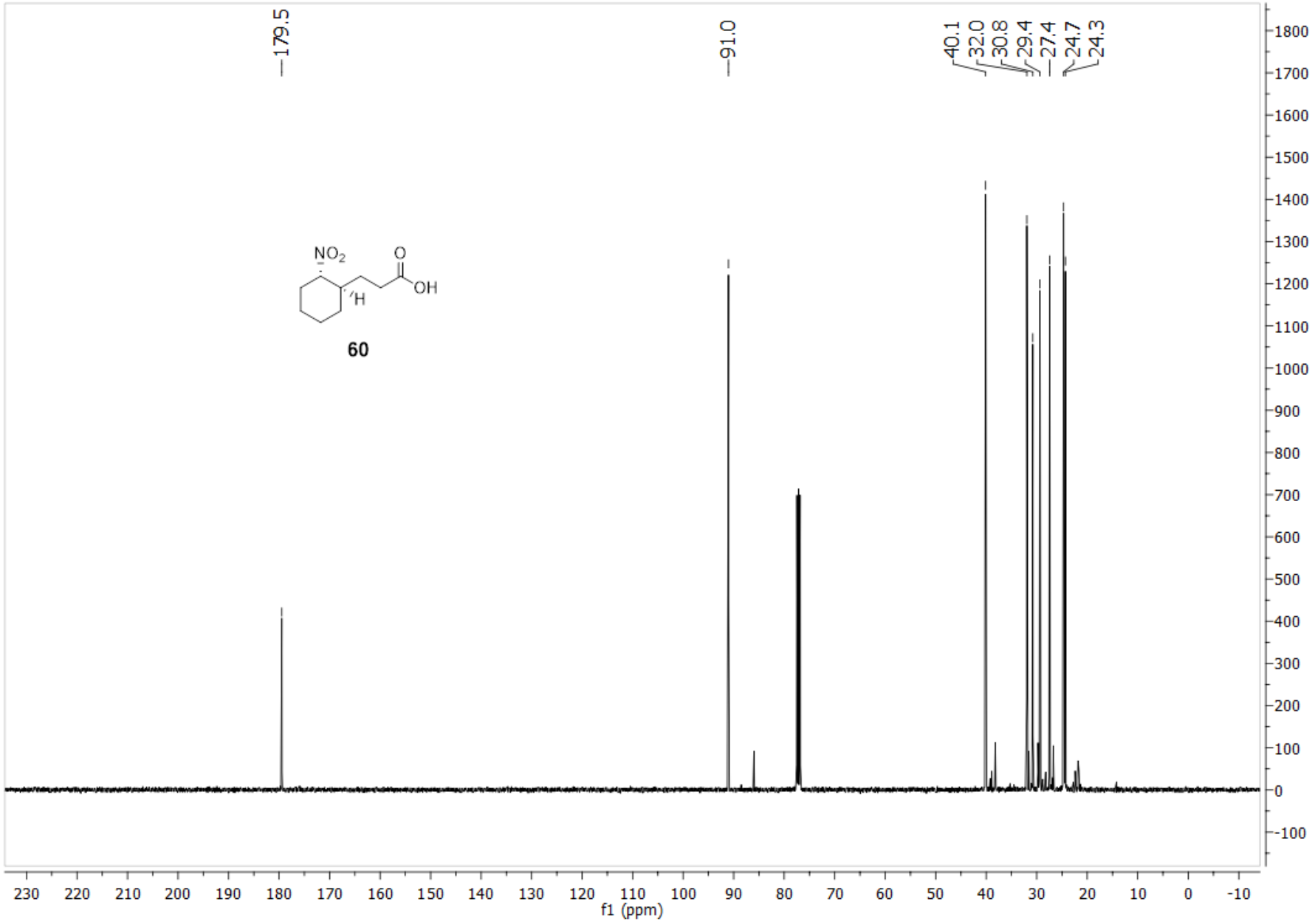
179.5
91.0
40.1
32.0
30.8
29.4
27.4
24.7
24.3
NO2
O
OH
H
60
f1 (ppm)

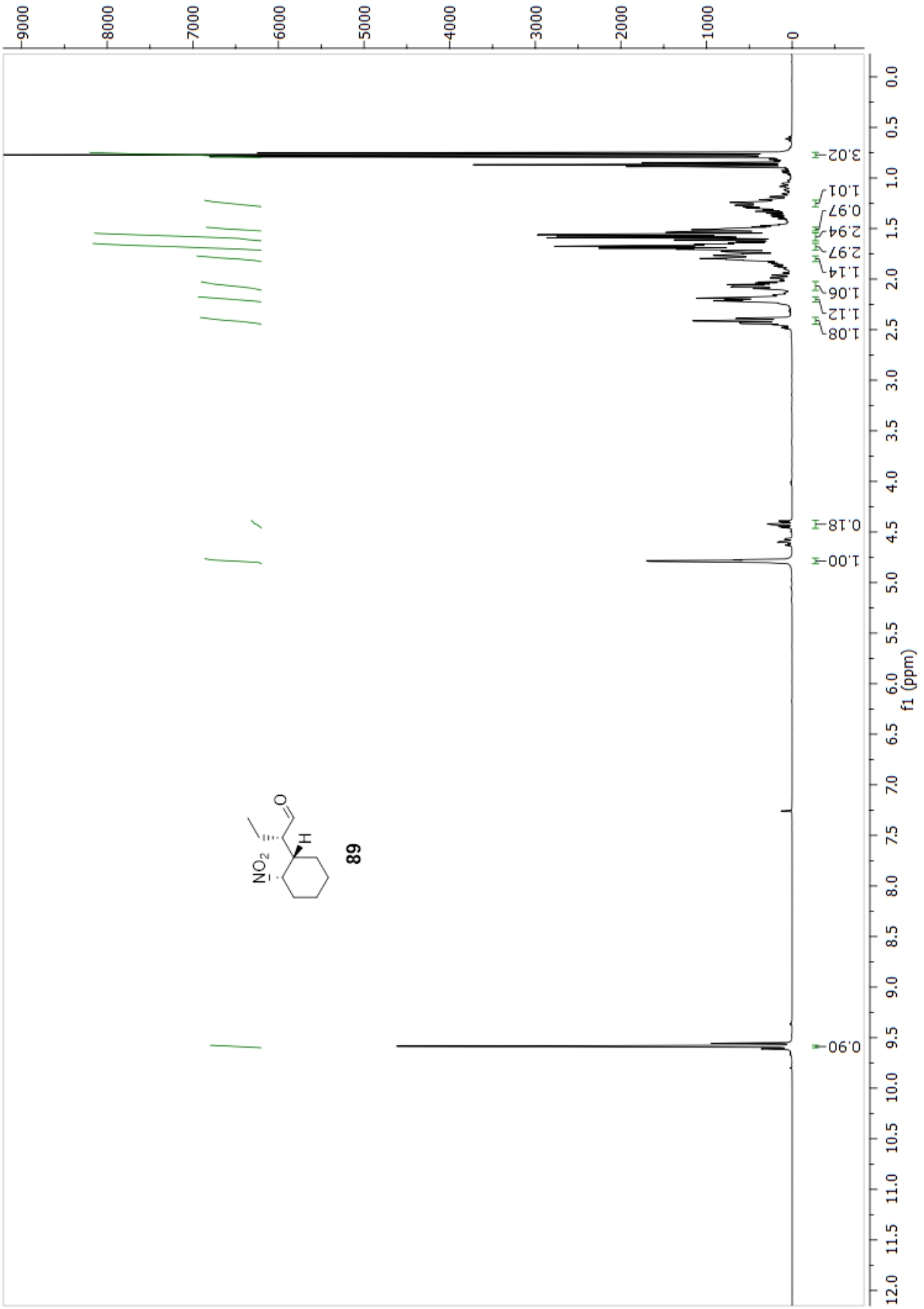
9000
8000
7000
6000
5000
4000
3000
2000
1000
0
3.02
1.01
0.97
2.94
2.97
1.14
1.06
1.12
1.08
0.18
1.00
0.90
0.0
0.5
1.0
1.5
2.0
2.5
3.0
3.5
4.0
4.5
5.0
5.5
6.0
6.5
7.0
7.5
8.0
8.5
9.0
9.5
10.0
10.5
11.0
11.5
12.0
f1 (ppm)
O
H
NO2
89

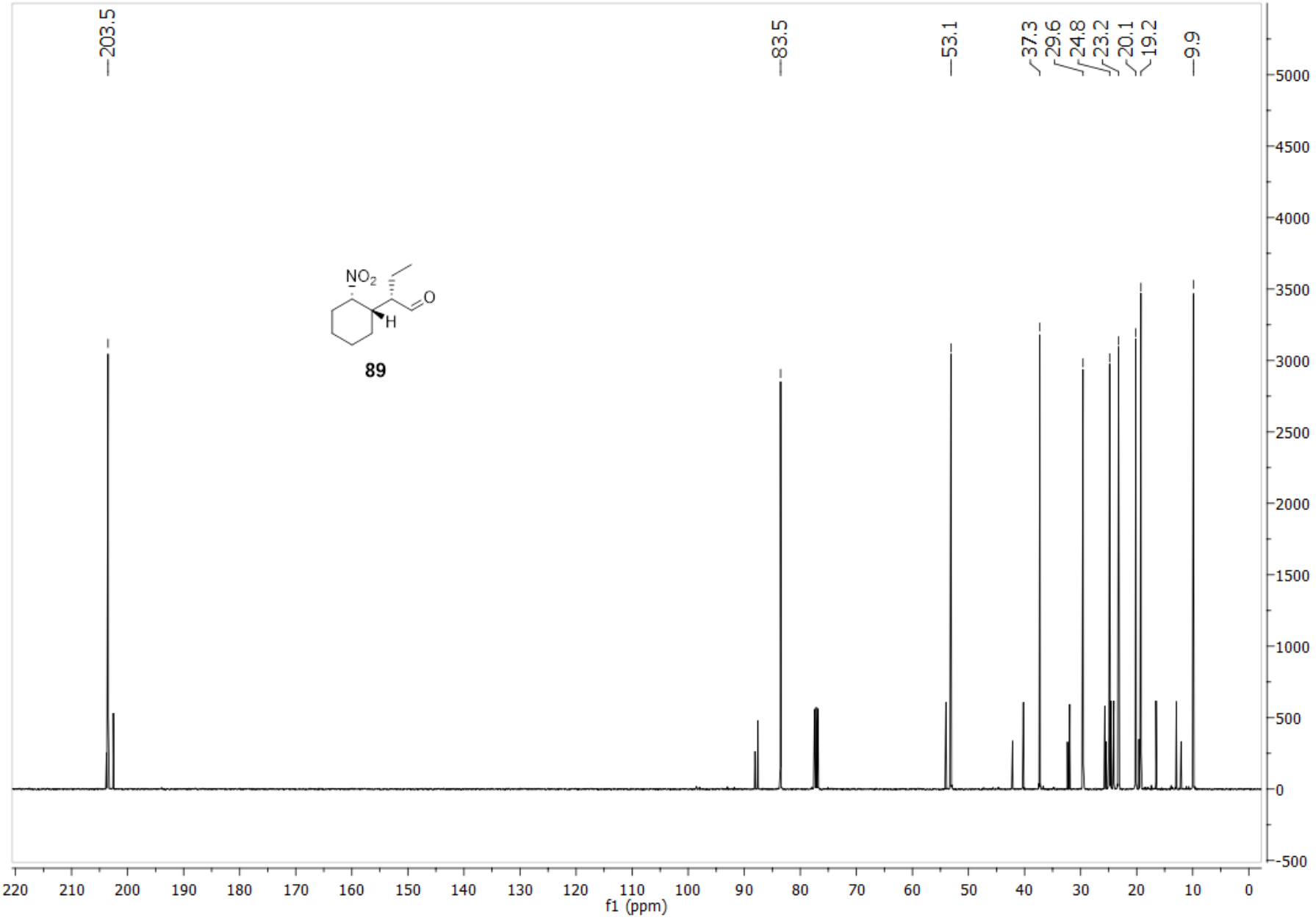
203.5
83.5
53.1
37.3
29.6
24.8
23.2
20.1
19.2
9.9
NO2
O
H
89
5000
4500
4000
3500
3000
2500
2000
1500
1000
500
0
-500
220
210
200
190
180
170
160
150
140
130
120
110
100
90
80
70
60
50
40
30
20
10
0
f1 (ppm)

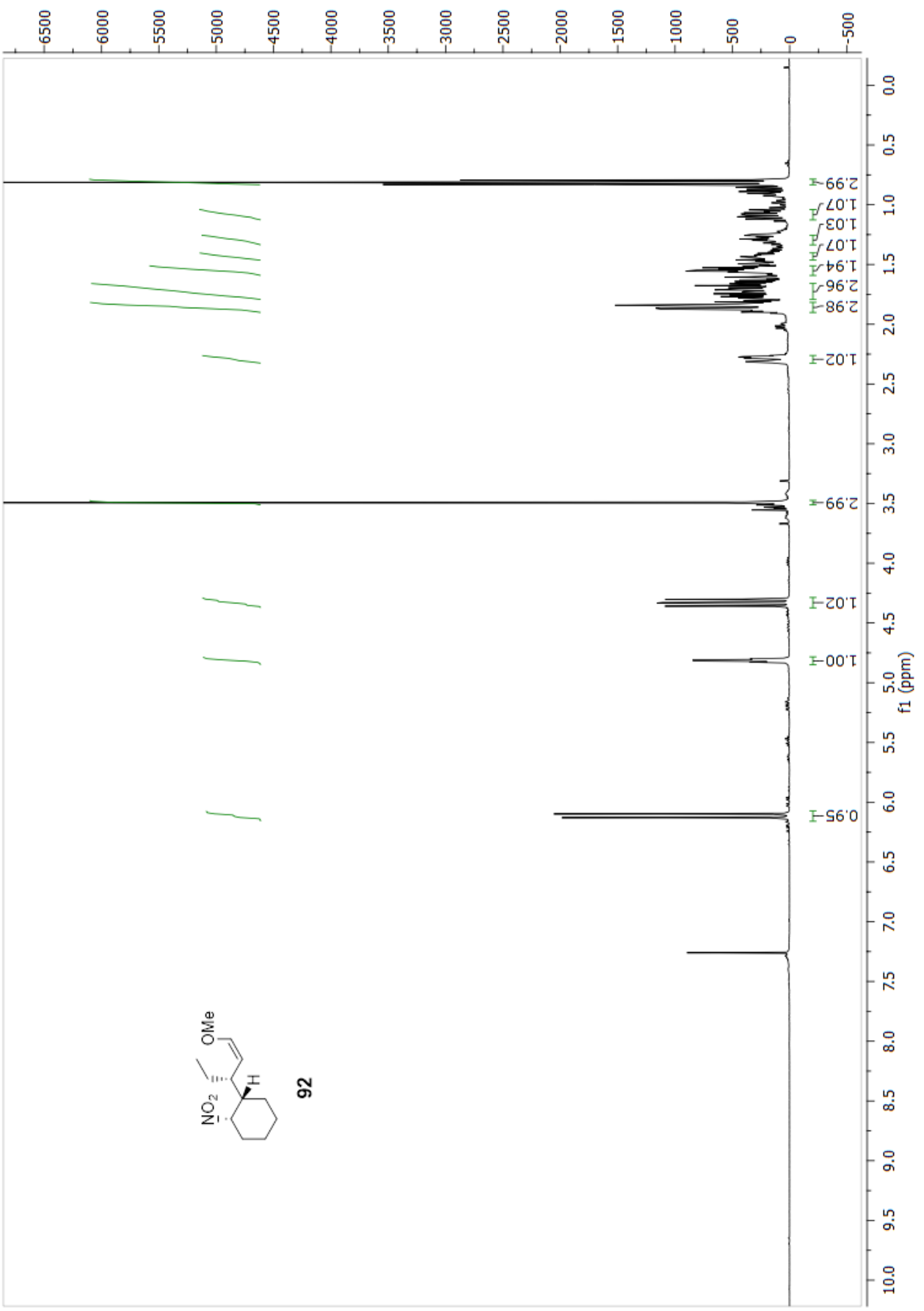
OMe
NO2
H
92
2.99
1.07
1.03
1.07
1.94
2.96
2.98
1.02
2.99
1.02
1.00
0.95
f1 (ppm)

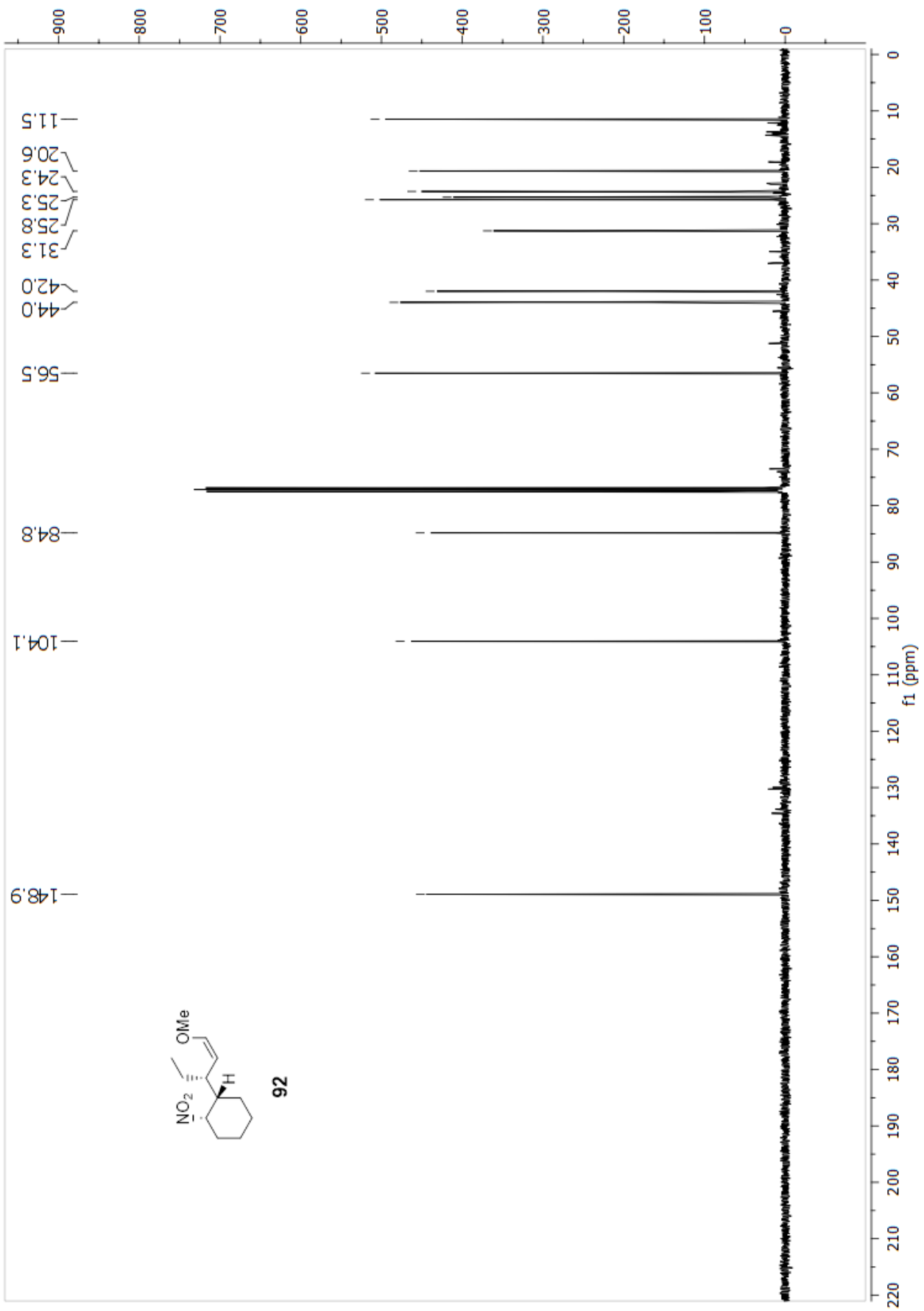
11.5
20.6
24.3
25.3
25.8
31.3
42.0
44.0
56.5
84.8
104.1
148.9
OMe
H
NO2
92
f1 (ppm)

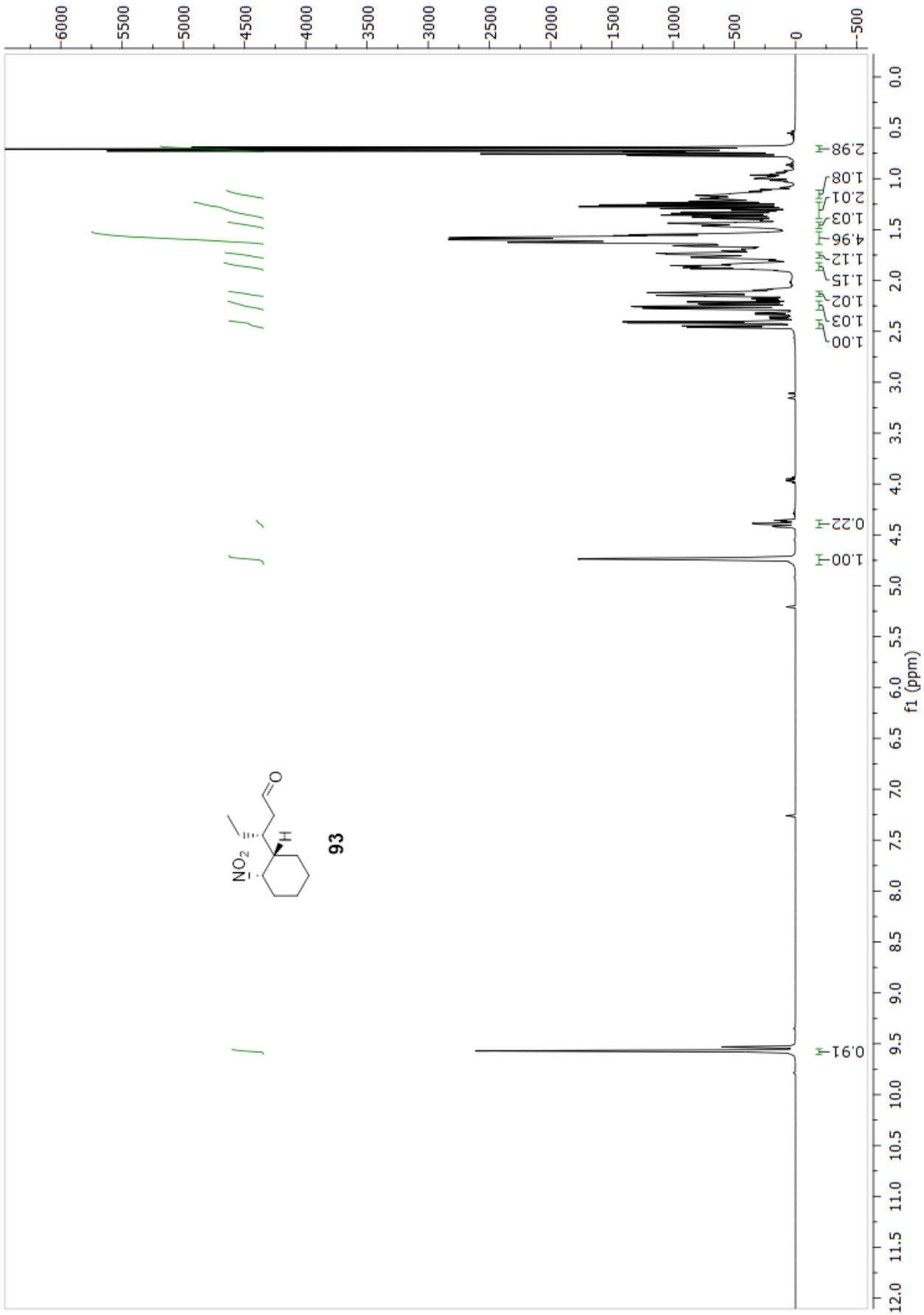
O
H
NO2
93
2.98
1.08
2.01
1.03
4.96
1.12
1.15
1.02
1.03
1.00
0.22
1.00
0.91
f1 (ppm)

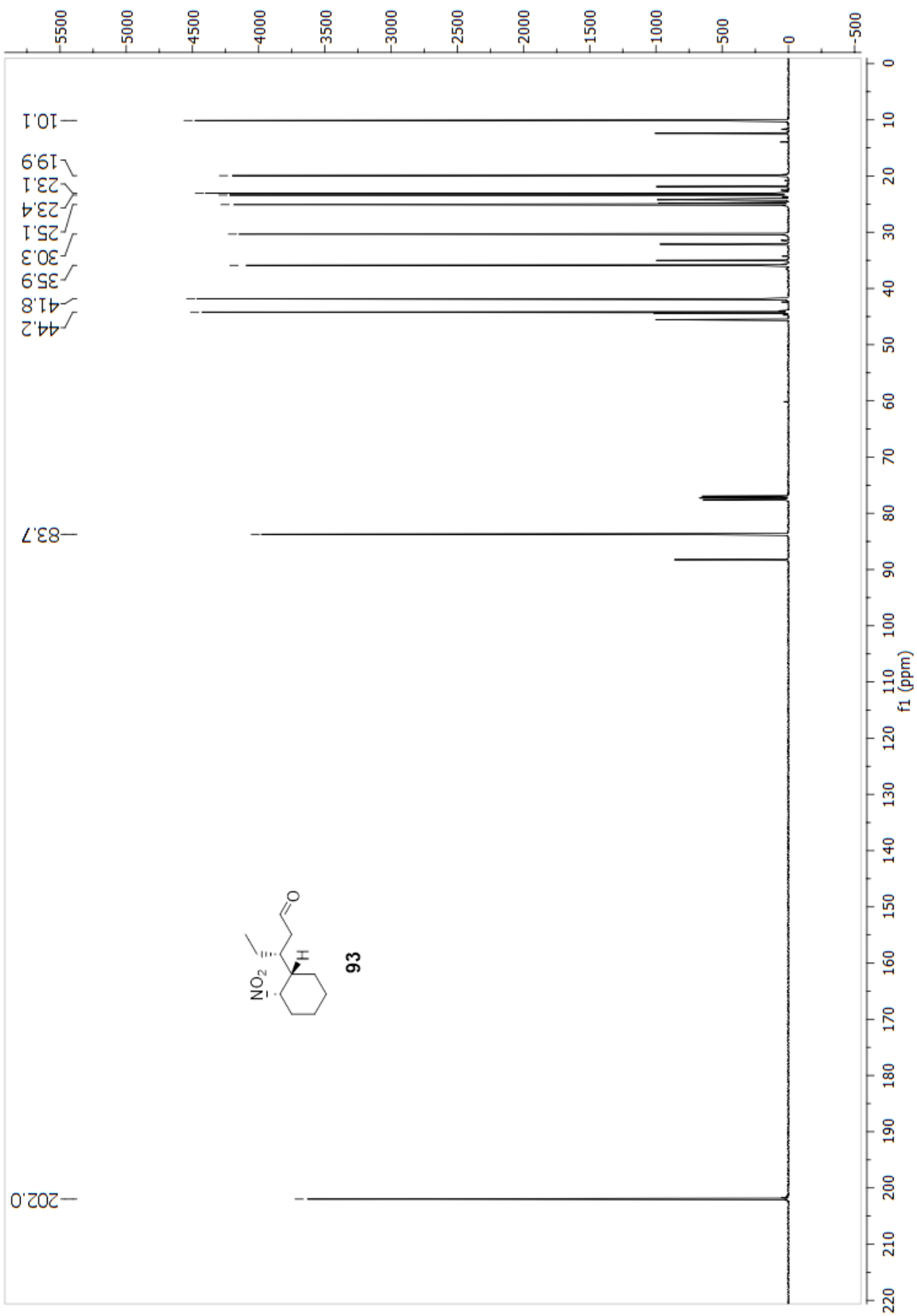
202.0
83.7
44.2
41.8
35.9
30.3
25.1
23.4
23.1
19.9
10.1
93
NO2
H
O
f1 (ppm)

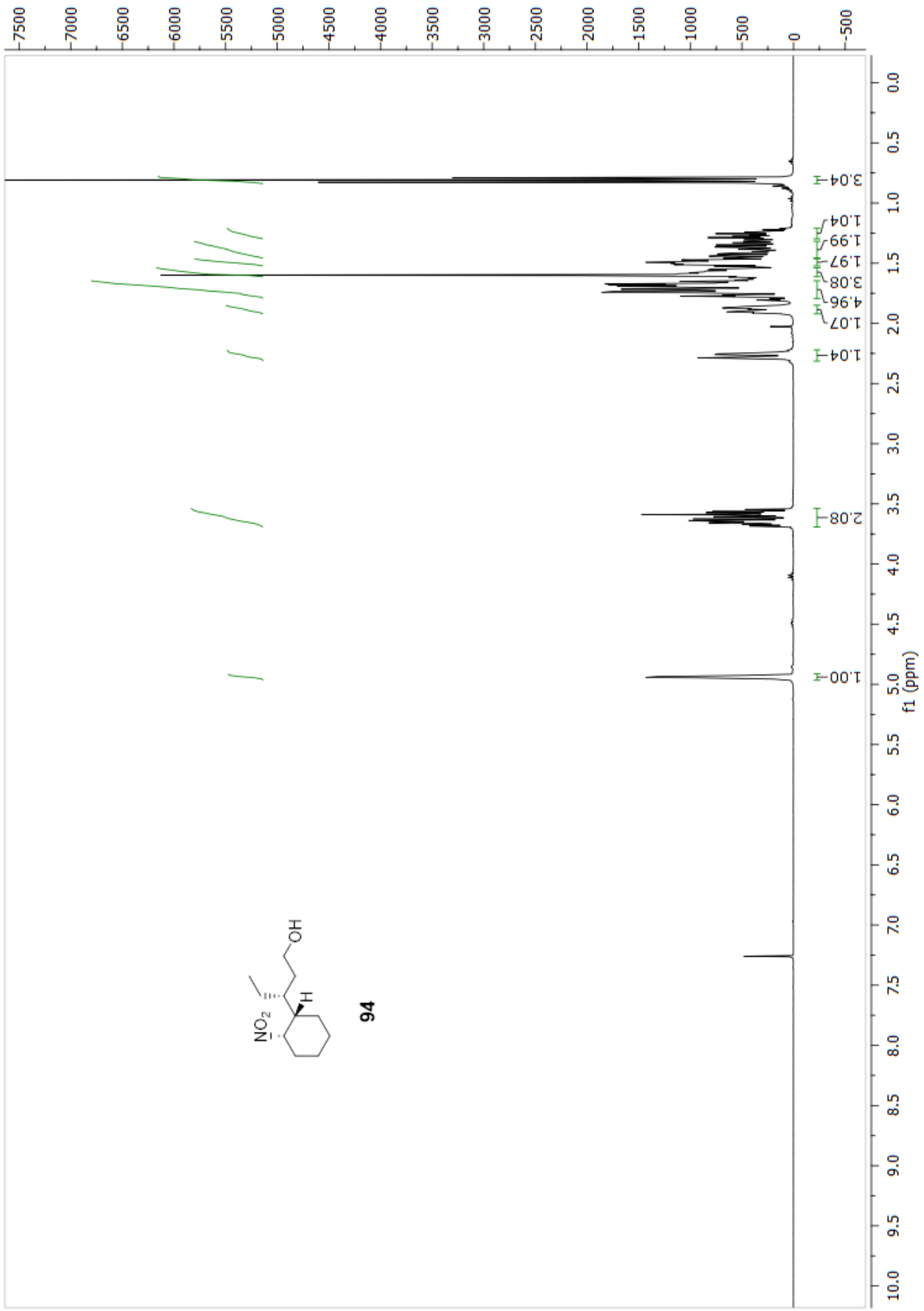
OH
H
NO2
94
3.04
1.04
1.99
1.97
3.08
4.96
1.07
1.04
2.08
1.00
f1 (ppm)

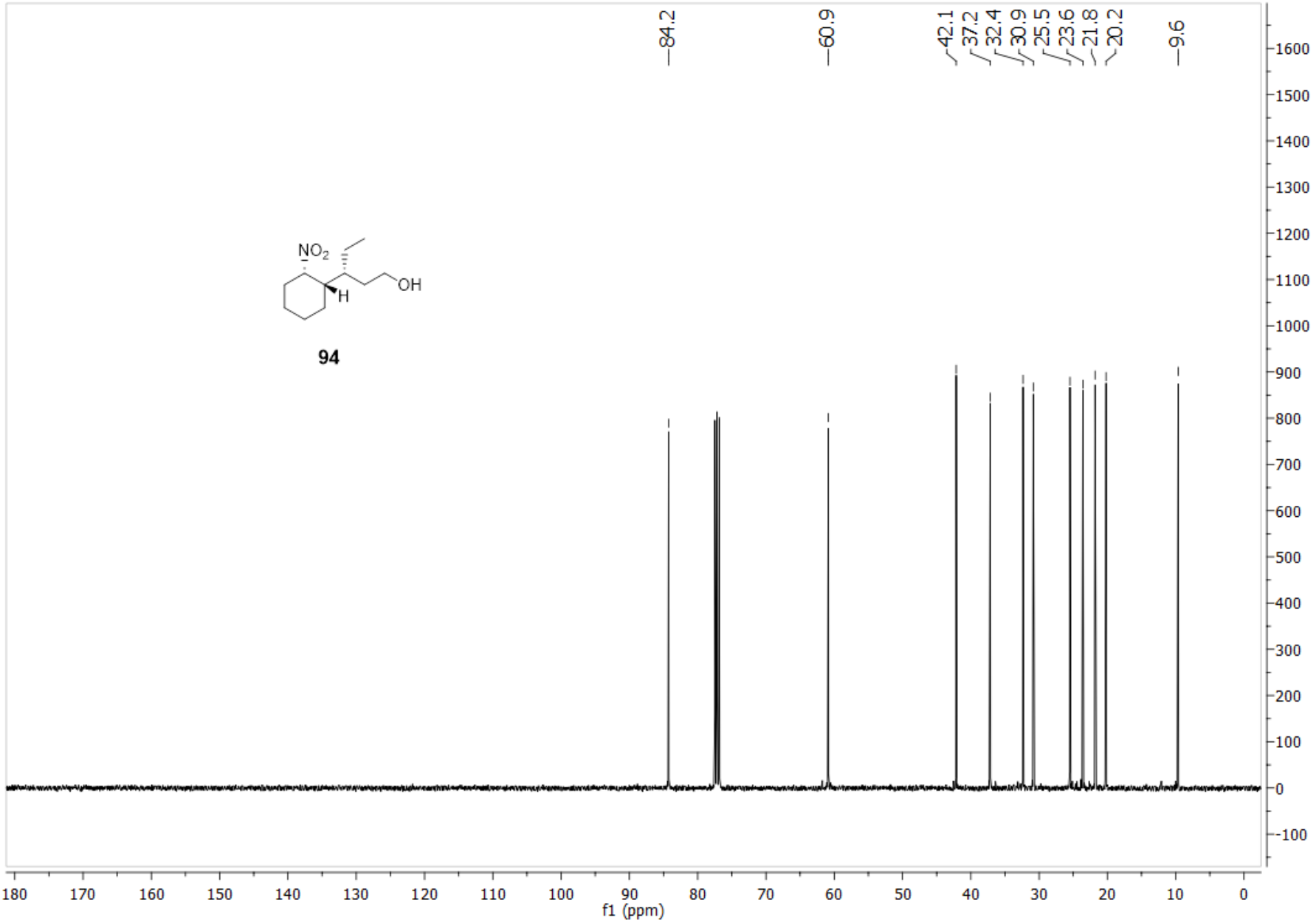
84.2
60.9
42.1
37.2
32.4
30.9
25.5
23.6
21.8
20.2
9.6
NO2
OH
H
94
f1 (ppm)

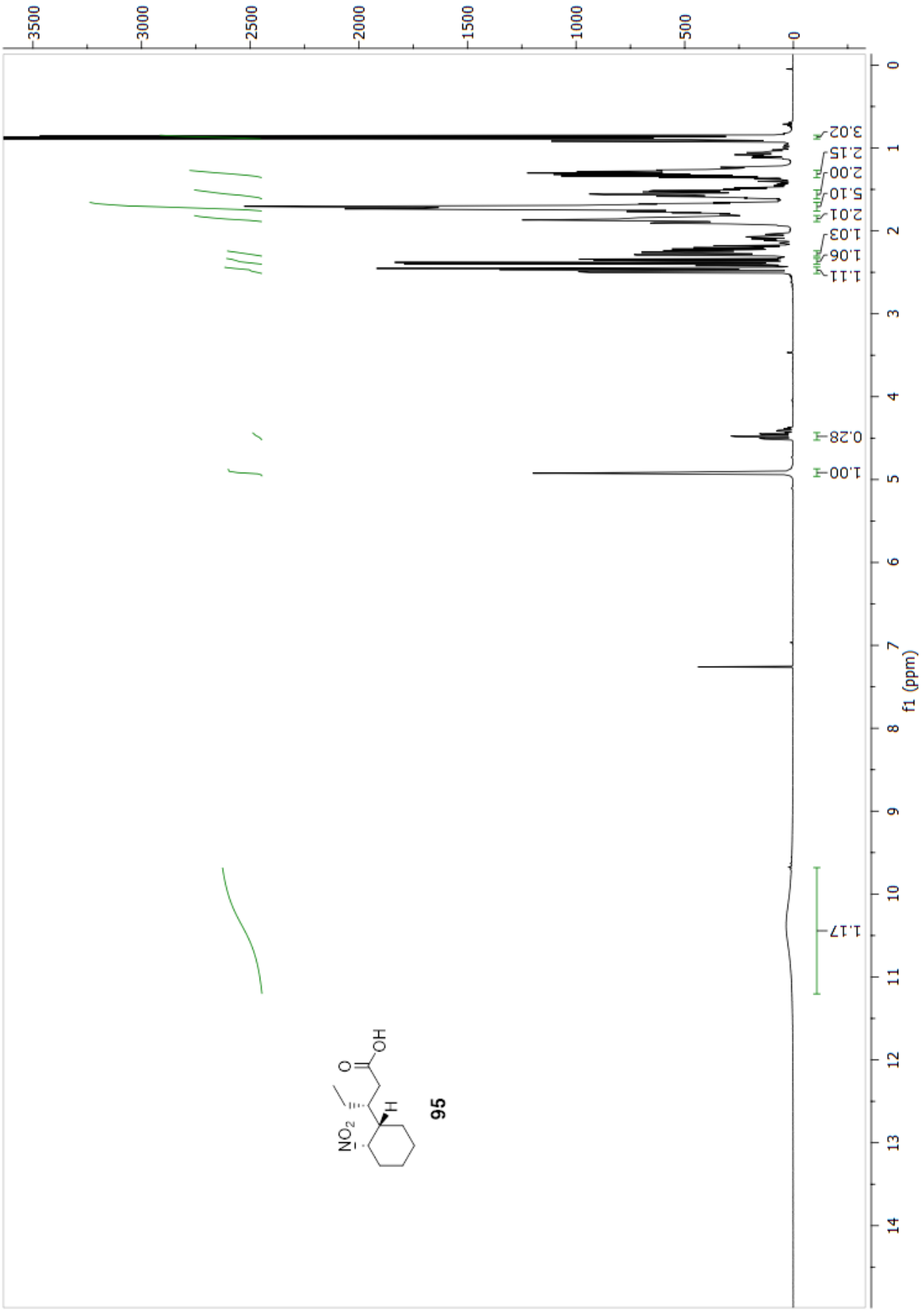
3500
3000
2500
2000
1500
1000
500
0
3.02
2.15
2.00
5.10
2.01
1.03
1.06
1.11
0.28
1.00
1.17
f1 (ppm)
OH
O
H
NO2
95

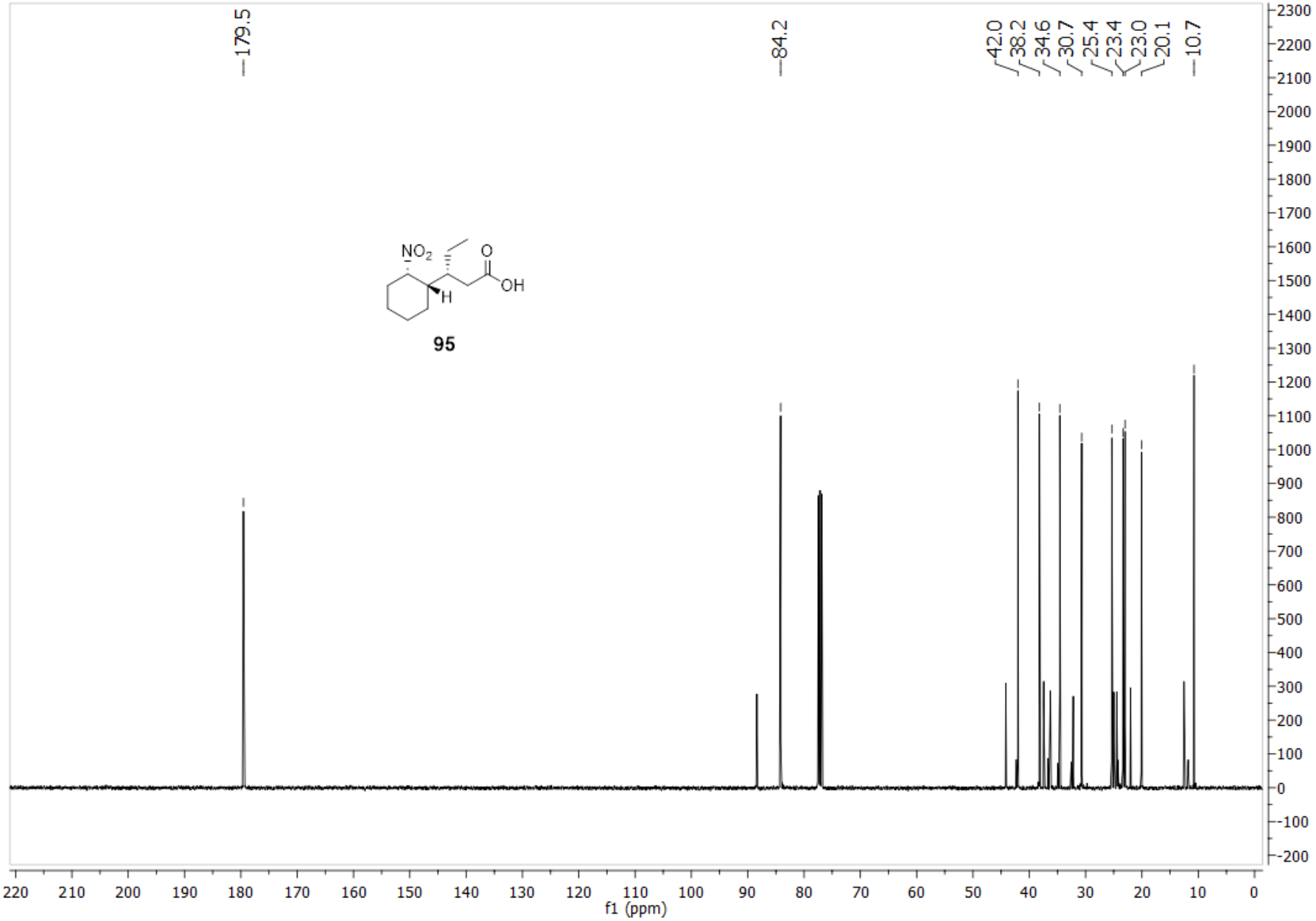
179.5
84.2
42.0
38.2
34.6
30.7
25.4
23.4
23.0
20.1
10.7
NO2
O
OH
H
95
f1 (ppm)

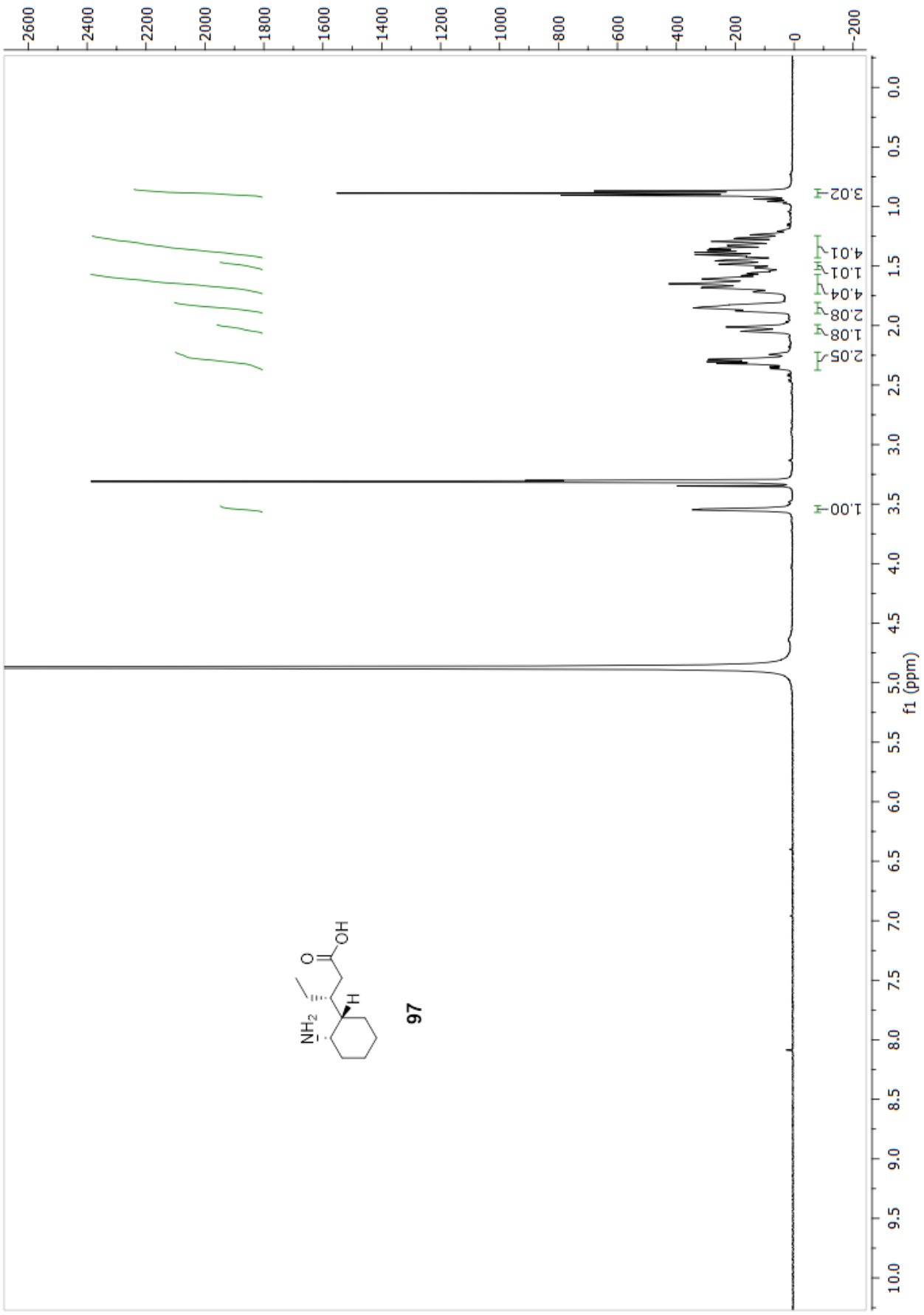
2600
2400
2200
2000
1800
1600
1400
1200
1000
800
600
400
200
0
-200
3.02
4.01
1.01
4.04
2.08
1.08
2.05
1.00
0.0
0.5
1.0
1.5
2.0
2.5
3.0
3.5
4.0
4.5
5.0
5.5
6.0
6.5
7.0
7.5
8.0
8.5
9.0
9.5
10.0
f1 (ppm)
NH2
O
OH
H

97

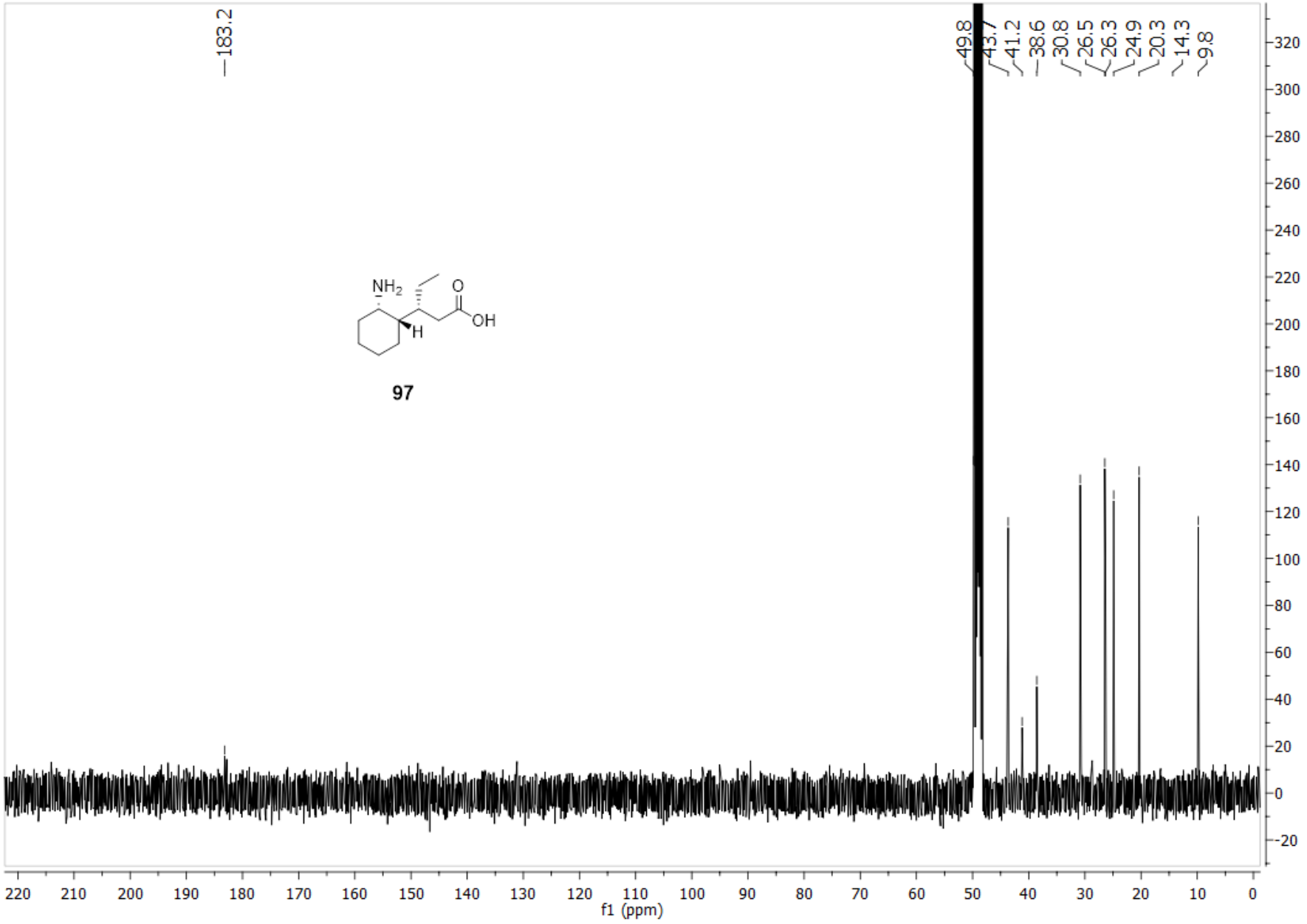
183.2
49.8
43.7
41.2
38.6
30.8
26.5
26.3
24.9
20.3
14.3
9.8
NH2
O
OH
H
97
f1 (ppm)

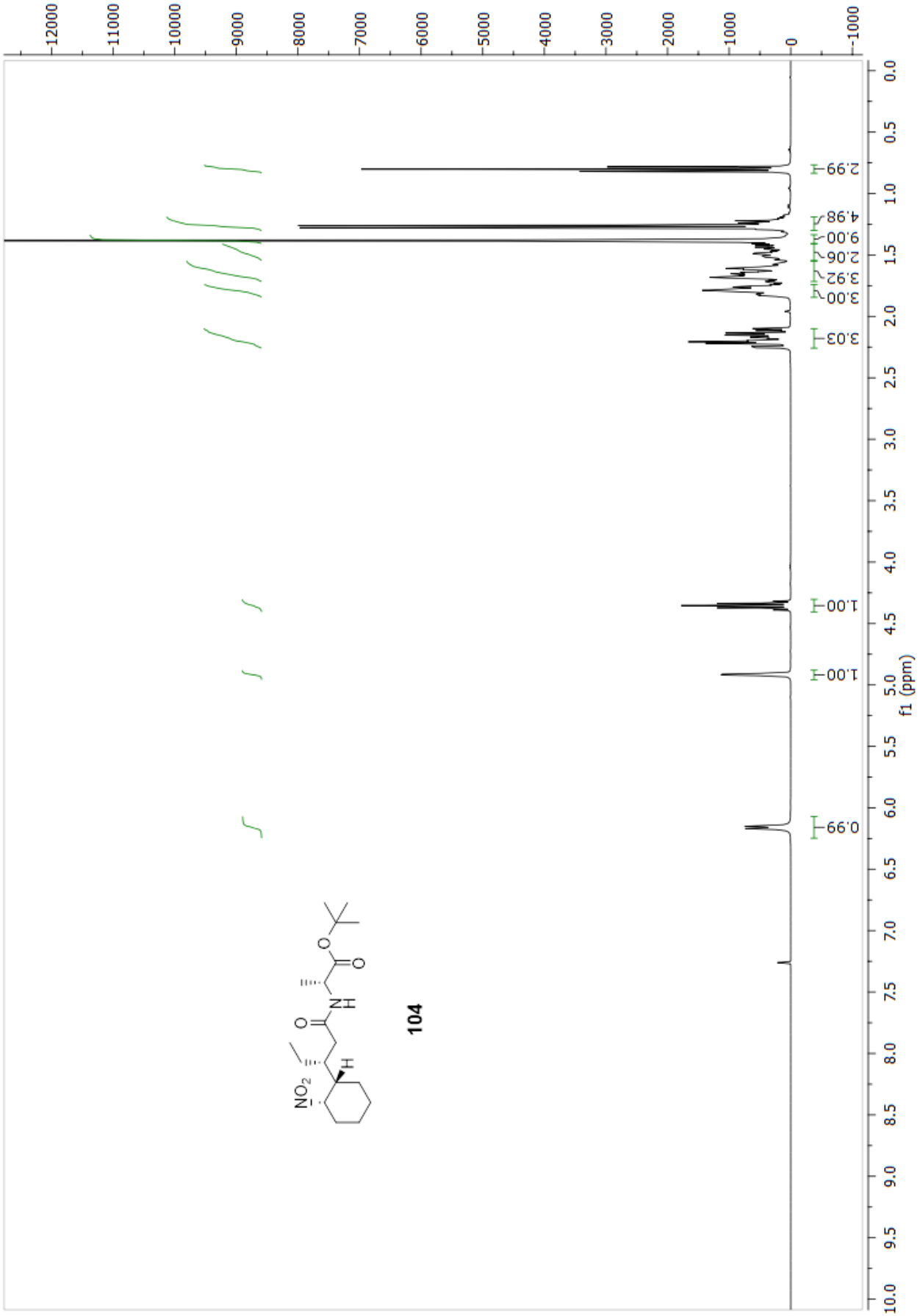
12000
11000
10000
9000
8000
7000
6000
5000
4000
3000
2000
1000
0
-1000
0.0
0.5
1.0
1.5
2.0
2.5
3.0
3.5
4.0
4.5
5.0
5.5
6.0
6.5
7.0
7.5
8.0
8.5
9.0
9.5
10.0
f1 (ppm)
2.99
4.98
9.00
2.06
3.92
3.00
3.03
1.00
1.00
0.99
O
O
N
H
O
O
NO2
H

104

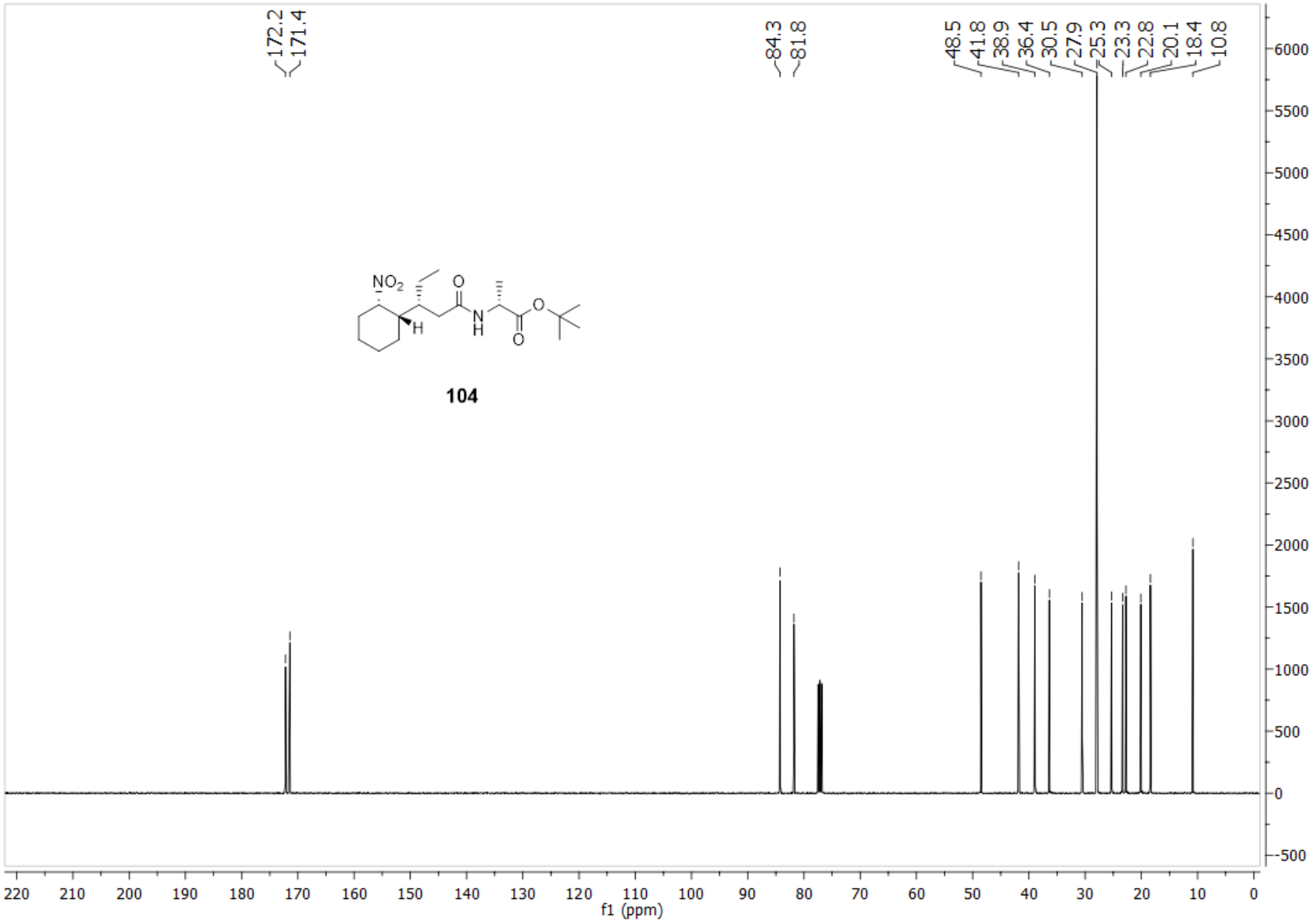
172.2
171.4
84.3
81.8
48.5
41.8
38.9
36.4
30.5
27.9
25.3
23.3
22.8
20.1
18.4
10.8
NO2
O
N
H
O
O
H
104
6000
5500
5000
4500
4000
3500
3000
2500
2000
1500
1000
500
0
-500
220
210
200
190
180
170
160
150
140
130
120
110
100
90
80
70
60
50
40
30
20
10
0
f1 (ppm)

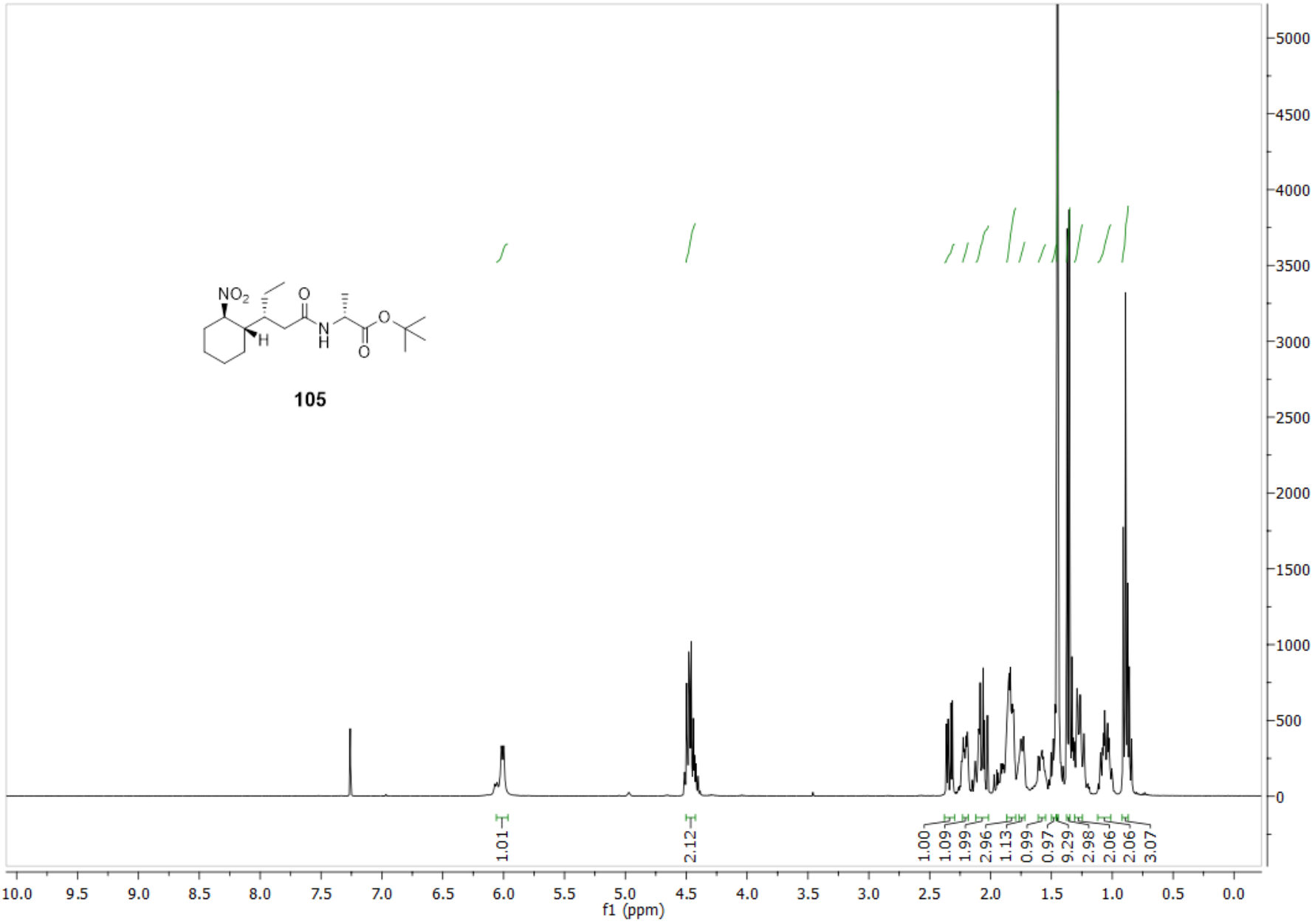
NO2
O
N
H
O
O
H
105
1.01
2.12
1.00
1.09
1.99
2.96
1.13
0.99
0.97
9.29
2.98
2.06
2.06
3.07
5000
4500
4000
3500
3000
2500
2000
1500
1000
500
0
10.0
9.5
9.0
8.5
8.0
7.5
7.0
6.5
6.0
5.5
5.0
4.5
4.0
3.5
3.0
2.5
2.0
1.5
1.0
0.5
0.0
f1 (ppm)

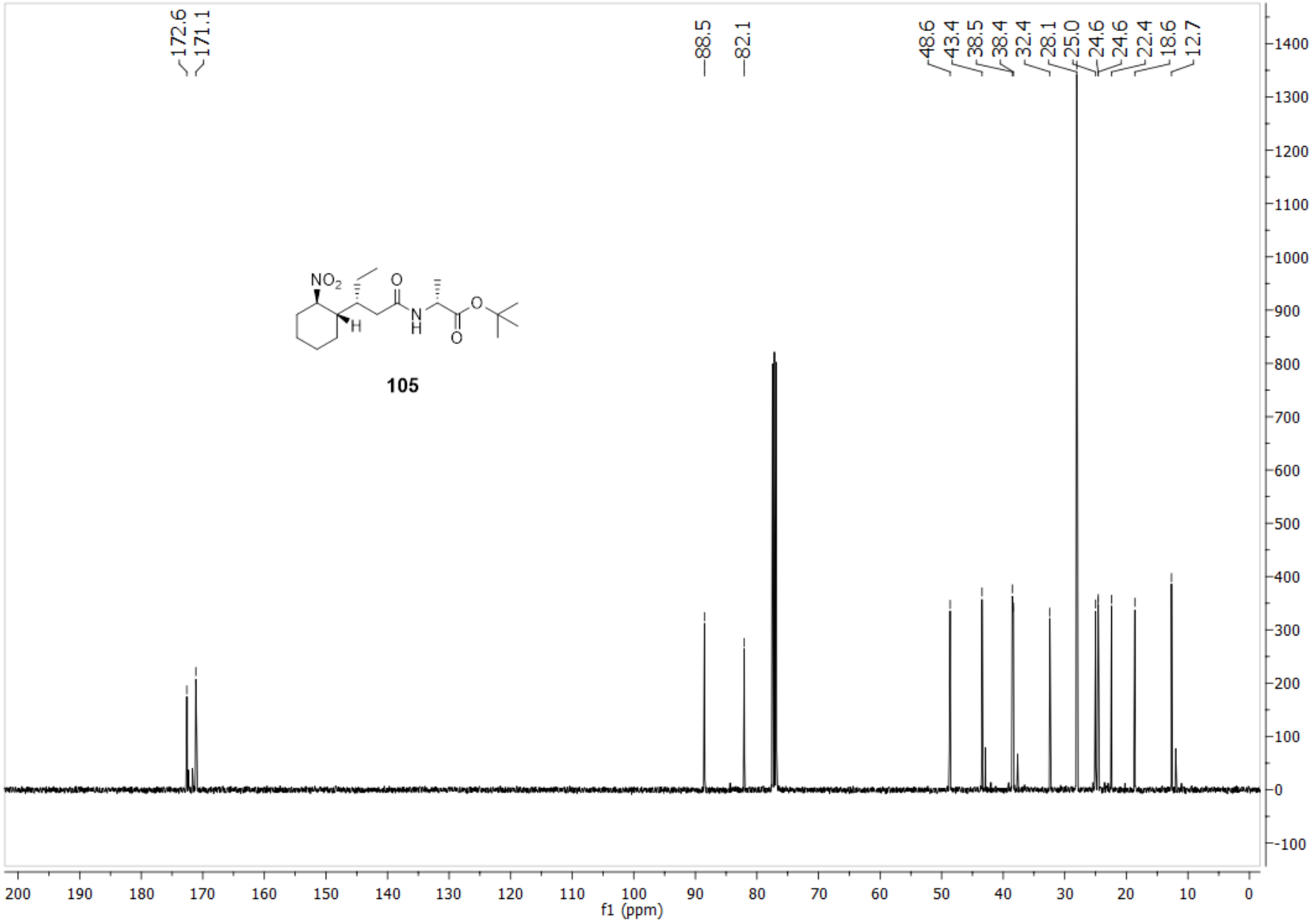
172.6
171.1
88.5
82.1
48.6
43.4
38.5
38.4
32.4
28.1
25.0
24.6
24.6
22.4
18.6
12.7
NO2
O
N
H
O
O
H
105
f1 (ppm)

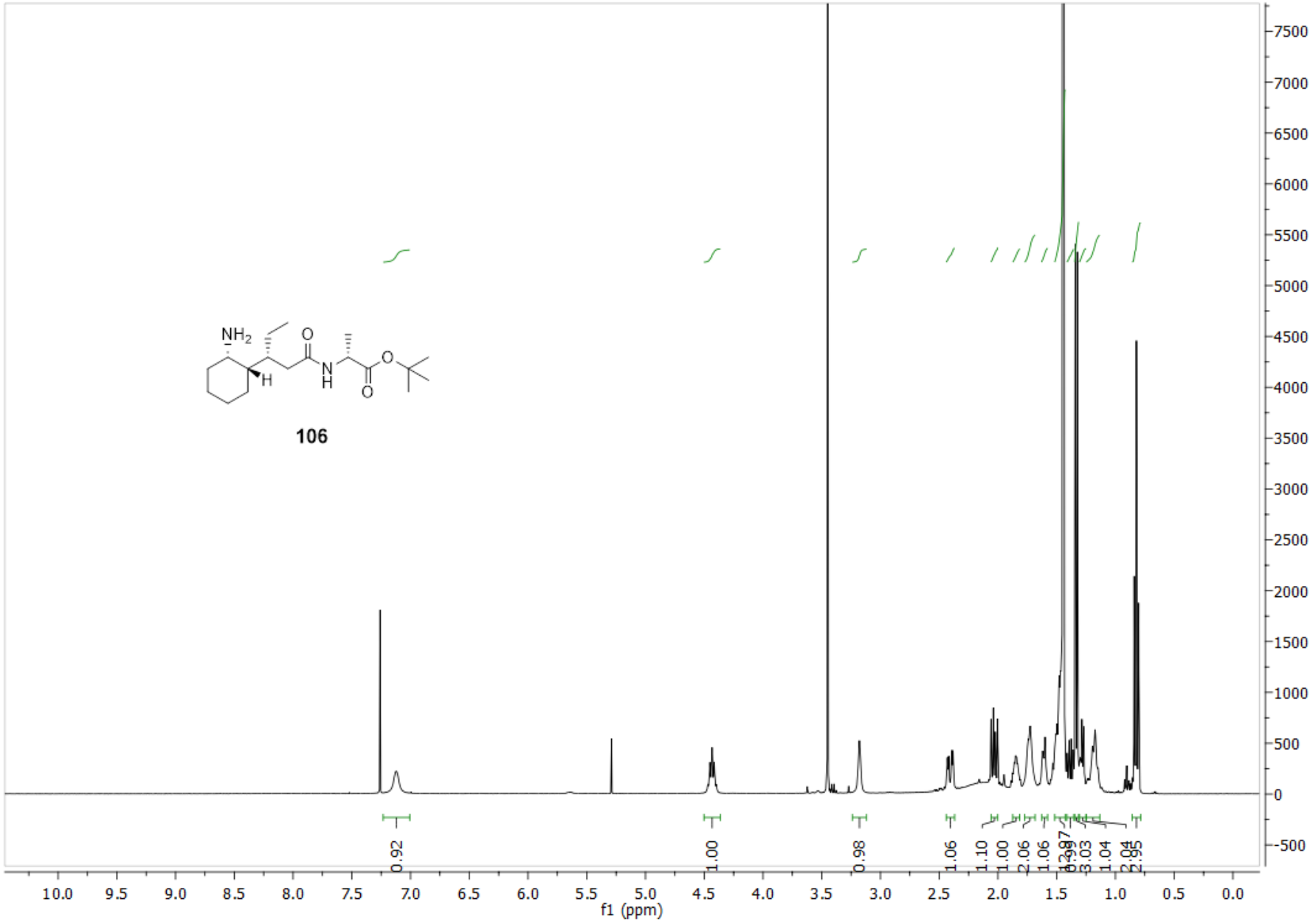
NH2
O
N
H
H
O
O
106
7500
7000
6500
6000
5500
5000
4500
4000
3500
3000
2500
2000
1500
1000
500
0
-500
0.92
1.00
0.98
1.06
1.10
1.00
2.06
1.06
4.97
3.03
1.04
2.04
2.05
10.0
9.5
9.0
8.5
8.0
7.5
7.0
6.5
6.0
5.5
5.0
4.5
4.0
3.5
3.0
2.5
2.0
1.5
1.0
0.5
0.0
f1 (ppm)

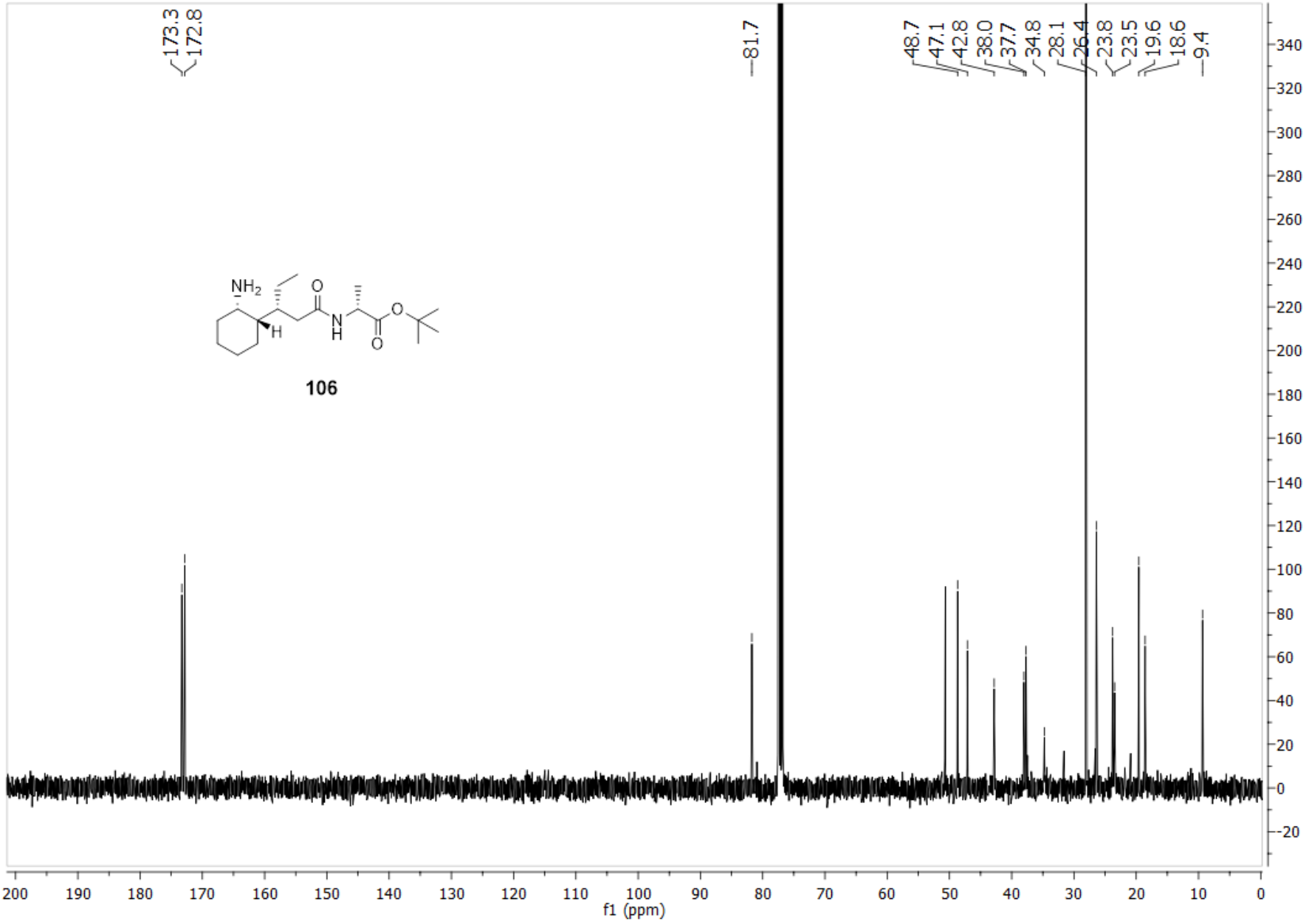
173.3
172.8
81.7
48.7
47.1
42.8
38.0
37.7
34.8
28.1
26.4
23.8
23.5
19.6
18.6
9.4
NH2
H
N
H
O
O
O
106
f1 (ppm)

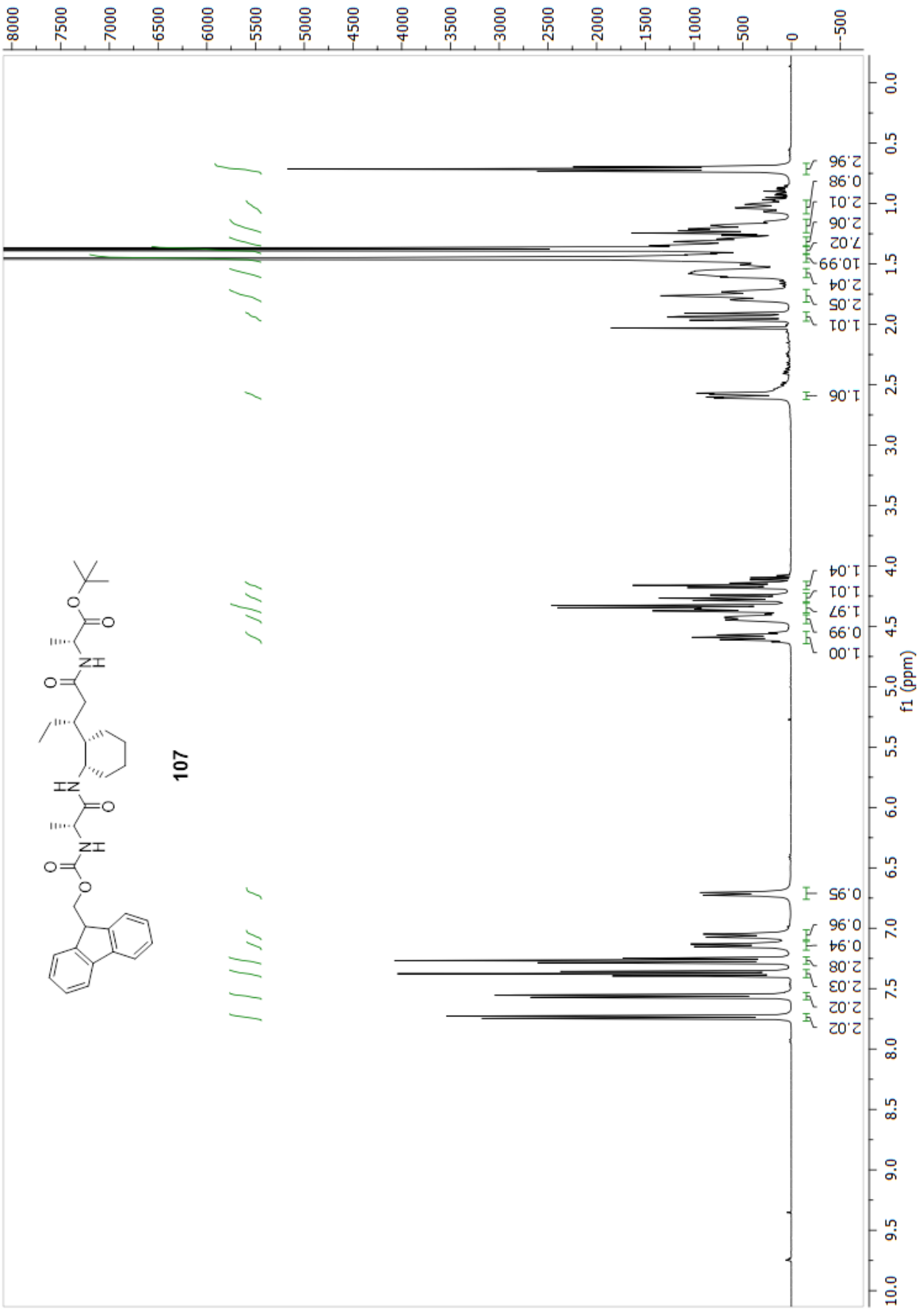
107
f1 (ppm)

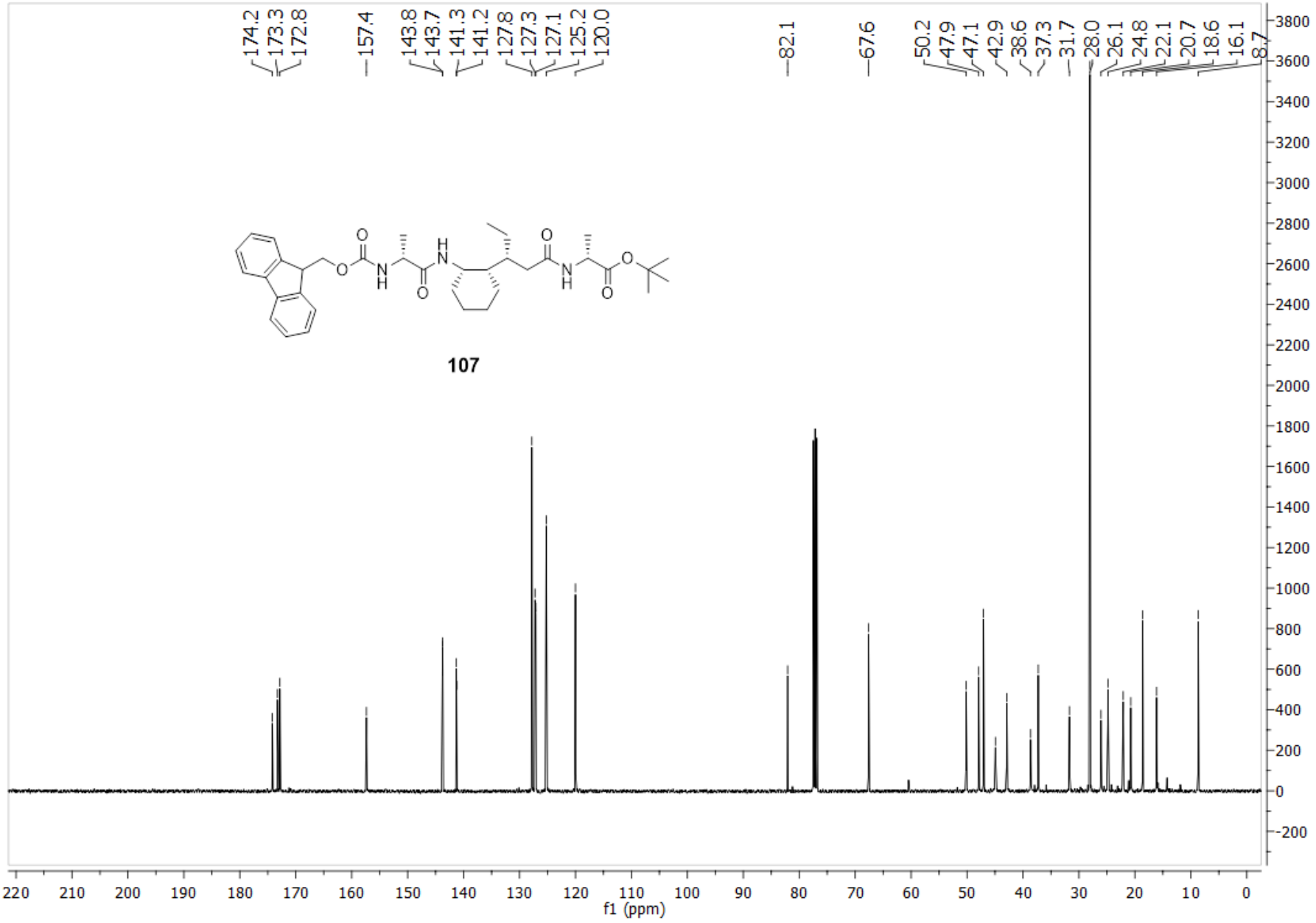
174.2
173.3
172.8
157.4
143.8
143.7
141.3
141.2
127.8
127.3
127.1
125.2
120.0
82.1
67.6
50.2
47.9
47.1
42.9
38.6
37.3
31.7
28.0
26.1
24.8
22.1
20.7
18.6
16.1
8.7
107
f1 (ppm)

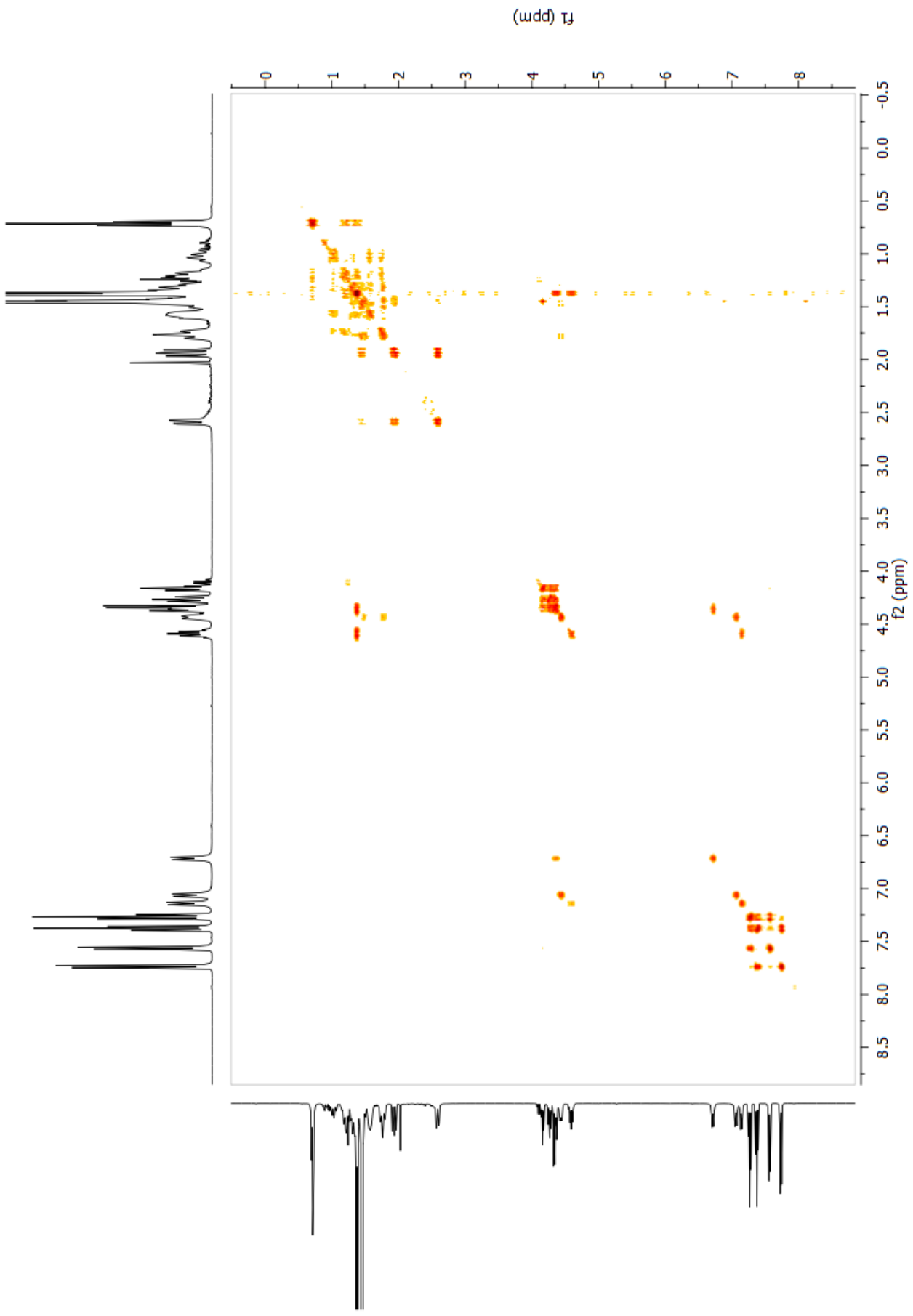

Figure 7.1: COSY NMR spectrum for trimer **107.** Recorded at rt, in an 8.0 mM solution in $CDCl_3$ (400 MHz).

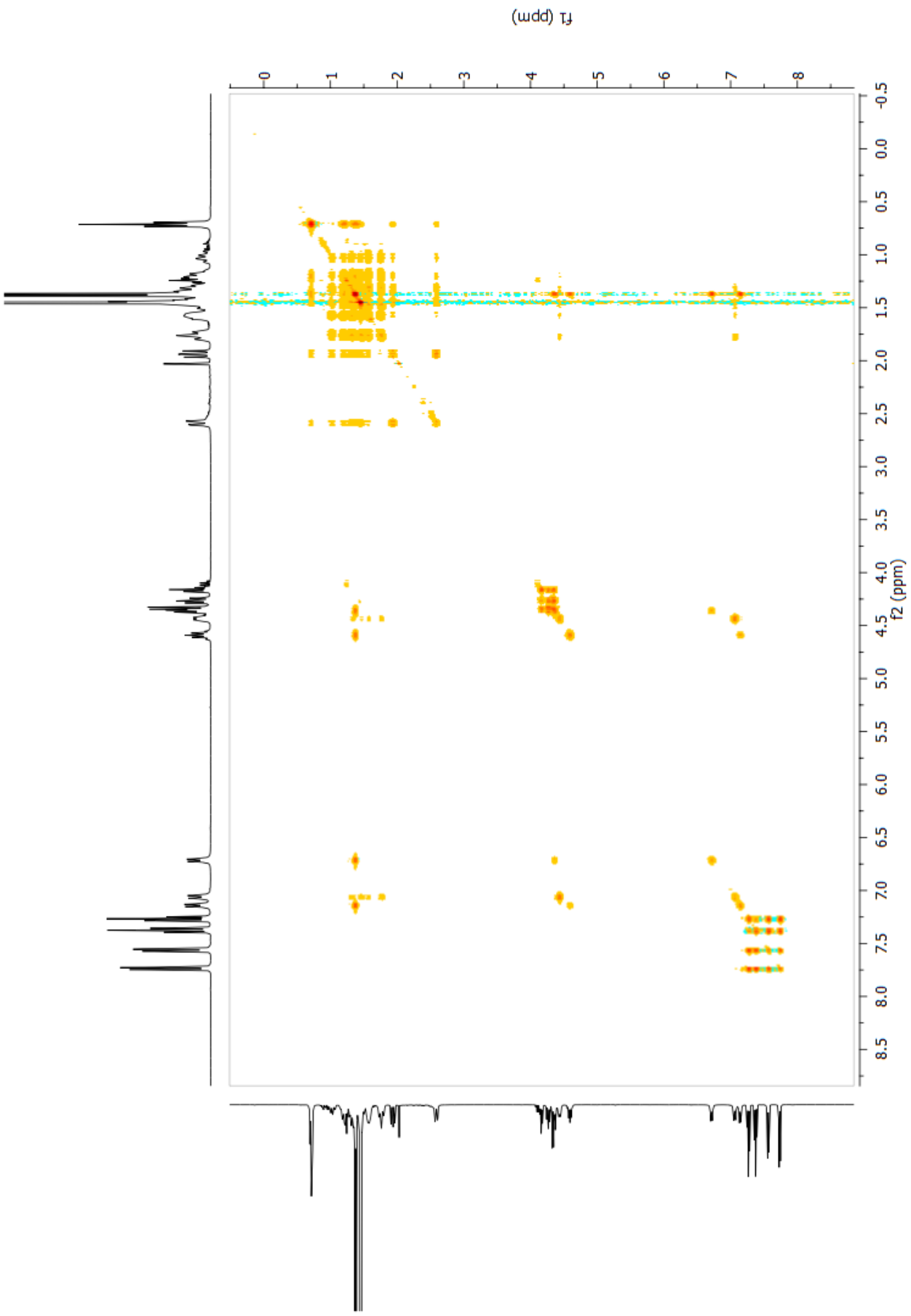

Figure 7.2: TOCSY NMR spectrum for trimer **107.** Recorded at rt, in an 8.0 mM solution in $CDCl_3$ (400 MHz).

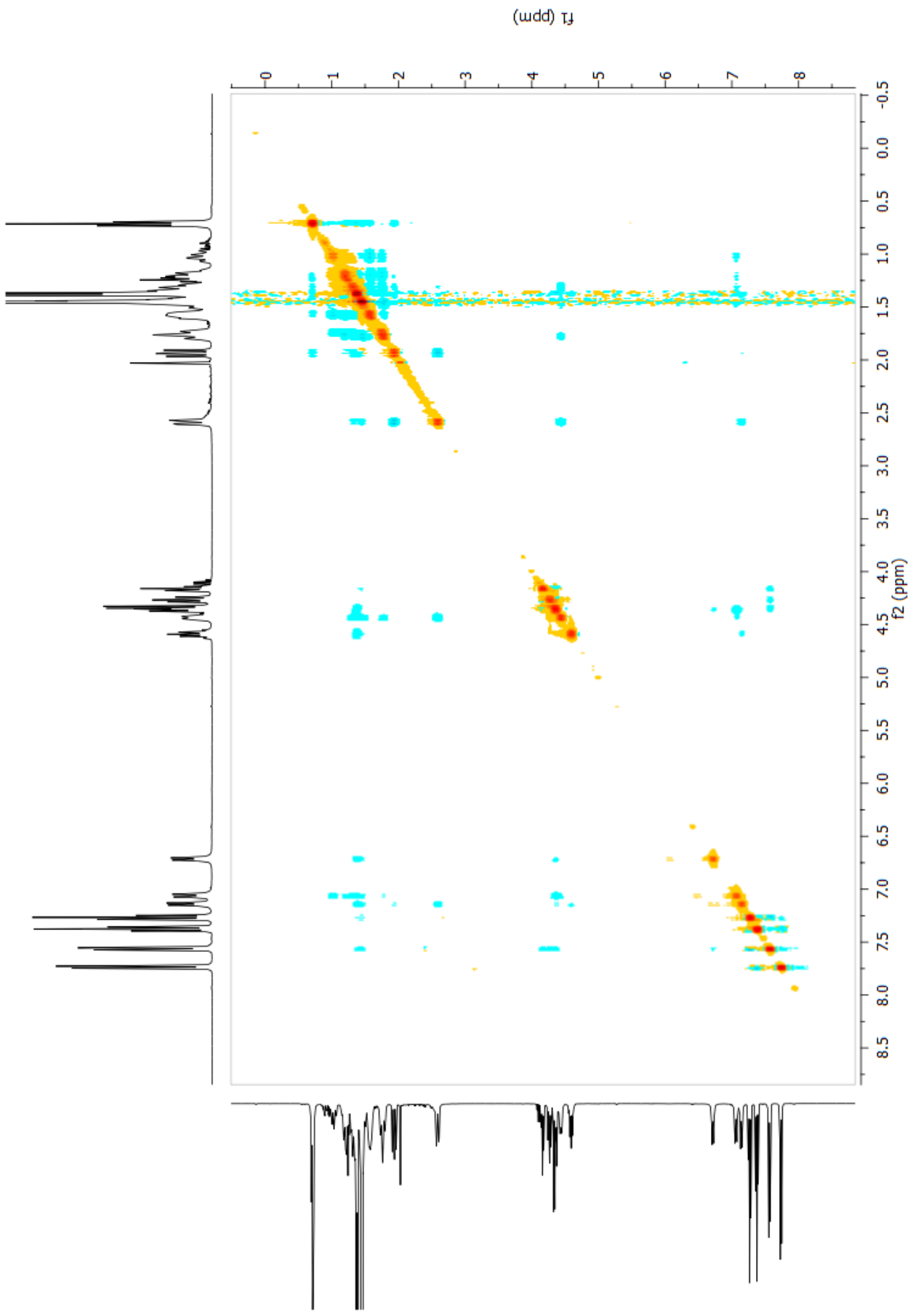

Figure 7.3: ROESY NMR spectrum for trimer **107.** Recorded at rt, in an 8.0 mM solution in $CDCl_3$ (400 MHz).

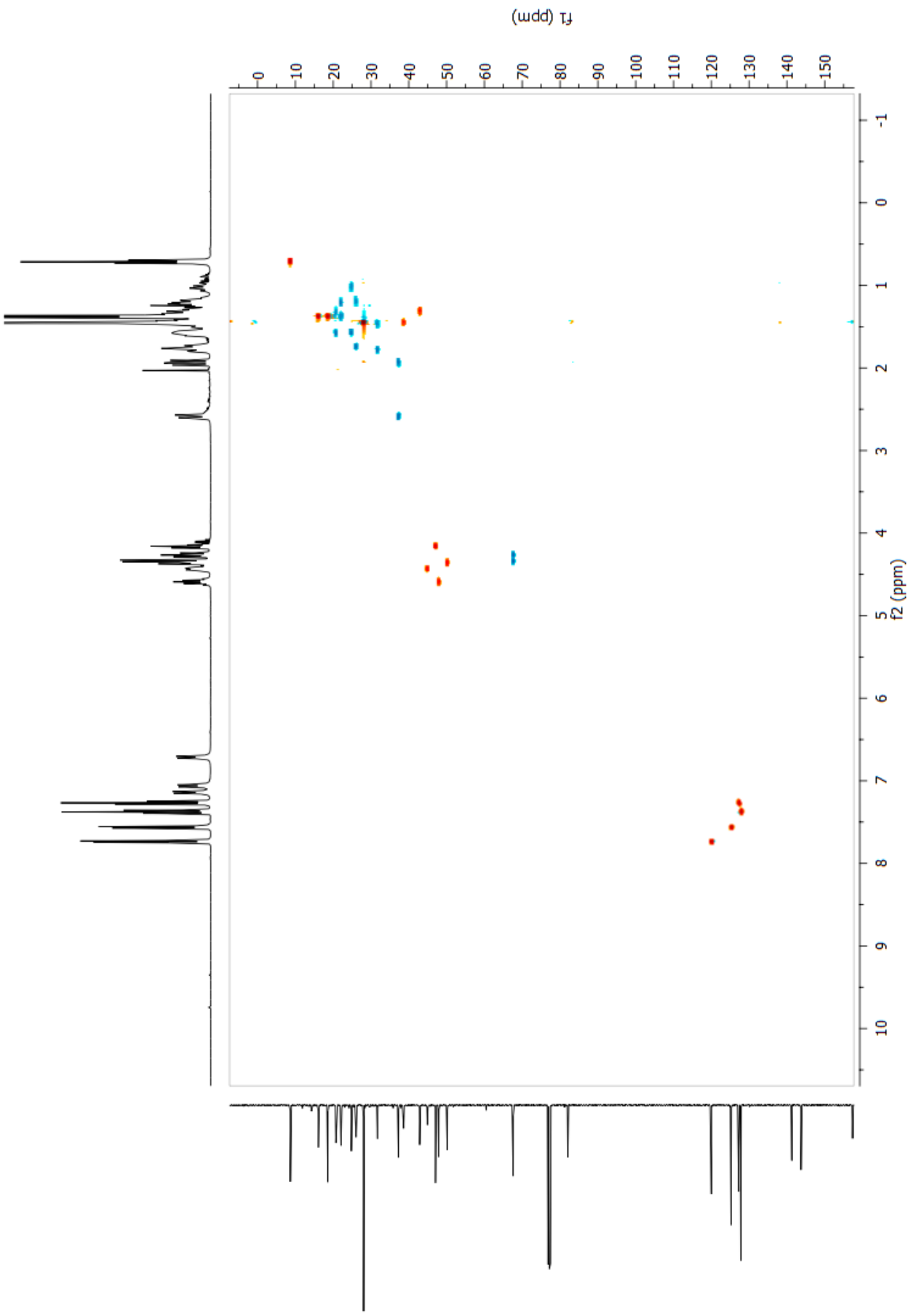

Figure 7.4: HSQC NMR spectrum for trimer **107.** Recorded at rt, in an 8.0 mM solution in $CDCl_3$ (400 MHz).

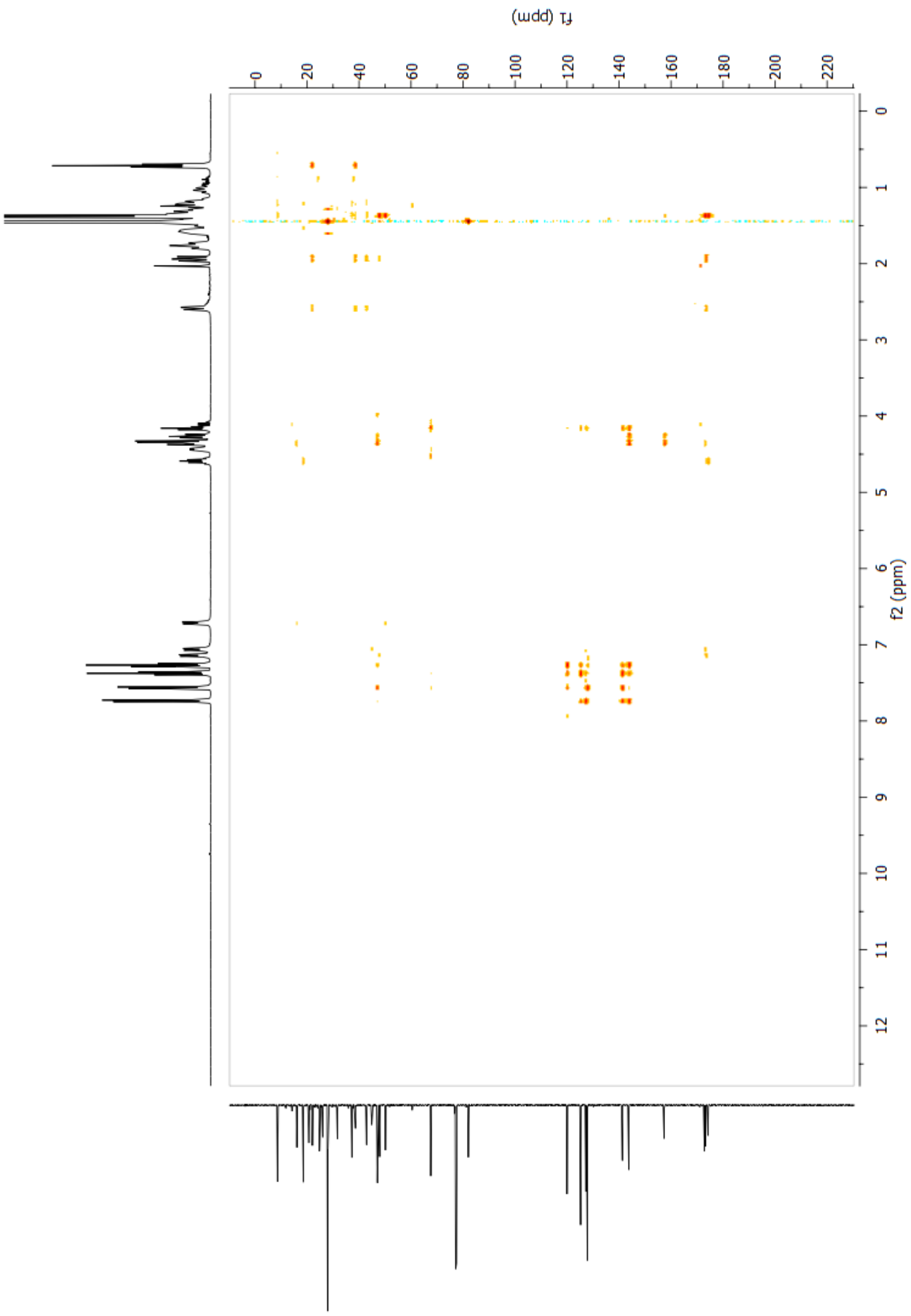

Figure 7.5: HMBC NMR spectrum for trimer **107.** Recorded at rt, in an 8.0 mM solution in $CDCl_3$ (400 MHz)

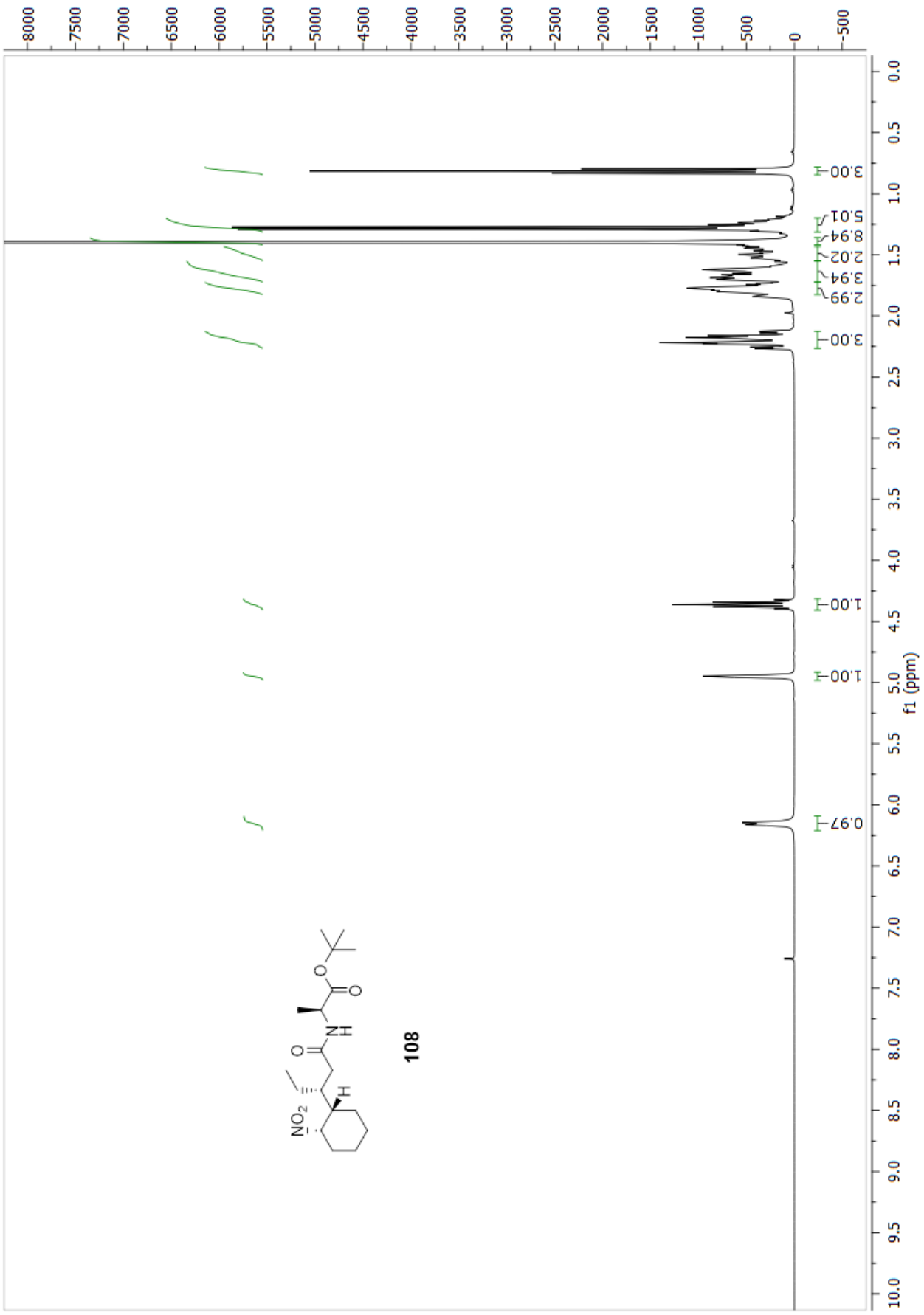

108

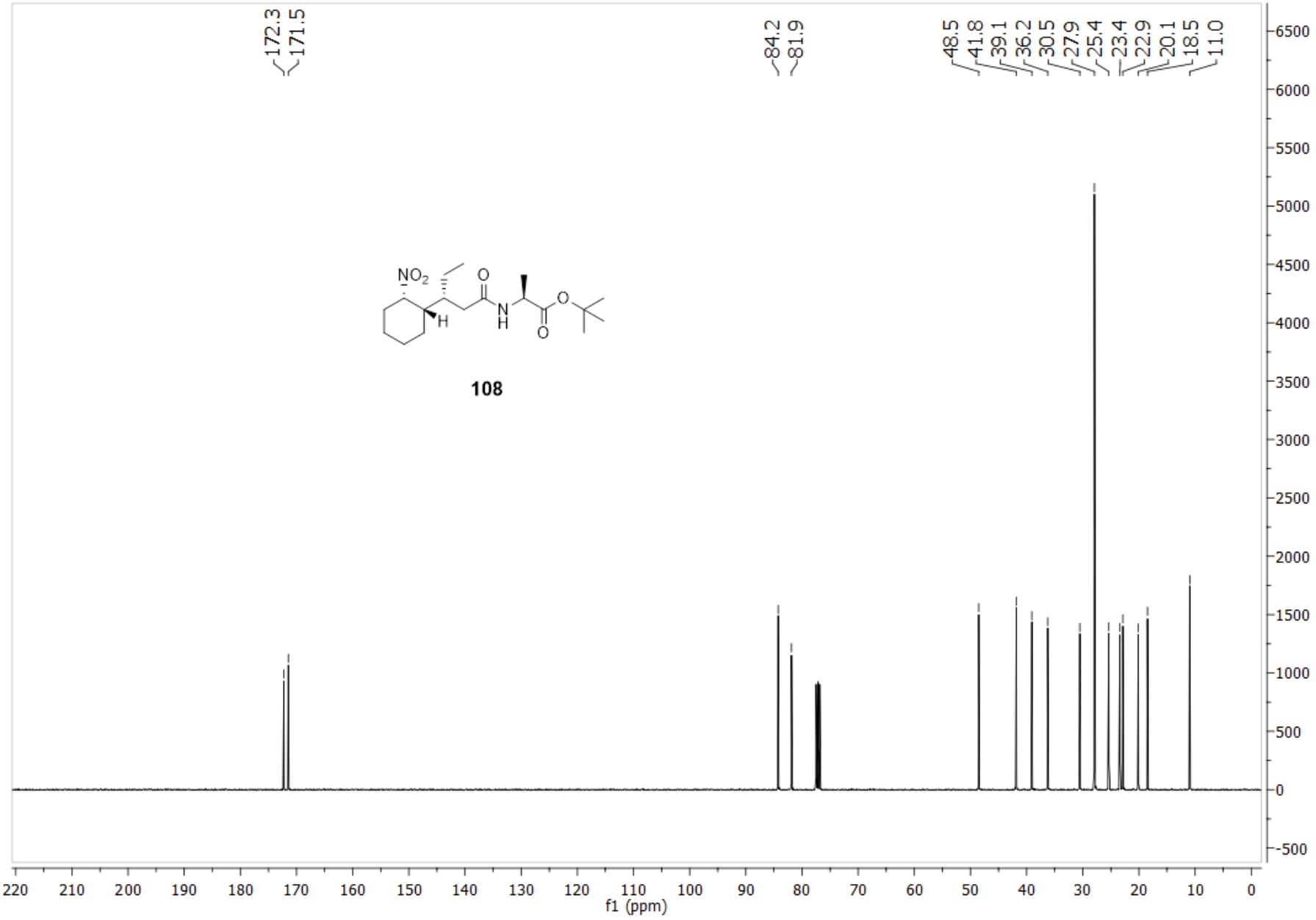
172.3
171.5
84.2
81.9
48.5
41.8
39.1
36.2
30.5
27.9
25.4
23.4
22.9
20.1
18.5
11.0
NO2
O
N
H
O
O
H
108
f1 (ppm)

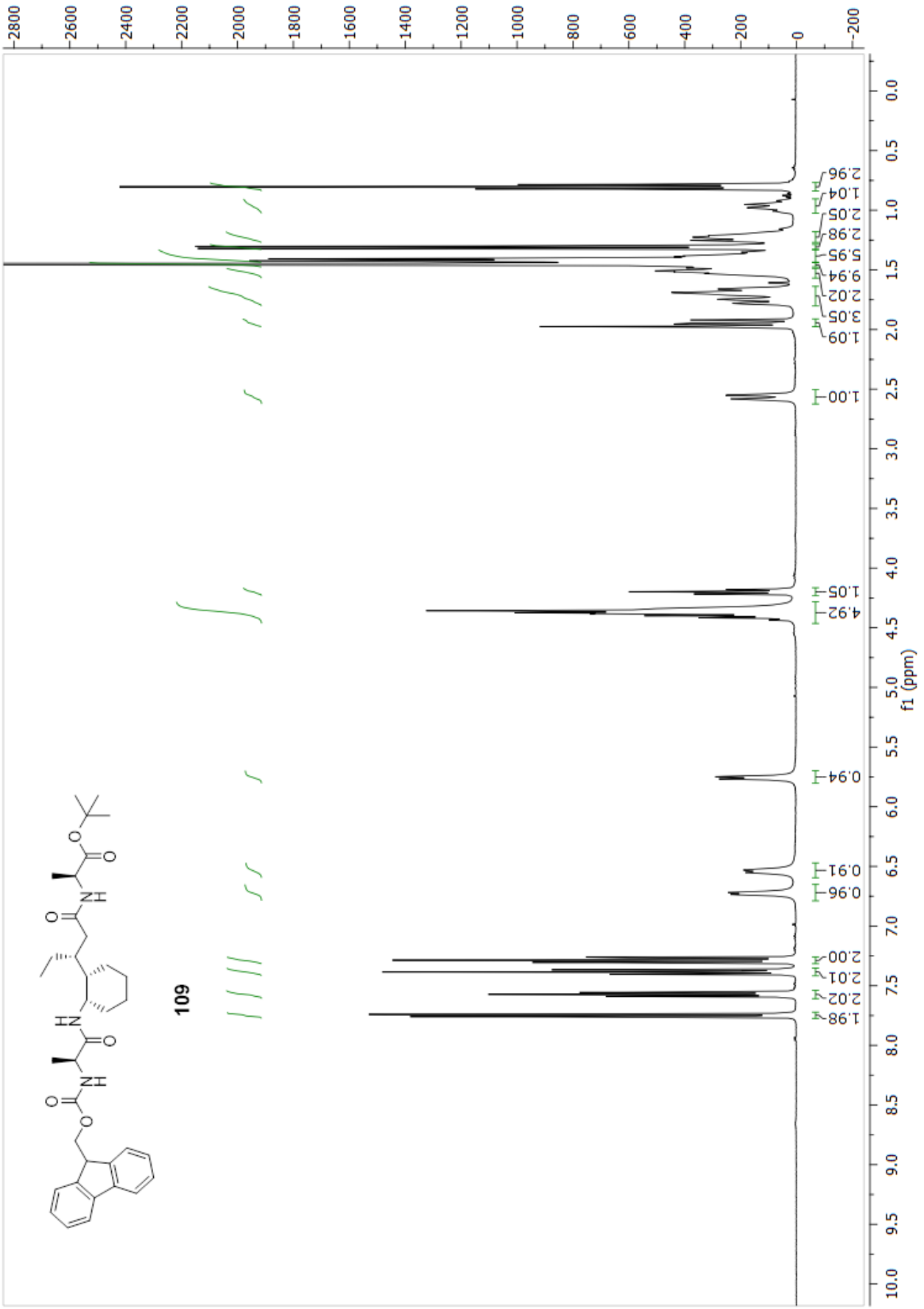
109
f1 (ppm)

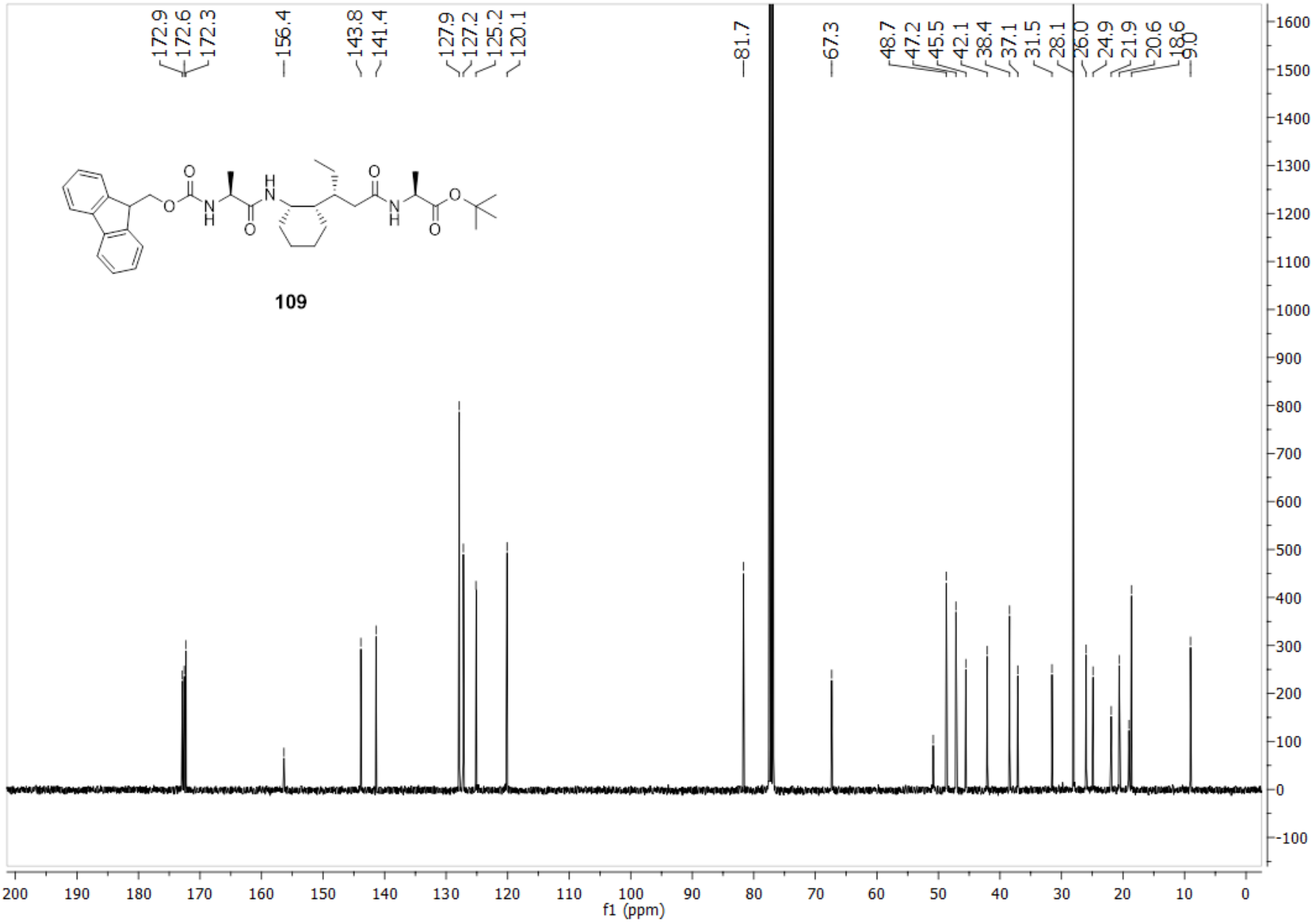
172.9
172.6
172.3
156.4
143.8
141.4
127.9
127.2
125.2
120.1
81.7
67.3
48.7
47.2
45.5
42.1
38.4
37.1
31.5
28.1
26.0
24.9
21.9
20.6
18.6
9.0
109
f1 (ppm)

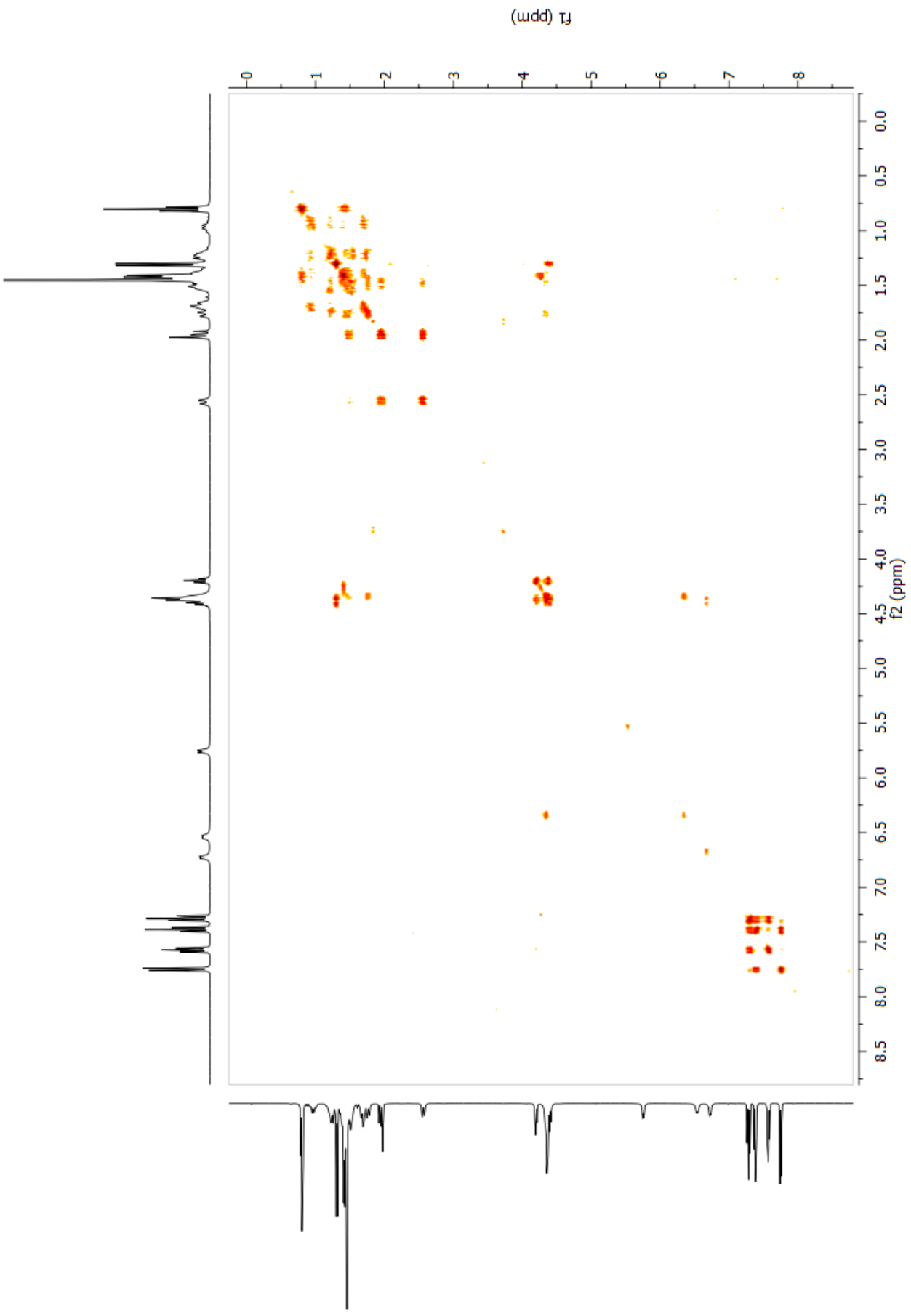

Figure 7.6: COSY NMR spectrum for trimer **109.** Recorded at rt, in an 8.0 mM solution in $CDCl_3$ (400 MHz)

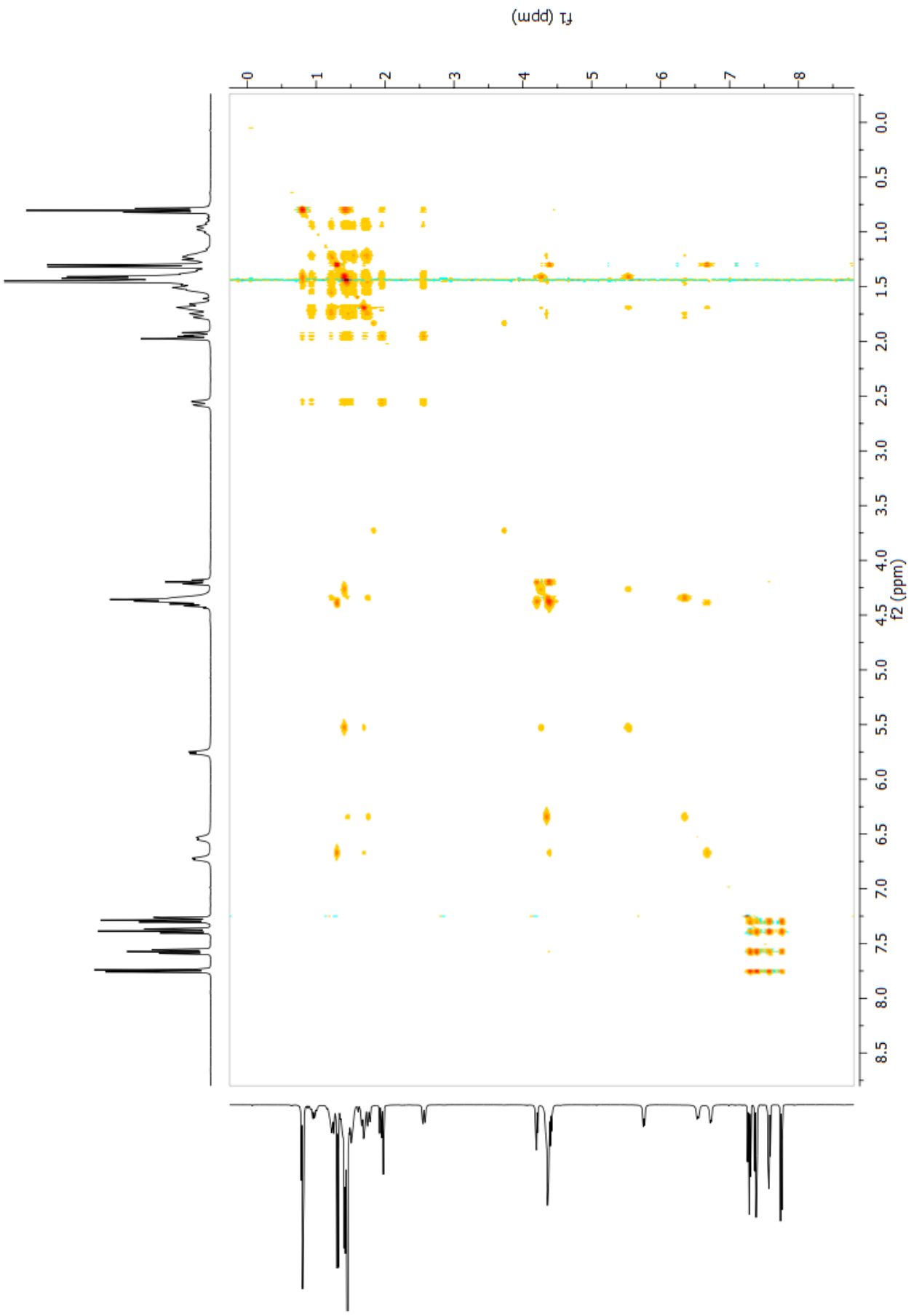

Figure 7.7: TOCSY NMR spectrum for trimer **109.** Recorded at rt, in an 8.0 mM solution in $CDCl_3$ (400 MHz)

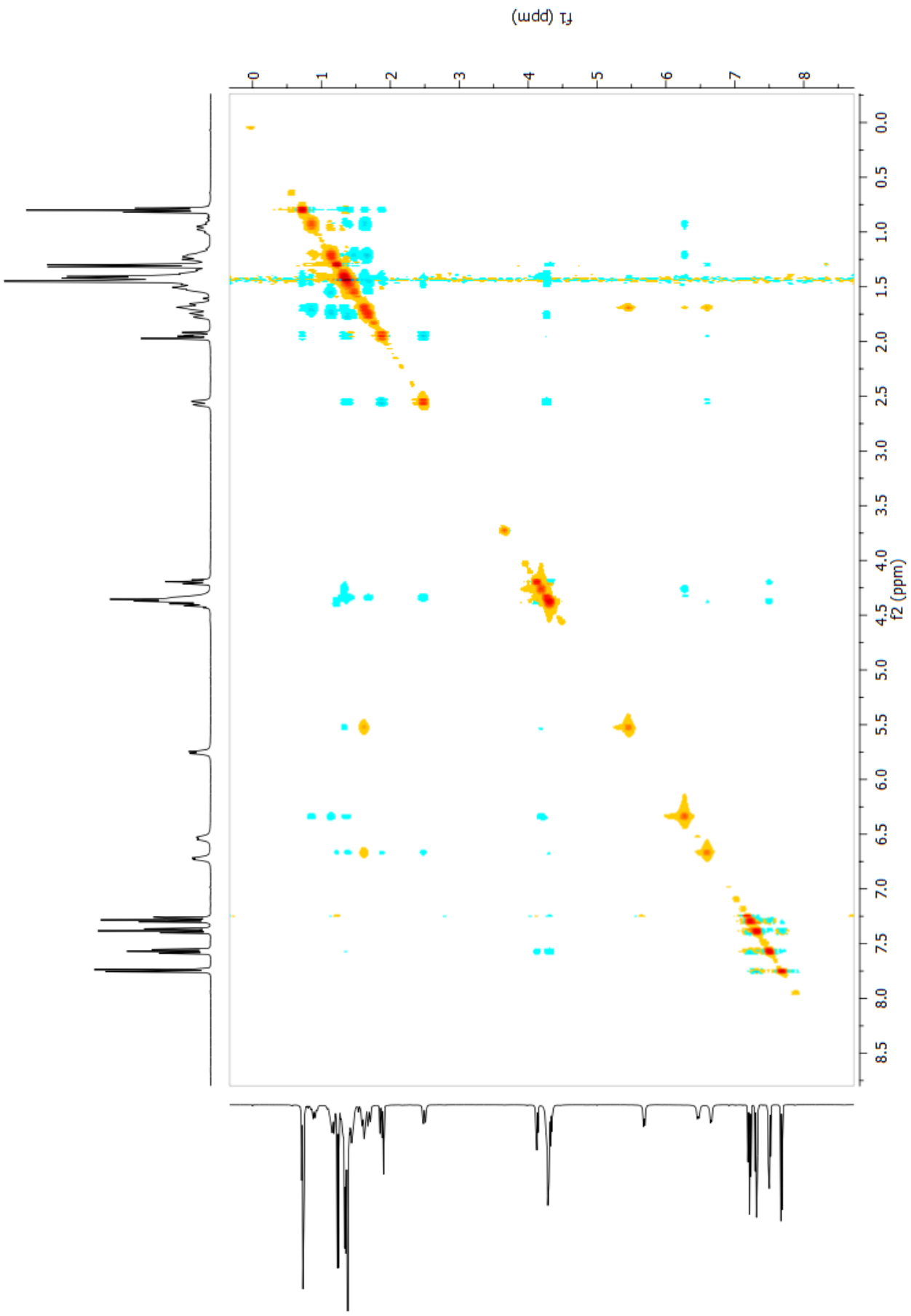

Figure 7.8: ROESY NMR spectrum for trimer **109.** Recorded at rt, in an 8.0 mM solution in $CDCl_3$ (400 MHz)

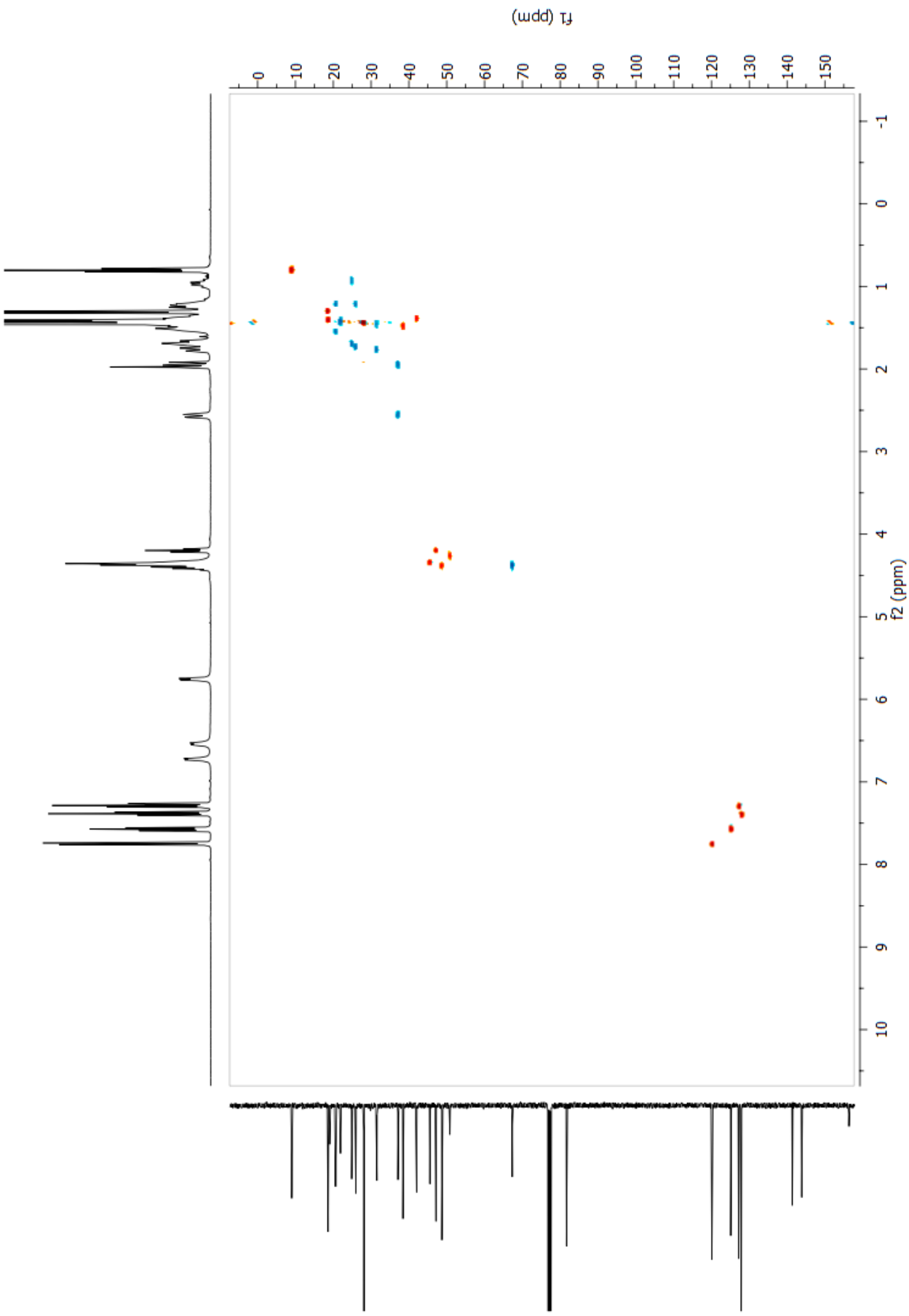

Figure 7.9: HSQC NMR spectrum for trimer **109.** Recorded at rt, in an 8.0 mM solution in $CDCl_3$ (400 MHz)

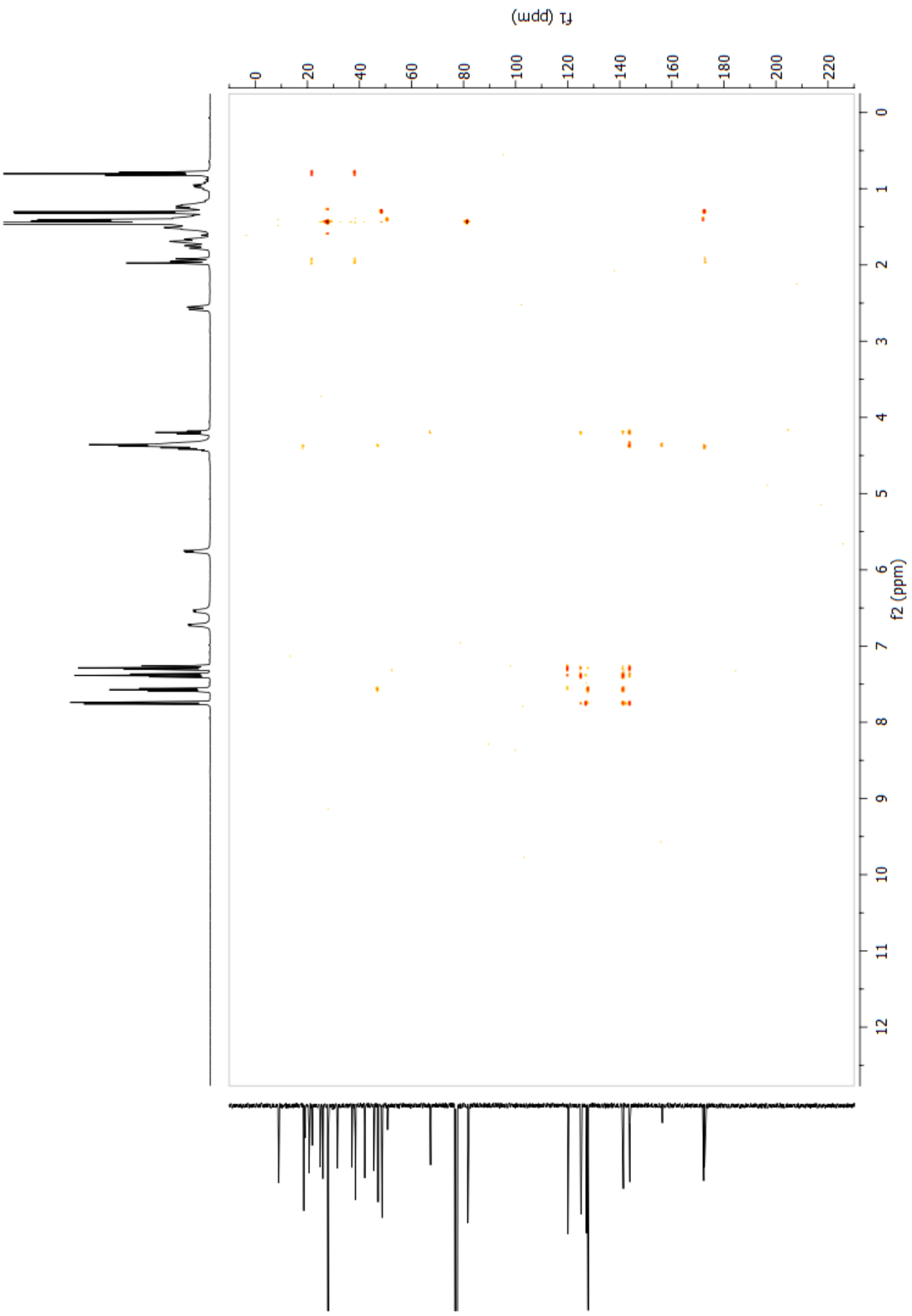

Figure 7.10: HMBC NMR spectrum for trimer **109.** Recorded at rt, in an 8.0 mM solution in $CDCl_3$ (400 MHz)

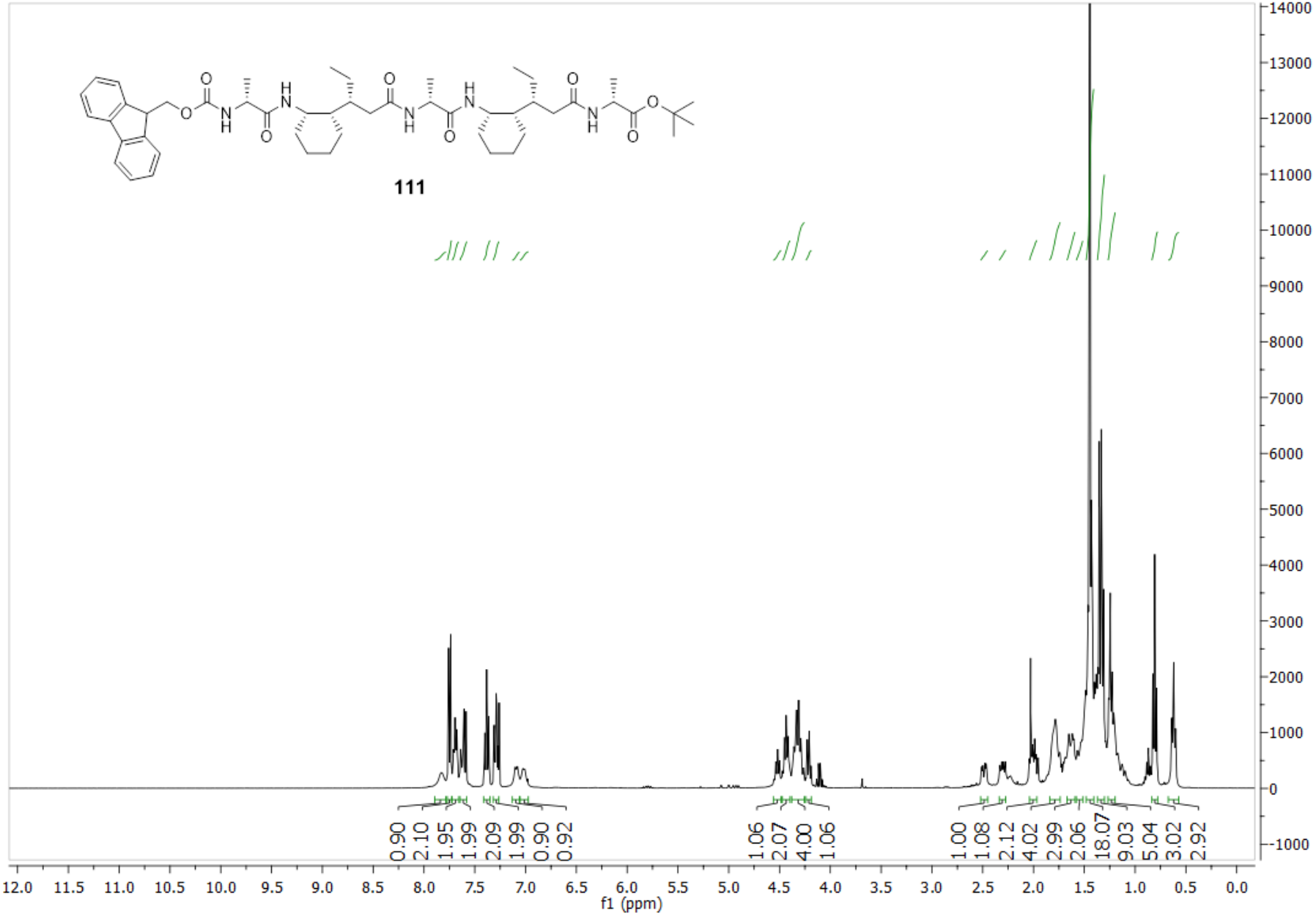
111
0.90
2.10
1.95
1.99
2.09
1.99
0.90
0.92
1.06
2.07
4.00
1.06
1.00
1.08
2.12
4.02
2.99
2.06
18.07
9.03
5.04
3.02
2.92
f1 (ppm)

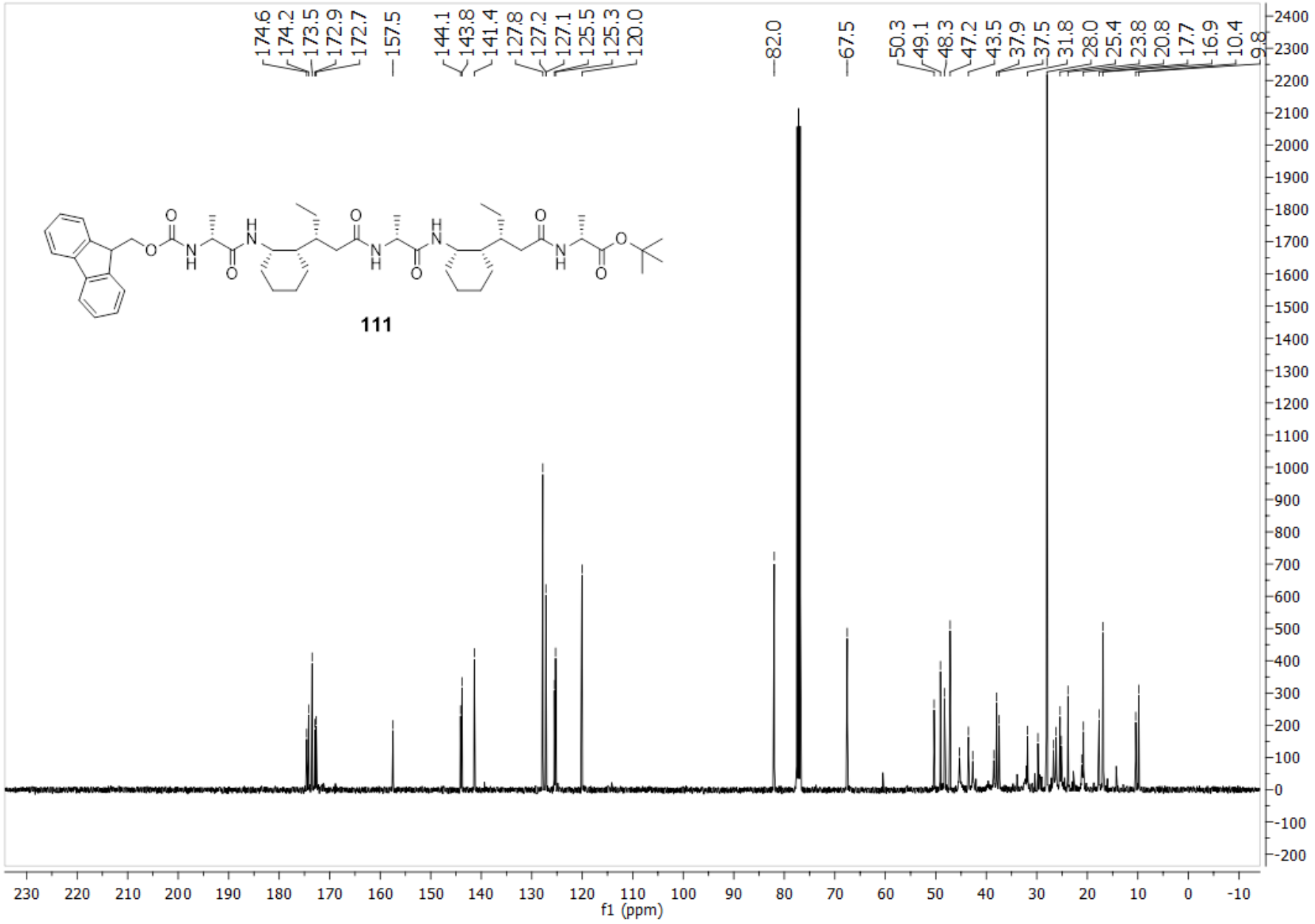
174.6
174.2
173.5
172.9
172.7
157.5
144.1
143.8
141.4
127.8
127.2
127.1
125.5
125.3
120.0
82.0
67.5
50.3
49.1
48.3
47.2
43.5
37.9
37.5
31.8
28.0
25.4
23.8
20.8
17.7
16.9
10.4
9.8
111
f1 (ppm)

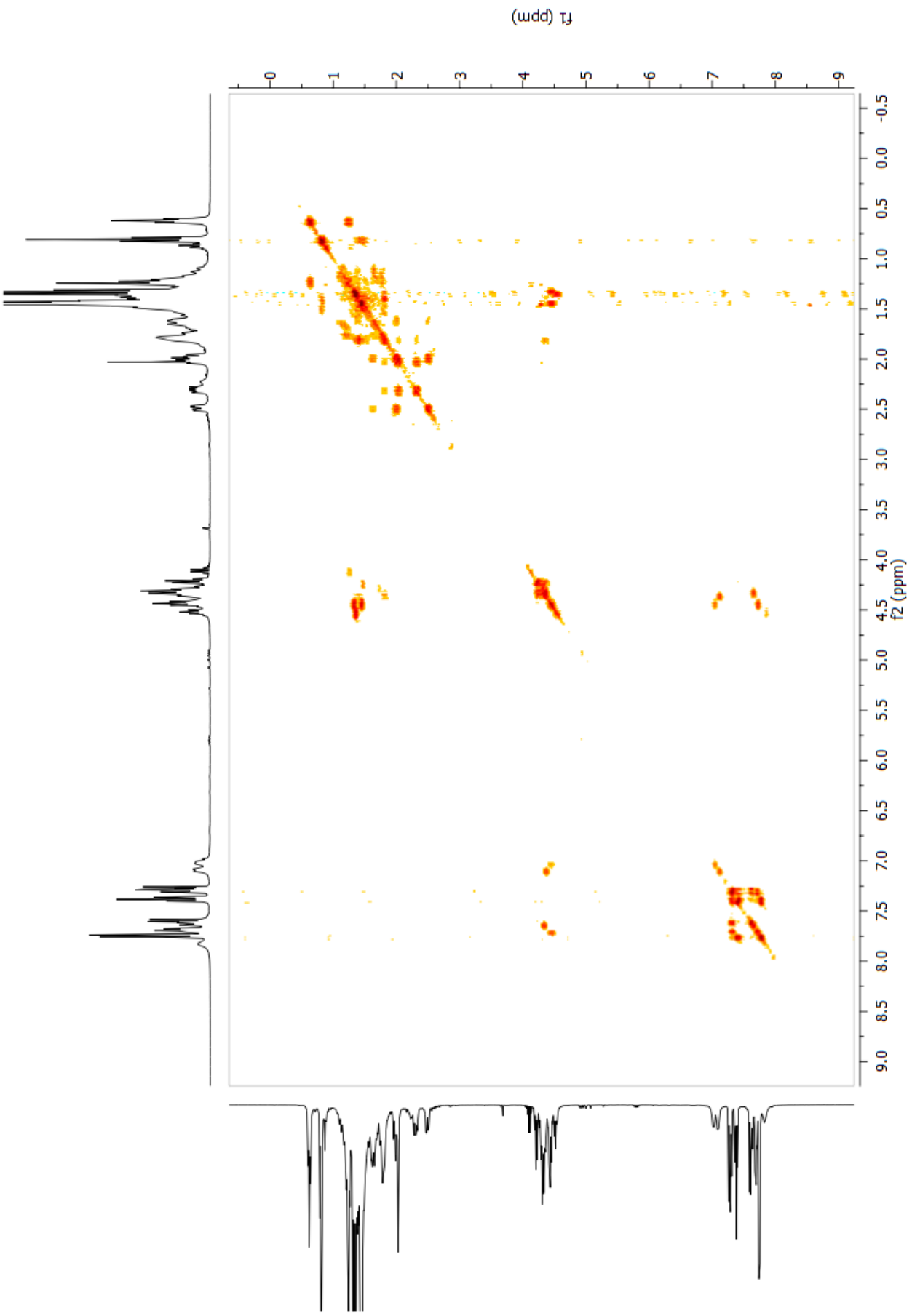

Figure 7.11: COSY NMR spectrum for pentamer **111.** Recorded at rt, in an 8.0 mM solution in $CDCl_3$ (400 MHz)

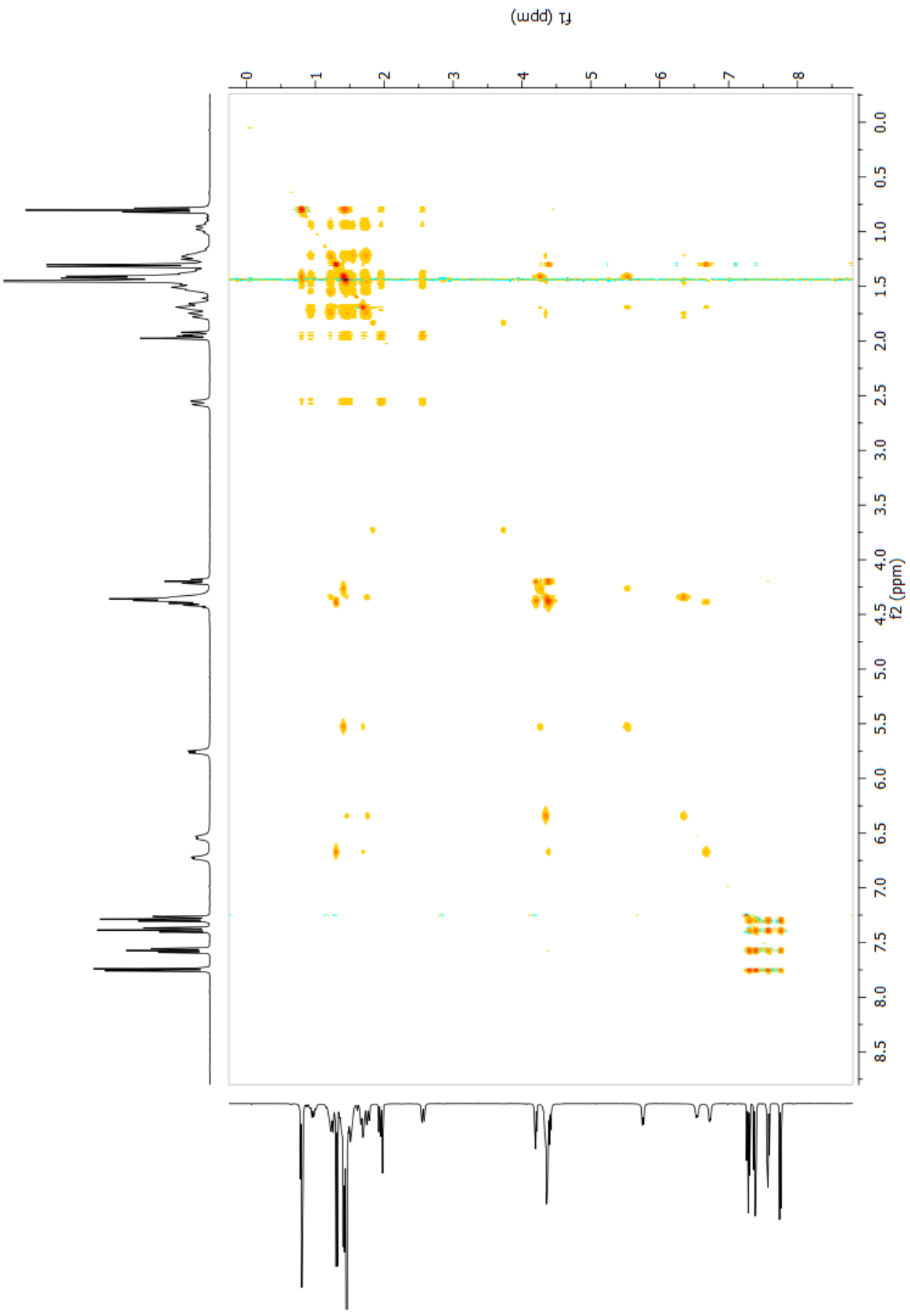

Figure 7.12: TOCSY NMR spectrum for pentamer **111.** Recorded at rt, in an 8.0 mM solution in $CDCl_3$ (400MHz)

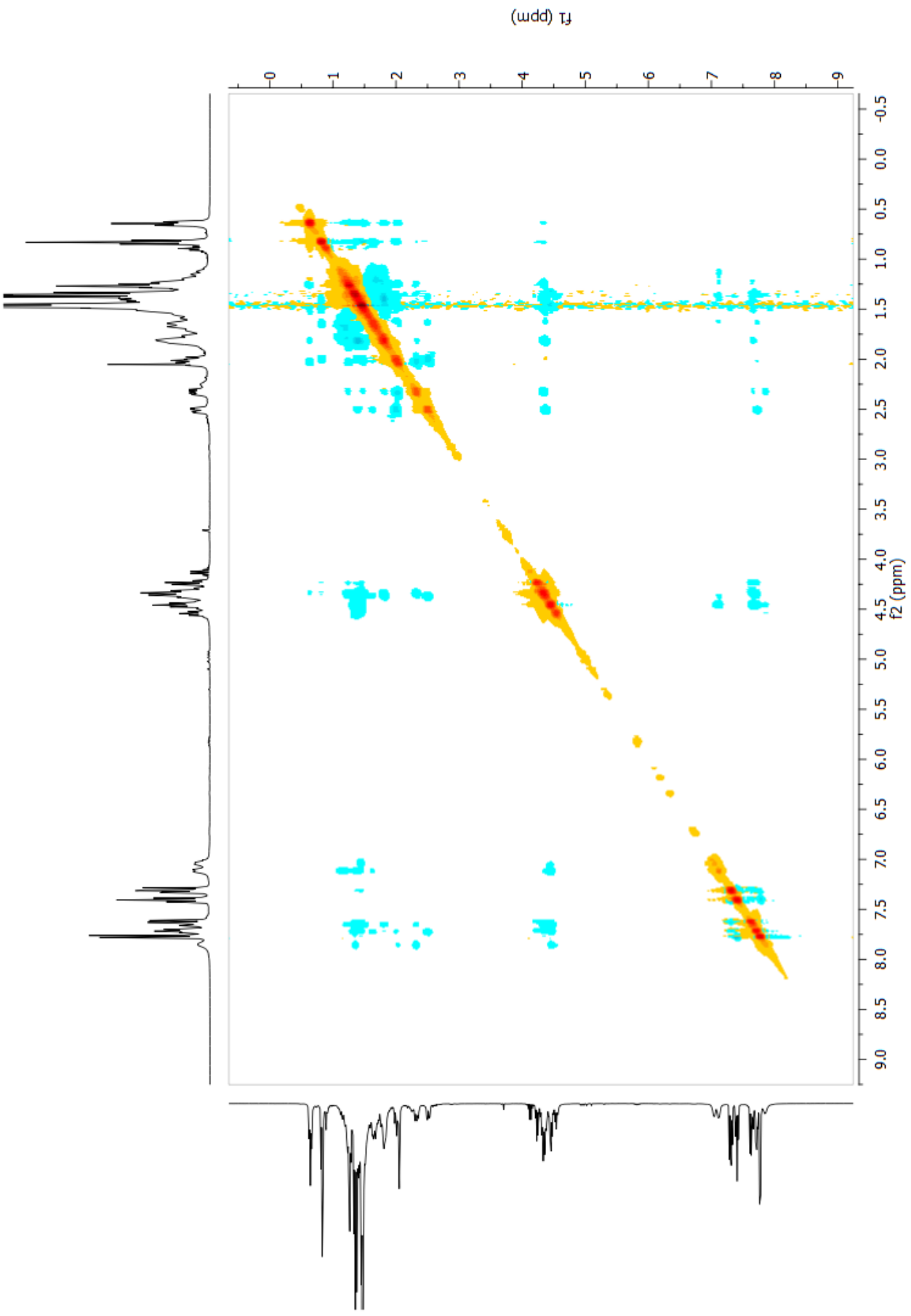

Figure 7.13: ROESY NMR spectrum for pentamer **111.** Recorded at rt, in an 8.0 mM solution in $CDCl_3$ (400MHz)

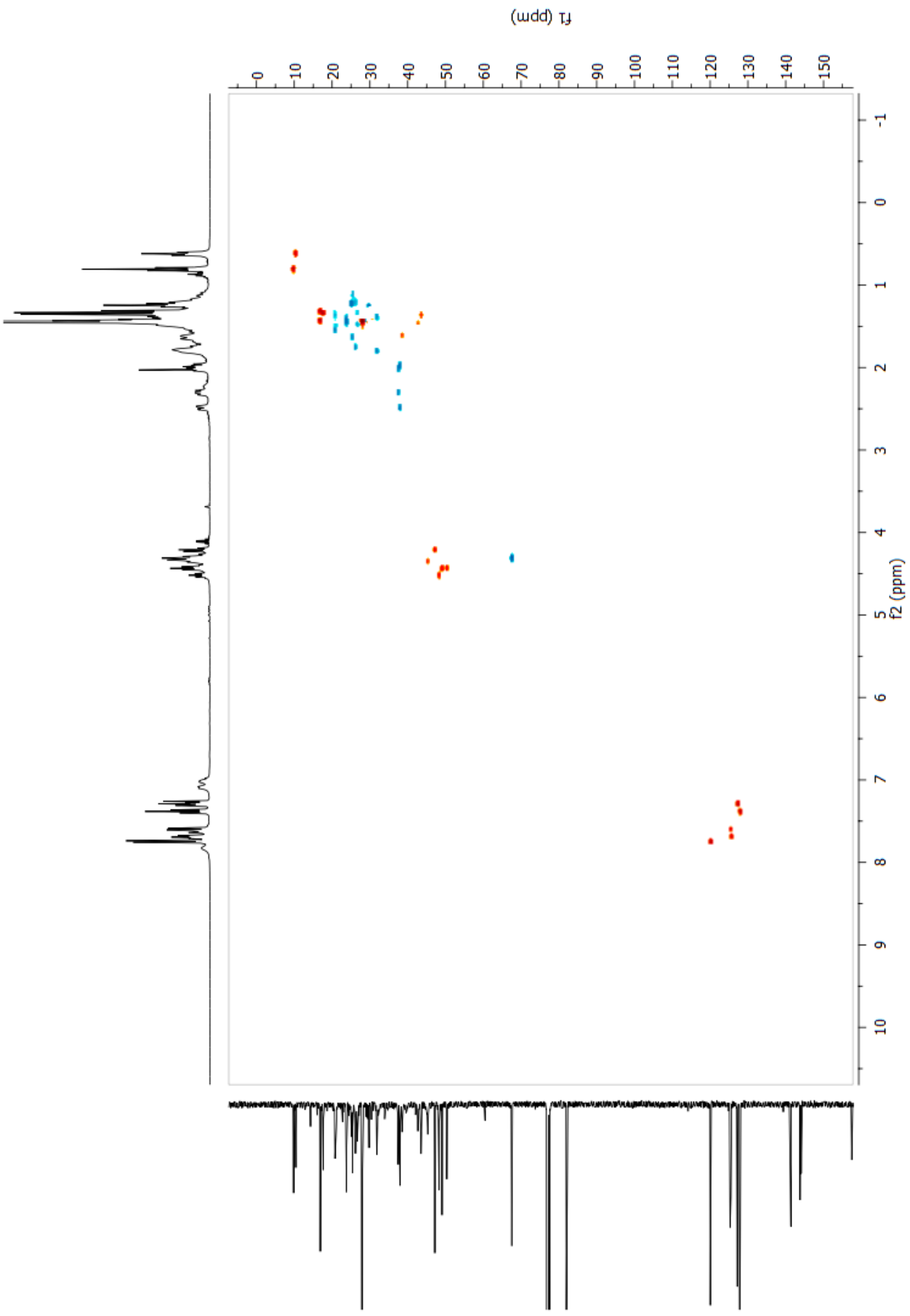

Figure 7.14: HSQC NMR spectrum for pentamer **111.** Recorded at rt, in an 8.0 mM solution in $CDCl_3$ (400 MHz)

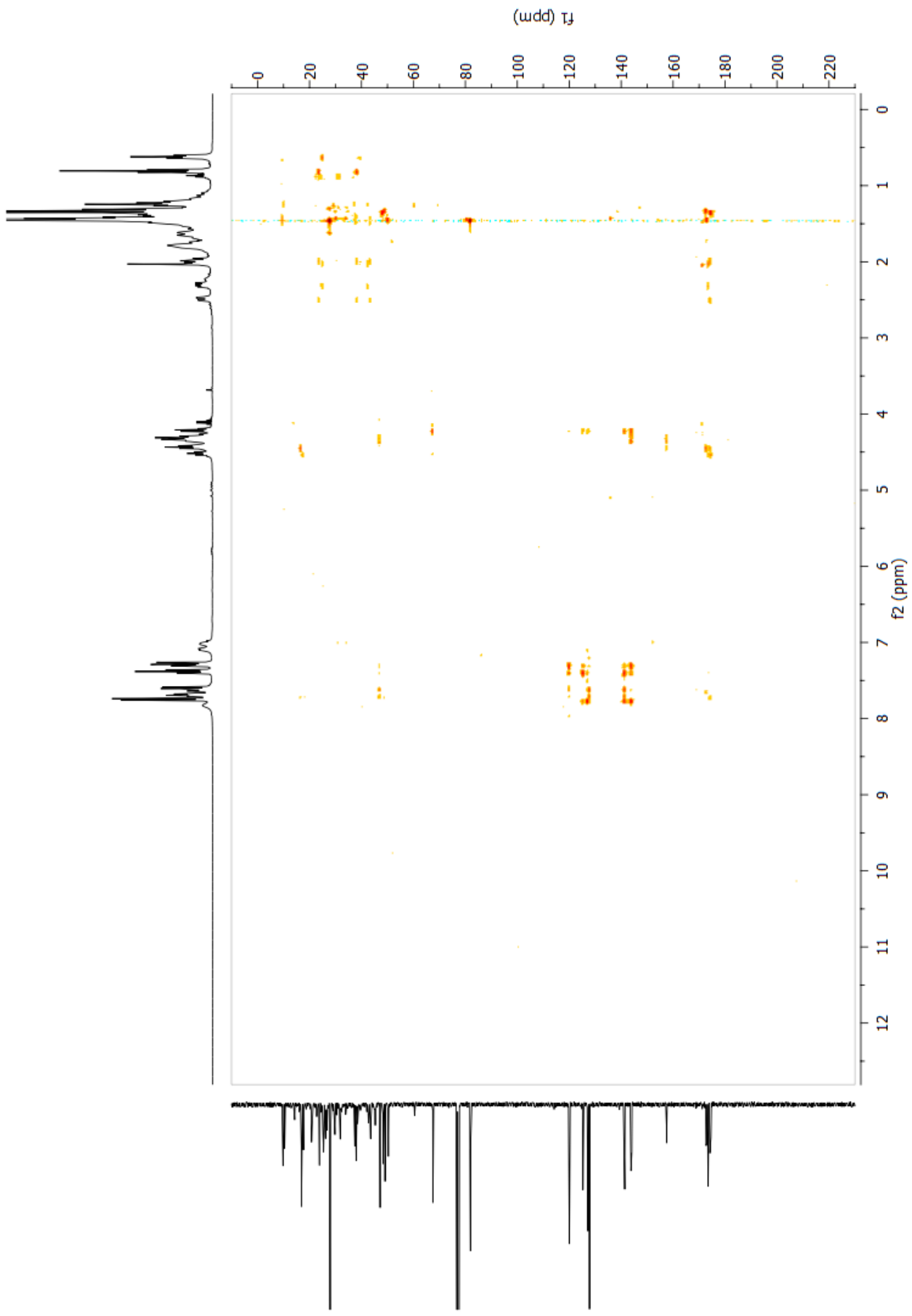

Figure 7.15: HMBC NMR spectrum for pentamer **111.** Recorded at rt, in an 8.0 mM solution in $CDCl_3$ (400MHz)

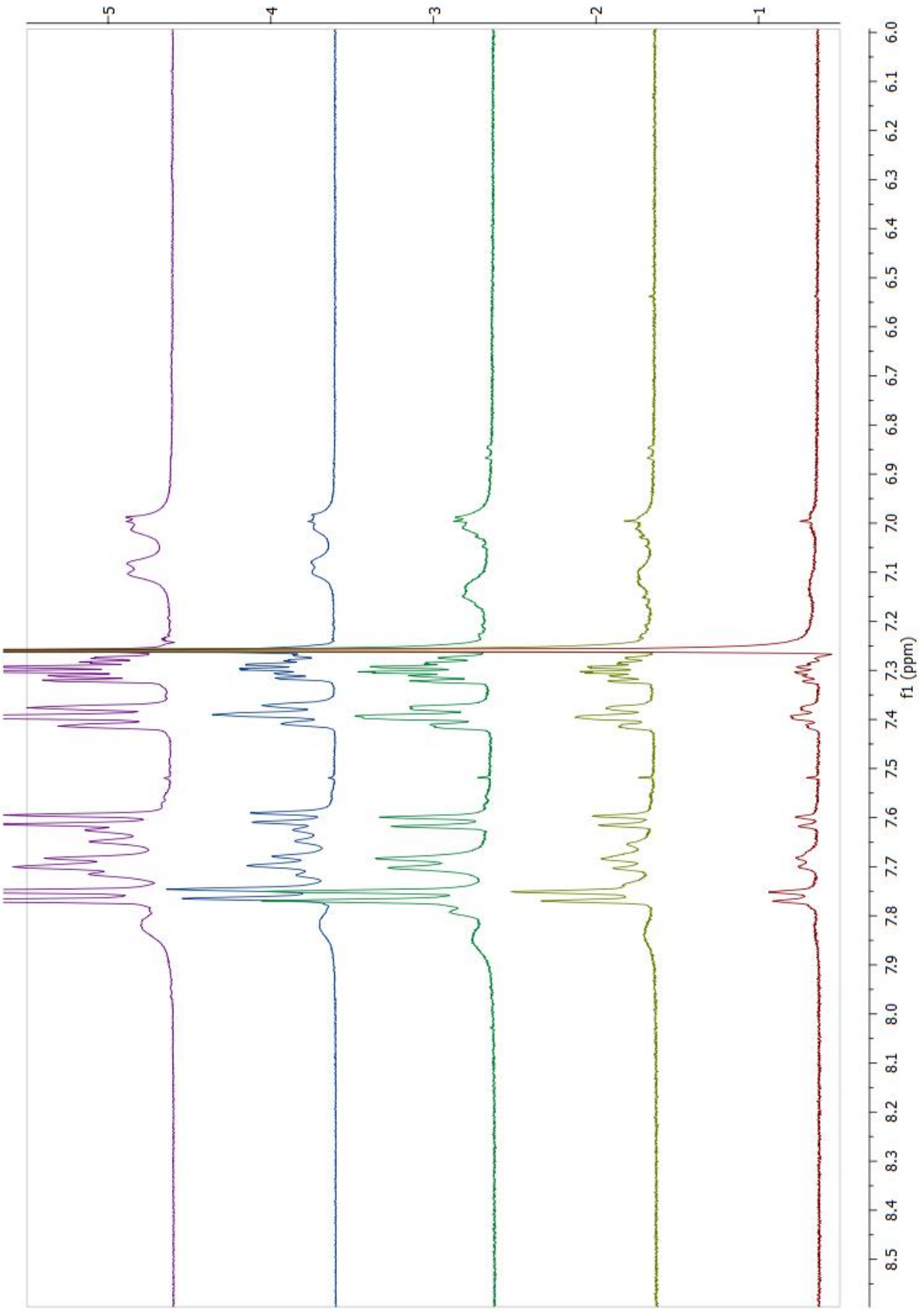

Figure 7.16: ^{1}H NMR Aggregation control studies for pentamer **111**. Recorded at rt, in 16, 8, 4, 2 and 1 mM solutions in $CDCl_3$ (400 MHz).

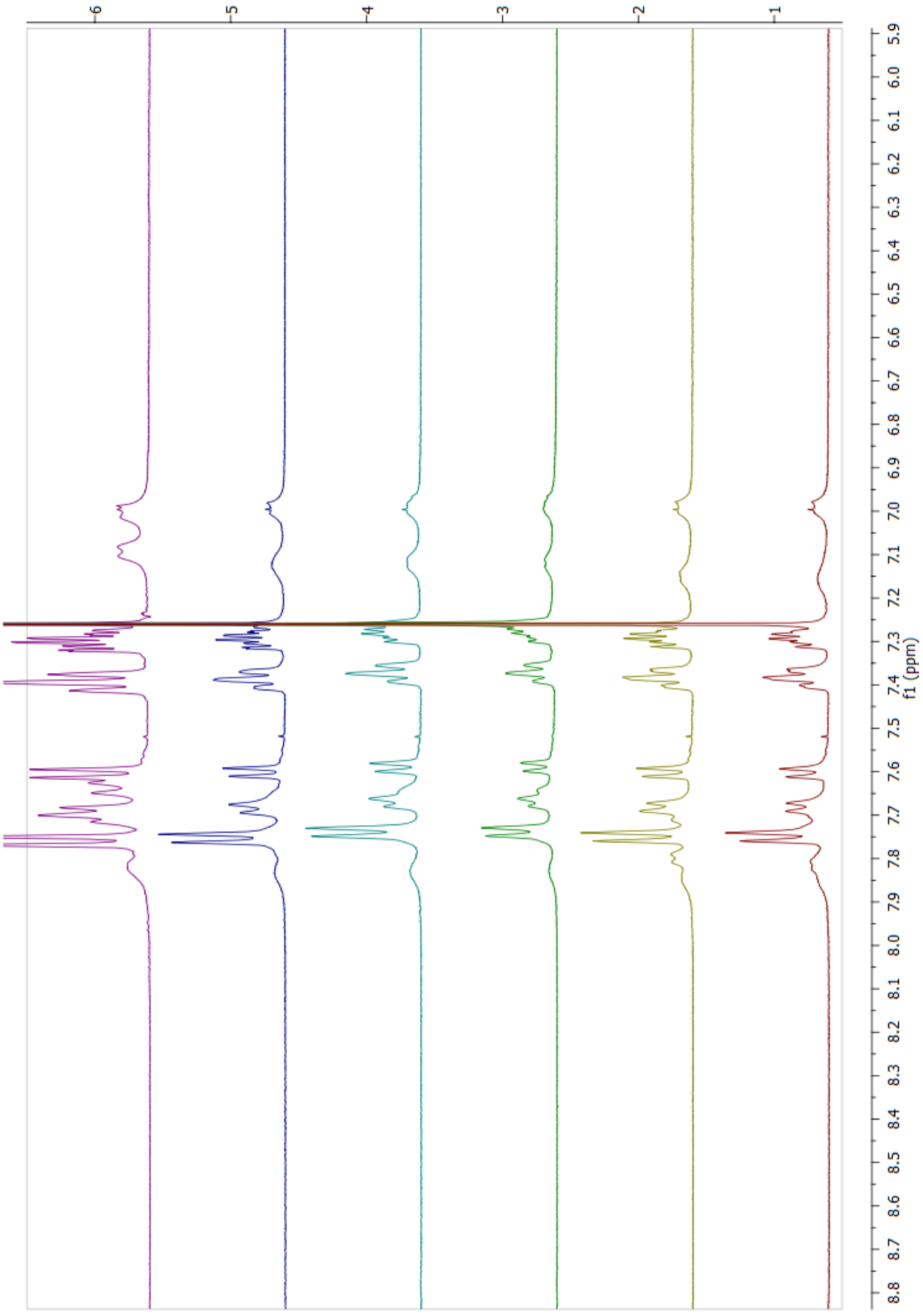

Figure 7.17: ^{1}**H** NMR DMSO titration studies for pentamer **111**. Recorded at rt, with 0.5, 10, 25, 50 and 100 µL d_6-DMSO added to solutions in $CDCl_3$ (400 MHz)

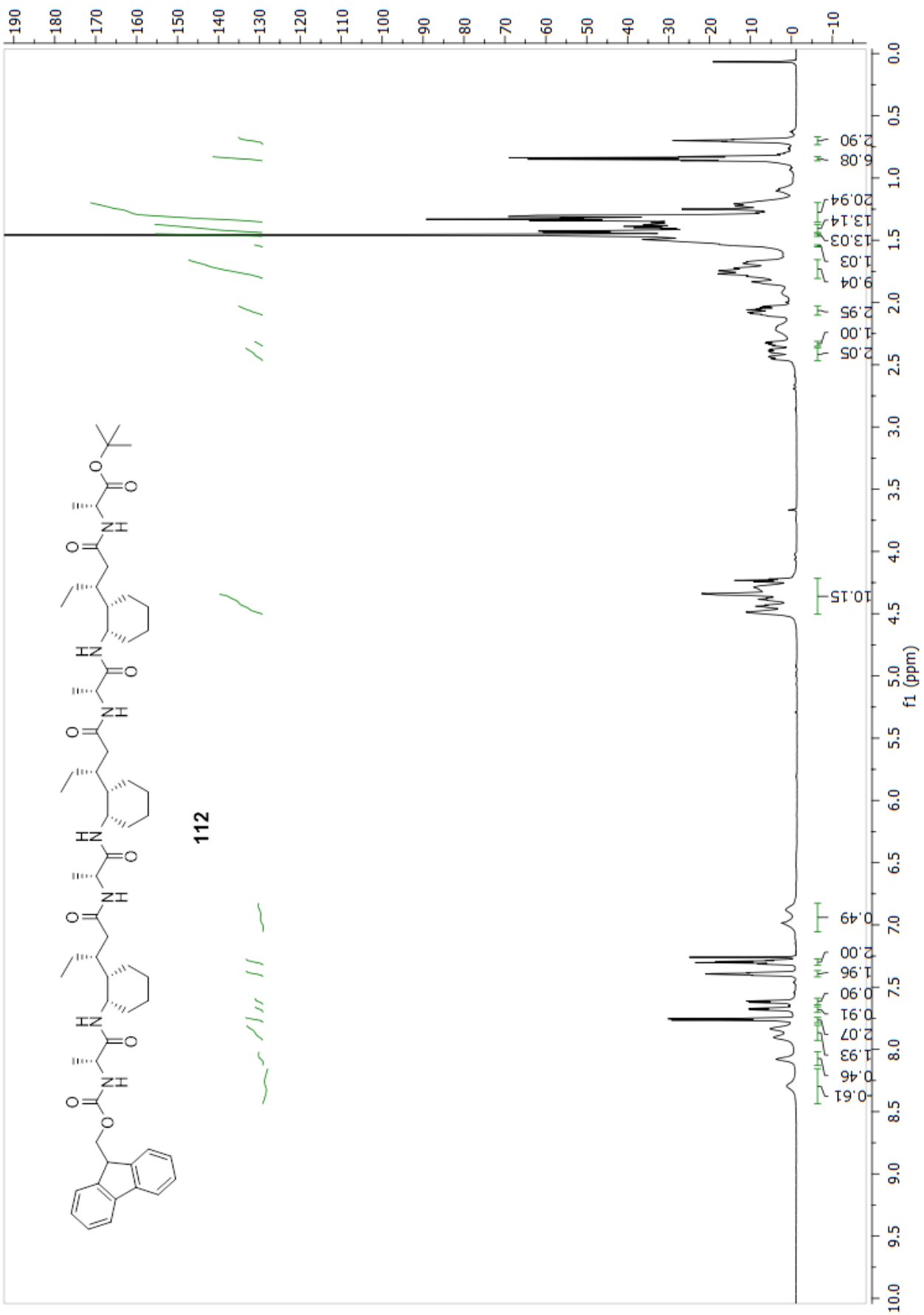
112
f1 (ppm)

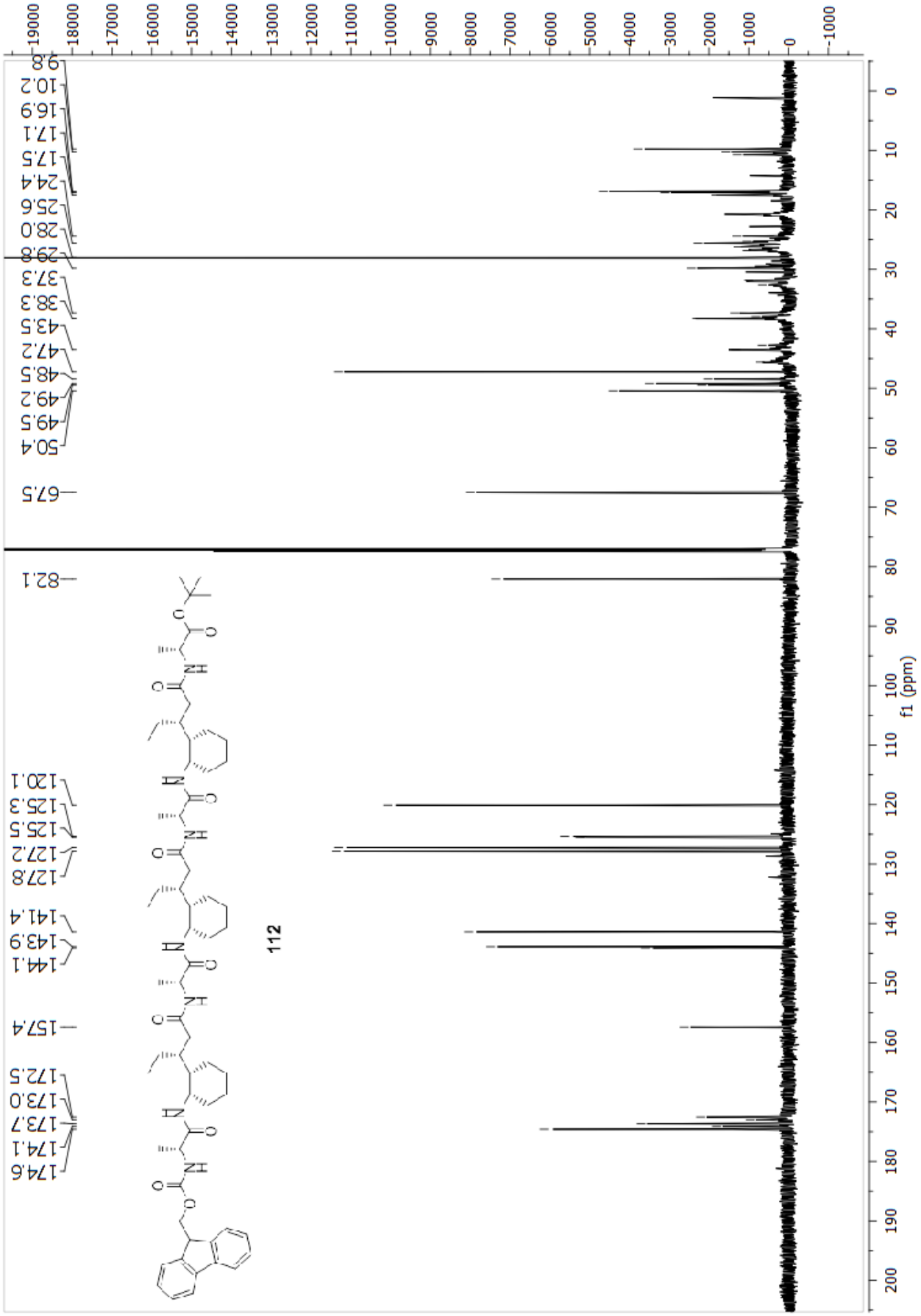
112
f1 (ppm)

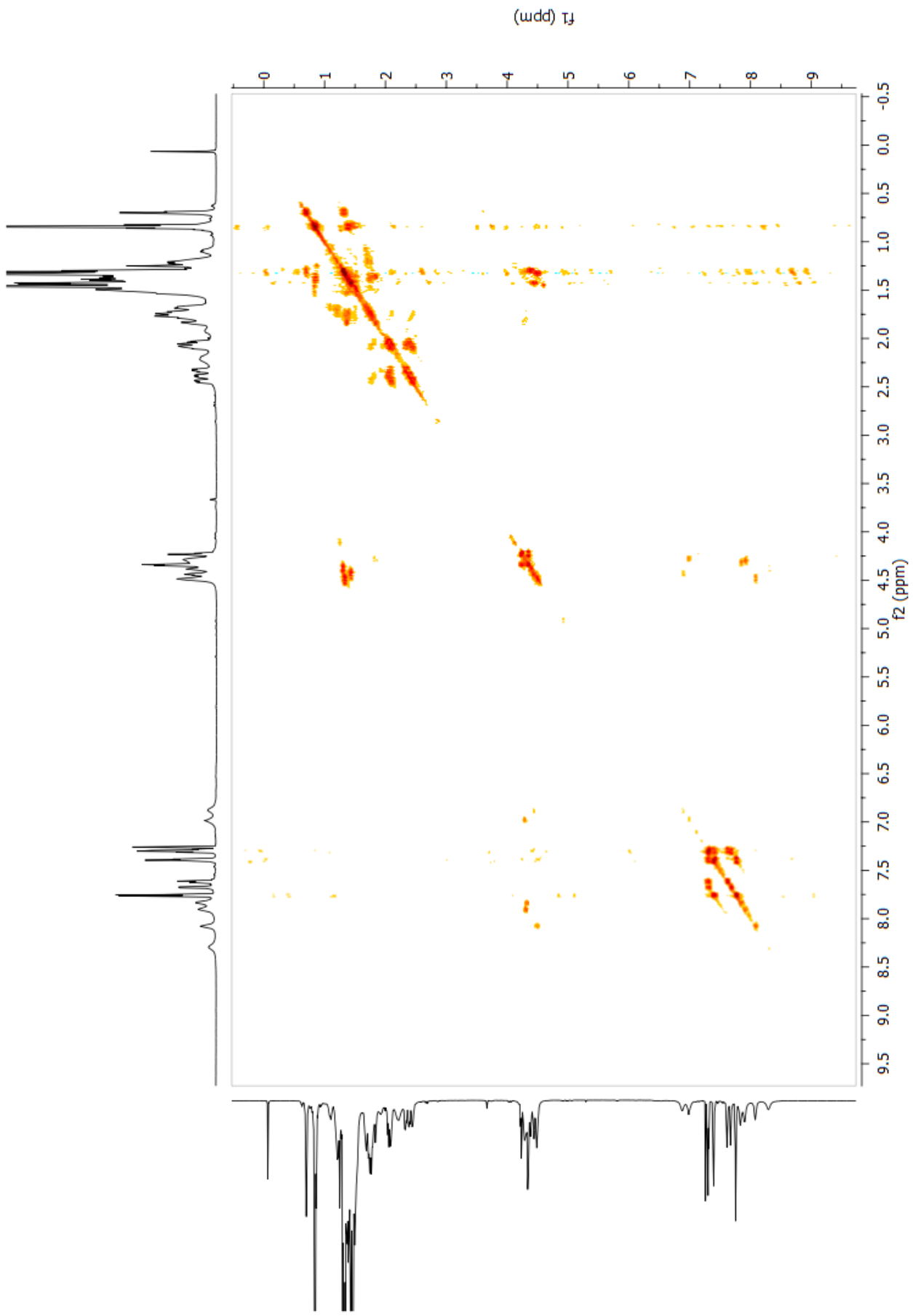

Figure 7.18: COSY NMR spectrum for heptamer **112.** Recorded at rt, in an 8.0 mM solution in $CDCl_3$ (400 MHz)

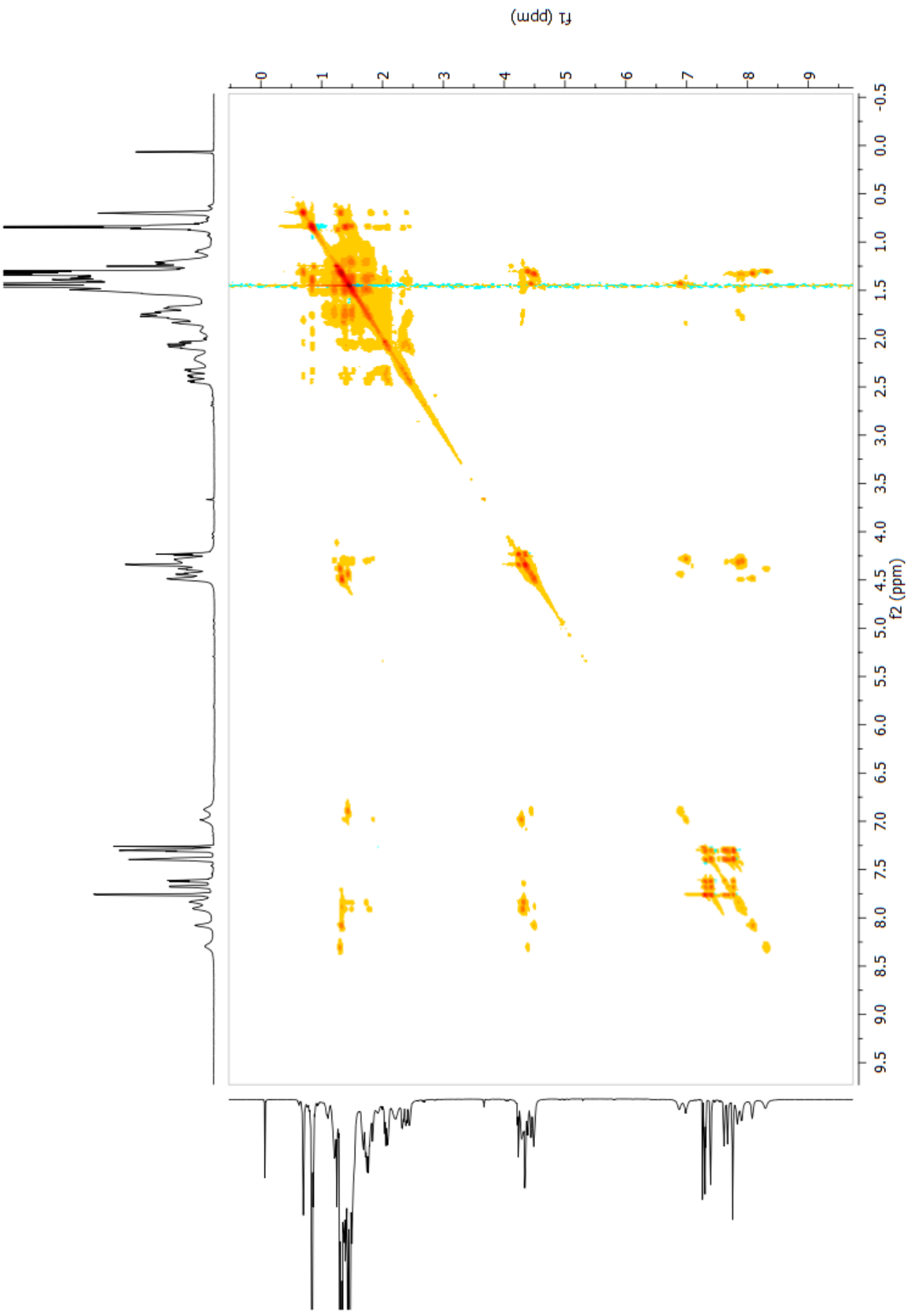

Figure 7.19: TOCSY NMR spectrum for heptamer **112.** Recorded at rt, in an 8.0 mM solution in $CDCl_3$ (400MHz)

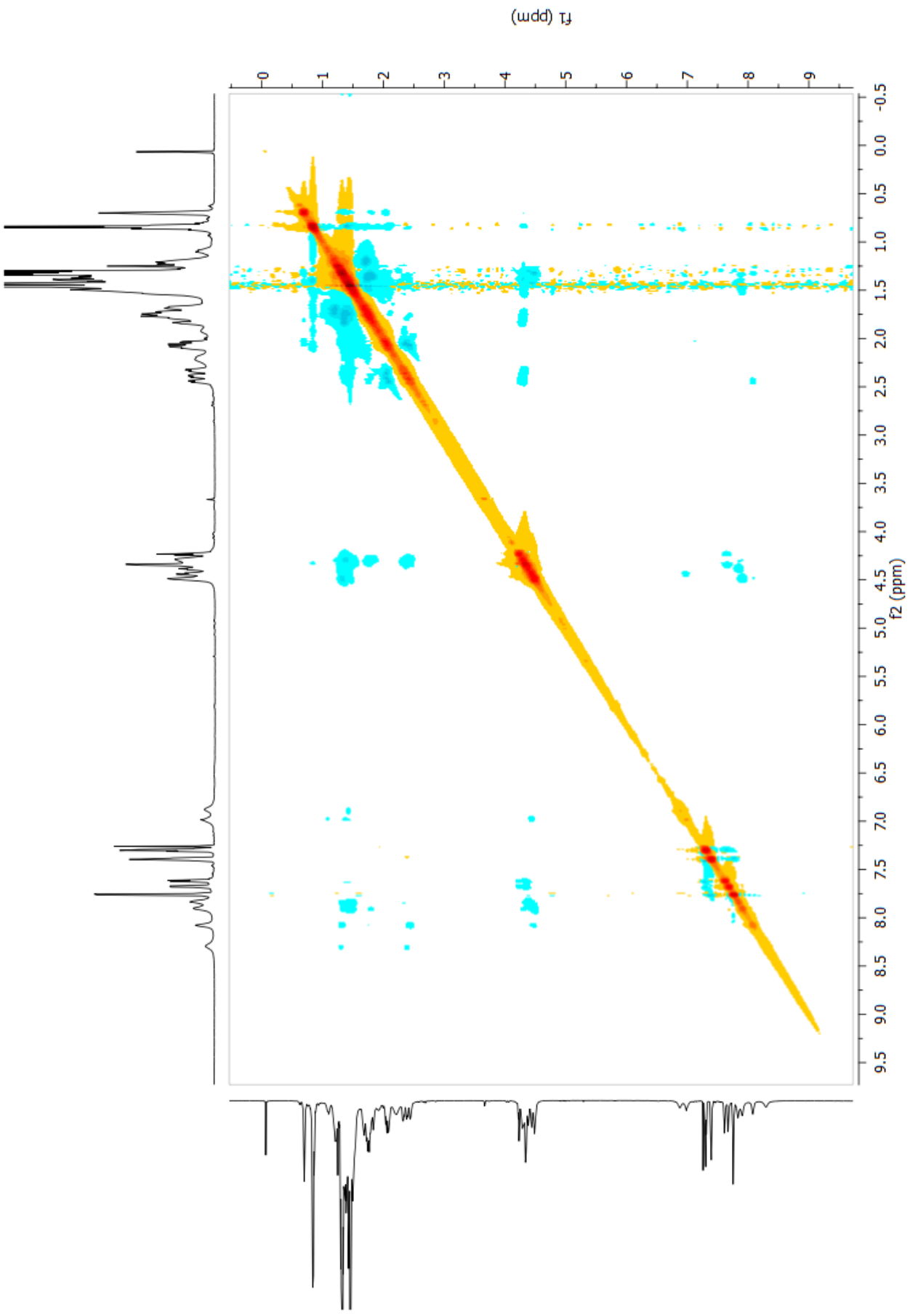

Figure 7.20: ROESY NMR spectrum for heptamer **112.** Recorded at rt, in an 8.0 mM solution in $CDCl_3$ (400MHz)

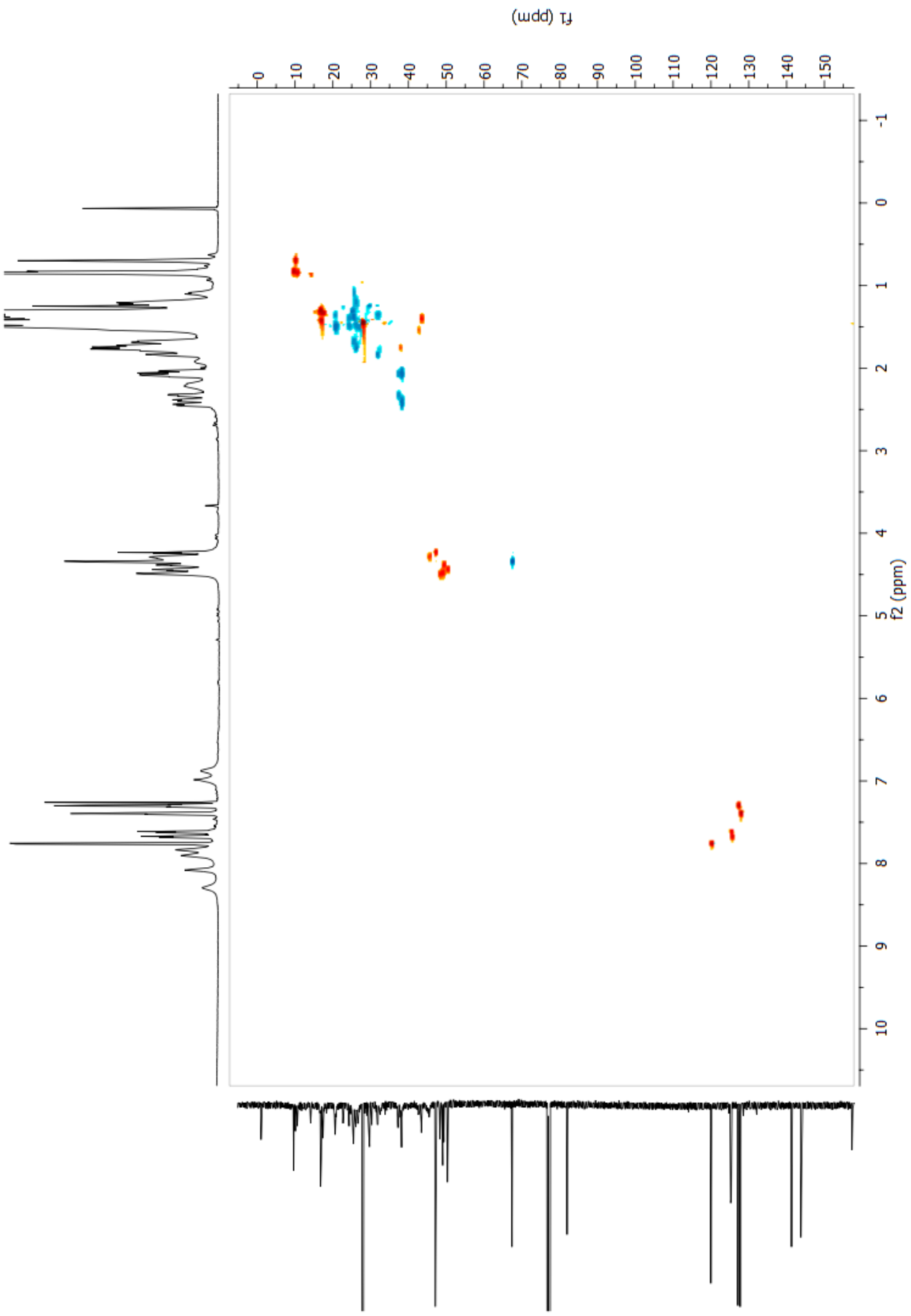

Figure 7.21: HSQC NMR spectrum for heptamer **112.** Recorded at rt, in an 8.0 mM solution in $CDCl_3$ (400 MHz)

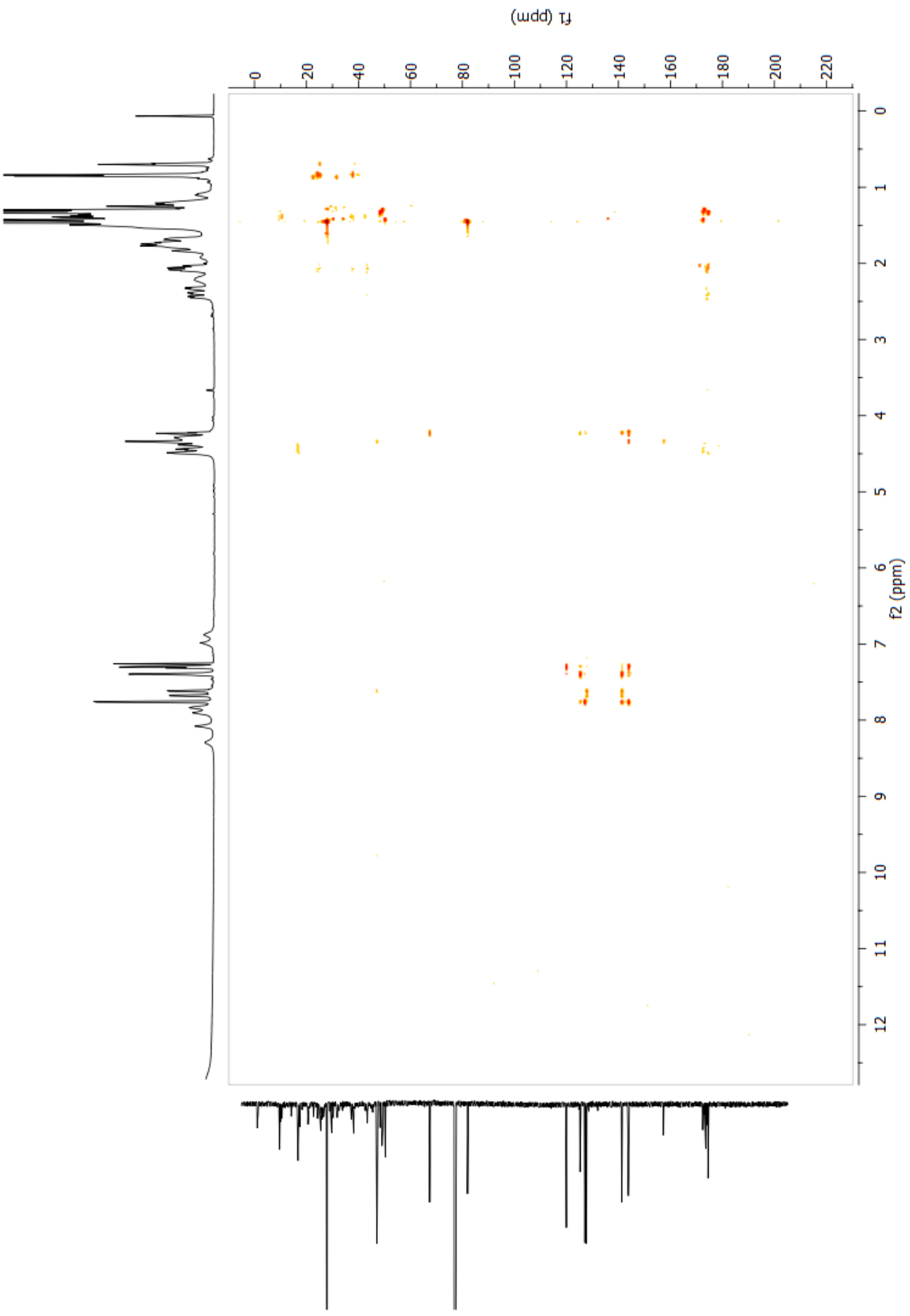

Figure 7.22: HMBC NMR spectrum for heptamer **112.** Recorded at rt, in an 8.0 mM solution in $CDCl_3$ (400MHz)

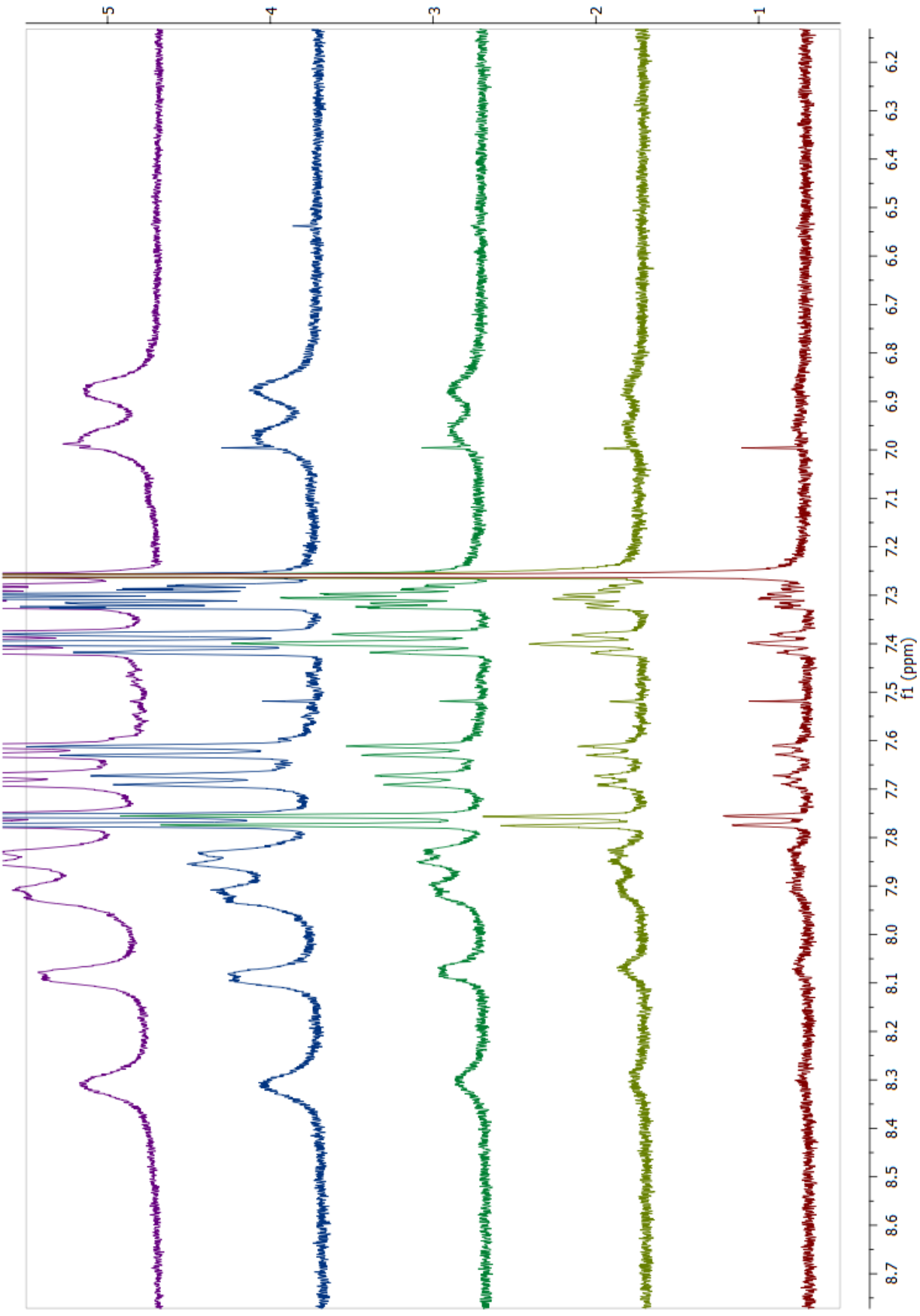

Figure 7.23: ^{1}H NMR Aggregation control studies for heptamer **112**. Recorded at rt, in 16, 8, 4, 2 and 1 mM solutions in $CDCl_3$ (400 MHz)

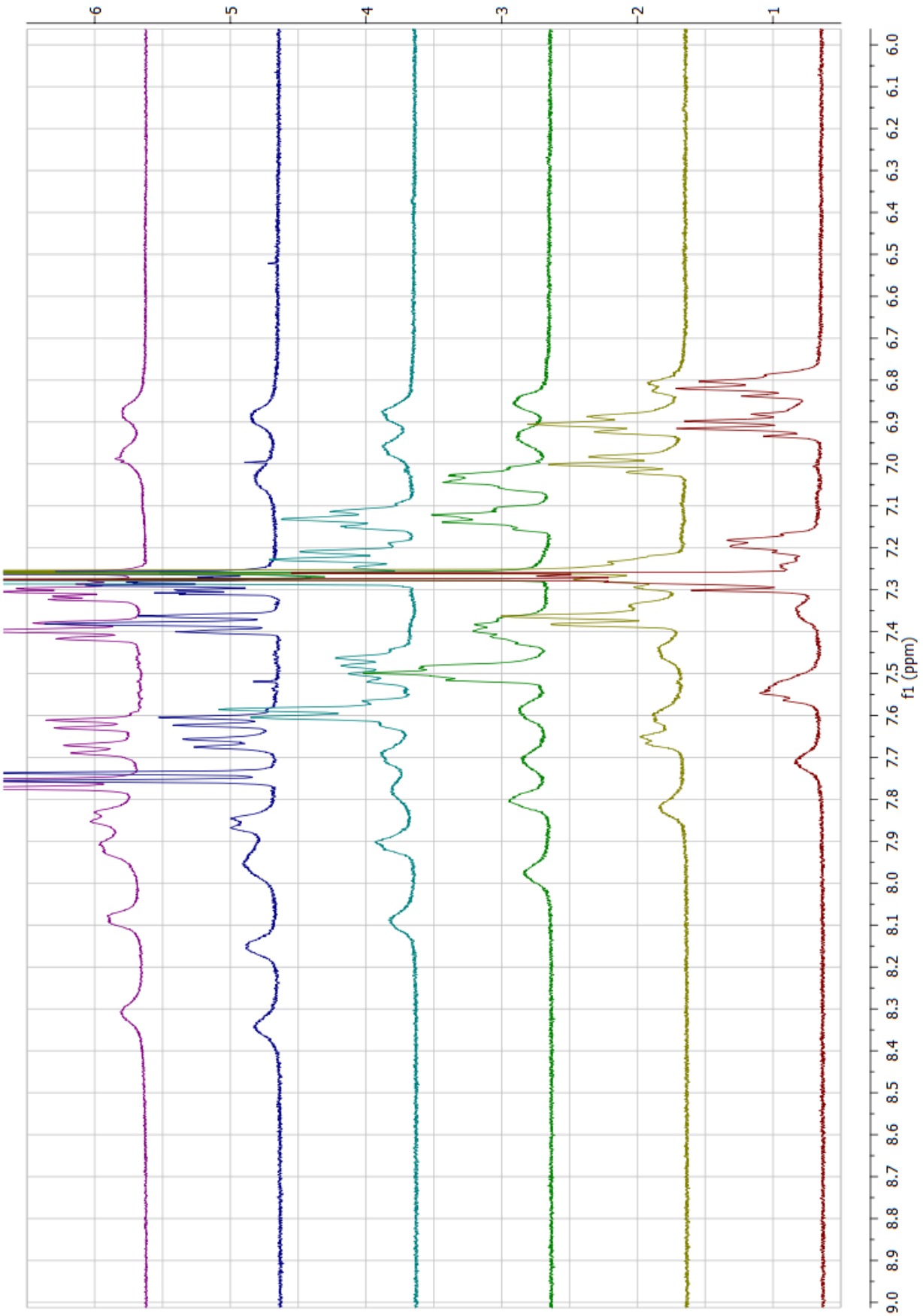

Figure 7.24: ^{1}**H** NMR DMSO titration studies for heptamer **112**. Recorded at rt, with 0.5, 10, 25, 50 and 100 µL d_6- DMSO added to solutions in $CDCl_3$ (400 MHz)

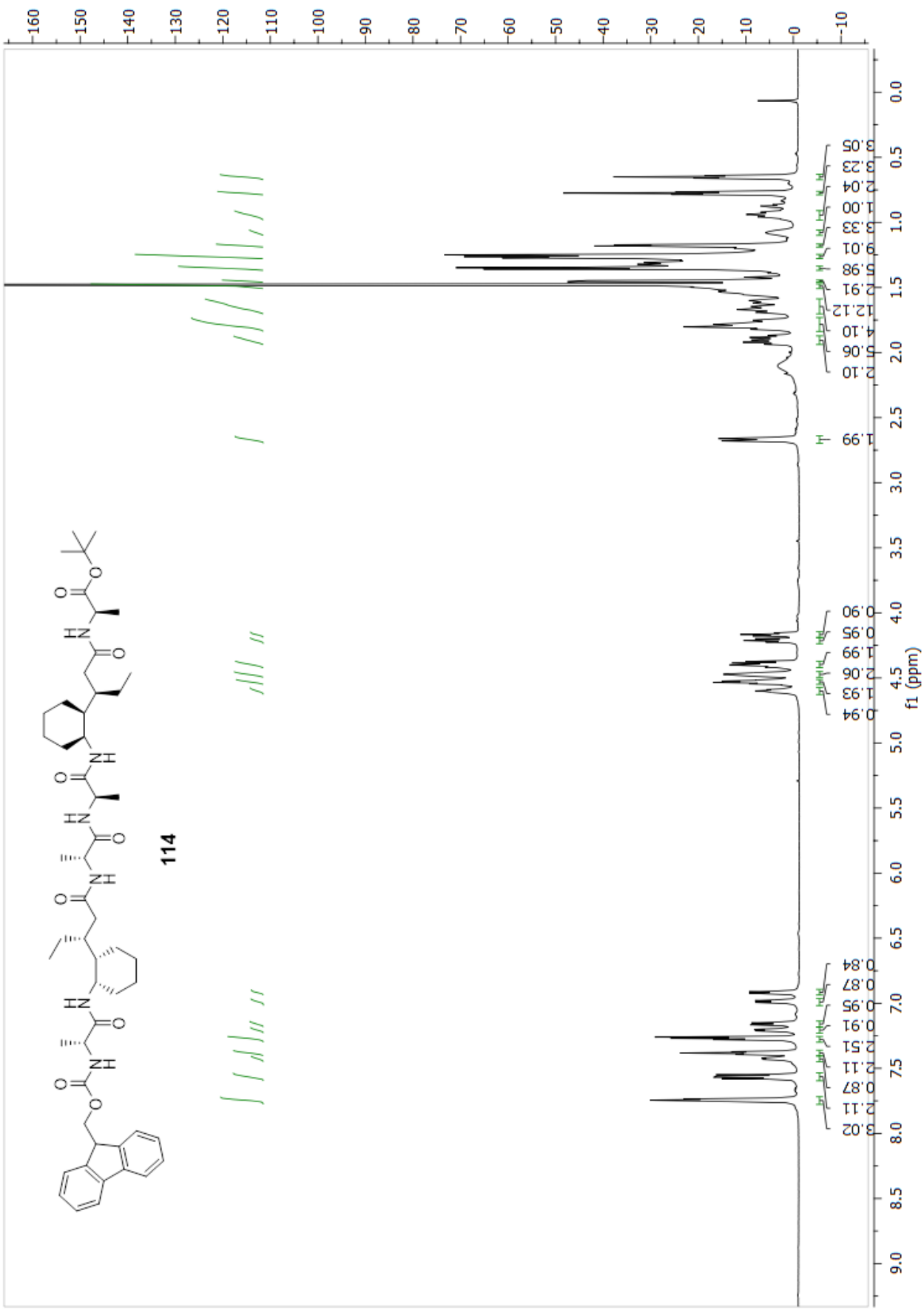
114
f1 (ppm)

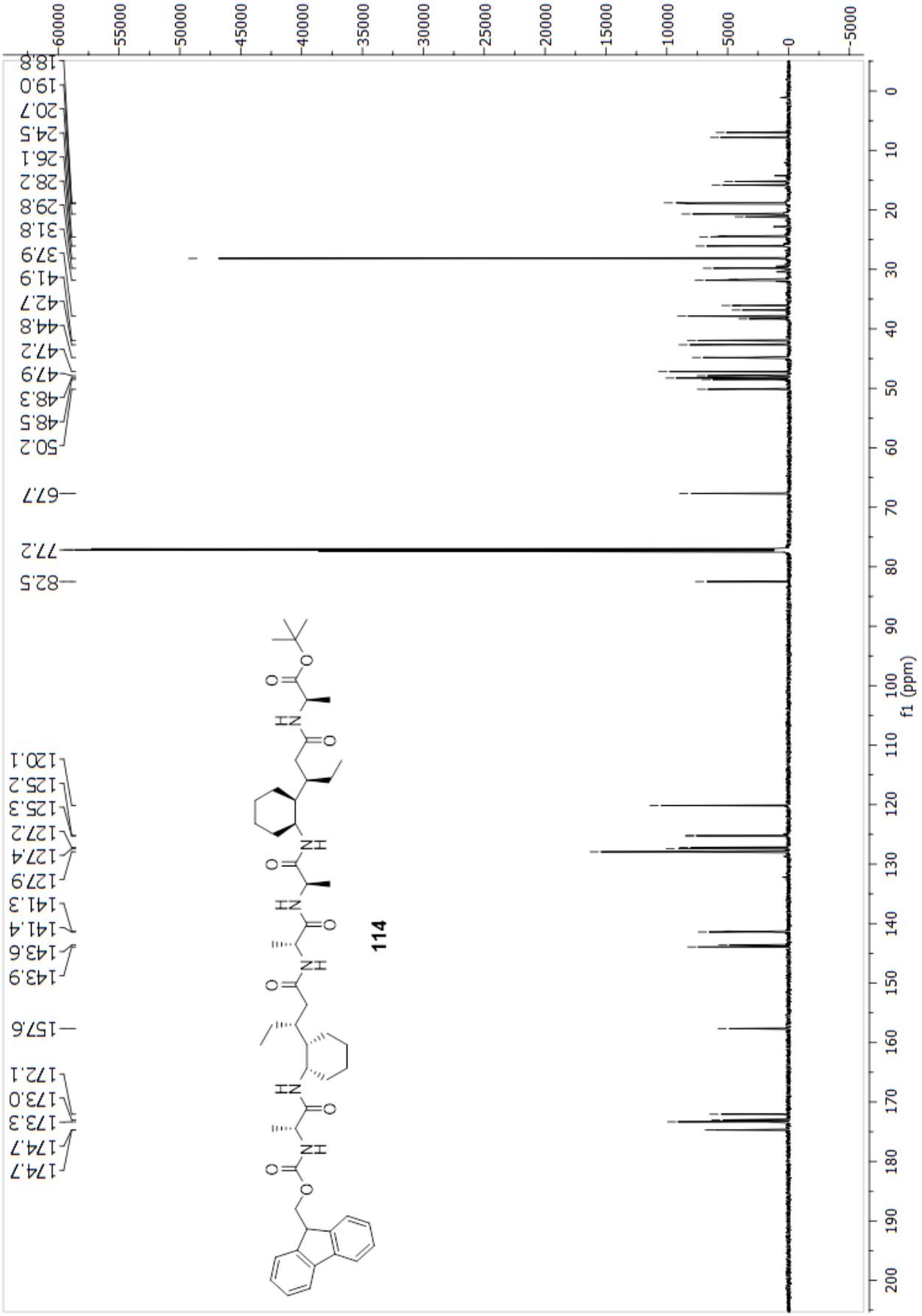
114
f1 (ppm)

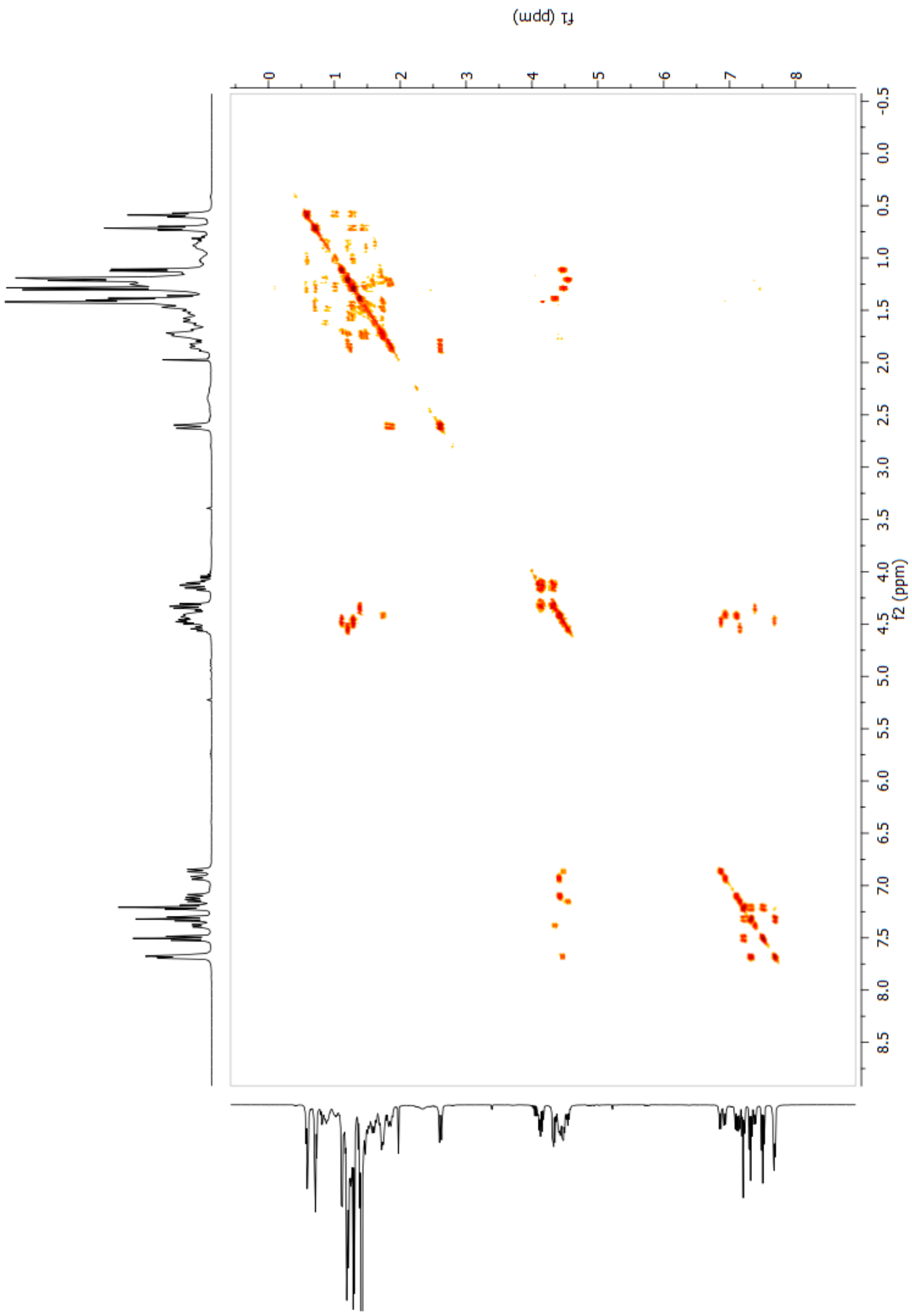

Figure 7.25: COSY NMR spectrum for hexamer **114.** Recorded at rt, in an 8.0 mM solution in $CDCl_3$ (400 MHz)

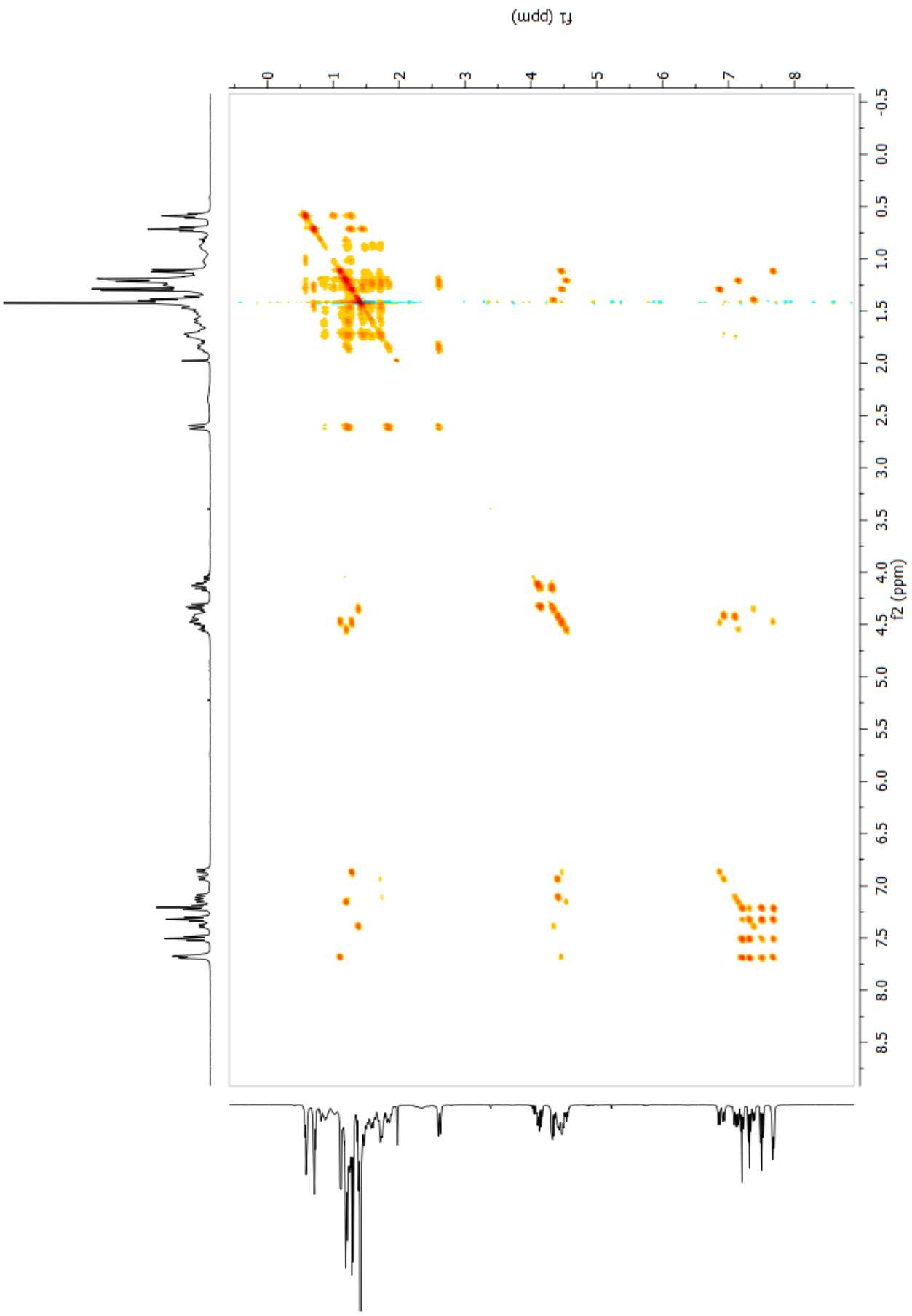

Figure 7.26: TOCSY NMR spectrum for hexamer **114.** Recorded at rt, in an 8.0 mM solution in $CDCl_3$ (400MHz)

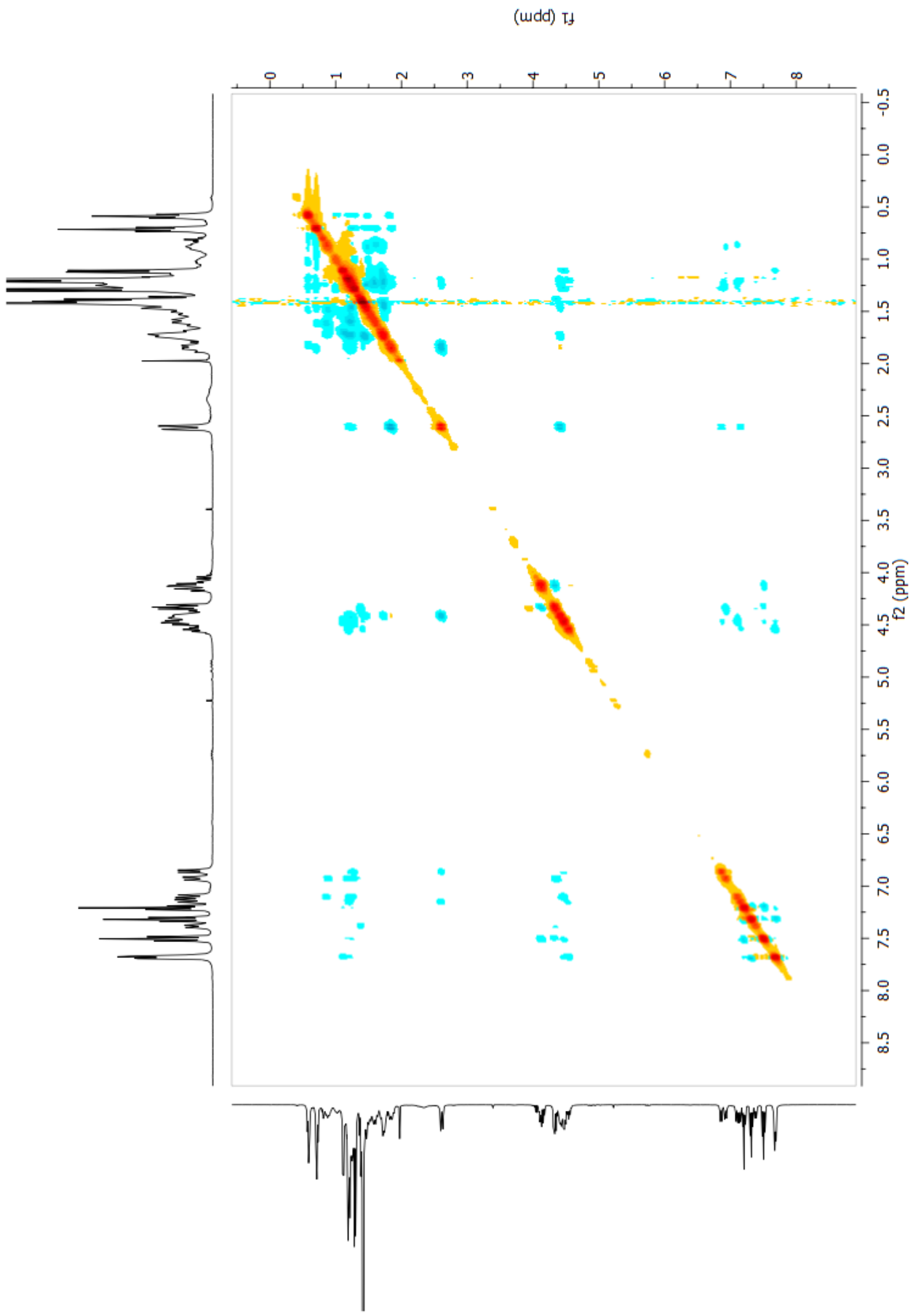

Figure 7.27: ROESY NMR spectrum for hexamer **114.** Recorded at rt, in an 8.0 mM solution in $CDCl_3$ (400MHz)

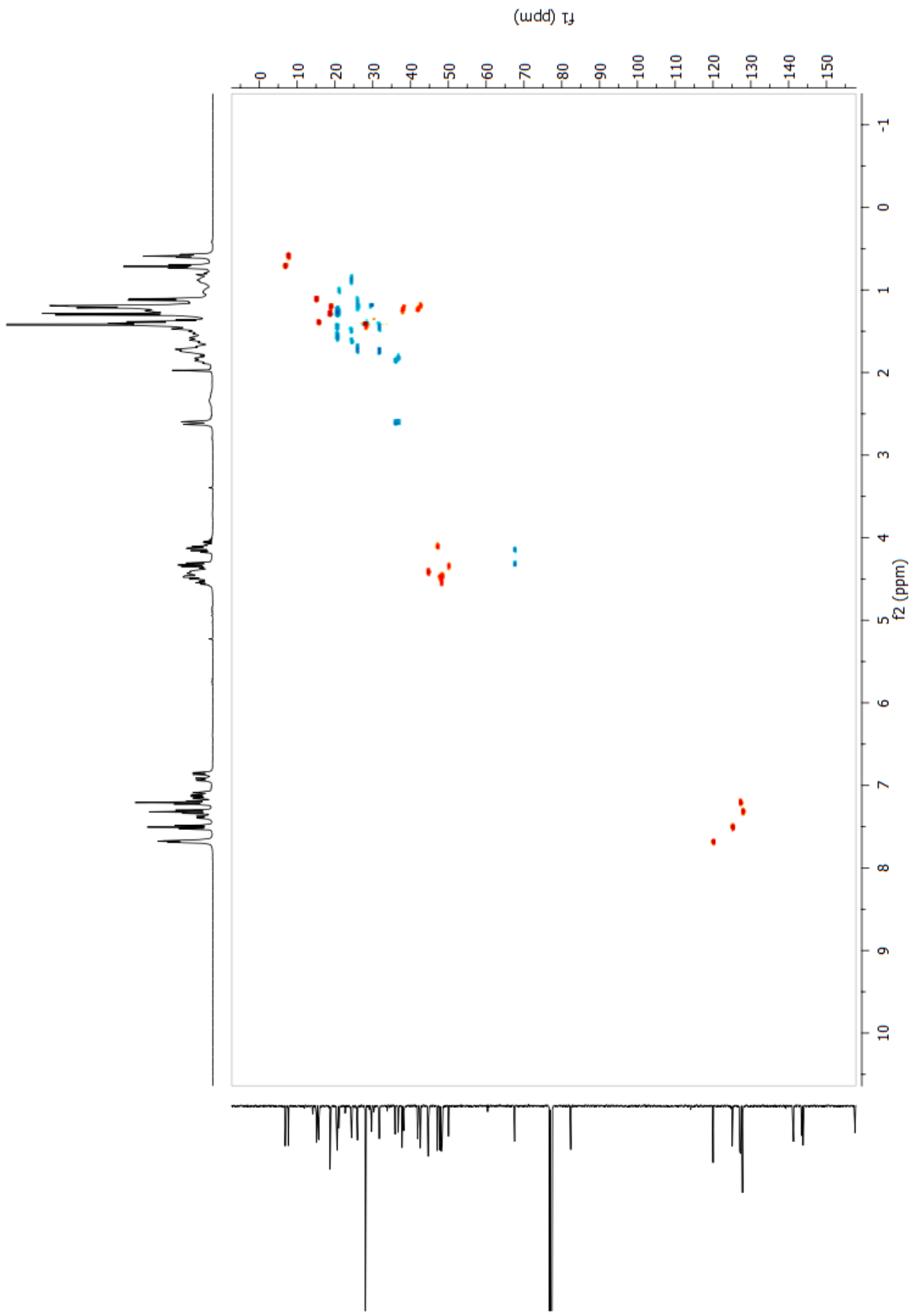

Figure 7.28: HSQC NMR spectrum for hexamer **114.** Recorded at rt, in an 8.0 mM solution in $CDCl_3$ (400 MHz)

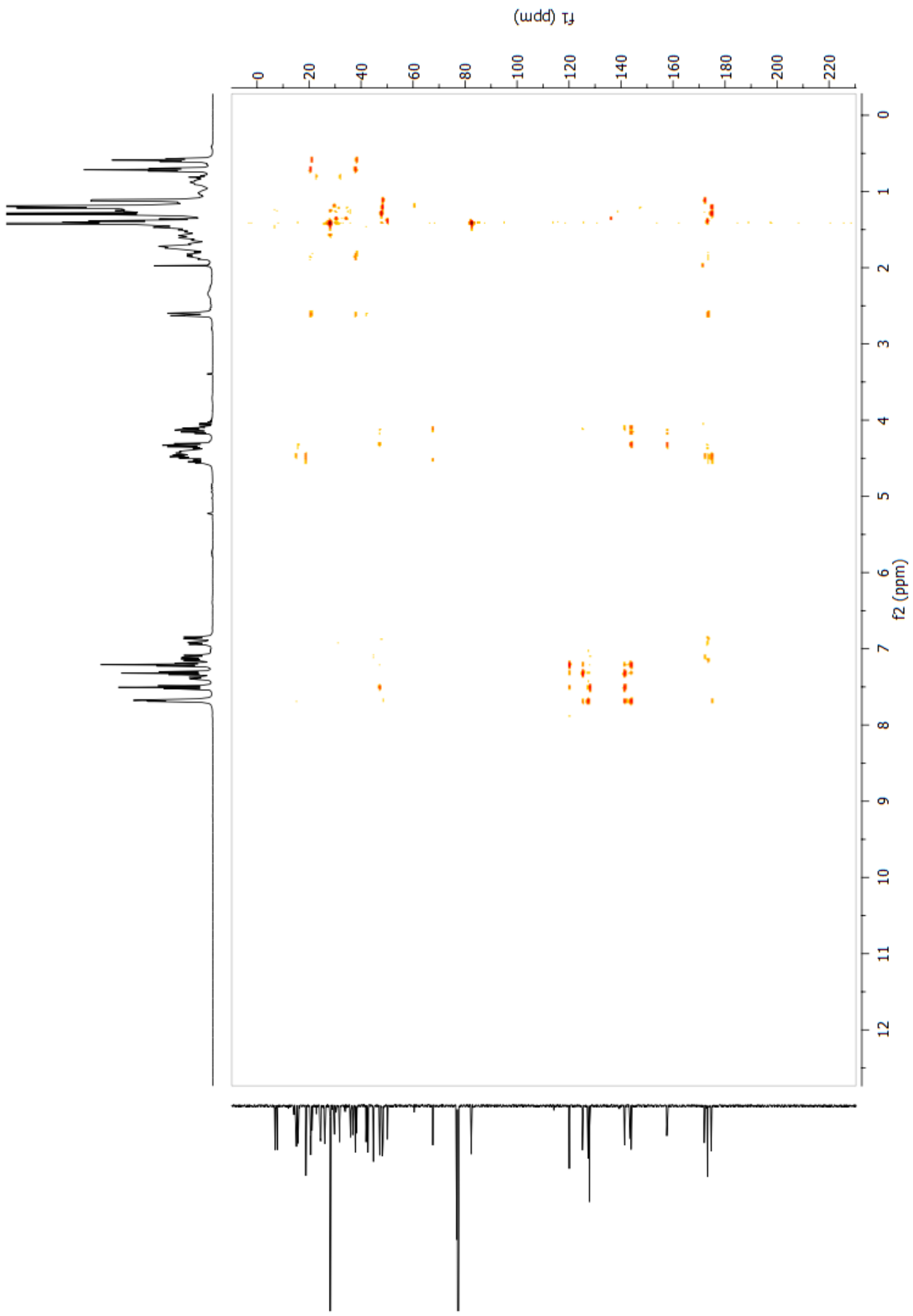

Figure 7.29: HMBC NMR spectrum for hexamer **114.** Recorded at rt, in an 8.0 mM solution in $CDCl_3$ (400MHz)

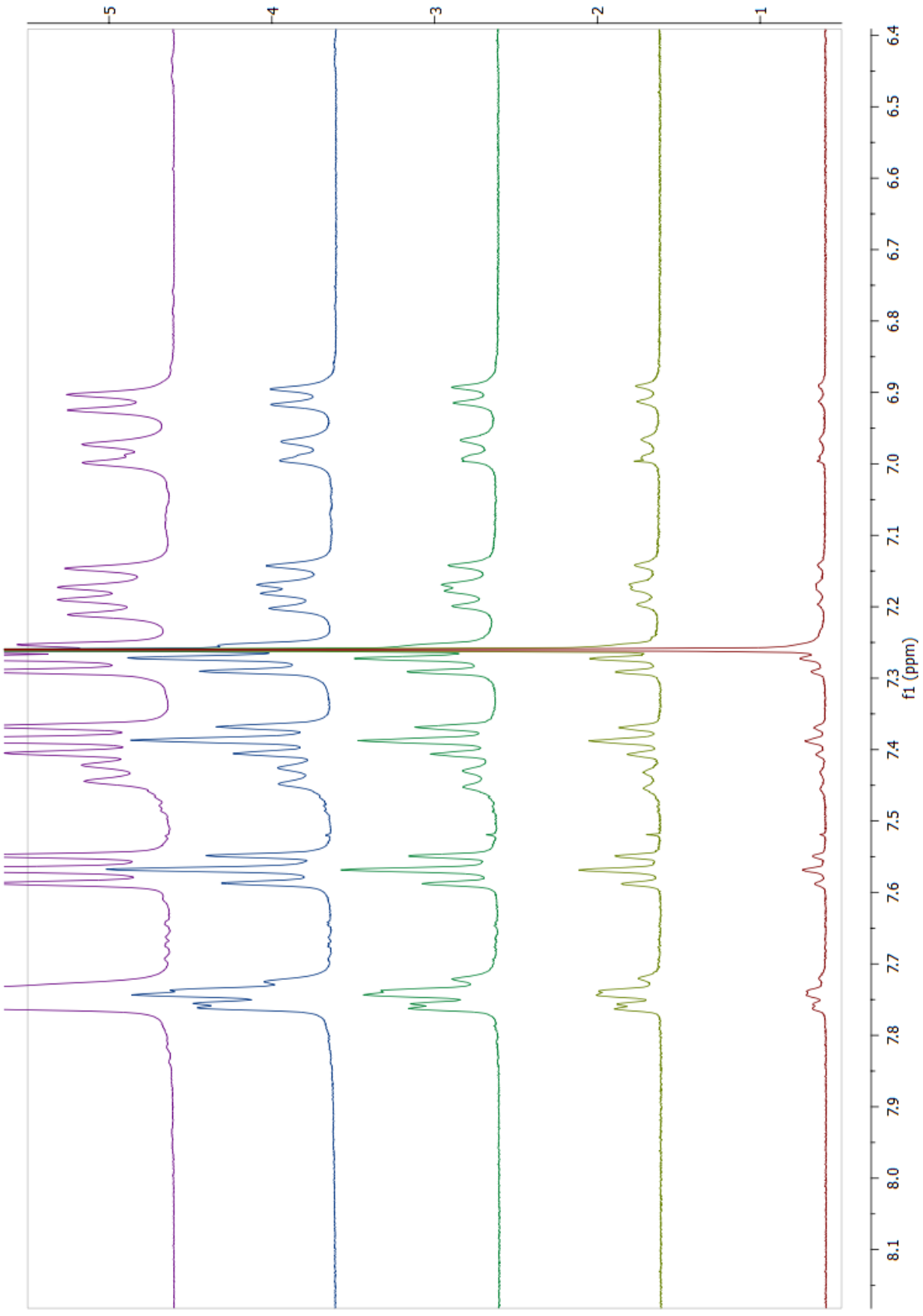

Figure 7.30: ^{1}H NMR Aggregation control studies for hexamer **114**. Recorded at rt, in 16, 8, 4, 2 and 1 mM solutions in $CDCl_3$ (400 MHz)

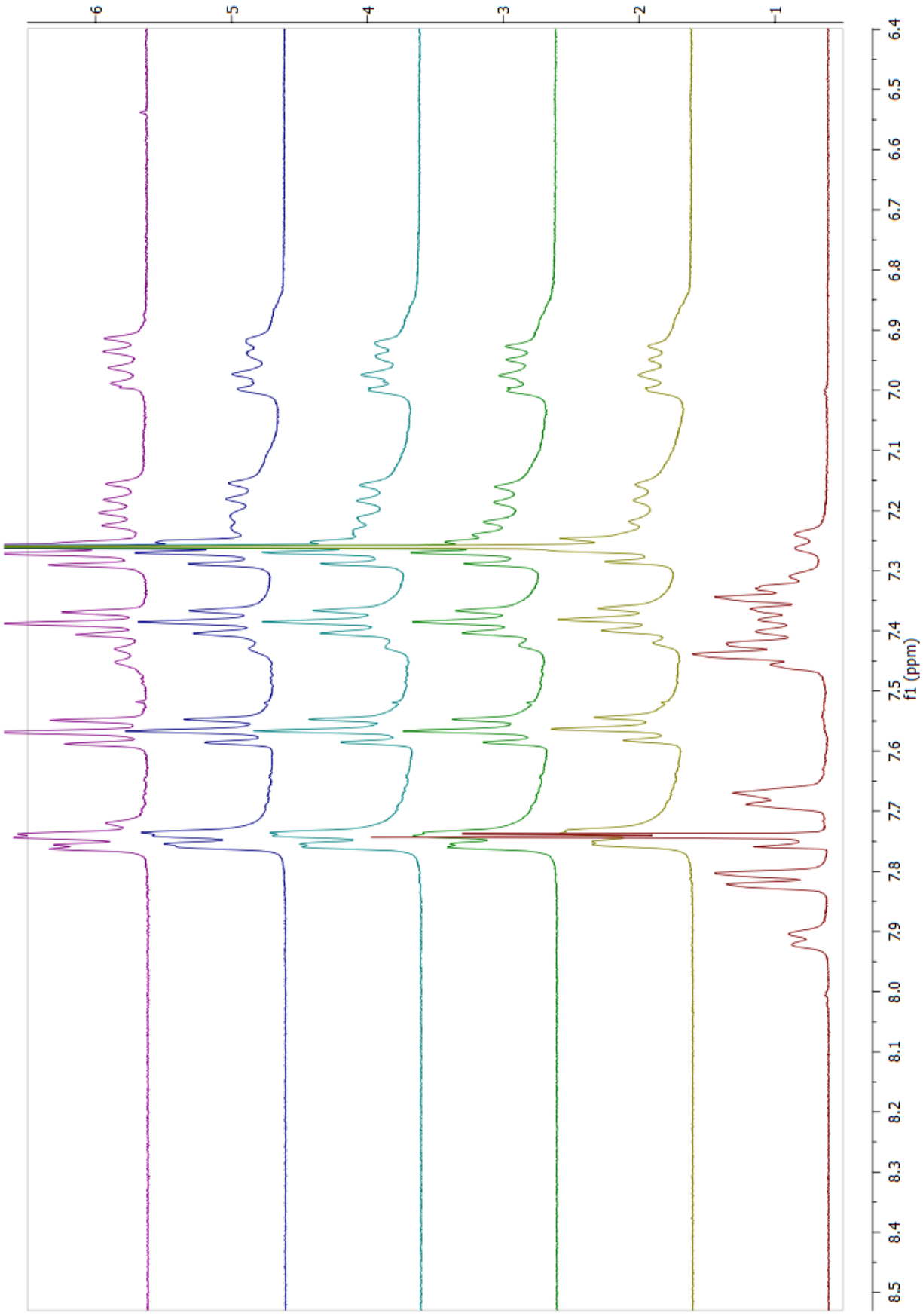

Figure 7.31: ^{1}H NMR DMSO titration studies for hexamer **114**. Recorded at rt, with 0.5, 10, 25, 50 and 100 µL d_6- DMSO added to solutions in $CDCl_3$ (400 MHz)

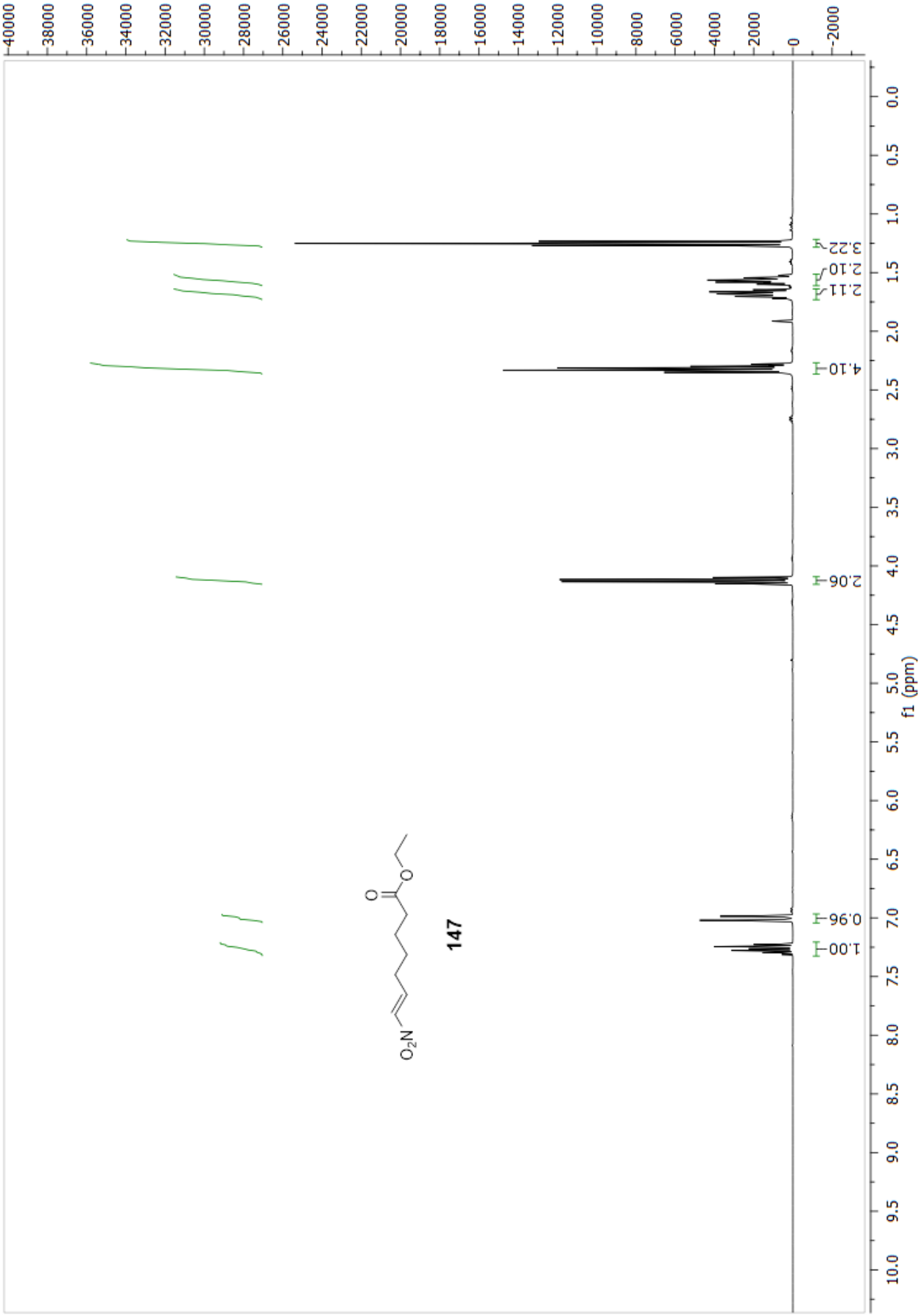
147
3.22
2.10
2.11
4.10
2.06
0.96
1.00
f1 (ppm)

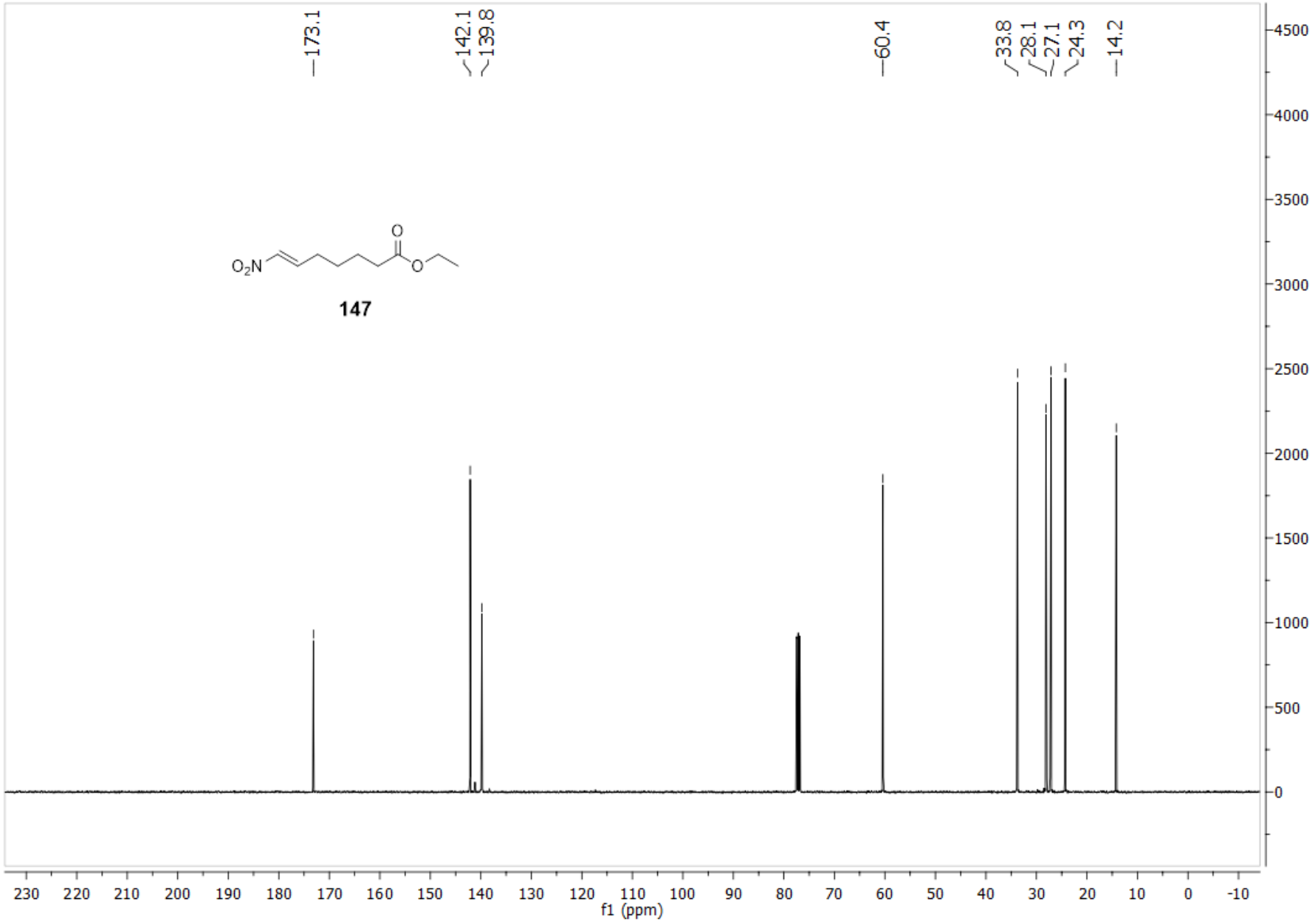
173.1
142.1
139.8
60.4
33.8
28.1
27.1
24.3
14.2
O
O2N
O
147
4500
4000
3500
3000
2500
2000
1500
1000
500
0
230 220 210 200 190 180 170 160 150 140 130 120 110 100 90 80 70 60 50 40 30 20 10 0 -10
f1 (ppm)

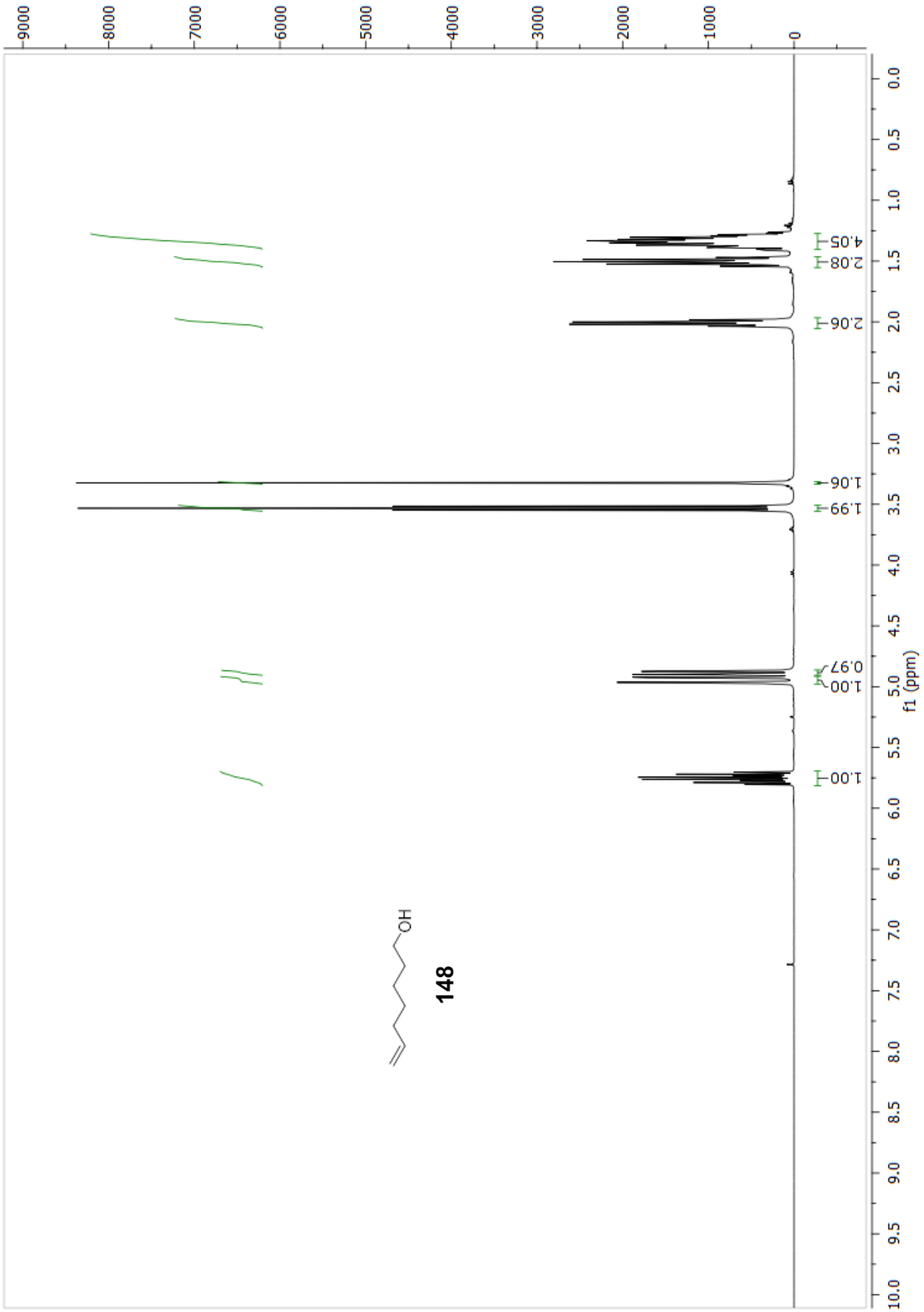
OH
148
4.05
2.08
2.06
1.06
1.99
1.00
0.97
1.00
f1 (ppm)

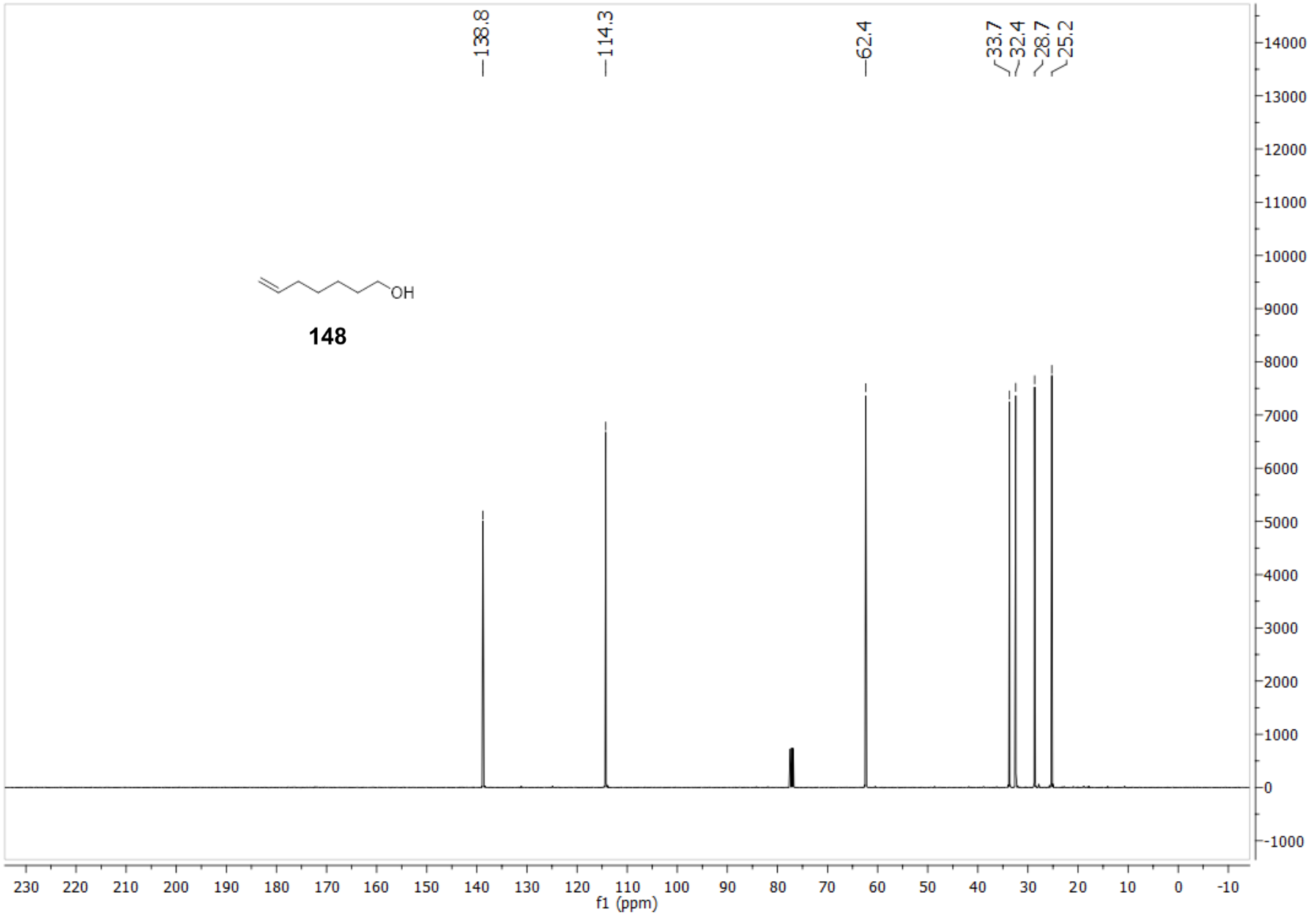
138.8
114.3
62.4
33.7
32.4
28.7
25.2
OH
148
14000
13000
12000
11000
10000
9000
8000
7000
6000
5000
4000
3000
2000
1000
0
-1000
230 220 210 200 190 180 170 160 150 140 130 120 110 100 90 80 70 60 50 40 30 20 10 0 -10
f1 (ppm)

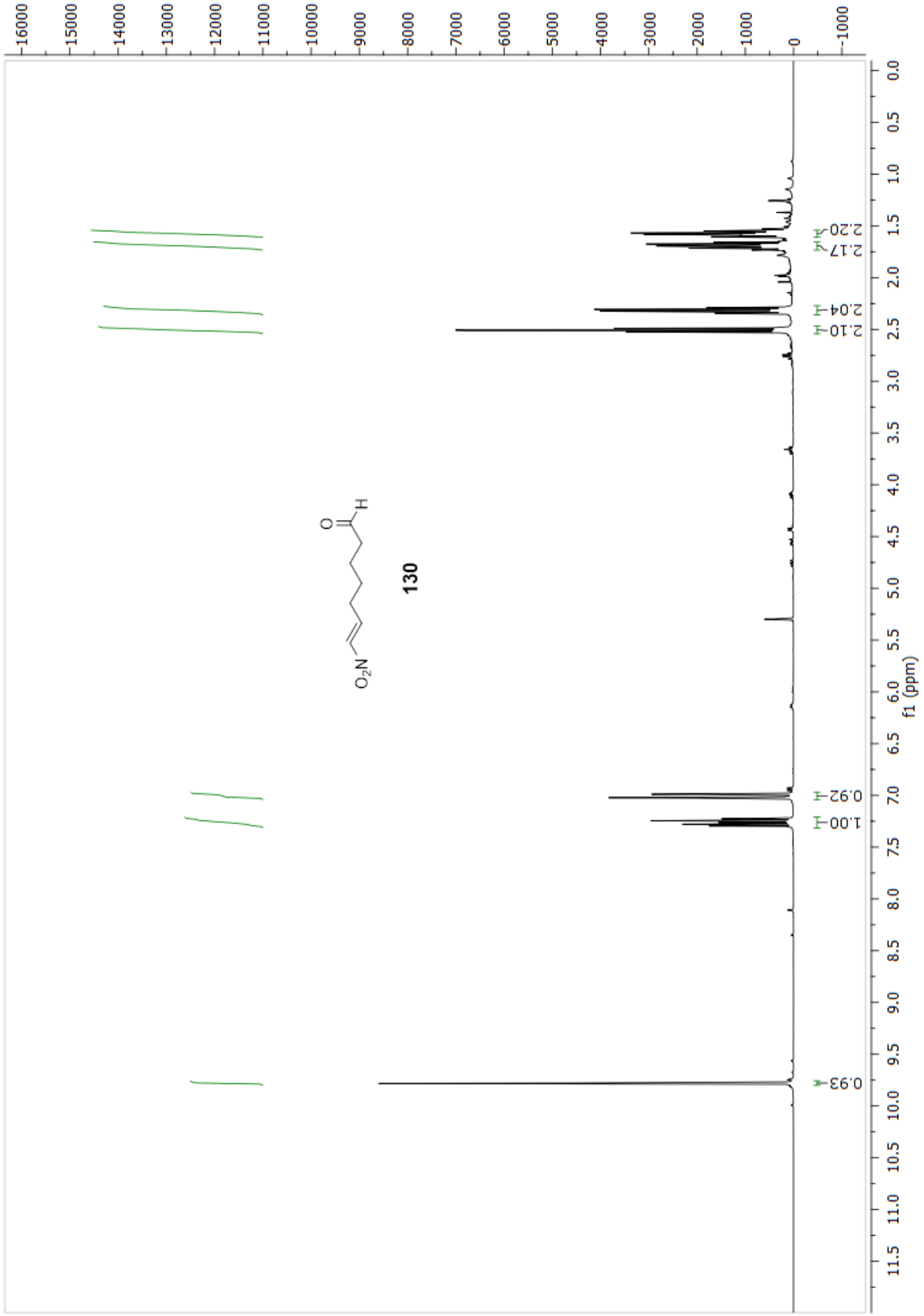
130
O
H
O2N
0.93
1.00
0.92
2.10
2.04
2.17
2.20
f1 (ppm)

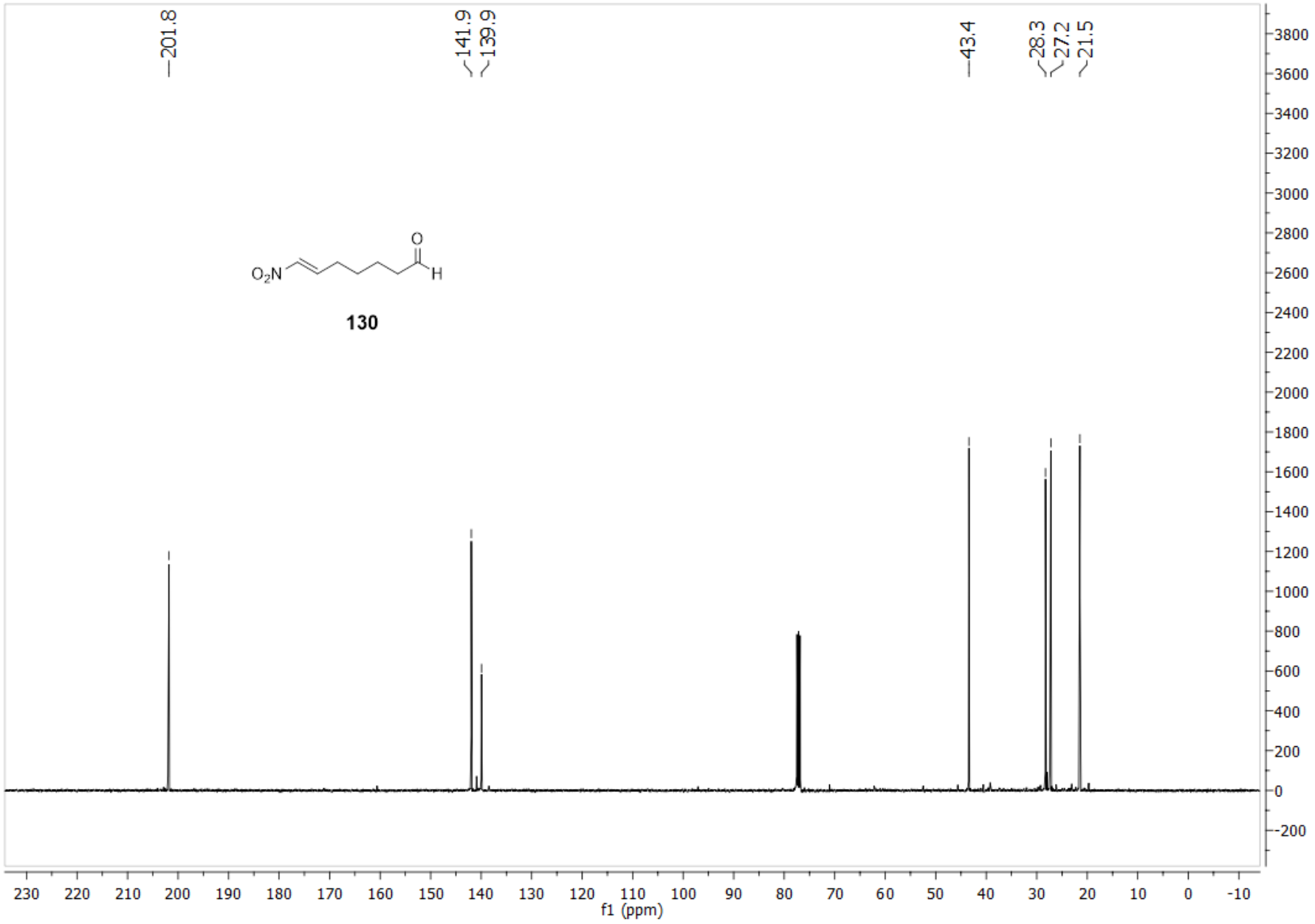
201.8
141.9
139.9
43.4
28.3
27.2
21.5
O
O2N
H
130
f1 (ppm)

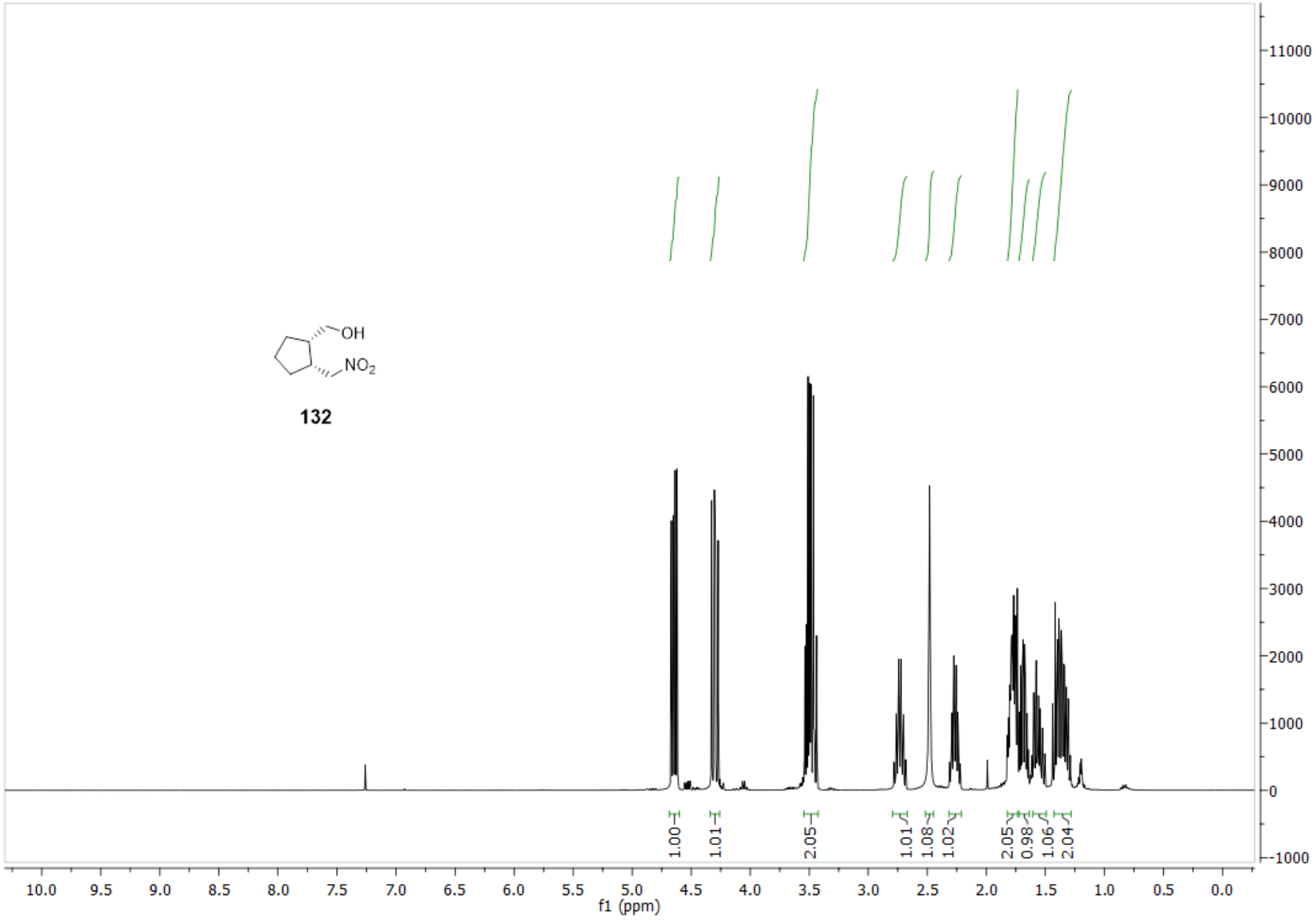
OH
NO2
132
1.00
1.01
2.05
1.01
1.08
1.02
2.05
0.98
1.06
2.04
f1 (ppm)

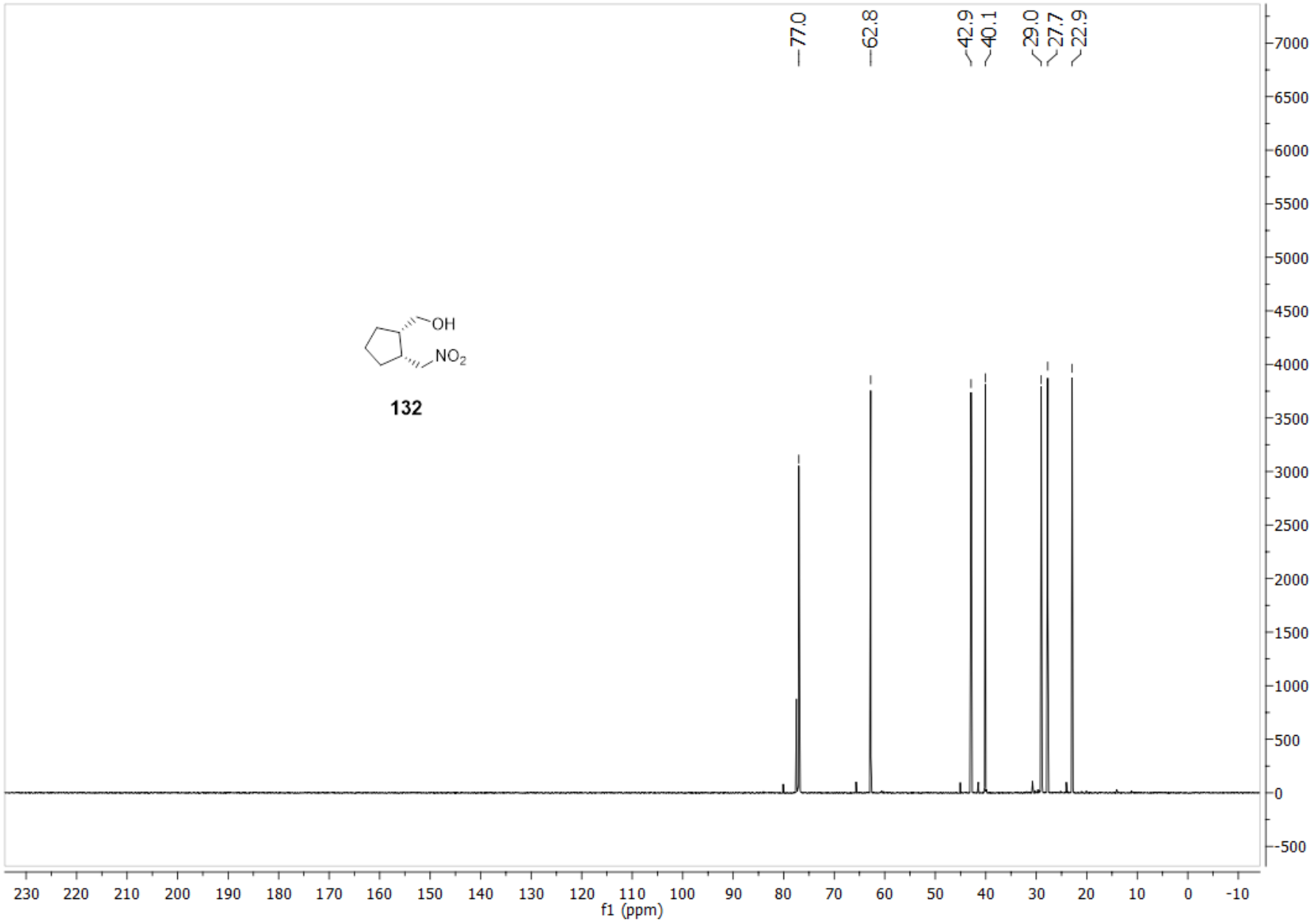
77.0
62.8
42.9
40.1
29.0
27.7
22.9
OH
NO2
132
f1 (ppm)

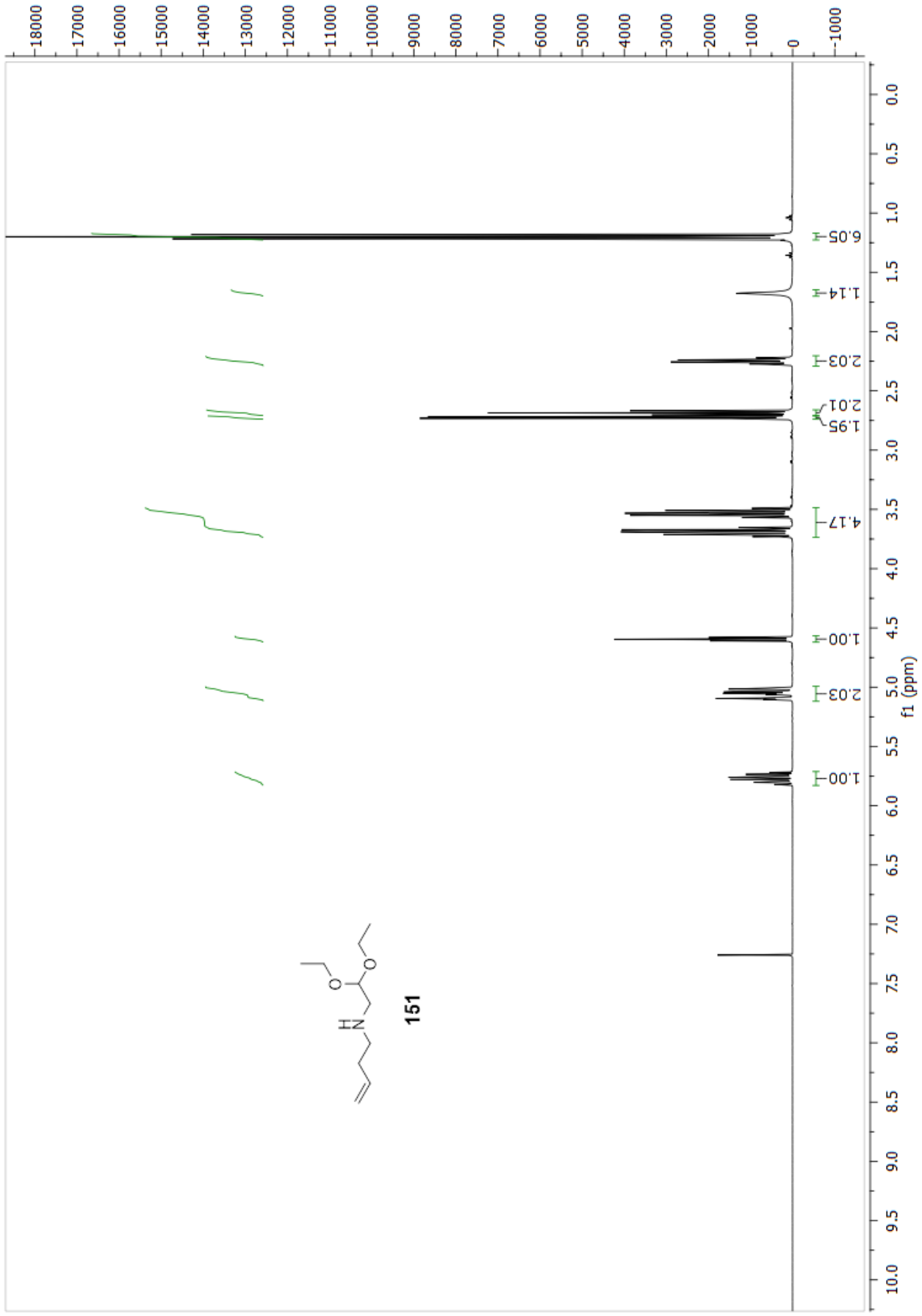
151
6.05
1.14
2.03
1.95
2.01
4.17
1.00
2.03
1.00
f1 (ppm)

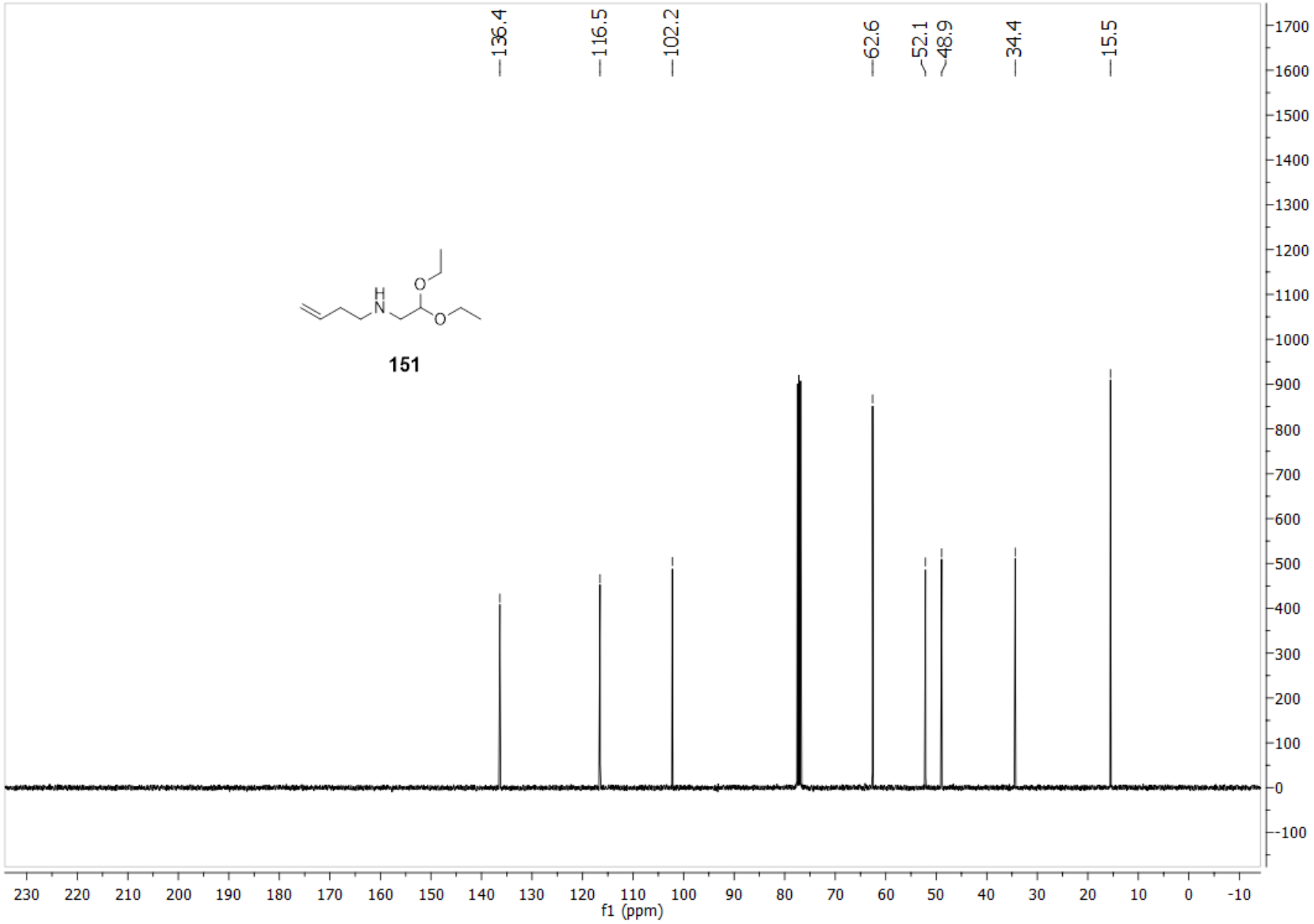
136.4
116.5
102.2
62.6
52.1
48.9
34.4
15.5
151
f1 (ppm)

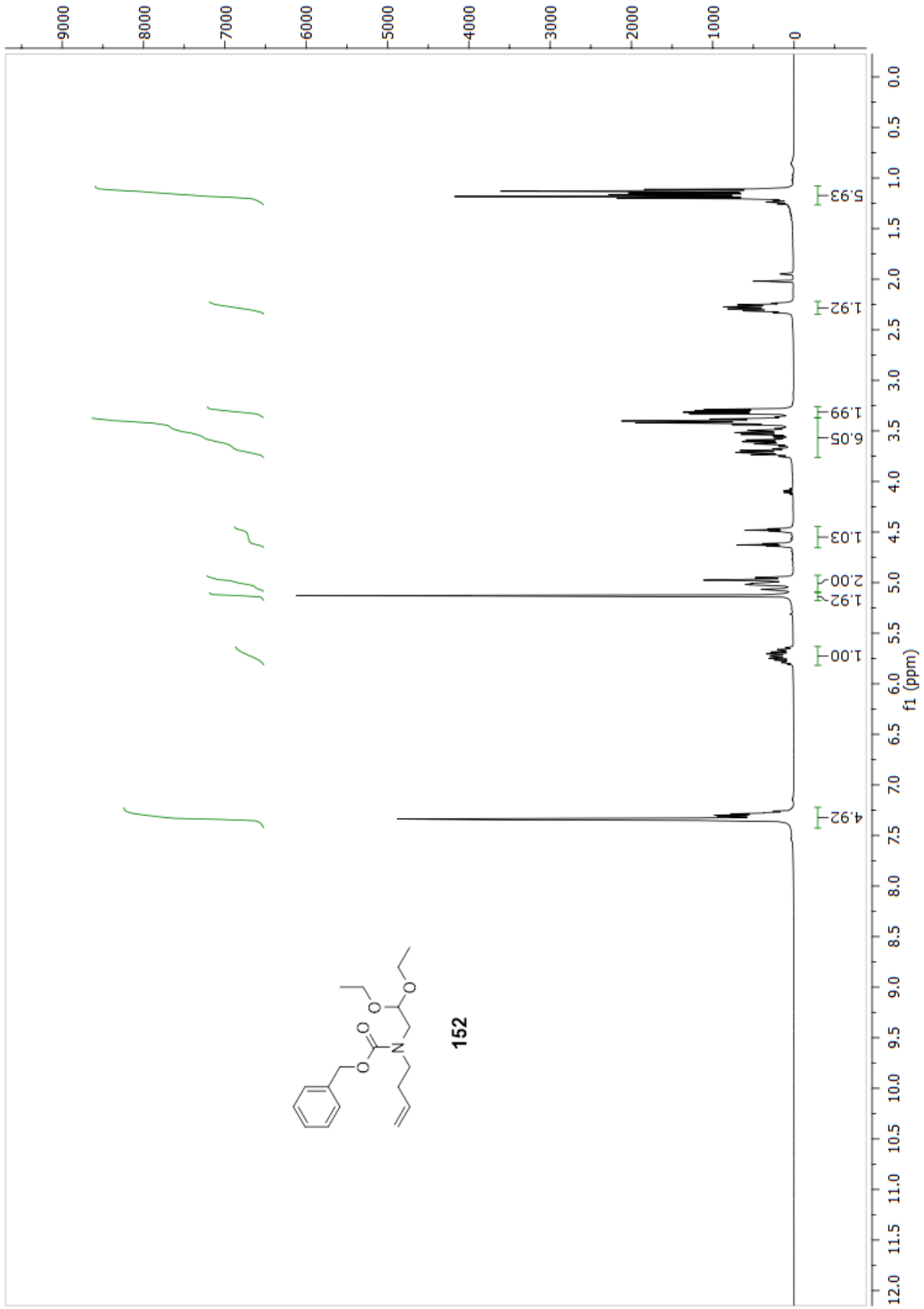
9000
8000
7000
6000
5000
4000
3000
2000
1000
0
0.0
0.5
1.0
1.5
2.0
2.5
3.0
3.5
4.0
4.5
5.0
5.5
6.0
6.5
7.0
7.5
8.0
8.5
9.0
9.5
10.0
10.5
11.0
11.5
12.0
f1 (ppm)
5.93
1.92
1.99
6.05
1.03
1.92
2.00
1.00
4.92
O
O
O
O
N
O

152

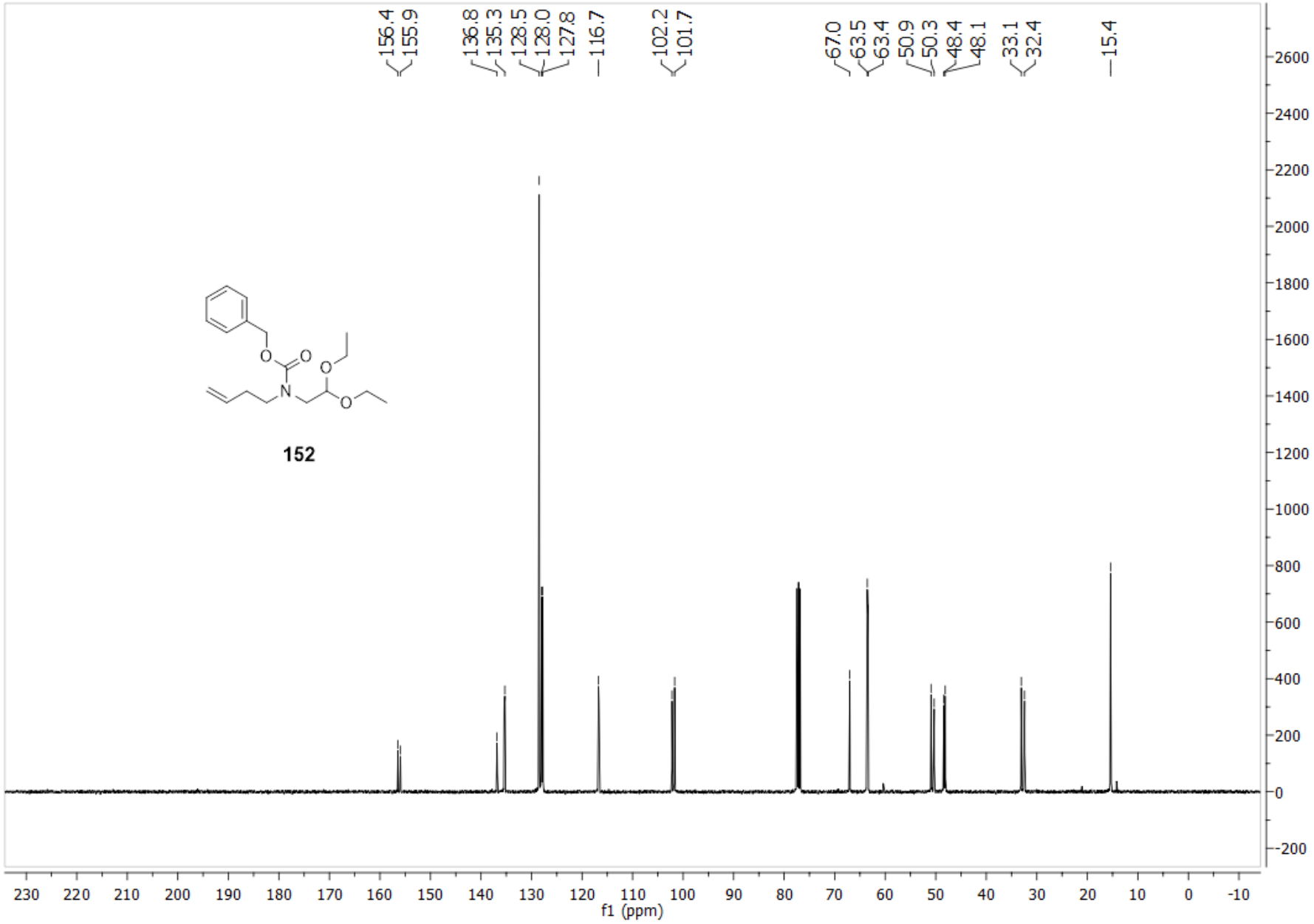
156.4
155.9
136.8
135.3
128.5
128.0
127.8
116.7
102.2
101.7
67.0
63.5
63.4
50.9
50.3
48.4
48.1
33.1
32.4
15.4
152
f1 (ppm)

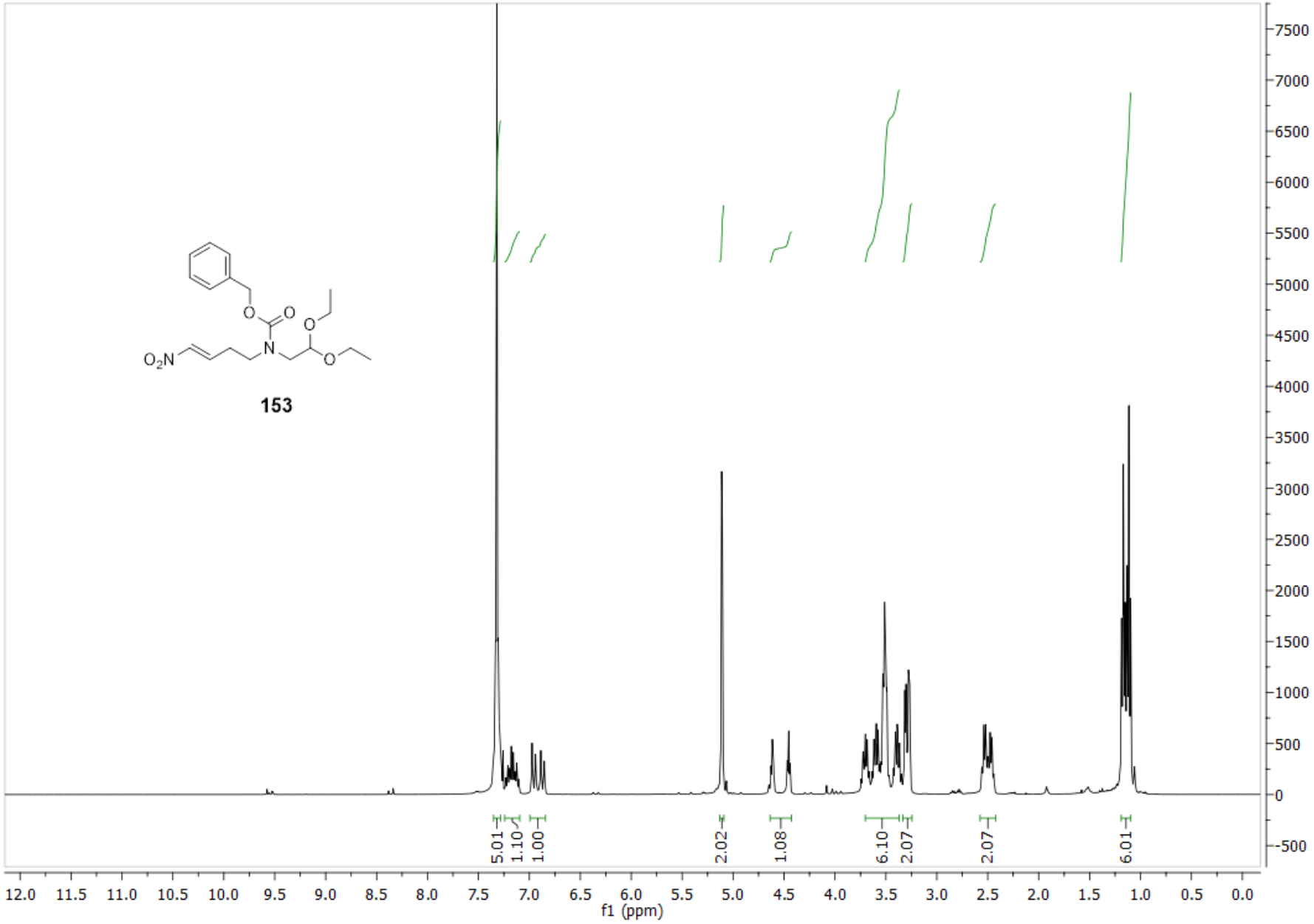
153
5.01
1.10
1.00
2.02
1.08
6.10
2.07
2.07
6.01
f1 (ppm)

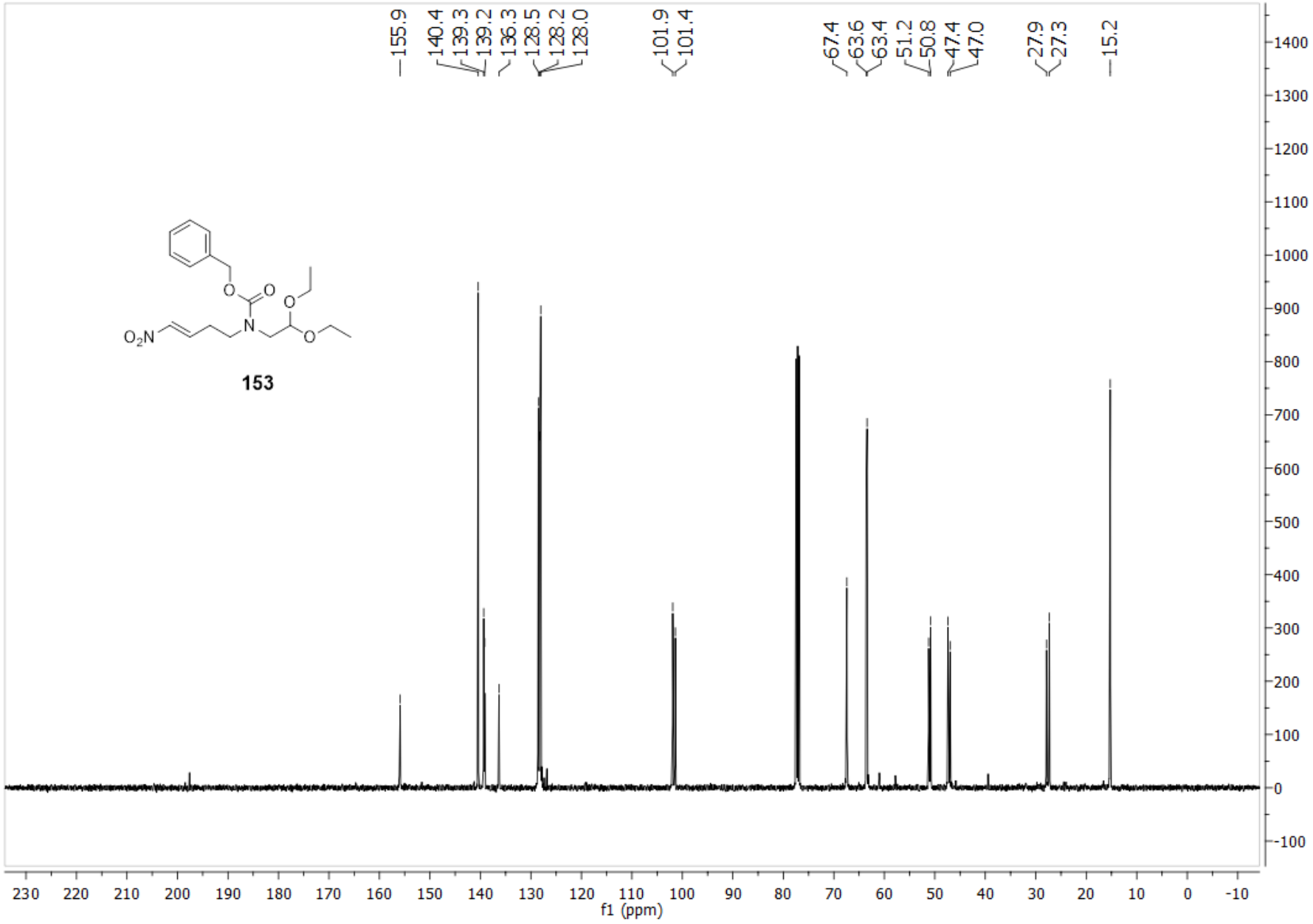
155.9
140.4
139.3
139.2
136.3
128.5
128.2
128.0
101.9
101.4
67.4
63.6
63.4
51.2
50.8
47.4
47.0
27.9
27.3
15.2
O2N
153
f1 (ppm)

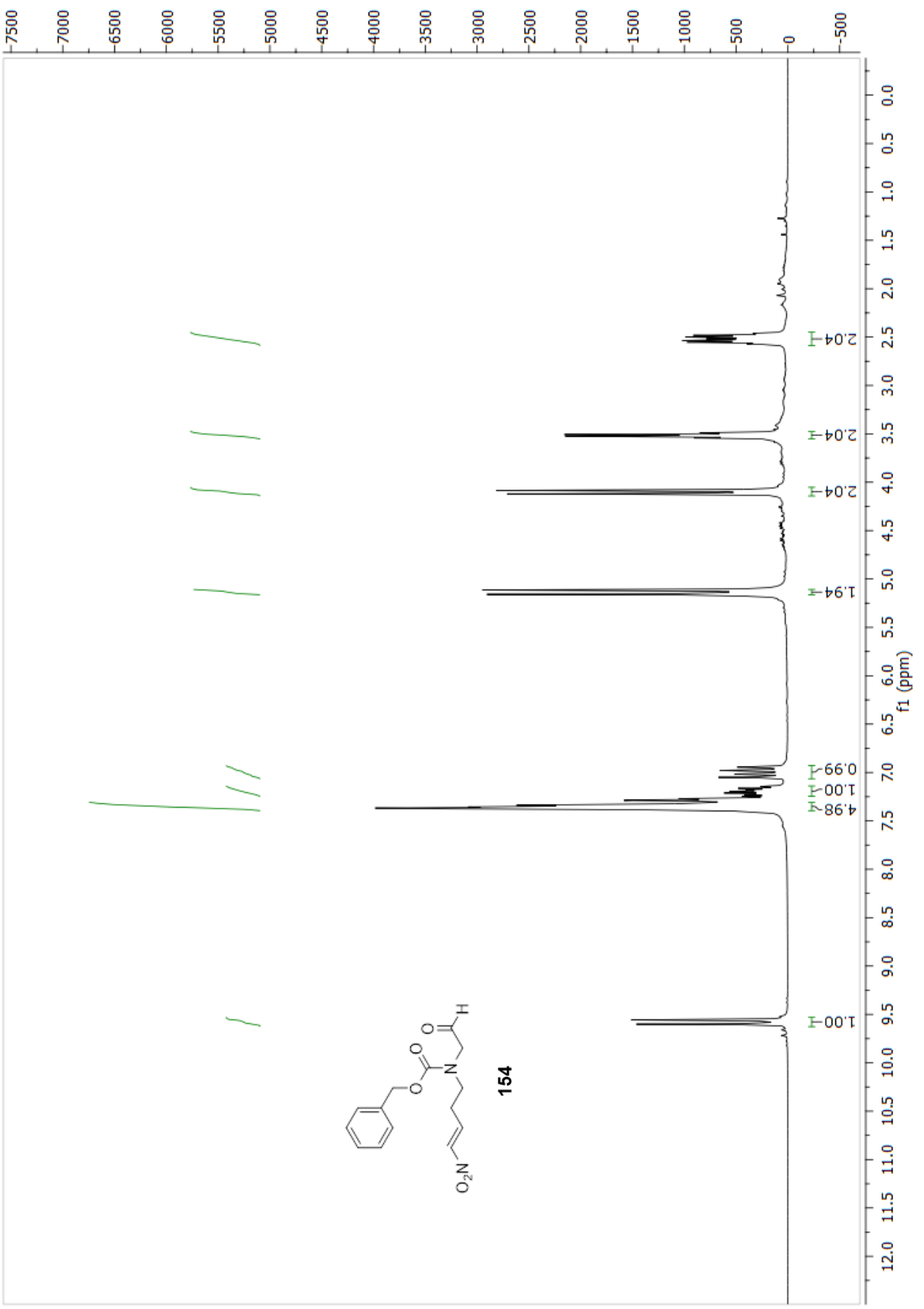
154
f1 (ppm)
2.04
2.04
2.04
1.94
0.99
1.00
4.98
1.00

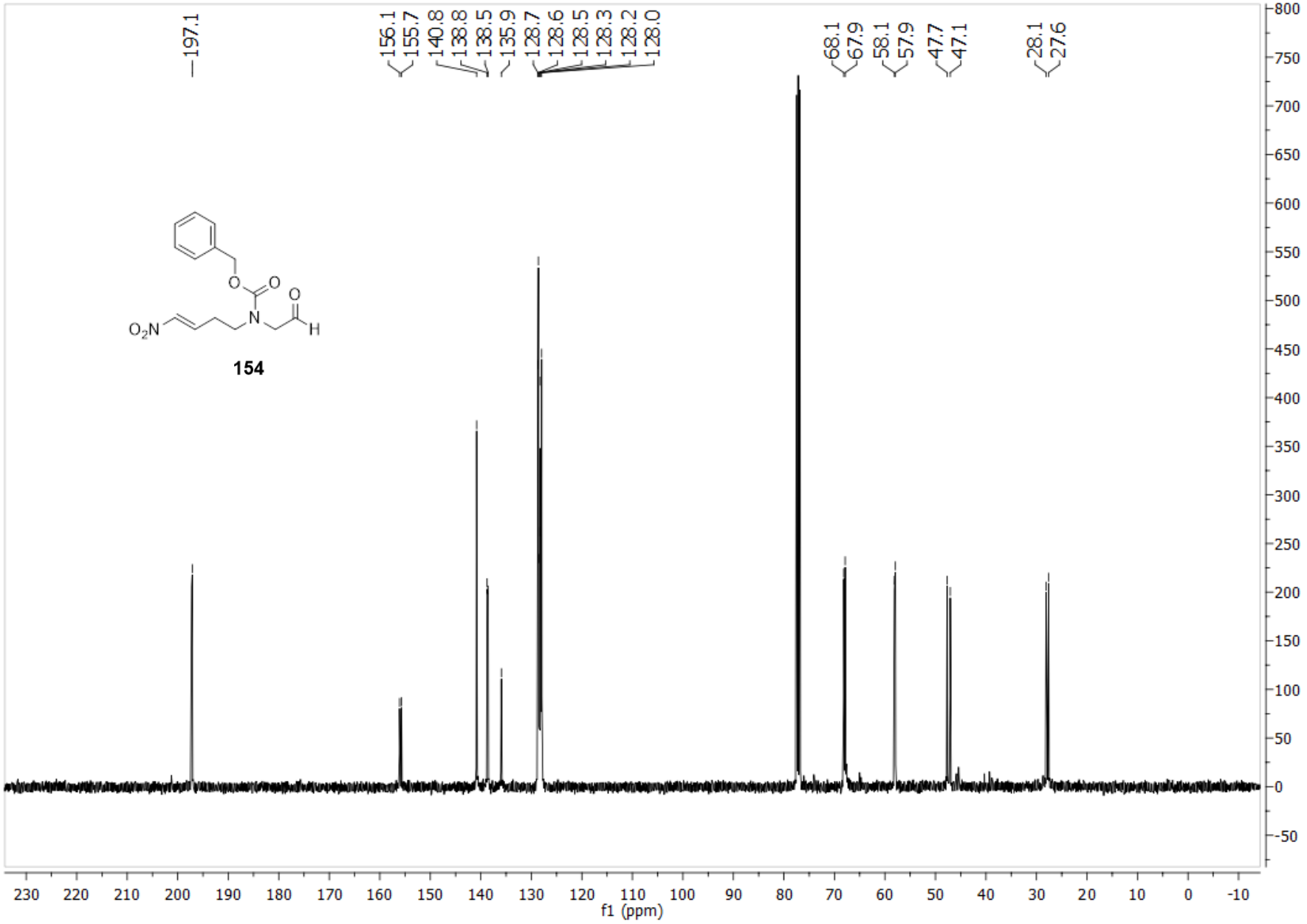
197.1
156.1
155.7
140.8
138.8
138.5
135.9
128.7
128.6
128.5
128.3
128.2
128.0
68.1
67.9
58.1
57.9
47.7
47.1
28.1
27.6
O
O
O
N
O2N
H
154
f1 (ppm)

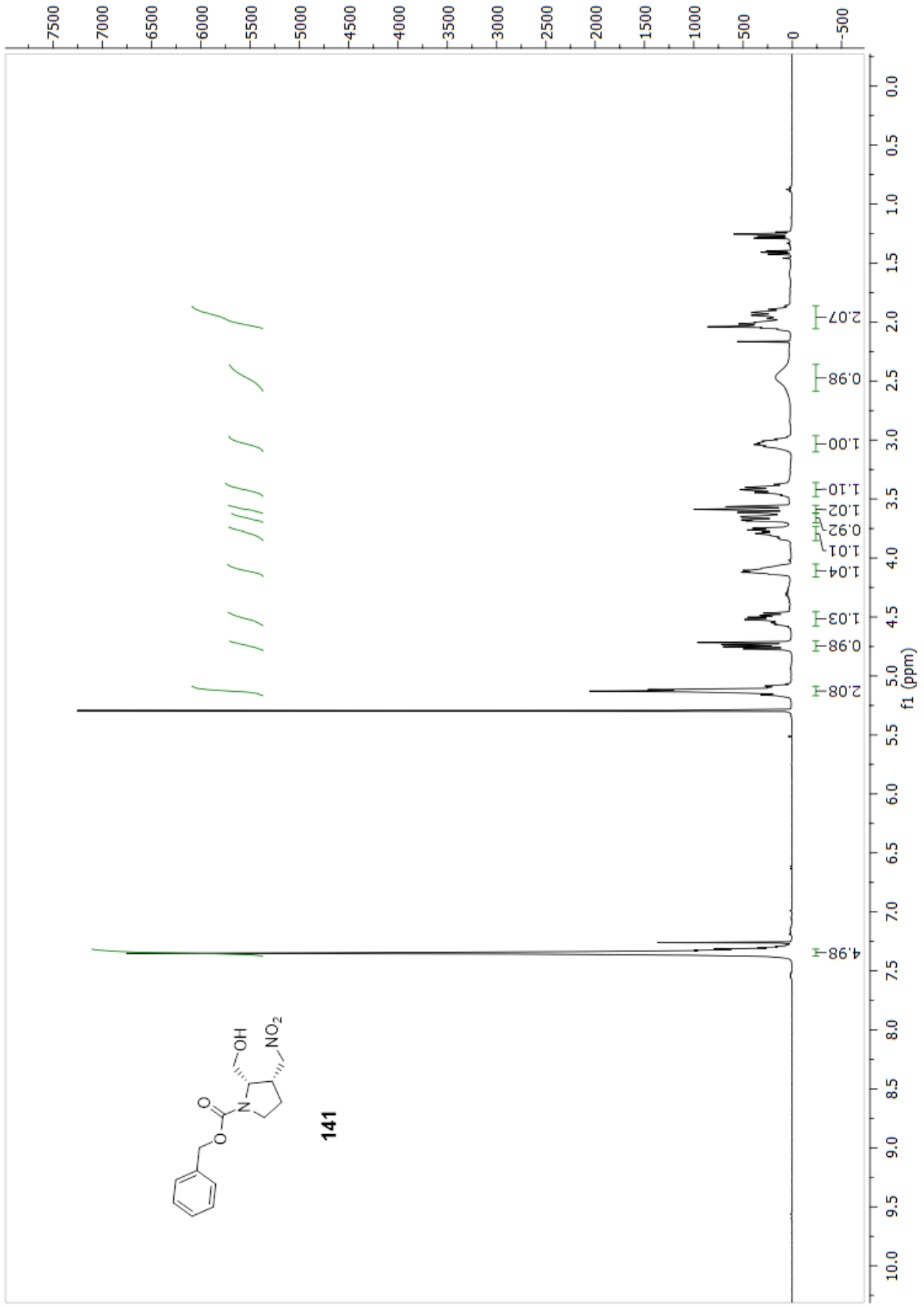
141
OH
NO2
O
N
O
4.98
2.08
0.98
1.03
1.04
1.01
0.92
1.02
1.10
1.00
0.98
2.07
f1 (ppm)

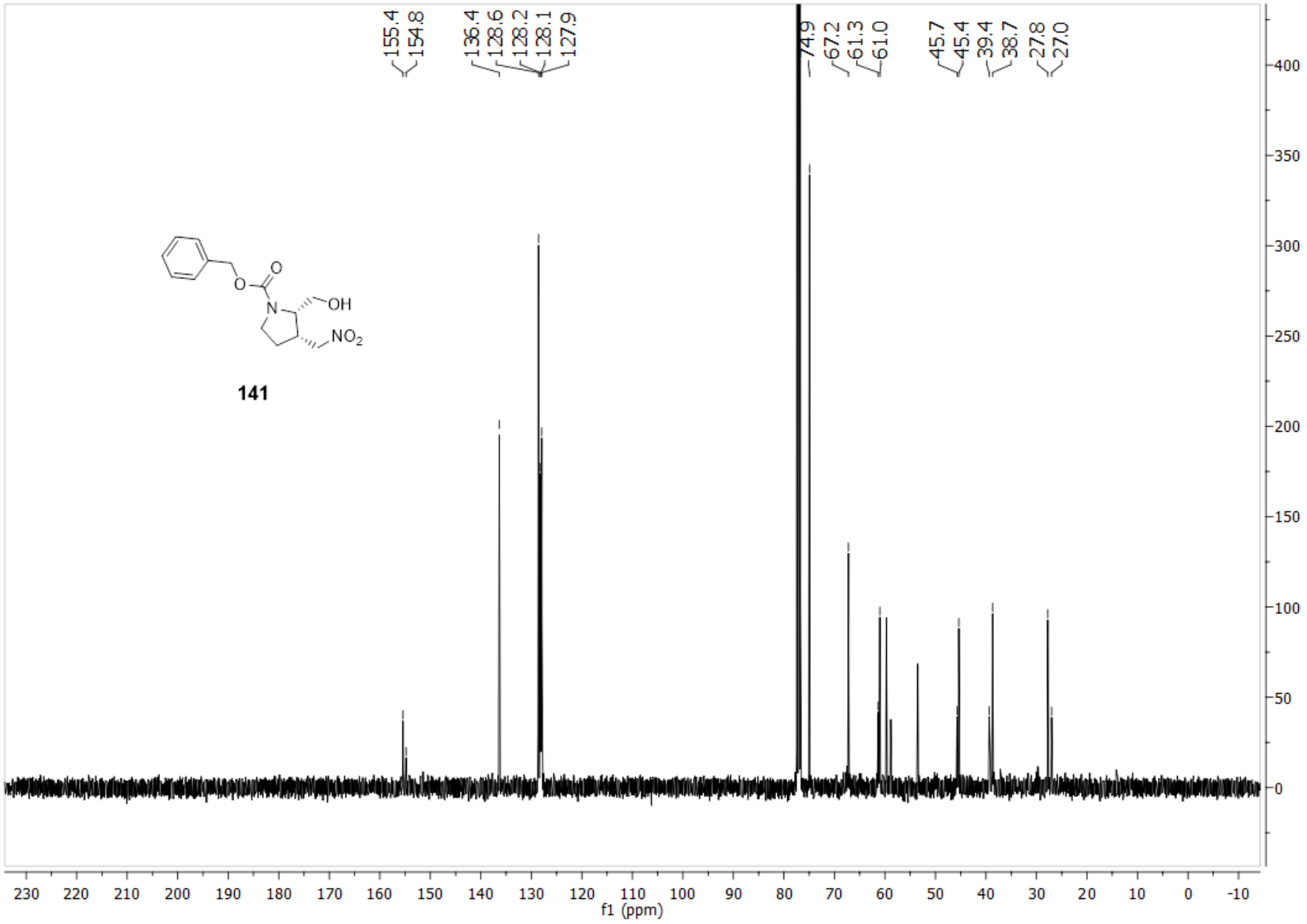
155.4
154.8
136.4
128.6
128.2
128.1
127.9
74.9
67.2
61.3
61.0
45.7
45.4
39.4
38.7
27.8
27.0
OH
NO2
141
f1 (ppm)

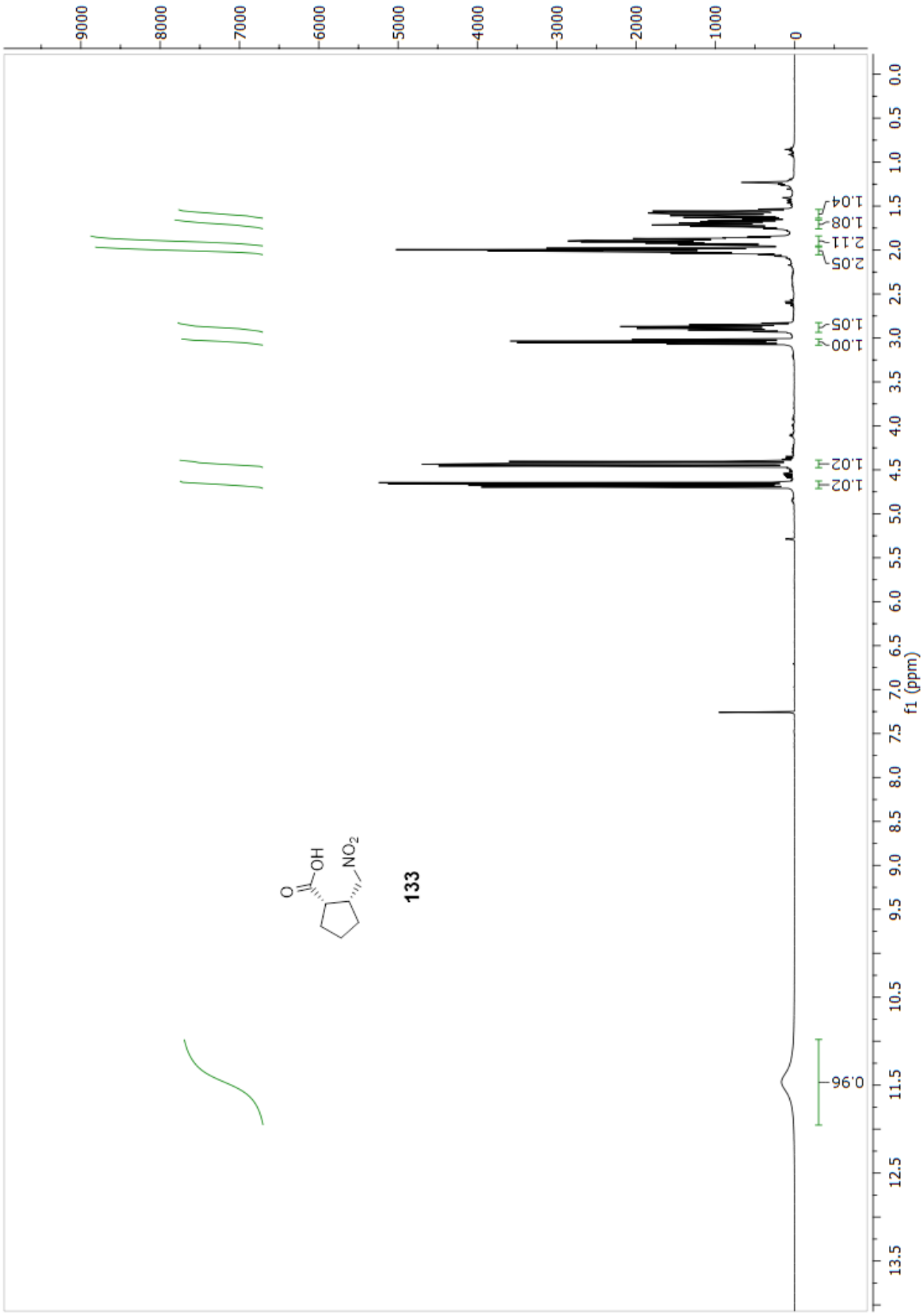
OH
O
NO2
133
f1 (ppm)
0.96
1.02
1.02
1.00
1.05
2.05
2.11
1.08
1.04

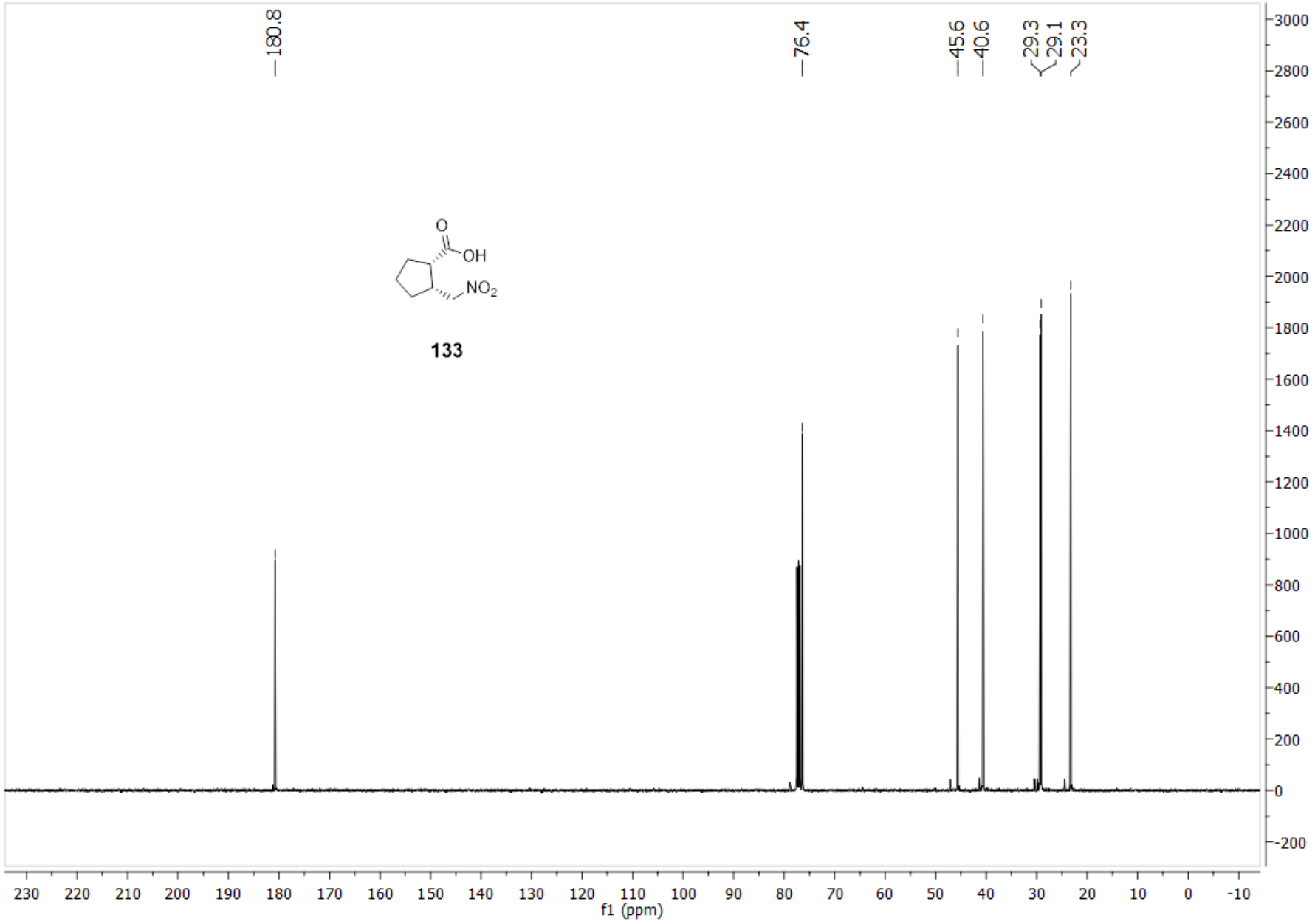
180.8
76.4
45.6
40.6
29.3
29.1
23.3
O
OH
NO2
133
f1 (ppm)

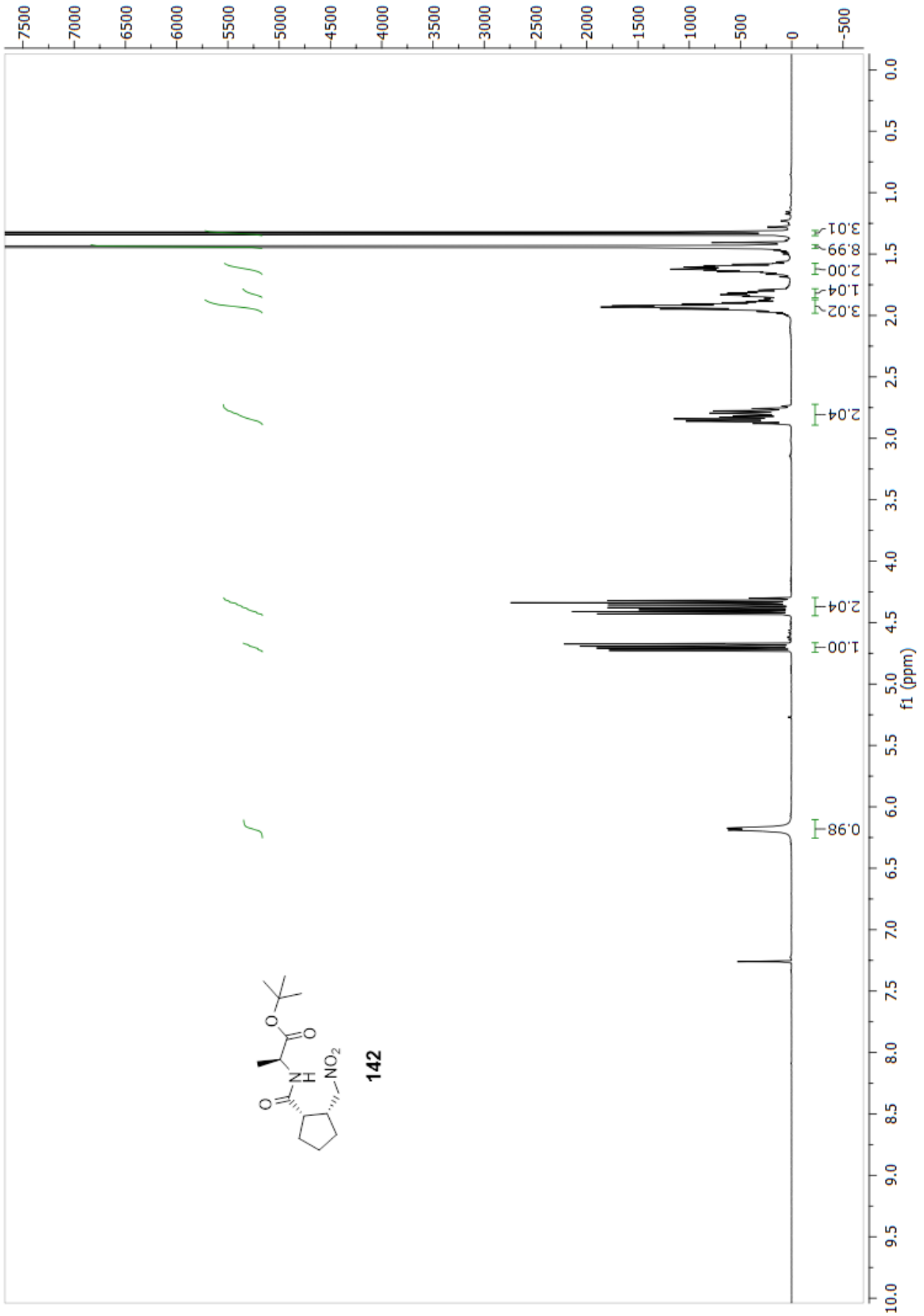
7500
7000
6500
6000
5500
5000
4500
4000
3500
3000
2500
2000
1500
1000
500
0
-500
3.01
8.99
2.00
1.04
3.02
2.04
2.04
1.00
0.98
0.0
0.5
1.0
1.5
2.0
2.5
3.0
3.5
4.0
4.5
5.0
5.5
6.0
6.5
7.0
7.5
8.0
8.5
9.0
9.5
10.0
f1 (ppm)
O
O
O
N
H
O
NO2

142

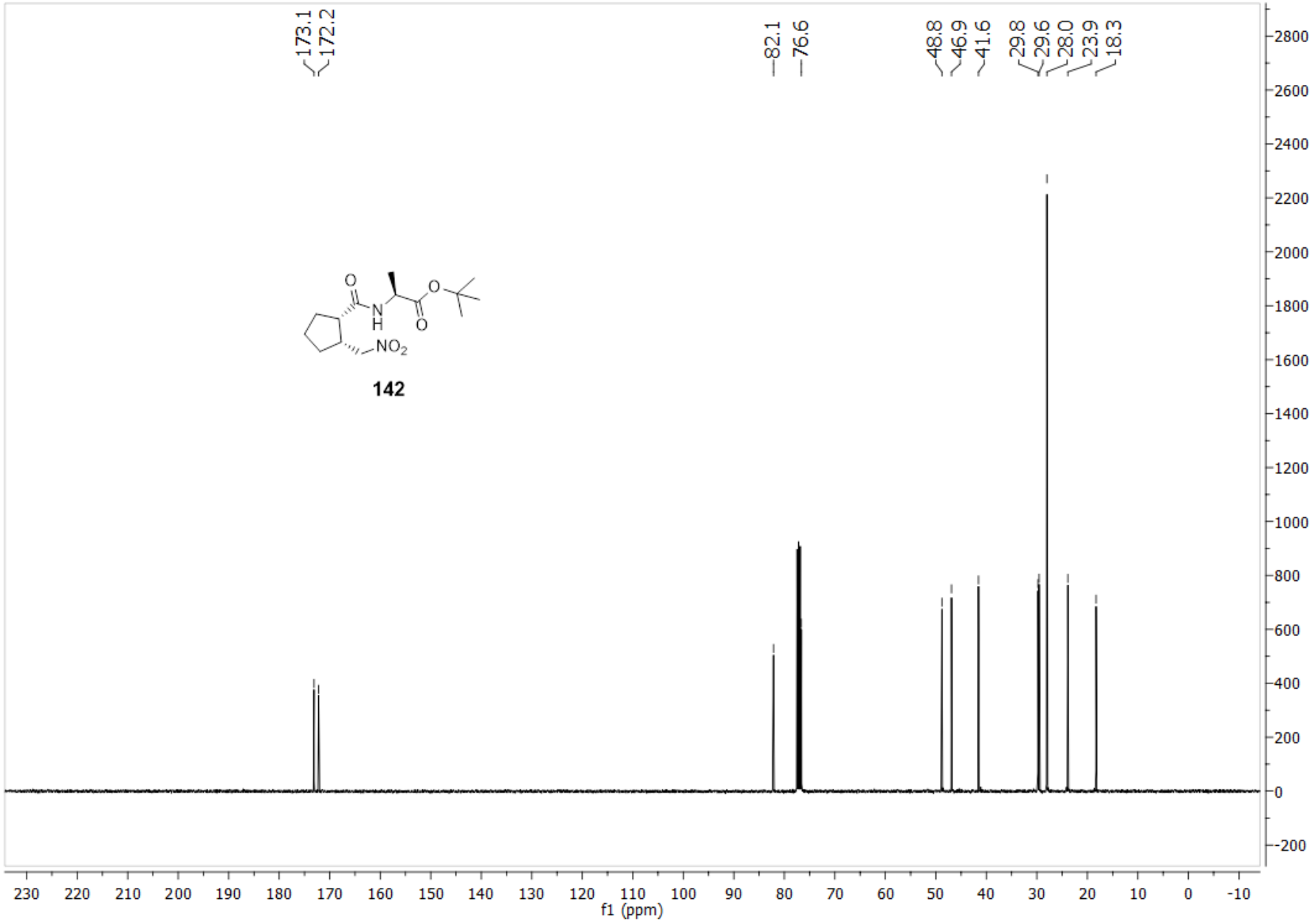
173.1
172.2
82.1
76.6
48.8
46.9
41.6
29.8
29.6
28.0
23.9
18.3
O
N
H
O
O
NO2
142
f1 (ppm)

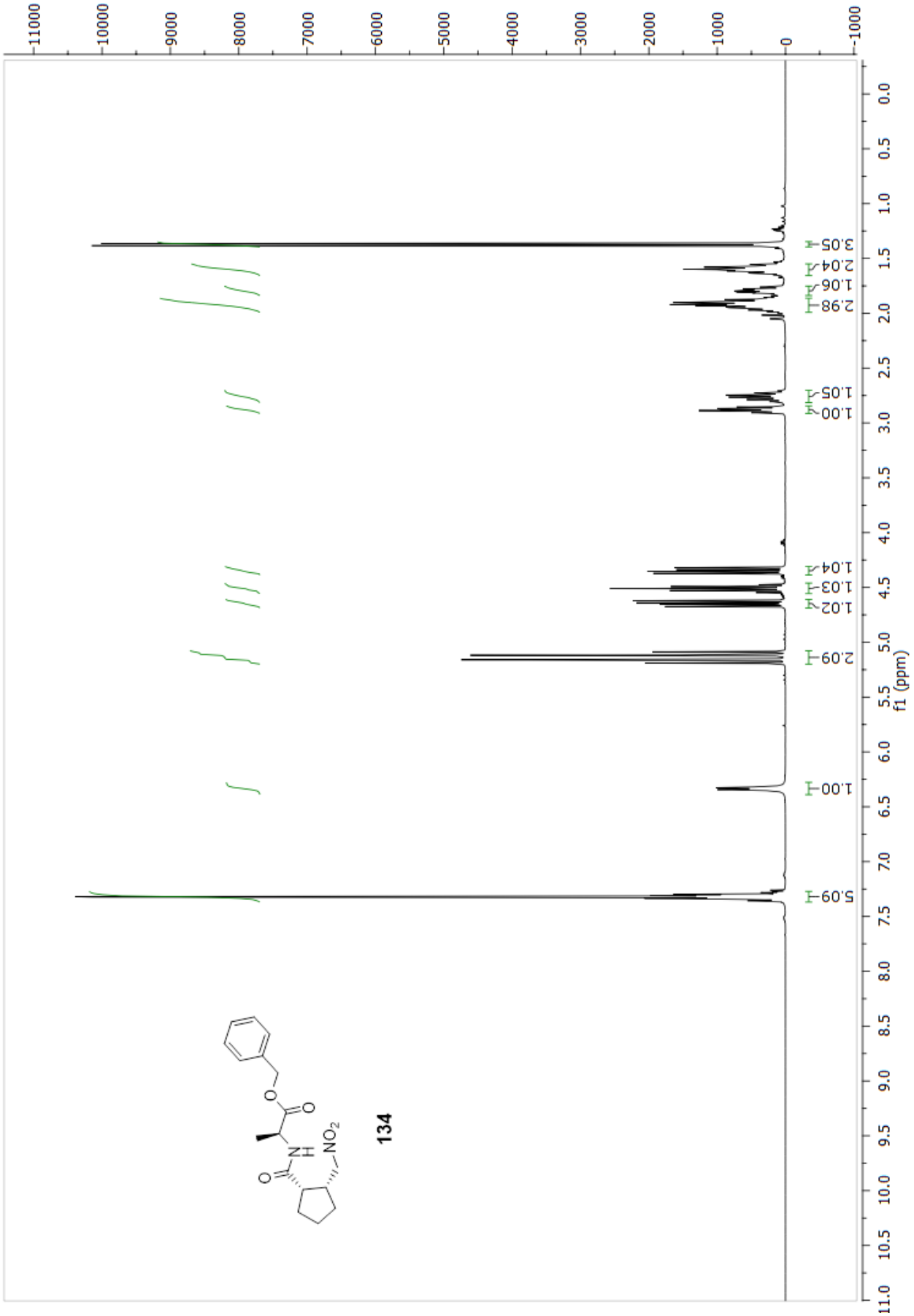
134
5.09
1.00
2.09
1.02
1.03
1.04
1.00
1.05
2.98
1.06
2.04
3.05
f1 (ppm)

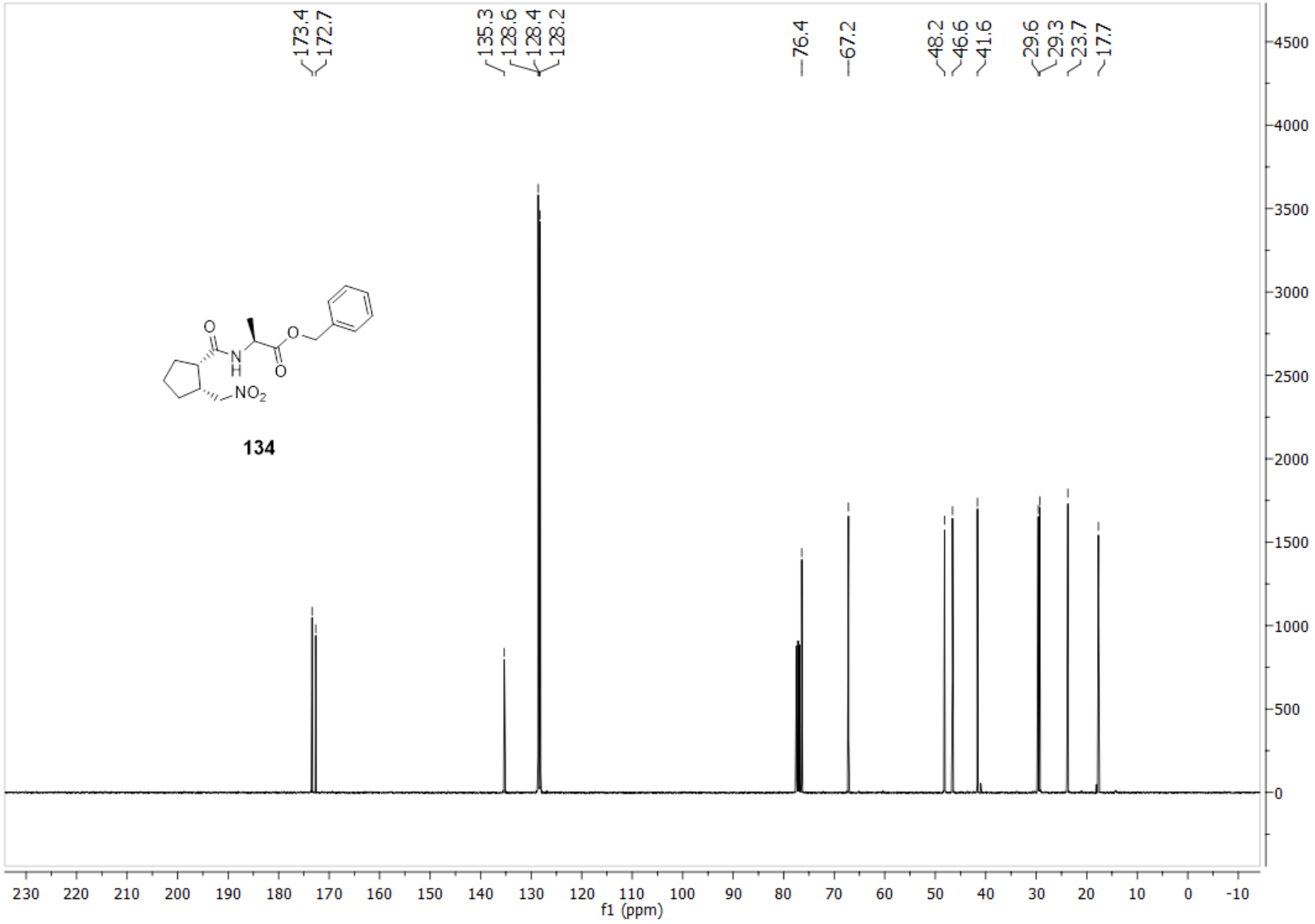
173.4
172.7
135.3
128.6
128.4
128.2
76.4
67.2
48.2
46.6
41.6
29.6
29.3
23.7
17.7
O
N
H
O
O
NO2
134
4500
4000
3500
3000
2500
2000
1500
1000
500
0
230 220 210 200 190 180 170 160 150 140 130 120 110 100 90 80 70 60 50 40 30 20 10 0 -10
f1 (ppm)

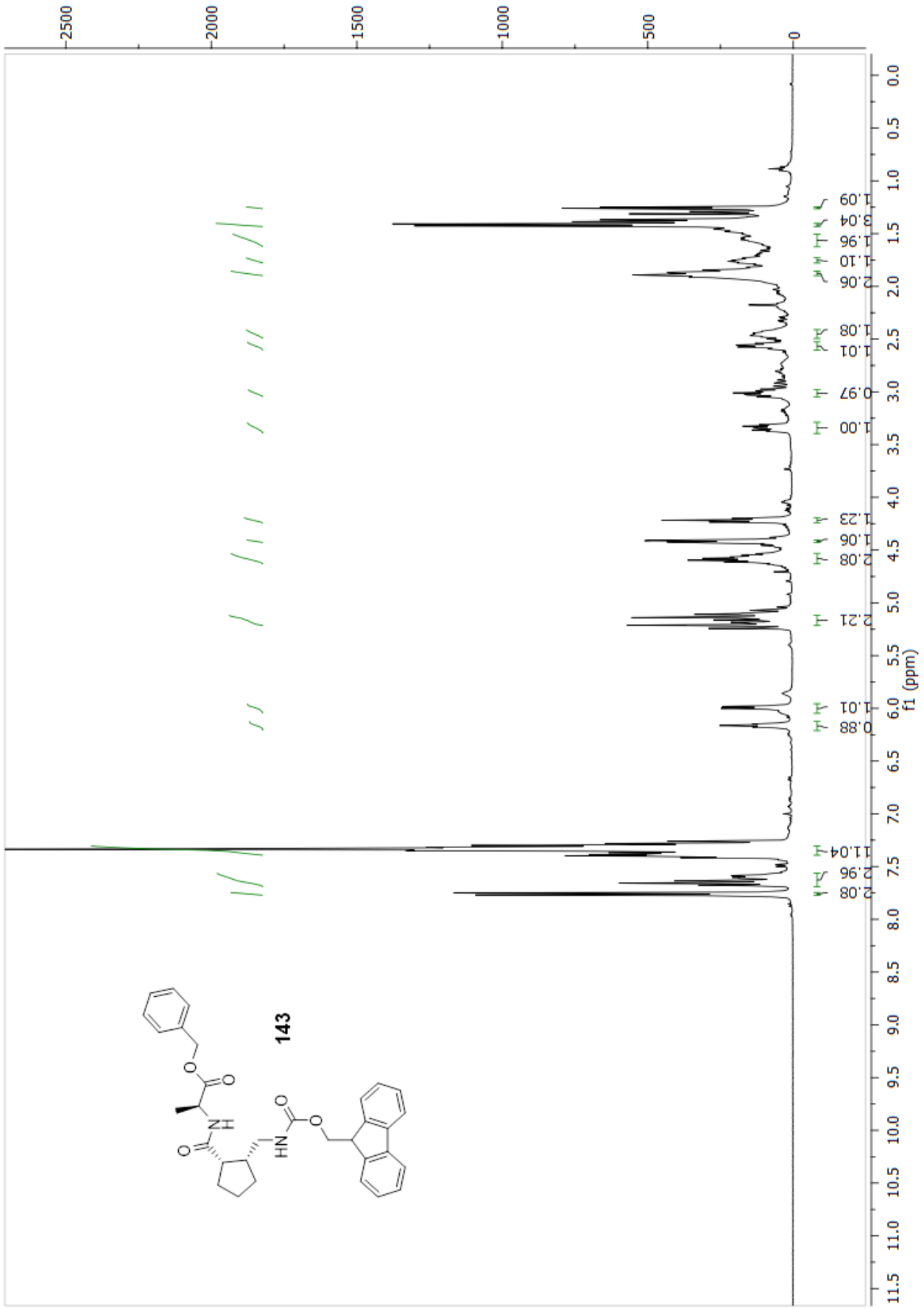
143
f1 (ppm)

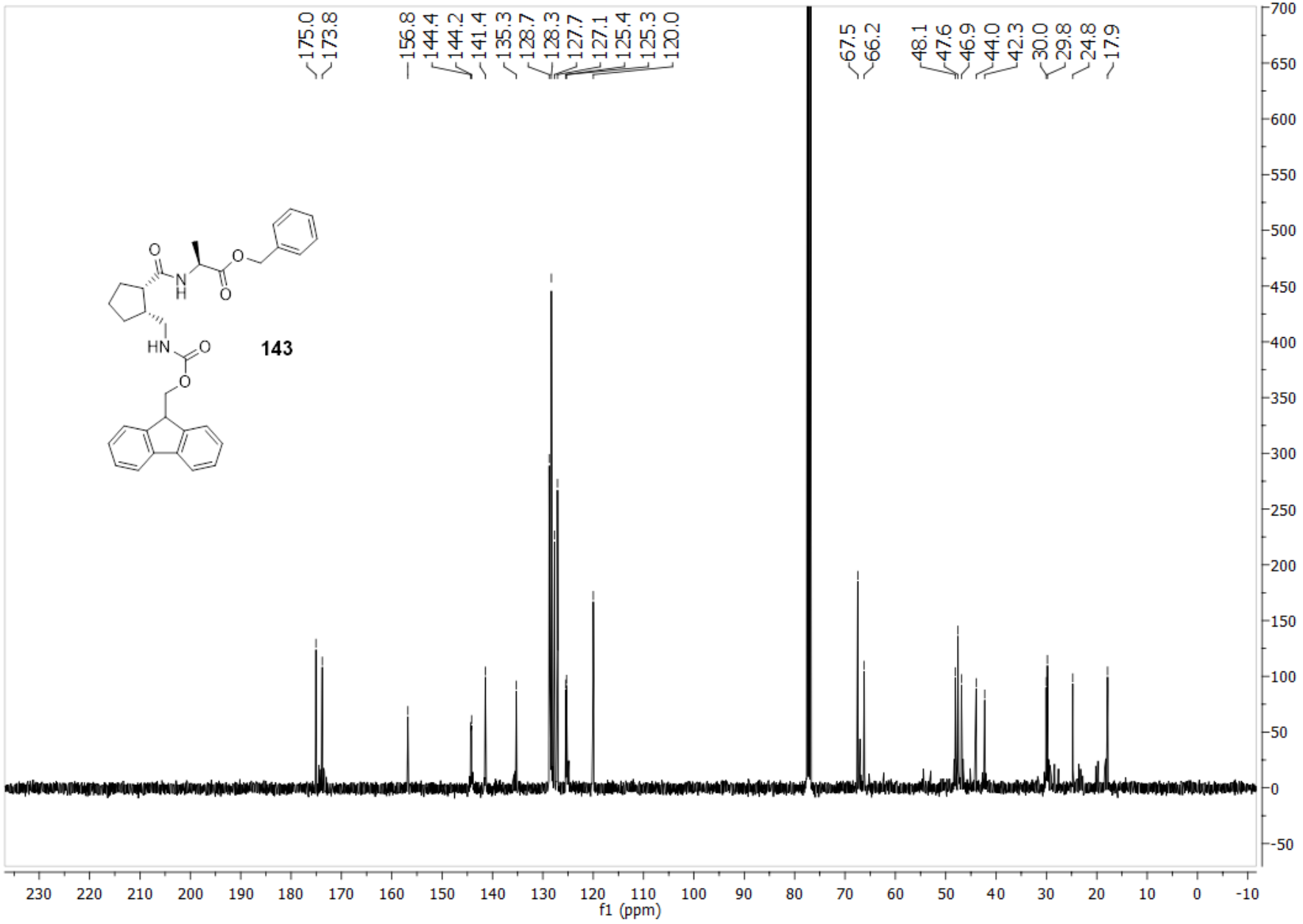
175.0
173.8
156.8
144.4
144.2
141.4
135.3
128.7
128.3
127.7
127.1
125.4
125.3
120.0
67.5
66.2
48.1
47.6
46.9
44.0
42.3
30.0
29.8
24.8
17.9
143
f1 (ppm)

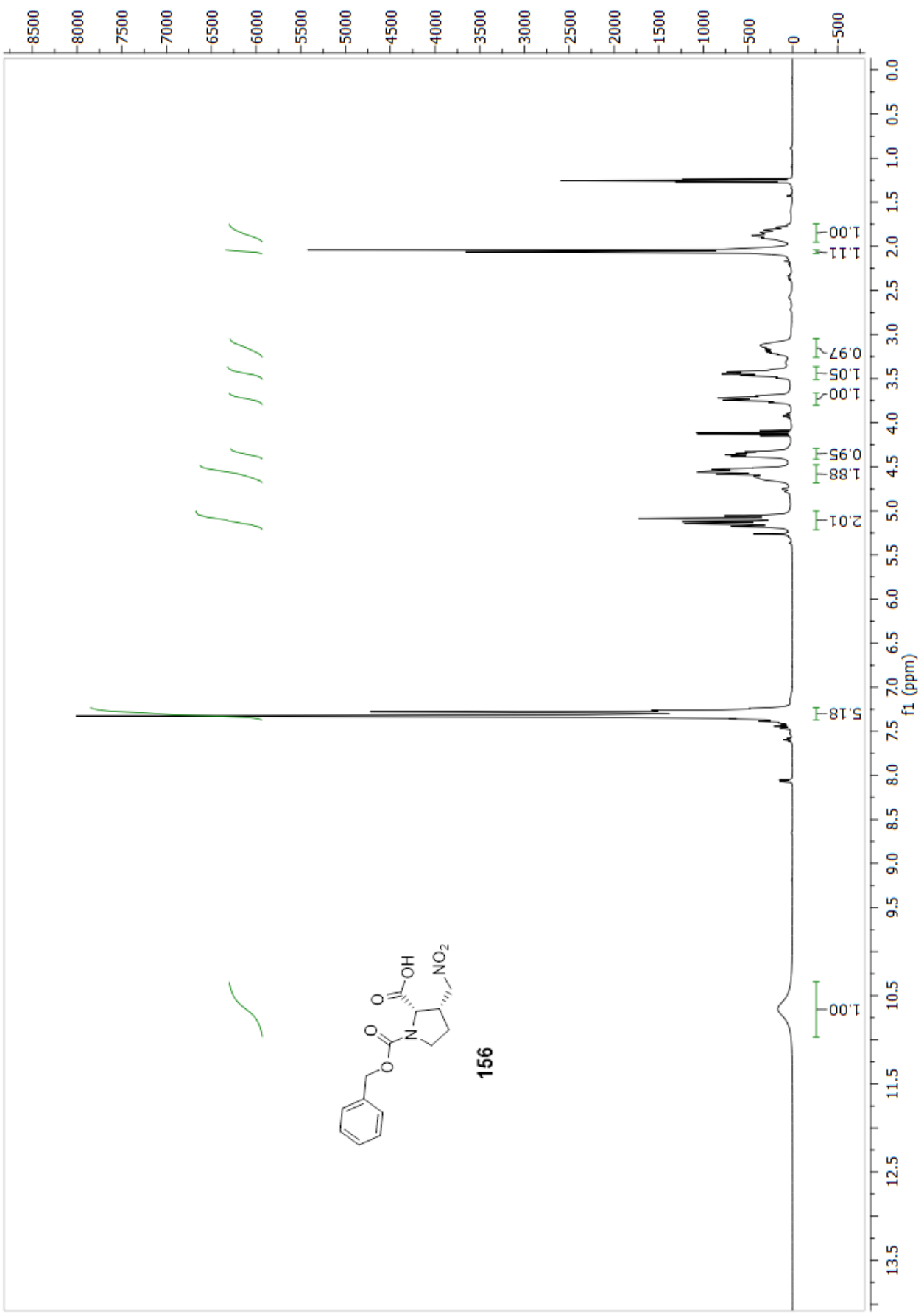
156
f1 (ppm)
5.18
2.01
1.88
0.95
1.00
1.05
1.00
0.97
1.11
1.00

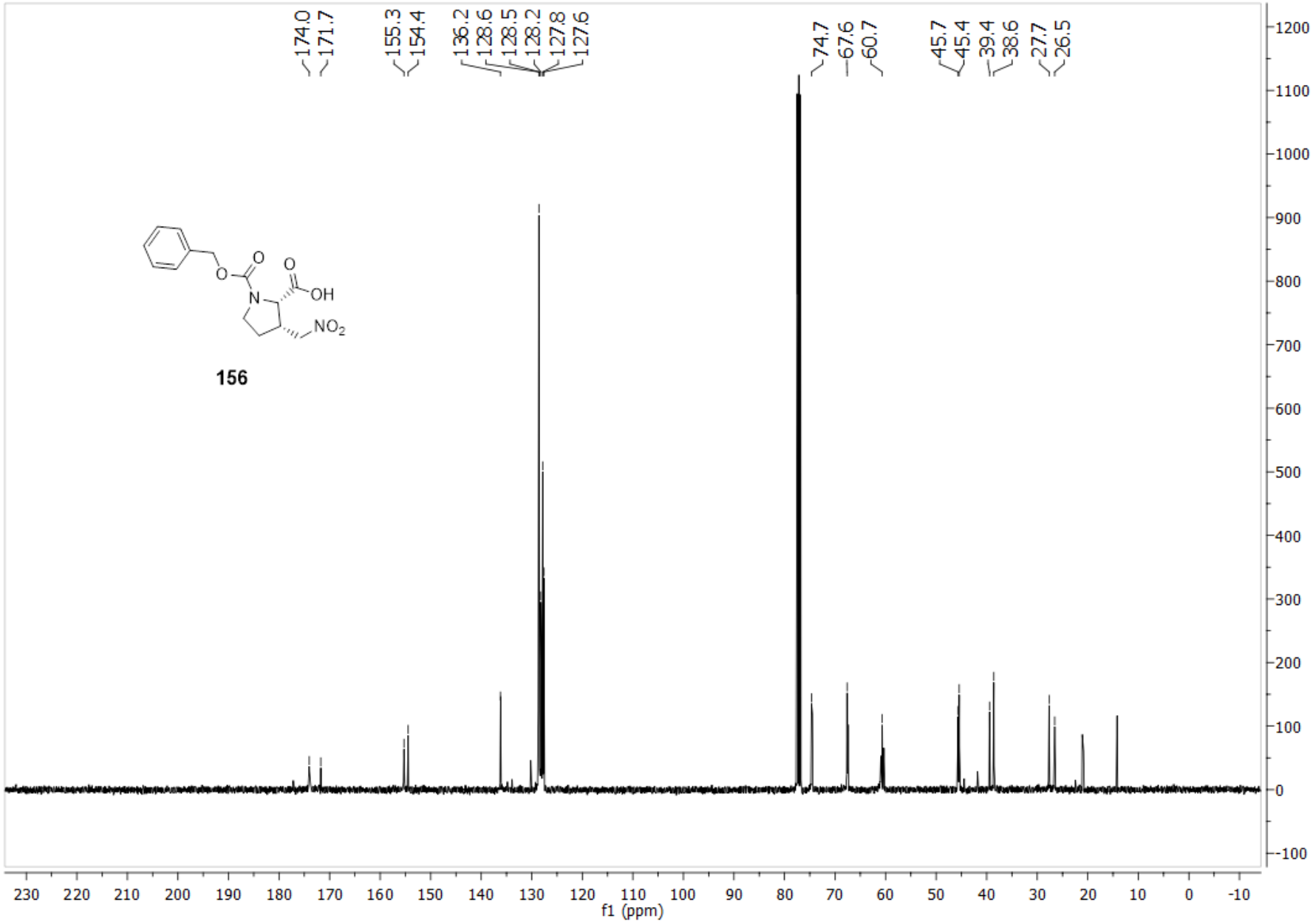
174.0
171.7
155.3
154.4
136.2
128.6
128.5
128.2
127.8
127.6
74.7
67.6
60.7
45.7
45.4
39.4
38.6
27.7
26.5
O
O
O
OH
N
NO2
156
f1 (ppm)

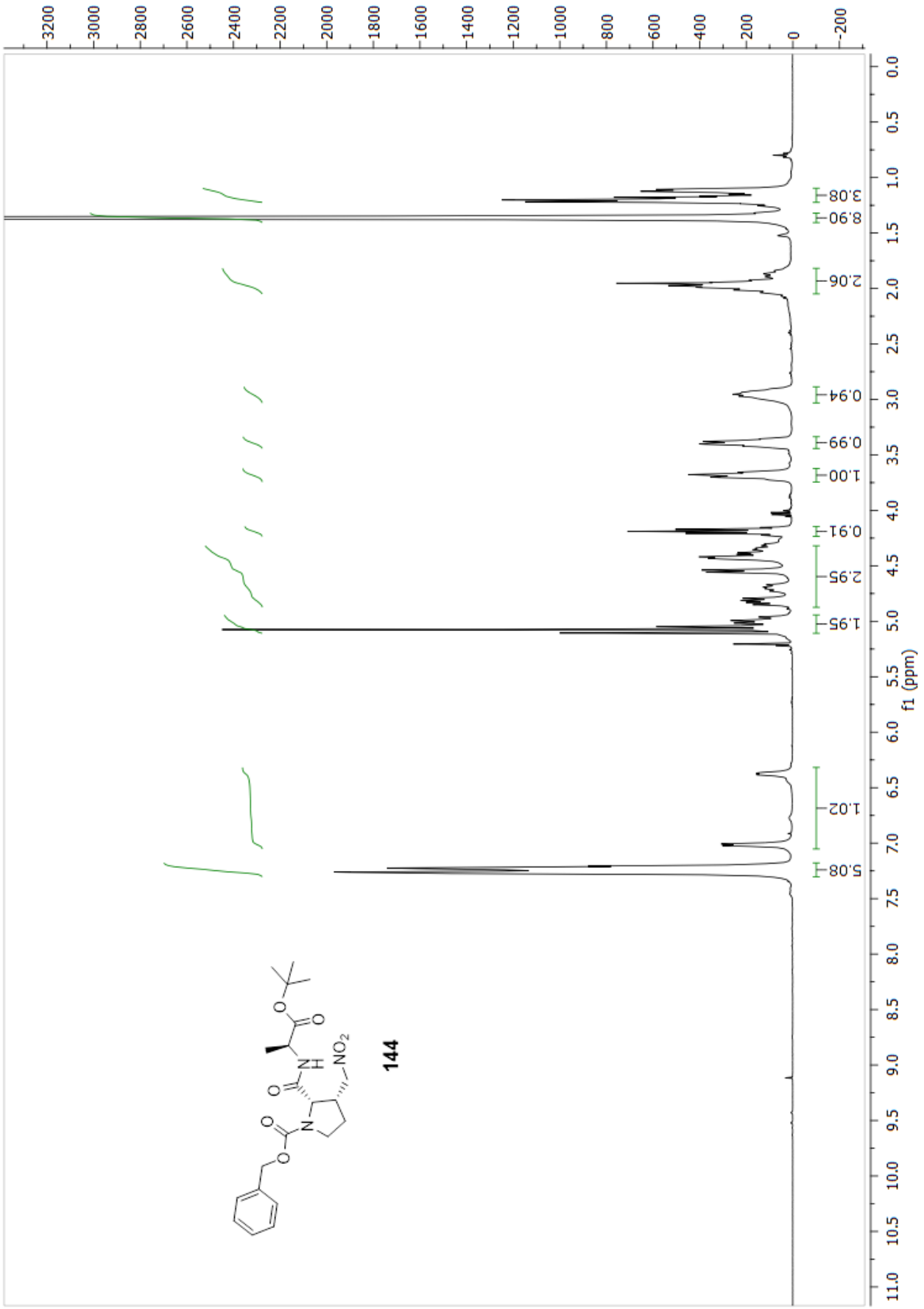
144
f1 (ppm)
3.08
8.90
2.06
0.94
0.99
1.00
0.91
2.95
1.95
1.02
5.08

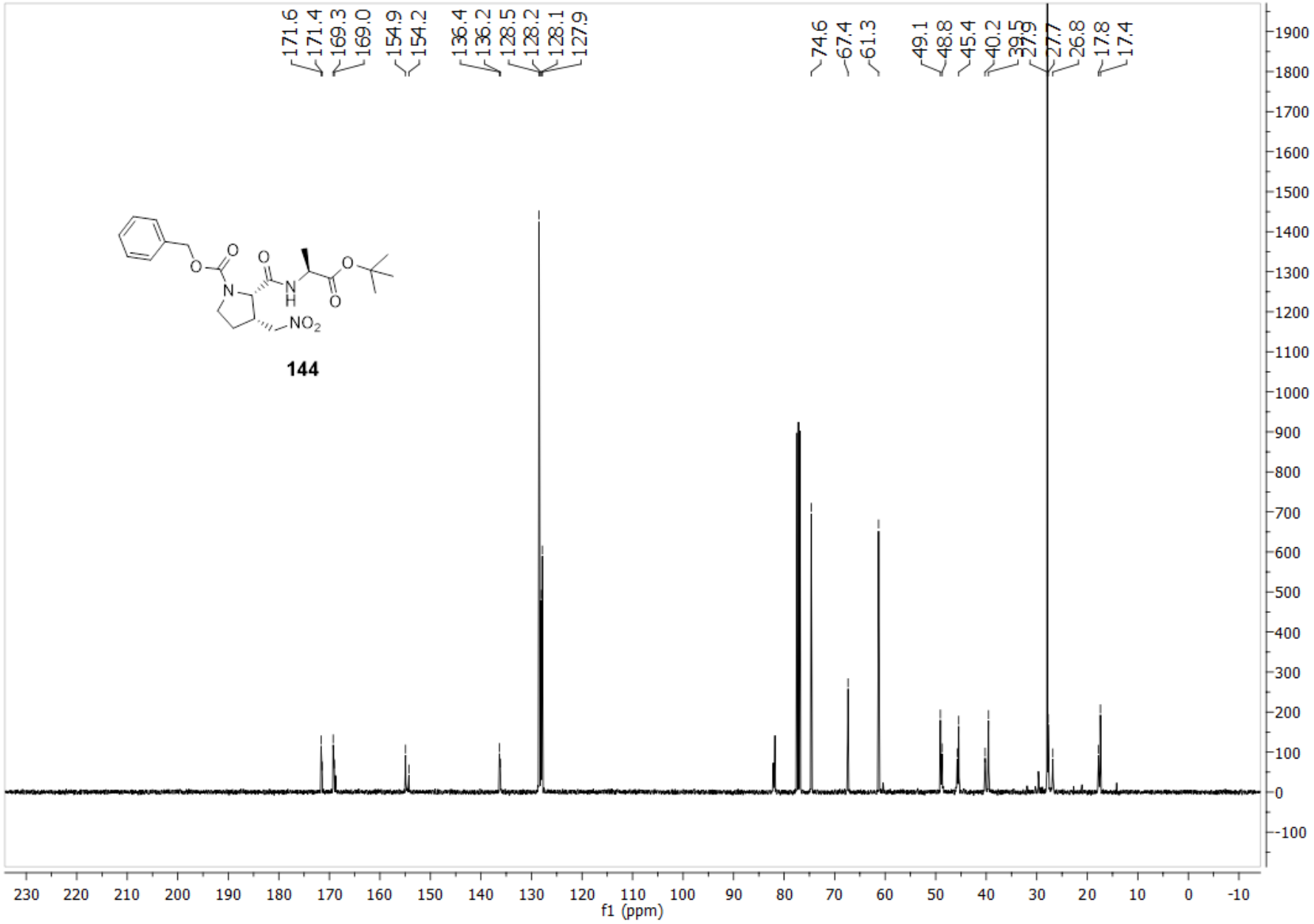
171.6
171.4
169.3
169.0
154.9
154.2
136.4
136.2
128.5
128.2
128.1
127.9
74.6
67.4
61.3
49.1
48.8
45.4
40.2
39.5
27.9
27.7
26.8
17.8
17.4
144
f1 (ppm)

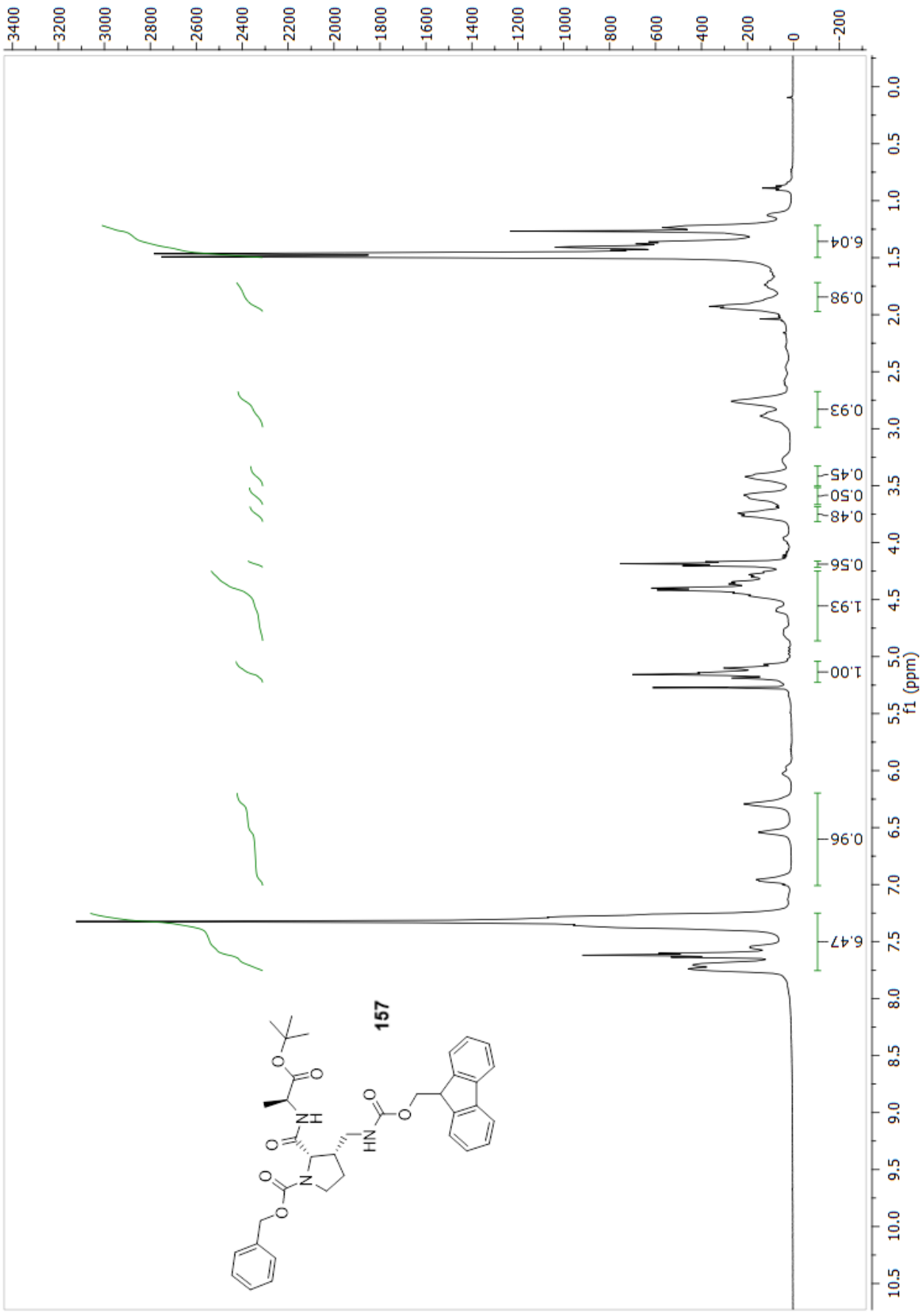
157
6.04
0.98
0.93
0.45
0.50
0.48
0.56
1.93
1.00
0.96
6.47
f1 (ppm)

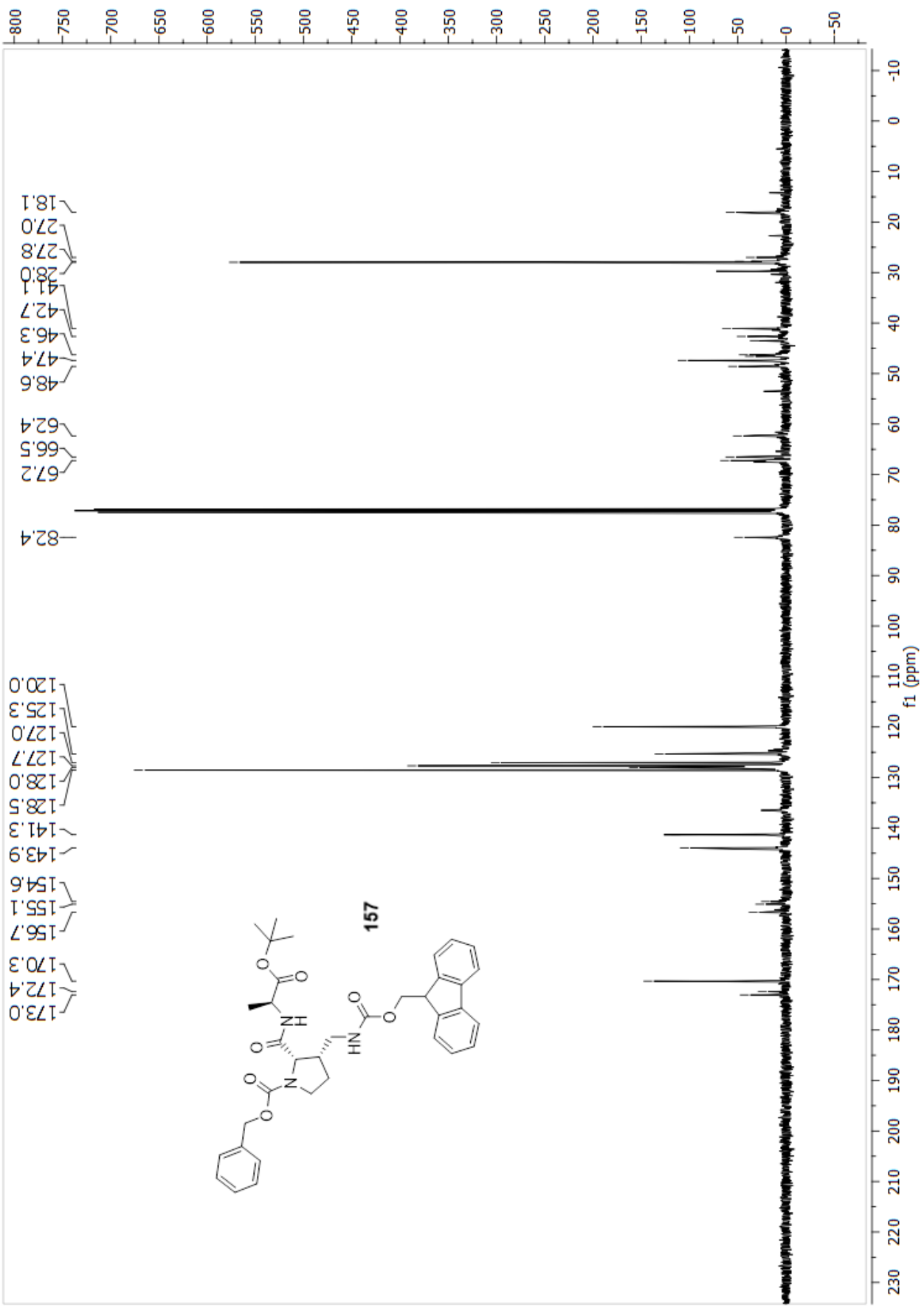
157
173.0
172.4
170.3
156.7
155.1
154.6
143.9
141.3
128.5
128.0
127.7
127.0
125.3
120.0
82.4
67.2
66.5
62.4
48.6
47.4
46.3
42.7
41.1
28.0
27.8
27.0
18.1
f1 (ppm)

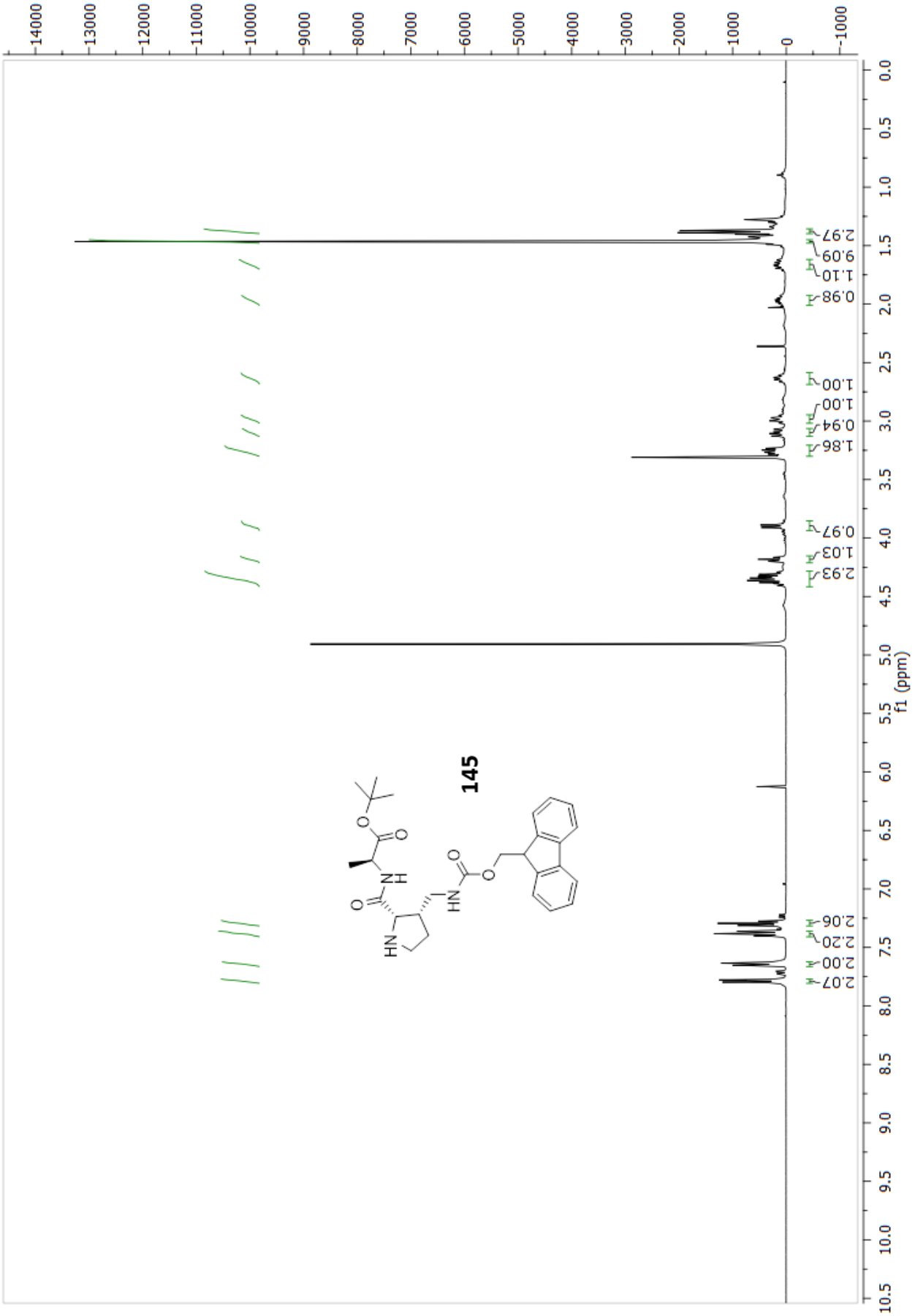
145
f1 (ppm)

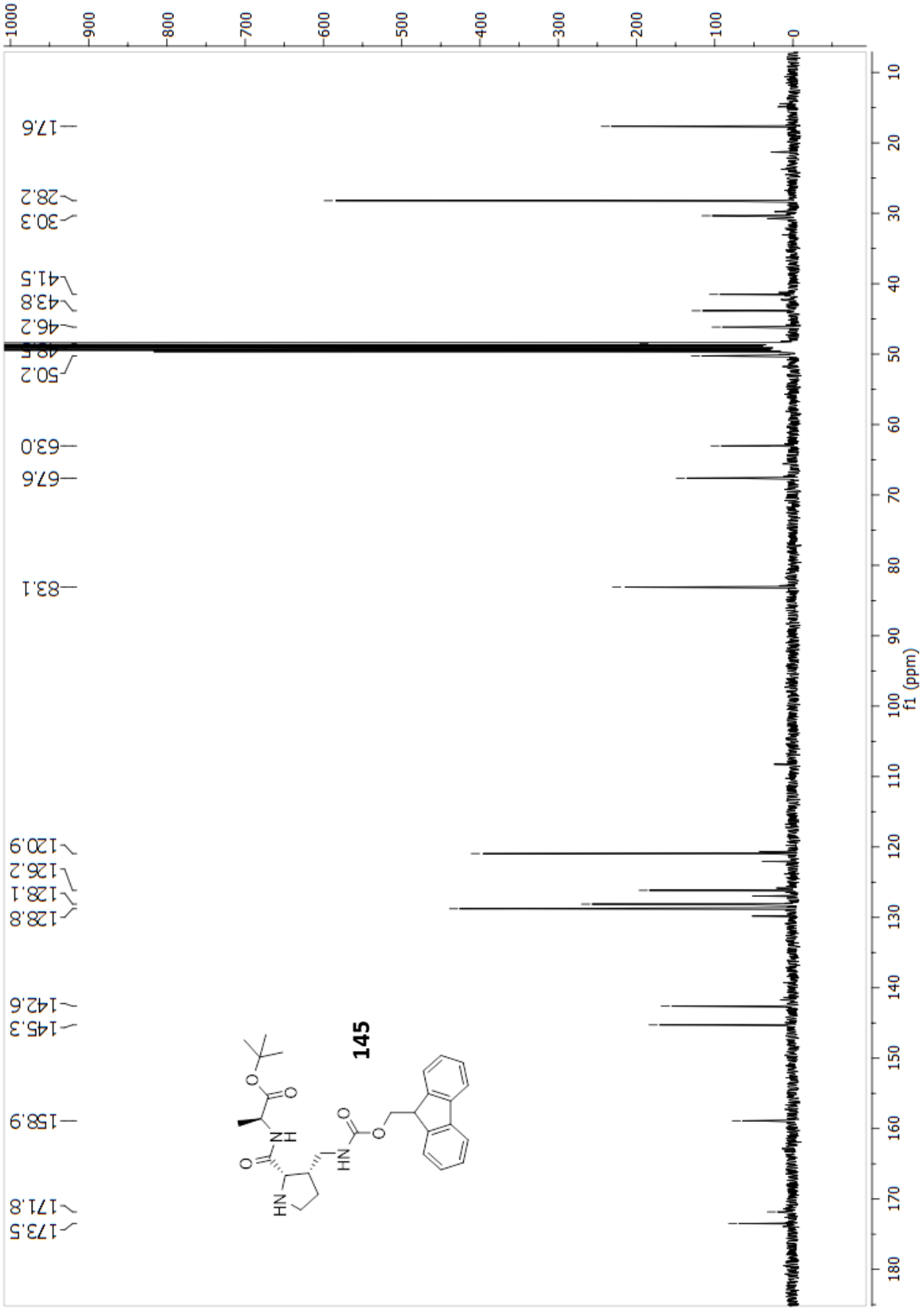
145
f1 (ppm)

7.2 – Chiral HPLC

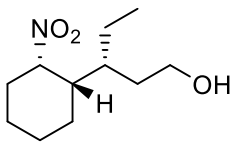

94

major enantiomer tR = 12.4 min, minor enantiomer tR = 14.8 min, 98% ee.

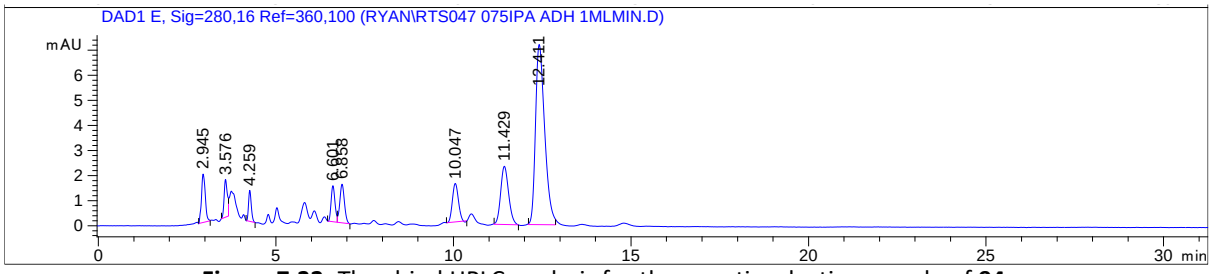

Figure 7.32: The chiral HPLC analysis for the enantioselective sample of **94**.

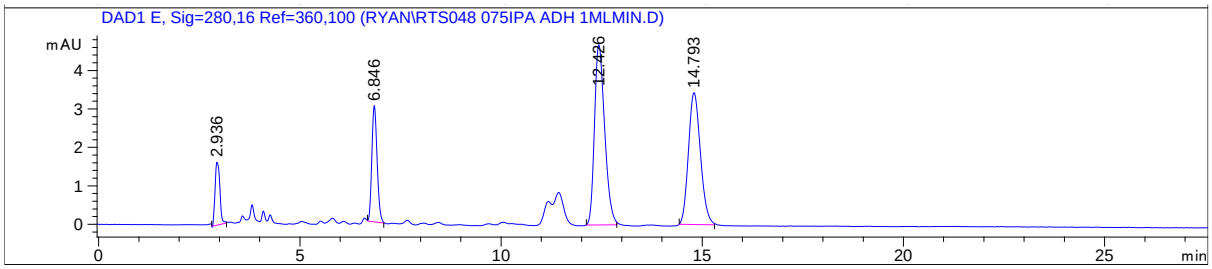

Figure 7.33 : The chiral HPLC analysis for the racemic sample of **94**.

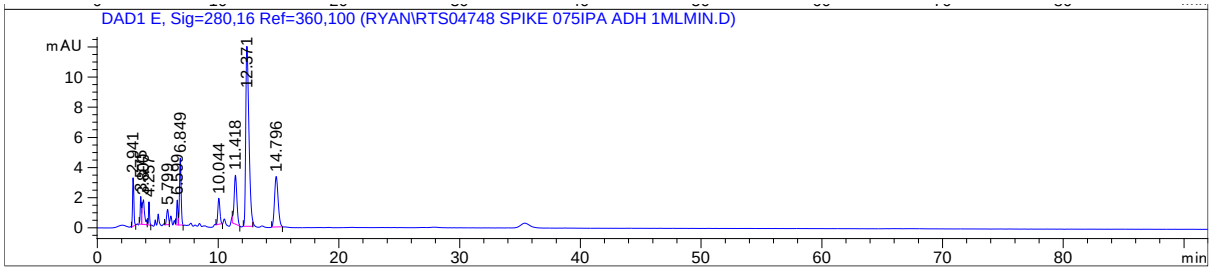

Figure 7.34: The chiral HPLC analysis for the spiked sample of **94**.

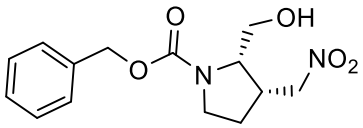

141

major enantiomer tR = 27.1 min, minor enantiomer tR = 24.1 min, 80% ee.

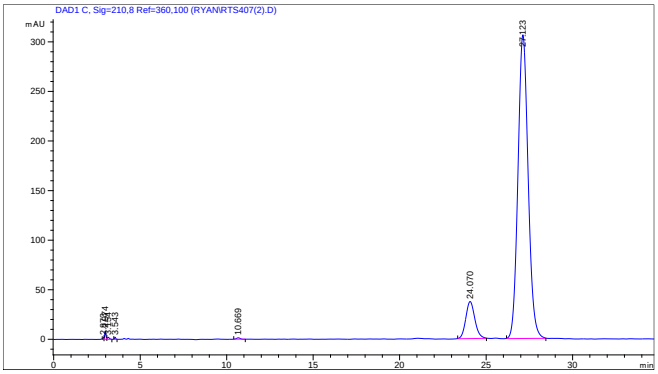

Figure 7.35: The chiral HPLC analysis for the enantioselective sample of **141**.

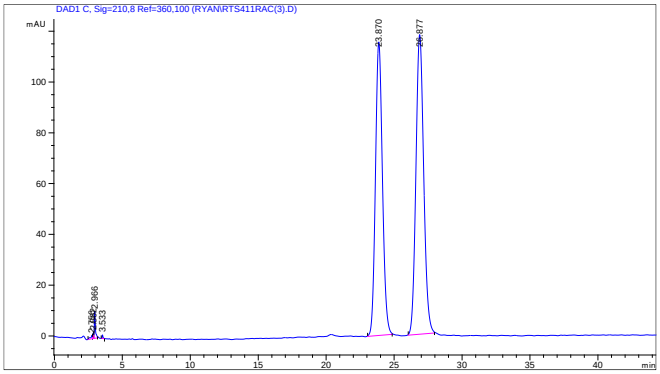

Figure 7.36: The chiral HPLC analysis for the racemic sample of **141**.

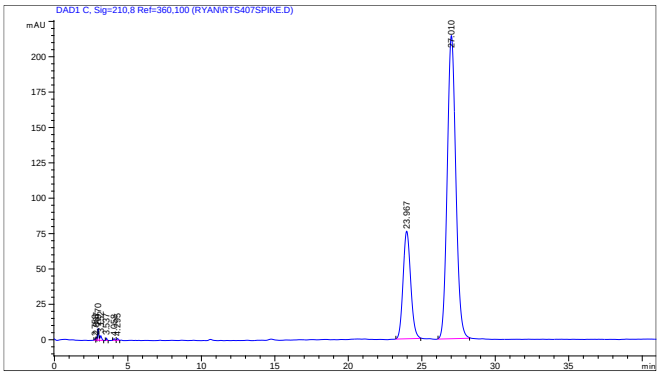

Figure 7.37: The chiral HPLC analysis for the spiked sample of **141**.

7.3 – Circular Dichroism

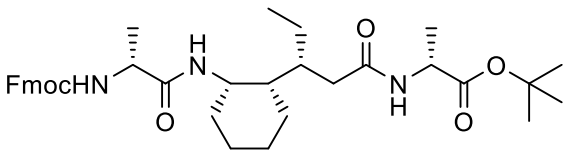

107

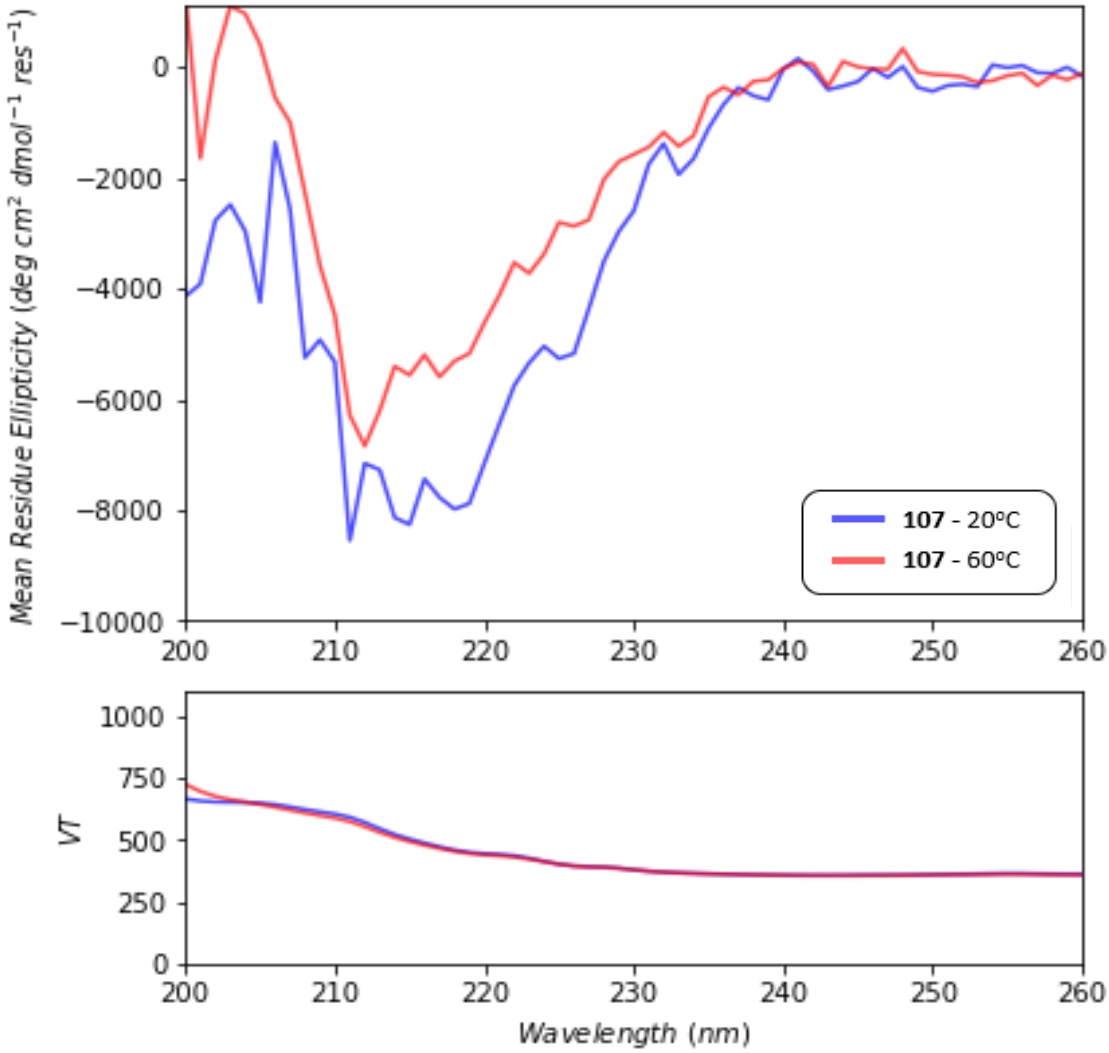

Figure 7.38: The CD spectra for **107** at 20°C and 60°C.

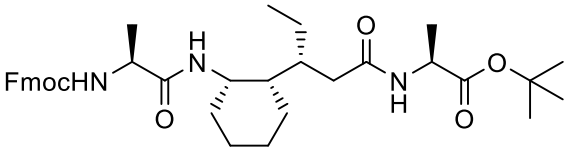

109

]

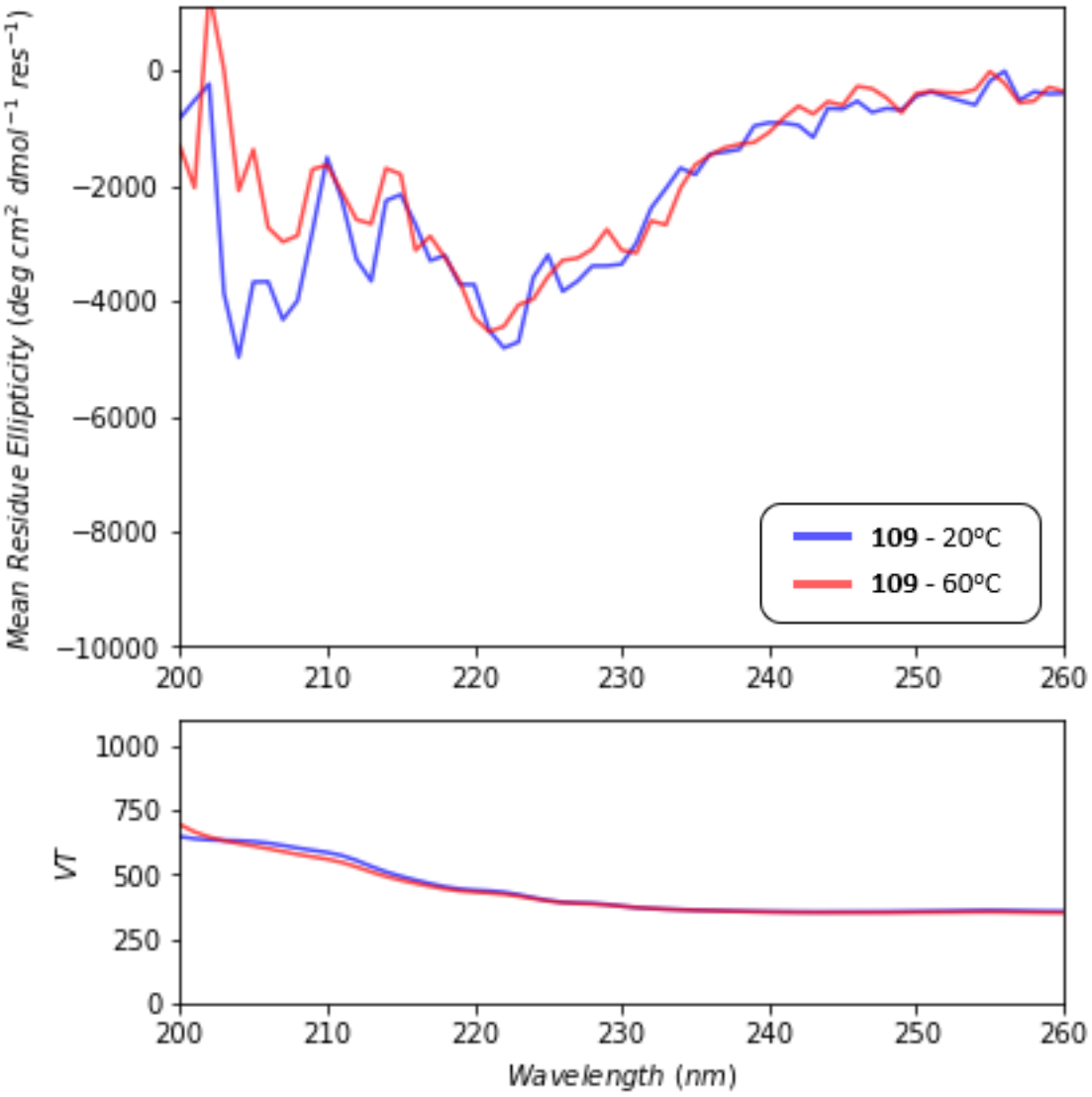

Figure 7.39: The CD spectra for **109** at 20°C and 60°C.

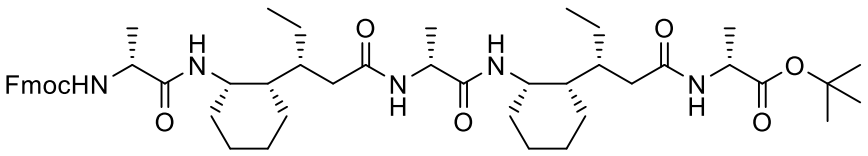

111

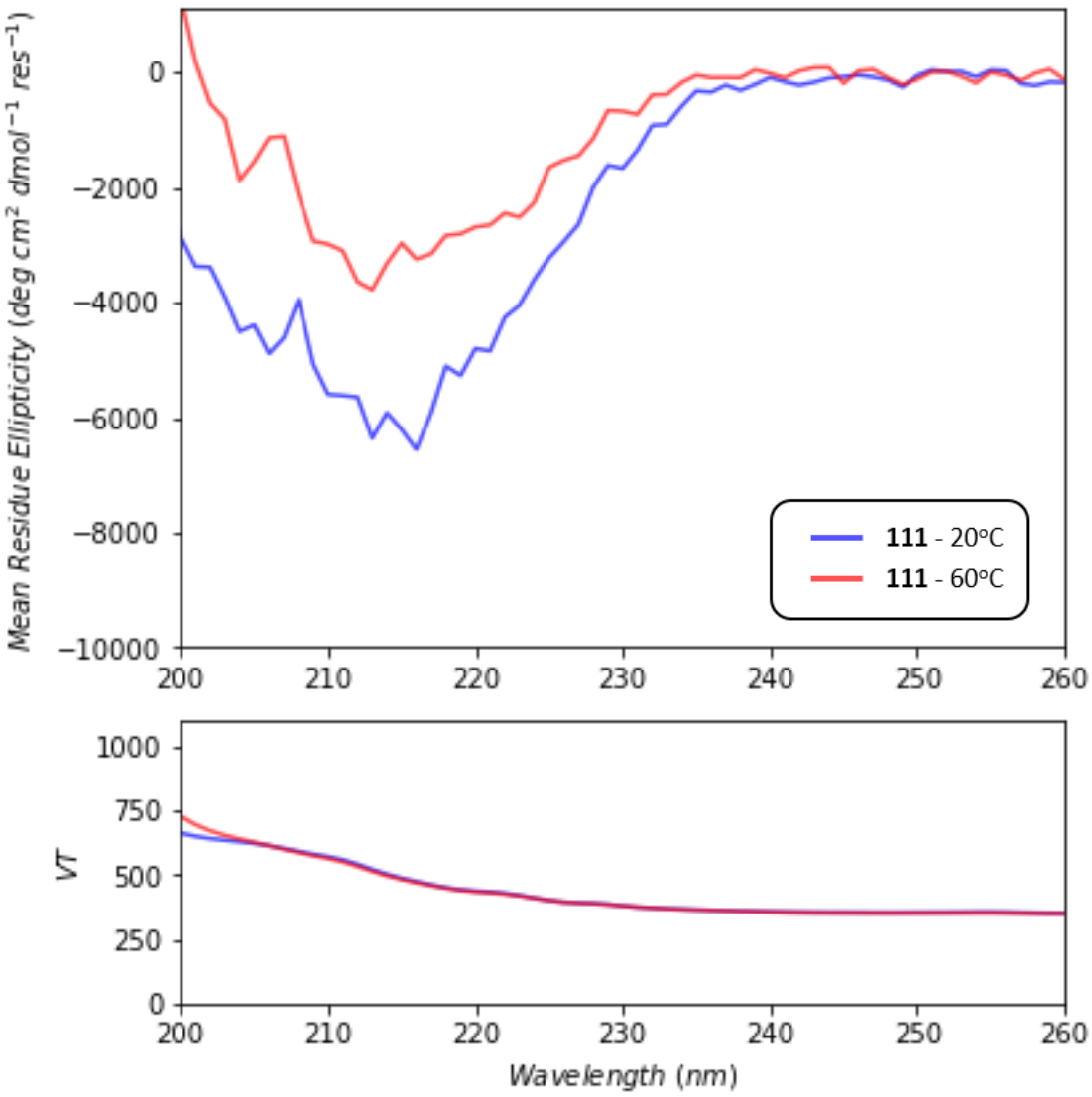

Figure 7.40: The CD spectra for **111** at 20°C and 60°C.

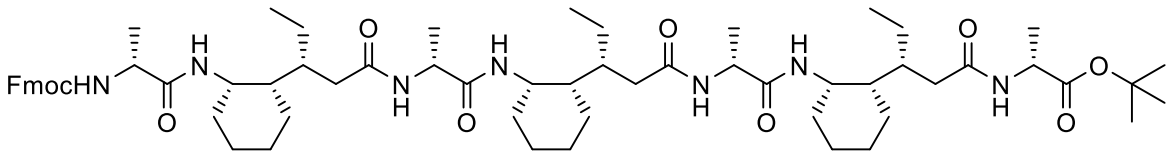

112

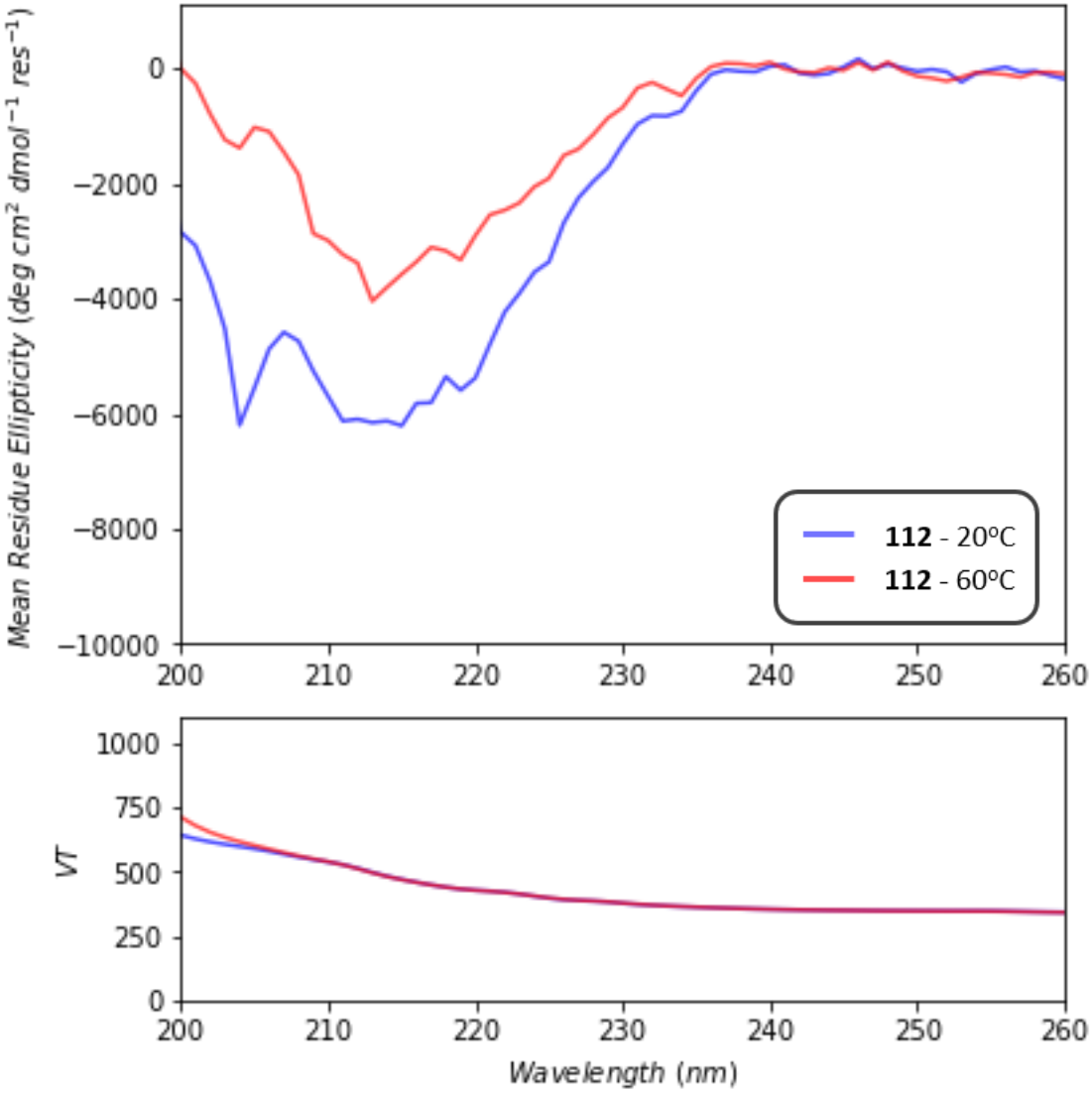

Figure 7.41: The CD spectra for **112** at 20°C and 60°C.

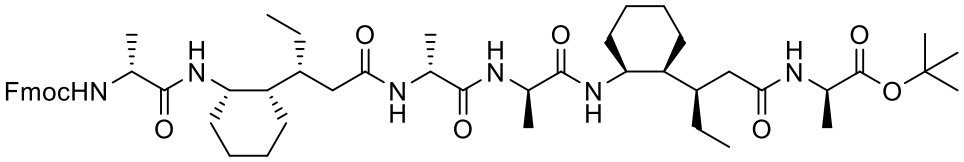

114

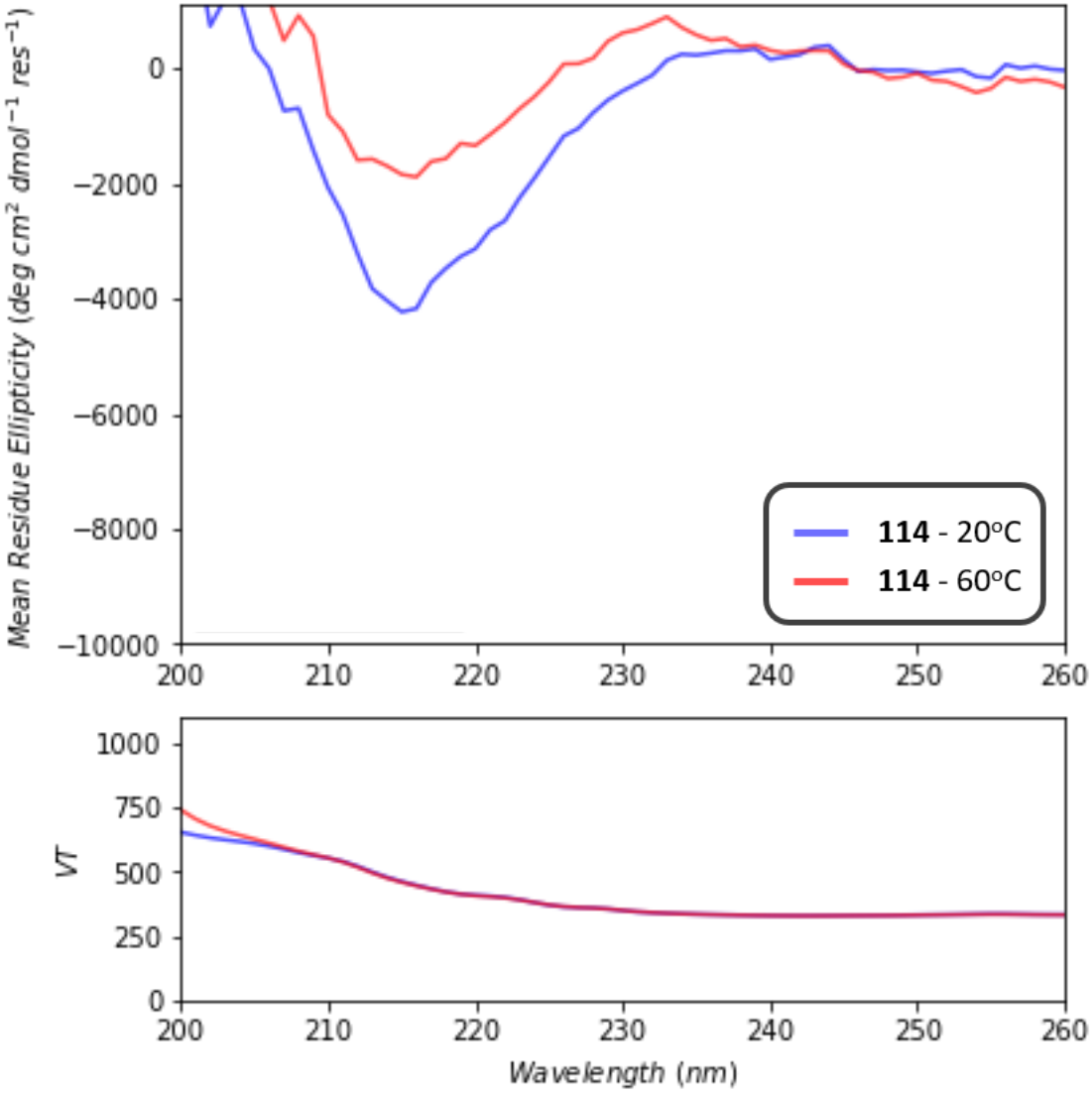

Figure 7.42: The CD spectra for **114** at 20°C